

# INDIAN JOURNAL OF PHYSICS

VOL. XIII

AND

## PROCEEDINGS

OF THE

*Indian Association for the Cultivation of Science, Vol. XXII.*

(Published in Collaboration with the Indian Physical Society)

### BOARD OF EDITORS

D. M. BOSE, PH.D. M. N. SAHA, D.Sc., F.R.S. K. PROSAD, M.A.

S. K. MITRA, D.Sc.

P. N. GHOSH, PH.D., Sc.D., *Secretary.*

(With Twenty-one Plates)

PRINTED AT THE CALCUTTA UNIVERSITY PRESS, SENATE HOUSE, CALCUTTA,  
BY BHUPENDRALAL BANERJEE AND PUBLISHED BY THE SECRETARY,  
INDIAN ASSOCIATION FOR THE CULTIVATION OF SCIENCE,

210, Bowbazar Street, Calcutta.  
1939,

Price Rs. 12 or £1-2-6.



## CONTENTS OF VOL. XIII

### PART I

	PAGE
1. The Propagation and the Total Reflection of Electromagnetic Waves in the Ionosphere—By M. N. Saha and K. B. Mathur	...      1
2. Raman Spectra of Co-ordination Compounds—By Bholanath Roy	...      13
3. Crystal Structure of Diphenylamine, Part I—By Jagattaran Dhar	...      27
4. The Internal Pressure in Liquids—By M. F. Soonawala	...      31
5. A New Theory of Lapse Rate—By D. Subrahmanyam	...      43
6. Further Studies of F-region at Allahabad—By R. R. Bajpai and B. D. Pant      ...      ...      ...      ...      ...      57	

### PART II

7. Jupiter's Atmosphere—By A. C. Banerji and Nizamuddin	...      73
8. A Note on the Transmutation Function for Deuterons—By P. L. Kapur      ...      ...      ...      ...      ...      87	
9. A Study of Sulphur Allotropes by the X-ray Diffraction Method (Part II)—By S. R. Das and K. Ghosh	...      ...      ...      ...      ...      91
10. The Fringe of the Atmosphere and the Ultra-violet Light Theory of Aurora and Magnetic Disturbance—By S. K. Mitra and A. K. Banerjee      ...      ...      ...      ...      ...      107	

### PART III

11. Band Spectrum of Antimony Monoxide—By A. K. Sen Gupta	...      145
12. On the Raman Effect in Camphor—By B. M. Anand and S. Narain	...      159
13. An experimental Study of Parabolic Wire Reflectors on a Wave- length of about 3 Metres—By A. K. Dutta, M. K. Chakravarty and S. R. Khastgir      ...      ...      ...      ...      ...      167	
14. On the Absorption and Emission Spectra of Rare Earth Crystals—By P. C. Mukherji      ...      ...      ...      ...      ...      185	
15. Measurement by means of the Electrometer Triode—By J. A. N. Thacs	...      199
16. An Improved form of Vacuum Arc Mercury still for Laboratories—By M. V. Sivaramakrishnan      ...      ...      ...      ...      ...      205	
17. On the Raman Spectrum of <i>o</i> -Diphenyl-benzene—By S. K. Mukerji and S. Abdul Aziz      ...      ...      ...      ...      ...      209	
18. On the Origin of the Colour of Paramagnetic Ions in Solution, II. Fine Structure of the Absorption Bands—By D. M. Bose and P. C. Mukherji      ...      ...      ...      ...      ...      219	

## Contents

### PART IV

	PAGE
19. New Measurements of Aluminium Monoxide Bands—By Debeshchandra Roy ... ... ... ...	231
20. A Simple Method of Coating Optical Surface, with Aluminium—By M. V. Sivaramakrishnan ... ... ... ...	241
21. Raman Spectrum of Diphenyl in the Solid State—By S. A. Aziz ...	247
22. Studies of the Ionosphere at Calcutta—By J. N. Bhar ..	253
23. Dynamics of the Pianoforte String and the Hammer Part III (General Theory)—By Mohinimohan Ghosh .	277
24. Surface Tension and Lindemann Frequency—By L. Sibaiya and M. Rama Rao . . . .	293
25. Liquid Drops—By L. D. Mahajan ... . . .	299

### PART V

26. Evaporation from Earthen Jugs—By Hazarilal Gupta and Abinash Chandra ... ... ... ...	305
27. Absorption Spectra of Compounds of Phosphorus—Sh. Nawazish Ali ...	309
28. Linear Extension of reflected Image produced by a Surface Traversed by Waves—By F. C. Auluck ... . . .	321
29. Isotope Effect in Band Spectrum of Tin monoxide—By P. C. Mahanti and A. K. Sen Gupta .. . . .	331
30. On the polarised Fluorescence of Organic Compounds—By Sachindra Mohan Mitra	349

### PART VI

31. Raman Effect in Arsenates and heat of Dissociation of AsO—By S. M. Mitra ... . . . .	391
32. On the Influence of Foreign Substances on the Absorption of the Dyestuffs in solution—By Sachindra Mohan Mitra ... . . .	397
33. A week Radio-active Substance (preliminary note)—Rajendralal De ...	407
34. A Note on the maintenance of Electron Emission in Cossor Valves after the low Tension supply is disconnected—By N. S. Pandya and P. D. Pathak ... . . . .	409
35. On the London-van der Waals forces between two Disc-like Particles—G. P. Dube and H. K. Das Gupta ... . . . .	411
36. Pressure Waves and Boundary Surfaces in the free Atmosphere—By D. S. Subrahmanyam ... . . . .	419
37. Raman Spectra of Coumarins and Chromones—By (Miss) Assema Mookerjee and Jagannath Gupta ... . . . .	439
38. Supersonic Velocities in Gases and Vapours—By S. K. Kulkarni Jatkar ... . . . .	445
39. Unusual Solar Activity—By Md. Salauddin and B. G. Narayan ... . . .	451
Supplementary : Presidential Address of the Indian Physical Society.	

## AUTHOR INDEX

		<b>PAGE</b>
Ali, Sh. Nawazish	... Absorption Spectra of Compounds of Phosphorus	... ... 309
Anand, B. M. and Narain, S.	On the Raman Effect in Camphor	... 159
Auluck, F. C.	... Linear Extension of reflected Image produced by a Surface traversed by Waves	... 321
Aziz, S. Abdul	... Raman Spectra of Diphenyl in Solid State See also Mukerji, S. K.	... 247
Bajpai, R. R. and Pant, B. D.	Further studies of F-region at Allhabad	... 57
Banerji, A. C. and Nizamuddin	Jupiter's Atmosphere	... ... 73
Banerjee, A. K.	... See Mitra, S. K.	
Bhar, J. N.	... Studies of the Ionosphere at Calcutta	... 253
Bose, D. M. and Mukherjee, P. C.	On the Origin of the Colour of Paramagnetic Ions in Solution, II. Fine Structure of Absorption Bands	... ... 219
Chakravarty, M. K.	... See Dutta, A. K.	
Chandra, Abinash	... See Gupta, Hazarilal.	
Das, S. R. and Ghose, K.	A Study of Sulphur Allotropes by X-ray diffraction Method (Part II)	... ... 91
Das Gupta, H. K.	... See Dube, G. P.	
De, Rajendralal	... A Weak Radioactive Substance (preliminary note)	... ... ... 407
Dhar, Jagattaran	... Crystal Structure of Diphenylamine, Part I	... 27
Dube, G. P. and Das Gupta, H. K.	On the London-van der Waals force between two Disc-like Particles	... ... 411
Dutta, A. K., Chakravarty M. K. and Khastgir, S. R.	An Experimental Study of Parabolic Wire Reflectors on a Wave-length of about 3 Metres	... ... ... 167
Ghosh, Mohinimohan	Dynamics of the Pianoforte String and the Hammer, Part III (General Theory)	... 277
Gupta, Hazarilal and Chandra, Abinash	Evaporation from Earthen Jugs	... ... 305
Gupta, Jagannath	... See Mookerjee, Aseema.	
Kapur, P. L.	... A note on the Transmutation Function for Deuterons	... ... ... 87

*Author Index*

		<b>PAGE</b>
Khastgir, S. R.	... See Dutta, A. K.	
Kulkarni Jatkar, S. K.	... Supersonic Velocities in Gases and Vapours	445
Mahajan, L. D.	... Liquid Drops	299
Mahanti, P. C. and Sen Gupta, A. K.	Isotope Effect in Band Spectrum of Tin Monoxide	331
Mathur, K. B.	... See Saha, M. N.	
Mitra, S. K. and Banerjee, A. K.	The Fringe of the Atmosphere and the Ultra-violet Light Theory of Aurora and Magnetic Disturbance	107
Mitra, Sachindra Mohan	On the polarised Fluorescence of Organic Compounds	349
	Raman Effect in Arsenates and heat of Dissociation of AsO	391
	On the Influence of Foreign Substance on the Absorption of the Dyestuffs in Solution	397
Mookerjee, (Miss) Aseenia and Gupta, Jagannath	Raman Spectra of Coumarins and Chromones	439
Mukherjee, P. C.	... On the Absorption and Emission Spectra of Rare Earth Crystals	185
	See also Bose, D. M.	
Mukherji, S. K. and Aziz S. Abdul	On the Raman Spectra of o-Diphenylbenzene	209
Narain, S.	... See Anand, B. M.	
Narayan, B. G.	... See Salaruddin, Md.	
Nizamuddin	... See Banerjee, A. C.	
Pant, B. D.	... See Bajpai, R. R.	
Pandya, N. S. and Pathak P. D.	A note on the maintenance of Electron Emission in Cossor Valves after the low Tension supply is disconnected	409
Pathak, P. D.	... See Pandya, N. S.	
Rama Rao, M.	... See Sibaiya, L.	
Roy, Bhulanath	... Raman Spectra of Co-ordination Compounds	13
Roy, Debeschandra	... New Measurements of Aluminium Monoxide Bands	231
Saha, M. N. and Mathur, K. B.	The Propagation and the Total Reflection of Electromagnetic Waves in the Ionosphere	1
Salaruddin, Md. and Narayan, B. G.	Unusual Solar Activity	451
Sen Gupta, A. K.	... Band Spectrum of Antimony Monoxide	145
Sibaiya, L. and Rama Rao, M.	Surface Tension and Lindemann Frequency	293

*Author Index*

vii

	PAGE
Sivaramakrishnan, M. V.	An Improved Form of Vacuum Arc Mercury still for Laboratories ... ... 205
Subrahmanyam, D. S.	A Simple Method of Coating Optical Surfaces with Aluminium ... ... 241
Soonawala, M. F.	A New Theory of Lapse Rate ... ... 43
Thaes, J. A. N.	Pressure Waves and Boundary Surfaces in the free Atmosphere ... ... 419
	The Internal Pressure in Liquids ... ... 31
	Measurement by means of the Electrometer Triode ... ... 199



## SUBJECT INDEX

SUBJECT	AUTHOR	PAGE
Absorption and Emission Spectra of Rare Earth Crystals.	P. C. Mukherjee	185
Absorption Spectra of Compounds of Phosphorus	Sh. Nawazish Ali	200
Absorption of the Dyestuffs in solution, On the Influence of Foreign Substances on the	Sachindra Mohan Mitra	397
Band Spectrum of Antimony Monoxide.	A. K. Sen Gupta	145
Bands of Aluminium Monoxide, New Measurements	Debeshchandra Roy	231
Band Spectrum of Tin Monoxide, Isotope Effect in	P. C. Mahanti and A. K. Sen Gupta	331
Colour of Paramagnetic Ions in Solution, II. Fine Structure of the Absorption Bands, On the Origin of the	D. M. Bose and P. C. Mukherjee	219
Electrometer Triode, Measurements by means of the	J. A. N. Thaes	199
Evaporation from Barthen Jugs	Hazarilal Gupta and Abinash Chandra	305
Fringe of the Atmosphere and the Ultra-violet Light Theory of Aurora and Magnetic Disturbance	S. K. Mitra and A. K. Banerjee	107
F-region at Allahabad, Further Studies of	R. R. Bajpai and B. D. Pant	57
Ionosphere, The Propagation and Total Reflection of Electromagnetic Waves in the	M. N. Saha and K. B. Mathur	1
Ionosphere at Calcutta, Studies of the Jupiter's Atmosphere	J. N. Bhar	253
Lapse Rate, A New Theory of	A. C. Banerji and Nizamuddin	73
Linear Extension of reflected Image produced by a Surface traversed by Waves	D. Subrahmanyam	43
Liquids, the Internal Pressure in Liquid drops	F. C. Auluck	321
London-van der Waals Forces between two Disc-like Particles, on the	M. F. Soonawala L. D. Mahajan G. P. Dube and H. K. Das Gupta	31 299 411

**Subject Index**

SUBJECT	AUTHOR	PAGE
Maintenance of Electron Emission in Cossor Valves after the low Tension supply is disconnected, A note on the	N. S. Pandya and P. D. Pathak	409
Optical Surfaces, A Simple Method of Coating with Aluminium	M. V. Sivaramakrishnan	241
Parabolic Wire Reflectors, An Experimental Study with Wave-length of about 3 Metres	A. K. Dutta, M. K. Chakravarti and S. R. Khastgir	167
Pianoforte String and the Hammer, Dynamics of the, Pt. III. (General Theory)	Mohinimohan Ghosh	277
Polarised Fluorescence of Organic Compounds, On the	Sachindra Mohan Mitra	349
Pressure Waves and Boundary Surfaces in the free Atmosphere	D. S. Subrahmanyam	419
Raman Spectra of Co-ordination Compounds	Bholanath Roy	13
Raman Effect in Camphor, On the	B. M. Anand and S. Narain	159
Raman Spectrum of o-Diphenylbenzene, On the	S. K. Mukerji and S. Abdul Aziz	209
Raman Spectra of Diphenyl in the Solid State	S. A. Aziz	247
Raman Effect in Arsenates and heat of Dissociation of AsO	S. M. Mitra	391
Raman Spectra of Coumarins and Chroinones	(Miss) Aseema Mookerjee, and Jagannath Gupta	439
Radioactive Substance, A Weak, (preliminary note)	Rajendralal De	407
Solar Activity, Unusual	Md. Salaruddin and B. G. Narayan	451
Structure of Diphenylamine Crystal, Part I	Jagattaran Dhar	27
Sulphur Allotropes, A Study by the X-ray Diffraction Method (Part II)	S. R. Das and K. Ghosh	91
Supersonic Velocities in Gases and Vapours	S. K. K. Jatkar	445
Surface Tension and Lindemann Frequency	L. Sabaiya and M. Rama Rao	299
Transmutation Function for Deuterons, A Note on the	P. L. Kapur	87
Vacuum Arc Mercury still for Laboratories, An Improved Form of	M. V. Sivaramakrishnan	205

# THE PROPAGATION AND THE TOTAL REFLECTION OF ELECTROMAGNETIC WAVES IN THE IONOSPHERE

By M. N. SAHA, D.Sc., F.R.S.

AND

K. B. MATHUR, M.Sc.

**ABSTRACT.** A critical review is given in this article of Prof. S. N. Bose's paper published in this journal. It is shown that when the collision frequency is taken to be zero, his method gives us the same result for the propagation of wireless waves as that of the earlier workers. The conditions of reflection which he has deduced for the case where collision cannot be neglected appear to require revision.

The propagation and the total reflection of electromagnetic waves in the ionosphere has been the subject of numerous investigations within the last ten years, a full bibliography of which is given under the references. A critical review of these papers shows that there are many points connected with this problem which have not yet received adequate explanation. In his pioneering work on the magnetoionic theory, Appleton (1932) did not actually solve the relevant Maxwellian Equations but expressions were obtained for the refractive index from a calculation of the dielectric constant of the medium, which is supposed to consist of a number of free electrons and ions. The displacement of these under the magnetic field which is limited by collisions with neutral particles and positive ions constitutes the displacement current, which is necessary to calculate the complex dielectric constant. Appleton's method is usually known as the ray theory of propagation of the electromagnetic waves. The refractive index comes out in general to be a complex quantity and has two different values depending upon the state of polarisation of the wave. Further it is a function of the electron concentration and collisional frequency, both of which are functions of height. Consequently the wave equation becomes too complex for solution. From the analysis, it follows that the original wave splits up into two ordinary and extraordinary, which are propagated with different velocities, as in a doubly refracting medium. He supposes that in the case when collisions can be neglected, the wave gets reflected from the layer where the refractive index becomes equal to zero. This enabled him to obtain the conditions of reflection involving the electron concentration and the frequency of the wave, which are now well-known and have received verification at least in the case of the F-layer.

A number of other methods has been proposed of which we may mention that of Försterling and Lassen (1933), Saha, Rai and Mathur (1938) and that of Hartree (1931) developed further by Booker (1935). The works of these authors lead to the same value of refractive index as that of Appleton, though originally they aimed at obtaining different results.

Recently Prof. S. N. Bose (1938) of Dacca has tackled the same problem by the method of characteristics, used for wave propagation by Hadamard, Debye and others. He confirms in general the conclusions of the previous investigators when collisions can be neglected, but gives new results when the collisions cannot be neglected. His results are, however, expressed in rather unfamiliar symbols, hence it is difficult to compare them with those of earlier workers and apply them to the elucidation of outstanding problems. The object of this paper is to examine his methods and results critically, to express them in a language easily comprehensible to workers on the ionosphere, and to find out how far the results obtained are new.

As we have to make a constant comparison between Bose's paper and the paper previously published by Saha, Rai and Mathur as well as those of other workers, we will refer to the latter as paper I.

The fundamental equations for propagation can be written as

$$\frac{1}{c} \frac{\vec{dE}}{dt} - \text{Curl } \vec{H} = - \frac{\rho V}{c} \quad \dots \quad (1)$$

$$\frac{1}{c} \frac{\vec{dH}}{dt} + \text{Curl } \vec{E} = 0 \quad \dots \quad (2)$$

$$\text{Div } \vec{H} = 0 \quad \dots \quad (3)$$

$$\text{Div } \vec{E} = \rho \quad \dots \quad (4)$$

These equations may be compared with (1.1) of paper I. Bose has used  $E$ ,

while in paper I,  $\vec{D}$  was used. But  $\vec{D} = \vec{KE} + \vec{P}$ ,  $K=1$ , and  $\vec{P} = \vec{NeV}$ , where  $V$  is the velocity of electrons.  $\vec{P}$  is therefore the displacement current, a term denoted by Bose by the symbol  $\theta$ . For his  $\theta_0$ , which is electrical density, we have used  $\rho$ . The fundamental equations used here, are of the same form as those of Booker.<sup>5</sup> The equations satisfy the conditions of continuity

$$\frac{d\rho}{dt} + \text{Div } (\rho V) = 0 \quad \dots \quad (5)$$

Let us now suppose (see Bose, p. 122) that every quantity vary as  $e^S$ , where  $S$  is the phase. For a plane wave

$$S = ip \left[ t - \frac{(lx + my + nz)}{c} \right]$$

where  $p$  is the pulsatance  $= 2\pi f$ ,  $f$  being the frequency of the wave,  $(l, m, n)$  direction-cosines of the wave-normal,  $q$  = refractive index. In general,  $(l, m, n)$  and  $q$  may be functions of  $(x, y, z)$ . Anyhow, no limitation is put on the form of  $S$  except that it is a function of  $(x, y, z, t)$ . Then the above equations reduce to

$$\frac{\dot{S}}{c} \vec{E} - (\vec{\Delta S} \times \vec{H}) = - \frac{\dot{P}}{c} \quad \dots (1')$$

$$\dot{S} \vec{H} + (\vec{\Delta S} \times \vec{E}) = 0 \quad \dots (2')$$

$$(\vec{\Delta S} \cdot \vec{H}) = 0 \quad \dots (3')$$

$$(\vec{\Delta S} \cdot \vec{E}) = p \quad \dots (4')$$

$$\dot{S}p + (\vec{P} \cdot \vec{\Delta S}) = 0 \quad \dots (5')$$

Here the supposition is that if  $\vec{E} = E_0 e^S$ ,  $E_0$  is a slowly-varying function of  $(x, y, z, t)$ , i.e.,

$$E_0 \dot{S} \gg \frac{dE_0}{dt}, \quad E_0 S_x \gg \frac{dE_0}{dx}$$

From (2), by scalar multiplication with  $H$ , we have

$$(\vec{E} \cdot \vec{H}) = 0 \quad \dots (6)$$

From (1), by scalar multiplication with  $H$ , we have

$$(\vec{P} \cdot \vec{H}) = 0 \quad \dots (7)$$

(4), (6), (7) show that  $\vec{E}$ ,  $\vec{P}$ ,  $\vec{\Delta S}$  are all normal to  $\vec{H}$ , and hence lie in the plane perpendicular to  $\vec{H}$ . But neither  $\vec{E}$ , nor  $\vec{P}$  are in general normal to  $\vec{\Delta S}$ , but from (1) we have

$$\frac{1}{c} (\vec{S} \vec{E} + \vec{P}) = (\vec{\Delta S} \times \vec{H}) \quad \dots (8)$$

i.e., the vector  $\vec{S} \vec{E} + \vec{P}$  is normal to both  $\vec{\Delta S}$  and  $\vec{H}$ .

To find out  $\vec{P}$ , we take the equation of motion of the electrons and ions. Let the displacement of these particles due to the radio-wave be  $u = (\xi, \eta, \zeta)$ . Then the equation of motion is

$$\ddot{\vec{m}}\vec{u} = e\vec{E} - g\vec{u} + \frac{e}{c}(\vec{u} \times \vec{h}) \quad \dots \quad (9)$$

This is a vector equation, identical with equation (1.3) of our paper I, and equation on p. 131 of Bose. Now we have

$$\vec{P} = Ne\vec{u}, \quad \vec{P} = Ne\vec{u}$$

Hence replacing  $\vec{u}$  by  $\vec{P}/Ne$ , we have

$$\ddot{\vec{P}} + v\dot{\vec{P}} = \frac{Ne^2}{m}\vec{E} + (\vec{P} \times \vec{h}) \quad \dots \quad (10)$$

Or using the symbols in (1.4) of paper I and putting  $\vec{P} = \vec{P}_0 e \vec{S}$

we have  $(\vec{S} + v)\vec{P} = \vec{P}_0^2 \vec{E} + (\vec{P} \times \vec{p}_h)$   $\dots \quad (10')$

where  $\vec{p}_h = \frac{e\vec{h}}{mc}$ ,  $\vec{P}_0^2 = \frac{Ne^2}{m}$ .

This is a vector equation and is equivalent to three different equations.

### THE EQUATION OF PROPAGATION

Multiplying (10) by  $\Delta \vec{S}$  vectorially, we have

$$\frac{\dot{\vec{S}}}{c}(\Delta \vec{S} \times \vec{H}) + \Delta \vec{S} \times (\Delta \vec{S} \times \vec{E}) = 0$$

since

$$(\Delta \vec{S} \times \vec{H}) = \frac{1}{c}(\vec{S} \cdot \vec{E} + \vec{P})$$

$$\begin{aligned} \Delta \vec{S} \times (\Delta \vec{S} \times \vec{E}) &= \Delta \vec{S} \cdot (\Delta \vec{S} \cdot \vec{E}) - \vec{E}^2 (\Delta^2 \vec{S}) \\ &= \rho \Delta \vec{S} - \vec{E} \Delta^2 \vec{S} \end{aligned}$$

Here  $\Delta^2 S$  means  $(\Delta S)^2$ . We have

$$\left( \frac{\dot{S}^2}{c^2} - \Delta^2 S \right) \vec{E} + \frac{\vec{P} \cdot \dot{S}}{c^2} + \rho \Delta S = 0 \quad \dots (11)$$

Now making use of the equations (5) and (10), we get the following vector-equation in  $\vec{P}$

$$\frac{\vec{P} \cdot \dot{S}}{c^2} = \frac{1}{p_0^2} \left[ \frac{\dot{S}^2}{c^2} - \Delta^2 S \right] \left[ (\dot{S} + v) \vec{P} - (\vec{P} \times \vec{p}_h) \right] = \frac{\vec{\Delta S} \cdot (\vec{P} \cdot \vec{\Delta S})}{\dot{S}} \quad \dots (12)$$

This is equivalent to three equations, and the operations which we have carried out here is similar to those in § 2 of our paper I.

The three vector equations (12), can be written out in a form more convenient for work by introducing some fresh notation. Here we are closely following Bose's procedure on pp. 137-138 of his paper.

We put

$$\begin{aligned} g(S) &= \frac{\dot{S}^2}{c^2} - \Delta^2 S \\ p(S) &= \dot{S}(\dot{S} + v) + p_0^2 \\ L(S) &= \left( \frac{\dot{S}^2}{c^2} - \Delta^2 S \right) \left[ \dot{S}(\dot{S} + v) + p_0^2 \right] + p_0^2 \Delta^2 S \\ &= g(S) p(S) + p_0^2 \Delta^2 S \end{aligned} \quad \dots (13)$$

(12) can now be written as

$$\vec{L}(S) \vec{P} - \dot{S} g(S) (\vec{P} \times \vec{p}_h) = p_0^2 \vec{\Delta S} \cdot (\vec{P} \cdot \vec{\Delta S}) \quad \dots (14)$$

Writing out in full, we have

$$\begin{aligned} \dot{P}_x [L(S) - p_0^2 S_x^2] + \dot{P}_y [T_x - S_x S_y p_0^2] + \dot{P}_z [-T_y - S_x S_z p_0^2] &= 0 \\ \dot{P}_x [-T_x - S_x S_y p_0^2] + \dot{P}_y [L(S) - p_0^2 S_y^2] + \dot{P}_z [T_x - S_x S_z p_0^2] &= 0 \\ \dot{P}_x [T_y - S_x S_z p_0^2] + \dot{P}_y [-T_x - S_x S_y p_0^2] - \dot{P}_z [L(S) - S_z^2 p_0^2] &= 0 \end{aligned} \quad \dots (15)$$

where  $\vec{T} = (T_x, T_y, T_z) = -\dot{S} g(S) \vec{p}_h$

Since the equations hold simultaneously, the determinant of their co-efficients vanish. From this condition we get after some work

$$L^3(S) - L^2(S) \Delta^2 S p_0^2 + L(S) \dot{S}^2 g^2(S) p_0^2 - \dot{S}^2 g^2(S) p_0^2 (\vec{\Delta S} \cdot \vec{p}_h)^2 = 0 \quad \dots (16)$$

Now

$$(\Delta S \cdot p_h) = p_h \Delta S \cdot \cos \alpha.$$

where  $\alpha$  is the angle between  $p_h$  the direction of the external magnetic field, and  $\Delta S$  the wave normal. Further, since

$$L(S) - p_0^2 \Delta^2 S = g(S) p(S)$$

we find that  $g(S)$  cancels out as a common factor. Equation (16) reduces to

$$p(S) L^2(S) - S^2 g(S) p_h^2 L(S) - S^2 g(S) p_h^2 p_0^2 \Delta^2 S \cos^2 \alpha = 0 \quad \dots \quad (17)$$

(16) and (17) are identical with the equations given by Bose on p. 142.

Bose points out that from equation (17), we can calculate the value of the refractive indices. As (17) is a quadratic equation we get two values for the refractive indices,  $q_1$  and  $q_2$ . But he does not proceed further to find out the actual values of  $q_1$ , and  $q_2$ , and compare them with the results of earlier investigators. This we now proceed to do, and we shall show that we get the same value for  $q_1$  and  $q_2$  as obtained on p. 63 of paper I for the o- and x-waves.

Let us put

$$q = \frac{c}{\lambda} |\Delta S| \quad \text{and} \quad S = i p$$

This is equivalent to taking

$$S = i p t \mp \frac{i p}{c} \int q (l dx + m dy + n dz)$$

and for vertical propagation

$$S = i p t \mp \frac{i p}{c} \int q dz$$

Now  $(ql, qm, qn)$  may be any functions of  $(x, y, z)$ ;  $q$  may be called the refractive index.  $p = \frac{1}{i} S$  is constant, and prescribed by the conditions of the experiment. Then it can be easily verified that if we put

$$r - q^2 = x, \quad r - \frac{iv}{p} = \delta, \quad r = p_0^2/p^2$$

we have for vertical propagation, i.e.,  $S_x = S_y = 0$ ,  $S_z = r$ ,

$$L(S) = -\frac{p^4}{c^2} (r - x\beta) \quad g(S) = -\frac{p^2}{c^2} x \quad p(S) = p^2(r - \beta)$$

and equation (17) reduces to

$$C' x^2 + xr[2\beta(\beta - r) + \omega^2 \sin^2 \alpha] - r^2(r - \beta) = 0 \quad \dots \quad (18)$$

Here  $C'$  is the quantity

$$C' = \beta(\beta^2 - \omega^2) - r(\beta^2 - \omega^2 \cos^2 a)$$

defined in equation (2.18) of paper I.

It can be shown after some work that the roots of equation (18) are given by

$$C'x = C'(1 - q^2) = -r\beta(r - \beta) - \frac{r\omega^2}{2} \sin^2 a \left[ 1 \pm \sqrt{1 + \frac{4(r - \beta)^2 \cos^2 a}{\omega^2 \sin^4 a}} \right] \dots \quad (19)$$

We get from (19)

$$C'q^2 = (r - \beta)(\omega^2 - \beta^2 + r\beta) - \frac{r\omega^2}{2} \sin^2 a \left[ 1 \pm \sqrt{\frac{4(r - \beta)^2 \cos^2 a}{\omega^2 \sin^4 a}} \right] \dots \quad (20)$$

If we neglect collisions, i.e., put  $\beta=1$ , we can easily deduce that (20) reduces to the values of  $q_o$  and  $q_x$  given in (3.10) of paper I. Hence we have proved that for vertical propagation, Bose's treatment gives the same result as that of earlier workers.

#### CONDITIONS FOR REFLECTION OF THE E. M. WAVE FROM THE IONOSPHERE

Let us now critically examine Bose's work as far as it deals with the conditions of reflection of the o- and x-waves from the ionosphere. In the original treatment of Appleton, it was supposed that the waves get reflected when  $q$ , the refractive index, becomes zero, in the cases where collision frequency can be neglected. This gives the well-known conditions of reflection.

o-wave 
$$\frac{Ne^2}{m} = p^2 \dots \quad (21)$$

x-wave 
$$\frac{Nc^2}{m} = p^2 \pm pp_h$$

It is supposed that the reflection represented by + sign does not occur, as the x-wave gets totally reflected from a lower height corresponding to the negative sign. Under these suppositions, we should have for Allahabad for  $f=4$  Mc./sec.

$$f_o^* - f_e^* = 65 \text{ Mc/sec.}$$

While this has been verified in general, Pant and Bajpai (1937), at Allahabad obtained on several occasions, difference of a quite different order :—it was found that for  $f=4$  Mc/sec.

$$f_c^o - f_c^r = 14 \text{ Mc/sec.}$$

This was explained by R. N. Rai (1937) from the idea that waves are returned from the ionosphere, when their group-velocity of propagation becomes zero. From this, he deduced when collisions can be neglected, in addition to the Appleton condition, a new condition of reflection

$$\frac{Ne^2}{m} = p^2 \frac{p_h^2 - p_L^2}{p^2 - p_L^2} \quad \dots \quad (22)$$

This gives us exactly

$$f_c^o - f_c^r = 14 \text{ Mc/sec.}$$

Thus the new condition explains completely the result obtained by Pant and Bajpai.

The question now rises : Both Appleton's criterion ( $q=0$ ), as well as that used by Rai (group-velocity=0) are, at best, assumptions. Can they be substantiated as direct deductions from theory? Further, when the collisional damping cannot be neglected, what will be the condition of reflection? This is the problem which Bose sets about to solve. His procedure is as follows :

By squaring equation (2), we have

$$\frac{S^2}{c^2} H^2 = (\Delta S \times E)^2 = (\Delta S)^2 E^2 - (\Delta S \cdot E)^2$$

$$\text{Hence } \frac{H^2}{E^2} = \frac{c^2 \Delta^2 S}{S^2} - \frac{(\Delta S \cdot E)^2 \cdot c^2}{E^2 \cdot S^2} = q^2 (1 - \cos^2 \theta) \quad \dots \quad (23)$$

where  $\theta$  is the angle between  $\Delta S$  and  $E$ . In general,  $\theta$  is a definite quantity.

Bose has assumed that reflection takes place when  $H=0$  or when  $E$  becomes parallel to  $\Delta S$ . These conditions reduce to  $q=0$  and  $q=\infty$  respectively.

From (23) we have

$$H=0 \quad \text{when } q=0$$

$$\text{and} \quad E=0 \quad \text{when } q=\infty$$

The propagation loses its wave character either when  $H=0$ , or  $E=0$ . We can therefore suppose that the wave will be reflected either when  $q=0$ , or  $q=\infty$ . The former gives us the conditions of Appleton (equation 21), and the latter gives us Rai's condition.

Bose has further tried to obtain more general conditions of reflection when damping cannot be neglected. (Equations on p. 132, 133 again on p. 139 and 140.) His condition for the o-wave is

$$\frac{dS}{dt} = -\frac{v}{2} \pm i \sqrt{p_0^2 - v^2/4}$$

He concludes that from this the train totally reflected has the form

$$\text{Exp} \left[ -\frac{v}{2} t \pm i \sqrt{p_0^2 - v^2/4} t \right]$$

and puts

$$p_c^2 = p_0^2 - v^2/4.$$

This takes the place of  $p^2 = p_0^2$  for the o-wave.

Similarly he obtains results for the x-wave on p. 133, and 135, which take the place of

$$p_0^2 = p^2 \pm pp_h, \quad p_0^2 = p^2 \frac{p^2 - p_h^2}{p^2 - p_{12}^2}$$

These results obtained by Bose are equivalent to putting the complex values of  $q$  for the o and x-waves given by formula (20) equal to zero and infinity. This is shown in Appendix (1), and the work is due to Mr. R. N. Rai.

But it is difficult to agree with this procedure because when  $q$  is complex, the conditions of reflection are no longer given by either  $q=0$ , or  $q=\infty$ .

For in general, when  $q$  is complex we can put  $q = \mu + i \frac{ck}{p}$

and it has been shown, that we have for the quasi-transverse as well as quasi-longitudinal regions

$$\mu^2 = \frac{1}{2} \left\{ \sqrt{X^2 + Y^2} + X \right\} \quad \dots \quad (25)$$

$$\frac{c^2 k^2}{p^2} = \frac{1}{2} \left\{ \sqrt{X^2 + Y^2} - X \right\}$$

where  $X$  and  $Y$  are function of electron-concentration, and collisional damping. For the o-wave in the equatorial region, we have

$$X = 1 - \frac{r}{1 + \delta^2}, \quad Y = \frac{r\delta}{1 + \delta^2}$$

The forms (25) show that  $\mu^2$  and  $\frac{c^2 k^2}{p^2}$  can never be negative. This is at once clear if one looks at the curves drawn for various values of  $v$ , and  $r$

by M. Taylor (1938) and Goubau (1935). For the o-wave it is found that for a fixed value of  $v$ ,  $\mu$  gradually decreases with  $r$ , and ultimately takes a small value  $>0$ , and varying very slowly. For the x-wave, the first part of the curve is similar, but then  $\mu$  rises abruptly, reaches a steep maximum at the point corresponding to  $\mu=\infty$  and then drops out very much as in the  $\mu$ -curve for the o-wave.

But it should be emphasised that these curves give no idea of the actual variation of  $\mu^2$  with  $z$ , because  $\mu^2$  is a function of  $N$  (the number of electrons), and  $v$ , the collisional damping, both of which vary continuously with height. For finding out the actual variation of  $\mu^2$  with height, we can adopt two procedures—we can take a number of curves of the type drawn by Goubau or M. Taylor for varying values of  $v$ , plot them on cardboards, and then cut the cardboards along the curves. These may then be arranged in a three-dimensional array, behind each other, so that X-axis corresponds to  $N$ , the Y-axis to  $v$ , and the Z-axis to  $\mu^2$ . We have then to take a section through the three dimensional profile of the  $\mu^2$ -surface, corresponding to the actual conditions in the atmosphere.

The other procedure would be to plot  $\mu^2$ -values taking some theoretical values for  $v$  and  $N$ , the electron concentration.  $N$  can be calculated from Chapman's formula for a simple region which has been shown by Saha and Rai (1938) to hold for the general case when radiation need not be monochromatic and  $v$  can be calculated from the kinetic gas theory, by taking  $T=\text{constant}$ , or  $T$  varying according to some assumed law.

In general,  $\mu^2=1$  in the non-deviating region, and variations will occur only in the deviating region. The curve will be usually smooth, but may show sudden fluctuations when we pass through irregular banks of ions or electrons, such as may likely be produced by minor causes. When we come to the simple region,  $\mu^2$  will vary continuously from unity to a small value, depending on  $p$ . These calculations are being carried out by the junior author.

These arguments tell us that both  $\mu^2$  and  $\left(\frac{c^2 k^2}{p^2}\right)$  the real and imaginary parts of  $q$ , are essentially positive, and they can be zero, only in the ideal case when  $\delta$ , the collision frequency is zero. Hence it is not possible to put  $q=0$ , and deduce any condition from it. In the same way, we cannot put  $q=\infty$ , when  $q$  is complex.

#### R E F E R E N C E S

Appleton (1932) : *J. Elec. Engrs.*, **71**, 642.

Booker (1936) : *Proc. Roy. Soc. A.*, **188**, 235.

Bose (1938) : *Ind. Journ. Phys.*, **21**, 121.

Fosterling & Lassen (1933) : *Ann. d. Physik.*, **18**, 26.

Goubaud (1935) : *Zs. f. H. F. T.*, **45**, 181.

Hartree (1931) : *Proc. Camb. Phil. Soc.*, **27**, 143.

Pant & Bajpai (1937) : *Science & Culture*, **2**, 409.

Rai (1937) : *Proc. Nat. Inst. Sci. India*, **3**, 307.

Saha, Rai & Mathur (1938) : *Proc. Nat. Inst. Sci. India*, **4**, 53.

Taylor (1933) : *Proc. Roy. Soc.*, **48**, 245.

### A P P E N D I X - I

Equation (20) can be written as

$$C'q_o^2 = t(\omega^2 + \beta t) - \frac{r\omega^2}{2} \sin^2 \alpha \left[ 1 - \sqrt{1 + \frac{4t^2 \cos^2 \alpha}{\omega^2 \sin^4 \alpha}} \right] \quad \dots \quad (i)$$

$$C'q_x^2 = t(\omega^2 + \beta t) - \frac{r\omega^2}{2} \sin^2 \alpha \left[ 1 + \sqrt{1 + \frac{4t^2 \cos^2 \alpha}{\omega^2 \sin^4 \alpha}} \right] \quad \dots \quad (ii)$$

Where

$$t = (r - \beta)$$

Now

$$q_o^2 = o$$

When

$$t = o$$

or

$$r - \beta = o$$

or

$$p^2 - ivp - p_0^2 = o$$

or

$$p = \frac{iv}{2} \pm \sqrt{p_0^2 - v^2}/4$$

Therefore the critical frequency is given by

$$p_c = \sqrt{p_0^2 - v^2}/4 \quad \dots \quad (iii)$$

$$q_x^2 = o \quad \text{when} \quad t^2 = \omega^2$$

or

$$t = \pm \omega$$

or

$$p^2 - ivp - p_0^2 \pm pp_h = o$$

putting

$$p' = p - \frac{iv}{2} \pm \frac{pp_h}{2},$$

we have

$$\begin{aligned} p'^2 &= \frac{p_h^2}{4} - \frac{\nu^2}{4} \mp \frac{ivp_h}{2} + p_0^2 \\ &= (a+ib)^2 \end{aligned}$$

where  $a = \left[ \frac{1}{2} \left\{ \frac{p_h^2}{4} - \frac{\nu^2}{4} + p_0^2 + \sqrt{\left( \frac{p_h^2}{4} - \frac{\nu^2}{4} + p_0^2 \right)^2 + \frac{\nu^2 p_h^2}{4}} \right\} \right]^{\frac{1}{2}}$

The critical frequency is given by

$$p_c = a \mp p_h/2 \quad \dots \quad (v)$$

$q_0^2$  and  $q_x^2$  are equal to infinity when

$$C' = 0$$

or  $\beta(\beta^2 - \omega^2) - r(\beta^2 - \omega^2 \cos^2 a) = 0$

After simplification and rearrangement, we have

$$ip(ip + \nu) + \frac{p_0^2 [(ip + \nu)^2 + p_h^2 \cos^2 a]}{[(ip + \nu)^2 + p_h^2]} = 0$$

which reduces to

$$p_0^2 = p^2 - \frac{p^2 - p_h^2}{p^2 - p_h^2 \cos^2 a} \quad \dots \quad (vi)$$

when  $\nu = 0$

Here we see that the conditions (iv) (v) (vi) are the same as those obtained by Bose.

# RAMAN SPECTRA OF CO-ORDINATION COMPOUNDS

BY BHOLANATH ROY,

(Received for publication, Dec. 12, 1938)

## Plate I.

### INTRODUCTION.

In the present paper is reported an investigation of the Raman spectra of two co-ordination compounds,  $[\text{Pt}(\text{en})_3] \text{Cl}_4$  and  $[\text{Pt}(\text{en})_2] \text{Cl}_2$ , where en represents ethylene diamine having the formula  $\text{C}_2\text{H}_4(\text{NH}_2)_2$ , with the object of verifying some of the predictions of the quantum theory as to the nature of the co-ordination bonds in such compounds. We shall give in the introduction an account of the co-ordination compounds first studied by Werner and of the various theories proposed to account for their structure culminating in the quantum mechanical theory of such bonds proposed by Pauling. A typical example of the so-called co-ordination compounds of Werner is  $[\text{Pt}(\text{NH}_3)_6]\text{Cl}_4$ . Here the Pt atom is capable of holding not only the four chlorine atoms by its electrovalency, but it can also further combine with six of such apparently stable molecules like  $\text{NH}_3$ . In solution all the four Cl atoms are found to be ionized while the six  $\text{NH}_3$  molecules are found to be attached to be the central atom by non-ionizable bonds. The characteristic properties of such complexes have been summarized by Sidgwick as follows :—

1. Their structures appear so be quite independent of the rules of valency according to which the numerical value of the valency of an atom element is primarily determined by the group in the periodic table to which it belongs. In these compounds the structure is determined rather by the tendency of four or six atoms or groups to arrange themselves round a central atom.
2. In them a univalent atom or group of atoms, such as Cl or NO can be replaced by apparently saturated molecules like  $\text{H}_2\text{O}$  or  $\text{NH}_3$ , without affecting the stability of the complex.
3. Such replacements are always accompanied by a change in the ionization of the molecule. Thus, taking the above complex compound  $[\text{Pt}(\text{NH}_3)_6]\text{Cl}_4$ , we find that the  $\text{NH}_3$  molecules can be replaced one by one along with the diminution in the number of the Cl ions in the outer group until  $[\text{Pt}(\text{NH}_3)_2\text{Cl}_4]$  is reached which is neutral. Here every  $\text{NH}_3$  molecule in the complex group  $\text{Pt}(\text{NH}_3)_6^{++++}$

is replaced by a Cl atom with a consequent diminution of the positive charge of the compound. Further replacement of  $\text{NH}_3$  molecules by Cl makes the resultant compound negatively charged. Finally we have the double salt  $\text{K}_2\text{PtCl}_6$  if the later stage of replacements by Cl ions is effected by KCl solution.

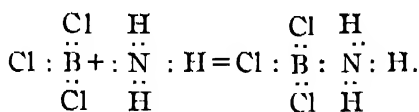
Werner<sup>4</sup> proposed to explain these phenomena by assuming that round the central atom of the complex there is a tendency for groups of atoms or molecules to attach themselves in definite numbers (usually six, sometimes four or eight). These groups occupy the first co-ordination sphere of combination of the central atom, and together with the latter form a co-ordination complex ; the complex molecule might also contain other atoms or groups occupying a second sphere, which are less firmly attached, e.g., in the above-mentioned compound, the  $\text{NH}_3$  molecules are attached to the first sphere of Pt and satisfy the co-ordination number six, while the four Cl atoms are attached to the second sphere. Experimentally the groups attached to the second sphere were distinguished by the fact that they were ionized by water, while those forming part of the co-ordination complex were not. Later X-ray analysis<sup>3</sup> of the crystalline structures of some of these co-ordination compounds of platinum confirmed Werner's theory.

Werner himself did not give any picture of the nature of the forces which held the groups of atoms to the first co-ordination sphere. Kossel, who had successfully explained the formation of polar compound by electrical forces tried to apply the same ideas to explain the formation of complex molecules. But his views were generally not accepted, and so it is unnecessary to go into the details of his theory.

Later Sidgwick<sup>5</sup> gave a new interpretation of the nature of the bonds which hold atoms or atomic groups to the first co-ordination sphere of the central atom. According to modern electrical theories only two kinds of bonds are possible, viz., electrovalent and covalent, the one due to the transference and the other due to the sharing of electrons between two atoms—the former is ionizable, the latter is not. Sidgwick supposes that the co-ordination bonds being non-ionizable belong to the latter type. But they must arise in a way different from the ordinary covalent bonds, since their number is not related to the periodic group of the central atom, and they can combine with atoms (like N in  $\text{NH}_3$  or O in  $\text{OH}_2$ ) which have already completed a stable number of electrons. In the normal covalency it is assumed that each of the two atoms contributed an electron to the link. Sidgwick extended the idea by supposing that both the electrons may be provided by one of the atoms. According to him the conditions for the formation of a co-ordination link are that we should have : (i) one atom which has a pair of valency electrons to offer, and (ii) another which has room for one or more pair of electrons in its valency groups. He called the former atom the donor and the latter atom the acceptor.

As an example of such formation he considered the combination of  $\text{NH}_3$  with

$\text{BCl}_3$ . In the former the N atom, which has five electrons in its valency group, of which three are shared with the three H atoms, leaving a pair of electrons to share, is the donor ; in the latter the B atom which has all its valency electrons shared with the three Cl atoms, and has two vacant places in its valency group, is the acceptor. Their combination was represented thus :



In this compound the atoms B and N assume a maximum covalency or co-ordination number of four, and round each an octet valency shell is completed.

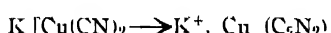
We can consider the application of Sidgwick's theory to the case of regular co-ordination compound like  $[\text{Cr}(\text{NH}_3)_6]\text{Cl}_3$ . Here the Cr atom stripped of its three valency electrons forms the ion  $\text{Cr}^{++}$  with a stable core of 21 electrons (of which three are in  $3d$  shell). It has no valency group left and the core is stable, as proved by the stability of the chromic salts. This ion can form a series of co-ordination links with  $\text{NH}_3$  molecules, in the following way—the N atom has five electrons in its valency group of which three are shared with the three H-atoms leaving a pair of electrons free to form co-ordination bonds with the central atom. It is assumed that in the case of these types of compounds the stable size of the valency group is 12 as opposed to 8 in the previous case considered, and therefore 6 molecules of  $\text{NH}_3$  will be taken up. In the case of one of the  $\text{NH}_3$  molecules being removed from the first co-ordination sphere, it takes away with it the two shared electrons which it contributed ; the Cl atom which replaces it moves from the second to the first co-ordination sphere. It can only supply one electron to the link, the other has to be supplied by the central atom. Thus the electrovalency of the latter is reduced by one, giving instead of  $[\text{Cr}(\text{NH}_3)_6]^{++}$ , the ion  $[\text{Cr}(\text{NH}_3)_5\text{Cl}]^{++}$ , or the salt  $[\text{Cr}(\text{NH}_3)_5\text{Cl}]\text{Cl}_2$ . The same change would occur for every replacement of a whole molecule in the complex by a univalent radical. Thus the peculiar change of electrovalency noted by Werner in this class of compounds is explained. The chief assumption in the above theory is of the existence of a stripped atom with a stable core round which a new valency shell of 12 electrons can be formed by six stable molecules sharing pairs of electrons with it. In case one of the latter is replaced by a univalent radical, one of the shared electrons is supplied by the central atom. Besides  $\text{Cr}^{++}$  other ions of elements belonging to the various transition groups like  $\text{Fe}^{++}$ ,  $\text{Fe}^{+++}$ ,  $\text{Co}^{+++}$ ,  $\text{Ni}^{++}$ ,  $\text{Pt}^{++++}$ , etc., form stable co-ordination compounds.

On this interpretation of the co-ordination bond, Bose<sup>6</sup> proposed an empirical rule, known as Bose-Sidgwick rule for calculating the magnetic moments of complex compounds. Sidgwick<sup>7</sup> has defined the effective atomic number (E.A.N.) of a central atom thus : To the atomic number of the element are

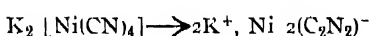
added all the electrons shared with the attached atoms or atomic groups (in every strictly covalent or homopolar bond, e.g., like CN, Cl, OH, etc., the number of shared electrons is one, and in every co-ordination bond, e.g., with molecules like NH<sub>3</sub>, H<sub>2</sub>O, CO<sub>2</sub>, etc., it is two). The original complex is usually an ion, and so we add to this the number of its negative electrovalency (if electronegative), or subtract from this its positive electrovalency (if electropositive). The number thus obtained is called the effective atomic number of the central atom. Bose-Sidgwick rule now runs thus : If the E. A. N. of the central atom be Z', and the number of electrons in the next inert-gas configuration be Z, then Z-Z' measures the magnetic moment of the complex in Bohr magnetons. This rule has been found valid for a large number of co-ordination compounds belonging to the transition group of elements. In certain cases it is found to fail, e.g., [Fe(II<sub>2</sub>O)<sub>6</sub>]SO<sub>4</sub> has the same magnetic moment as the anhydrous FeSO<sub>4</sub> though according to the above rule it ought to have been diamagnetic. Here it is supposed that in [Fe 6H<sub>2</sub>O] the force between the Fe<sup>+</sup> ion and the water molecule is of a purely electrostatic nature, and constitutes the so called ion-dipole bond.

In a subsequent paper Bose<sup>8</sup> gave a detailed picture of how in such complexes, the spin moments of the unpaired electrons of the co-ordinating atom are neutralised. Starting with the double cyanides of the iron group he showed that the following complex cyanides are all diamagnetic, i.e., in them the unpaired electrons in the third shell of the central atom have been neutralised by forming covalent bonds with free electrons of the associated (CN) groups.

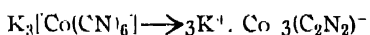
Unpaired electrons in the 3d shells of the central atom.



1



2



3

In each case it will be seen that there are as many (C<sub>2</sub>N<sub>2</sub>)<sup>-</sup> groups attached to the central paramagnetic atom as there are unpaired electrons in the 3rd shell of the latter. That these form covalent bonds is shown by the Raman spectra of solutions of many of these complex cyanides, whose frequencies vary from 300 cm.<sup>-1</sup> to 700 cm.<sup>-1</sup>. Further in them the single frequency of the (CN) group alters in number and in amount, which speaks in favour of the existence of the (C<sub>2</sub>N<sub>2</sub>) group.<sup>9</sup> On the basis of this observed fact Bose has developed a theory of the nature of the valency bond between the central atom and the associated groups in all classes of co-ordination compounds, which to a certain extent gives a detailed picture of Sidgwick's theory of co-ordination bond.

The above theory, however, only gives information about the nature of the chemical bond in co-ordination compounds, but it says nothing about the arrangements of the attached atoms or atomic groups in space surrounding the central atom. Also the theory is empirical, and is not based on any theoretical foundation.

For some years past attempts have been made to obtain a quantum-mechanical interpretation of the covalent bond, and thereby also to account for the spatial arrangements of different attached atoms or atomic groups round the central atom. Heitler and London<sup>10</sup> were the first to give a satisfactory quantum-mechanical picture of the nature of the covalent bond in the hydrogen molecule. They showed that a covalent bond is formed by two electrons belonging to two atoms entering into a covalent bond moving in a binuclear orbit with anti-parallel spins and therefore with zero magnetic moment. Pauling applied<sup>11</sup> this to the interpretation of covalent bonds in polyatomic molecules. He showed that in such molecules in which the attached atoms are monovalent, electron-pair bonds equal in number to the valency of the central atom are formed due to directional properties of wave-functions associated with different valence electrons of the central atom. These individual wave-functions project out in particular directions from the central atom and so have especial affinity for the attached atoms located in those directions.

Pauling showed that an *s*-electron can give rise to no directional effect, while the *p*-electrons can give rise to three wave functions  $p\sigma$ ,  $p\pi_+$ ,  $p\pi_-$  which project markedly along directions which are mutually perpendicular to one another. Such directional properties of *p*-wave functions go to explain the structures of  $\text{H}_2\text{O}$ ,  $\text{NH}_3$  molecules. In the case of the carbon atom ( $1s^2 2s^2 2p^2$ ), it is assumed that for the purpose of forming quadrivalent bonds that electrons on the outer shell of carbon are distributed in  $2s2p^3$  orbits. Pauling showed that it is possible to form four linear combinations of these from  $sp^3$  wave-functions ( $sp^3$  hybridization) resulting in wave-functions which project along directions which make tetrahedral angles with one another. Such wave-functions are peculiarly suited to account for the tetrahedral bonds of the carbon atom, e.g., in  $\text{CH}_4$ ,  $\text{CCl}_4$ , etc. Pauling then extended his theory to the case of transition-group elements, which have the characteristic that the outer valency groups (e.g.,  $4s^2$  in the case of the first transition group) are augmented by the addition of unpaired inner  $3d$  electrons so that *d*-wave functions also come into play. He showed that in addition to  $sp^3$  hybridization giving rise to tetrahedral bonds, new  $sp^3d\gamma^2$  wave-functions suited for attaching six corner atoms octahedrally arranged (i.e., at the six face-centres of a cube at whose centre the central atom is placed) can be formed. This is in agreement with the experimental fact that co-ordination numbers of six associated with octahedral arrangements are particularly characteristics of the transitional elements. It may be noted in passing that such an arrangement is usually the case also when six atoms or atomic groups are distributed round a central atom without giving rise to covalent bonds, e.g., in the case of a hydrated

crystal, the metallic ion is usually surrounded by six molecules of  $H_2O$  arranged octahedrally. Such ion dipole bonding does not come under the present theory. Pauling also shows that in addition to the tetrahedral bonds due to  $sp^3$  combinations four bonds all in a plane and corresponding to the four corners of a square can be formed by  $sp^2d\gamma$  hybridizations.

The basis of Pauling's theory of the co-ordination bond is that the central atom has directional wave-functions respectively along six and four special directions, along which are present an equal number of atomic groups each with a free  $s$ -electron. Thus respectively six and four co-ordination bonds are formed, each containing one electron contributed by the central atom and the other by a co-ordinated group. To illustrate, let us take, (i)  $K_3Co(CN)_6$ , which dissociates into  $3K^+$ ,  $[Co^{---}(CN)_6]$ . Co has nine electrons (outside the closed  $2s^2 2p^6$  shell) and receives three electrons from the K atoms (this is the weakest part of Pauling's theory in which it is necessary to assume that the metallic atom can receive up to four additional electrons); further six electrons are contributed by the (CN) groups, giving a total of 18 electrons. But of this 18, 12 go to form the  $sp^3d\gamma^2$  bonds, leaving 6 electrons which are housed in the  $d\gamma^3$  orbits in pairs and thus completely neutralising the paramagnetic moment of the complex. (ii)  $K_2 [Ni(CN)_4]$  dissociates into  $2K^+$ ,  $[Ni^{---}(CN)_4]$ ; the total number of available electrons is, from Ni  $-\underline{12}$ , and 4 from the 4 (CN) groups. Out of the total number of 16 electrons, 8 go to form the four pairs of covalent bonds, while the remainder 8 are housed in the  $3d$  shell of Ni. If the bond is tetrahedral ( $sp^3$ ), the 8 electrons in the  $3d$  shell of Ni will give rise to a paramagnetic moment of 2 Bohr's magnetons, which is contrary to experimental results.

Ni.			Ni.		
$3d$	$4p$	$4s$	$3d$	$4p$	$4s$
++	++	++	++	++	++
++	++		++	++	
++	++		++		
unpaired + +	(A)		++		
			++	(B)	
(Paramagnetic)			(Diamagnetic)		

Pauling therefore boldly predicted that the bond is tetragonal ( $sp^2d\gamma$ ), in which there are only 8 free places available in the  $3d$  shell of Ni to house the remaining 8 electrons, so that the resulting complex is diamagnetic. Later X-ray analysis of the structure of  $Ba.[Ni(CN)_4]$  has verified<sup>12</sup> Pauling's prediction.

Pauling's theory in spite of certain questionable assumptions, is capable of predicting the arrangement of (CN) groups in the complex cyanides, but it fails to account for the diamagnetism of certain complex hexamine compounds like  $[Co(NH_3)_6]Cl_3$ ,  $[Pt(NH_3)_6]Cl_4$ , etc., in which according to Bose-Sidgwick rule each  $NH_3$  molecule contributes two electrons to form a co-ordination bond with the central atom. If we suppose that each  $NH_3$  molecule, which is diamagnetic, contributes only one electron to a co-ordination bond, the rest molecule will become paramagnetic, and therefore the complex cannot be diamagnetic. Van Vleck<sup>13</sup> has shown that it is possible to realise all the results predicted from Pauling's theory, from the theory of molecular orbitals as developed by Hund, Mulliken and others, without making any doubtful assumptions made by Pauling, and also without postulating the existence of directed electron pair bonds. This theory is sufficiently general to include the case of purely electrostatic ion-dipole interaction between the central ion<sup>1</sup> and the associated groups. Though the case of hexamine compounds have not been treated in detail, it appears probable that further development of mathematical analysis will enable the treatment in detail of molecular orbitals in which both the electrons come from an associated group.

So far the verification of the theory of co-ordination bonds has been (i) from magnetic evidence, (ii) from X-ray analysis, (iii) from chemical and optical isomers. The assumption of covalent bonds in co-ordination compounds can also be verified by the study of the Raman spectra of the latter, which when performed satisfactorily enables us to find out the symmetry of the complex group.

There have been several investigations of the Raman spectra of these complex compounds belonging to the iron group in solutions; of the cyanides by Damaschun,<sup>14</sup> Samuel and Khan;<sup>15</sup> of the hexamines by S. Dutta,<sup>16</sup> and Damaschun;<sup>14</sup> but due to the fact that these compounds are strongly coloured, the Raman spectra obtained have never been satisfactory.

Mathieu<sup>17</sup> has recently investigated the Raman spectra of two practically colourless complexes of platinum,  $[Pt en_3] Cl_4$  and  $[Pt en_2] Cl_2$ , both of which are diamagnetic. The Raman spectra obtained by Mathieu, which will be discussed in detail later, do not appear to be in agreement with the theory discussed above. It was thought worthwhile to re-investigate in detail these two compounds and compare the results obtained with the theoretical predictions.

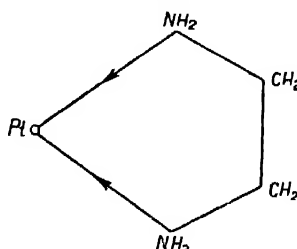


FIGURE 1.

Both the above compounds are Werner co-ordination compounds. Now it is well-known that ethylenediamine is a chelate compound, occupying in space two positions, i.e., it behaves as two independent molecules with a covalent link between. Each (en) group forms with the platinum a chelate ring, as shown below :

Now Pt has 10 valence electrons ( $5d^8 6s^2$ ). Let us now take the case of  $[Pt\text{ en}_3]\text{Cl}_4$ . As it dissociates in aqueous solution into  $[Pt\text{ en}_3]^+$   $4\text{Cl}^-$  each of the Cl-ion receives an electron which must come from the Pt atom. The complex therefore exists in the form  $[Pt^{+4+}\text{en}_3^-]$ . Now since the compound is diamagnetic, the  $Pt^{+4+}$  ion in the complex must have from Bose-Sidgwick rule, 18 electrons in its  $5d^{10} 6s^2 6p^6$  orbits. Hence the three (en) groups must supply  $18 - 6 = 12$  electrons to the co-ordination, i.e., each (en) group supplies 4 electrons, two from each of the  $\text{NH}_2$  groups. If the six  $\begin{pmatrix} \text{CH}_2 \\ | \\ \text{NH}_2 \end{pmatrix}$  groups are distributed octahedrally round the Pt (i.e., at the face-centres of a cube), as shown in the diagram, then the bonds must be of  $sp_3d_{\gamma^2}$  type which require 12 of the 18 electrons [of these 2 go to the 6s-shell, 6 to the 6p-shell, and 4 to the 5d-shell,] leaving the remaining six to fill the  $d_{\gamma^3}$  orbits. This makes the compound diamagnetic, which it actually is.

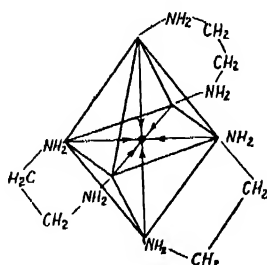


FIGURE 2.

In the case of  $[Pt\text{ en}_2]\text{Cl}_2$  (a case of tetra-co-ordination), Bose-Sidgwick rule fails. Owing to the formation of two Cl-ions, the Pt atom loses 2 electrons leaving 8 outer electrons on it. To this are added 8 electrons due to co-ordination with the 2 (en) molecules. It has now 16 outer electrons. Then according to

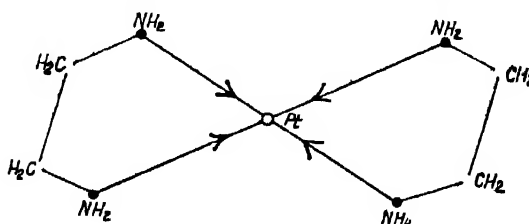


FIGURE 3.

the same argument as applied to the case of  $K_2 [Ni(CN)_4]$  it can be shown that if the bonds be of  $sp^3$  type the compound becomes paramagnetic; and if of the  $sp^2d_2$  type, it becomes diamagnetic, which it actually is. Hence the attached groups are expected to be arranged at the corners of a square.

Mathieu studied both these compounds and reported four Raman lines for  $[Pt\ en_3]Cl_4$  and two for  $[Pt\ en_2]Cl_2$ , which as we shall see, cannot be explained either by our theory, or by his theory.

#### E X P E R I M E N T A L.

The substances used in the investigations were prepared in the laboratory according to methods given for  $[Pt\ en_3]Cl_4$  by Werner<sup>18</sup> and for  $[Pt\ (en)_2]Cl_2$  by Jorgensen.<sup>19</sup>

Both the compounds are highly soluble in water. Each of them was dissolved in conductivity water to form a concentrated aqueous solution. It was then poured into a properly cleaned Wood's tube, bent and drawn out into a horn-shape at one end, and provided with a plane window at the other. The light from a mercury arc was focussed on the tube by a powerful condenser, and the light scattered transversely and emerging from the plane window was limited by further apertures to eliminate as much as possible any parasitic light, and then focussed by a good short-focussed ophthalmoscope lens on to the slit of the spectrograph. Also some portions of the tube was painted black to cut off all extraneous light. Suitable screens were placed all around the arrangement to cut off external light. To improve the illumination a parabolic metallic reflector was placed behind the arc, and also a plane mirror behind the Wood's tube to reflect back all the light that passed through the tube. The spectrograph used was a Hilger two-prism spectrograph of large light-gathering power, with the optical parts of glass, and having a dispersion of about  $27 \text{ \AA. U. per mm.}$  in the region of  $4358 \text{ \AA. U.}$  A bottle containing a 5% solution of *m*-dinitrobenzene in benzene was interposed between the condenser and the tube to absorb the Hg lines  $4047 \text{ \AA. U.}$  and  $4077 \text{ \AA.}$  so that  $4358 \text{ \AA. U.}$  was the only exciting line. The scattered spectra were all photographed on Ilford Golden Isozenith plates suitably "backed" to prevent photographic halation.

For studying the polarisation of the  $[Pt\ en_3]Cl_4$ , a Wollaston double-image prism was interposed between the ophthalmoscope lens and the slit of the spectrograph, whereby the emerging scattered radiation was resolved into its vertical and horizontal components. As the power of resolution of the prism is limited, the plane window of the Wood's tube was also painted black, leaving only a narrow horizontal strip through which alone the scattered radiation could come out of the tube. The two components were then distinctly separated, and both photographed simultaneously. In this way, the polarisation picture of the  $[Pt\ en_3]Cl_4$  was obtained. To distinguish between the two components, however, a polarisation picture was also taken, under identical conditions, of  $CCl_4$ , whose complete data are known.

## RESULTS AND DISCUSSIONS.

The spectograms are reproduced in plate I. It can be seen from them that 10 Raman lines have been recorded for each compound. They are given in tables I and II. Also the Raman lines obtained with ethylenediamine the lines with the same compounds as observed by Mathieu are given in the two tables for comparison.

TABLE I.

Raman lines for $[Pt\text{ en}_3]\text{Cl}_4$			Raman lines for ethylenediamine		
Observed by	Author.	Mathieu.	*	Relative intensity	Recorded by Mathieu.
284 $\text{cm}^{-1}$ (D)		250 $\text{cm}^{-1}$	4	469 $\text{cm}^{-1}$	470 $\text{cm}^{-1}$
472 "		439 "			
561 "	(I)	515 "	2		
595 "	(P)	550 "	4		
869 "		840 "		833 "	850 "
976 "		960 "		982 "	
1198 "		1064 "		1100 "	1090 "
1336 "				1301 "	
				1352 "	1
1450 "		1450 "		1453 "	2
1692 "	(water)				1464 "

D=depolarised.

P=polarised.

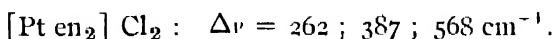
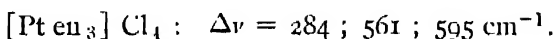
TABLE II.

Raman lines for $[Pt\text{ en}_2]\text{Cl}_2$			Raman lines for ethylenediamine		
Observed by author. <sup>++</sup>	Relative intensity,	*	Relative intensity	Recorded by Mathieu.	
262 $\text{cm}^{-1}$	4				
387 "	1				
469 "	1	469 $\text{cm}^{-1}$	1	470 $\text{cm}^{-1}$	
568 "	4				
875 "	2	833 "	2	850 "	
1015 "	1	982 "	1		
1170 "	2	1100 "	2	1090 "	
1316 "	1	1301 "	1		
		1352 "	1		
1441 "	2	1443 "	2	1464 "	
1685 "					
(water)					

\* Taken from Chaudhuri, B. K., *Ind. J. Phys.*, **11**, 203 (1937).

++ The values of  $\Delta\nu$  reported by Mathieu are  $225 \text{ cm}^{-1}$  and  $525 \text{ cm}^{-1}$ .

Thus we have obtained for



It may be seen from above that some of the frequencies due to ethylenediamine have been affected by the co-ordination with Pt. Most remarkable is the case of the  $1100 \text{ cm}^{-1}$  line which has been shifted to  $1198 \text{ cm}^{-1}$  and  $1170 \text{ cm}^{-1}$  respectively in  $[\text{Pt en}_3]\text{Cl}_4$  and  $[\text{Pt en}_2]\text{Cl}_2$ . The  $1100 \text{ cm}^{-1}$  line may be due to the mode of vibration of ethylenediamine as shown in the figure, because as reported by Chaudhuri,<sup>20</sup> the line is highly polarised, and also it is not due to the C-C vibration.

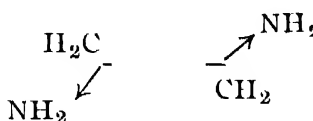


FIGURE 4.

As the Pt is co-ordinated at the two ends through the two ( $\text{NII}_1$ ) groups, it is natural that this frequency should be adversely affected. It is also evident from above that Mathieu's obtaining 4 lines with  $[\text{Pt en}_3]\text{Cl}_4$  is due to his date or ethylenediamine being incomplete, as it does not contain the  $982 \text{ cm}^{-1}$  line, and for which reason he assigned the  $978 \text{ cm}^{-1}$  line to  $[\text{Pt en}_3]\text{Cl}_4$ . With  $[\text{Pt en}_2]\text{Cl}_2$  he obtained only two lines; probably he did not give sufficiently long exposure and so a third line which is diffuse and feeble was not recorded by him. Also his value of  $\Delta\nu$  differ in many cases widely from our values; for, as seen from his paper, he did not take any comparison spectrum, and so probably used a dispersion formula to calculate the wave-lengths, and some error may have been introduced in the calculations: in the present investigation an iron-spectrum was taken for comparison, and the frequency shifts were calculated after careful microscopic measurements.

For an octahedral type of molecule there are six normal modes of vibration, three of them being permitted in the Raman effect. Of these one is polarised and single, and the other two are depolarised and also doubly and triply degenerate respectively.

This result has been arrived at by Yost, Stefiens and Gross,<sup>21</sup> Redlich, Kurz and Rosenfeld,<sup>22</sup> Wilson Jr.,<sup>21</sup> and also Nagendranath.<sup>23</sup> All the four methods are however different. The former two used the central force method, while the latter two used the valence-force potential method. The compound  $[\text{Pt en}_3] \text{Cl}_4$  is however slightly different from the usual octahedral molecule

considered by the above authors, for, in this case every two alternate co-ordinating groups (the two  $\text{CH}_2$  in every ethylenediamine molecule) have a covalent link between them. Indeed for this reason Mathieu assumed that each (en) acts as a single molecule co-ordinated from its centre of gravity to the central atom, whereby he reduces the octahedral model to a plane triangular one as shown below. It will be shown however that

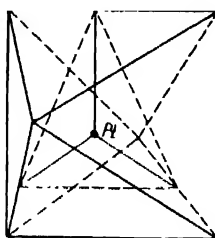


FIGURE 5.

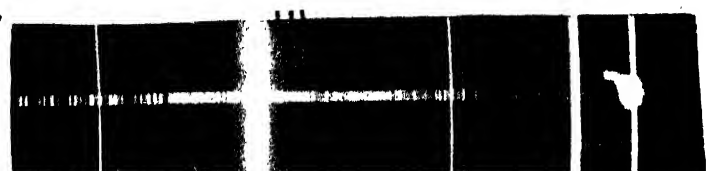
this assumption is incorrect.

As mentioned above, three lines  $\Delta\nu = 284, 561, 595 \text{ cm}^{-1}$  have been obtained with  $[\text{Pt en}_3] \text{Cl}_4$  of which the farthest one is strongly polarised, while the other two are depolarised.

Now Yost, Steffens and Gross from their theoretical treatment gave a relation between the three Raman frequencies of an octahedral model, which is,

$$\nu_1^2 = \nu_2^2 + \frac{3}{2}\nu_3^2.$$

From their assignment,  $\nu_1$  is expected to be the polarised line, while  $\nu_2$  and  $\nu_3$  refer to the depolarised lines ( $\nu_2 > \nu_3$ ). According to Nagendra-nath's treatment (by the valence-force potential method) the relation should not hold, at least accurately. Actually it does not hold rigorously even for Yost's values with  $\text{SF}_6$ . Substituting the Raman frequencies of  $[\text{Pt en}_3] \text{Cl}_4$  in Yost's relation we get the value for  $\nu_1^2, 561^2 + \frac{3}{2} \cdot 284^2 = 660^2$ . And 660 is greater than the observed value 595 by 11%. The agreement is however not bad, as even in a freely co-ordinated compound like  $\text{SF}_6$  the disagreement is about 16%. So  $[\text{Pt en}_3] \text{Cl}_4$  should have on the above grounds an octahedral symmetry. But from Mathieu's triangular model, three Raman lines are to be expected with the same polarisation characters as with the octahedral model, though there is no frequency relation in the former. But this approximate validity of the frequency relation cannot be regarded as conclusive evidence in favour of the octahedral arrangement ; for the deduction of the above relation is based on the assumption of a pure central force field in the molecule, which is doubted by many authors. The final evidence is however furnished by our results obtained with  $[\text{Pt en}_2] \text{Cl}_2$ . If  $[\text{Pt en}_2] \text{Cl}_2$  be a case of tetra-co-ordination, then there are two models possible



Raman Spectra

(a)  $\text{Pt}(\text{en})_4\text{Cl}_4$   
(b)  $\text{Pt}(\text{en})_2\text{Cl}_2$



for it, *viz.*, tetrahedral or tetragonal, of which the latter is to be expected from our calculations above. In the tetrahedral model, 4 Raman lines are expected. In the latter model 3 lines are expected. Again according to Mathieu's assumption the model should be linear, as shown below :

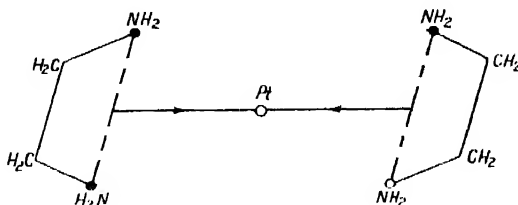


FIGURE 6.

Such a model can give rise to only one Raman line<sup>2</sup>, and in fact this is what Mathieu predicted. But he reported to have got two lines. Actually we obtained with it Raman lines,  $\Delta\nu = 262, 387, 568 \text{ cm}^{-1}$ . As the spectrum obtained was very weak it was extremely difficult to study the polarisation characters of the lines. As this is not necessary, we did not study it. The 3 lines obtained with  $[\text{Pt en}_2] \text{Cl}_2$  cannot be explained by any of the suggested models except the tetragonal one. So we have to discard Mathieu's hypothesis that an ethylenediamine molecule acts as if co-ordinated at one point (its centre of gravity) to the central atom. Hence it follows also that Mathieu's proposed structure for  $[\text{Pt en}_2] \text{Cl}_4$  is to be discarded in favour of the octahedral model.

To summarise our results, it may now be concluded that,

1. If an ethylenediamine molecule is co-ordinated to a central atom, then it will form a chelate ring, *i.e.*, be co-ordinated at two points, and its two groups will vibrate along the co-ordination bonds, independent of one another, in spite of the covalent link between them,
2. In  $[\text{Pt en}_2] \text{Cl}_4$  the three ethylenediamine molecules have their six  $\begin{pmatrix} \text{CH}_2 \\ | \\ \text{NH}_2 \end{pmatrix}$  groups arranged octahedrally round the Pt atom.
3. In  $[\text{Pt en}_2] \text{Cl}_2$  the two ethylenediamine molecules have their four groups arranged at the corners of a square.

Also the peripheral groups cannot be held to the central atom by polar bonds, as vibrations along such bonds cannot be recorded in the Raman effect.

This is we believe the first instance in which the quantum theory of co-ordination bond has been verified in detail by investigations of Raman spectra. Investigations with similar transparent co-ordination compounds of the transitional groups of elements are necessary to obtain further confirmation. It may be noted that these investigations also confirm Sidgwick's hypothesis of the contribution of two electrons by an associated group to a co-ordination bond.

This investigation was undertaken at the suggestion of Prof. D. M. Bose. My grateful thanks are due to him for providing me with facilities for work and for many helpful discussions. I am also indebted to Dr. S. C. Sirkar for guidance during the experimental portion of the work.

## SUMMARY.

The Raman spectra of the two co-ordination compounds of  $[Pt\text{ en}_2]\text{Cl}_2$  and  $[Pt\text{ en}_2]\text{Cl}_2$  in aqueous solutions have been investigated and the frequencies and polarisations of the lines due to the vibrations of the complexes  $[Pt(\text{en})_3]$  and  $[Pt(\text{en})_2]$  have been determined. The frequencies obtained are

- (i) for  $[Pt(\text{en})_3]$ ,  $\Delta\nu = 284(D)$ ,  $561(D)$  and  $595(P)\text{ cm}^{-1}$ .
- (ii) for  $[Pt(\text{en})_2]$ ,  $\Delta\nu = 262$ ,  $387$  and  $568\text{ cm}^{-1}$ .

It is shown that the results obtained are compatible with the predictions of the theory of valence bonds in this class of compounds, which was first developed by Sidgwick and later interpreted upon a quantum mechanical basis by Pauling and others.

PALIT LABORATORY OF PHYSICS,  
UNIVERSITY COLLEGE OF SCIENCE,  
92, UPPER CIRCULAR ROAD,  
CALCUTTA.

## REFERENCES.

- <sup>1</sup> Kossel, W., *Ann. der Physik.*, **49**, 229 (1916).
- <sup>2</sup> Lewis, G. N., *J. Amer. Chem. Soc.*, **38**, 762 (1916).
- <sup>3</sup> Wyckoff, *The Structure of Crystals*.
- <sup>4</sup> Werner, A., *Zs. f. Anorg. Chemie*, **3**, 267 (1893).
- <sup>5</sup> Sidgwick, N. V., *J. C. S.*, **123**, 725 (1923).
- <sup>6</sup> Bose, D. M., *Zeits. f. Phys.*, **35**, 219 (1925).
- <sup>7</sup> Sidgwick, N. V., *Electronic Theory of Valency*, p. 163.
- <sup>8</sup> Bose, D. M., *Zeits. f. Phys.*, **65**, 677 (1930).
- <sup>9</sup> Bose, D. M., *Ind. J. Phys.*, **9**, 277 (1934).
- <sup>10</sup> Heitler, W. and London, F., *Zeits. f. Phys.*, **44**, 455 (1927).
- <sup>11</sup> Pauling, L., *J. Amer. Chem. Soc.*, **55**, 1363 (1933).
- <sup>12</sup> Van Vleck, J. H., and Sherman, A., *Rev. of Mod. Phys.*, **1**, 167 (1933).
- <sup>13</sup> *Loc. cit.*
- <sup>14</sup> Damaschun, I., *Zs. f. Phys. Chem.*, **B**, **16**, 81 (1932).
- <sup>15</sup> Samuel, R., and Khan, M. J., *Zs. f. Phys.*, **84**, 87 (1933).
- <sup>16</sup> Bose, D. M., and Dutta, S., *Nature*, **128**, 725 (1932).
- <sup>17</sup> Mathieu, J. P., *Jour. de Phys.*, **8**, 169 (1937); *Comptes Rendus*, **204**, 682 (1937).
- <sup>18</sup> Werner, A., *Festschrift der Naturforsch. Gesell. (Zurich)*, **62**, 558 (1917).
- <sup>19</sup> Jorgensen, S. M., *Journal f. Pract. Chemie*, **34**, 510 (1886).
- <sup>20</sup> Chaudhuri, B. K., *Ind. J. Phys.*, **11**, 203 (1937).
- <sup>21</sup> Yost, D. M., Steffens, C. C., and Gross, S. T., *J. Phys.*, **2**, 311 (1934).
- <sup>22</sup> Redlich, O., Kurz, T., and Rosenfeld, P., *Zs. Phys. Chem. B.*, **19**, 231 (1932).
- <sup>23</sup> Nagendranath, N. S., *Ind. Acad. Sci. Proc.*, **1A**, 250 (1934).
- <sup>24</sup> Wilson, E. B., *Jour. Chem. Phys.*, **2**, 432 (1934).

# CRYSTAL STRUCTURE OF DIPHENYLAMINE, PART I

BY JAGATTARAN DHAR

Department of Physics and Mathematics,  
Indian School of Mines, Dhanbad.

(Received for publication, Dec. 20, 1939)

## Plate II.

**ABSTRACT.** Goniometric measurements on diphenylamine crystals reveal that they belong to monoclinic holohedral class with the following elements :—

$$a : b : c = 1.01 : 1 : 2.78$$

and

$$\beta = 91^\circ 30'$$

From X-ray measurements the cell dimensions are obtained as  $a_0 = 14.0 \text{ \AA}$ ;  $b_0 = 13.9 \text{ \AA}$ ;  $c_0 = 39.5 \text{ \AA}$  whence the axial ratio is  $1.01 : 1 : 2.84$ . The number of molecules per unit cell comes out to be 32.

## I. INTRODUCTION.

Crystals of diphenyl,<sup>1</sup> *p*-diphenylbenzene,<sup>2</sup> *p*-diphenyldiphenyl,<sup>3</sup> diphenylethane<sup>4</sup> (dibenzyl), diphenylethylene<sup>5</sup> (Stilbene), diphenylacetylene<sup>6</sup> (tolane), diphenylketone<sup>7</sup> (Benzophenone), Benzil,<sup>8</sup> etc., have been studied for their structure by X-rays and by the method of magnetic<sup>9</sup> susceptibility. In all of them the benzene nucleus is found to be a planar hexagon of each side  $1.41 \text{ \AA}$ . The molecules of diphenyl, *p*-diphenylbenzene and *p*-diphenyldiphenyl conform to a planar and linearly extended structure. In dibenzyl, however, owing to the  $\text{CH}_2$  linkage intervening the two benzene nuclei the molecule has a three dimensional space structure. Benzil is found to correspond to the structure of dibenzyl. In Stilbene the molecules are shown to have a nearly planar form in striking contrast to the shape of the dibenzyl molecule in which the benzene rings are almost at right angles to the plane of the central zig-zag. Preliminary measurements on tolane suggest that it is closely similar to the stilbene structure. In the Benzophenone molecule, the two benzene rings are found to be inclined to each other at about  $135^\circ$  and the carbon atom linking the two nuclei lies at the intersection of the planes of the two rings.

In diphenylamine the intervening linkage is NH and so its structure cannot be assumed, *a priori*, to be similar to any of the structures referred to. A structural study of the diphenylamine crystal is expected to throw some light as to how this intermediate linkage of atoms other than the linkage of the aliphatic carbon will affect the structure, and has consequently been undertaken. In this paper we

propose to report only the morphology of the crystal and the X-ray findings as regards the unit cell.

## 2. GONIOMETRIC STUDY.

Dr. Fraenkel and Dr. Landau's diphenylamine is crystallised out of alcohol by slow evaporation lasting over several days. This gives rise to thin plates bounded by prism or pyramidal faces. The plates, whenever thick, are invariably cleaved on the flat broad face. Very seldom crystals grow the same prismatic or pyramidal faces. A large number of crystals are, first of all, examined by the Fuess horizontal circle goniometer and later by the Czapski two-circle theodolite goniometer. For recognising uniquely the flat face of the plate-like crystals, a Laue photograph with the heterogeneous X-ray beam (from Philips Metalix X-ray tube) normal to the flat face is taken and the Gnomonic points of the Laue spots are drawn. It is concluded therefrom that the flat face may be either (010) or (001). It is later on conclusively proved by taking a rotation photograph normally to the flat face that the flat face of the crystal is the *c*-face (001). The various faces of the crystal with their interfacial angles are then stereographically projected on a Wulff's net. The stereographic projection shows that the diphenylamine crystal belongs to the monoclinic holohedral class quite in agreement with the observation by Bodewig.<sup>10</sup> The result is as follows :—

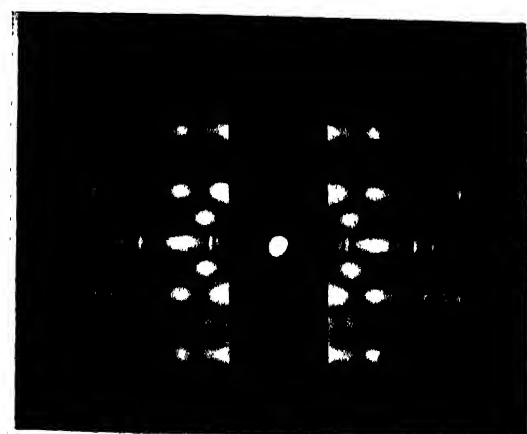
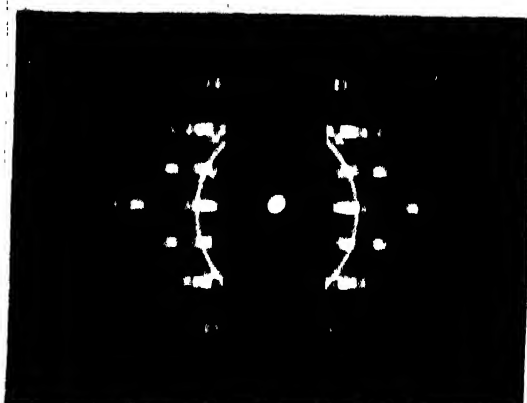
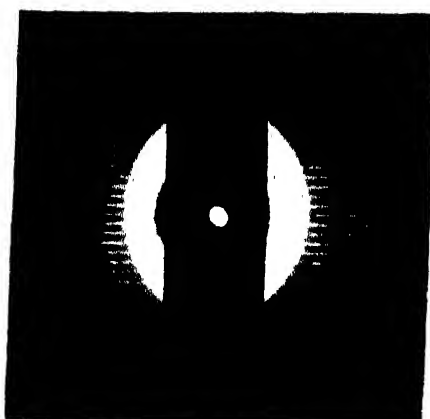
TABLE I.

Planes.	Angles observed	Angles calculated.	Planes.	Angle observed	Angle calculated.
(001) $\wedge$ (110) =	88° 15'	88° 56'	(110) $\wedge$ (111) =	90° 0'	90° 7'
(001) $\wedge$ (111) =	74° 0'	74° 58'	(110) $\wedge$ (221) $\equiv$	90° 10'	90° 15'
(001) $\wedge$ (223) =	67° 30'	68° 32'	(110) $\wedge$ (223) =	90° 0'	89° 56'
(001) $\wedge$ (221) =	81° 15'	81° 50'	(110) $\wedge$ (112) =	89° 50.	89° 52'
(001) $\wedge$ (112) =	62° 30'	62° 36'	(110) $\wedge$ (225) =	89° 40'	89° 46'
(001) $\wedge$ (225) =	56° 0'	57° 15'	(110) $\wedge$ (332) =	89° 0'	89° 31'
(001) $\wedge$ (332) =	82° 30'	81° 35'	(110) $\wedge$ (011) =	49° 0'	48° 27'
(001) $\wedge$ (011) =	70° 0'	70° 36'	(221) $\wedge$ (011) =	44° 30'	44° 18'
(110) $\wedge$ (110) =	90° 40'	90° 38'			

The axial ratio is found to be  $a : b : c = 1.01 : 1 : 2.78$  and  $\beta = 91^\circ 30'..$

## 3. X-RAY STUDY.

At first, a rotation photograph of the diphenylamine crystal mounted normal to the flat face, is taken. It reveals only the row lines very prominently which

(i) about  
 $a$  axis(ii) about  
[110](iii) about  
[11-1]

Rotation photographs of diphenylamine.



suggest that in this particular case the flat face is a *c*-face (001). The cell dimensions are then determined from rotation photographs about the two crystallographic axes lying in the (001) face of the crystal as well as about the zone-axes [110] and [114] in a cylindrical camera of diameter 8·25 cms. Copper K<sub>α</sub> radiation from a Hadding tube was used for the purpose. The rotation photographs are exhibited in the accompanying plate II. It is indeed remarkable that in the rotation photographs about the crystal axes the odd layer lines would be much less intense than the even layer lines. The following values have thus been found for the axial lengths :—

$$a_0 = 14\cdot0 \text{ \AA} ; b_0 = 13\cdot9 \text{ \AA} ; c_0 = 39\cdot5 \text{ \AA}$$

$\beta$  is assumed to be the same as that obtained from stereographic projection.

In the third column of table I, the interfacial angles are calculated on the above cell dimensions as obtained from X-ray measurements.

The specific gravity of the crystal is determined by the well-known flotation method from a solution of ZnSO<sub>4</sub> in water and is found to be 1·18. As the molecular weight of diphenylamine is 169, the number of molecules per unit cell comes out to be 32. Further work is in progress.

#### ACKNOWLEDGMENT.

The work was conducted partly at the Indian School of Mines, Dhanbad, and partly at the University of Dacca. I am indebted to the Principal and Dr. B. B. Banerji, of the Indian School of Mines, Dhanbad, as well as to Prof. S. N. Bose and Dr. K. Banerjee, of the University of Dacca, for kindly granting me the requisite facilities.

#### REFERENCES.

- <sup>1</sup> Dhar, *Ind. J. Phys.*, **7**, 43 (1932).
- <sup>2</sup> Pickett, *Nature*, **131**, 513 (1933); *Proc. Roy. Soc. A*, **142**, 332 (1933).
- <sup>3</sup> Pickett, *Journ. Am. Chem. Soc.*, **58**, 2299 (1936).
- <sup>4</sup> Dhar, *Ind. J. Phys.*, **9**, 1 (1934); Robertson, *Proc. Roy. Soc. A*, **146**, 473 (1934) and *Proc. Roy. Soc. A*, **150**, 348 (1935).
- <sup>5</sup> Robertson and Woodward, *Proc. Roy. Soc. A*, **162**, 568 (1937).
- <sup>6</sup> Robertson, Prasad and Woodward, *Proc. Roy. Soc. A*, **164**, 187 (1936).
- <sup>7</sup> Banerjee and Haque, *Ind. J. Phys.*, **12**, 87 (1938).
- <sup>8</sup> Banerjee and Sinha, *Ind. J. Phys.*, **11**, 409 (1938).
- <sup>9</sup> Krishnan and Banerjee, *Proc. Roy. Soc. Phil. Trans. A.*, **234**, 265 (1935); Lonsdale and Krishnan, *Proc. Roy. Soc. A*, **156**, 597 (1936); Krishnan and Banerjee, *Proc. Roy. Soc. Phil. Trans. A.*, **234**, 265 (1935).
- <sup>10</sup> Bodewig, *Zell. f. Kryst.*, **3**, 411 (1879).



# THE INTERNAL PRESSURE IN A LIQUID

By M. F. SOONAWALA, M.Sc.

(Maharaja's College, Jaipur)

(Received for publication, January 11, 1938)

**ABSTRACT.** The equation of state for water is derived under certain limiting conditions from thermodynamical considerations. The internal pressure is thence deduced. Values of compressibility are calculated, and compared with the observed ones.

The problem of the determination of the internal pressure in a liquid presents problems quite different from that of a gas. For, while in the latter case, pressure manifests itself as the effect of molecular bombardment on the surface of the containing vessel, no such action takes place in a liquid. The conditions at the surface of a liquid are totally different from those prevailing in the interior. As a molecule approaches the surface, its velocity is considerably diminished, and even annulled, due to the forces of cohesion between it and the neighbouring molecules. The surface acts as an effective barrier, which prevents the transmission of the pressure of the molecular impact on the one side of it to the other side beyond the surface. What the thickness of the barrier is, we cannot very well determine. However, if we can calculate the free energy of the molecules in a liquid, we can deduce a value of the internal pressure. We require for this purpose a knowledge of the potential energy of the molecules of the liquid. The relation between the free energy  $F$ , and the total energy  $E$ , of a system is given by the equation <sup>1</sup>

$$e^{-\frac{F}{kT}} = \int e^{-\frac{E}{kT}} d\Omega ; [d\Omega = dq_1 \cdot dq_2 \dots dp_1 \cdot dp_2 \dots] \quad \dots \quad (i)$$

$q$ 's and  $p$ 's are the positional and the impulse co-ordinates of the system, and  $k$  is the Boltzmann constant. The energy  $E$  is made up of two parts : the kinetic energy,

$$E_{kin} = \frac{1}{2m} (\dot{p}_1^2 + \dot{p}_2^2 + \dots) \quad \dots \quad (ii)$$

and the potential energy,  $E_{pot}$ . The kinetic energy will be a function of the velocities only ; while, it can safely be assumed that the potential energy is a function of the co-ordinates only. Evaluating the integral for the kinetic energy for all possible velocities,<sup>2</sup>

$$F = -k N T \cdot \ln \left( \frac{c}{h^3 N} \right) - \frac{3}{2} k N T \cdot \ln (2\pi m k T) - k T \cdot \ln \int e^{-\frac{E_{\text{pot}}}{k T}} dq_1 dq_2 \dots ; \quad N$$

is the number of molecules in a gram-molecule. ... (iii)

The equation of state is obtained from the relation,<sup>3</sup>

$$p = -\frac{\partial F}{\partial v} = k T \cdot \frac{\partial}{\partial v} \left\{ \ln \int e^{-\frac{E_{\text{pot}}}{k T}} dq_1 dq_2 \dots \right\} \quad \dots \quad (\text{iv})$$

When the potential energy is zero, as in a perfect gas, this leads to the gas equation,

$$p = k N T \cdot \frac{\partial}{\partial v} \left\{ \ln \int dv \right\} = \frac{k N T}{v} = \frac{R T}{v} \quad \dots \quad (\text{v})$$

If a relation between the potential energy and the volume can be established for a liquid, it may be possible to evaluate the integral of state,

$$\int e^{-\frac{E}{k T}} \cdot d\Omega.$$

Laplace's theory of capillarity assumes the latent heat of a liquid to yield the potential energy. The relation is

$$U = 2mL \quad \dots \quad (\text{vi})$$

where  $m$  is the mass of a molecule of the liquid,  $U$  its potential energy, and  $L$ , the latent heat of the liquid. The total energy of the molecule will be

$$E = \frac{1}{2}mv^2 + U = \frac{1}{2}m(c^2 - b), \quad \dots \quad (\text{vii})$$

where

$$b = \frac{2U}{m} \quad \dots \quad (\text{viii})$$

A more general formulation of the energy is given by <sup>4</sup>

$$E = \frac{1}{2}m(c^2 - b - \beta), \quad \dots \quad (\text{ix})$$

$$\text{where } \beta = \frac{2kT}{m} \cdot \ln \left\{ 4\pi \sqrt{\frac{m}{\pi kT}} \cdot I \right\} \quad \dots \quad (\text{x})$$

$k$  is Boltzmann's constant, and

$$p = \frac{16\pi^2 m^2}{h^2} \quad \dots \quad (\text{xi})$$

$h$  is Planck's constant, and  $I$  the integral referred to. The integral of state is then given by

$$\int e^{-\frac{E}{k T}} \cdot d\Omega = \int e^{-\frac{1}{2} \frac{m}{k T} (c^2 + b + \beta)} \cdot d\Omega. \quad \dots \quad (\text{xii})$$

We give below an investigation on these lines for water, because the relevant data are available for it in a form fuller than for any other liquid. The density,  $\rho$ , and hence the specific volume of water, has been well determined for all temperatures from  $0^{\circ}\text{C}$  to  $365^{\circ}\text{C}$ , the critical temperature. We can, therefore, deduce relationships between  $I$  and the specific volume,  $1/\rho$ , on the one hand, and between  $b$  of (viii) and the specific volume on the other. The graph, figure 1, closely suggests a relation  $b^2 = c\rho^3$ , with the value  $1.94 \times 10^7$  for the constant  $c$ . A better approximation is had of the form

$$b^2 \left( \frac{I}{\rho} - a \right)^3 = c.$$

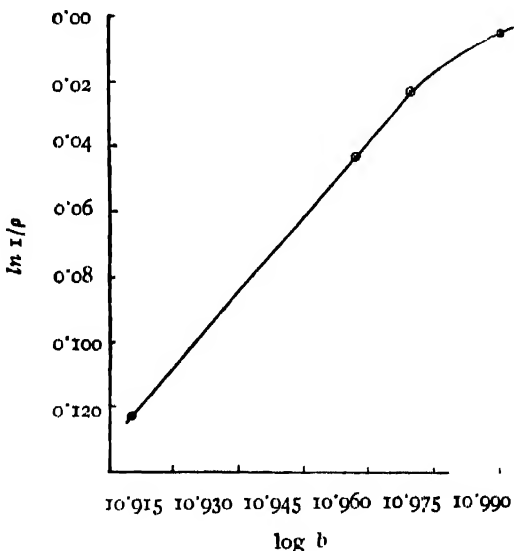


FIGURE 1.

We further know that, at the critical temperature, though  $b=0$ , the density  $\rho=0.329$ ; which leads us to conclude that the true relation is of the form

$$(b+a_1)^2 \cdot \left( \frac{I}{\rho} - a \right)^3 = c \quad \dots \quad (\text{xiii})$$

Ordinarily,  $a_1$  is much smaller than  $b$ . The correctness of this relation is seen from the following table. The last column shows the calculated value  $a$ , taking  $1.94 \times 10^7$  for the value of  $c$ , and 850 for  $a_1$ . The value of  $a$  is satisfactorily constant, the mean being  $-0.09$ .

TABLE I.

$b$	$x/\rho$	$b^{-\frac{2}{3}}$	$a$
$0.94 \times 10^{-6}$	1.000	$4.66 \times 10^{-8}$	1.0
9.77 "	1.0044	4.714	" -0.09
9.30 "	1.0227	4.872	" -0.08
9.04 "	1.0435	4.965	" -0.08
8.06 "	1.1312	5.360	" -0.09

If  $M$  is the molecular weight of the liquid,  $M/\rho$  will be the volume of a gram-molecule of it. We shall henceforth put

$$M\left(\frac{x}{\rho} - a\right) = v - M \cdot a = x \quad (\text{xiv})$$

We can, similarly deduce a relation between the integral  $I$  and  $\rho$ , or,  $x$ .

Figure 2 shows the relation between  $\log(a-I)$  and  $\frac{x}{M}$ .

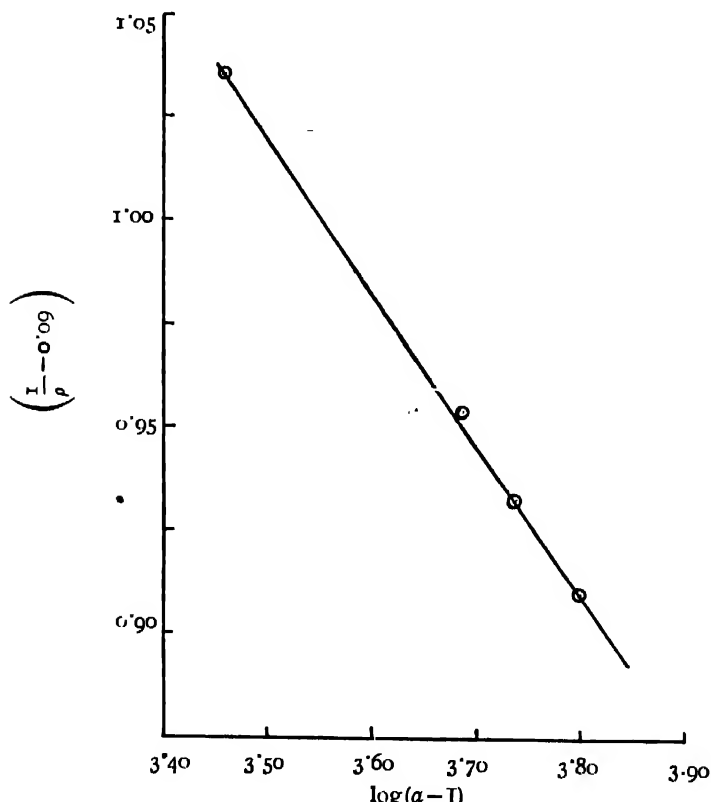


FIGURE 2.

It indicates the relation

$$I = a \left\{ 1 - e^{-nx} \right\} \quad \dots \quad (xv)$$

where  $a = 9800$ , and  $n = 0.33$ .

The integral of state can now suitably be transformed. Thus,

$$\begin{aligned} & \int e^{\frac{1}{2} \frac{m}{kT}} \left\{ b + \frac{2kT}{m} \cdot \ln \left( 4p \cdot \sqrt{\frac{m}{2\pi kT}} \cdot I \right) \right\} \cdot dv \\ &= \int 4p \cdot \sqrt{\frac{m}{2\pi kT}} \cdot I \cdot e^{\frac{1}{2} \frac{m}{kT}} \cdot b \cdot dv \\ &= \int 4p \cdot \sqrt{\frac{m}{2\pi kT}} \cdot I \cdot e^{\frac{1}{2} \frac{m}{kT}} \cdot (B \cdot x^{-\frac{3}{2}} - a_1) \cdot dx, \\ & \quad \text{from (xiii) and (xiv)} \\ &= 4p \cdot \sqrt{\frac{m}{2\pi kT}} \cdot e^{\frac{1}{2} \frac{ma_1}{kT}} \cdot a \int \left( 1 - e^{-nx} \right) \cdot e^{\frac{1}{2} \frac{mB}{kT} \cdot x^{-\frac{3}{2}}} \cdot dx \\ &= A \int e^{cx^{-\frac{3}{2}}} \cdot dx - A \cdot \int e^{cx^{-\frac{3}{2}} - nx} \cdot dx \quad \dots \quad (xvi) \end{aligned}$$

where

$$A = 4ap \cdot \sqrt{\frac{m}{2\pi kT}} \cdot e^{-\frac{1}{2} \frac{ma_1}{kT}} \quad \dots \quad (xvii)$$

and

$$c = \frac{1}{2} \frac{mB}{kT} = \frac{1}{T} \times 0.037 \quad \dots \quad (xviii)$$

Neither of the above two integrals can be easily evaluated. For, changing the variable to  $y$  defined by

$$y = cx^{-\frac{3}{2}},$$

$$\int e^{cx^{-\frac{3}{2}}} dx = -\frac{2}{3} C + \frac{2}{3} \int y^{-\frac{5}{2}} e^y dy \quad \dots \quad (xix)$$

which cannot be evaluated except as a series, when convergent. We can, however, study the integral (i) under certain limiting conditions.

Firstly, let

$$cx^{-\frac{3}{2}} \ll nx, \quad \dots \quad (xx)$$

as would be the case near the normal value of  $x$ , viz., 16.2. Then,

$$\int e^{cx - \frac{3}{2} - nx} dx = \int e^{-nx} dx = -\frac{e^{-nx}}{n}; \quad \dots \text{ (xxi)}$$

and,  $e^{-\frac{F}{kT}} = \Lambda \left\{ x + \frac{e^{-nx}}{n} \right\}; \quad \dots \text{ (xxii)}$

giving  $-\frac{F}{kT} = \ln \Lambda + \ln \left\{ x + \frac{e^{-nx}}{n} \right\}$

and,  $p = -\frac{\partial F}{\partial v} = -\frac{\partial F}{\partial x} = \frac{1 - e^{-nx}}{x + \frac{1}{n \cdot e^{nx}}} \cdot k \cdot N \cdot T., \quad \dots \text{ (xxiii)}$

$$= \frac{RT}{x}, \quad \dots \text{ (xxiv)}$$

to a first approximation, R being the gas constant, and N the number of molecules per gram-molecule. This resembles the ordinary gas equation, excepting that  $x$  replaces the volume. The effect of the correction terms in (xxiii) is to reduce the pressure lower than that given by (xxiv).

Secondly, let  $x$  be so small that

$$cx^{-\frac{3}{2}} \gg nx \quad \dots \text{ (xxv)}$$

Then, on substituting

$$\begin{aligned} cx^{-\frac{3}{2}} &= y, \\ \int e^{cx^{-\frac{3}{2}}}.dx &= -\frac{2}{3}c^{\frac{3}{2}} \int y^{-\frac{5}{3}}.e^y dy \\ &= -\frac{2}{3}.c^{\frac{3}{2}} \left[ y^{-\frac{5}{3}}.e^y + \frac{5}{3} \left\{ e^y.y^{-\frac{2}{3}} + \frac{8}{3} \left( e^y.y^{-\frac{1}{3}} + \frac{1}{3} \int y^{-\frac{4}{3}}.e^y dy \right) \right\} \right] \\ &= -\frac{2}{3}.c^{\frac{3}{2}}.y^{-\frac{5}{3}}.e^y \cdot \left\{ 1 + \frac{5}{3} \cdot \frac{1}{y} + \frac{5}{3} \cdot \frac{8}{3} \cdot \frac{1}{y^{\frac{2}{3}}} + \dots \right\} \\ &= -\frac{2}{3}.c^{\frac{3}{2}}.y^{-\frac{5}{3}}.e^y, \quad \text{to the approximation assumed in (xxv).} \end{aligned}$$

$$= -\frac{2}{3} \cdot \frac{1}{c} \cdot x^{\frac{5}{2}} \cdot e^{cx^{-\frac{3}{2}}} \quad \dots \text{ (xxvi)}$$

Therefore,

$$\begin{aligned}
 & \int e^{cx^{-\frac{3}{2}}}.dx - \int e^{cx^{-\frac{3}{2}} - nx}.dx \\
 &= \int e^{cx^{-\frac{3}{2}}}.dx - \int e^{cx^{-\frac{3}{2}}}(1 - nx)dx \\
 &= n \int x \cdot e^{cx^{-\frac{3}{2}}}.dx
 \end{aligned} \quad \dots \quad (\text{xxvii})$$

Here,

$$\begin{aligned}
 & \int x \cdot e^{cx^{-\frac{3}{2}}}.dx \\
 &= -\frac{2}{3c} \cdot x^{\frac{7}{2}} \cdot e^{cx^{-\frac{3}{2}}} + \frac{2}{3c} \int x^{\frac{5}{2}} \cdot e^{cx^{-\frac{3}{2}}}.dx
 \end{aligned} \quad \dots \quad (\text{xxviii})$$

and

$$\begin{aligned}
 & \int x^{\frac{5}{2}} \cdot e^{cx^{-\frac{3}{2}}}.dx \\
 &= -\frac{2}{3c} \cdot x^5 \cdot e^{cx^{-\frac{3}{2}}} + \frac{5}{3c} \int x^4 \cdot e^{cx^{-\frac{3}{2}}}.dx \\
 &= -\frac{2}{3c} \cdot x^5 \cdot e^{cx^{-\frac{3}{2}}} - \frac{10}{9} \cdot \frac{1}{c^2} \cdot x^{\frac{13}{2}} \cdot e^{cx^{-\frac{3}{2}}} + \frac{80}{27} \cdot \frac{1}{c^3} \cdot x^8 \cdot e^{cx^{-\frac{3}{2}}} \quad \dots \quad (\text{xxix}) \\
 &\therefore \int x \cdot e^{cx^{-\frac{3}{2}}}.dx \\
 &= -\frac{2}{3c} \cdot x^{\frac{7}{2}} \cdot e^{cx^{-\frac{3}{2}}} \left\{ 1 - \frac{2}{3c} \cdot x^{\frac{5}{2}} - \frac{10}{9c^2} \cdot x^3 + \frac{160}{27c^3} \cdot x^{\frac{9}{2}} + \dots \right\} \\
 &= -\frac{2}{3c} \cdot x^{\frac{7}{2}} \cdot e^{cx^{-\frac{3}{2}}}, \quad \text{to the approximation (xxv).} \quad \dots \quad (\text{xxx})
 \end{aligned}$$

Then from (xvi),

$$\begin{aligned}
 e^{-\frac{F}{kT}} &= A \left\{ \int e^{cx^{-\frac{3}{2}}}.dx - \int e^{cx^{-\frac{3}{2}} - nx}.dx \right\} \\
 &= A \cdot n \cdot \int x \cdot e^{-cx^{-\frac{3}{2}}}.dx \\
 &= -A \cdot n \cdot \frac{2}{3} \cdot \frac{1}{c} \cdot x^{\frac{7}{2}} \cdot e^{cx^{-\frac{3}{2}}} \quad \dots \quad (\text{xxxii})
 \end{aligned}$$

Hence

$$-\frac{F}{kT} = \ln\left(-\frac{\frac{n}{3}\Delta n}{c}\right) + \frac{7}{2}\ln x + cx^{-\frac{3}{2}}; \quad \dots \text{ (xxxii)}$$

and,

$$\begin{aligned} p &= -\frac{\partial F}{\partial x} = N.k.T. \left\{ \frac{7}{2} \cdot \frac{1}{x} - \frac{3}{2} \cdot c \cdot x^{-\frac{5}{2}} \right\} \\ &= \frac{RT}{x} \left\{ \frac{7}{2} - \frac{3}{2} \cdot c \cdot x^{-\frac{3}{2}} \right\} \\ &= -RT \cdot \frac{3}{2} \cdot c x^{-\frac{5}{2}} \end{aligned} \quad \dots \text{ (xxxiii)}$$

This indicates a large negative pressure, tending to infinity as  $x$  approaches the value zero. Such a negative pressure would be accounted for by the forces of cohesion ; though, how it could attain values large enough to attain to infinity, would not be similarly explained. If this infinitely large force of cohesion between the molecules is to be avoided, we should suppose a change to come over the nature of the forces of interaction between the molecules approaching closer and closer.

We can also investigate the intermediate region, where,

$$nx = cx^{-\frac{3}{2}} \quad \dots \text{ (xxxiv)}$$

Then

$$\begin{aligned} &\int e^{cx^{-\frac{3}{2}}} dx - \int e^{cx^{-\frac{3}{2}} - nx} dx \\ &= \int e^{cx^{-\frac{3}{2}}} dx - x \\ &= \frac{e^{nx}}{n} - x. \end{aligned} \quad \dots \text{ (xxxv)}$$

Hence,

$$e^{-\frac{F}{kT}} = A \left\{ \frac{e^{nx}}{n} - x \right\}; \quad \dots \text{ (xxxvi)}$$

and,

$$-\frac{F}{kT} = \ln A + \ln \left\{ \frac{e^{nx}}{n} - x \right\}; \quad \dots \text{ (xxxvii)}$$

giving,

$$p = R.T.n \cdot \frac{\frac{e^{nx}}{n} - 1}{\frac{e^{nx}}{n} - nx}, \quad \dots \text{ (xxxviii)}$$

This indicates a region of positive pressure, but of instability, as shown by the increase of volume with pressure.

It may be of interest to investigate the influence of  $\beta$  in (ix) on our results. If we assume  $\frac{1}{2}mb$  to be the potential energy, as in (vii), we have the following resulting equations :

$$\begin{aligned} e^{-\frac{F}{kT}} &= \int e^{\frac{1}{2} \cdot \frac{mb}{kT}} \cdot dv = \int e^{\frac{1}{2} \cdot \frac{m}{kT} (Bx^{-\frac{3}{2}} - a_1)} \cdot dx \\ &= e^{-\frac{1}{2} \cdot \frac{ma_1}{kT}} \int e^{\frac{1}{2} \frac{mB}{kT} \cdot x^{-\frac{3}{2}}} \cdot dx \\ &= e^{-\frac{1}{2} \cdot \frac{ma_1}{kT}} \int e^{cx^{-\frac{3}{2}}} \cdot dx \\ &= C \int e^{cx^{-\frac{3}{2}}} \cdot dx \quad \dots \text{ (xxxix)} \end{aligned}$$

where  $c$  has the same significance as in (xviii).

$$\text{When } x \ll 1, \quad \dots \text{ (xl)}$$

$$e^{-\frac{F}{kT}} = -\frac{2}{3} \cdot \frac{C}{c} \cdot x^{\frac{5}{2}} \cdot e^{cx^{-\frac{3}{2}}} \quad \dots \text{ (xli)}$$

$$\text{and } p = -\frac{2}{3}RTcx^{-\frac{5}{2}}, \quad \dots \text{ (xlii)}$$

a result identical with (xxxiii).

$$\text{When } cx^{-\frac{3}{2}} \ll 1, \quad \dots \text{ (xliii)}$$

$$\begin{aligned} \int e^{cx^{-\frac{3}{2}}} \cdot dx &= \int (1 + cx^{-\frac{3}{2}} + \dots) \cdot dx \\ &= x - \frac{2}{3}c \cdot x^{-\frac{1}{2}} - \dots \quad \dots \text{ (xliv)} \end{aligned}$$

$$\text{Hence, } e^{-\frac{F}{kT}} = C (x - \frac{2}{3}cx^{-\frac{1}{2}} - \dots) \quad \dots \text{ (xlv)}$$

$$\begin{aligned} \text{and } p &= \frac{RT}{x}, \quad \dots \text{ (xlivi)} \\ \text{as in (xxiv)} \end{aligned}$$

The introduction of  $\beta$  in (ix) is thus seen to have no effect upon the salient features of our results. These would be represented by an isothermal of the form shown in figure 3.

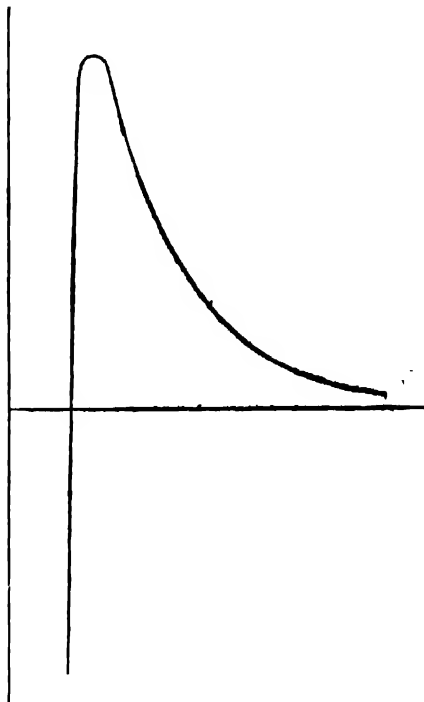


FIGURE 3.

At a temperature of  $27^\circ\text{C}$ . (xxiv) denotes a pressure of the order of 1,500 atmospheres to exist in the liquid. The compressibility of water at pressures of 1, 500, and 1000 kilograms per square cm. has values  $45 \cdot 3 \times 10^{-6}$ ,  $38 \cdot 1 \times 10^{-6}$ , and  $33 \cdot 6 \times 10^{-6}$ , respectively,<sup>5</sup> the unit of pressure being 1 kgm. per sq. cm. Basing ourselves on equation (xxiv), if  $p$  is the internal pressure when the external pressure is one atmosphere,

$$\frac{45}{38} = \frac{p+500}{p} \quad \dots \quad (\text{xlvii})$$

which yields a value of  $p$  of the order of 2,700 atmospheres.

For a change  $\Delta p$  in the pressure  $p$ , the corresponding change in the volume is

$$\Delta v = \frac{\partial v}{\partial p} \cdot \Delta p = \frac{x^2}{RT} \cdot \Delta p \quad \dots \quad (\text{xlviii})$$

At  $20^\circ\text{C}$ ., the proportionate change in the volume for a change of pressure by an amount 1 kgm per sq. cm. is

$$\frac{\Delta v}{v} = -\frac{x^2}{RTv} \cdot \Delta p = 5 \cdot 9 \times 10^{-4} \quad \dots \quad (\text{xlix})$$

This is seen to differ from the experimental value,  $45.3 \times 10^{-6}$ , by as much as a factor of 13. However, (xxiv) would diminish the compressibility with pressure. The change in compressibility  $C$  with the pressure  $p$  would be given by

$$\Delta C = \frac{\partial C}{\partial p} \cdot \Delta p = \frac{\Delta p}{p^2} = \left( \frac{x}{RT} \right)^2 \cdot p \quad \dots \quad (1)$$

For a change of 500 kgm/sq. cm., this works out to  $2 \times 10^{-4}$ , while the experimentally determined value is  $0.7 \times 10^{-5}$ .

This is a sufficient indication that the approximation is far from correct under normal conditions. What it exactly implies is not difficult to understand. The pressures, as calculated above, are the internal pressures in a liquid. Such an internal pressure can be conceived as the force acting on a unit area within the liquid on one side of it due to the action of the molecules on the other side of the area. This area would be subjected to the bombardment of the molecules in consequence of their thermal agitation, which would cause a pressure in the direction of impact of the molecules. On the other hand, a pressure would be exerted upon the area in the opposite direction due to the molecules on one side of it exerting a pull upon those on the other side. If this latter pressure due to the cohesion of the molecules is much smaller than the pressure due to the molecular impact, the approximation of (xx) holds good : while, when converse is the case it is the approximation (xxv) which obtains. The above comparison of the calculated and observed values of the several relevant constants indicates that the pressure is not purely thermal ; but the force of cohesion also exists in the liquid to an appreciable extent. It would necessitate the introduction of a further modification in the amount of the potential energy within the liquid, because on the assumption of the truth of (ix), we are led to values of compressibility not entirely in agreement with observations.

## R E F E R E N C E S.

- <sup>1</sup> Max Planck : *Theory of Heat* (English translation) ; p. 244 ; eq. (403).
- <sup>2</sup> *Ibid* ; p. 284 ; eq. (474).
- <sup>3</sup> *Ibid* ; pp. 77, 78 ; eqs. (112), (115).
- <sup>4</sup> M. F. Soonawala : *Ind. Jour. Phys.*, **10**, 362 (1936).
- <sup>5</sup> W. H. J. Childs : *Physical Constants*, p. 19.



# A NEW THEORY OF LAPSE-RATE\*

By D. S. SUBRAHMANYAM

A. C. College, Guntur

(Received for publication, February 4, 1939)

**ABSTRACT.** A new type of vertical motion of air different from penetrative convection is discussed. For small vertical displacements the motion is assumed to be similar to that in long gravitational waves, the volume of an element remaining constant during the displacement. Vertical motion of this type is the result of differences of pressure set up in the vertical direction and the pressures on an element in the other principal directions do not alter during the process of small displacement. As a result of the change in pressure, the molecular energy of the element is altered which results in a change of temperature, and consequently in a lapse-rate.

There is close agreement between the value of the lapse-rate deduced for small displacements without acceleration and the mean lapse-rates in the free atmosphere observed at different stations under normal conditions, so that the theory of mass motion developed may be taken to be a true picture of what is happening in the free atmosphere. If the type of motion described here can be called cumulative convection, the free atmosphere may be said to be normally in 'cumulative equilibrium.'

An explanation is also obtained for the ascent of air masses in a cyclone and their descent in an anticyclone. These movements are due to gradients of pressure in the vertical direction and the condition for motion is that when the lapse-rate is greater than the equilibrium rate, the acceleration is upwards, and when it is less than that, it is downwards.

## I. INTRODUCTION

It is found as a result of investigations with sounding balloons, that the rate at which temperature decreases with height is quite uniform in the free atmosphere, from a height of about 3 km. from the ground up to the tropopause. There is fall in temperature below 3 km. also but the lapse-rate is not regular, probably due to local disturbances and fluctuations that arise at the surface of the earth. But in the free atmosphere the lapse-rate is practically constant, the temperature-height curves of any ascent being almost linear, and the value about  $6^{\circ}\text{C}$ . to  $7^{\circ}\text{C}$ . per km.

The decrease of temperature with height in the troposphere is explained to be due to the convection that is taking place in it. Calculating on the basis that the atmosphere is in adiabatic equilibrium, the lapse-rate

\* Communicated by L. Ramakrishna Rao to the Indian Physical Society.

$\left( - \frac{dT}{dy} \right)$  is found to be equal to  $g \cdot \frac{A}{C_p}$  for dry air where  $g$  is the acceleration due to gravity,  $A$ , the reciprocal of the mechanical equivalent of heat and  $C_p$ , the specific heat at constant pressure. Substituting the values of these constants, the above adiabatic lapse-rate is found to be  $9.86^{\circ}\text{C. per km.}$ , which is much higher than the observed value mentioned above. The theoretical value obtained for ascending saturated air is less than the above value, but it is not a constant, as it depends upon the temperature of the air. If the atmosphere be in equilibrium for ascending saturated air, the lapse-rate should vary considerably from place to place and time to time, depending upon the temperature at the surface of the earth; it should also vary with height. But observations, as already stated, are rather different. Besides, the theory of ascending saturated air cannot be applied to regions where air masses are found to be descending as in anticyclones. The stability of air is usually discussed with reference to the adiabatic lapse-rates and the conclusion reached is that a dry atmosphere is in stable, unstable or neutral equilibrium, according as the lapse-rate is less than, greater than, or equal to the dry adiabatic lapse-rate and that saturated air is stable for downward motion when the lapse-rate is less than the dry adiabatic, but unstable for upward displacements unless the lapse-rate is less than the saturated adiabatic.<sup>1</sup> No satisfactory explanation has so far been given as to why the rate should be uniform throughout the free atmosphere up to the tropopause and fairly constant in value irrespective of time and place. There may be several factors like radiation and eddy diffusion, as discussed by Douglas,<sup>2</sup> which tend to produce a constant rate, but up till now, no theoretical value has been obtained which agrees with observations.<sup>3</sup>

Closely connected with lapse-rate are some other phenomena which too have not yet received satisfactory explanation. The centre of a cyclone is found to be a comparatively cold region and yet air masses are found to move upwards in it. An anticyclone may be warm, yet air masses are found to descend downwards in it though the lapse-rate is less than the dry adiabatic. These peculiar phenomena cannot evidently be explained by the hypothesis of penetrative convection. They are therefore attributed to be due to differences of pressure in the vertical direction and the term 'cumulative convection'<sup>4</sup> is applied to the large movements of air that take place in these cases. Yet there has been no theoretical calculation of what the lapse-rate should be in such a type of motion.

An attempt is made in this paper to develop a theory of lapse-rate (which may be said to be the lapse-rate for cumulative convection) for vertical motion of air due to difference of pressure, assuming the motion to be like that in long gravitational waves. The aid of the kinetic theory of gases is also sought for a simple relationship that obtains between pressure exerted by a gas in any

direction and the kinetic energy of the molecules of the gas in that direction. The results obtained seem to be in fair agreement with observations.

## 2. LONG WAVES

The idea of long waves, the wave-length of which is very great as compared to the height of disturbance, is very useful in understanding the picture of air motion presented in this paper. Vertical motion of air in the case of long waves is easily seen to be different from that of penetrative convection. In the latter case, an element of air is considered to be warmer and therefore lighter than its surroundings, to be displaced from one layer to another, and then to expand adiabatically to attain the pressure there. The surroundings are considered to be practically undisturbed except for filling up the space vacated by the element. Motion of air in the case of long waves would be entirely different. Here there is motion on a large scale. Vast sheets of air rise or fall. And as they do so, two neighbouring elements in the same horizontal plane will move together and the difference in their vertical displacements will be negligibly small. The consequence of it is that there is no question of expansion of the element sideways suddenly as it rises. Even if there be a slight difference in the vertical displacements of these two elements, the result will not be (in the first place) expansion sideways, but mass motion, in a horizontal direction, the velocity of motion depending upon the rate of variation of pressure with distance.

This leads to an important assumption that is made in the development of the theory that there is little tendency for an element of air to change its volume as it is displaced slightly from one point to another in the vertical direction. This assumption may be considered to be not unreasonable in the light of what has been stated above, when the displacements are small. All displacements in the vertical direction therefore, according to the theory presented here, take place at constant volume, the displacements of the air elements being small.

## 3. RELATION BETWEEN MOLECULAR ENERGY AND PRESSURE

There is a very simple relation in the kinetic theory of gases between the pressure exerted by a gas on an element of area and the kinetic energy of the molecules of the gas in a direction normal to the area.

If  $n$  be the number of molecules per c.c. of the gas,  $m$ , the mass of a molecule, and  $\bar{v}^2$  the average of the squares of the velocity components of the gas in the direction of the Y axis, the pressure exerted on an element of area in the XZ plane (which we may say is the pressure in the Y direction) is

$$P_y = n, m \cdot \bar{v}^2 \quad \dots (1)$$

But if the kinetic energy possessed by the molecules per unit volume of the gas in this direction be called  $E_y$ ,

$$E_y = \frac{1}{2} n.m.v^2 \quad (2)$$

$$P_y = 2 \cdot E_y \quad (2a)$$

or

$$dP_y = 2 \cdot dE_y \quad (2b)$$

#### 4. THEORY OF MASS MOTION OF AIR (CUMULATIVE CONVECTION)

Mass motion of air between two points which are close to each other is due to the difference of pressures between the two points in the direction of the line that joins them. The importance of considering direction for the pressure arises from the fact that in the case of vertical motion of an element of air in a gravitational field, the pressure alters very rapidly with height. Let  $P_x$ ,  $P_y$ ,  $P_z$ , be the pressures at the point A (the co-ordinates of which are  $x$ ,  $y$ ,  $z$ ) in the three principal directions. Let B be a point the co-ordinates of which are (for the sake of simplicity)  $x$ ,  $y + dy$ ,  $z$ . Let the initial pressure at this point in the three directions be  $P'_x$ ,  $P'_y$ ,  $P'_z$ . If we assume that there is static equilibrium in the beginning, we know that

$$P_x = P_y = P_z,$$

$$P'_x = P'_y = P'_z \text{ and}$$

$$P_y = P'_y + \rho g dy \quad (\rho, \text{ being the density at A}).$$

Let us now examine what takes place if there is a little accumulation and therefore some excess of pressure at A, so that

$$P_y > P'_y + \rho g dy.$$

There will be motion upwards, the equation for vertical motion being

$$\frac{Dv_0}{Dt} + g + \frac{1}{\rho} \frac{\partial P_y}{\partial y} = 0 \quad \dots \quad (3)$$

where  $v_0$  represents the mass velocity of the gas in the vertical direction and,  $\frac{Dv_0}{Dt}$  represents the acceleration of the element (following its motion).

Hence  $-\frac{1}{\rho} \frac{\partial P_y}{\partial y} = g + \frac{Dv_0}{Dt}.$

The value of  $-\frac{\partial P_y}{\partial y}$ , when there is accumulation below, will be greater

than the value it would have in static equilibrium and consequently  $\frac{Dv_0}{Dt}$  will be positive, the acceleration being upward. If on the other hand there is accumulation at the higher point B,

$$P_y < P'_y + \rho g dy.$$

the accelerated motion is downwards, and in

$$-\frac{\partial P_y}{\partial y} = \rho g + \rho \frac{Dv_0}{Dt}$$

$\frac{Dv_0}{Dt}$  is negative.

We shall now investigate the motion of an element. Let us assume for definiteness that the accumulation is below and that the motion is upwards. Let the element at A reach B in a short time,  $dt$ , the whole volume remaining constant in this process. As the element moves upwards, the value of  $P_y$  alters at a very rapid rate as it moves against a gravitational field of force, and its molecular energy in the vertical direction also diminishes at the same rate. But there is no such variation of pressure laterally as the surrounding elements also come up with it. Hence by the time the element reaches B, the energy corresponding to one degree of freedom only becomes less while that corresponding to the other degrees of freedom remains practically constant. Due to the law of equipartition of energy, however, there may be a transference of energy taking place between that degree and the other degrees which will tend to make the kinetic energy and hence the pressure equal in all directions. But since any such equalization should be preceded by a decrease in the Y direction, we shall assume that in a very short interval of mass motion of the gas, the pressures and therefore the energies are different in different directions. We shall thus assume that for the element in vertical motion as pictured here  $P_x$  and  $P_z$  do not alter but  $P_y$  alone alters during a small displacement of the element.

For a small displacement  $dy$ , the change in the value of  $P_y$  may be taken to be  $dP_y = \frac{\partial P_y}{\partial y} dy$  ... (4)

$$\text{By equation (3)} \quad \frac{\partial P_y}{\partial y} = -\rho \left( g + \frac{Dv_0}{Dt} \right) \quad \dots \quad (5)$$

It may be noted in this connection that the effect of the rotation of the earth is ignored as the change it produces in the motion is negligible in comparison with  $g$  as pointed out by Brunt.<sup>5</sup> It is further assumed that the element has no motion in any other direction than the Y direction, in order to simplify the theory and study the effect of only the vertical motion on the element.

Now from equations (4) and (5) we have

$$dP_y = -\rho \left( g + \frac{Dv_0}{Dt} \right) dy \quad \dots \quad (6)$$

and consequently from equation (2b)

$$dE_y = -\frac{1}{2} \rho \left( g + \frac{Dv_0}{Dt} \right) dy \quad \dots \quad (7)$$

This is the change in the kinetic energy of the molecules of the element in the vertical direction per unit volume due to the displacement  $dy$ . Since we have assumed that there is no change in pressures in the other directions, the energies corresponding to all the other degrees of freedom of the molecules are not altered during this displacement. The change in the total kinetic energy per unit volume of the molecules of the element  $dE$  will be therefore equal to  $dE_y$ , and this does not alter in value due to any subsequent redistribution between all the different degrees of freedom of the molecules.

Therefore the change in the total kinetic energy of the molecules of the gas per unit volume

$$dE = -\frac{1}{2} \rho \left( g + \frac{Dv_0}{Dt} \right) dy \quad \dots \quad (8)$$

The corresponding change of temperature  $dT$  suffered by the element may be easily computed applying the first law of thermodynamics :

$$dT = \frac{dE}{J \cdot C_v} \quad \dots \quad (9)$$

where  $J$  is the mechanical equivalent of heat and  $C_v$  the specific heat of air at constant volume (the displacement having been considered to take place at constant volume). Therefore from equations (8) and (9) we have for the rate of change of temperature of the element with height

$$\frac{dT}{dy} = -\frac{1}{2 \cdot J \cdot C_v} \left( g + \frac{Dv_0}{Dt} \right) \quad \dots \quad (10)$$

Let us assume that the acceleration  $\frac{Dv_0}{Dt}$  is zero when the atmosphere is in equilibrium. We shall call the corresponding rate at which an element falls in temperature with height the equilibrium lapse-rate. The equilibrium lapse-rate is thus equal to

$$-\frac{dT}{dy} = \frac{g}{2 \cdot J \cdot C_v} \quad \dots \quad (11)$$

Substituting the values,  $C_v$  (for dry air) = .1715. Cal. per gm. (the value for damp air does not differ materially from this),

$$J = 4.185 \times 10^7 \text{ ergs. per cal.}$$

and

$$g = 981.0 \text{ cm. per sec. per sec.}$$

We have  $-\frac{dT}{dy}$  from equation (11) equal to

$$\begin{aligned} & \frac{981}{2 \times 4.185 \times 10^7 \times 0.1715} \\ &= 6.836 \times 10^{-5} \text{ C. per cm.} \\ &= 6.836 \text{ C. per km.} \end{aligned}$$

This is easily seen to be one-fifth of what is usually called the auto-convection gradient.<sup>6</sup>

The value 6.836 C. per km. is the rate at which an element of air would fall in temperature as it is displaced upwards vertically through a short distance as part of a vast sheet or layer of air, the volume of the element remaining constant during the small vertical displacement. Continuous vertical motion of air itself may be considered to take place in successive short steps, each step consisting of two stages :

(i) The stage in which an element undergoes a vertical displacement according to the way stated above.

(ii) The stage in which adjustments take place in a horizontal level, with expansion or contraction of the element sideways. But these changes in volume cannot be so sudden as to be completely adiabatic, because what may result in a horizontal direction as a consequence of this type of convection is a gradient of pressure which produces a wind. Hence the change of volume which an element undergoes at the new level is very likely to be isothermal. Consequently the lapse rate in an atmosphere in which such motion takes place will not differ appreciably from the value calculated above. Observations of the free atmosphere go to show that this type of (cumulative) convection is playing an important part in the movements of air masses in our atmosphere.

## 5. COMPARISON WITH OBSERVATIONS IN THE FREE ATMOSPHERE

Individual observations in the troposphere above a height of about 3 km. show that the temperature decreases at a uniform rate with height, the

temperature-height curves being almost straight lines. This itself is in agreement with the result deduced above. Besides, the mean value of the lapse-rate obtained from a number of observations taken at different stations in the middle latitudes is found to agree quite satisfactorily with the result calculated above. The following table gives the mean lapse-rates observed at different stations in the middle latitudes. It is obtained from a table given by Dines who made use of Gold's values.

TABLE I ?

(Mean Lapse-rates)

Height in km.	Petrograd.	Scotland.	Berlin.	England S.E.	Paris	Vienna.	Pavia.
	Deg. A.	Deg. A.	Deg. A.	Deg. A.	Deg. A.	Deg. A.	Deg. A.
13.5	-0.1	-0.2	0.6	-0.2	0.2	0.0	-1.3
12.5	-2.7	-0.2	-1.0	0.1	0.2	-1.3	-0.3
11.5	-0.3	-1.1	0.9	0.8	0.7	0.1	2.4
10.5	1.3	0.7	2.7	2.6	4.1	3.4	4.2
9.5	3.1	3.6	4.9	5.3	5.7	5.1	4.6
8.5	5.4	5.4	6.3	6.1	6.9	6.7	6.6
7.5	7.3	7.8	7.7	7.1	7.4	7.6	7.3
6.5	6.2	7.0	7.1	7.1	7.1	7.6	8.2
5.5	6.5	7.0	6.9	7.0	6.7	6.8	6.8
4.5	5.9	6.4	6.2	6.9	6.2	6.3	6.7
3.5	5.6	5.6	5.9	6.0	5.5	5.7	5.9
2.5	5.4	5.7	4.8	5.5	4.7	5.4	6.3
1.5	4.3	5.0	5.1	4.8	4.0	4.6	5.6

In calculating the mean value of the lapse-rate in the troposphere, we must exclude observations below a height of 3 km., as this region is subject to many local disturbances and fluctuations and the lapse-rates are irregular. Also we should not take the region in which the tropopause rises and falls, as the mean value in it would be obviously misleading. Hence, below are given the mean lapse rates at different stations calculated from the values lying between the thick lines in the above table.

		Free troposphere between.	Mean lapse-rate.
Petrograd	...	3 km. - 8 km.	6°30 Deg. A. per km.
Scotland	...	do.	6°66 "
Berlin	...	3 km. - 9 km.	6°68 "
England S.E.	...	do.	6°70 "
Paris	...	do.	6°63 "
Vienna	...	do.	6°78 "
Pavia	...	do.	6°92 "
		Mean	6°71 "

The equilibrium lapse rate is theoretically deduced to be 6°.836 C. per km. The agreement between the above mean observed value and the theoretical value is very close and we may therefore conclude that the ' free troposphere ' (lying between 3 km. and the tropopause) in the middle latitudes, to which belong the stations in the above table. is normally in equilibrium for mass motion of the type discussed in this paper (*i.e.*, for cumulative convection).

Mean lapse-rates of the free atmosphere obtained at Agra<sup>8</sup> and<sup>9</sup> Poona in India are given below. The mean for Poona is calculated for lapse-rates between 3 and 15 geodynamic kilometres and that for Agra between 3 and 14 gkm. The mean values for the free atmosphere (6°.87 C. and 6°.35 C. respectively per km.) show fair agreement with the theoretical value deduced.

TABLE II.

Height in gkm.	Lapse-rate (Poona) (1928-'31).	Lapse-rate (Agra, (1925-'28).
14-15	eg. C.	Deg. C.
13-14	6.7	...
12-13	8.0	6.3
11-12	8.3	7.1
10-11	8.2	7.0
9-10	8.1	6.9
8-9	7.8	6.7
7-8	7.2	6.7
6-7	6.8	6.3
5-6	5.9	6.1
4-5	5.6	6.2
3-4	5.8	6.1
Mean/gkm.	7.02	6.48
Mean/km.	6.88	6.35

6. LAPSE-RATES IN ASCENDING AND DESCENDING CURRENTS OF AIR (CYCLONIC AND ANTI-CYCLONIC SYSTEMS)

In the discussion made above on the equilibrium lapse-rate it is assumed that  $\frac{Dv_0}{Dt}$  is equal to zero. Now we may take up for consideration the cases when

it is not equal to zero. If we call  $\frac{Dv_0}{Dt}$  the vertical acceleration of the element,

we see that there is a possibility for two cases in addition to the case of equilibrium: (i) The vertical acceleration may be positive or (ii) it may be negative. From equation (10)

$$-\frac{dT}{dy} = \frac{1}{2J.C_v} \left( g + \frac{Dv_0}{Dt} \right).$$

We see that in case (i) when  $\frac{Dv_0}{Dt}$  is positive (*i.e.*, the velocity increases with increase of height) the quantity within the parentheses will be greater than  $g$  and the lapse-rate will be higher in value than the equilibrium lapse-rate.

In cases (ii)  $\frac{Dv_0}{Dt}$  is negative (*i. e.*, the increase of velocity is down-ward) the quantity within parentheses becomes less than  $g$ , and the lapse-rate will be less than the equilibrium rate.

Thus we arrive at a new and interesting result that for upward motion of air with increasing velocity, the lapse-rate is higher and for downward motion with increasing velocity it is less than the equilibrium lapse-rate. It has already been stated that the acceleration will be upwards ( $\frac{Dv_0}{Dt}$  positive) when

there is accumulation below and downwards ( $\frac{Dv_0}{Dt}$  negative) when the accumulation is above. These conditions are found to obtain in cyclonic and anticyclonic systems respectively.

*Cyclonic systems* :—It is a widely observed fact that in a region of low pressure, there is an upward current of air, the velocity of which increases with height above the ground. The acceleration upward, in cases of strong convection on such occasions, becomes appreciable as compared to  $g$  and the lapse-rate should be accordingly affected. An example for upward acceleration quoted by Ramanathan<sup>10</sup> from Brunt, may be given in this connection. “An estimate of upward acceleration in hailstorms has been made by Brunt. He has shown that

in order to raise a spherical hail stone of radius 3 cm. in an ascending current, an upward vertical velocity exceeding 55 metres per sec. would be required. If this velocity is developed within a distance of 3 km, the acceleration will be  $50 \text{ cm/sec}^2$ ."

Thus in a region of low pressure the lapse-rate should be, according to the theory developed here, greater than the equilibrium lapse-rate.

*Anticyclonic systems* :—It is also known widely that in an anticyclone there is a downward motion of air ; but this does not seem to be as vigorous as the upward motion in a cyclone. Still since the downward motion is a result of accumulation in upper levels of air, and when an element of air moves under difference of pressure there is acceleration, it is quite possible that there is downward acceleration (however small) in anticyclonic systems in the free atmosphere.

Thus  $\frac{Dv_0}{Dt}$  becomes negative in these cases and the lapse rate becomes less than the equilibrium rate.

But since the convection in them is not so rapid as in cyclonic systems the difference from the equilibrium value will not be as great in them as in the latter.

These conclusions obtain confirmation from observations made in cyclones and anticyclones. Below is given a table showing the mean temperatures in cyclones and anticyclones. The results are due to Dines.<sup>11</sup>

TABLE III<sup>12</sup>

Height in km.	Cyclone—980 mb. Temperature.	Anticyclone—1026 mb. Temperature.
14	224 Deg. A.	215 Deg. A.
13	25	15
12	25	17
11	24	20
10	25	25
9	26	31
8	28	28
7	34	46
6	42	53
5	49	59
4	56	65
3	63	71
2	70	76
1	276	279

For the cyclone we may take the 'free troposphere' to be between 3 km. and 7 km. and for the anticyclone between 3 km. and 9 km. at the lowest. Then we have from the above table the following mean values for the lapse-rates :

TABLE IV

	Mean lapse-rate	Difference from calculated equilibrium rate (6°836)
Cyclone	7°25 C.	+0°414° C.
Anticyclone	6°67 C.	-0°166° C.

Some individual cases may also be quoted in support of this view. There was an anticyclone over Upper India between the 19th and the 26th of December, 1930. The sounding <sup>13</sup> on the 19th Dec., gave a mean lapse-rate (between 4 gkm. and 15 gkm.) of 6°·45 C. per gkm. and that on the 22nd, 6°·66 C. per gkm. The mean of these two values is 6°·56 C. per gkm. or 6°·43 C. per km., a value less than the theoretical value for equilibrium. (6°·836 C. per km.)

A cyclone crossed the East Coast (India) at Nellore on the 17th of November, 1933. Soundings <sup>14</sup> made during the period of the cyclone on 15th, 16th, 17th, 18th and 19th of that month at Madras observatory, 110 miles away, gave the mean lapse-rates 7·32, 7·15, 7·08, 7·64 and 7·47 deg. C. respectively per gkm. (between 3 gkm. and 15 gkm.) of the free atmosphere. The mean value is 7·33 deg. C. per gkm. or 7·19 deg. C. per km., which is clearly higher than the theoretical equilibrium lapse-rate.

Thus the result deduced theoretically that the lapse-rate should be greater in a cyclonic system and less in an anticyclonic system than the equilibrium rate is supported by observations of the upper atmosphere. We have therefore a satisfactory explanation for the ascent of (cold) air in a cyclone and the descent of air (which may be warm) in an anticyclone even when the lapse-rate is less than the adiabatic. These vertical motions may therefore be considered to be due to pressure differences set up in the vertical direction and not to convection of the penetrative type.

In conclusion, I wish to express my grateful thanks to Dr. J. Roy Strock, our Principal, and to Dr. H. H. Sipes, our Bursar, for the kind encouragement they gave me in my work. I am also highly obliged to Dr. I. Ramakrishna Rao of the University College, Waltair, who was kind enough to go through the paper and give me very valuable suggestions.

## R E F E R E N C E S

- <sup>1</sup> D. Brunt, *Physical and Dynamical Meteorology*, p. 41 and p. 64 (1934).
- <sup>2</sup> *Memoirs of the Roy. Met. Soc.*, 8, 159 (1930).
- <sup>3</sup> D. Brunt, *loc. cit.*, p. 20.
- <sup>4</sup> Shaw, *Dictionary of Applied Physics*, Vol. 3, p 72.
- <sup>5</sup> Brunt, *loc. cit.*, p. 165.
- <sup>6</sup> Brunt, *loc. cit.*, p. 47.
- <sup>7</sup> Geddes, *Meteorology*, p. 268.
- <sup>8</sup> *Mem. Ind. Met. Dept.*, 28, Part V (1930).
- <sup>9</sup> *Mem. Ind. Met. Dept.*, 28, Part IV (1934).
- <sup>10</sup> *Mem. Ind. Met. Dept.*, 28, Part V, 89 (1936).
- <sup>11</sup> *Phil. Trans. Roy. Soc. A*, 211, 253 (1911).
- <sup>12</sup> Geddes, *Meteorology*, p. 369.
- <sup>13</sup> N. K. Sur and J. C. Roy, *Sci. Notes, Ind. Met. Dept.*, 5, p. 23.
- <sup>14</sup> Ramanathan, *Mem. Ind. Met. Dept.*, 26, Part V, p. 79 (1936).



# FURTHER STUDIES OF F-REGION AT ALLAHABAD \*

BY R. R. BAJPAI

AND

B. D. PANT

Department of Physics, the University of Allahabad

(Received for publication, February 28, 1939)

Plates III, IV and V.

**ABSTRACT.** Results of measurement of virtual height of the F-region carried out (mostly at night) during 1937-38 session on several wave frequencies are described. It is found that the nature of the equivalent height change varies in a marked manner from day to day. Sometimes the virtual height shows three maxima during a single night. A good correlation has been found to exist between the hour of occurrence of minimum virtual height of the F-region and the hour at which the barometer at ground level reads maximum pressure. Occasionally echoes from ionized regions above the normal F-layer have been obtained. Occurrence of complex echoes is found to be associated with variation of one or other of the terrestrial magnetic elements. It is seen that contrary to the results obtained by many investigators the F-region exists till about 10 o'clock at night.

## INTRODUCTION.

The paper presents the results of some of the ionospheric investigations carried out at Allahabad during the 1937-38 session. The work was started with a view to predict maximum usable frequencies for broadcasting over various distances and to make a thorough study of the electron density and equivalent height variations in the F<sub>2</sub>-region. Our experience during the 1936-37 session had shown that the critical penetration frequency of the F<sub>2</sub>-region was always below 11 Mc/sec., so, keeping in mind the long time variation in the electron density of the ionospheric regions owing to the increased sun spot activity, we constructed a transmitter which enabled us to transmit pulses up to 13.6 Mc/sec., but we found that the 13.6 Mc/sec. waves were reflected by the region even up to 10 or 11 o'clock at night. Thus the measurement of ionization density was possible only during a limited period at night. Under such circumstances it was not possible for us to predict maximum usable frequencies for the major portion of day and we confined our attention only to the measurement of virtual height. Off and on we also measured the critical penetration frequency differences between the ordinary and the extra-ordinary waves.

\* Communicated by Prof. M. N. Saha, F.R.S.

The data collected in our laboratory from experimental transmissions on 4 Mc/sec. had shown the utility of such waves for regular broadcasting purposes in India. The All-India Radio also realised this fact and started broadcasts on 60 and 90 metre bands. The International Tele-communications Conference held at Cairo also came to similar conclusions and set apart such bands for broadcasting exclusively in the tropical and sub-tropical countries. In view of the importance of these waves, the virtual height measurements were generally carried out on such and a number of other wave lengths. The data presented here are based on automatic ( $P'$ , t) records and auxiliary visual observations. The day-time observations were confined only to few holidays, since on other days the disturbance level was very high. Experiments were also made to develop an automatic ( $P'$ , f) recording apparatus. In these experiments the transmitter and receiver were kept in tune manually. §1 gives a brief description of our apparatus while §2 contains our experimental results along with their discussion.

#### §1. APPARATUS.

The method used is that of Breit and Tuve.<sup>1</sup> The transmitter generates short wave-trains of radio-frequency 50 times per second. These waves fall on the receiver which is lying just on the side of the transmitter, both directly and after reflection from the upper ionized strata. The output from the receiver is fed to the vertically deflecting plates of an oscilloscope the horizontally deflecting plates of which are connected to a timebase synchronized with the frequency of the pulses.

The transmitter consists of a simple Hartley circuit. Modulation is effected by means of a valve in series with the oscillator. Normally the grid of the oscillator is kept so negative that no plate current flows through the oscillator and the modulator, but by the application of short unidirectional pulses generated by a thyratron and its associated circuit, the grid potential of the modulator is reduced to zero for short periods fifty times per second. It is during these periods that the transmitter oscillates and radiates the desired wave trains.

#### §2. EXPERIMENTAL RESULTS AND THEIR DISCUSSION.

(a) *Diurnal variation of Virtual Height.*—The ( $P'$ , t) records were usually taken throughout a month on several frequencies so that for any particular frequency eight or ten records distributed over the entire month were available. The graphs represent monthly average values of virtual height at the particular frequency mentioned. Generally an average of more than four values has been taken. In December, however, very few records could be taken so curves for the virtual height variation for a particular day and night have been given. The October data were also meagre. The rest of the curves are fairly good averages.

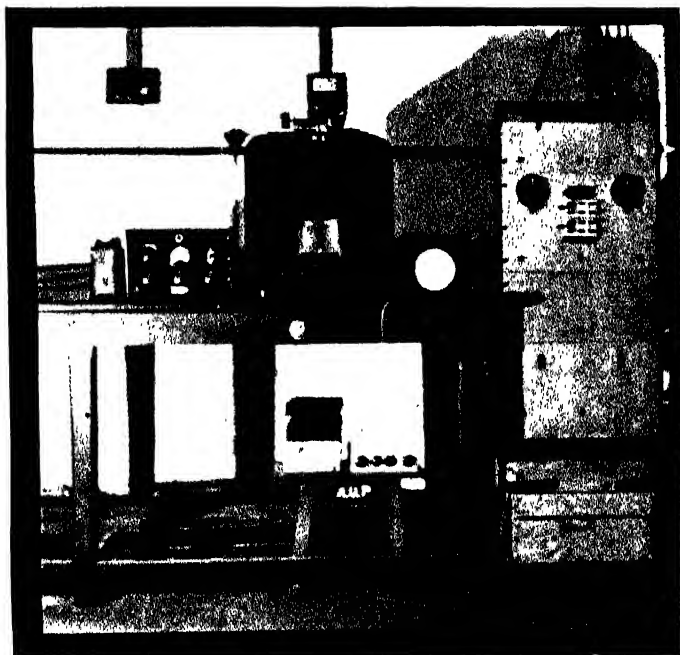


Fig. 1.  
Apparatus.



Figures 2, 3 and 4 show all these curves. Marked variations in the nature of equivalent height changes are noticed from day to day. Sometimes we find that during a single night there are three maxima in virtual height, while at others there are only two and yet on certain nights the virtual height remains constant almost throughout the night. We have reported elsewhere<sup>3</sup> the existence of similar maxima and minima in the electron density of the night F-region and it would have been interesting to correlate the two variations, but unfortunately we could not get electron density data during this period. It is therefore difficult to say if there is any relation between virtual height variations and the increase in electron density. It is still more difficult to explain the nature of these virtual height variations mentioned above, for they depend on the complicated meteorology of the upper atmosphere about which so little is known. We cannot say if these changes accompany some sort of atmospheric oscillation or are the result of some other cause unknown to us. Some of our records clearly show that increase in electron density of the night F-region takes place several times during the course of a single night. Figure 7 taken on December 10-11, 1937, at a frequency of 2.9 Mc/sec. shows that the waves ceased to be reflected at 0020 but they reappear-

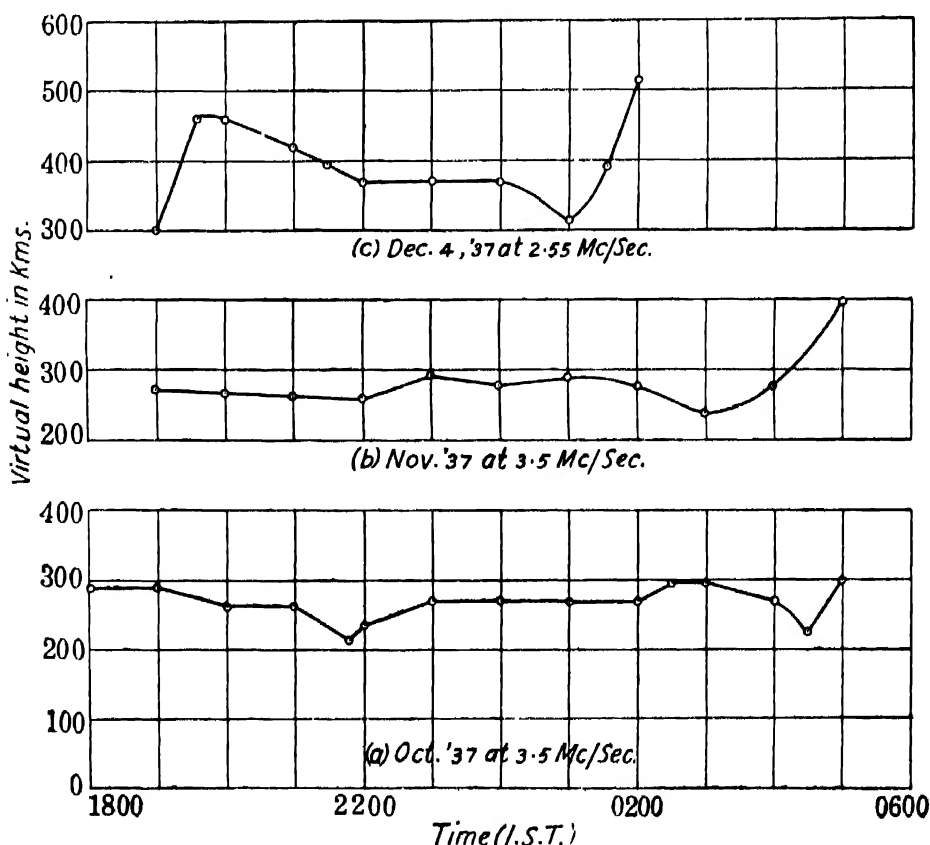
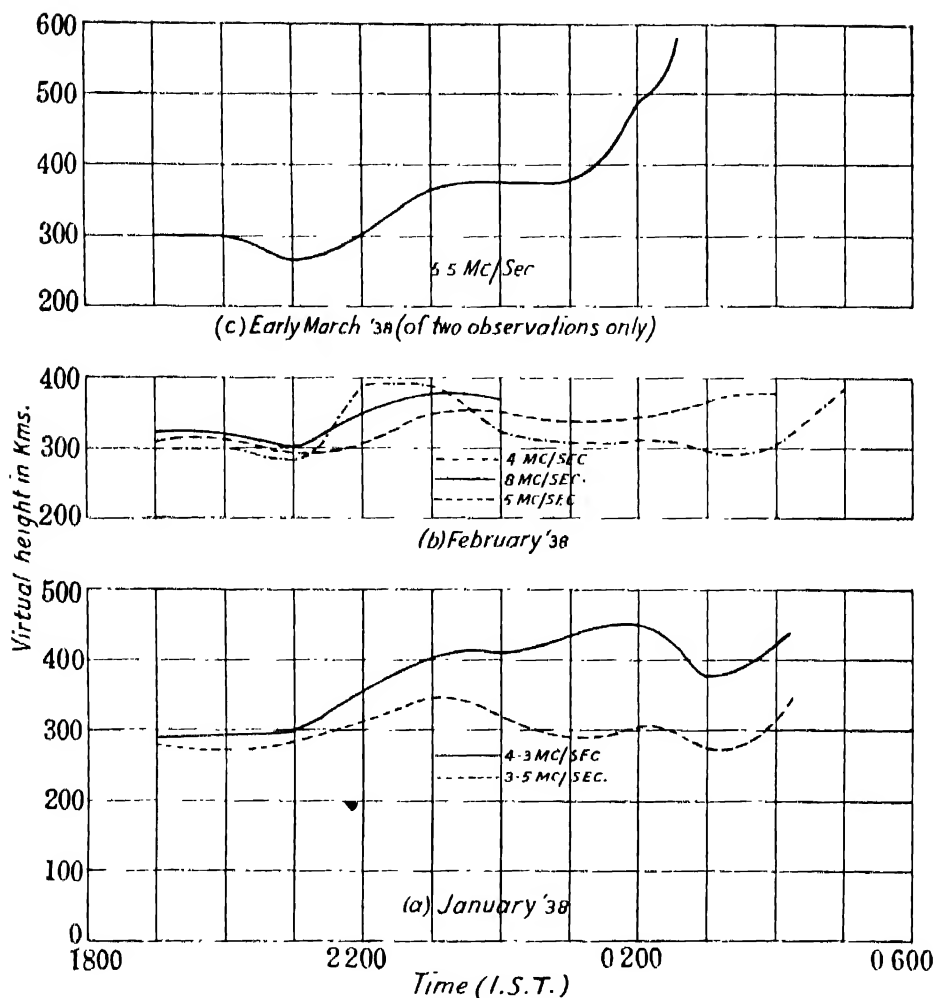


Fig 2. Showing mean virtual height of the F-region for the months and at the frequencies shown



*Fig. 3 Mean virtual height of F-region for the months and at the frequencies shown*

ed twice during the night before they began to be continuously reflected by increased ionization due to the incidence of the rays of the Sun in the morning. It unmistakably points out that between the hours 0130 and 0150, and 0245 and 0350, there was an increase in the electron density of the F-region which cannot be attributed to ionization due to ultra-violet light of the Sun. For understanding these short-time variations, as well as to gain an insight into the nature of variation of ionization density with height, it is very necessary that  $(P', f)$  curves should be determined as frequently as possible and the mean hourly values of maximum electron density, minimum virtual height and virtual heights on a number of other frequencies published, just as the data for earth's magnetic field are published.

Now variations in virtual height can occur either due to change in the electron density in the lower layers which have a retarding influence on the

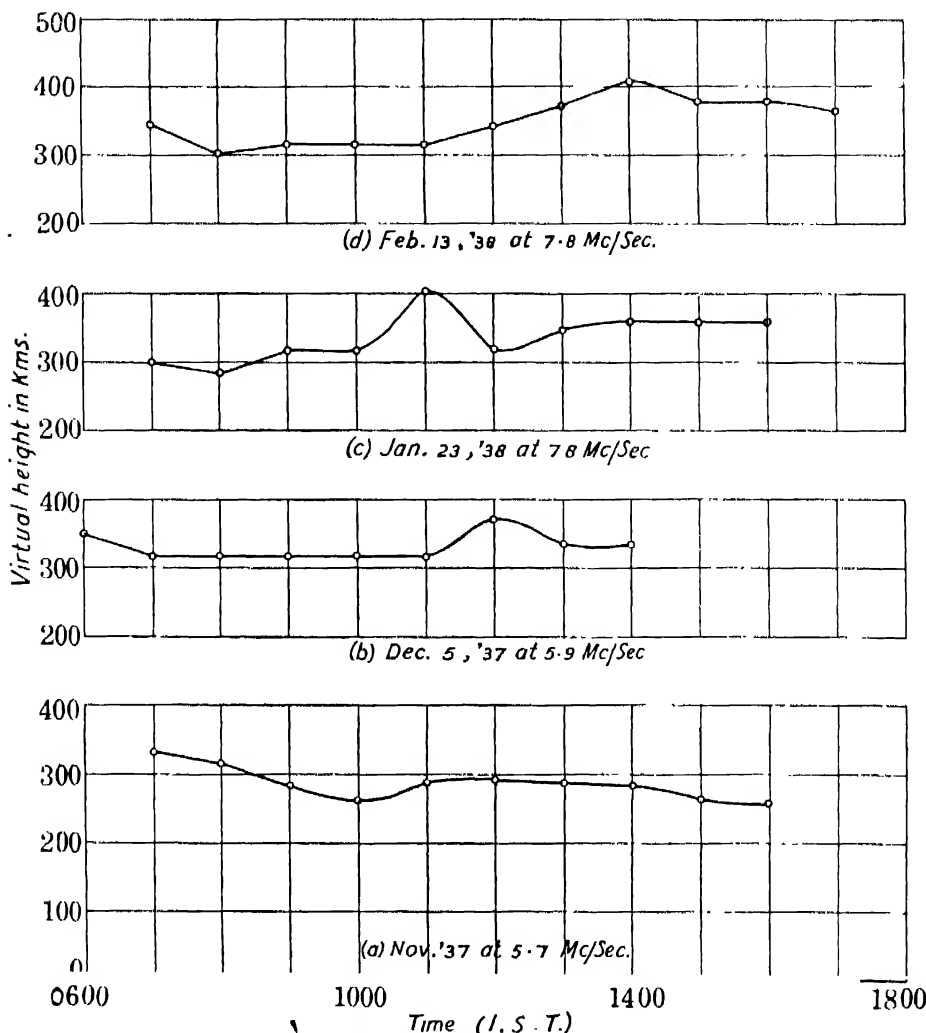


Fig 4. Showing day virtual height of the F<sub>2</sub>-region on the dates and frequencies given (a) gives mean virtual height

waves that pass through them, or due to changes in the real height of the layer. Figure 3 clearly shows that the variations in virtual height of the night F-region are similar in nature even when frequencies vary from 4 to 8 Mc/sec. This strongly suggests that the variations in the virtual height of the region are due to changes in the actual height of the layer itself. The conclusive proof of the movement of the layer can, however, be obtained only if the temporal rate of change of optical path which can be measured by Appleton's method<sup>3</sup> is found to be equal to the temporal rate of change of equivalent path.

#### (b) Seasonal Variation of Virtual Height.

Two curves showing the seasonal variation of the virtual height during the period of observation have also been drawn. Figure 5 (a) shows equivalent

heights as observed at seven o'clock in the evening on different days while Figure 5(b) gives the same for midnight. The curves also give an insight into the general difference in the values of the virtual height in the evening and at midnight. It is obvious that in general the virtual height at midnight is greater than that in the evening hours. This fact also shows that this difference in virtual height is to be expected on account of change in actual height, for otherwise we should expect greater retardation of the waves in the lower regions in the evening hours than that at midnight and hence a greater virtual height at the former hour.

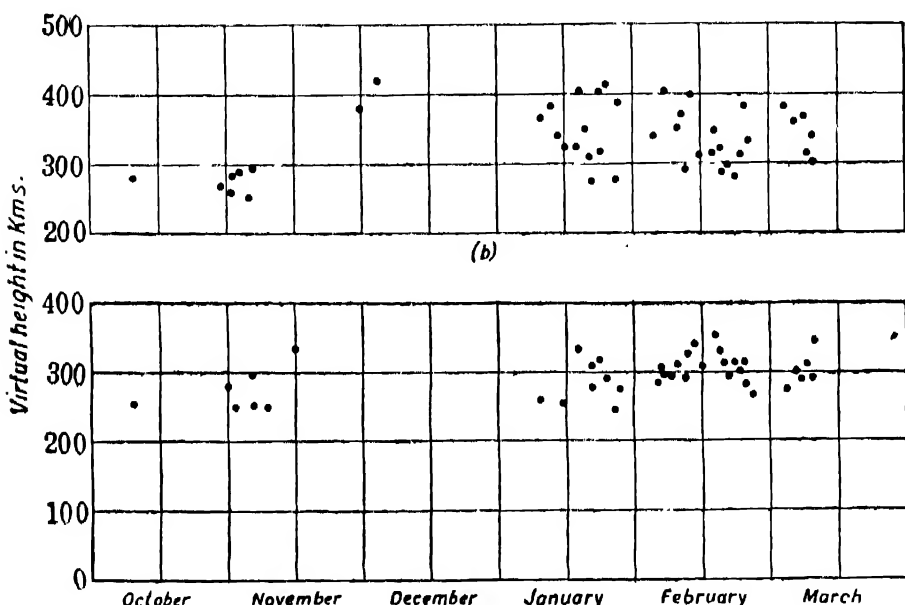


*Fig 5 Showing seasonal variation of the virtual height of the F-region at  
(a) 1900 and (b) midnight*

### *(c) Correlation of Barometric Pressure and Virtual Height*

Correlations of atmospheric pressure with ionospheric phenomena are not new. Ranzi<sup>1</sup> found correlation between increase in the E-region ionization after sunset and barometric depressions observed at the place of observation or north of it. Colwell<sup>5</sup> claims that under suitable conditions, the variations in the strength of a broadcasting station may be used to indicate the presence of cyclonic<sup>1</sup> anticyclonic regions with an accuracy of about ninety per cent for weather forecasting purposes. Martyn and Pulley<sup>6</sup> in Australia have found a strong correlation between E-layer average electron density at night and the ground level barometric pressure observed next morning. The latter authors have also found a correlation between the noon ionization density of the E-region and barometric pressure observed as before. They also pointed out that similar

correlations have not been reported from the northern hemisphere. Taking up the suggestion of these Australian investigators, Best, Farmer and Ratcliffe<sup>7</sup> tried to look up for this correlation in England, but their report shows that they did not find any such correlation.

Figures 2 and 3, especially figure 3(b), clearly show that in the evening between 2000 and 2200 there occurs a minimum in the virtual height of the F-region. We attempted to find out if any relationships exist between this minimum equivalent height and the maximum barometric pressure observed at ground level during the same night. The result is given in figure 6(b). 6(a) shows correlation between the time of occurrence of this minimum in virtual

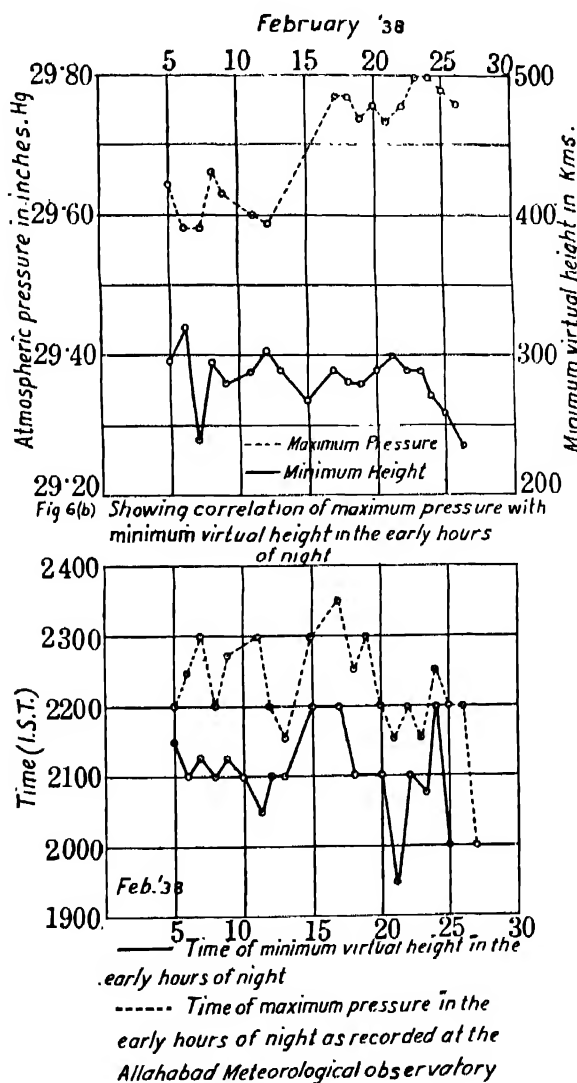


Fig 6(a) Showing Correlation of the time of minimum virtual height with that of maximum pressure in the early hours of night

height of the F-region and the time at which barometer at ground level was observed to read maximum pressure during night. The atmospheric pressure at Allahabad shows two maxima, one at about 10 or 11 o'clock in the night and the other at about the same time during the day. The observations reported in figure 6 refer to February, 1938. A glance at figure 6(b) shows that the relationship between minimum virtual height and maximum barometric pressure is none too good. If the two phenomena are directly connected, we should find days of greater pressure indicating lower minimum virtual height and *vice versa*. Such a variation, although to some extent seen in figure 6(b), is not always to be found. Figure 6(a), on the other hand, shows a very good correlation between the time of the minimum virtual height and the time of maximum pressure. The days on which the minimum virtual height occurs early, the maximum pressure also is seen to take place early. There is, however, no fixed time difference between the times of occurrence of the two phenomena. This and the rather poor relationship shown in figure 6(b) may be due to the fact that atmospheric oscillation is not the only process taking part in these changes but there are other processes also at work which we are ignoring. It may appear that the minimum virtual height may be due to reduction in the retardation suffered by the waves in the lower part of their path or to contraction due to cooling with the advance of night. We, however, think that if this is so, then instead of a minimum we should observe a continuous fall in the virtual height, for reduction in retardation and contraction due to cooling are expected to increase with the advance of night. It seems that perhaps the semidiurnal pressure variation and this minimum in virtual height are products of the same cause, possibly some sort of atmospheric oscillation. Further study of such correlations is expected to throw light on the vexed meteorological problem of semidiurnal pressure variation.

#### *(d) Complex Echoes and Formation of High Layers.*

Such echoes we have described and discussed in a number of previous communications.<sup>8</sup> We have ascribed them to partial reflection occurring at irregularly moving electron clouds and at other high layers different from the normal stratification. The occurrence of such reflections is, in general, associated with magnetic storms.<sup>9</sup> Kirby, Smith and Gilliland<sup>10</sup> report that during the first phase of an ionosphere storm, the regions extending from E-layer upwards get literally torn up into small irregularly moving electron clouds, the normal stratification being destroyed. They, however, think that this first turbulent phase of the storm is observable only in the auroral zone latitudes. Our observations of transient irregular echoes on the other hand clearly suggest the existence of a torn-up ionosphere and we think that such conditions prevail

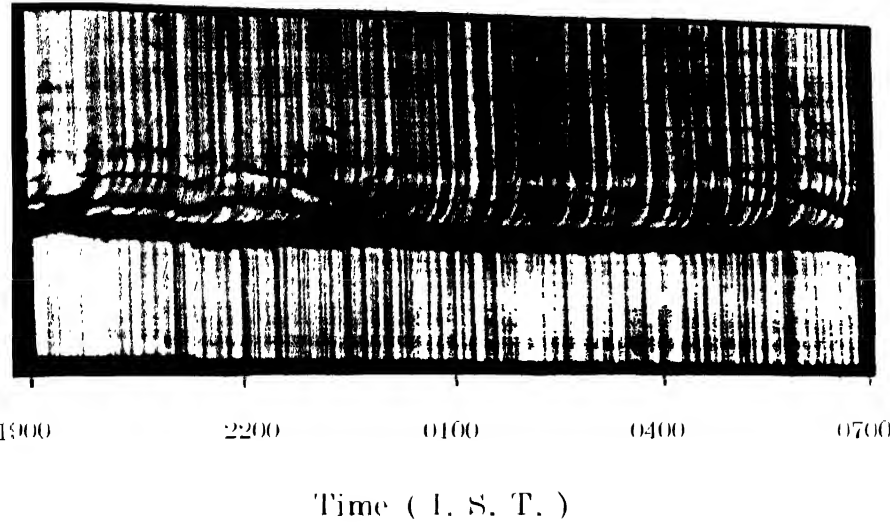
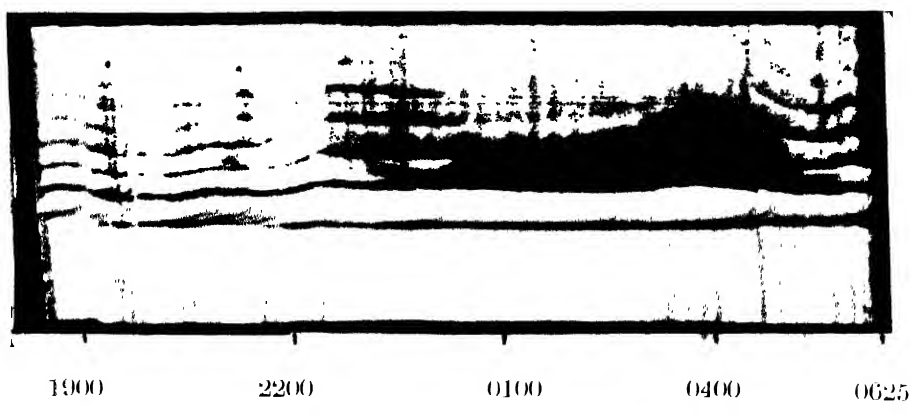
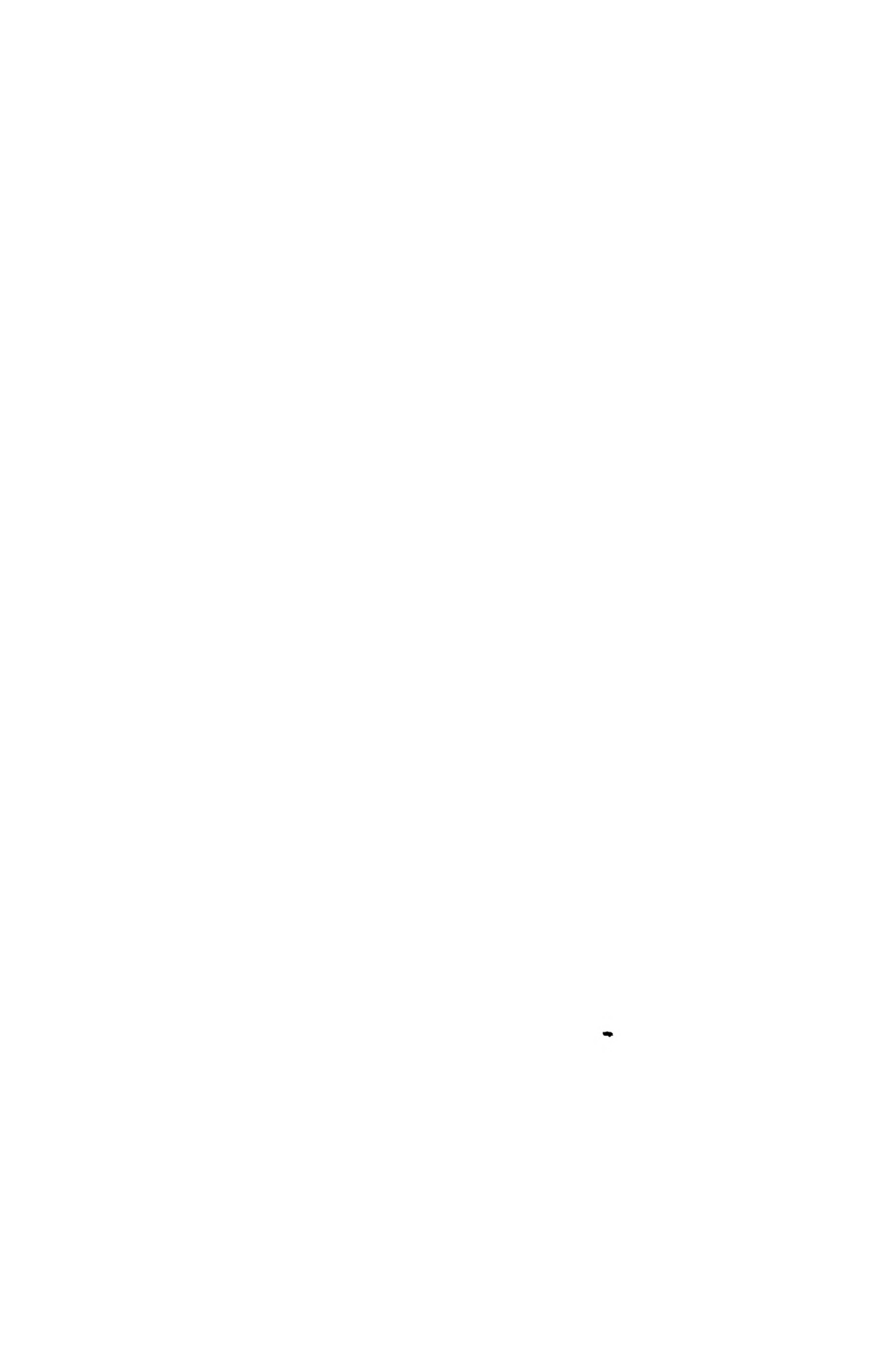


Fig. 7.



Time ( I. S. T. )

Fig. 8.



even at Allahabad. There is, however, a great difference in the intensity of the effect at the two latitudes. In the auroral zone the ionosphere gets disturbed and torn up down to the level of E-region and even lower when complete cessation of echoes occurs, but at Allahabad we notice such disturbance generally above the F-layer and the normal stratification of the ionosphere is not destroyed, for reflections from the normal F-region are received inspite of the irregular complex reflections. It is due to the fact that perhaps the ionizing and disturbing agency is unable to reach such low heights in lower latitudes.

Besides the irregular transient reflections taking place from ionization clouds, we also observe echoes from abnormal layers lasting for several hours. The virtual height from which such reflections take place changes even by 200 kms. during the course of a few hours. Figure 8 shows that at 2300 a reflection appeared from an equivalent height of about 650 kms. which at 2335 got reduced to only about 520 kms. Formation of such high layers and their movement has also been observed by Leiv Harang at Tromsø. Sometimes we have also observed that these abnormal layers instead of moving downwards move upwards with similar velocities. This upward movement we can ascribe to heating of the regions that generally takes place during the second phase of an ionosphere storm and which extends to latitudes far south of the auroral zone, but we have still to see as to what amount of increase in temperature will impart such high velocities to the upmoving layer. As for the downward movement of the layer, it is difficult to believe that the layer moves as a whole with such tremendous velocities as thought by some investigators. It seems that the ionizing agency moves lower down so that we are able to obtain reflections beginning from a greater height and ending at a lower one. Thus instead of the movement of the layer it appears to us that the ionizing agency travels down causing ionization in the lower heights.

In table I we have given the periods at night during which complex echoes were received along with the frequency at which observations were made. Table II gives a comparative statement of such echoes with reflections from E-layer and magnetic character of days as reported from the Colaba Observatory, Bombay. We observe that with the occurrence of complex echoes, the horizontal force may increase or decrease; the vertical force may remain quiet or it may be the only element of the earth's field to get disturbed. There are also occasions when all the three elements get simultaneously disturbed. Sometimes complexity occurs at the same time when the earth's field gets disturbed, while at other times the former takes place earlier. As it is now almost certain that the occurrence of complex echoes and disturbances in terrestrial magnetic field are due to irregularities in the upper ionized strata, and as our observations have shown that complex echoes are observed with different effects on the earth's magnetic field, it seems that every time when complex echoes are seen, the nature of the disturbance in the upper ionized regions is not the same.

TABLE I.

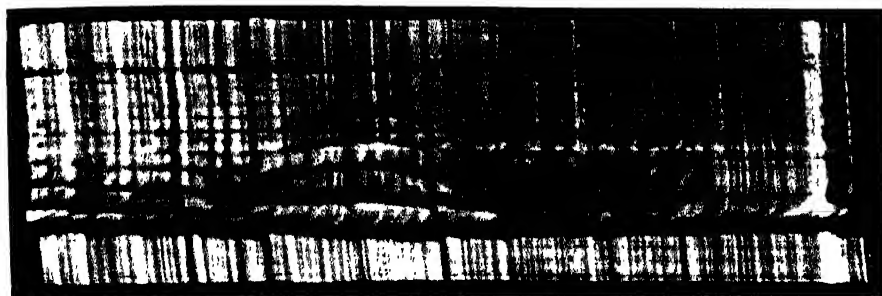
Date.	Frequency in Mc/sec. at which observations were made.	Time during which complex echoes appeared.
29-10-37	3'5	2330-2400
30-10-37	3'5	0000-0120
	3'5	1900-1940
18-1-38	2'8	0030-0520
	2'8	2030-2300
21-1-38	3'4	1930-2000
	3'4	2100-2400
27-1-38	3'5	0250-0320
9-2-38	6'0	0100-320
	6'0	0515-0650
13-2-38	5'4	2100-2400
14-2-38	5'4	0000-0050
15-2-38	5'4	2050-2400
18-2-38	7'8	2130-2350
19-2-38	5'4	2030-2400
20-2-38	5'4	0000-0155
	3'9	2020-2400
21-2-38	3'9	0000-0100
	3'9	2110-2400
22-2-38	3'9	0000-0100
23-2-38	5'5	1945-2030
	5'5	2148-2400
24-2-38	5'5	0000-0200
	5'5	0340-0430
	5'5	2230-2330
25-2-38	5'5	2235-2400
26-2-38	5'5	0000-0550
	3'5	2120-2400
27-2-38	3'5	0000-0145

TABLE II.

Date.	Ionospheric behaviour		Magnetic character as reported by the Colaba Observatory, Bombay.	REMARKS.
	Reflections from F-layer.	Complex echoes.		
29-10-37		C	Quiet	Complex echoes observed for about two hours.
1-12-37	I		Small	
10-12-37	I		Small	
10-1-38			Quiet	
12-1-38			Small	
13-1-38			Small	
15-1-38			Small	
17-1-38	E	C	Very great	At about 0245, the time of appearance of complex echoes, a sudden decrease in the vertical forces was noted and a similar increase in the horizontal force was also observed. The latter, however, remained disturbed throughout the night. The decrease in declination was observed at 0330.
18-1-38	E		Small	Reflections from E were present before disturbance in H. F. and V. F. was observed, but that in D took place afterwards.
20-1-38			Small	
21-1-38		C	Moderate	Sudden rise in H. F. during the existence of complex echoes.
22-1-38	E		Very great	Great disturbances in all the three elements lasting for several hours were noted in the magnetic elements; but when the peculiar disturbances in virtual height of the E-layer took place, the magnetic disturbances were over.
24-1-38			Small	Virtual height curve quite regular.
26-1-38	E		Moderate	Disturbance in H. F. and V. F. over several hours before the appearance of sporadic E-reflections in the early morning.
27-1-38	E		Small	

TABLE II (*contd.*).

Date.	Ionospheric behaviour.		Magnetic character as reported by the Colaba Observatory, Bombay.	REMARKS.
	Reflection from E layer.	Complex echoes.		
5-2-38	...	...	Quiet	Nothing unusual in virtual height curve.
6-2-38	...	...	Moderate	.. Increase in ionization of the E-region noted between 0015-0400, time coincides with disturbance in H. F.
7-2-38	...	...	Small	(P', t) curve quite regular.
8-2-38	...	C	Great	Strong complex echoes appeared in the last phase of the storm when H. F. began to increase after undergoing a decrease.
9-2-38	...	C	Small	Weak complexity. Time does not coincide with magnetic disturbance.
10-2-38	...	...	Small	(P', t) curve regular.
11-2-38	...	...	Small	(P', t) curve regular.
12-2-38	...	C	Small	Weak complexity. Time of beginning coincides with the time of disturbances in V. F., H. F. and D., but complexity continues for 2 hours afterwards.
13-2-38	...	C	Small	Weak complexity, but no time correlation.
15-2-38	...	C	Quiet	Sufficiently strong complexity observed.
17-2-38	...	...	Quiet	....
18-2-38	...	C	Quiet	Some small rise in H. F., a little before complexity appeared.
19-2-38	...	C	Quiet	Strong complex echoes observed. Examination of the magnetograms showed that H. F. was very quiet, but there were some disturbances in V. F.
20-2-38	...	C	Quiet	....
21-2-38	...	C	Quiet	....
22-2-38	...	C	Quiet	....
23-2-38	...	C	Small	Complex echoes appeared four times during the night; at the beginning of complexity small increase in H. F. noted.
24-2-38	...	C	Quiet	Complexity for less than an hour and just at that time a small rise in H. F. was noticed, otherwise the day was very quiet.
25-2-38	...	C	Small	Complexity found during the disturbed period as well as afterwards. It begins with deflections in H. F. and V. F.
26-2-38	E	C	Small	....



1900

2200

0100

0400

0700

Time ( I. S. T )

Fig. 9.



1900

2200

0100

0400

0700

Time ( I. S. T. )

Fig. 10.



## (e) Reflections from E-layer.

Table III gives the periods during which reflections from the E-layer were received with the frequency of the waves used in the experiments. The observations were generally carried out during night, hence the table gives such periods only during night-hours.

TABLE III.

Date.	Frequency in Mc/sec. at which observations were made.	Time during which reflections from the layer appeared.
30-10-37	3.5	1815-1830
...	3.5	2110-2230
9-11-37	8.0	2100-2145
1-12-37	2.9	1820-2400
2-12-37	2.9	0000-0020
10-12-37	2.9	1930-2000
12-1-38	2.9	1810-1920
13-1-38	2.8	1815-1910
17-1-38	2.8	1940-2040
18-1-38	2.8	0030-0245
...	2.8	0455-0630
22-1-38	3.5	2200-2330
23-1-38	3.5	0510-0620
26-1-38	3.5	1845-1930
27-1-38	3.5	0130-0240
28-1-38	3.5	0120-0230
21-2-38	3.9	1800-2000
26-2-38	3.5	1815-2310
...	3.5	0000-0620

(f) Existence of F<sub>1</sub>-region after Sun-set.

In a previous communication<sup>2</sup> we have reported that our ionization measurements showed us separate existence of F<sub>1</sub>-region till about 10 o'clock at night instead of till sun-set as reported by other investigators. The present investigations also gave us a similar evidence. Figure 9 obtained on January 27-28, 1938,

at a frequency of 3.5 Mc/sec. clearly shows that from the beginning of the record at 1850 three multiple reflections from a virtual height varying from 270 to 225 kms. were received, but at 2150 suddenly there appeared reflections from an equivalent height of about 360 kms. also simultaneous with previous reflections. For a period of about 20 minutes echoes from both the heights were seen but afterwards only the higher layer reflections remained. It seems that in the beginning the waves were reflected from the F<sub>1</sub>-region, then for about 20 minutes the x-wave was reflected from the F<sub>1</sub>-region while the o-wave was returned from the F<sub>2</sub>-region. Afterwards the reflections took place from the F<sub>2</sub>-region alone. Although this is not a conclusive proof that the two regions coalesced at the time of disappearance of reflections from the lower height, for it only means that the electron density in the region fell below that required to reflect the waves having a frequency of 3.5 Mc/sec., yet it points out that the F<sub>1</sub>-region existed at least till this hour.

#### *(g) Some Abnormalities.*

Sometimes, especially in the early morning hours, we have observed broad, diffuse and weak reflections coming from an equivalent height of 1000-1500 kms. On several occasions these reflections persisted for short periods even after echoes from the normal F-layer appeared.

We have also observed that during the early part of night, weak reflections persisted after the waves had penetrated the region. These would disappear if the frequency was raised by about 5 Mc/sec. and would not show penetration phenomena.

Several times we have seen that near the penetration frequency a single pulse instead of breaking up into only two components gets separated into three and even four components which disappear one by one as the frequency of the waves is raised.

#### *(h) Note on Figure 10.*

In a previous section we have mentioned Colwell's claim of predicting weather conditions from the knowledge of radio broadcast reception. Figure 10 taken on January 22-23, 1938, shows possibilities of similar predictions from direct ionospheric studies. We observe that unusual disturbances occurred in the virtual height of the F-region on this night and the abnormal E appeared twice. These disturbances were connected with a severe western disturbance and the weather on the following day was found to be extremely bad. The conditions of broadcast reception during this period were found to be very poor.

## ACKNOWLEDGMENTS.

We are indebted to Prof. M. N. Saha for his keen interest in these investigations and constant encouragement.

We are thankful to Dr. G. R. Toshniwal for his kindness in going through the paper and for suggestions about the presentation of the paper.

We express our sincere thanks to Dr. C. W. B. Normand, Director-General of Observatories, for supplying us with the pressure records taken at the Allahabad Meteorological Observatory ; to the Meteorologist-in-charge of the Colaba Observatory for regularly sending us reports on magnetic character of days and for lending us the required magnetograms ; and to Dr. N. K. Sur for supplying us information about the western disturbance referred to in § 2(i).

## REFERENCES.

- <sup>1</sup> Breit and Tuve, *Phys. Rev.*, **28**, 554 (1926).
- <sup>2</sup> Bajpai and Pant, *Ind. Jour. Phys.*, **12**, 211 (1938).
- <sup>3</sup> Appleton, *Proc. Phys. Soc.*, **42**, 321 (1930).
- <sup>4</sup> Ranzi, *Nature*, **130**, 545 (1932).
- <sup>5</sup> Colwell, *Proc. Inst. Rad. Eng.*, **21**, 721 (1933).
- <sup>6</sup> Martyn and Pulley, *Proc. Roy. Soc. A*, **184**, 455 (1936).
- <sup>7</sup> Best, Farmer and Ratcliffe, *Proc. Roy. Soc. A*, **184**, 96 (1938).
- <sup>8</sup> Toshniwal, Pant, Bajpai and Verma, *Proc. Nat. Acad. Sc. India*, **6**, 161 (1936) ; Toshniwal, Pant and Bajpai, *Proc. Nat. Inst. Sc. India*, **3**, 337 (1937) ; Pant and Bajpai, (in press).
- <sup>9</sup> Kirby, Smith and Gilliland, *Phys. Rev.*, **54**, 234 (1938).



# JUPITER'S ATMOSPHERE\*

By A. C. BANERJI

AND

NIZAMUDDIN

(Received for publication, Feb. 15, 1938)

**ABSTRACT.** In this paper the two models of Jupiter's atmosphere, *viz.*, adiabatic and isothermal, have been considered. The variability of the period of rotation of the atmosphere depending on the latitude and the variation of gravity have both been taken into account. The datum level of Jupiter is the effective radiating and absorbing layer--probably a cloud layer--at a certain height in the atmosphere. It has the observed temperature of  $150^{\circ}$  Absolute. The authors have investigated the relation between pressure and density at any depth below the datum level and at any height above the datum level, in each of the two cases, *viz.*, (1) when the atmosphere consists of methane only, and (2) when it consists of a mixture of one part of methane and six parts of hydrogen. Even taking the atmosphere to be in adiabatic condition below the datum level and in isothermal condition above the datum level the authors have found that the total thickness of the atmospheric layer cannot, in any case exceed 1900 kms., and possibly it is below 1300 kms.

Before 1923, it was widely believed that the four great planets were very hot and that a large fraction of their volume was occupied by gas. In 1923 and 1924 H. Jeffries<sup>1</sup> investigated the physical constitution of the outer planets and suggested that they were cold. This conclusion was subsequently corroborated by observation which indicated a surface temperature of  $150^{\circ}$  absolute, for Jupiter. In a subsequent paper he further suggested that the Jupiter was formed of a rocky core covered by a thick layer of ice and that there was an atmosphere of more than 6000 kilometres in depth surrounding this icy layer. In 1934, Wildt<sup>2</sup> showed that an extensive atmosphere surrounding the surface of Jupiter will involve great density which makes it highly improbable that such an atmosphere exists there. Wildt gave 600 kilometres as the maximum depth that may possibly be attained by isothermal hydrogen atmosphere obeying gas laws.

In 1937, M. Peek<sup>3</sup> investigated the physical state of Jupiter's atmosphere. He found even smaller values for the maximum depth for the atmosphere than was indicated by Wildt.

The datum level of Jupiter is not the planet's solid surface, but it is the

\* Communicated by the Indian Physical Society.

effective radiating and absorbing layer—probably a cloud layer—at a certain height in the atmosphere. The datum level does not rotate as a rigid body; on the other hand it is observed that the period of rotation depends upon the latitude. Peck has taken the observed temperature of  $150^{\circ}$  Absolute to be the temperature of the datum level. He has taken three models for Jupiter's atmosphere, viz., (1) the adiabatic, (2) the isothermal, and (3) a compromise in which an empirical relation is assumed between the depth and the lapse rate of temperature. In the first two cases for the purpose of numerical evaluation he has treated the atmosphere as though it was entirely composed of methane. In the third case not only he took methane in the unmixed state, but also in two mixed states with two different proportions of hydrogen. He investigated the relations between pressure, depth and density only at points below the datum level and not upwards in the atmosphere external to the datum level. He found that at a depth 25 kilometres below the datum level, atmosphere would probably become unrecognisable as such by the meteorologists.

In his investigation Peck has not considered the variability of the period of rotation of Jupiter's atmosphere. From observations of the spots near the pole the period is found to be about  $9^h 55^m$  while for the equatorial spots it is about  $9^h 50^m$ . It appears that there is a sort of relative motion or general circulation in Jupiter's atmosphere. No satisfactory reason can be given for this relative motion as the theory of general circulation of the atmosphere is still very imperfect.

We have assumed the following formula for angular velocity at any point in the planet's atmosphere :

$$\omega = \omega_0 \left[ 1 + a_2 \left( \frac{r}{R} \right)^2 \sin^2 \theta + a_4 \left( \frac{r}{R} \right)^4 \sin^4 \theta \right], \quad \dots \quad (1)$$

where  $r$  is the distance of the point from centre of Jupiter and  $\theta$  is the colatitude of the place. Here  $\omega_0$  is the angular velocity at points where  $\theta=0$  and  $R$  is the radius of the equatorial section of the datum level which is the stratum of the atmosphere that gives rise to the observed temperature  $150^{\circ}$  Absolute, and  $a_2$  and  $a_4$  are numerical constants. It may be mentioned here that spectroscopic observations<sup>1</sup> show that there is an equivalent atmosphere of one mile of methane and ten metres of ammonia at normal temperature and pressure above the visible photographic surface which we may take up as the datum level. The pressure at this level is calculated to be 0.335 atmosphere (earth's).

Some explanation seems to be necessary for the assumption of the above formula for the angular velocity. If the axis of  $z$  is the axis of rotation, we have the following equation for relative equilibrium :

$$\int \frac{dP}{\rho} = V + \int \omega^2 (xdx + ydy) = V + \frac{1}{2} \int \omega^2 d(x^2 + y^2), \quad (2)$$

where  $V$  is the potential of the extraneous forces. In order that this equation may be integrable we must have a functional relation between  $P$  and  $\rho$ , and between  $\omega$  and  $\sqrt{x^2 + y^2}$ , i.e.,  $r \sin \theta$ .

We have to choose positive powers of  $r \sin \theta$  in order that  $\omega$  may not become infinite when  $\theta=0$ . It will be seen later on that  $a_2$  is negative and numerically greater than  $a_4$ , consequently within the atmosphere whose depth is small compared to the planet's radius,  $\omega$  decreases as  $r$  increases along a radial line.

We have taken account of variation of gravity which was neglected by Peck. We have considered two models, (1) adiabatic, (2) isothermal. We have investigated the relation between pressure and density at any depth below the datum level and at any height above the datum level, in each of the two cases, viz., (1) when the atmosphere consists of methane only, and (2) when it consists of a mixture of hydrogen and methane. We have calculated the possible maximum depth of the atmosphere below the datum level and also its possible maximum height above the datum level. The density at the outer boundary of the atmosphere is taken to be the inter-stellar density,<sup>5</sup> viz.,  $10^{-26}$  c.g.s. units, and the density at the inner boundary of the atmosphere is taken to be the density of solid ammonia, viz., 0.82 c.g.s. units, to allow for maximum possible depths. Alternative calculations have also been made by taking the density at the inner boundary to be that of solid methane, i.e., 0.42 c.g.s. units in the first case and to be that of solid state of mixture, i.e., 0.27 c.g.s. units in the second case.

For the period of rotation in different regions we have taken the following data for the year 1928, from two papers<sup>6</sup> published by A. Stanley Williams in 1931, the data for later years being not available :—

Region (south Latitude).	Mean Latitude (south).	Rotational Period.
2°S to 16°S	8°S	9 <sup>h</sup> 50 <sup>m</sup> 19.2 <sup>s</sup>
27°S to 37°S	32°S	9 <sup>h</sup> 55 <sup>m</sup> 22.6 <sup>s</sup>
37°S to 55°S	46°S	9 <sup>h</sup> 55 <sup>m</sup> 9.8 <sup>s</sup>

From the three rotational periods we calculate three values for  $\omega$  which are assumed to hold at the mean latitudes of the three regions. These values are now substituted in formula (1). We thus get three equations which determine the values of  $a_2$ ,  $a_4$  and  $\omega_0$  :

$$a_2 = -0.06776 \text{ (numerical factor)} \quad (3)$$

$$a_4 = +0.05819 \text{ ( , , )}$$

$$\omega_0 = -\frac{2\pi}{35040} \text{ radians per sec.}$$

Our fundamental equations <sup>7</sup> of relative equilibrium are :—

$$\left. \begin{aligned} \frac{\partial P}{\partial r} &= \rho \cdot \frac{\partial V}{\partial r} + \rho \omega^2 s (1 - \mu^2) \\ \frac{\partial P}{\partial \mu} &= \rho \cdot \frac{\partial V}{\partial \mu} - \rho \omega^2 r^2 \mu \end{aligned} \right\} \quad \dots \quad (4)$$

Here  $r$  is the radial distance and  $\mu = \cos \theta$ , where  $\theta$  is the polar angle, and  $V$  is the gravitational potential due to Jupiter's mass, and  $\omega$  the angular velocity at any point of the atmosphere.

Taking Jupiter to be an oblate spheroid we find the expression for the gravitational potential <sup>8</sup> to be

$$V = \frac{GM}{r} \left[ 1 - \frac{3}{3} \cdot \frac{P_2}{5} \cdot \left( \frac{Re}{r} \right)^2 + \frac{3}{5} \cdot \frac{P_4}{7} \cdot \left( \frac{Re}{r} \right)^4 + \dots \dots \right]$$

where  $M$  is the mass of Jupiter,  $G$  the universal gravitation constant,  $R$  the semi-equatorial diameter,  $e$  the eccentricity of the Jupiter. Taking the semi-equatorial and semi-polar diameters of Jupiter <sup>9</sup> to be 71370 and 66620 kilometres respectively we find  $e^2$  to be .1287 and thus neglecting terms inside the bracket containing  $e^6$  (which is of the order .0001) and higher powers of  $e$ , we get

$$V = \frac{GM}{r} \left[ 1 - \frac{3}{3} \cdot \frac{P_2}{5} \cdot \left( \frac{Re}{r} \right)^2 + \frac{3}{5} \cdot \frac{P_4}{7} \cdot \left( \left( \frac{Re}{r} \right)^4 \right) \right] \quad \dots \quad (5)$$

We may remark here that as the extraneous forces are derived from a potential function, the equi-density surfaces are also equi-pressure and equi-temperature surfaces.

### I. ISOTHERMAL CASE

1. We shall now consider the isothermal model. In this case

$$P = \frac{\beta T}{\mu} \rho = K \rho \quad \text{where } K = \left( \frac{\beta T}{\mu} \right)$$

where  $\beta$  is the universal gas constant and its value is  $8.26 \times 10^7$  c.g.s. units.  $T$  is taken to be  $150^\circ$  Absolute which is the observed temperature for the datum level.

$$\text{Putting } P = K \rho \quad \text{and} \quad \omega = \omega_0 \left[ 1 + a_2 \left( \frac{r}{R} \right)^2 (1 - \mu^2) + a_4 \left( \frac{r}{R} \right)^4 (1 - \mu^2)^2 \right]$$

in our equations of relative equilibrium (4), we get

$$\frac{k}{\rho} \frac{\partial \rho}{\partial r} = \frac{\partial V}{\partial r} + \omega_0^2 r (1 - \mu^2) \left[ 1 + a_2 \left( \frac{r}{R} \right)^2 (1 - \mu^2) + a_4 \left( \frac{r}{R} \right)^4 (1 - \mu^2)^2 \right]^2$$

$$\frac{k}{\rho} \frac{\partial \rho}{\partial \mu} = \frac{\partial V}{\partial \mu} - \omega_0^2 r^2 \mu \left[ 1 + a_2 \cdot \left( \frac{r}{R} \right)^2 (1 - \mu^2) + a_4 \left( \frac{r}{R} \right)^4 (1 - \mu^2)^2 \right]^2$$

Multiplying the first of these equations by  $\delta r$  and the second by  $\delta \mu$  and then adding and integrating, we get

$$k \log \rho = V + \omega_0^2 r^2 \left[ \frac{1 - \mu^2}{2} + \frac{a_2^2}{2} (1 - \mu^2)^2 \left( \frac{r}{R} \right)^2 + \frac{a_2^2}{6} (1 - \mu^2)^3 \left( \frac{r}{R} \right)^4 + \frac{a_4 (1 - \mu^2)^3}{3} \left( \frac{r}{R} \right)^4 + \frac{a_2 a_4 (1 - \mu^2)^4}{4} \left( \frac{r}{R} \right)^6 + \frac{a_4^2}{10} (1 - \mu^2)^5 \left( \frac{r}{R} \right)^8 \right] + \text{constant} \dots \quad (7)$$

is the complete solution of the equations of relative equilibrium. The arbitrary constant can be eliminated by substituting the given conditions. In each case we shall only consider the variation of density along a definite radial line. Hence in evaluating the arbitrary constant we shall not change the value of  $\theta$ .

If  $\rho = \rho_0$  when  $r = r_0$ , we get from (5) and (7)

$$k \log \left( \frac{\rho}{\rho_0} \right) = GM \left[ \left\{ \frac{1}{r} - \frac{1}{r_0} \right\} - \frac{P_2}{5} \cdot (R^2 c^2) \left\{ \frac{1}{r^3} - \frac{1}{r_0^3} \right\} + \frac{3}{5} \frac{P_4}{7} \cdot (Re)^4 \times \left\{ \frac{1}{r^5} - \frac{1}{r_0^5} \right\} + \omega_0^2 \left[ \frac{(1 - \mu^2)}{2} \left\{ 2 - \frac{2}{r_0^2} \right\} + \frac{a_2}{2} \cdot \frac{(1 - \mu^2)^2}{R^2} \left\{ 4 - \frac{6}{r_0^4} \right\} + \frac{a_2^2}{6} \cdot \frac{(1 - \mu^2)^3}{R^4} \left\{ 6 - \frac{6}{r_0^6} \right\} + \frac{a_4}{3} \cdot \frac{(1 - \mu^2)^3}{R^4} \left\{ 6 - \frac{6}{r_0^6} \right\} + \frac{a_2 a_4}{4} \cdot \frac{(1 - \mu^2)^4}{R^6} \left\{ 8 - \frac{8}{r_0^8} \right\} + \frac{a_4^2}{10} \cdot \frac{(1 - \mu^2)^5}{R^8} \left\{ 10 - \frac{10}{r_0^{10}} \right\} \right] \dots \quad (8)$$

We shall take  $\rho_0$  to be the density at the datum level which is assumed to be an equi-density surface for which the observed temperature is  $150^\circ$  Absolute and pressure is  $0.335$  atmosphere (Earth's).<sup>10</sup>

(A) We shall first take the atmosphere to consist of methane only—in this case  $\mu = 16$  being the molecular weight for methane.

1. *Equatorial Plane.*—Let us first calculate here the density in the equatorial plane. In the equatorial plane  $\theta = \frac{\pi}{2}$ , and we shall take  $r_0 = R$  (equatorial radius of Jupiter's surface) for datum level in this plane, for the sake of convenience in our calculations, since the error involved is of the order we are neglecting. We assume that the total height of Jupiter's atmosphere is small compared to its radius. For a point in the equatorial plane within the atmosphere at a radial distance  $\delta R$  from the datum level we take  $r = R + \delta R$ .

Neglecting  $\left(\frac{\delta R}{R}\right)^2$  and higher powers of  $\left(\frac{\delta R}{R}\right)$  we get after simplification, for the value of  $\rho$  at  $r=R+\delta R$  in the equatorial plane from (5) and (7)

$$\log \left(\frac{\rho}{\rho_0}\right) = -\frac{GM}{KR} \left(\frac{\delta R}{R}\right) \left[ 1 + \frac{3e^2}{10} + \frac{9e^4}{56} \right] + \frac{\omega_0^2 R^2}{K} \left(\frac{\delta R}{R}\right) \left[ 1 + a_2 + a_4 \right]^2 \quad (9)$$

We take  $P_0$  to be the pressure at the datum level and its value is  $0.335$  atmosphere (Earth's), as given by Peck. Now from the relation  $P_0 = K\rho_0$ , where  $K = 7.75 \times 10^8$  c.g.s. units (in this case  $\mu = 16$ ) and 1 atmosphere <sup>11</sup> is equal to  $1013600$  dynes, and we find  $\rho_0 = 000438$  c.g.s. units.

We take the mass of Jupiter to be  $\frac{1}{1047.4}$  of Sun's mass as given by Russell.<sup>12</sup> Now Sun's mass is  $1.985 \times 10^{33}$  grammes as given by Eddington.<sup>13</sup> Thus Jupiter's mass is found to be  $1.896 \times 10^{30}$  grammes.

Here  $G$  is the universal gravitation constant and is equal to  $8.66 \times 10^{-8}$  c.g.s. units. Now for calculating the height of the outer boundary of the atmosphere we put  $\rho = 10^{-26}$  c.g.s. units, which is known to be the inter-stellar density. Then our equation becomes, on substituting the numerical values,

$$-22.6415 = -\frac{\delta R \times (-3.0403)}{10^6} \text{ (c.g.s. units)}$$

which gives the value of  $\delta R = 74.47 \times 10^5$  cms. =  $74.47$  kilometres.

Now for finding the depth of the atmosphere below the datum level, we take  $\rho$  to be the density of solid ammonia which is  $0.82$  (c.g.s units) in order to allow for the maximum possible depth. Then substituting the numerical values as before we get

$$3.2723 = -\frac{3.0403}{10^6} \times \delta R$$

which gives

$$\delta R = -10.76 \times 10^5 \text{ cms.}$$

The negative sign stands for the depth which comes out to be  $10.76$  kilometres.

Next taking  $\rho$  to be the density of solid methane, i.e.,  $0.42$  c.g.s units, we get  $9.81$  kilometres as the depth.

(ii) *Colatitude*  $\theta = 30^\circ$ .

We shall now calculate the density at any point in the radial line for which  $\theta = 30^\circ$ . As before we shall calculate the radial height of the atmosphere above the datum level, for which  $\rho = \rho_0$ , and also the depth of the atmosphere below this point along the radius. Here also for the sake of convenience in our calculations

we put  $r_0 = r_1$ , for the datum level, where  $r_1$  is the radial distance from the centre of Jupiter of the point on its surface for which  $\theta = 30^\circ$ , the error being of the order we are neglecting. For a point in the radial line  $\theta = 30^\circ$  within the atmosphere at a distance  $\delta r_1$  from the datum level we take  $r = r_1 + \delta r_1$ .

Putting  $r = r_1 + \delta r_1$  and  $\theta = 30^\circ$  in formula (7) and neglecting  $\left(\frac{\delta r_1}{r_1}\right)^2$

and higher powers of  $\left(\frac{\delta r_1}{r_1}\right)$ , we get

$$\log \left( \frac{\rho_0}{\rho} \right) = \frac{GM}{Kr_1} \times \left( -\frac{\delta r_1}{r_1} \right) \left[ 1 - \frac{P_2}{5} \cdot \left( \frac{R}{r_1} \right)^2 \cdot 3e^2 + \frac{3}{5} \cdot \frac{P_4}{7} \cdot \left( \frac{R}{r_1} \right)^4 \cdot 5e^4 \right] \\ + \frac{a_0^2 r_1^2 (1 - \mu^2)}{K} \times \left( \frac{\delta r_1}{r_1} \right) \left[ 1 + a_2 \cdot \left( \frac{r_1}{R} \right)^2 (1 - \mu^2) + a_4 \cdot \left( \frac{r_1}{R} \right)^4 (1 - \mu^2)^2 \right]^2 \dots \quad (10)$$

The values of  $i$ ,  $P_2$  and  $P_4$  are found to be

$$\left. \begin{aligned} r_1 &= 6.772 \times 10^9 \text{ cms.} \\ P_2 &= .625 \\ P_4 &= .0225 \end{aligned} \right\} \dots \quad (11)$$

Substituting the numerical values from (3) and (11) and putting  $\rho = 10^{-20}$  (c.g.s units) for the outer boundary of the atmosphere, we have

$$-22.6415 = -\frac{3.2678 \times \delta r_1}{10^6} \text{ (c.g.s. units)}$$

$$\therefore \delta r_1 = \frac{22.6415 \times 10^6}{3.2678} = 6.928 \times 10^6 \text{ cms.} \\ = 69.28 \text{ kms.}$$

i.e., the height comes out to be 69.28 kms. Similarly putting  $\rho = 0.82$  for the inner boundary we get, for the depth of the atmosphere,

$$3.2723 = -\frac{3.2678 \times \delta r_1}{10^6} \text{ (c.g.s. units)}$$

$$\therefore \delta r_1 = \frac{10^6 \times 3.2723}{-3.2678} = -1.001 \times 10^6 \text{ cms.} \\ = -10.01 \text{ kms.}$$

Therefore the depth is 10.01 kilometres.

Again taking  $\rho = 0.42$ , density of solid methane we get the equation

$$2.9817 = \frac{-3.2678 \times \delta r_1}{10^6}$$

or  $\delta r_1 = -9.12 \times 10^5 \text{ cms.} = -9.12 \text{ kms.}$

i.e., the depth is 9.12 kms.

(B) Next let us suppose the atmosphere to consist of a mixture of 1 part of methane and 6 parts of hydrogen.

In this case the value of  $\mu$  becomes 4 instead of 16. We substitute the new value of  $\mu$  in our equations and proceed as before.

(i) *Equatorial Plane*.—In the equatorial plane, the height of the atmosphere above the datum level is found to be 297.88 kms. The depth below the datum level is found to be 43.04 kilometres, if the density of inner boundary is taken to be 0.82, i.e., the density of solid ammonia.

Next if we take the density of the inner boundary to be the density of solid state of mixture, i.e., 0.27, we find the depth to be 36.71 kilometres.

(ii) *Colatitude  $\theta = 30^\circ$* .—Considering the extent of atmosphere in the radial line  $\theta = 30^\circ$ , and proceeding as before, we find that the height of the atmosphere above the datum level is 277.12 kilometres and the depth below the datum level is 40.04 kms., if we take the density of the inner boundary to be the density of solid ammonia.

Again if we take the density of the inner boundary to be the density of solid state of the mixture, i.e., 0.27, then we find the depth to be 34.15 kilometres.

## II. ADIABATIC MODEL

(C) In considering the adiabatic model also, we shall first assume that the atmosphere consists of methane alone. The relation between pressure and density in this case is

$$P = K_2 \rho^\gamma \quad \text{where } K_2 = \left( \frac{\beta T}{\mu} \right)^\gamma P^{1-\gamma};$$

here  $\gamma$  denotes the ratio of specific heats. We shall put  $\gamma = 1 + \frac{1}{\lambda}$ . For methane  $\mu = 16$  and now taking as before the value for the pressure  $P_0$  at the datum level in the equatorial plane, to be 335 atmosphere (Earth's) and  $T = 150^\circ$  Absolute, and substituting numerical values in (12), we find that  $K_2 = 7.884 \times 10^9$  c.g.s. units.

Now putting  $P = K_2 \rho^{\frac{1}{\lambda} + \frac{1}{\lambda}}$  in the fundamental equations (4) and integrating as before, we get

$$\begin{aligned} K_2(\lambda+1)\rho^{\frac{1}{\lambda}} &= \frac{GM}{r} \left[ 1 - \frac{3}{3} \cdot \frac{P_2}{5} \cdot \left( \frac{Rc}{r} \right)^2 + \frac{3}{5} \cdot \frac{P_4}{7} \cdot \left( \frac{Rc}{r} \right)^4 \right] + \omega_0^2 r^2 \\ &\quad \left[ \frac{(1-\mu^2)}{2} + \frac{a_2}{2} \cdot \left( \frac{r}{R} \right)^2 (1-\mu^2)^2 + \frac{a_4}{3} \cdot \left( \frac{r}{R} \right)^4 (1-\mu^2)^3 + \frac{a_2^2}{6} \cdot \left( \frac{r}{R} \right)^4 (1-\mu^2)^3 \right. \\ &\quad \left. + \frac{a_2 a_4}{4} \cdot \left( \frac{r}{R} \right)^6 (1-\mu^2)^4 + \frac{a_4^2}{10} \cdot \left( \frac{r}{R} \right)^8 (1-\mu^2)^5 \right] + \text{constant} \quad \dots \quad (13) \end{aligned}$$

As before the constant can be evaluated for a definite radial line from the given conditions. In this case the right hand side of equation (8) remains the

same and for the left-hand side we shall have  $k_2 (1+\lambda) \left( \rho^{\frac{1}{\lambda}} - \rho_0^{\frac{1}{\lambda}} \right)$  instead of  $k \log \left( \frac{\rho}{\rho_0} \right)$ .

(i) *Equatorial Plane.*—We shall first find the extent of the atmosphere in the equatorial plane. Putting

$$\rho = \rho_0, \quad r_0 = R, \quad \theta = \frac{\pi}{2} \quad \text{and} \quad r = R + \delta R$$

and proceeding exactly as in the isothermal case, we get

$$K_2 \left( 1 + \lambda \right) \left( \rho^{\frac{1}{\lambda}} - \rho_0^{\frac{1}{\lambda}} \right) = -23.56 \times 10^2 \times \delta R.$$

On substituting the values of  $K_2$  and  $\lambda$ , we get

$$\left( \rho^{\frac{1}{\lambda}} - \rho_0^{\frac{1}{\lambda}} \right) = -\frac{\delta R}{10^6} \times 0.6896.$$

For finding the height of the outer boundary, we put  $\rho = 10^{-26}$  (c.g.s. units),

so that  $\left( \rho^{\frac{1}{\lambda}} - \rho_0^{\frac{1}{\lambda}} \right) = 0.9828$  (c.g.s. units), and the height is given by

$$\delta R = \frac{0.9828 \times 10^6}{0.6896} = 14.25 \times 10^5 \text{ cms} = 14.25 \text{ kms.}$$

of the atmosphere below the datum level, we first put  $\rho = 0.82$ , which gives

$$\left( \frac{1}{\rho^\lambda} - \frac{1}{\rho_0^\lambda} \right) = .8438 \text{ so that the depth } -\delta R = \frac{.8438 \times 10^6}{.06896} = 122.4 \times 10^5 \text{ cms.} \\ = 122.4 \text{ kms.}$$

Next taking  $\rho$  to be density of solid methane  $0.42$  we find that

$$\left( \frac{1}{\rho^\lambda} - \frac{1}{\rho_0^\lambda} \right) = .6726 \text{ (c.g.s. units) so that the depth } (-\delta R) \text{ comes out to be} \\ 97.54 \text{ kms.}$$

(ii) Colatitude  $\theta = 30^\circ$ .—Next let us find the extent of atmosphere in colatitude  $\theta = 30^\circ$ . Proceeding exactly as in the isothermal case and substituting

the values of  $K_2$  and  $\lambda$  we get  $\left( \frac{1}{\rho^\lambda} - \frac{1}{\rho_0^\lambda} \right) = -\frac{\delta r_1 \times .07413}{10^6}$  where  $\delta r_1$  has the same meaning as before.

Putting  $\rho = 10^{-2.6}$  c.g.s. units, for the height of the outer boundary, we get  
 $\delta r_1 = \frac{10^6 \times .09828}{.07413} = 13.26 \times 10^5 \text{ cms.} = 13.26 \text{ kms.}$

Similarly putting  $\rho = 0.82$  for the density of the inner boundary, we get, for the depth below the datum level.

$$-\delta r_1 = \frac{10^6 \times .8438}{.07413} = 113.9 \times 10^5 \text{ cms.} = 113.9 \text{ kms.}$$

Again putting  $\rho = 0.42$  for the density of the inner boundary we find the depth below the datum level to be  $90.74$  kms.

(D) Next let us consider the case of the atmosphere consisting of a mixture of 1 part of methane and 6 parts of hydrogen. In this case the value of  $\mu = 4$  and  $1 + \frac{1}{\lambda} = 1.4$ . Consequently  $\lambda = \frac{5}{2}$ .

With these new values for  $\mu$  and  $\lambda$  we find that value of  $K_2$  in this case is  $1.191 \times 10^{11}$  (c.g.s. units).

(i) Equatorial Plane.—Our equation giving the density in the equatorial plane remains the same in form as in C (i) except that the values of  $K_2$  and  $\lambda$  will be changed, and we get

$$K_2 (1 + \lambda) \left( \frac{1}{\rho^\lambda} - \frac{1}{\rho_0^\lambda} \right) = -23.56 \times 10^2 \times \delta R$$

Substituting the numerical values of  $K_2$  and  $\lambda$  and putting  $\rho=10^{-26}$  c.g.s. units, we get, for the height of the atmosphere above the datum level,

$$\delta R = \frac{.04535 \times 10^8}{.5657} = 8.09 \times 10^6 \text{ cms.} = 80.9 \text{ kms.}$$

Similarly for the depth below the datum level, we get

$$-\delta R = \frac{.8784 \times 10^8}{.5657} = 15.53 \times 10^7 \text{ cms.} = 15.53 \text{ kms.}$$

by taking  $\rho=0.82$  (c.g.s. units) at the inner boundary.

Next putting the density at the inner boundary to be  $0.27$  (c.g.s. units), i.e., the density of solid state of the mixture, we get  $-\delta R = \frac{.5471 \times 10^8}{.5657} = 967.4$  kms. as the depth below the datum level.

(ii) Colatitude  $\theta=30^\circ$ .—Similarly we can find the density at any point in the radial line  $\theta=30^\circ$ , by proceeding exactly in the same way as in the isothermal case. We get

$$K_2(1+\lambda) \left( \frac{1}{\rho^\lambda} - \frac{1}{\rho_0^\lambda} \right) = -25.33 \times 10^2 \times \delta R ;$$

$$\text{substituting for } K_2 \text{ and } \lambda, \text{ we get } \left( \frac{1}{\rho^\lambda} - \frac{1}{\rho_0^\lambda} \right) = -\frac{.608 \times \delta R}{10^8} .$$

Putting  $\rho=10^{-26}$  (c.g.s. units), we get for the height of the atmosphere above the datum level,  $\delta R = \frac{.04535 \times 10^8}{.608} = 74.59 \times 10^5 \text{ cms.} = 74.59 \text{ kms.}$

Similarly putting  $\rho=0.82$  (c.g.s. units) for the density of the inner boundary, we get  $-\delta R = \frac{.8784 \times 10^8}{.608} = 14.45 \times 10^7 \text{ cms.} = 1445 \text{ kms.}$  as the depth below the datum level.

Again putting  $\rho=0.27$  (c.g.s. units) for the density of the inner boundary we

get  $-\delta R = \frac{10^8 \times .5471}{.608} = 899.7 \text{ kms.}$  as the depth below the datum level.

We now give below our results in a tabular form.

TABLE I

## Atmosphere of Methane alone

	Isothermal		Adiabatic	
	Equatorial plane,	Colatitude $\theta = 30^\circ$	Equatorial plane,	Colatitude $\theta = 30^\circ$
Height in kms. above the datum level	74'47	69'28	14'25	13'26
Depth in kms. below the datum level, taking the density at the inner boundary to be that of solid methane.	9'81	9'72	97'54	96'74
Depth in kms. below the datum level, taking the density at the inner boundary to be that of solid ammonia.*	10'76	10'01	122'4	113'9

TABLE II

## Atmosphere consisting of a mixture of 1 part of Methane and 6 parts of Hydrogen

	Isothermal		Adiabatic	
	Equatorial plane,	Colatitude $\theta = 30^\circ$	Equatorial plane,	Colatitude $\theta = 30^\circ$
Height in kms. above the datum level	297'88	277'12	80'19	74'59
Depth in kms. below the datum level, taking the density at the inner boundary to be that of solid state of mixture.	36'71	34'15	967'4	869'7
Depth in kms. below the datum level, taking the density at the inner boundary to be that of solid ammonia.*	43'04	40'01	1553	1445

Assuming the atmosphere to consist of a mixture of 1 part of methane and 6 parts of hydrogen, the probable thickness of the atmosphere in the equatorial plane appears to be about 334 kms. under isothermal condition and 1050 kms.

\* To allow for maximum possible depths we have also calculated them by assuming the density at the inner boundary of the atmosphere to be that of solid ammonia, although only traces of ammonia are revealed by the spectroscope.

under adiabatic condition. The datum level in Jupiter's atmosphere probably consists of a cloud layer as mentioned before ; so from analogy of terrestrial conditions, it will not perhaps be unreasonable to assume that from the inner boundary (solid surface of Jupiter) of the atmosphere to the datum level, the atmosphere is adiabatic and from the datum level to the outer boundary of the atmosphere the atmosphere is isothermal. With this assumption the total thickness of Jupiter's atmosphere will be about 1200 kilometres. This is quite a plausible figure. We cannot extend our terrestrial analogy too far and we have no evidence to show that there is any region in Jupiter's atmosphere in which temperature steadily increases with height due to ionization.

UNIVERSITY OF ALLAHABAD,  
ALLAHABAD, INDIA.

#### R E F E R E N C E S.

- <sup>1</sup> M. N., **83**, 350, 1931, and **84**, 531 (1931).
- <sup>2</sup> *Offenluchungen der Universitäts-Sternwarte zu Göttingen*, No. 10, 1334.
- <sup>3</sup> M. N., **97**, 574 (1937).
- <sup>4</sup> *Nature*, **135**, 719 (1935).
- <sup>5</sup> *Dominion Astrophysical Observatory*, Vol. V, No. 3, p. 174.
- <sup>6</sup> M. N., **94**, 240 (1934), and **94**, 672 (1934).
- <sup>7</sup> M. N., **93**, 391 (1933).
- <sup>8</sup> *Analytical Statistics* by Routh, Vol. II, 153, 1908.
- <sup>9</sup> *Spherical Astronomy* by W. M. Smart, 405, 1931.
- <sup>10</sup> M. N., **97**, 176 (1937).
- <sup>11</sup> *Thermodynamics* by Birtwistle, 91, 1931.
- <sup>12</sup> *Astronomy* by Russel, Dugan and Stewart, 362, 1926.
- <sup>13</sup> *The Internal Constitution of Stars* by Eddington, 395, 1926.



# A NOTE ON THE TRANSMUTATION FUNCTION FOR DEUTERONS\*

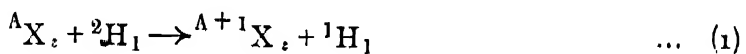
By P. L. KAPUR

Physics Department, University of the Punjab, Lahore

(Received for publication, Feb. 28, 1939.)

**ABSTRACT.** It is shown that there is a limit to the validity of the picture of 'partial entry' of deuterons in the Coulomb potential barrier of bombarded nuclei in nuclear reactions in which the neutron of the deuteron is captured and that this limit comes out very beautifully from the theory published by the author in a previous paper. A graph showing the relation of the total energy of the out-going proton to the energy of the incident deuteron for different values of the potential barrier is also plotted.

In a previous paper<sup>1</sup> the author (1937) calculated the probability of the deuteron through the potential barrier of the bombarded nucleus, when reactions of the type



are involved, on the picture proposed by Oppenheimer and Phillips (1935) which takes into account the large size and the small binding energy of the deuteron. The underlying physical idea is that for reactions such as (1) it is not essential for the deuteron to penetrate as a whole into the bombarded nucleus giving rise to, on Bohr's picture (1936), an intermediate system  ${}^{A+2}Y_{+1}$  which disintegrates into  ${}^{A+1}X$ , with the emission of a proton. All that is essential for such reactions is that there must be an appreciable probability of the neutron in the deuteron coming within the range of interaction of the bombarded nucleus, and this can happen, on account of the large size of the deuteron, even when the deuteron centre of mass is beyond the range of specifically nuclear forces. Once there, the neutron undergoes a reaction with the nucleus resulting in its absorption. On this picture, which may be called that of 'partial entry' in contradistinction to that of 'complete entry' in which the bombarding particle penetrates as a whole before giving rise to the nuclear reaction, the intermediate state is the final state in so far as the number of constituent particles in the final nucleus is concerned.

\* Communicated by the Indian Physical Society.

<sup>1</sup> This paper will be referred to as K1 in the text.

If the deuteron were a rigid system of charge equal to the protonic charge and mass equal to that of the proton or the neutron (the difference between the proton and neutron mass is neglected) its classical distance of nearest approach would be given by  $E = Ze^2/X_2$  where  $E$  is its kinetic energy,  $Z$  the atomic number of the bombarded nucleus, and  $X_2$  the distance of the proton for the nucleus. But now on account of its small binding energy and the fact that the neutron is not influenced by the coulomb repulsion the deuteron centre of the mass penetrates a little farther, that is to say, the proton is *dragged* into the coulomb potential 'mountain' of the nucleus along a 'valley' created by the presence of the neutron. The critical value of the incident energy for which the proton of the deuteron is dragged along up to the surface of the nucleus is obviously given by

$$E_c = \frac{Ze^2}{R} - I \quad \dots \quad (2)$$

where  $I$  is the binding energy of the deuteron and  $R$  the radius of the nucleus. For energies less than  $E_c$  the proton does not come within the range of interaction of the nuclear forces, so that the intermediate state is the final state. But for energies greater than  $E_c$  the proton also comes under the influence of nuclear forces and we get an intermediate nucleus  $^{A+2}Y_{z+1}$  which disintegrates into a proton and a residual nucleus  $^{A+1}Y_z$ . In other words, for energies greater than  $E_c$  we pass from the picture of 'partial entry' to that of 'complete entry.' This limit for the validity of the picture of 'partial entry' for the case of deuteron is not at once evident in  $K_1$ ; it shall be shown, nevertheless, that the above physical condition is incorporated in the method employed therein.

Keeping the same notation as employed in  $K_1$  the path of the deuteron in the  $x, y$  plane ( $x$  and  $y$  denote respectively the distances of the proton and the neutron from the nucleus) is given by  $x = y = 0$  up to a point  $x = y = X_1$  and then by equation (14) of  $K_1$  till the neutron reaches the nucleus and the proton is at a distance  $X_0$ ; that is to say, that up to the point  $x = y = X_1$  the deuteron is still a deuteron, but having reached this point it no longer moves as a deuteron. The distances  $X_0$  and  $X_1$  are determined by

$$\frac{Ze^2}{IX_0} = \beta^2 + \rho - 1 \quad \dots \quad (3)$$

and

$$(Ze^2/IX_1 - \rho)^{\frac{1}{2}} = \beta - 1 \quad \dots \quad (4)$$

where  $\rho = E/I$  and  $\beta$  is determined from the equation

$$\frac{z-\beta}{(\beta^2+2\rho-z)^{\frac{1}{2}}} = \tan \left[ \frac{(\beta^2+2\rho-z)^{\frac{1}{2}}(\beta^2-\beta+\rho-1)}{\beta(\beta^2-2\beta+\rho+1)} - \gamma \frac{(\beta^2+2\rho-z)^{\frac{3}{2}}}{\beta} \right] \dots (5)$$

with  $\gamma = \frac{IR}{Ze^2}$ ;  $R$  being the radius of the nucleus. As can be easily seen from (5) the upper limit to the value which  $\beta$  can have is  $\beta=2$ . From (3) and (4) one easily obtains

$$\frac{Zc^2}{IX_1} - \frac{Zc^2}{IX_0} = \frac{1}{2}(\beta-2)^2 \dots (9)$$

which is a positive definite form.

Hence  $X_1 \leq X_0$ . The equality sign holds only when  $\beta=2$ ; so that one can regard  $X_1$  as the 'break-up' distance for the deuteron of energy  $E$ , because up to this distance it moves as a deuteron and it is only after reaching this point that it begins to break up, the neutron moving towards the nucleus and finally reaching it, while the proton moves away on account of the coulomb repulsion and is at a distance  $X_0$  when the neutron reaches the nucleus.

Now obviously as the proton is dragged in to a distance  $X_1$  due to the binding energy  $I$  of the deuteron, we have

$$\frac{Zc^2}{X_1} - \frac{Zc^2}{X_2} \leq 1 \dots (7)$$

where  $X_2$  is the classical distance of approach. The equality sign gives us the upper limit to the drag. Taking the equality sign in (7) we obtain with the help of (4)

$$\beta = 0 \text{ or } 2,$$

so that the maximum value that  $\beta$  can have is 2: and we have already pointed out that equation (5) which is used to determine  $\beta$  for a given  $\rho$  has no solution for  $\beta \geq 2$ . When  $\beta = 2$ , (4) yields

$$\frac{Zc^2}{X_1} = I + E_r$$

which is the same as (2). In other words, this upper limit to the value of  $\beta$  as determined from equation (5) just corresponds to the limit of the validity of the picture of 'partial entry' for the case of deuterons.

Further as  $X_1$  represents the break-up distance and so the turning point for the proton of the deuteron, (6) gives us the kinetic energy of the proton in terms of the binding energy of the deuteron when the neutron reaches the nucleus,

i.e., in terms of the energy with which the proton is ejected out. For  $\beta=2$ , the proton is ejected with just zero kinetic energy. The total energy of the leaving proton depends through  $\beta$  upon the incident energy and the relation between the two is shown in the accompanying graph. The total energy of the ejected proton is given by (4) and is seen to be greater than  $E = Zc^2/X_2$ , this extra energy being derived from the binding energy of the deuteron.

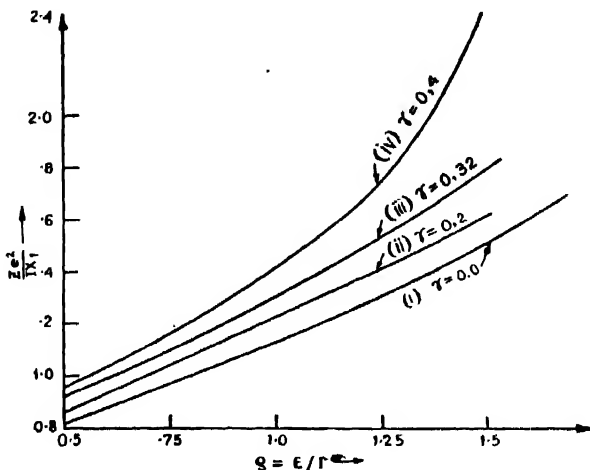


FIGURE I

Curves showing the relation between the energy of the incident deuteron and that of the outgoing proton in reactions of type (1) for different values of  $\gamma = \frac{IR}{Ze^2}$ . The curves (i), (ii), (iii) and (iv) are for  $\gamma = 0.0$ ,  $0.2$ ,  $0.32$ , and  $0.4$  respectively. All energies are measured in terms of the binding energy of the deuteron.

R INSTITUTE OF SCIENCE

Bohr, N., Nature, **137**, 344 (1936).Kapur, P. L., Proc. Roy. Soc. A., **163**, 553-568 (1937).Oppenheimer, J. R., and Phillips, M., Phys. Rev., **48**, 500-502 (1935).

# A STUDY OF SULPHUR ALLOTROPES BY THE X-RAY DIFFRACTION METHOD (PART II)\*

*White Sulphur, Black Sulphur and Colloidal Sulphur Suspensions in Water*

BY S. R. DAS

AND

K. GHOSH

(Received for publication, March 17, 1939)

Plates VI and VII

**ABSTRACT** It has been reported previously<sup>1</sup> by one of the authors † (S. R. D.) that white sulphur prepared from the hydrolysis of  $S_2Cl_2$  possesses a new structure which is really different from those of the well-known crystalline modifications and the name  $S_w$  was suggested for this form. The present paper describes two other methods of preparation of  $S_w$ , namely, (i) from "chilled" liquid sulphur and (ii) from the sublimes of sulphur. The colour of  $S_w$  prepared from the first method depends on the temperature of the liquid sulphur. Thus, it is white from 119°C to 221°C and grey from 242°C to 325°C, and white again from 360°C up to the boiling point of sulphur. In the first region the liquid is mobile, and changes to highly viscous state in the second stage and finally becomes mobile again in the third stage. The three regions of temperature, mentioned above, are not sharply demarcated from one another. Further studies were made as to the stability of  $S_w$  at different temperatures. It is shown that at higher temperatures insoluble  $S_w$  converts into soluble  $S_a$  with a rate increasing with the temperature. It is suggested that a layer of  $SO_2$  is present in the insoluble varieties of  $S_a$  and  $S_w$ . Chemical evidences of the existence of  $SO_2$  layer is also given. It is further suggested that under certain physical conditions which are not yet known,  $SO_2$  layer on the crystallites is in some way responsible for the formation of the unstable  $S_w$  variety. It has also been found that if  $SO_2$  layer is removed from the  $S_w$  crystallites, it is at once converted into soluble  $S_a$ .  $S_w$  prepared from the sublimes of sulphur is

\* Communicated by the Indian Physical Society.

† Some of the preliminary works on sulphur, published by the senior author in Part I, had been carried out in collaboration with Mr. K. Ray, M. Sc., and these results were reported in several brief notes in *Science and Culture* (Vol. II, p. 108, 1936 and Vol. II, No. 12, 1937). Later on Mr. Ray being totally off from the field the results were critically revised by Das with a new camera specially constructed for this purpose, with the effect that the accuracy of these measurements was greatly increased. The paper (Part I) was entirely written by Das based on those revised data.

found to be more stable than what was prepared from frozen liquid sulphur, but still its stability is of much lower order than  $S_\omega$  obtained by the hydrolysis of  $S_2Cl_2$ .

The structure of colloidal sulphur particles was studied by allowing a fine beam of X-Rays to pass through running drops of colloidal solution suspended in water, and it is found that the colloidal particles in water are really crystalline in character like ordinary orthorhombic sulphur ( $S_a$ ).

## I. INTRODUCTION

In a previous communication<sup>1</sup> by one of the authors, the results of X-Ray investigations on the structures of the various allotropes of sulphur were described. Amongst other points, it was reported that white sulphur prepared by the hydrolysis of  $S_2Cl_2$  really possesses a characteristic crystalline structure, in opposition to the prevalent views which describe it as an amorphous allotrope of the element. The name  $S_\omega$  was suggested to represent this allotrope and the new structure possessed by it will be referred to an  $\omega$ -structure or  $\omega$ -phase of sulphur in the present paper.

The study of white sulphur has hitherto been so neglected that no information about its physical properties can be obtained from the existent literature. Really of all the allotropes of sulphur, it is the least known modification at the present moment.

Even the standard text books<sup>2</sup> on chemistry only mention the name of white sulphur with a scanty description of its method of preparation with no reference to the properties of this important allotrope. Naturally, therefore, it was thought important, and interesting too, to undertake a thorough and systematic study of the physical characteristic of  $S_\omega$ .

It was simply stated in the first communication that  $S_\omega$  is easily converted into  $S_a$  at about 88°C. The present paper chiefly aims at describing the results of investigations on the transition phenomenon, i.e., its dependence on the period of heating and the temperature. Two other methods of preparing  $S_\omega$  are also reported, for example, we have seen that (i) the insoluble part of chilled liquid sulphur, which was previously known as  $S_\mu$ , is actually found to be  $S_\omega$  and (ii) the insoluble part of the sublimate obtained by condensing vapour of sulphur on a cold surface is also  $S_\omega$ .

In the present paper we have also presented the results of our later investigations on colloidal suspension of sulphur.

## 2. THE METHODS OF PREPARATION OF $S_\omega$

### (i) From "Chilled" Liquid Sulphur

A quantity of sulphur recrystallised from a clear solution in carbon disulphide was heated in a hard glass test tube with the help of an electric heater.

The temperature of the heater could be controlled by adjusting the resistance in the circuit and the temperature could easily be maintained at any point within  $2^{\circ}\text{C}$ .

In the actual experiment, the sulphur was maintained at a certain fixed temperature for about an hour and the liquid was subsequently poured in an agate mortar. The liquid was thus suddenly cooled to the room temperature or "chilled" as it is called. The liquid sulphur solidifies as soon as it is poured out; the colour of the solids obtained depends on the temperature at which the liquid sulphur is kept before the actual solidification sets in.

Liquids kept at temperatures lying near the melting point give yellow solids like ordinary roll sulphur, whereas those at temperatures in the neighbourhood of the boiling point, freeze into chocolate brown solids. At intermediate temperatures we obtain solids of all shades of colours passing from bright yellow to chocolate brown.

In every case the solid so obtained is treated repeatedly with  $\text{CS}_2$  to wash away the soluble part which is known by the chemists as  $\text{S}_{\lambda}$ .

We prepared a cell of the insoluble part and mounted it on the carrier<sup>1</sup> and exposed in the manner described in the previous communication (Part I). Another important point which is worth mentioning, is that the insoluble part is first found to be plastic, but it very soon hardens up into a brittle solid. The colour of this insoluble sulphur is also peculiar in the respect that in some cases the substance is obtained as a white mass, while in some other cases its colour is found to be grey. We have given a chart in Table I which will show our observations on this point. It will be noticed there that the whole temperature range in which sulphur exists in the form of a liquid may be divided into three regions. The insoluble part separated from the frozen liquid in the first region extending from the melting point of sulphur up to  $221^{\circ}\text{C}$  is white. This region is also marked by the mobile state of sulphur, but near the higher temperature end of this range, the viscosity of the liquid commences to increase. In the second region extending from  $242^{\circ}\text{C}$  to  $352^{\circ}\text{C}$  the viscosity of the liquid sulphur rises to the maximum; but again it diminishes at the higher temperature end. The colour of the insoluble part derived from liquid in this region is grey. In the whole of the third region, which begins with the termination of the second and extends right up to the boiling point of sulphur, the liquid is mobile, but the mobility is appreciably less than that in the first region. The insoluble portion obtained in this region is again white. We must remember, however, that the three regions of temperature mentioned above are not sharply demarcated from one another, but each region merges in a continuous and gradual manner into its neighbouring region or regions.

The structure of the insoluble sulphur prepared from liquid sulphur at any temperature from the melting point to the boiling point is of the  $\text{S}_{\omega}$  type, quite irrespective of the colour of the substance.

TABLE I

Temperature of the liquid.	Colour and consistency of the liquid.	Colour of the insoluble part derived from the frozen liquid
1. 144°C	Yellow and transparent, mobile.	White.
2. 177°C	Yellow and transparent, mobile	White.
3. 195°C	Red and transparent, slightly viscous.	White.
4. 200°C	Red and transparent, viscous.	White,
5. 221°C	Bright red and almost opaque, viscous	White.
6. 242°C	Deep red and opaque, very viscous	Grey.
7. 253°C	Dark red and opaque, very viscous.	Grey.
8. 299°C	Opaque and black, less viscous.	Grey.
9. 318°C	Opaque and black, still less viscous	Grey.
10. 352°C	Opaque and black, mobile	Grey.
11. 381°C	Opaque and black, mobile	White.
12. 413°C	Opaque and black, mobile.	White.
13. 431°C	Opaque and black, mobile.	White.
14. 445°C	Opaque and black, boiling.	White.

Diverse colours of sulphur after different physical treatments and prepared by different physical or chemical processes present a quite perplexing problems, the solution of which has not been attempted as yet. It may be suggested that impurities of various kinds may be the root-cause of these "strategic" colours of the substance. That the presence of impurities, even in very minute quantities, influences the colour of a substance to a large extent, is now definitely known. But the case of sulphur seems to be quite inexplicable on this simple theory. For example, had the colour of the insoluble sulphur, separated from frozen liquid sulphur, been due to the presence of impurities, its colour would

not have changed as shown in the chart. We would, rather, expect  $S_\omega$  of one and the same colour in every case or it should have gradually passed from one colour at the lowest temperature to another at the highest temperature through all possible shades at the intermediate temperatures. The colour of the *entire solid mass* on the other hand, obtained by freezing a quantity of liquid sulphur, changes in a continuous manner as has been mentioned before.

We like to add another point in this connection. It has been observed during the whole course of our investigation that the colour of a heated specimen of  $S_\omega$  changes to a greenish one, the greenish colour getting deeper as the conversion of  $S_\omega$  into  $S_a$  progresses. At present, we are unable to present any plausible explanation for the colour change of sulphur.

A comparison of the photographs (Figures 1 and 2) of this insoluble variety with the diffraction pattern of  $S_\omega$  prepared from  $S_2Cl_2$  shows clearly that its structure is identical with that of  $S_\omega$ . Also the measurements of the Bragg-spacings (Table V) to which the rings in the pattern correspond agree well with those of  $S_\omega$  derived from  $S_2Cl_2$ . Thus we conclude that the insoluble part "Chilled" liquid sulphur is not amorphous but possesses an  $\omega$ -structure.

Several photographs were also taken with specimens of frozen liquid sulphur which were neither treated with carbon disulphide, nor powdered in a mortar.

These specimens, therefore, contained both the soluble and the insoluble parts. The pattern in this case consisted of a superposed spectrum due to both  $S_\omega$  and  $S_a$ . The  $S_a$  rings showed some local intensifications and thus indicated a want of perfectly random orientation of the  $S_a$  crystal grains which must, therefore, have been large in size. The  $S_\omega$  rings, on the other hand, were quite uniform in intensity, proving thereby that the  $S_\omega$  crystallites were very small, *i.e.*, smaller than  $10^{-3}$  cm. in each direction.

The method just described furnishes the easiest way of preparation of  $S_\omega$ . But, as will be shown in a later section (Sec. 3), this method has a great disadvantage. Because, we have seen that  $S_\omega$  prepared in this manner is very unstable and converts completely into  $S_a$  within about 30 hours, whereas  $S_\omega$  prepared from  $S_2Cl_2$  is highly stable; this point was also reported before (Part I).<sup>1</sup>

#### (ii) Preparation of $S_\omega$ from the Sublimate of Sulphur

Recrystallised sulphur was heated at a temperature lying within the range 300°C to 444°C (the latter being the boiling point of sulphur). But sulphur gives off copious amounts of vapour even at 300°C, which may be condensed on any cold surface. The heating, in this case, was performed exactly in the same way as described in (i).

A porcelain crucible lid was placed over the mouth of the test tube which had a portion projecting above the electric heater. This part was, therefore, at a much lower temperature. When the heating continued for a few hours, vapours of sulphur were found to condense partly on the side of the cooler part of the test tube and partly on the crucible-lid placed over the mouth of the test tube. If the temperature of the liquid were raised higher, a larger portion of the vapour condensed on the lid which was cooled with the help of a filter paper soaked in water. Sometimes, we found it more advantageous to use a number of lids, one replacing the other as soon as it got heated. The thin layer of the sublimate was scraped out and collected.

The colour of the sublimate was whitish yellow and at the time of scraping it was found to be quite plastic. But the plasticity was soon lost. This type of plasticity is a peculiarity of sulphur. Whenever liquid sulphur or vapour of sulphur is suddenly quenched to a low temperature, the element, wholly or partly (depending upon the physical conditions such as the temperature of the liquid sulphur and that of the quenching bath), passes through this unstable plastic state. The plastic material finally transforms into a hard brittle polycrystalline mass, insoluble in  $\text{CS}_2$ .

The insoluble part of the frozen liquid sulphur, soon after freezing, is also plastic and a thin film may easily be prepared from it on pressing. In some of the experiments on this insoluble form of sulphur, films prepared in this manner were used.

The sublimate of sulphur collected in the way mentioned above was treated with carbon disulphide and the insoluble part was used for taking the diffraction photographs. The pattern (Fig. 3) shows that this also has the  $\omega$ -structure. But this method of preparation of  $\text{S}_\omega$  is very tedious, for, the process is very slow, but methods may be devised for a quicker collection.

### 3. TRANSITION OF $\text{S}_\omega$ INTO $\text{S}_\alpha$

The result of a preliminary study on the transition of  $\text{S}_\omega$  into  $\text{S}_\alpha$  was reported in Part I. It was observed that at  $88^\circ\text{C}$  a specimen of  $\text{S}_\omega$  completely transformed into  $\text{S}_\alpha$  within 36 hours. The problem has, subsequently, been investigated in a systematic way, in order to determine the lowest temperature at which the transformation may take place. Our experiments in this line were first performed with  $\text{S}_\omega$ , prepared by the hydrolysis of  $\text{S}_2\text{Cl}_2$ . It was found that a specimen of  $\text{S}_\omega$ , prepared 12 months ago, produced a pure  $\text{S}_\omega$  pattern, but the photograph taken after 19 months since the preparation of the specimen, exhibited the rings of both  $\text{S}_\omega$  and  $\text{S}_\alpha$ , thus establishing that even at the room temperature ( $30^\circ\text{C}$ ) a certain percentage of  $\text{S}_\omega$  had converted by that time into  $\text{S}_\alpha$ . The Bragg-spacings corresponding to the rings in its pattern are given in table IV.

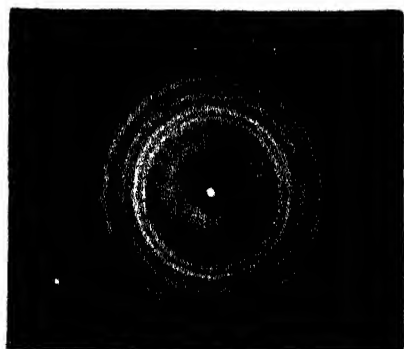


Fig. 1

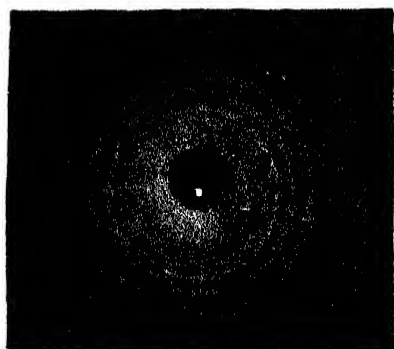
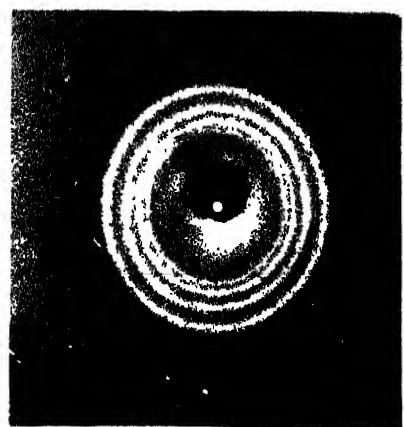
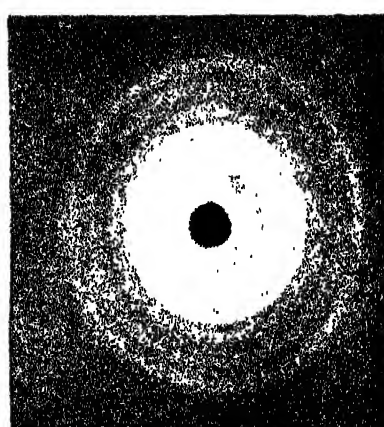


Fig. 2



15 3



118

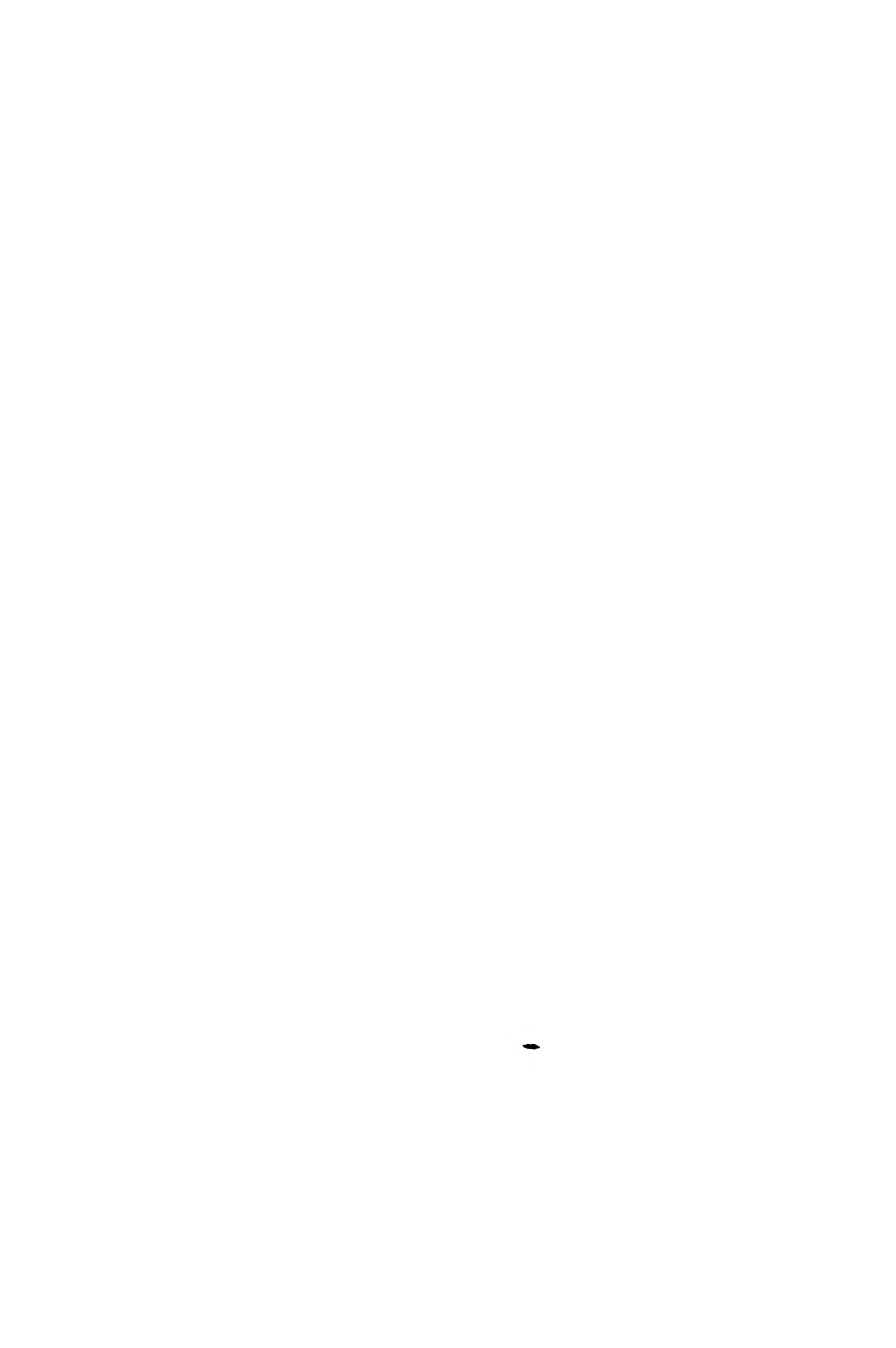
## Powder diagrams.

Fig. 1 Insoluble part of 'chilled' liquid sulphur-white ( $S_{\alpha}$ )

Fig. 2 " " " " " " " " " " gray ( S<sub>w</sub> )

Fig. 3 " " " the sublimate of sulphur ( $S_2$ )

Fig. 4 S<sub>1</sub> heated for two hours at 97.5°C pure (S<sub>1</sub>)



If  $S_\omega$  be kept at a higher temperature, the same transformation takes place more rapidly and may be detected in fewer hours, with the help of its diffraction pattern.

Figures 4, 5, 6 and 7 illustrate the effect of heating a specimen of  $S_\omega$  at  $97^{\circ}5^\circ\text{C}$  for 2, 5, 15 and 20 hours respectively. Figure 4 only shows a pure  $\omega$ -pattern, Figure 5 is a superposed spectrum due to  $S_\omega$  and  $S_\alpha$ , whereas figure 6 exhibits a pure  $\alpha$ -pattern. So a complete transformation at this temperature took place within 15 hours. Figure 7 shows the effect of further heating a specimen which already converted entirely into  $S_\alpha$ . There have appeared a large number of sharp intense spots on the photograph indicating the growth of the crystal grains. This diffraction pattern resembles exactly what was also observed in the case of a heated specimen of orthorhombic sulphur as discussed in Part I.

In Table II, we represent a chart which summarizes the results of heating a specimen of  $S_\omega$  prepared from  $S_2\text{Cl}_2$  for 21 hours, at various different temperatures. Table III, on the other hand, summarizes our observations in the case of a specimen of  $S_\omega$  heated for various periods at the fixed temperature of  $97^{\circ}5^\circ\text{C}$ .

The method of ascertaining the nature of the pattern in all these cases consisted in comparing the Bragg-spacings and intensities of the rings in any pattern with those of pure  $S_\alpha$  and  $S_\omega$ . It was observed in each case that the spacings of any specified ring agreed with that of a ring either of the  $\alpha$  pattern

TABLE II

Temperature of specimen.	Period of heating.	Approx. percentage of solubility.	Nature of diffraction pattern.
$54^{\circ}4^\circ\text{C}$	21 hours	0	Pure $S_\omega$ pattern
$63^{\circ}0^\circ\text{C}$	21 hours	0	Pure $S_\omega$ pattern.
$63^{\circ}9^\circ\text{C}$	21 hours	10	Weak $\alpha$ & strong $\omega$ pattern.
$71^{\circ}0^\circ\text{C}$	21 hours	60	$\alpha$ & $\omega$ patterns almost equally strong
$73^{\circ}1^\circ\text{C}$	21 hours	80	Strong $\alpha$ & weak $\omega$ pattern.
$74^{\circ}5^\circ\text{C}$	21 hours	88	Strong $\alpha$ & weak $\omega$ pattern.
$79^{\circ}0^\circ\text{C}$	21 hours	90	Strong $\alpha$ & very weak $\omega$ pattern.
$79^{\circ}5^\circ\text{C}$	21 hours	95	Pure $\alpha$ pattern.
$90^{\circ}7^\circ\text{C}$	21 hours	100	Pure $\alpha$ pattern.

TABLE III

Period of heating.	Temp. at which the specimen was heated.	Colour of the heated specimen.	Percentage of soluble variety	Nature of diffraction pattern.
2 hours	97.5°C	Yellow	0.9	Pure $\omega$ pattern.
5 hours	97.5°C	Dirty yellow	5.8	Strong $\omega$ and very weak $\alpha$ -pattern.
10 hours	97.5°C	Greenish yellow	51.3	$\omega$ and $\alpha$ patterns almost equally strong.
15 hours	97.5°C	Greenish yellow	85.5	Pure $\alpha$ pattern.
20 hours	97.5°C	Greenish grey	98.1	Pure $\alpha$ -pattern with sharp spots.

or of the  $\omega$ -pattern. No ring appeared, which could not be identified in this way. Table IV shows clearly the results of classifying the rings into the appropriate patterns. Columns 1 and 2 show the spacings and intensities of the rings obtained in the cases of pure  $S_\alpha$  and  $S_\omega$  respectively.

In Table V, we have collected the Bragg-spacings of  $S_\omega$  prepared from (a)  $S_2Cl_2$ , (b) frozen liquid sulphur, and (c) the sublimate of sulphur. The table also gives in Column 4 the Bragg-spacings of the rings in the pattern of the insoluble part present in a specimen of  $S_\omega$  heated for 24 hours at 79°C. It will be seen that the insoluble part so obtained is  $S_\omega$ .

Conversion of  $S_\omega$  into  $S_\alpha$  has been studied also with  $S_\omega$  prepared as the insoluble fraction of solidified liquid sulphur which is maintained at different temperatures before the solidification. For this purpose, several specimens of  $S_\omega$  were prepared from liquid sulphur kept at each of the following temperatures—144°C, 177°C, 195°C, 212°C, 290°C, 318°C, 381°C, 431°C, 444°C. The patterns obtained in the case of any specimen by an exposure of about ten hours, starting immediately after the preparation of the specimen, are exactly similar to the  $S_\omega$  pattern.

Another set of photographs was taken with  $S_\omega$  prepared from the liquid sulphur at the abovementioned temperatures. In this case each of the specimens was first kept at the room temperature for about eleven hours after its preparation and was exposed, at the end of that period, for about ten hours. The observations made are summarized in Table VI which shows that  $S_\omega$  prepared in this way is highly unstable and converts considerably into  $S_\alpha$  within a few hours, even at the room temperature.

TABLE IV

Spacings in Å. units

Recrystallised $S_a$ .	Pure $S_w$ from $S_2Cl_2$ .	$S_w$ heated at 62°C for 24 hrs.	$S_w$ heated at 68.9°C for 21 hrs.	$S_w$ heated at 79°C for 24 hrs.	$S_w$ heated at 97.5°C for 2 hrs.	$S_w$ heated at 97.5°C for 5 hrs.	$S_w$ heated at 97.5°C for 15 hrs.	$S_w$ from $S_2Cl_2$ after 12 months since the preparation at the room tempera- ture.	$S_w$ from $S_2Cl_2$ after 17 months since the preparation at the room temper- ature.
5.66		5.74	5.72		5.71	5.70			
	4.50	4.48	4.49		4.47	4.49		4.18	
	4.02	3.97			3.98			4.01	
3.84		3.84	3.88		3.91	3.88			3.84
	3.56	3.51	3.55		3.54	3.55		3.56	3.57
3.45			3.47			3.47			
3.14*		3.17	3.15		3.19	3.16			
	3.07	3.06	3.08		3.06	3.09		2.95	3.01
2.84		2.86	2.86		2.87	2.87			
	2.71				2.70			2.70	2.71
2.64			2.63			2.65			
2.41		2.66							
2.30									
2.26									
2.12						2.11			
1.98	2.10	2.10			2.09		2.10		

Similar experiments were performed also with  $S_w$  prepared from the sublimes of sulphur. In this case, the substance is found to be more stable than what was prepared from frozen liquid sulphur. But still, its stability is of much lower order than that of  $S_w$  obtained by the hydrolysis of  $S_2Cl_2$ . An adequate explanation of this anomaly regarding the variable stability, under similar physical conditions, of one and the same crystalline phase of a substance, derived from different

\* It has lately been found that the ring corresponding to the spacing  $3.14\text{\AA}$  in the pattern of  $S_a$  resolves into two rings on further resolution, which correspond to the spacings  $3.20\text{\AA}$  and  $3.10\text{\AA}$ . In Part I the spacing  $3.14\text{\AA}$  was reported to be that of the  $(210)$  plane; the identification was, therefore, not correct in that case.

TABLE V  
(Spacings of  $S_w$  in Å. U.)

From $S_2Cl_2$	From chilled liquid.	From sublimate.	Insoluble part of a specimen of $S_w$ heated at $70^\circ C$ .
4.59	4.59	4.51	4.49
4.02	3.99	4.05	4.02
3.56	3.53	3.56	3.55
3.07	3.05	3.05	3.06
2.71		2.68	2.69
2.10		2.10	2.11

sources, is not readily possible. Further investigations are in progress to elucidate the point. But we may suggest that probably the mechanical disturbance made on the substance during the process of separating the soluble and the insoluble parts, which consisted in powdering the frozen solid in a mortar and in treating repeatedly with  $CS_2$ , tells upon the stability of the crystalline  $\omega$ -phase which is actually an unstable configuration at the ordinary temperatures. There are other instances of this type of enhanced structural transformation of unstable crystalline phases by the influence of mechanical disturbances.

This point will be discussed in a future communication with reference to later observations on the stability of  $S_w$  and some other results obtained in this Laboratory.

TABLE VI  
(Insoluble part of frozen liquid sulphur exposed after  $11\frac{1}{2}$  hours since its preparation)

Temp. of the liquid sulphur.	Period of heating	Nature of the pattern.
$161^\circ C$	10 hours	$S_\alpha$ rings with intense spots on the rings
$182^\circ C$	10 hours	Intense $S_\alpha$ rings and one $S_w$ ring
$201^\circ C$	10 hours	Mixture of $S_\alpha$ and $S_w$ patterns.
$220^\circ C$	10 hours	Mixture of $S_\alpha$ and $S_w$ patterns.
$265^\circ C$	10 hours	$S_w$ pattern and one $S_\alpha$ ring.
$286^\circ C$	10 hours	Pure $S_\alpha$ pattern.
$328^\circ C$	10 hours	Pure $S_\alpha$ pattern.
$352^\circ C$	10 hours	Pure $S_\alpha$ pattern.
$391^\circ C$	10 hours	Pure $S_\alpha$ pattern.
$413^\circ C$	10 hours	Pure $S_\alpha$ pattern.
$440^\circ C$	10 hours	$S_\alpha$ rings with intense spots.

Fig. 5

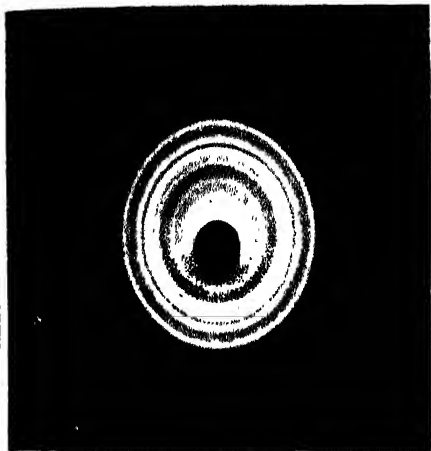


Fig. 6

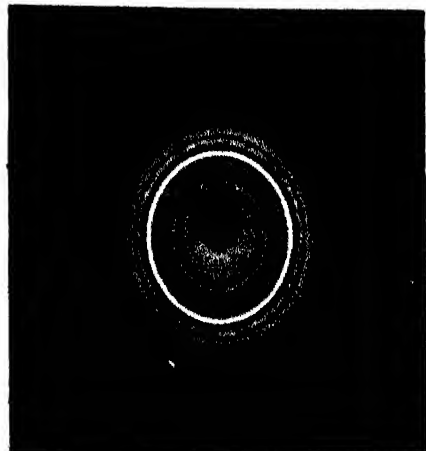


Fig. 7

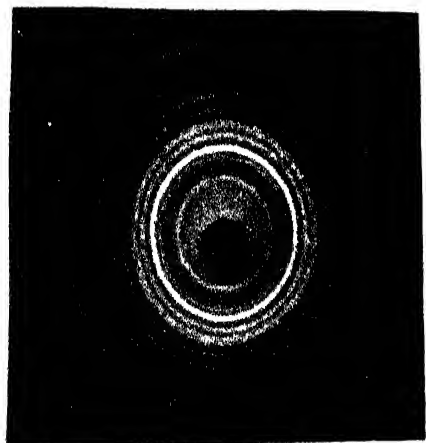
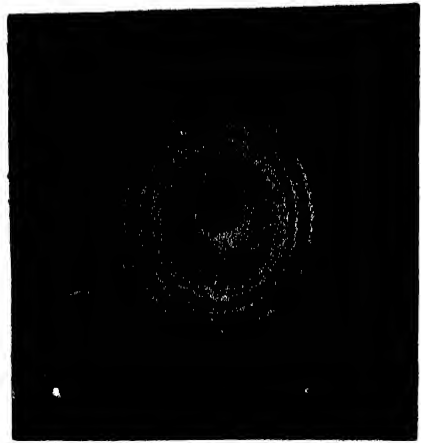


Fig. 8



## Powder diagrams.

Fig. 5  $S_{\omega}$  heated for 5 hours at  $97.5^{\circ}\text{C}$  ( $S_{\omega}$  &  $S_{\alpha}$ )Fig. 6 " " 15 " " (pure  $S_{\alpha}$ )Fig. 7 " " 20 " (  $S_{\alpha}$  rings & dots )Fig. 8 Insoluble part of a specimen of  $S_{\omega}$  heated for 24  
hours at  $79^{\circ}\text{C}$  ( c. t. table II )



## *Study of Sulphur Allotropes by the X-ray Diffraction Method 101*

### **ANOTHER METHOD OF STUDYING THE CONVERSION OF $S_{\omega}$ INTO $S_{\alpha}$ —THE METHOD OF SOLUBILITY IN CS<sub>2</sub>**

It was reported previously<sup>1</sup> that  $S_{\omega}$  is insoluble in the common solvent for sulphur, *i.e.*, CS<sub>2</sub>. But when  $S_{\omega}$  transforms into  $S_{\alpha}$  at elevated temperatures,  $S_{\alpha}$  so obtained goes completely into solution in CS<sub>2</sub>. This fact furnishes us with another method for the detection of the conversion of  $S_{\omega}$  into  $S_{\alpha}$ . The X-Ray diffraction method has one drawback in this matter, because, unless a considerable portion, say, about 10% of  $S_{\omega}$ , is converted into  $S_{\alpha}$ , the sharp rings of  $S_{\alpha}$  do not easily appear in the diffraction photographs. In the charts presented in Tables II and III, the third and 4th column respectively give the percentages of the soluble  $S_{\alpha}$  present in the heated specimens of  $S_{\omega}$ . It is to be noted in Table II that at 62°C, heat-treatment for a period of 21 hours converts about 6% of  $S_{\omega}$  into  $S_{\alpha}$  as is revealed by the solubility test, whereas the diffraction photograph in that case shows only an  $\omega$ -pattern. Similarly at 70°C, heat-treatment for a period of 21 hours converts 95% of  $S_{\omega}$  into  $S_{\alpha}$ , *i.e.*, the specimen still contains about 5% of  $S_{\omega}$ , but the diffraction photograph shows only a pure  $\alpha$ -pattern.

#### *The nature of the insoluble part present in a heated specimen of $S_{\omega}$*

In order to see the real nature of the insoluble part present in a specimen of  $S_{\omega}$  which has partially converted into  $S_{\alpha}$ , we took the diffraction photograph of such a sample of sulphur derived from a quantity of  $S_{\omega}$  which had been heated at 79°C for about 21 hours. As Table II shows, about 95% of the heated specimen is soluble in CS<sub>2</sub>. After thoroughly washing away the soluble part with CS<sub>2</sub>, a diffraction photograph was taken with the remaining insoluble part. The photograph exhibited a pure  $\omega$ -pattern. The spacings of the rings are given in Table V, and the pattern is produced in Figure 8.

*Thus we may conclude that at higher temperatures insoluble  $S_{\omega}$  converts into soluble  $S_{\alpha}$  with a rate increasing with the temperature.*

The matter is somewhat different when the conversion of  $S_{\omega}$  occurs at temperatures near about the room temperature, *i.e.*, in the vicinity of 30°C. Here we find that the specimen retains its insolubility even after the complete conversion into  $S_{\alpha}$ . In this case, therefore, the conversion of  $S_{\omega}$  into  $S_{\alpha}$  cannot be detected by the solubility test.

### **5. THE INFLUENCE OF NH<sub>4</sub>OII ON THE CONVERSION OF $S_{\omega}$ INTO $S_{\alpha}$**

The fact that NH<sub>4</sub>OII may convert insoluble  $S_{\alpha}$  into soluble  $S_{\alpha}$ , inspired us to see if insoluble  $S_{\omega}$  might be converted into soluble  $S_{\omega}$  by the same process.

We have seen in the previous section that by the process of heating at a sufficiently high temperature, a quantity of  $S_\omega$  may be converted into a mass of soluble sulphur which, however, no longer possesses the original  $\omega$ -structure. The restoration of solubility and the structural transformation go hand-in-hand at high temperatures and appear to be the two effects of one common cause.

A quantity of  $S_\omega$  was powdered and the powder was moistened with and immersed in liquor ammonia in a stoppered bottle. After 3 or 4 hours the powder was dried and its solubility was tested with  $CS_2$ . It was found that the powder went into solution. The diffraction pattern of a specimen of this powder (without any treatment with  $CS_2$ ) indicated that the substance had completely converted into  $S_\alpha$ . The observation was quite astonishing, because here we find the influence of a chemical on a structural transformation. The authors do not know of any other example of this type. The failure of this method has rendered almost impossible to prepare a specimen of soluble  $S_\omega$ . *Thus  $S_\omega$ , whenever it occurs, is always an insoluble modification of sulphur.*

The action of heat at sufficiently high temperatures has been described in Section 4. There also, one and the same process brings about the structural transformation simultaneously with the solubility of the substance. This fact, therefore, naturally suggests that the structural transformation and the solubility are but two effects of one common cause.

The insolubility of the various forms of sulphur including  $S_\omega$  has already been suggested (Part I) to be due to the presence of a layer of  $SO_2$  on the surface of the small crystallites of the insoluble varieties of sulphur. This conclusion was drawn as a generalisation of the fact that  $SO_2$  is always involved in the process of preparation and comes in contact with the element whenever an insoluble variety of sulphur ( $S_\alpha$  or  $S_\omega$ ) is prepared. The physical influence of heat and the chemical influence of  $NH_4OH$  in restoring solubility to insoluble  $S_\alpha$  also furnished a further evidence in favour of this idea. The action of  $NH_4OH$  on  $S_\omega$  was not studied at that moment. But the result of the experiment made later on and described above shows that  $NH_4OH$  is able to remove the insolubility also of  $S_\omega$  but at the same time its peculiar structure is lost with the appearance of the  $\alpha$ -structure.

We have obtained another evidence for the existence of  $SO_2$  in all the insoluble varieties of sulphur irrespective of their structures. It is known that the decolorisation of a solution of potassium permanganate is a very delicate test for  $SO_2$  which reduces the permanganate. The test, in our case, was made in the following simple way : a sufficiently dilute solution of  $KMnO_4$  was taken in a test tube half filled with the solution and closed with a piece of cork. A quantity of hardened plastic sulphur, prepared a few days back and almost completely insoluble in  $CS_2$ , was placed inside the test tube.

The permanganate solution was then warmed. The colour of the solution gradually faded away and ultimately the solution became colourless. Similar experiments were performed with  $S_w$  and recrystallised  $S_a$ . In the case of  $S_w$  the solution lost its colour exactly as in the case of hardened plastic sulphur. But recrystallised  $S_a$  was found to be quite unable to bring about the above colour change. The decolorisation in these cases is supposed to be due to the  $SO_2$  molecules set free by heat from the surface of the crystallites. One point should be mentioned here that if the solutions are heated strongly so that the liquid boils, decolorisation may be caused also by recrystallised  $S_a$ . In that case sulphur combining with oxygen dissolved in the water or given out by  $KMnO_4$  may produce  $SO_2$  which may then cause the decolorisation. So special care was taken in warming the solution.

All these observations strongly support the  $SO_2$ -hypothesis in explaining the insolubility of all the insoluble types of sulphur. We have, again, no reason to suppose a different cause for the insolubility of  $S_w$ . But as in the case of  $S_w$  the characteristic structure is also associated with its insolubility, we should assume that  $SO_2$ , which is responsible for the insolubility, is also responsible for its peculiar structure. The exact mechanism by which a layer of  $SO_2$  on the surface may influence the structure inside the crystallites is yet unknown.

But this far we can say that though the mere presence of  $SO_2$  guarantees the insolubility of sulphur obtained by any process, it never guarantees an  $\alpha$ -structure. Its presence is necessary, but not sufficient for the formation of  $S_w$ . This explains the simultaneity of the structural transformation of  $S_w$  with the appearance of solubility. The presence of  $SO_2$  is the common cause, with which the insolubility of sulphur is invariably associated and which, under certain circumstances yet unknown, leads also to the formation of the peculiar structure of  $S_w$ .

In this connection attention must be drawn also to the following facts :—

(a) The conversion of  $S_w$  into insoluble  $S_a$  at lower temperatures, shows that the structure of  $S_w$  is *unstable even in the presence of  $SO_2$* . Thus the presence of  $SO_2$  again is no guarantee for the stability of  $S_w$ .

(b) The insolubility of  $S_w$  cannot be due to the peculiar structure possessed by it. For, in that case,  $S_w$  could not convert into *insoluble  $S_a$*  at the ordinary temperatures. Because the insolubility of  $S_a$  requires  $SO_2$ .

(c) The structure of  $S_w$  cannot be due to  $SO_2$  being placed inside the lattice. For, in that case, the crystallites of  $S_w$ , formed as a result of the transformation of  $S_w$ , would have been so imperfect that sharp diffraction rings, as were actually obtained, would have been quite impossible. The expulsion of  $SO_2$  molecules from inside the lattice would produce some vacant points in it and would severely

disturb the structure, as a result the structure would become highly unstable, and consequently would have completely been shattered. And as the molecules are not sufficiently mobile, specially at the room temperature, rebuilding of a regular structure, i.e.,  $S_a$ , is not so quickly possible. With this idea, of course, we may explain the other peculiarities of  $S_w$  and for this reason it was suggested previously in a note.<sup>1</sup> But it becomes difficult to understand the action of  $NH_4OH$  in removing the  $SO_2$  molecules from inside the lattice. It is not possible for  $NH_4OH$  to penetrate into the lattice of  $S_w$  and remove, by way of chemical combination, the molecules of  $SO_2$ .

Further investigations are in progress to determine the structure and real nature of  $S_w$  and will shortly be published.

#### 6. BLACK SULPHUR AND SULPHUR PRECIPITATED FROM A SOLUTION OF SODIUM THIOSULPHATE

Mellor<sup>1</sup> has mentioned that several authors noticed a black variety of sulphur which has also been called metallic sulphur. The present authors have also observed that if a quantity of sulphur (Flower of S, recrystallised or precipitated sulphur) is boiled in a basin or a test tube, always a black residue is left inside the vessel. We have obtained this residue even from sulphur repeatedly crystallised from a solution in  $CS_2$ . We obtained a very good powder diagram with this black substance which was suspected to be another variety of sulphur. But a chemical analysis kindly made by Prof. P. R. Ray has revealed that it contains a mixture of sulphur with silica and sulphides of iron and nickel. We have, therefore, given up further studies on this substance.

It is well known that when a solution of sodium thiosulphate (ordinary "hyj o" salt) is acidulated, the salt decomposes and sulphur is set free, a part of which is precipitated as a gummy solid and a part remains in the colloidal suspension. The gummy deposit produces a pure  $S_a$  pattern, indicating that the substance contains small  $S_a$  crystallites, just like the gummy deposits of colloidal sulphur prepared by the action of  $H_2S$  on sulphurous acid. No peculiarity has been noticed with this substance.

#### 7. THE STUDY OF STRUCTURE OF SULPHUR PARTICLES IN COLLOIDAL SUSPENSION IN WATER

(By Drop Method)

It has been reported previously<sup>1</sup> that the spontaneous solid deposits of colloidal sulphur, formed as a result of a very slow process of sedimentation, as well as the electrolytic deposit obtained on addition of a requisite quantity of  $NH_4OH$  of proper concentration to the colloidal solution, are crystalline and their structures are exactly similar to that of orthorhombic sulphur or  $S_a$ .

## *Study of Sulphur Allotropes by the X-ray Diffraction Method 105*

In order to arrive at a definite conclusion about the real nature of the colloidal sulphur particles in the state of suspension, several attempts were made also to study the solution by X-ray diffraction method, but they were all unsuccessful.

Recently<sup>5</sup> we have been able to come to a very definite conclusion as regards the nature of colloidal sulphur particles suspended in water. A totally new method of studying less volatile liquids by the X-ray diffraction method has been developed, which involves in exposing the liquid in small drops to the incident radiation. With the arrangements made, it was possible to control the size of the drops, which in our experiments was of the order of a m.m. We found that in the case of a colloidal solution of sulphur, a drop of the abovementioned size remained, on an average, undisturbed and practically unchanged for more than half an hour, inspite of the mechanical disturbances due to the constant working of the pumps and other sources.

It is also worth mentioning here that no change in the quality of the solution was noticed and we have also not been able to observe any trace of coagulation of sulphur particles and the consequent quick deposition of sediments in the colloidal solution under the influence of X-rays. To test this point a set of preliminary experiments was necessary. For, if the deposition of sulphur takes place in this condition, any crystalline pattern obtained may be due to the deposits and no definite conclusion regarding the nature of the suspended sulphur particles may be arrived at.

A quantity of the solution was enclosed in a thin-walled glass tube of about 1.5 m.m. bore. The tube was sealed at both ends and exposed to the X-rays (5 m.-amp. at 35 KV) for about 10 hours. No sign of sedimentation or any other change could be detected.

The photographs obtained with colloidal sulphur drops exhibited a crystalline pattern but the background was very diffuse owing to the scattering of X-rays by the water molecules in the solution. Measurements of the sharp rings and the visual estimation of the relative intensities definitely show that the colloidal particles in the state of suspension are also crystalline like ordinary  $S_a$ . This variety, as reported previously,<sup>1</sup> is insoluble in  $CS_2$ .

The authors desire to take this opportunity for expressing their respectful thanks to Professor Dr. B. B. Ray for the interest he has taken in the work.

KHAJRA LABORATORY OF PHYSICS,  
UNIVERSITY COLLEGE OF SCIENCE,  
92, UPPER CIRCULAR ROAD,  
CALCUTTA.

R N F R H N C E S

<sup>1</sup> S. R. Das, *Ind. Jour. Phys.*, **12**, 163 (1938); *Science and Culture*, **1** (1936).

<sup>2</sup> Partington, *Inorganic Chemistry*; Mellor, *Modern Inorganic Chemistry*, etc.

<sup>3</sup> S. R. Das and K. Ray, *Science and Culture*, **2**, 168 (1937).

<sup>4</sup> Mellor, *A Comprehensive Treatise on Inorganic Chemistry*, Vol. X.

<sup>5</sup> S. R. Das and K. Ghosh, *Science and Culture*, **4** (1938).



# THE FRINGE OF THE ATMOSPHERE AND THE ULTRA-VIOLET LIGHT THEORY OF AURORA AND MAGNETIC DISTURBANCES\*

BY PROF. S. K. MITRA

AND

MR. A. K. BANERJEE

(Received for publication, March 30, 1939.)

**ABSTRACT.** An atmosphere in isothermal equilibrium has no natural limit, an atmosphere in adiabatic equilibrium has, however, one. Beyond this "inner" adiabatic atmosphere lies the outer atmosphere formed by molecules "evaporated" from the outer surface of the "inner" atmosphere. The fringe region lies at the farther limits of this outer atmosphere, where the molecules moving without any collision describe orbits of enormous dimensions.

Taking atomic oxygen and molecular nitrogen as the upper atmosphere constituents the height of the critical level or level of negligible collision is calculated by the authors and is found to be 770 km. Above 930 km. there is practically no collision between the atoms.

Ionization of the atoms in the fringe region by solar ultra-violet radiation will diminish the rate of escape owing to their entanglement with the earth's magnetic field. Critical velocities of escape of oxygen ions from different latitudes of the earth are calculated.

The increase with height of the viscous drag of the earth measured by kinematical viscosity  $\eta/\rho$  is taken into account and it is shown that the atmosphere rotates with the earth so long as there is appreciable collision between atoms.

Molecular densities at different levels of the fringe region are estimated. The merging of the fringe region into interstellar space takes place between 2000 and 2500 km. above the earth's surface.

Existence of super-elastic collisions between an excited (metastable) atom and a neutral particle extends the fringe region. Of the various metastable states of the constituent particles only those of oxygen atoms are capable of producing any effect by super-elastic collisions. It is found that roughly about  $10^4$  atoms in the  ${}^1S$  state and  $10^6$  atoms in the  ${}^1D$  state suffer collisions per second with other atoms. The atoms in the  ${}^1S$  state can shoot a neutral oxygen atom to a height of about 14,000 km. above earth's centre while an atom in the  ${}^1D$  state can shoot it to a height of about 9,500 km. The density distribution in the fringe region and the merging with the interstellar space (which takes place at about 2500 km. above the earth's surface) are found to be only slightly modified by the presence of these high speed particles.

By considering the motion of ions in the earth's magnetic and gravitational fields, taking into account the variations of  $g$  and  $H$  with altitude and also considering the rotation of the earth magnet it is found that an ion starting at the equator at 12 o'clock noon at 40,000 km. height

\* Communicated by the Indian Physical Society.

and descending along the magnetic line of force with a velocity of 1 km/sec will enter the earth's atmosphere at 12-54 local hour. Bearing of the above results on the Ultra-violet light theory of Aurorae and magnetic storms as suggested by Hulbert (the essential feature of which is the distillation of speedy ionized particles from lower to higher latitudes by the earth's magnetic field) is discussed.

If it is assumed that the high speed atoms are ionized at a height of about 40,000 km. the time of descent as calculated above by the authors agrees with that calculated by Hulbert. Analysis shows, however, that by no known means particles from lower levels can reach 40,000 km. level to which they must rise in order to reach the auroral latitude. Again according to Hulbert the particles driven upwards by super-elastic collisions will be ionized in three hours. Recent calculations on atomic absorption coefficient of oxygen shows, however, that the time required should be several orders higher than that assumed by Hulbert.

## C O N T R I N T S

### PART I

#### Fringe of the Atmosphere and its Extension

- §1. Introduction.
- §2. Atmosphere in Isothermal and in Adiabatic Equilibrium—Natural Limit of the Atmosphere.
- §3. Critical Level.
- §4. Effect of Ionization on the Rate of Escape of Molecules from the Earth's Atmosphere.
- §5. Rotation of the Earth—Viscous Drag.
- §6. Fringe of the Atmosphere.

Extension of the Fringe Region by super-elastic collisions. Possible sources of super-elastic collisions. Calculation of the number of metastable oxygen atoms. Average molecular density in the fringe region.

### PART II

#### The Ultra-violet light theory of Aurorae and Magnetic Storms

- §1. Introduction.
  - §2. Motion of Ions in Gravitational-Magnetic Field.
  - §3. Effect of Variation of  $g$  and  $H$  on Ion Paths.
  - §4. Rotation of the Earth-Magnet—Time of arrival of the ions in high latitudes. Average path of an ion.
  - §5. The Ultra-violet Light theory of Aurorae and Magnetic Disturbances.
  - §6. Summary and Conclusion.
- References.

L I S T O F S Y M B O L S

$a$ —Earth's radius.

$A(n, l)$ —A constant, depending on the orbit in which the electron is captured.

$$C = \sqrt{\frac{M}{HR}}.$$

$c$ —Velocity of light (Part II, §2).

$c', c'$ —Velocities of two colliding gas molecules (Part I, §3).

$E$ —Energy required to ionize an atom (Part II, §5); Intensity of the electric field generated by the rotation of the magnetic lines of force of the earth (Part II, §4).

$E_r, E_\theta$ —Components of the electric field  $E$ ,

$e$ —Charge on an ion.

$g$ —Acceleration due to gravity at a distance  $r$  from the centre of the earth.

$g_0$ —Acceleration due to gravity at the surface of the earth.

$H$ —Intensity of the earth's magnetic field at a distance from the centre of the earth.

$H_r, H_\theta$ —Components of  $H$ .

$H_0$ —Intensity of the earth's magnetic field at the surface of the earth.

$h$ —Planck's constant.

$I(\nu)_0$ —Intensity of solar radiation of frequency  $\nu$  outside the earth's atmosphere.

$k$ —Boltzmann's constant.

$M$ —Magnetic moment of the earth.

$m$ —Molecular or atomic weight (Part I, §3), weight of an ion (Part II).

$m_1, m_2$ —Molecular or atomic weights.

$N$ —Total number of atoms in a column of 1 sq. cm. cross-section above the critical level.

$n$ —Molecular density.

$n_0$ —Molecular density at the datum level.

$p$ —Pressure at any particular level.

$p_0$ —Pressure at the datum level.

$q$ —Number of ions formed per sec. in a column of 1 sq. cm. cross-section above the critical level.

$q_+$ —Number of positive ions in the column.

$q_-$ —Number of electrons in the column.

$$q_0 = \frac{mg}{KT} \cdot r_0.$$

$$q'_0 = \frac{mg}{KT} \cdot r_0 - 2.$$

- q*—Number of ions recombining per second in a column of 1 sq. cm. cross-section above the critical level.
- q(n, l)*—A constant, depending on the orbit of capture.
- R*—Radius of curvature of the helical path of an ion.
- r*—Radius vector (distance from the centre of the earth).
- r<sub>0</sub>*—Distance of the datum level from the centre of the earth.
- T*—Temperature of the gases of the atmosphere (in absolute degrees).
- T<sub>s</sub>*—Temperature of the sun (in absolute degrees).
- t*—Time (in seconds).
- u<sub>a</sub>*—Gravitational magnetic drift velocity of an ion.
- V*—Relative velocity of two colliding gas molecules (Part I, §3), Relative velocity of an ion ( $= v - u_a$ ) (Part I, §2). Energy in volts (Part I, §6).
- v*—Velocity of an atom or molecule (Part I, §3). Velocity of an ion (Part II, §§2, 3, 4).
- v'*—Electromagnetic drift velocity.
- Z*—Effective atomic number of an ion.
- z*—Height above the datum level.
- a*—Recombination coefficient of ions and electrons.
- $4\pi\beta$ —Solid angle subtended by the sun at the earth.
- γ*—Ratio of specific heat at constant pressure to the specific heat at constant volume (Part I, §2); a constant (Part I, §4).
- γ<sub>1</sub>*—A constant.
- η*—Coefficient of viscosity of a gas.
- θ*—Angular co-ordinate (Part I, §3); Angle made by *r* with the axis of the earth (Part II, §4).
- θ<sub>0</sub>*—Co-latitude of the place where a particular magnetic line of force terminates on the earth's surface.
- λ<sub>0</sub>*—Wavelength of radiation corresponding to frequency *v<sub>0</sub>*.
- v*—Frequency of radiation.
- v<sub>0</sub>*—Threshold frequency for dissociation or ionization of an atom.
- ρ<sub>1</sub>, ρ<sub>2</sub>*, etc.—Densities of gases at a particular level of the atmosphere.
- (ρ<sub>1</sub>)<sub>0</sub>, (ρ<sub>2</sub>)<sub>0</sub>*—Densities of gases at the datum level.
- σ*—Molecular diameter.
- τ(v)*—Absorption per atom of radiation of frequency *v*.
- τ<sub>0</sub>*—Limiting value of *τ(v)* at *v=v<sub>0</sub>*.
- φ*—Angular co-ordinate (Part I, §3). Total angular shift of an ion path due to electromagnetic drift. (Part II, §4).
- χ*—Angular measure (in degrees from the poles) of the region of escape of ions from the earth's atmosphere.
- ψ(v)*—Ionization probability.
- ω*—Angular velocity in the helical motion of an ion.
- Ω*—Angular velocity of rotation of the earth.

§1 INTRODUCTION

It is now conventional to divide the atmosphere into three regions—the Lower, the Middle and the Upper Atmosphere. The lower atmosphere, which is the same as the Troposphere, extends from the ground level to a height of 10 to 15 km.; the middle atmosphere, from 15 to 100 km., includes the Stratosphere lying immediately above the Troposphere and also the Ozonosphere between 25 and 45 km. The atmosphere from 100 km. above is called the Upper Atmosphere and is more or less ionized. Besides these three regions, one should also consider the "fringe" region of the upper atmosphere which is supposed to exist beyond the so-called limit of the upper atmosphere. Attention to this "fringe" region of the atmosphere was first drawn by Johnstone Stoney.<sup>1</sup> The fringe has recently awakened new interest owing to its being a possible source of speedy charged particles which may be the cause of magnetic storms, aurorae, etc.<sup>2</sup> The purpose of the present paper is to make a critical study of the origin and properties of the fringe region (Part I) and to examine how far the charged particles originating in it by the action of the ultra-violet rays of the sun may be a contributory cause of the above-named geophysical phenomena (Part II).

PART I. FRINGE OF THE ATMOSPHERE AND  
ITS EXTENSION

. §2. ATMOSPHERE IN ISOTHERMAL AND IN ADIABATIC  
EQUILIBRIUM; NATURAL LIMIT OF THE ATMOSPHERE

Let us consider the idealised case of a gaseous atmosphere above a non-rotating earth undisturbed by solar rays. Such an atmosphere, if left to itself, would, after a sufficient time, attain a state of isothermal equilibrium. Under equilibrium condition, the constituent gases at different heights would be distributed according to the law

$$\left. \begin{aligned} \rho_1 &= (\rho_1)_0 e^{-\frac{m_1 g}{kT} \cdot z} \\ \rho_2 &= (\rho_2)_0 e^{-\frac{m_2 g}{kT} \cdot z} \\ &\text{etc.} \quad \text{etc.} \end{aligned} \right\} \dots \quad (1)$$

where

$\rho_1, \rho_2$ , etc. are the densities of the different gases at a height  $z$  above the earth's surface;

$(\rho_1)_0, (\rho_2)_0$ , etc. are the densities of the different gases at the surface of the earth ;  
 $m_1, m_2$ , etc. are the molecular weights of the constituent gases ;

$T$  is the constant absolute temperature of the atmosphere.

It is easily seen from eqn. (1) that the density of the atmosphere diminishes exponentially so that  $\rho$  attains zero value only at infinity. Such an atmosphere, as long as it obeys gas kinetic laws, will not have any natural limit.

Secondly, we may consider the idealised case of the opposite extreme in which the whole mass of the atmosphere is subject to turbulence (caused by heating, etc.) and possesses convective motions throughout its entire height. Under such circumstances the atmosphere may be said to be in adiabatic equilibrium as opposed to isothermal equilibrium. The adiabatic equilibrium is brought about by the movement of masses of air from lower to higher level and *vice versa*, without any loss or gain of heat.

From the general equation of equilibrium of the atmosphere

$$\frac{\partial p}{\partial z} = -g\rho$$

we get

$$k\gamma\rho^{\gamma-1} \frac{\partial \rho}{\partial z} = -gz$$

by applying the adiabatic law  $p=k\rho^\gamma$ .

Integrating we get

$$\frac{k\gamma}{\gamma-1} (\rho_0^{\gamma-1} - \rho^{\gamma-1}) = gz \quad \dots (2)$$

where  $\rho_0$  is the density of the gas at the surface of the earth ;

$\gamma$  is the ratio of the specific heat at constant pressure to the specific heat at constant volume.

Thus equation (2) expresses the law according to which density and temperature fall off with height. In contrast with equation (1) we find that  $\rho$  becomes zero at a finite value of  $z$  given by

$$\left. \begin{aligned} z &= \frac{k\gamma\rho_0^{\gamma-1}}{g(\gamma-1)} \\ &= \frac{\rho_0\gamma}{g\rho_0(\gamma-1)} \end{aligned} \right\} \quad \dots (3)$$

We thus see that in the case of an atmosphere in adiabatic equilibrium we can conceive of a natural limit. If, for instance, we assume that the entire terrestrial atmosphere is in adiabatic equilibrium, its natural limit can easily be calculated

and is found to lie at a height of about 29 km.<sup>3</sup> above the surface of the earth ( $\rho_0 = 0.001205 \text{ gm/cm}^3$ ,  $\gamma = 1.4$ ,  $p_0 = 760 \text{ mm.}$ ).

Further considerations show that the surface at the outer limit of the atmosphere—though a natural upper boundary of the atmosphere in the lower region in adiabatic equilibrium—will not be a surface separating a region of perfect vacuum above and a region containing gas molecules below. Molecules from the adiabatic atmosphere below will be constantly evaporating, as it were, due to thermal agitation, across the surface of separation to the vacuous space above in much the same way as liquid molecules escape from the body of a liquid to the space above its surface. Thus the region above the natural limit will contain molecules and this region may be called the “outer atmosphere.” If we assume that there is appreciable, though small, collisions between the molecules, then these will be distributed according to equation (4) provided the temperature is taken to be constant.

$$\left. \begin{aligned} \rho_1 &= (\rho_1)_0 e^{-\frac{m_1 g}{kT} a \left( \frac{z}{a+z} \right)} \\ \rho_2 &= (\rho_2)_0 e^{-\frac{m_2 g}{kT} a \left( \frac{z}{a+z} \right)} \\ &\text{etc.} \quad \text{etc.} \end{aligned} \right\} \dots \quad (4)$$

The outlying region of this “outer atmosphere,” in which collisions are few and far between, may be called the spray or fringe of the atmosphere. The level at which the transition from the outer atmosphere to the spray region occurs will, of course, depend on the temperature, pressure and other factors of the “outer atmosphere.”

In this fringe region of the atmosphere, molecules will move freely with the velocity acquired at the last collision in the lower region and subject only to the pull of gravity will describe parabolic, elliptic or hyperbolic paths according to the magnitude and direction of their velocities. Molecules with hyperbolic orbits will, of course, escape from the earth and the velocity necessary for such escape will be given by

$$v^2 \geq \frac{2ga^2}{r}$$

where

$v$  = velocity of the molecule ;

$g$  = acceleration due to gravity at the level from which the molecule escapes ;

$a$  = the earth's radius ;

$r$  = distance of the level of escape from the centre of the earth.

If the idealised conditions described above were applicable to the earth, then we would have the following picture of the atmosphere : The constituent

gases are thoroughly mixed and the atmosphere is in adiabatic equilibrium up to a height of about 29 km. which is the natural limit of the atmosphere with lapse rate of about  $10^{\circ}$  per km. This region in which the temperature falls linearly with height is the "inner atmosphere." Beyond this is the "outer atmosphere" formed of molecules evaporated from the inner atmosphere. The outer atmosphere is in isothermal equilibrium and its outlying regions form the spray of the atmosphere where there is practically no collision and the molecules describe parabolic, elliptic or hyperbolic paths round the earth. As mentioned in the Introduction, it is this last named region of the atmosphere which will form the subject matter of our study in the following sections

### §3. CRITICAL LEVEL

The picture of the ideal adiabatic atmosphere given above is unfortunately widely different from the actual condition of the atmosphere. The lapse rate for instance is only about  $5^{\circ}\text{C}/\text{km}$ . instead of about  $10^{\circ}\text{C}/\text{km}$ . Again if the loss and gain of heat by radiation and absorption by each element of the atmosphere for a permanent atmospheric arrangement be considered, it can be shown that on the assumption of a uniform constitution of the atmosphere, the adiabatic state could not extend to a height greater than given by  $p = \frac{1}{2} p_0$ , where  $p_0$  is the surface pressure. If the atmosphere be not uniform the height of the adiabatic layer increases and for the actual constitution of the atmosphere (containing varying amount of water vapour at different heights), it has been shown by Gold<sup>4</sup> that the height of the adiabatic layer should lie between  $p = \frac{1}{2} p_0$  and  $p = \frac{1}{4} p_0$  (*i.e.*, between  $z = 5\frac{1}{2}$  km. and  $z = 10\frac{1}{2}$  km.). Above this adiabatic layer we have the outer atmosphere and here also recent observations show that the condition is far from isothermal, due principally to the photo-chemical and photo-ionizing action of the solar-rays. The outer atmosphere, the base of which is approximately isothermal and is to be identified with the stratosphere, thus extends to great heights, and it is near the outside (boundary) of this region that we shall look for the "fringe" region of the outer atmosphere. The collisional frequency in this region is negligible and the molecules have either a chance to escape or to describe closed paths round the earth or to fall back to the earth after describing parabolic orbits and reaching enormous heights from the earth's surface.

The first attempt to calculate the height at which collisions begin to have negligible effect was made by Milne<sup>5</sup> and was later followed up by J. E. Jones.<sup>6</sup> It has been shown by the latter that the failure of previous workers to estimate the height of the "ceiling of the atmosphere" or the level above which there is very little chance of a collision is due to their assumption of uniform molecular density along the free path of a molecule. At high altitudes of the atmosphere the free path of a molecule is appreciably large and the molecular density also

decreases rapidly upwards. Along the free path of a molecule, therefore, the molecular density is liable to change appreciably. Thus account should be taken of the fact that the probability of collision of a molecule is a function not only of its velocity but also of its origin and direction of motion, since the molecular density will vary in different manners in different directions.

Milne and Jones start with the well-known expression of Tait for the probability of collision of a molecule of given velocity  $c$ —

$$\theta(c) = n\sigma^2 \sqrt{\frac{m^3}{8\pi k^3 T^3}} \int_0^\infty \int_0^\pi \int_0^{2\pi} e^{-\frac{mc'^2}{2kT}} c'^2 V.d.c. \sin\theta d\theta. d\phi.$$

where  $n$  = molecular density ;

$\sigma$  = molecular diameter ;

$m$  = molecular weight ;

$c, c'$  = velocities of the colliding molecules ;

$V$  = relative velocity between the colliding molecules and is given by  $V^2 = c^2 + c'^2 - 2cc' \cos\theta$  ;

$\theta, \phi$  = angular co-ordinates of the direction of motion.

The expression can be put in the form :—

$$\theta(c) = \sqrt{\frac{\pi n \sigma^2}{c \frac{m}{2kT}}} \psi \left( c \sqrt{\frac{m}{2kT}} \right)$$

where  $\psi$  is a function of the form  $\psi(x) = xc^{-x^2} + (2x^2 + 1) \int_0^x e^{-y^2} dy \dots (5)$

In order to evaluate the above equation, we require a knowledge of the various constants  $n, \sigma$ , etc.  $n$  in particular varies with height and the usual expression for its variation is given in eqn. (1). When we are considering the conditions at great heights we have got to take into account the change in the pull of gravity as well as the attraction of the mass of air which varies with height, as one goes outwards. Taking these factors into consideration Milne shows that a more correct expression for  $n$  at great heights in the outer atmosphere, assuming a constant temperature, is given by—

$$n = n_o \left( \frac{r_o}{r} \right)^2 e^{-q_o' \left( 1 - \frac{r_o}{r} \right)} \dots (6)$$

where  $n_o$  = molecular density at a level at a distance  $r_o$  from the earth ;

$n$  = molecular density at the level at a distance  $r$  where collision is being considered ;

$$q_o' = \frac{mg}{kT} \cdot r_o - 2 = q_o - 2.$$

The estimate of the height of the "critical level" is now made by the help of equations (5) and (6) and introducing the idea of the "cone of escape." Let us suppose that an observer ascends gradually upwards from a level where molecular density is small but appreciable. If the molecules were opaque, then the hemispherical sky above the observer would appear to him absolutely opaque, a line drawn from the observer towards any direction would pass through many molecules, one behind the other. If the observer continues his ascent, he will reach a level where the molecules overhead will gradually thin away and will ultimately just fill the sky, i.e., a line drawn upwards will pass through only one molecule whereas a line drawn in any other direction will still pass through more than one molecule. Mounting still higher, he will find his sky overhead gradually clearing up and he will "see" a cone with its axis vertical within which his sky will be clear. It is obvious that this cone will open out with height and the observer will finally have his whole sky clear. This cone, the axis of which is vertical and the angle of which increases with height, is the "cone of escape" of the molecules. A molecule moving within the solid angle of this cone will have some chance of escaping without a collision.  $\theta$ , the semi-vertical angle of the cone of escape, is shown by Jones to be related to  $r$  and  $c$  by the equation

$$e^{q_o' \frac{r_o}{r}} - 1 = \frac{q_o' c q_o' \cos \theta c^2 m}{2k'T \sqrt{\pi n_o \sigma^2 r_o} \psi \left( c \sqrt{\frac{m}{2k'T}} \right)} . \quad \dots \quad (7)$$

The lowest estimate of the level above which a molecule may escape without a collision is easily obtained from eqn. (7) by putting  $\theta = 0$  and  $c = \infty$ .

Thus

$$e^{q_o' \frac{r_o}{r_c}} - 1 = \frac{q_o' e^{q_o'}}{\pi n_o \sigma^2 r_o} . \quad \dots \quad (8)$$

Jones and Milne used eqn. (8) to calculate the levels of escape of hydrogen and helium, which at the time they wrote the papers were believed to be the constituents of the upper atmosphere. Assuming the temperature of the outer atmosphere to be  $219^{\circ}\text{K}$  they obtained the values of the levels of escape of the above two gases to be 1521 km. and 630 km. respectively (heights measured from above the stratosphere, 20 km. from the surface of the earth). We now know that the assumptions of Milne and Jones regarding the constituents as well as the temperature of the upper atmosphere are wrong. According to modern concep-

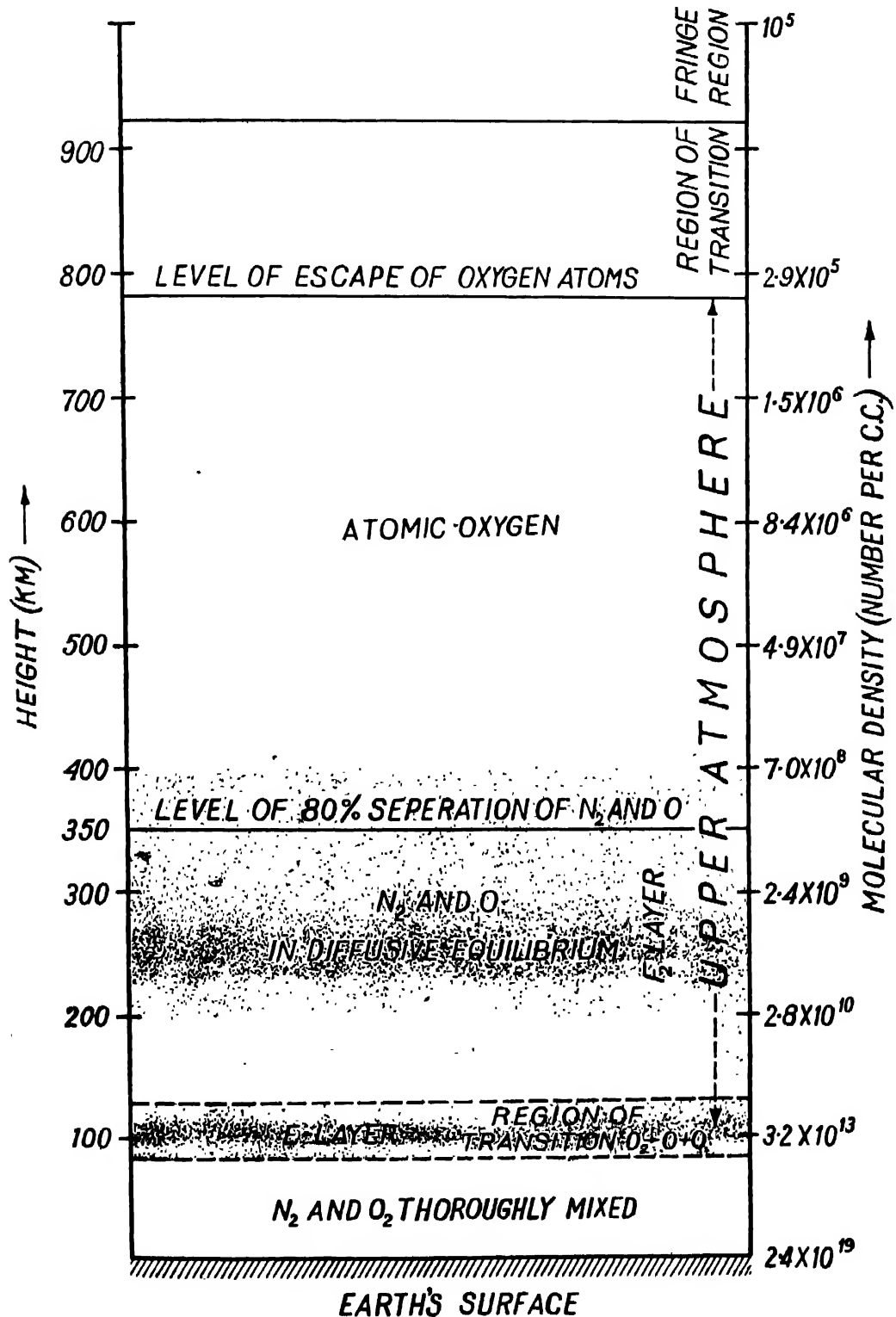


FIGURE I

tions, the atmosphere above 100 km. consists of molecular nitrogen and atomic oxygen and is at a high temperature.<sup>7</sup> Further, explorations by radio waves as well as observations on the meteorological phenomena afford us means of estimating the molecular density at 100 km. level. We can, therefore, calculate the minimum heights of the levels of escape of the above two gases by taking 100 km. level as the datum level and also assuming the most probable temperature. Taking<sup>8</sup>  $(n_o)_O = 6.963 \times 10^{12} / \text{c.c.}$ ,  $(n_o)_{N_2} = 2.543 \times 10^{13} / \text{c.c.}$ ,  $\sigma_o = 2.63 \times 10^{-8} \text{ cm.}$ ,  $\sigma_{N_2} = 3.8 \times 10^{-8} \text{ cm.}$ ,  $T = 1000^\circ \text{K}$ , we find the level of escape of  $N_2$  and of  $O$  to be 410 km. and 671 km. respectively (heights measured from above 100 km. level). These values, as mentioned before, give a lower estimate of the height of the level of escape. To estimate the upper limit of this level, from above which molecules may emerge to form the spray, we make  $\theta$  approach  $90^\circ$ . Putting  $\theta = 85^\circ$  the levels for  $N_2$  and  $O$  are found to be 485 km. and 831 km. (above the 100 km. level). It is to be noted that all the molecules above this level which avoid collisions will not escape from the atmosphere. Only those molecules which move with velocities greater than  $\frac{2ga^2}{r}$  will get rid of the earth's attraction. This critical velocity for escape of a molecule from the top of the earth's atmosphere is calculated to be about 11 km./sec. ( $r = 7378 \text{ km.}$ ,  $a = 6378 \text{ km.}$ ,  $g = 732 \text{ cm./sec.}^2$  at 1000 km. level). The distribution of the constituent gases and molecular density at different altitudes of the atmosphere are shown in Figure 1.

#### §4. EFFECT OF IONIZATION ON THE RATE OF ESCAPE OF MOLECULES FROM THE EARTH'S ATMOSPHERE

In the previous section we have seen that a neutral particle requires a velocity of about 11 km./sec. to overcome the pull of gravity and escape from the earth's atmosphere. We have not considered, however, the possibility of the atoms and molecules in the fringe region being ionized by the ultra-violet radiation of the sun. The motion and distribution of the particles, if ionized, will be profoundly influenced by the earth's magnetic field. The critical velocity for escape of these ionized particles and its variation with latitude may be estimated after the elaborate calculations of Störmer<sup>9</sup> on the trajectories of charged particles coming from infinity towards a magnetic dipole. His calculations show that there is a space  $Q_\gamma$  characterized by a certain value of  $\gamma$ , an integration constant, within which the charged particles cannot enter. For  $\gamma < -1$ , no charged corpuscle can reach the magnetic dipole. For  $\gamma$  lying between  $-1$  and  $0$ , charged particles from infinity may reach the magnetic dipole. There is, however, a toroidal space round the dipole where they cannot enter. The meridional curve of this space is given by—

$$r = \frac{\sqrt{\gamma_1^2 + \sin^2 \chi - \gamma_1}}{\sin \chi} \quad \dots \quad (9)$$

where  $\gamma_1 = -\gamma$ ;

$\chi$  = the angle which the radius vector  $r$  makes with the magnetic axis  $z$ ;

$r$  = the radius vector measured in units of length  $C = \sqrt{\frac{M}{HR}}$ ,  $M$  being the magnetic moment of the dipole;

and  $HR = \frac{m}{e}v$ , where  $v$  is the velocity of the charged particle.

The maximum angular distance  $\chi_1$  of the zone within which the charged particles may enter the earth's atmosphere (the earth is regarded as a small sphere of radius  $a$  placed round the magnetic dipole) is obtained by finding the intersection of the toroidal surface with a sphere of radius  $a$ . This is shown in Figure 2. It can be shown from eqn. (9) that  $\chi_1$  is given by

$\sin \chi_1 = \sqrt{2\gamma_1 a}$ , [  $a$  is measured in unit of length  $C = \sqrt{\frac{M}{HR}}$  ] or since the maximum value of  $\gamma_1$  is 1,

$$\sin \chi_1 = \sqrt{\frac{2a}{C}}, [ a \text{ measured in cms.} \dots (10) ]$$

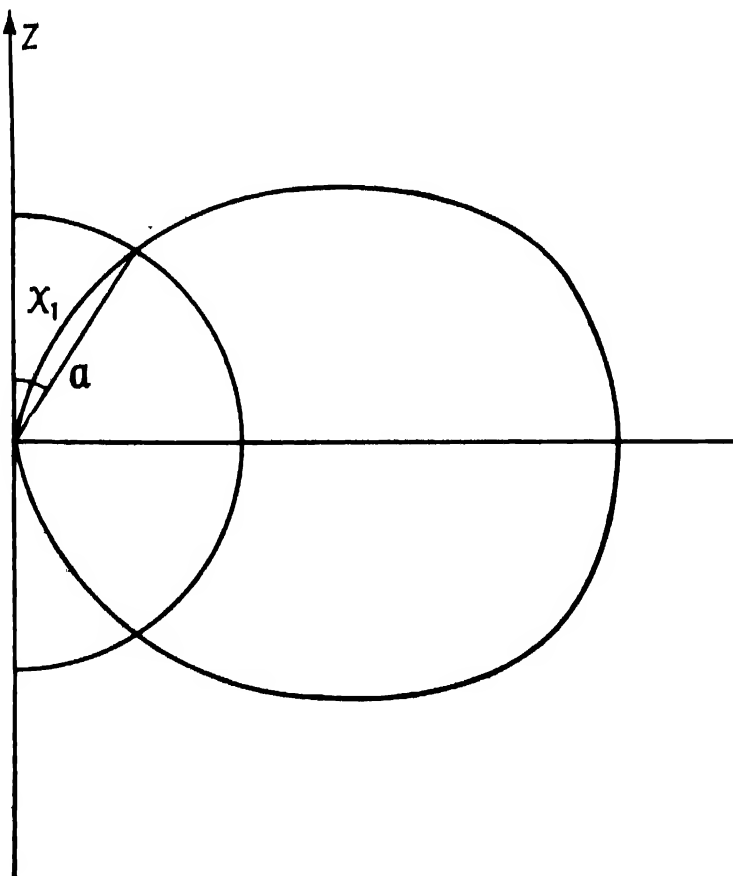


FIGURE 2

The case of charged particles escaping from the earth's atmosphere being exactly complementary to that of Störmer's, we can calculate the value of  $\chi_1$  giving the zone from which a charged particle having a given velocity  $v$  can escape from the earth's atmosphere to infinity. Table I is prepared following the above method, and shows that the velocity required by an ion of atomic oxygen to disentangle itself from the earth's magnetic field is much greater than that required for a neutral atom. Whereas the required velocity for a neutral particle is independent of the latitude, that for a charged particle is not so. The critical velocity increases with decreasing latitude.

TABLE I

Co-latitude $\chi_1$ (in degrees)	$HIR = \frac{m}{e} \cdot v$	$C = \sqrt{\frac{M}{HIR}}$ (cm.).	Velocity of escape (cm./sec.).
5°.5	$3.344 \times 10^3$	$1.585 \times 10^{11}$	$2 \times 10^6$
8°.3	$1.672 \times 10^4$	$7.087 \times 10^{10}$	$10^7$
14°.8	$1.672 \times 10^6$	$2.242 \times 10^{10}$	$10^8$
27°.2	$1.672 \times 10^6$	$7.087 \times 10^9$	$10^9$
54°.35	$1.672 \times 10^7$	$2.242 \times 10^9$	$10^{10}$
90°	$4.18 \times 10^7$	$1.418 \times 10^9$	$2.5 \times 10^{10}$

In calculating the rate of escape of molecules, particularly of light gases like hydrogen or helium, no account has hitherto been taken of the possibility of ionization of the atoms in the fringe region and their subsequent entanglement in the magnetic field. If this is taken into consideration, the rate of escape will be greatly diminished. The rate will also be different for different latitudes. To make an estimate of the actual rate of escape taking this process of ionization into account we require a precise knowledge of the "ionization probability" of the gaseous constituents of the atmosphere, the possible sources of particles possessing the requisite speed and their distribution at different levels. Lack of necessary data prevents us from attempting such quantitative calculation.

#### §5 ROTATION OF THE EARTH—VISCOSUS DRAG

An interesting point that is to be considered is the possibility of different layers of the atmosphere at different heights moving with different angular velocities on account of insufficient viscous drag. The expression for the coefficient of viscosity of a gas being  $\eta = \frac{1}{3} N m c \lambda$ , it would appear that the viscosity is independent of pressure. The above expression will, of course, hold as long as the gas

obeys gas kinetic laws,<sup>9</sup> i.e., as long as collisional frequency is appreciable. It may be noted here that in experimental investigations on the viscosity of a gas at low pressure, with laboratory apparatus, the coefficient of viscosity falls to a low value at low pressure. It may be shown, however,<sup>10</sup> that this is due to the size of the vessel becoming comparable with the mean free path of the gas molecules. As long as the size of the apparatus is large compared with the mean free path (as is the case for the atmosphere covering the earth), the coefficient of viscosity should remain independent of pressure. The effective drag of one layer of the gas upon the other depends not on the coefficient of viscosity alone but on the so-called coefficient of kinematical viscosity<sup>11,12</sup> which is defined as  $\frac{\eta}{\rho}$ . It would then appear that the drag of one layer upon another is actually greater in the high atmosphere than in the lower atmosphere. We give a curve (Figure 3) showing the relation between the change of kinematical viscosity with height from 100 km. level for the atmospheric distribution assumed above.

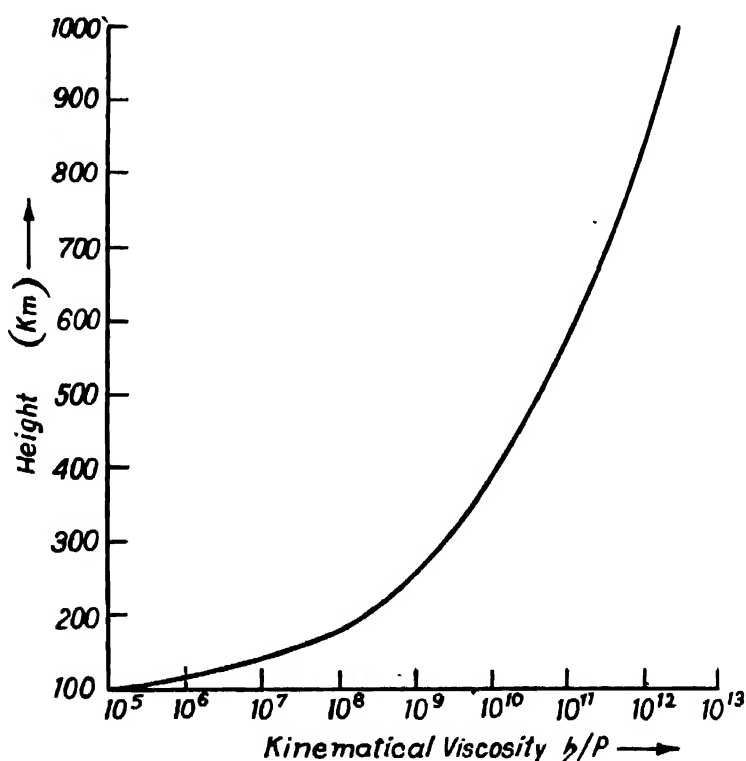


FIGURE 3

We are, therefore, justified in assuming that up to the limit of the outer atmosphere within which collisions are appreciable the air molecules participate in the

rotation of the earth. A molecule leaving the lower region from the level of escape and moving in the fringe region with the velocity acquired at the last collision, will, therefore, have a component of velocity in the direction of rotation of the earth. As a consequence of this the trajectory of such a molecule will experience a curvature opposite to the direction of rotation of the earth, i.e., the longitude at which the molecule will return to the atmosphere from the fringe region will be different from that at which it left the level of escape.

#### §6. FRINGE REGION OF THE ATMOSPHERE

We have already referred in §2 to the fringe or the spray region of the atmosphere where molecules move freely with the velocity acquired at the last collision in the lower region. Being subject only to the pull of gravity they describe parabolic, elliptic or hyperbolic paths according to the magnitude and direction of their velocity. It is evident from what has been said in §3 that the spray region begins from above the critical level. It is possible to calculate the average number of particles per c.c. between any two heights in the spray region from a knowledge of the density and the temperature round the level of escape. We proceed to carry out the calculation on the assumption that the level of escape begins from about 800 km., and that the molecular density and temperature here are  $3 \cdot 0 \times 10^5$ /c.c. and  $1000^\circ\text{K}$ . The atmospheric constituent, here, is practically wholly atomic oxygen.

TABLE II

Region ( $Z_2 - Z_1$ ) in km. above earth's surface.	Velocity (km./sec.).		Number crossing/cm. <sup>2</sup> of 1000 km. level.		Average density (Molecules per c.c.).
	$v_2$	$v_1$	$n_2$	$n_1$	
1250-1000	1.87	1.5	$7.8 \times 10^{12}$	$10^{13}$	$1.0 \times 10^5$
1500-1250	2.6	1.87	$4 \times 10^9$	$7.8 \times 10^9$	$3.0 \times 10^4$
1750-1500	3.15	2.6	$2.4 \times 10^8$	$4 \times 10^9$	$8.0 \times 10^3$
2000-1750	3.59	3.15	$1.38 \times 10^7$	$2.4 \times 10^8$	$4.5 \times 10^2$
2250-2000	3.95	3.59	$1.07 \times 10^6$	$1.38 \times 10^7$	$2.3 \times 10$
2500-2250	4.27	3.95	$9.2 \times 10^4$	$1.07 \times 10^6$	$2.0$
2750-2500	4.54	4.27	$9.9 \times 10^2$	$9.2 \times 10^4$	$1.0 \times 10^{-1}$
3000-2750	...	...	...	...	...

Assuming a Maxwellian distribution in the region of the level of escape and also taking the variation of 'g' with height into account Table II is prepared, giving the average molecular density at different levels of the region. The source of particles in the fringe region is assumed to be the molecules between 800-1000 km. level. The second column gives the range of velocity required to send the molecules flying within the region concerned;  $v_1$  is the initial velocity required to send the particle above the lower level of the zone and  $v_2$  above the upper level. The third column gives the number of particles per square cm. crossing the 1000 km. level,  $n_2$  corresponding to those that reach the upper level and  $n_1$  to the lower. The last column gives the average molecular density at different altitudes of the spray or fringe region beginning from 800 km.

#### EXTENSION OF THE FRINGE REGION BY SUPER-ELASTIC COLLISIONS

From Table II it will be seen that the molecular density in the spray region rapidly diminishes with increasing height and at 2500 km. from the earth's surface, the density falls to 1 molecule per c.c. which is the order of density in the inter-stellar space. According to Hulbert,<sup>2</sup> however, the spray region may extend to heights much beyond this, if it be assumed that a certain fraction of the molecules in the region of the level of escape acquire high velocity due to super-elastic collisions. There are, according to Hulbert,  $10^{16}$  molecules in a vertical column per sq. cm. in the fringe region (according to Hulbert the fringe region begins from 450 km. but as we have seen in §3 this should be from 770 km.). These  $10^{16}$  molecules suffer  $10^{11}$  collisions per sec. A fraction ( $10^{-8}$ ) of these is of the super-elastic kind which impart velocities of the order of 10 km./sec. to the neutral particles. Such particles rise to heights of 40,000-50,000 km. above the centre of the earth, in about 3 hours time. Hulbert utilizes these high-velocity particles for explaining the upper atmosphere phenomena like aurorae and magnetic storms. These he suggests are due to the high-flying particles getting ionized by the solar ultra-violet rays and reaching the higher latitudes by being entangled by the earth's magnetic field. We will in the following sections discuss in some detail the above-mentioned assumptions of Hulbert on which this attractive theory of magnetic storms and aurorae is based.

We will discuss the matter in two steps:—

1. Firstly, we will discuss the spectroscopic processes which in the region round the level of escape may lead to the production of high-velocity particles by super-elastic collisions and calculate the number of the high velocity particles produced per second thereby, and

2. Secondly, the motion of these particles, when ionized, in the magnetic field of the earth.

#### POSSIBLE SOURCES OF SUPER-ELASTIC COLLISIONS

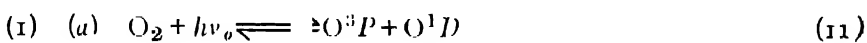
In the super-elastic type of collision, the encounter takes place between a neutral and an excited particle. The excited particle might give up whole or part of its energy to the neutral particle and the latter may thus acquire speed corresponding to the energy lost by the excited particle. In order to estimate the number and the speed of the high-velocity particles it is necessary first to study the nature of the excited particles. Now an ordinary excited atom or molecule has a spontaneous chance of coming down to a lower state of energy with emission of radiation. This chance is very high—in other words, the life of an atom in an excited state is very small. In fact both theoretical considerations and experimental results show that the life of an ordinarily excited atom is of the order of  $10^{-9}$  to  $10^{-10}$  sec. It is thus obvious that in order that the particle may lose its energy by collision instead of by spontaneous radiation, the average number of collisions per sec. must be of the same order as the inverse of the life of the excited atom. Now in the region of the atmosphere we are considering, the collisional frequency is much smaller than the inverse of the average life of ordinary excited atoms or molecules, that is, several orders less than  $10^8$  or  $10^9$ /sec. The excited particles which may possibly suffer super-elastic collisions cannot, therefore, be of the ordinary excited types, but must be of the metastable type for which the life is very much longer. We will thus have to enquire about the possible metastable states to which the atoms and molecules present in the outer atmosphere may be excited and which by superelastic collisions could produce high-speed neutral particles. The particles in the upper atmosphere which it is necessary to consider are N<sub>2</sub>, N and O. It is now definitely established<sup>13</sup> that molecular oxygen, as such, is not present in the high levels of the atmosphere owing to the dissociative action of the solar ultra-violet rays. Recent spectroscopic studies of the light of the night sky seem to show that N<sub>2</sub> is also dissociated, producing atomic nitrogen.<sup>14,15</sup> The extent to which this dissociation is effected and the relative proportions of N<sub>2</sub> and N have not yet been quantitatively worked out. We will consider below, in some detail, the metastable states of these three gases.

#### ATOMIC OXYGEN

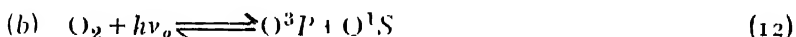
The presence of metastable oxygen atoms in the upper atmosphere in the <sup>1</sup>S and <sup>1</sup>D states is well established by spectroscopic evidence. The famous

green line  $\lambda 5577$  and the two red auroral lines  $\lambda 6300$  and  $\lambda 6363$  are due to the transitions  ${}^1S - {}^1D$  and  ${}^1D - {}^3P_{1,2}$ . The life of oxygen atom in these states ( ${}^1S$  and  ${}^1D$ ) has been found by wave-mechanical calculations by Condon<sup>16</sup> to be  $5$  and  $1.3 \times 10^2$  secs. respectively.

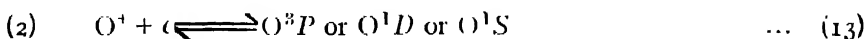
It may be interesting to discuss how oxygen atoms are brought to these metastable states. Chance of such transitions occurring by direct absorption is extremely small. It is sometimes suggested that though direct absorption may be inoperative, the atom may be brought to the metastable state through a roundabout process. According to A. K. Das,<sup>17</sup> the atom may be raised to a higher energy level by a direct absorption of radiation and then come down to a metastable state. A study of the energy-level diagram of oxygen atom shows, however, that there is no such higher energy level to which the atom may be raised from the ground-state and from which it may drop directly to a metastable state. It is possible, of course, to reach these metastable states by several steps, but obviously the number of atoms reaching the metastable states by this process will be extremely small. It seems that the most likely process by which the atom may be excited to metastable states are photo-dissociation and/or recombination of oxygen ions with electrons according to the following scheme :—



$$\lambda_o = 1750\text{\AA}$$



$$\lambda_o = 1325\text{\AA}$$



There is experimental evidence<sup>18</sup> that the first of the two absorption processes actually occurs. The second absorption process, though quite likely, has not yet been observed experimentally.

With regard to the recombination process it would appear that owing to the presence of ions in the outer region it is to be the most likely process of producing metastable oxygen atoms.

#### MOLÉCULAR NITROGEN

The existence of nitrogen molecules in the metastable state  $A^3\Sigma_g^+$  is evinced by the Vegard-Kaplan band systems observed in the light of the night sky. The transitions corresponding to these bands are given by  $A^3\Sigma_g^+ \rightarrow X^1\Sigma$  and are ordinarily forbidden.

The process by which  $N_2$  molecules attain the  $A^3\Sigma_g^+$  state is as follows: By direct absorption of solar ultra-violet radiation  $N_2$  molecules are raised to higher energy-levels (for instance  $X^1\Sigma \rightarrow a^1\pi_u$ ,  $X^1\Sigma \rightarrow b$ ,  $X^1\Sigma \rightarrow b$ ,  $X^1\Sigma \rightarrow c$ ,  $X^1\Sigma \rightarrow f$ ,  $X^1\Sigma \rightarrow g$ ,  $X^1\Sigma \rightarrow h$ ) and are finally ionized ( $X^1\Sigma \rightarrow \Lambda^1$ ).

$N_2$  ions combine with electrons to form  $D$ ,  $C^3\pi_u$ ,  $B\pi_g$ . These by spontaneous transition and emission of  $IV^{+ve}$ ,  $II^{+ve}$  and  $I^{+ve}$  bands drop to  $A^3\Sigma_g^+$  level. Being highly metastable it can give up its energy by collision or by spontaneous radiation in a region where the interval between collisions is much larger than the average life.

Active nitrogen<sup>19</sup> which is sometimes suggested as the source of metastable oxygen atoms may also produce high-speed particles by super-elastic collisions. Our knowledge of active nitrogen both as regards its nature and origin and also its possible presence in the upper atmosphere is extremely meagre. It is, therefore not possible to consider in detail the possible effect of active nitrogen on the production of high-speed particles.

#### ATOMIC NITROGEN

The following photo-dissociation processes may convert nitrogen molecules to nitrogen atoms:—



$$\lambda = 1273 \text{ \AA}$$



$$\lambda_o = 1124 \text{ \AA}.$$

No such continuous absorption corresponding to these processes has yet been observed in the laboratory for  $N_2$ . Only very recently spectroscopic evidence regarding the presence of atomic nitrogen in the metastable state has been adduced by the discovery of lines corresponding to the transitions  $^2D \rightarrow ^4S$ , and  $^2P \rightarrow ^4S$  in the night sky spectrum. The third forbidden line of atomic nitrogen lines is the infra-red and has not yet been investigated.

Nitrogen atoms in metastable states might be obtained by the above photo-dissociation processes or by the predissociation of nitrogen molecules in highly excited vibrational states, as has been suggested by Saha.<sup>20</sup>

In Table III are given the velocities and heights which may be attained by oxygen atoms and nitrogen molecules respectively if they suffer super-elastic collisions with  $O$ ,  $N$ , and  $N_2$  molecules in various metastable states.

TABLE III

Source.	Energy (in electron-volts).	Velocity (in km./sec.) imparted to		Height (in km.) attained (above earth's centre).	
		O	N <sub>2</sub>	O	N <sub>2</sub>
O	$^1D - ^3P$	2	4.89	3.7	9,500
	$^1S - ^3P$	4.2	7.09	5.36	14,000
N	$^3P - ^2D$	1.19	3.77	2.85	8,500
	$^2D - ^4S$	2.37	5.96	4.03	10,000
N <sub>2</sub>	$^2P - ^4S$	3.56	6.53	4.93	12,000
	$N_2 A^3\Sigma_u^- \rightarrow N^1\Sigma_g^+$	6.15	8.58	6.10	23,000
	Active N <sub>2</sub> $\rightarrow N^1\Sigma_g^+$	9.71	10.79	8.13	37,000
					19,000

Of the various metastable states shown in Table III the highest energies for super-elastic collision are given by the metastable  $A^3\Sigma_u^+$  state of N<sub>2</sub> and also by the active nitrogen. But since N<sub>2</sub> is confined more or less below the region of escape owing to diffusive separation, particles suffering super-elastic collisions with such N<sub>2</sub> molecules will not be able to attain great heights. The metastable states of atomic oxygen seem, therefore, to be the most probable sources of the high-speed particles of Hulbert. Atomic nitrogen if it exists can be expected to reach the highest levels on account of its being lighter than atomic oxygen and will undoubtedly lie above the level of escape. But it will be seen from Table III that the energy of its metastable states is on the whole smaller than the  $^1S - ^3P$  energy of atomic oxygen. In order, therefore, to estimate the number of particles shot up by super-elastic collisions, it will suffice to calculate the number of oxygen atoms in the  $^1S$  state. This we proceed to do below.

#### CALCULATION OF THE NUMBER OF METASTABLE OXYGEN ATOMS

Since the most likely process by which oxygen atoms may be excited to the  $^1S$  state is that of recombination of negative oxygen ions with electrons as shown in equation (13), we will have to calculate, in the first instance, the number of O-ions produced per sec. in a column of 1 sq. cm. cross-section above 770 km., i.e., above the level of escape.

The number of ions produced per second in a column of 1 sq. cm. cross-section above 770 km. level may be calculated, making the simplifying assumption that the ionizing radiation is very little diminished in intensity by the slight

absorption it suffers in its passage through the spray region. (This is consistent with the picture of the spray region given before, namely, that above the critical level there is very little screening of one atom by another.) Thus the number of ions produced per second, in the column, is given by

$$q = N \int_{v_0}^{\infty} I(v)_0 \psi(v) dv \quad \dots \quad (14)$$

where  $N$  = total number of atoms in the column ;

$I(v)_0$  = intensity of the ionising radiation outside the earth's atmosphere ;

$\psi(v)$  = ionization probability =  $\frac{\tau(v)}{hv}$  where  $\tau(v)$  = absorption per atom.

Assuming the sun to be radiating like a black body at a temperature  $T_s$ ,

$$I(v)_0 = \frac{8\pi\beta h v^3}{c^2} e^{-\frac{hv}{kT_s}}$$

where  $4\pi\beta$  is the solid angle subtended by the sun at the earth. Thus

$$q = N \cdot \frac{8\pi\beta}{c^2} \int_{v_0}^{\infty} v^2 e^{-\frac{hv}{kT_s}} \tau(v) dv$$

which comes to

$$q = N \cdot \frac{8\pi\beta \tau_0 v_0^2 k T_s}{c^2 h} e^{-\frac{hv_0}{kT_s}}$$

where  $\tau_0$  corresponds to the threshold frequency  $v_0$ .

Taking the value for  $\tau_0$  as given by Saha and Rai <sup>21</sup> ( $2.81 \times 10^{-17}$ ) we get the number of oxygen ions formed per second in the column to be given by

$$q = 5.667 \times 10^8.$$

If Chapman's <sup>22</sup> value for  $\tau_0 (3.5 \times 10^{-16})$  is taken, then

$$q = 5.043 \times 10^9.$$

Thus we find that about  $5.7 \times 10^8$  to  $5 \times 10^9$  atoms out of the total  $10^{16}$  atoms are ionized per second.

Next we will find how many of these ionized atoms recombine per second to form neutral atoms in the excited  ${}^1S$  state. This number is given by

$$q = q_+ q_- \alpha \quad \dots \quad (15)$$

where  $q_+$  = number of positive ions ;

$q_-$  = number of electrons ;

$\alpha$  = recombination coefficient for capture in the excited  ${}^1S$  state.

In the absence of any experimental value for the coefficient of recombination, we have to fall back upon theoretical value. The recombination coefficient is given by

$$\alpha = q(n, l) \sqrt{\frac{2eV}{m}} \quad \dots \quad (16)$$

where  $e.V$  = the energy of the recombining electron and  $q(n, l)$  is cross-section for electron capture in the particular orbit and is given by

$$q(n, l) = \frac{A(n, l) \times 10^{-20} \cdot Z^2}{V} \quad \dots \quad (17)$$

$Z$  is the effective atomic number and  $A(n, l)$  a factor depending on the orbit in which the electron is captured.

We take the value of  $A(n, l)$  for the  ${}^1S$  state from the theoretical curves given by Morse and Stueckelberg.<sup>23</sup> Thus for a temperature of  $1000^\circ K$ ,  $V = 13 e.v.$  and we have, taking  $Z=3$ ,

$$q(n, l) = \frac{0.35 \times 10^{-20}}{13} \cdot 3^2$$

and consequently

$$\alpha = 4.969 \times 10^{-13}.$$

Thus the number of ions recombining per sec. in the  ${}^1S$  state is given by

$$\begin{aligned} q &= [5.7 \times 10^8]^2 \times 4.969 \times 10^{-13} \\ &= 1.6 \times 10^5, \text{ taking } q=5.7 \times 10^8 \\ \text{or} \quad &= [5.04 \times 10^9]^2 \times 4.696 \times 10^{-13} \\ &= 1.3 \times 10^7, \text{ taking } q=5.04 \times 10^9. \end{aligned}$$

#### AVERAGE MOLECULAR DENSITY IN THE FRINGE REGION

We next consider how many of these  $10^5$  to  $10^7$  atoms suffer super-elastic collisions per sec. The mean free-path of an atom round the 800 km. level or so is on the average about 150 km. The thermal velocity corresponding to  $1000^\circ K$  is about 2 km./sec. So that in the region between 770 km. and 930 km. an atom suffers one encounter in about 75 secs. The life of the atom in the  ${}^1S$  state being .5 sec., one atom only out of 150 suffers an encounter per sec. On an average, therefore,  $10^3$  to  $10^5$  atoms per sec. receive high velocity due to super-elastic collisions. Roughly we can take that about  $10^4$  atoms are shot up per sec. per sq. cm. in the spray region. Considering now the oxygen atoms in  ${}^1D$  state we find that only  $10^3$  to  $10^5$  atoms out of the  $10^5$  to  $10^7$  atoms in the  ${}^1S$  state suffer super-elastic collisions per sec. in the column above 770 km. level. Thus most of the atoms in the  ${}^1S$  state come down to the  ${}^1D$  state by

emitting the green line. The life in the  ${}^1D$  state being much longer ( $10^2$  secs.) these atoms come down to the ground state by super-elastic collisions. Thus it may be taken that roughly  $10^6$  atoms with  $4.89$  km./sec. velocity ( ${}^1D - {}^3P$ ) and  $10^4$  atoms with  $7.09$  km./sec. velocity are shot out per sec. through each sq. cm. area of  $1000$  km. level. We have to see, therefore, how the density distribution in the spray region is modified by these high-flying atoms reaching  $8500$  and  $14000$  km. respectively. Table IV is prepared after the method followed in preparing Table II and depicts how the super-elastic collisions affect the merging of the atmosphere with the inter-stellar space. This occurs at a distance somewhat greater from the centre of the earth than when the effects of super-elastic collisions are not considered.

TABLE IV

Region ( $Z_2 - Z_1$ ) in kms. above earth's surface.	Number crossing per cm. <sup>2</sup> of datum level at $Z = 1000$ km.	Average density (Molecules per c.c.)
1750-1500	$4 \times 10^9$	$8.0 \times 10^3$
2000-1750	$2.4 \times 10^8$	$4.5 \times 10^2$
2250-2000	$1.48 \times 10^7$	25
2500-2250	$2.07 \times 10^6$	5
3000-2500	$1 \times 10^6$	3
4000-3000	$10^4$	$10^{-1}$

## PART II. THE ULTRA-VIOLET THEORY OF AURORAE AND MAGNETIC STORMS

### § I. INTRODUCTION

In Part I we have calculated the number of atoms which are shot up across the level of escape and which ultimately contribute to the formation of the spray region. We have not considered the effect of ionization of these particles which would undoubtedly occur by the absorption of the ultra-violet radiation of the sun. As mentioned in the introduction the ionized particles will in general proceed polewards and might contribute to the production of aurorae and magnetic storms.<sup>2</sup> We now proceed to consider these phenomena in some detail.

We have seen that  $10^6$  oxygen atoms with velocity of  $5.0$  km./sec. and  $10^4$  atoms with velocity of  $7.0$  km./sec. will be shot across every sq. cm. surface from the region of escape into the outer atmosphere. In the absence of any other physical process, these high-speed atoms will attain heights of  $8500$  km. and  $14000$  km. respectively from the centre of the earth. The super-elastic collisions will thus extend the spray region to about  $14000$  km.

We will now consider the effect of ionizing solar radiation. Such ionization by the incident solar ultra-violet radiation will profoundly modify the motion and distribution of the high-flying particles. The magnetic field of the earth will cause the ionized particles to spiral round the magnetic lines of force and lead them towards the polar regions of the earth. We discuss first in some detail the path of a charged particle when it is subject simultaneously to the influence of the terrestrial magnetic field and also to the pull of gravity.

## §2. MOTION OF IONS IN GRAVITATIONAL-MAGNETIC FIELD

Let us consider the simple case of an ion moving in a constant magnetic field  $H$  with velocity  $v_0$ . If the velocity  $v_0$  be in a direction making an angle  $\theta$  with the magnetic line of force, it will have components  $v_0 \cos \theta$  and  $v_0 \sin \theta$  along and at right angles to the magnetic line of force. The component along the magnetic line of force will remain unaffected by the magnetic field but the component at right angles to the field will make the ion spiral round the magnetic line of force. Let the component at right angles to the magnetic field be denoted by  $v$ ; then the equation of motion of the ion is

$$m \cdot \frac{dv}{dt} = \frac{e[v \times H]}{c}, \quad \dots \quad (18)$$

The motion described by (18) is the motion with constant velocity  $v$  in a circle of radius  $R$  given by

$$R = \frac{mc}{He} \cdot v. \quad \dots \quad (19)$$

The angular velocity in the circular path is

$$\omega = - \frac{eH}{mc}. \quad \dots \quad (20)$$

Thus component  $v_0 \sin \theta (=v)$  of the ion makes it move in a helical path of radius  $R \left( = \frac{mc}{He} \cdot v \right)$  while the component  $v_0 \cos \theta$  simply leads the ion along the magnetic line of force.

Let us now consider the additional effect due to the presence of the gravitational field on the ion paths.<sup>24</sup> The force equation in this case becomes

$$m \frac{dv}{dt} = F + \frac{e[v \times H]}{c} \quad \dots \quad (21)$$

where  $F = mg$  is the force due to pull of gravity.

To transform eqn. (21) in the form of eqn. (18) we suppose a velocity  $u_g = \frac{c[F \times H]}{eH^2} = c \cdot \frac{mg}{eH}$  to be imparted to the ion. The velocity of the ion is now given by  $V = (v - u_g)$  and eqn. (21) may be written

$$m \frac{dV}{dt} = e[V \times H]$$

and consequently

$$\begin{aligned} R &= \frac{mc}{He} \cdot V \\ &= \frac{mc}{He} (\overset{\rightarrow}{v}^2 - 2u_g v + \overset{\rightarrow}{u_g}^2)^{\frac{1}{2}}. \end{aligned}$$

Thus the effect of the force  $F = mg$  is firstly to change the radius of the circular path  $R$  from  $\frac{mc}{He} \cdot v$  to  $\frac{mc}{He} (\overset{\rightarrow}{v}^2 - 2u_g v + \overset{\rightarrow}{u_g}^2)^{\frac{1}{2}}$  and secondly to make the helical path advance in a direction at right angles both to  $g$  and to  $H$  with a velocity  $u_g = \frac{mg}{He} \cdot c$ .

It is easy to see, therefore, that the atoms as soon as they are ionized in the spray region will, owing to the component of velocity at right angles to the magnetic field, begin to trace cycloidal paths, *i.e.*, they will spiral round the magnetic lines of force and have at the same time a drift towards the east for positive ions and towards the west for electrons and negative ions. The ions and electrons will be led at the same time by the component of velocity along the line of force towards the north pole or south pole according to the direction of motion at the time of ionization.

### §3. EFFECT OF VARIATION OF $g$ AND $H$ ON ION PATHS

In calculating the helical paths of ions and electrons in the fringe region, we have not taken into account the variation of  $g$  and  $H$  with altitude. These variations will affect three things : (a) the radius of curvature of the cycloidal path of the ion,  $R$  ( $= \frac{mc}{He} \cdot V$ ), (b) the angular velocity of rotation in the cycloidal path  $\omega$  ( $= - \frac{eH}{mc}$ ) and (c) the gravitational-magnetic drift velocity  $u_g$  ( $= c \cdot \frac{mg}{He}$ ).

(a) As the ion descends downwards H increases continually inversely as the cube of the distance of the point under consideration from the centre of the earth. The radius of curvature of the ion path thus decreases continually downwards.

(b) As H increases downwards, the angular velocity of rotation will increase in the same rate as that of (a).

(c) Since  $g$  varies inversely as the square and H inversely as the cube of distance from the centre of the earth and since these are in the numerator and denominator respectively in the expression for the drift velocity, the drift velocity will decrease owing to the relatively greater increase of H.

Simply stated the above results mean that as the ion comes downwards, the pitch of the helical path becomes smaller and smaller, the rotation in the orbit becomes faster and faster and the helical path tends more and more to be confined to one particular line of force. We give below a Table showing the variation of R,  $\omega$ ,  $u_d$  for a typical case. [V=1 km./sec.,  $m=16 \times 1.062 \times 10^{-24}$  gm.]

TABLE V

Height above earth surface Z (in km.).	$g$ (cm./sec. <sup>2</sup> ).	H (Gauss)	R (cm.).	$\omega$ (radian/sec.).	$u_d$ (cm./sec.).
1,000	732.6	.37	$4.48 \times 10^2$	$2.43 \times 10^2$	3.28
2,000	568	.253	$6.56 \times 10^2$	$1.52 \times 10^2$	3.73
3,000	452	.174	$9.52 \times 10^2$	$1.05 \times 10^2$	4.31
4,000	370	.128	$1.3 \times 10^3$	$7.7 \times 10^1$	4.81
5,000	308	.095	$1.74 \times 10^3$	$5.74 \times 10^1$	5.36
10,000	148.6	.0286	$5.8 \times 10^3$	$1.72 \times 10^1$	8.64
20,000	57.3	.0054	$3.1 \times 10^4$	3.23	17.74
40,000	18.6	.0007	$2.29 \times 10^5$	.43	39.06

Figures 4, 5 and 6 are drawn showing the variation of R,  $\omega$  and  $u_d$  with height as the ion comes downwards.

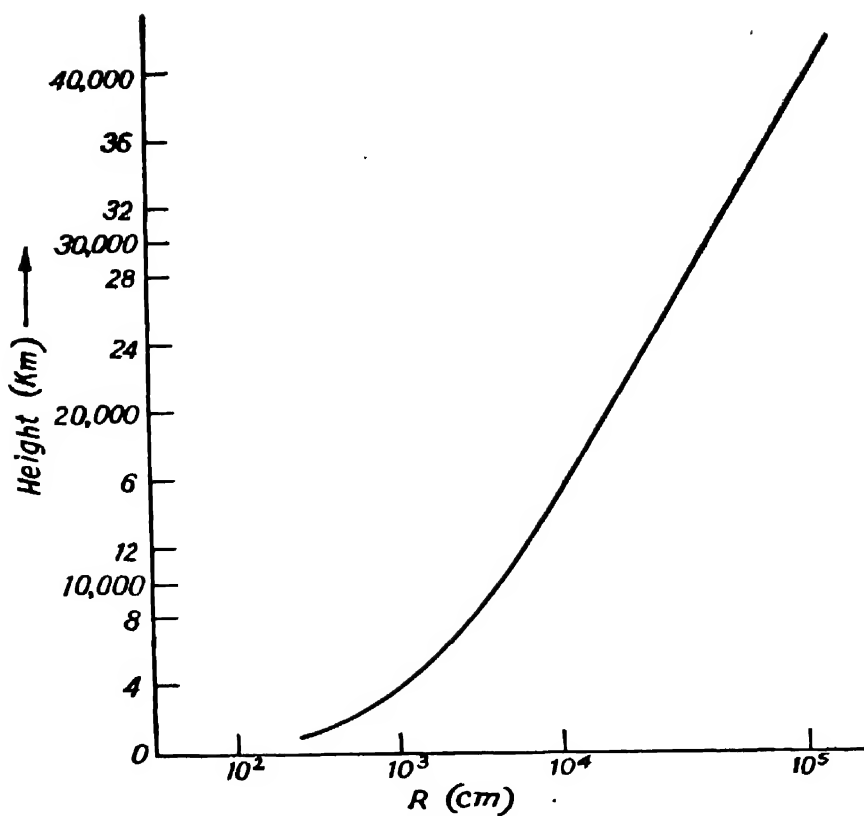


FIGURE 4

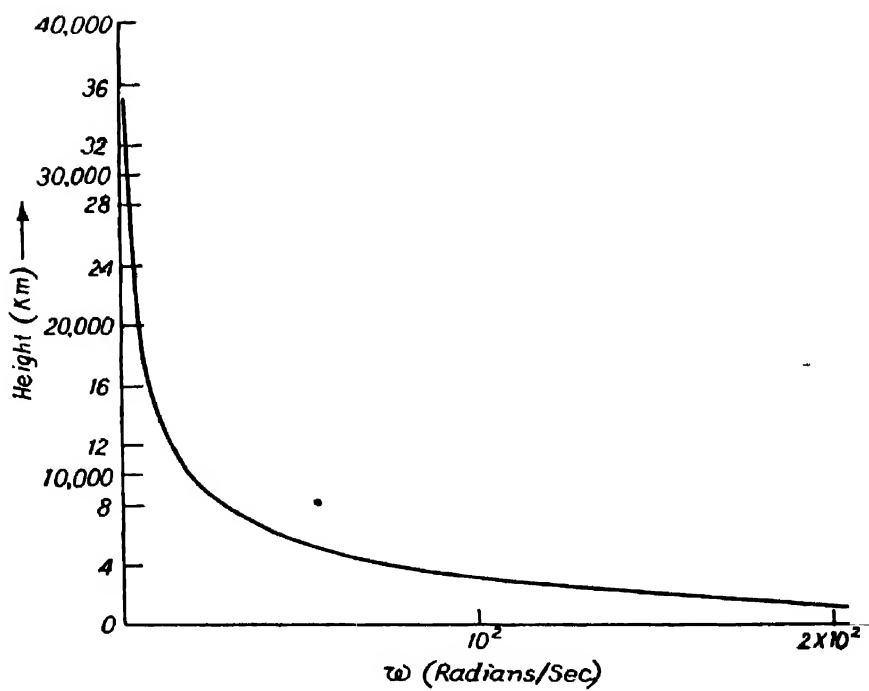


FIGURE 5

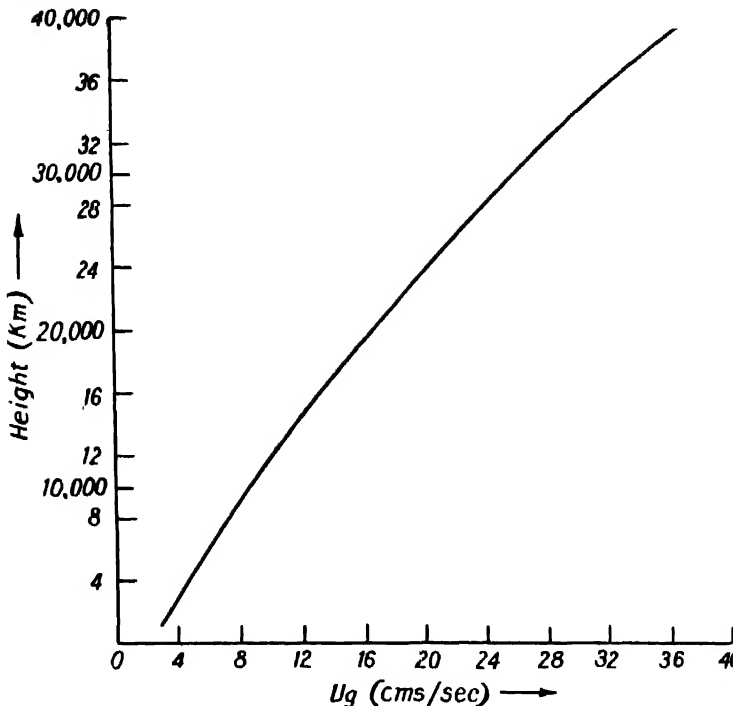


FIGURE 6

#### §4. ROTATION OF THE EARTH MAGNET-TIME OF ARRIVAL OF THE IONS IN HIGH LATITUDES

In the above discussion, the tacit assumption has been made that the earth is not rotating. If, however, the earth's rotation is taken into account, then the motion of the lines of force causes certain complications in the motion of the ion, which we will now consider. It is obvious in the first place that uncharged particles will not participate in the peripheral motion of the earth's atmosphere because by our assumption the particles in the "spray" are moving in the region of no collision and their motion is determined only by the initial velocities acquired by them during the last super-elastic collision. This is not so for charged particles, that is, for ions and electrons. Such particles in their cycloidal motion round the magnetic lines of force will be subject to the electric force which is developed due to the motion of the magnetic lines of force of the rotating earth magnet. In order to determine how the motion will be affected, we start with the well-known Lorentz equation

$$E = [v \times H] \quad (22)$$

where  $E$  is the electric field generated by the motion of the magnetic field  $H$  with velocity  $v$ .

Since the earth may be regarded as a magnet rotating round its axis (neglecting the inclination of the geographical to the magnetic axis) at any point above the surface of the earth, there will be developed an electric field of intensity given by the above equation. It may be shown, after Swann,<sup>25</sup> that the rotation of the earth-magnet attributes an electric polarisation  $P = \frac{[(\Omega \times r) \times I]}{c}$  to it. For points outside the earth's surface, this gives rise to an electric field having components<sup>26</sup>

$$\left. \begin{aligned} E_r &= \frac{M\Omega}{4\pi c a^2} \cdot \frac{a^4}{r^4} (1 - 3 \cos^2 \theta) \\ E_\theta &= -\frac{2M\Omega}{4\pi c a^2} \cdot \frac{a^4}{r^4} \sin \theta \cos \theta \end{aligned} \right\} \quad \dots \quad (23)$$

where  $\theta$  is the angle made by  $r$  with the axis of the earth, and obviously the magnetic field has components

$$\left. \begin{aligned} H_r &= \frac{2M}{4\pi r^3} \cdot \cos \theta \\ H_\theta &= \frac{M}{4\pi r^3} \cdot \sin \theta \end{aligned} \right\}. \quad \dots \quad (24)$$

The motion of the ion in this crossed electro-magnetic field will, therefore, impart a drift velocity to the ion given by

$$\begin{aligned} v' &= c [E \times H] \\ &= (\Omega r) \frac{\vec{a}^2}{r^2} \frac{1 + \cos^2 \theta}{1 + 3\cos^2 \theta}. \end{aligned} \quad \dots \quad (25)$$

Eqn. (25) shows that when  $r \gg a$ ,  $v' \approx 0$  and for  $r = a$ , and  $\theta = 90^\circ$ ,  $v' = \Omega a$ , i.e., rotational velocity of the earth. In other words, an ion at a distance of several earth-radii from the earth will move spiralling round the magnetic line of force of a nearly stationary earth, but as it descends, it will gradually experience a drag as if it is beginning to participate in the earth's rotation. This drift velocity will have an important effect on the final position of the arrival of the ion near the surface of the earth. If the ion participated in the full velocity of the rotation of the earth, then the ion could have glided down a particular line of force and would have arrived at the meridian on which the line of force in question strikes the earth. If, however, we assume that the ion is not participating in the rotation of the earth, then the particle would arrive at a meridian  $\Phi = \left( \frac{360 \times t}{24 \times 60 \times 60} \right)^\circ$  west of the meridian at which the line

of force strikes a non-rotating earth. If, however, the ion participates only partly in the peripheral velocity of the earth, then it will arrive at a meridian which is intermediate between the above two. It is easy to calculate the amount of the shift, *i.e.*, to calculate at what local hour an ion would arrive at the surface of the earth if we know the hour at which it was ionized and also its speed at the moment of ionization

The eastward velocity experienced by an ion at a distance  $r$  from the earth's centre due to the rotation of the earth magnet is

$$(\Omega_1) \frac{a^2}{r^2} \frac{1 + \cos^2 \theta}{1 + 3\cos^2 \theta}$$

so that the angular velocity at the point under consideration is

$$\Omega_1 \frac{a^2}{r^2} \frac{1 + \cos^2 \theta}{1 + 3\cos^2 \theta}$$

Obviously this angular velocity varies at each point of the downward course of the ion as  $r$  changes, so that the total angle turned through is

$$\int_{t_1}^{t_2} \frac{\Omega u^2}{r^2} \frac{1 + \cos^2 \theta}{1 + 3\cos^2 \theta} \cdot dt = \int_{s_1}^{s_2} \frac{\Omega u^2}{r^2} \frac{1 + \cos^2 \theta}{1 + 3\cos^2 \theta} \frac{ds}{v}, \quad \dots \quad (26)$$

where  $(t_2 - t_1)$  is the time of descent along the magnetic line of force, and  $v$  is the velocity along the magnetic line of forces. Knowing the equation of a magnetic line of force

$$\frac{\sin^2 \theta}{\sin^2 \theta_o} = \frac{a}{r}$$

the above integration can be performed graphically.

$\Phi$ , the total angle turned through, being known, it is easy to calculate at what local hour the ion will return to the earth's atmosphere. This is given by

$$t = \frac{24 \times 60 \times 60}{360^\circ} \times \Phi^\circ \text{ secs.}$$

It is found by calculation that an atom ionized at 12 o'clock at 40,000 km. at equator and descending along the magnetic line of force with 1 km./sec. velocity will return to the atmosphere at about 12-54 local hour, *i.e.*, about 54 minutes behind. If the atom be ionized at 1,000 km. it will reach the top of the atmosphere at about 12-30 P.M.

## THE AVERAGE PATH OF AN ION

We may now discuss the nature of the average path followed by an ion as it proceeds from the equator to higher latitudes due to the combined effect of the following velocities :

(1) Velocity along the magnetic line of force of magnitude  $v$ .

(2) Gravitational-magnetic drift velocity  $u_g$  at right angles to  $g$  and  $H$  of

magnitude  $\frac{mg}{Hc} \cdot c$  (opposite direction for electrons).

(3) Velocity  $v'$  due to rotation effect of the earth-magnet of magnitude

$$\Omega \cdot \frac{a^2}{r} \cdot \frac{1 + \cos^2 \theta}{1 + 3\cos^2 \theta} \text{ in the direction of rotation}$$

where  $r$ =distance from the centre of the earth;

$\theta$ =angle made by  $r$  with the axis of the earth;

$g$ =acceleration due to gravity at the point under consideration;

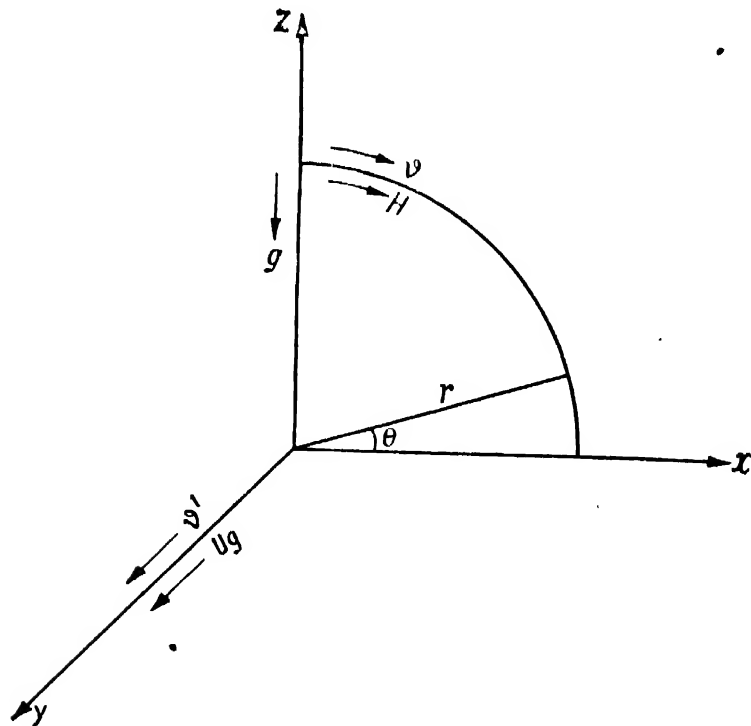


FIGURE 7

$a$ =radius of the earth ;

$H$ =magnetic field of the earth at the point under consideration;

$\Omega$ =angular velocity of the rotation of the earth.

(The component velocities are shown in Figure 7.)

The velocity  $v$  has components  $v \sin \theta$  and  $-v \cos \theta$  along  $x$  and  $z$  axes respectively. Thus the velocity components for an ion are

$$\left. \begin{aligned} \dot{x} &= v \sin \theta \\ \dot{y} &= c \frac{mg_o}{eH_o a} \frac{r}{1 + \cos^2 \theta} + \Omega \frac{a^2}{r} \frac{1 + \cos^2 \theta}{1 + 3\cos^2 \theta} \\ \dot{z} &= -v \cos \theta \end{aligned} \right\} \quad \dots \quad (27)$$

$$\therefore g = g_o \frac{a^2}{r^2}$$

$$H = H_o \frac{a^3}{r^3} (1 + \cos^2 \theta)$$

or the velocity of the ion at the point under consideration is

$$\begin{aligned} V &= (\dot{x}^2 + \dot{y}^2 + \dot{z}^2)^{\frac{1}{2}} \\ &= \left[ v^2 + \left\{ c \frac{mg_o}{eH_o a} \frac{r}{1 + \cos^2 \theta} + \Omega \frac{a^2}{r} \frac{1 + \cos^2 \theta}{1 + 3\cos^2 \theta} \right\}^2 \right]^{\frac{1}{2}} \quad \dots \quad (28) \end{aligned}$$

In the above expression,  $v$  is constant for all altitudes and of the other two terms

$c \frac{mg_o}{eH_o a} \frac{r}{1 + \cos^2 \theta}$  and  $\Omega \frac{a^2}{r} \frac{1 + \cos^2 \theta}{1 + 3\cos^2 \theta}$  the former represents the effect of the

gravitational-magnetic drift velocity and the latter that of rotation of the earth-magnet. When  $r$  is very much larger than  $a$ , the second term becomes very small, in other words, the rotation of the magnetic field is negligible. If  $r$  is comparable with  $a$ , the second term becomes much greater than the first and the effect of rotation of the magnetic field begins to be appreciable. Thus at very high altitudes the ions will proceed along a magnetic line of force due as it were to a non-rotating earth, as the ions come to lower levels it begins to participate in the lateral motion of the lines of force and are carried with them in the direction of rotation of the earth.

Now the range of heights under consideration does not exceed 7 or 8 times the radius of the earth. It is easily seen that within this height the second term is always much greater than the first. In fact as we come downwards from

higher levels, the second term rapidly increases in value while the first term becomes small in comparison with the second. This means that the ions have always a tendency to participate in the transverse motion of the earth. This tendency increases as the ions come down and at heights of a few hundred kilometres from the earth the electrons and ions move with the earth as if they form a part of the outer atmosphere.

#### §5 THE ULTRA-VIOLET LIGHT THEORY OF AURORAE AND MAGNETIC DISTURBANCES

In the preceding sections we have studied the state of affairs at the farthest limits of the atmosphere on the basis of our most recent knowledge of the constituents and temperature of the upper atmosphere. We have found that the fringe region or region of free flight of the atmospheric particles begins from a height of about 800 km. from the earth's surface. Obviously the lightest constituent of the gases of the upper atmosphere will predominate in number in the fringe region. Hydrogen and helium being absent, as is now believed, the fringe will contain oxygen in the atomic state. The question of dissociation of nitrogen in the upper atmosphere is not yet definitely settled. We will now see how the present study enables one to test quantitatively the current ultra-violet light theory of aurorae and magnetic storms.

Firstly, we have seen that the highest energy available by a super-elastic collision is only 4·2 electron volts which can impart a velocity of about 7 km.-sec. to an oxygen atom. This velocity enables a particle to attain a height of about 14,000 km. above the earth's centre. We do not, therefore, find particles speedy enough to reach a height of 40,000 km. or so, as is demanded by the ultra-violet light theory to account for the maximum frequency of occurrence of aurorae at 67° latitude.

A remarkable feature of the auroral spectrum is that the intensity of the green line of oxygen and the negative bands of nitrogen are of the same order whereas in the spectrum of the night sky the nitrogen bands are very feeble. The ultra-violet light theory attempts to give an explanation of this on the supposition that neutral nitrogen molecules from the equatorial region are transported to high levels in the fringe region and by being ionized are thence guided to the polar regions; unfortunately, however, nitrogen, if it exists in the molecular state, will be confined far below the level of escape and will have, therefore, little chance of being transported from the equatorial to the polar region.

The number of high-speed particles thus crossing each sq. cm. area of the top of the atmosphere at the equatorial region and again entering the atmosphere at the polar region, as calculated in the present paper, is only  $10^4$

at the maximum; this is less by about three orders than the number assumed in the ultra-violet light theory of Hulbert.<sup>2</sup>

Coming now to the question of ionization of high-flying particles in the fringe region, here too we find some difficulty. The time for such a high-flying atom to get ionized by the ultra-violet rays of the sun is given by

$$t = \frac{E}{I_o(1 - e^{-\tau_0})} \quad (29)$$

where  $E$  = Energy required to ionize the atom;

$I_o$  = Intensity of ionizing solar ultra-violet radiation;

$\tau_0$  = Atomic absorption co-efficient.

We have as yet no experimental value of  $\tau_0$  for the process  $O^3P \rightarrow O^4S$  but taking the theoretical value of Saha and Rai,  $\tau_0 = 2.81 \times 10^{17}$ , we find it to be much less than the average value ( $3 \times 10^{11}$ ) assumed by Hulbert and Maris. The intensity of ultra-violet solar radiation within the limits  $\lambda = 912\text{\AA}$  to  $\lambda = 0$ , assuming the sun to be a black body radiator even in the ultra-violet portion is about  $6.6 \times 10^{-2}$  erg-sec.-cm.<sup>2</sup>. It can easily be calculated that the time required for an oxygen atom to be ionized is about  $3 \times 10^2$  hours. This is about a thousand times greater than the time of ionization as calculated by Hulbert. In other words, this would lead us to the conclusion that the oxygen atoms in their path in the fringe region have very little chance of being ionized. We may mention here, however, that all such calculations cannot be regarded as final since the extreme ultra-violet portion of the solar spectrum departs widely from that of a black-body radiator at  $6800^\circ\text{K}$  and is most probably of the nature of line emission.

McNish<sup>27</sup> in a recent paper has pointed out that on three occasions bright solar eruptions were not accompanied by magnetic storms and regards this as irreconcilable with the ultra-violet light theory. This argument against ultra-violet light theory requires, however, careful re-examination since the bright solar eruptions due to the intensification of a particular line does not necessarily mean enhancement of the ionizing radiation required to ionize the particles in the fringe region.

#### §6. SUMMARY AND CONCLUSION

The discussion and the analysis given in the previous sections show that the atmosphere may extend up to great heights if its fringe or the spray region is taken into account. The spray region begins from a level at which the molecules begin to experience negligible collision with one another. If, as is now usually believed, the higher regions of the atmosphere consist of atomic oxygen and is at a high temperature ( $1000^\circ\text{K}$ ), then it is found that the transition from the region

of collision to region of no collisions will occur between heights 770 km. and 930 km. The oxygen atoms escaping from this region and describing orbits—elliptic, hyperbolic or parabolic—round the earth will, in the absence of any disturbing effect, form the spray region of the earth's atmosphere. (The atoms with hyperbolic orbits will, of course, escape altogether from the earth's atmosphere.) The average density of atoms in the spray region will rapidly diminish with increasing height and its value will approach that of the interstellar space, viz., about one particle per c.c. at a height of 3000 km. from the surface of the earth.

If account is taken of super-elastic collisions which some of the atoms might suffer in the region of escape (770-930 km.) due to atoms or molecules in this region being excited to metastable states by the incident solar radiation, then the spray region is found to extend to the height of 14,000 km.

These results are at variance with the supposition which Hulbert makes for explaining aurora and magnetic storms. According to Hulbert super-elastic collisions might drive particles to heights of about 42,000 km. A critical examination of the possible modes of super-elastic collisions, in the light of the available spectroscopic knowledge, does not warrant the existence of particles speedy enough to reach such enormous heights.

We have seen that, in the highly rarefied atmosphere we are considering, only those atoms which can remain in the excited states for a sufficiently long time (*i.e.*, atoms and molecules in the metastable states) can have a chance of imparting high velocities to other particles. The metastable states which can effect this are the  $^1S$  for oxygen atom and the  $\Lambda^3\Sigma^+$  state of the nitrogen molecules. The energies of these states are, however, 4.2 ev and 6.15 ev and the velocity imparted by them to an oxygen atom are 7.1 km./sec. and 8.6 km./sec. respectively. Hulbert's particles reaching 42,000 km. height must receive sufficient energy to attain velocity of the order of 10 km./sec. (Note—At great altitudes a small excess of velocity takes the particle a long way up since  $g$  is very small at high levels.) Our present spectroscopic knowledge of the upper atmosphere does not indicate any source of metastable atoms with such high energy.

If the ionization of the particles thrown up by super-elastic collisions is taken into account, it is found that the ions will be entangled in the magnetic field of the earth and the combined action of the gravity and the magnetic field will lead them along magnetic lines of force from the equatorial to higher latitudes. Here again the average time ( $3 \times 10^3$  hours) taken for ionization of the particles calculated from the theoretical value of the absorption coefficient of atomic oxygen ( $\tau_0 = 2.81 \times 10^{-17}$  for the ionizing wavelength) is found to differ widely from that assumed by Hulbert.<sup>2</sup> Hulbert's particles are assumed to take about 3 hours for ionization while the calculation referred to above yields results which are about three orders higher than Hulbert's value. In order that Hulbert's hypothesis of

the production of aurorae and magnetic storms by the import of ions transferred from low to high latitudes be applicable, it is necessary to have atoms or molecules with absorption coefficients at least three orders higher than that of atomic oxygen and/or to have the ionizing radiation in the portion of the solar spectrum under consideration greater by the same amount than that calculated from black-body solar radiation.

In connection with the motion of the ions in the rotating magnetic field of the earth an interesting point arises. How will the lateral motion of the magnetic field of the rotating earth-magnet affect the motion of the ion? It is seen that this motion of the magnetic field will produce an electric field

according to the Lorentz equation  $E = \frac{[v \times H]}{c}$  and that the field will have the

effect of dragging the ions along with it round the earth; in other words, the ions in the spray region, unlike neutral particles, will partially participate in the rotation of the earth. The rotation effect at a height  $r$  will be  $\frac{a^2}{r^2} \frac{1 + \cos^2 \theta}{1 + 3\cos^2 \theta}$  of the rotational velocity of the lines of force at that

height. As the surface of the earth is approached, the dragging effect will increase and the rotational velocity of the ion will also approach the rotational velocity of the earth.

An important consequence of the entanglement of the ions with the magnetic lines of force will be the reduction of the rate of escape of molecules from the outer atmosphere of the earth. A neutral particle in the equatorial region having a velocity 11 km./sec. at a height 7000 km. from the earth's centre will escape from the attraction of the earth. The same particle, if ionized, will require a velocity of  $2.5 \times 10^5$  km./sec. in order to escape by disentangling itself from the earth's magnetic field.

A rough quantitative estimate of the various factors regarding the formation and ionization of the particles in the spray region shows that the assumptions underlying the ultra-violet theory of aurora and magnetic storms as postulated by Hulbert<sup>2</sup> do not show very satisfactory quantitative agreement with the available data of the high atmosphere. One may, however, expect that with the increase of our spectroscopic knowledge regarding the constituents of the high atmosphere new facts may emerge which would show the way out of the difficulty and would explain the discrepancies discussed in the paper.

## R E F E R E N C E S

- <sup>1</sup> Stoney, *Trans. Roy. Soc. Dublin*, **6**, 305 (1898) ; *Astrophys. Journal* (1898-1904) ; *Proc. Roy. Soc.*, **67**, 286 (1900).
- <sup>2</sup> Maris and Hulbert, *Phys. Rev.*, **33**, 412 (1929) ; Hulbert, *Phys. Rev.*, **38**, 1560 (1930).
- <sup>3</sup> Jeans, *Dynamical Theory of Gases*, Ch. XV, p. 350.
- <sup>4</sup> Gold, *Proc. Roy. Soc.*, **82**, 43 (1909).
- <sup>5</sup> Milne, *Trans. Camb. Phil. Soc.*, Vol. 22, No. 26, p. 483.
- <sup>6</sup> Jones, *Trans. Camb. Phil. Soc.*, Vol. 22, No. 28, p. 535.
- <sup>7</sup> Martyn and Pulley, *Proc. Roy. Soc.*, **184**, 455 (1936).
- <sup>8</sup> Mitra and Rakshit, *Ind. Jour. Phys.*, **12**, 47 (1938).
- <sup>9</sup> Störmer, *University Observatory, Oslo, Publication No. 10* (1934).
- <sup>10</sup> Loeb, *Kinetic Theory of Gases*, p. 240.
- <sup>11</sup> Chapman and Milne, *Q. J. Roy. Met. Soc.*, **46**, 392 (1920).
- <sup>12</sup> Eddington, *Internal Constitution of Stars*, p. 281.
- <sup>13</sup> Majumdar, *Ind. Jour. Phys.*, **12**, 75 (1938).
- <sup>14</sup> Kaplan, *Nature*, **141**, 1139 (1938).
- <sup>15</sup> Bernard, *Nature*, **141**, 1140 (1938).
- <sup>16</sup> Condon, *Astrophys. Journal*, **79**, 217 (1934).
- <sup>17</sup> A. K. Das, *Gelands. Beitr. Geophysik*, **49**, 241 (1937).
- <sup>18</sup> Ladenburg and Van Voorhis, *Phys. Rev.*, **43**, 315 (1933).
- <sup>19</sup> Vegard, *Dic. Naturwissenschaften*, **39**, 639 (1938).
- <sup>20</sup> Saha, *Proc. Nat. Inst. Sc. India*, Vol. I, No. 3, p. 227.
- <sup>21</sup> Saha and Rai, *Proc. Nat. Inst. Sc. India*, **4**, 319 (1938).
- <sup>22</sup> Chapman, *Proc. Roy. Soc.*, **132**, 353 (1931).
- <sup>23</sup> Morse and Strickelberg, *Phys. Rev.*, **36**, 16 (1930).
- <sup>24</sup> Page, *Phys. Rev.*, **33**, 553 (1929).
- <sup>25</sup> Swann, *Bull. Nat. Research Council (Washington)*, Vol. 4, Part 6, No. 24, p. 75 (1922).
- <sup>26</sup> Page, *Phys. Rev.*, **33**, 23 (1929).
- <sup>27</sup> McNish, *Phys. Rev.*, **52**, 155 (1937).

# BAND SPECTRUM OF ANTIMONY MONOXIDE (SbO)

By A. K. SENGUPTA

(Received for publication, April 14, 1939)

## Plate VIII

**ABSTRACT.** The present paper reports the vibrational structure analysis of the emission band spectrum of the diatomic molecule, SbO, in the region  $\lambda_{3200}-\lambda_{6800}$ . The bands have been assigned to two systems designated as the more refrangible and the less refrangible systems of the molecule and are due respectively to  $^2\Sigma \rightarrow ^2\Pi$  and  $^2\Pi \rightarrow ^2\Pi$  transitions. They have a common lower state which shows a separation of  $2372 \text{ cm}^{-1}$ , between its  $\Pi$ -components. From analogy with the other members of the group V(b) oxides, this common lower state seems in all probability to be the ground state of the molecule in question.

## INTRODUCTION

During the last few years attempts have been made to obtain the band spectra associated with the oxides of group V(b) elements in the periodic table and to interpret them in the light of recent developments in the theory. At present our knowledge of the spectra of  $\text{NO}^1$ ,  $\text{PO}^2$  and  $\text{AsO}^3$  has much advanced. But for the remaining two oxides of the group, namely,  $\text{SbO}^4$  and  $\text{BiO}^5$ , there are available only the preliminary reports of analysis of their spectra.

It is well known that the bands of  $\text{NO}^1$  are observed under different modes of excitation and consist of four systems, designated as  $\beta$ ,  $\gamma$ ,  $\delta$  and  $\epsilon$  bands. All of them have a common lower state, which is a  $^2\Pi$  state with a separation of  $121 \text{ cm}^{-1}$ . In the case of  $\text{PO}^2$ , only one ultra-violet system, analogous to the  $\gamma$ -bands of  $\text{NO}$ , has so far been thoroughly analysed. The lower state of this system is also a  $^2\Pi$  state with a separation of  $224 \text{ cm}^{-1}$ . For  $\text{AsO}^3$ , two band systems are however known. They have also a common lower  $^2\Pi$  state with a separation of  $1026 \text{ cm}^{-1}$ . In each of these three molecules, the lowest  $^2\Pi$  state corresponds to the ground state of the molecule in question.

For  $\text{SbO}^4$ , only a preliminary analysis of the bands photographed under the dispersion of a Hilger E. I spectrograph has been reported by Mukherji who recorded a large number of single-headed bands in the region  $\lambda_{3300}-\lambda_{6000}$  and arranged them into four independent and apparently singlets system designated by him as A, B, C and D bands. He published the following band head equations :—

A bands :

$$\nu = 29749.4 + 586(v' + \frac{1}{2}) - 6.5(v' + \frac{1}{2})^2 - 824.3(v'' + \frac{1}{2}) + 5.9(v'' + \frac{1}{2})^2$$

B bands :

$$\nu = 26600.4 + 573(v' + \frac{1}{2}) - 4.5(v' + \frac{1}{2})^2 - 813.0(v'' + \frac{1}{2}) + 3.3(v'' + \frac{1}{2})^2$$

C bands :

$$\nu = 24317.4 + 586(v' + \frac{1}{2}) - 6.5(v' + \frac{1}{2})^2 - 813.0(v'' + \frac{1}{2}) + 3.3(v'' + \frac{1}{2})^2$$

D bands :

$$\nu = 20655.7 + 565(v' + \frac{1}{2}) - 3.5(v' + \frac{1}{2})^2 - 808.0(v'' + \frac{1}{2}) + 3.8(v'' + \frac{1}{2})^2.$$

From a comparison of the values of the vibrational coefficients, Mukherji was of opinion that A and C bands have a common upper state while B and D bands have a common lower state which in all probability corresponds to the ground state of the molecule. He could not, however, correlate the levels associated with the D bands with those of the other three systems.

From experimental evidences since the emitter of these bands is known to be the normal diatomic antimony oxide molecule, one would expect its band systems to arise from transitions between doublet electronic states as in the case of homologous molecules, NO, PO and AsO. In view of this, it is of interest to enquire whether the four systems, into which Mukherji has classified the observed bands, are themselves independent doublet systems arising from transitions between similar electronic states whose resultant separation is practically negligible or they are widely separated components of one or more doublet systems. It is further found that the intensity distribution in A and D bands is apparently unusual. Although such unusual distribution of intensity is not rare, it is worth while to enquire whether the quantum-numbers of bands in these two systems have been correctly assigned. With these objects in view, the present investigation was taken up.

#### E X P E R I M E N T A L

For light source the flame of an arc between antimony and carbon electrodes, as previously used by Mukherji,<sup>4</sup> was employed. The bands were photographed also with a Hilger E. 1 quartz spectrograph but with a slit finer in width than that used by the latter author. For photographing the bands in the region beyond  $\lambda 3800$ , a Hilger E. 52 glass spectrograph was used. The dispersion of the spectrographs are as follows :—

Hilger E. 1  $6.5 \text{ \AA/mm.}$  at  $\lambda 3300$  to  $49.0 \text{ \AA/mm.}$  at  $\lambda 6500$ .

Hilger E. 52  $6.8 \text{ \AA/mm.}$  at  $\lambda 4500$  to  $24.8 \text{ \AA/mm.}$  at  $\lambda 6700$ .

For obtaining the best definition of the band heads, Ilford fine-grained plates were used. An effective exposure of about an hour was necessary to develop the bands with sufficient intensity.

Measurements of band heads were carried out with a Gaertner Precision Comparator in the usual way adopting iron arc lines as reference standards.

#### DESCRIPTION OF THE SPECTRUM

The bands are degraded to the red and lie in the region  $\lambda_{3200}-\lambda_{6800}$ . Due to overlapping of neighbouring sequences the appearance of the spectrum seems complicated. It is, however, found that the stronger bands in the region  $\lambda_{3200}-\lambda_{4700}$  show double heads. Such a feature is also noticeable in a few cases on plates taken by Mukherji. On the other hand the bands lying on the longer wave-length side of  $\lambda_{4700}$  do not show such double heads, even on spectrograms taken with the glass spectrograph. Had these bands belonged to the same system which includes those on the shorter wave-length side, one would have expected to observe also the doublet nature of their heads. This evidently indicates that the absence of double heads is not due to want of the irresolution with the present dispersion.

It is, therefore, likely that the bands in the region  $\lambda_{3200}-\lambda_{4700}$  form one system while those on the longer wave-length side of  $\lambda_{4700}$  belong to a different system. The vibrational analysis of the bands given in the present paper confirms this view. For convenience we shall refer hereafter to these two systems as the more refrangible and the less refrangible bands of SbO.

#### THE MORE REFRANGIBLE BANDS

These bands form two sub-systems, fairly wide apart. The more refrangible and the less refrangible components are denoted as (a) and (b) respectively.

The (0, 0) band of the (a) sub-system is a strong band at  $v=26479 \text{ cm}^{-1}$ . The two bands (1, 0) and (0, 1) are almost of equal intensity. On the other hand while the (2, 0) band is fairly intense, the (0, 2) band is totally absent, although the band (2, 4) of this sequence ( $v'-v''=-2$ ) appears with noticeable intensity. Similar features are also observed in the sequences  $\Delta v = \pm 3$ . The intense bands of this sub-system show in most cases double heads, the shorter wave-length component being comparatively weaker in intensity (Figure 1).

It may here be noted that the double heads where observable are due to R-form and Q-form branches, since their interval shows a tendency to increase with increasing  $v''$  or with decreasing  $v'$ .

The (0, 0) band of the (b) sub-system is a strong band at  $v=24205 \text{ cm}^{-1}$ . The bands of the different sequences are distributed in a manner very similar to that of the (a) sub-system and also show double heads in favourable cases.

It is thus found that the interval between the (0, 0) bands of the two sub-systems is  $2274 \text{ cm}^{-1}$ .

Table I includes the data of these bands together with their  $v'$  and  $v''$ -assignments. For comparison Mukherji's classification is also included. It will be seen that Mukherji's "B" and "C" bands are but the two sub-systems (a) and (b). His assignment of ( $v'$ ,  $v''$ ) values to these bands remains, therefore, unaltered. But his A-system which was fragmentary does no longer exist as an independent system. In fact almost all the comparatively stronger bands belonging to it have been included in either of the above two sub-systems. Hence the anomaly in the intensity distribution in Mukherji's A-system is apparent.

The "Q" heads are represented within the limits of experimental error by the following formula :

$$v = \left\{ \begin{array}{l} 20504.0 \\ 24322.0 \end{array} \right\} + 582.0 (v' + \frac{1}{2}) - 6.50 (v' + \frac{1}{2})^2 - 817.0 (v'' + \frac{1}{2}) + 5.40 (v'' + \frac{1}{2})^2$$

Table II gives the difference between observed and computed wave numbers. Large differences are found for all bands associated with the vibrational level  $v' = 0$ . This level, therefore, seems to be perturbed.

The following five heads which were recorded by Mukherji have not, however, been observed on our plates :

$\lambda 3430.0$  [A (2, 2)],  $\lambda 3583.1$  [A (1, 6)],  $\lambda 3786.1$  [C (4, 0)],  $\lambda 4451.9$  [C (4, 5)],  $\lambda 4352.9$  [C (5, 5)].

Incidentally it may be mentioned that the first three of these heads are not also included in the wave-length data of Eder and Valenta.<sup>6</sup> In addition to these discrepancies, it is further found that the heads at  $\lambda 3469.6$  and  $\lambda 3567.9$ , which Mukherji assigned as A(0, 1) and A(0, 2) bands, are in all probability due to condensation of partially resolved line structure of bands preceding them. In fact they could not be included in the band system under consideration.

TABLE I  
The more Refrangible Band System of SbO

$\lambda$ in air	$\nu$ in vacuo	Assignment.	Type of Head.	Mukherji's Assignment.
3248.37	30775.8	a(10, 1)	Q	
3286.76	30436.4	a(11, 2)	Q	
3325.67	30060.04	a(12, 3)	Q	
3366.45	29696.4(l)	a(13, 4)	Q	
3373.61	29633.4	a(11, 3)	Q	
3402.40	29382.6	a(7, 1)	Q	A(1, 1)

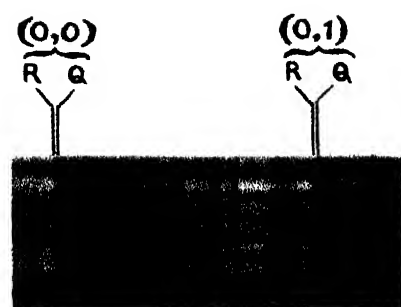


Fig. 1.

b (0, 0) and b (0, 1) bands of the more refrangible band system of SbO showing R and Q heads.



TABLE I (*contd.*)

$\lambda$ in air.	$\nu$ in vacuo.	Assignment.	Type of Head	Mukherji's Assignment
3459·74	28895·7	a(6, 1)	R	
3460·60	28888·5	a(6, 1)	Q	
3475·15	28767·5(l)	a(9, 3)	R	
3476·29	28757·3(l)	a(9, 3)	Q	
3496·26	28593·8	a(7, 2)	R	
3497·31	28585·3	a(7, 2)	Q	A, L, 2
3517·78	28418·9(l)	a(10, 4)	Q	
3521·58	28388·3,L	a(5, 1)	Q	
3552·00	28145·1	a(3, 0)	Q	A(3, 1) B(3, 0)
3587·57	27868·4	a(4, 1)	Q	
3620·72	27611·0	a(2, 0)	R	
3621·71	27603·4	a(2, 0)	Q	B(2, 0)
3623·15	27592·5	a(5, 2)	Q	
3655·65	27347·1	a(3, 1)	R	
3656·80	27338·6	a(3, 1)	Q	B(3, 1)
3672·20	27223·9(l)	a(9, 5)	Q	A(0, 3)
3687·33	27112·2	b(7, 1)	Q	
3695·01	27055·9	a(1, 0)	R	
3696·45	27045·3	a(1, 0)	Q	B(1, 0)
3730·80	26796·3	a(2, 1) & (5, 3)	Q	B(2, 1)
3755·95	26616·9(l)	b(6, 1)	Q	B(3, 2)
3766·32	26543·6	a(3, 2)	Q	
3774·00	26489·6	a(0, 0)	R	B(0, 0)
3776·00	26475·6	a(0, 0)	Q	
3799·60	26311·1	b(7, 2)	Q	A(1, 5)
3810·62	26235·0	a(1, 1)	Q	
3823·55	26146·3(l)	b(10, 4)	Q	
3827·62	26118·5(l)	b(5, 1)	R	
3829·03	26108·9(l)	b(5, 1)	Q	

TABLE I (*contd.*)

$\lambda$ in ang.	$\nu$ in vacue.	Assignment.	Type of Head	Mukherjee's Assignment.
3864.02	25872.5	b(3, 0)	Q	
3871.81	25820.4(l)	b(6, 2)	Q	
3894.84	25667.8	a(0, 1)	Q	B(0, 1)
3904.59	25603.7	b(4, 1)	R	C(4, 1)
3905.88	25595.2	b(4, 1)	Q	
3939.67	25440.3	a(1, 2)	Q	
3945.40	25338.8	b(2, 0)	R	
3946.71	25330.4	b(2, 0)	Q	C(2, 0)
3940.14	25314.8	b(5, 2)	Q	
3965.28	25211.8	a(2, 3)	Q	B(2, 3)
3986.20	25078.9	b(3, 1)	R	C(3, 1)
3987.90	25068.8	b(3, 1)	Q	
4007.01	24949.2	b(9, 5)	Q	B(3, 4)
4033.83	24785.2	b(1, 0)	R	
4035.00	24776.2	b(1, 0)	Q	C(1, 0)
4074.96	24533.2	b(2, 1) & b(5, 3)	R & Q	C(2, 1)
4076.72	24522.6	b(2, 1)	Q	
4091.00	24437.0	a(2, 4)	Q	
4116.82	24283.8	b(3, 2)	R	
4119.05	24270.6	b(3, 2)	Q	C(3, 2)
4128.19	24216.9	b(0, 0)	R	
4130.22	24205.0	b(0, 0)	Q	C(0, 0)
4169.65	23976.1	b(1, 1)	R	
4171.44	23965.8	b(1, 1)	Q	C(1, 1)
4259.36	23471.1	a(3, 6)	Q	
4270.30	23411.0	b(1, 1)	R	
4272.74	23397.6	b(0, 1)	Q	C(0, 1)
4297.72	23261.6	a(4, 7)	Q	
4312.85	23180.0	b(1, 2)	R	

TABLE I (*contd.*)

$\lambda$ in air.	$\nu$ in vacuo.	Assignment.	Type of Head.	Mukherji's Assignment.
4314.81	23169.5	b(1, 2)	Q	C(1, 2)
4358.09	22939.4	b(2, 3)	Q	C(2, 3)
4361.10	22923.6	a(2, 6)	Q	
4395.27	22745.4	a(3, 7)	R	
4398.50	22728.7	a(3, 7)	Q	D(4, 0)
4669.21	21410.9	b(2, 5)	Q	
4715.64	21200.1	b(3, 6)	Q	

TABLE II

(O-C) Values

More Refinable Band System of SbO

$v'/v''$	0	1	2	3	4	5	6	7
0	a { -0.7 b { +0.7 { 0.0 { +2.9 { +1.1 { +1.1 { +0.8 { +0.2	{ -2.3 { -0.5 { -4.1 { -1.3 { +0.2 { -0.5 { -0.5 { +2.7 { +0.3	{ -3.4 { -2.2 { -3.4 { -2.2 { -3.3 { -3.7 { -0.1 { -0.1					
1								
2				{ -3.3 { -3.7	{ -4.3 { x	{ x { -4.6	{ -2.5 { x { +2.0 { +3.0	{ +1.0 { x
3								
4								
5								
6								
7								
8								
9				P { +14.2 { x		P { +17.6 { +14.9		

TABLE II (contd.)

$r'/r''$	0	1	2	3	4	5	6	7
10		$\left\{ \begin{array}{l} +0.7 \\ -x \end{array} \right.$			$\left\{ \begin{array}{l} -2.4 \\ -3.0 \end{array} \right.$			
11			$\left\{ \begin{array}{l} -2.3 \\ -x \end{array} \right.$	$\left\{ \begin{array}{l} -0.7 \\ -x \end{array} \right.$				
12				$\left\{ \begin{array}{l} +0.3 \\ -x \end{array} \right.$				
13					$\left\{ \begin{array}{l} -2.9 \\ + \end{array} \right.$			

## THE LESS REFRANGIBLE BANDS

The system lies above  $\lambda 4500$  and extends towards the red end of the spectrum. It consists of a fairly large number of single-headed bands degraded towards the higher wave-length side.

The bands are grouped under two sub-systems, the arrangement of each group being the same. It is found that the components of the corresponding bands of the two sub-systems are at a distance of about  $2139 \text{ cm.}^{-1}$  apart. The analysis shows that the  $(o, o)$  bands of both the sub-systems are absent. But the intensity of the bands along both  $v' = o$  and  $v'' = o$  progressions increases till it attains a maximum and then diminishes. The bands of the  $v'' = o$  progression are, in general, stronger than those belonging to the  $v' = o$  progression.

In Table III the wave-length and the wave-number data of the bands together with their vibrational assignments are given. The two sub-systems are denoted by (a) and (b) as in the previous system. Mukherji's classification is also included for comparison.

The following equation has been obtained in the usual manner to represent the bands in the two sub-systems :

$$v = \frac{20667.5}{18528.5} + 560.0(v' + \frac{1}{2}) - 5.00(v' + \frac{1}{2})^2 - 817.2(v'' + \frac{1}{2}) + 5.38(v'' + \frac{1}{2})^2$$

Table IV includes the O-C values calculated with the help of the above equation.

It is evident from Table III that in the case of the 'a' components the present analysis is in close agreement with that given by Mukherji. But for the 'b' components a large number of new bands have been recorded. A re-examination of plates taken by Mukherji also shows their presence on them.

TABLE III

## The Less Refrangible Band System of SbO

$\lambda$ in air.	$\nu$ in vacuo.	Assignment.	Mukherji's Assignment
4504.70	22192.4	a(3, 0)	D(3, 0)
4562.04	21013.9	a(4, 1)	D(4, 1)
4573.03	21861.1	a(7, 3)	
4617.35	21651.9	a(2, 0)	D(2, 0)
4675.03	21384.3	a(3, 1)	D(3, 1)
4739.80	21105.0	a(1, 0)	D(1, 0)
4795.80	20845.8	a(2, 1)	D(2, 1)
4920.13	20291.1	a(1, 1)	D(1, 1)
4935.92	20050.0	a(2, 0)	D(2, 0)
5012.36	19826.5	a(6, 5)	
5047.03	19805.8	a(3, 3)	D(3, 3)
5065.05	19737.7	a(0, 1)	D(0, 1)
5107.16	19574.9	a(7, 6)	
5126.30	19501.8	a(3, 2) & b(5, 2)	D(1, 2)
5189.00	19263.0	a(2, 3)	D(2, 3)
5252.15	19034.5	a(3, 4)	D(3, 4)
5277.70	18942.4	a(0, 2)	D(0, 2)
5318.80	18796.0	a(1, 5)	D(4, 5)
5344.68	18705.0	b(2, 1)	
5341.25	18717.0	a(1, 3)	D(1, 3)
5406.37	18491.6	a(2, 4)	D(2, 4)
5505.57	18158.4	a(0, 3)	D(0, 3)
5572.80	17939.3	a(1, 4)	D(1, 4)
5638.80	17729.4	a(2, 5)	D(2, 5)
5679.46	17602.4	b(0, 1)	
5733.38	17436.9	b(7, 6)	
5750.70	17384.4	a(0, 4)	D(0, 4)
5757.93	17362.6	b(1, 2)	

TABLE III (*contd.*)

$\lambda$ in air.	$\nu$ in vacuo.	Assignment.	Mukherji's Assignment.
5776.96	17305.4	a(4, 7)	
5837.69	17125.3	b(2, 3)	
5949.45	16803.6	b(0, 2)	
5958.79	16777.3	a(3, 7)	
6015.20	16620.2	a(0, 5)	D(0, 5)
6029.99	16579.2	b(1, 3) & a(4, 8)	
6071.37	16466.2	a(8, 11)	
6105.63	16373.8	a(5, 9)	
6113.15	16353.7	b(2, 4)	
6240.19	16020.7	b(0, 3)	..
6304.79	15856.6	a(4, 9)	..
6325.58	15804.5	b(1, 4)	..
6381.53	15665.0	a(5, 10)	...
6412.03	15591.4	b(2, 5)	..
6459.21	15477.5	a(6, 11)	..
6537.80	15291.4	a(7, 12)	..
6559.13	15241.7	b(0, 4)	..
6591.60	15166.6	b(4, 7)	..
6618.84	15104.2	a(8, 13)	..
6647.03	15040.2	b(1, 5)	..

## CORRELATION OF THE TWO SYSTEMS

A comparison of the band head equations for the two systems shows that the vibrational constants in their final states are practically identical in magnitude. This leads one to conclude that the two systems have a common lower level. In analogy with the homologous molecules NO, PO and AsO, this lower level is very likely a  $^2\Pi$  state. The appearance of close double heads in the more refrangible system suggests that its upper level is either a  $^2\Sigma$  or a  $^2\Delta$  state. The intensity distribution and the general appearance of this system bears a very

TABLE IV

Less Refrangible Band System of SbO

### (i) -C) Values

close resemblance to the  $\Lambda$ -bands of AsO described very fully by Connelly<sup>1</sup> who has suggested a  $^2\Sigma$  state as its upper level. It, therefore, seems very probable that the upper level of the more refrangible band system of SbO is also a  $^2\Sigma$  state. In that case, the separation of  $2272 \text{ cm}^{-1}$ , between the two sub-systems is the doublet separation of the lower  $^2\Pi$  state.

The separation of the two sub-systems of the less refrangible bands is about  $2139 \text{ cm}^{-1}$ , which is less than that for the more refrangible bands by  $133 \text{ cm}^{-1}$ . It seems likely that the doublet separation of the upper level of the former system has this value. The absence of double heads as well as the magnitude of the separation suggests that it is very likely a  $^2\Pi$  state. The intensity distribution of this system bears a close resemblance to that of the  $\beta$ -bands of NO,<sup>1</sup> which is also due to a  $^2\Pi \rightarrow ^2\Pi$  transition.

Hence the electronic transitions concerned in the two systems may be diagrammatically represented as shown in Fig. 2.

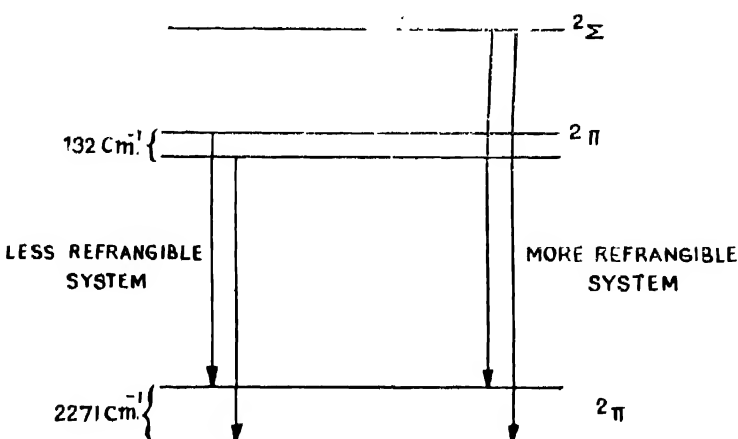


FIG. 2.

The doublet separation of  $2272 \text{ cm}^{-1}$ , in the lower state of SbO, is so far the highest found in the case of diatomic oxide molecules.

It is well-known that the doublet interval in the  $^2\Pi$  ground states of NO, PO and AsO are  $121 \text{ cm}^{-1}$ ,  $224 \text{ cm}^{-1}$ , and  $1026 \text{ cm}^{-1}$ , respectively. A separation larger than  $1026 \text{ cm}^{-1}$  is, therefore, expected in the case of SbO.

It is interesting to note further that the molecules NS<sup>+</sup> and PO which have the same number of electrons have practically identical doublet separations in their  $^2\Pi$  ground levels. On the other hand in the ground state of SnCl<sup>+</sup> with 67 electrons the separation is about  $2360 \text{ cm}^{-1}$ . A doublet separation of  $2272 \text{ cm}^{-1}$  seems, therefore, a very probable value in the ground state of SbO, which has 59 electrons.

## ACKNOWLEDGMENT

The author desires to offer his best thanks to Prof. P. N. Ghosh for continual interest and encouragement in the course of the investigation and to Dr. P. C. Mahanti for many helpful discussions.

## REFERENCES

- <sup>1</sup> Jevons, W., *Report on Band Spectra of Diatomic Molecules* (1932).
- <sup>2</sup> Ghosh, P. N. and Ball G. N., *Z. f. Phys.*, **71**, 362 (1931); Sen Gupta, A. K., *Proc. Phys. Soc.*, **47**, 247 (1935).
- <sup>3</sup> Connally, F. C., *Proc. Phys. Soc.*, **46**, 790 (1934), Jenkins, F. A. and Strait, L. A., *Phys. Rev.*, **47**, 136 (1935).
- <sup>4</sup> Mukherji, B. C., *Z. f. Phys.*, **70**, 552 (1931).
- <sup>5</sup> Ghosh, C. S., *Z. f. Phys.*, **86**, 241 (1933).
- <sup>6</sup> Röder, J. M. and Valenta, E., *Atlas Typischer Spektren* (1928).
- <sup>7</sup> Fowler, A. and Bakker, C. J., *Proc. Roy. Soc.*, **136**, 28 (1932).
- <sup>8</sup> Jevons, W., *Proc. Roy. Soc.*, **110** 365 (1926).

SPECTROSCOPIC RESEARCH LABORATORY,  
APPLIED PHYSICS DEPARTMENT,  
UNIVERSITY COLLEGE OF SCIENCE,  
92, UPPER CIRCULAR ROAD,  
CALCUTTA.



## ON THE RAMAN EFFECT IN CAMPHOR \*

BY B. M. ANAND

AND

S. NARAIN

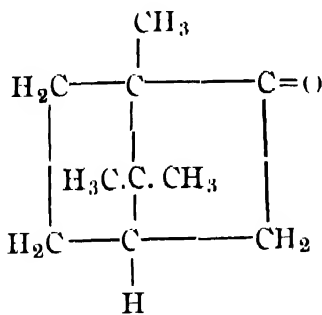
(Received for publication, February 15, 1939)

## Plate IX

**ABSTRACT.** The Raman spectrum of camphor has been studied in the crystalline state and in its saturated solutions in carbon tetrachloride, carbon disulphide, chloroform, methyl alcohol and acetic acid. The characteristic Raman frequencies of camphor in the solid state are 512, 653, 1182, 1450, 1738 and 2937 cm.<sup>-1</sup>. When dissolved in the first three solvents, about twenty frequencies, including the above, are observed. In the last two solvents the number of lines observed is small. Important Raman frequencies are ascribed to the corresponding vibrations in the camphor molecule.

## INTRODUCTION

The Raman effect has been a very useful tool in the study of molecular constitutions. Camphor



is an important organic compound which has not been studied in great detail. Jatkar and Padmanabhan<sup>1</sup> have studied camphor in its saturated solution in  $\text{CCl}_4$ , while Thosar and Bawa Kartar Singh<sup>2</sup> have observed its Raman spectrum in the solid state. In the present paper Raman effect of camphor in the crystalline state and in its saturated solutions in five solvents is given.

The characteristic frequencies of a solute molecule may be displaced due to the influence of the solvent molecule. Some new frequencies may appear due to the relative vibrations and interactions of the solute and the solvent molecules.

#### EXPERIMENTAL ARRANGEMENTS

The experimental arrangements have been previously given by one of us.<sup>3,4</sup> A high light gathering power ( $f/3.5$ ) spectrograph by Carl Leiss was used. Chemicals were Merck's extra pure samples or B. D. H. analytical reagents.

#### RESULTS

Table I gives the frequency shifts of camphor in the solid state and in solution. Table II gives a summary of the result, along with the result, of previous workers for comparison. Plate IX gives the enlargements of the negatives.

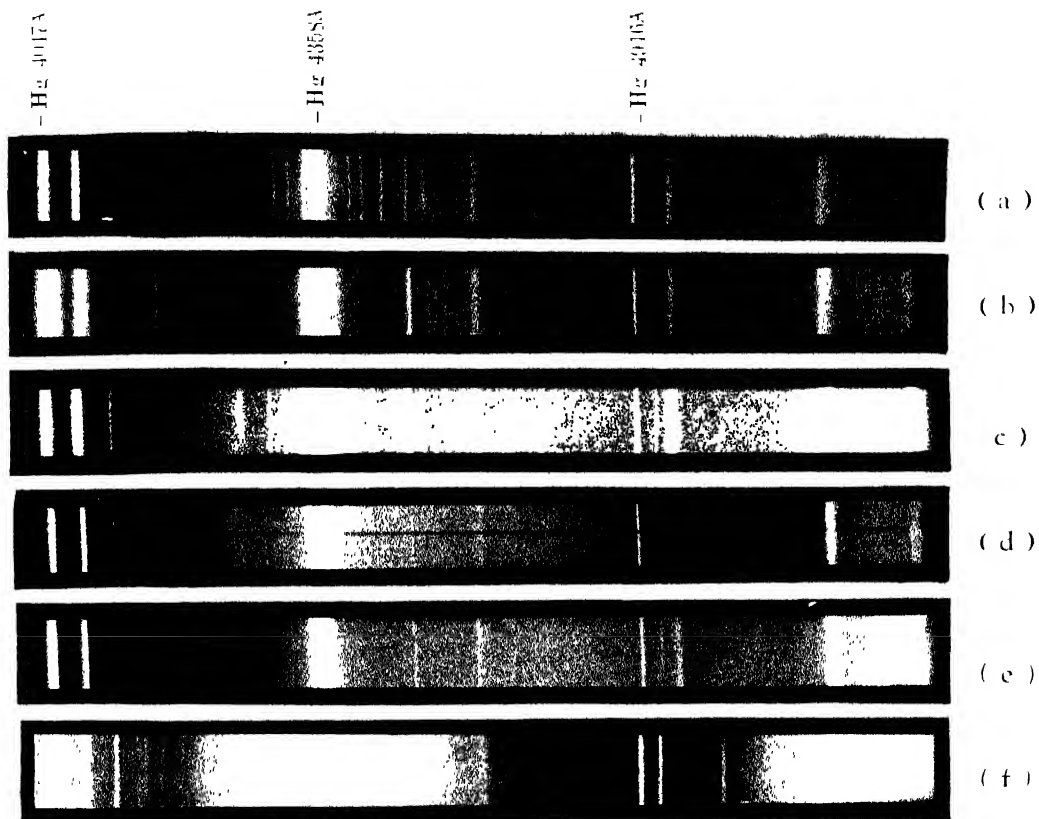
#### DISCUSSION

In the solid state only the most prominent lines of camphor make their appearance. The greater number of lines in solution may be due to overtones and combinations. The small number of lines observed in solutions of camphor in methyl alcohol and acetic acid is due to the continuous background which invariably accompanies the Raman spectra of camphor in these two solvents.

Table II shows a fair degree of agreement between our results for the mean values of  $\Delta\nu$  for camphor in solution and those of Jatkar and Padmanabhan, except for the new frequencies 122, 295, 472, 610, 2776, 3106  $\text{cm.}^{-1}$  observed by us.

Out of the six lines observed by us in the crystalline state, the three—653 (3s), 1450 (1s) and 2937 (3b)—agree with those found by Thosar and Singh. Their other three lines are comparatively weak and do not appear in our plates. It may be mentioned that they gave an exposure of 96 hours using  $\lambda_{4046}$  as the exciting line, while our exposure was for 12 hours employing  $\lambda_{4358}$ . The line 1738  $\text{cm.}^{-1}$  due to  $\lambda_{4046}$  falls in the region of  $\lambda_{4358}$  and, therefore, has not been recorded by them.

Some of the prominent frequencies are given below : 2941  $\text{cm.}^{-1}$  is a fairly intense broad band showing structure. It is observed in the solid state as well as



Raman Spectra of Camphor.

- ( a ) Solution saturated in  $\text{CCl}_4$
- ( b ) " " "  $\text{CS}_2$
- ( c ) " " "  $\text{CHCl}_3$
- ( d ) " " "  $\text{CH}_3\text{OH}$
- ( e ) " " "  $\text{CH}_3\text{COOH}$
- ( f ) Crystalline state



TABLE I(a)

Camphor in  $\text{CCl}_4$ 

$$\nu_a = 24702 \text{ cm.}^{-1}$$

$$\nu_b = 24515 \text{ cm.}^{-1}$$

$$\nu_c = 22938 \text{ cm.}^{-1}$$

$$\nu_d = 18310 \text{ cm.}^{-1}$$

No.	$\nu$	T	$\Delta\nu$	Exciting $\nu$	No.	$\nu$	T	$\Delta\nu$	Exciting $\nu$
1	24587	1b	115	a	23	22552	od	386	c
2	24488	1b	217*	a	23	22481	2s	157	c
3	24380	2b	313*	a	24	22400	Band of three eq. lines	538	c
4	24295	1b	220*	b	35	22345	od	603	c
5	24117	2b	455*	a	26	22200	2s	618	c
6	24105	1s	320*	b	27	22136	1s	704	c
7	24058	2s	647	a	28	22182	1b	786*	c
8	23997	1s	705	a	29	22152	1b	786*	c
9	23940	1d	575	b	39	22081	1b	854	c
10	23911	1d	604	b	31	22035	1b	913	c
11	23865	1d	650	b	32	21991	1b	947	c
12	23848	1d	667	b	33	21938	1d	1000	c
13	23792	1d	910	a	34	21847	2b	1091	c
14	23758	1d	914	a	35	21735	2b	1153	c
15	23396	1s	-458*	c	36	21747	2b	1191	c
16	23349	1s	-311*	c	37	21658	1s	7380	c
17	23152	1s	-214*	c	38	21493	2s	1439	c
18	22825	1s	113	c	39	21191	2s	1739	c
19	22721	2s	217*	c	40	20150	1b	2782	c
20	22675	od	263	c	41	10072	1b	2066	c
21	22623	2s	315	c					

(i) Mean  $\Delta\nu$  for solvent  $\text{CCl}_4$ : 217, 315, 457, 756, 786  $\text{cm.}^{-1}$

(ii) Mean  $\Delta\nu$  for solute camphor: 114, 263, 386, 538, 603, 653, 704, 854, 912, 946, 1000, 1091, 1153, 1191, 1280, 1439, 1739, 2782, 2966  $\text{cm.}^{-1}$

TABLE I(b)

Camphor in CS<sub>2</sub>

No.	$\nu$	I	$\Delta\nu$	Exciting $\nu$	No.	$\nu$	I	$\Delta\nu$	Exciting $\nu$
1	24051	3s	651*	a	15	22232	1s	706	c
2	23097	1d	705	a	16	22132	1b	866 *	c
3	23010	1b	605	b	17	22081	1b	857	c
4	23861	1b	841	a	18	22003	1b	935	c
5	23705	1b	937	a	19	21923	1b	1015	c
6	23580	1b	-651*	c	20	21831	1b	1104	c
7	23536	1b	1166	a	21	21778	4b	1160	c
8	23190	1b	1005	b	22	21749	4b	1180	c
9	20777	1b	261	c	23	21630	1b	1308	c
10	22613	1b	295	c	24	21176	1b	1462	c
11	22541	1b	307	c	25	21104	2s	1744	c
12	22462	1s	176	c	26	20310	4b	2036	c
13	22383	1s	555	c	27	19824	1s	3114	c
14	22283	3s	655*	c					

(i) Mean  $\Delta\nu$  for solvent CS<sub>2</sub> : 653, 866 cm.<sup>-1</sup>(ii) Mean  $\Delta\nu$  for solute camphor : 261, 205, 307, 476, 555, 605, 705, 840, 936, 1015, 1100, 1163, 1180, 1308, 1403, 1714, 2028, 3114 cm.<sup>-1</sup>

TABLE I(c)

Camphor in CHCl<sub>3</sub>

No.	$\nu$	I	$\Delta\nu$	Exciting $\nu$	No.	$\nu$	I	$\Delta\nu$	Exciting $\nu$
1	24055	1bd	647	a	15	23011	2b	927	c
2	23573	1bd	-635*	c	16	21977	2b	961	c
3	23293	1bd	-355*	c	17	21604	od	1034	c
4	23809	2s	129	c	18	21828	1b	1110	c
5	22669	3s	260*	c	19	21724	2b	1214*	c
6	22562	3s	376*	c	20	21467	2bd	1471*	c
7	22456	1s	482	c	21	21181	2s	1757	c
8	22365	2b	573	c	22	20160	2s	2778	c
9	22315	2d	623	c	23	19998	3b	2940	c
10	22305	3s	633*	c	24	18059	2b	251	d
11	22250	3s	682*	c	25	17045	2b	365	d
12	22221	1d	717	c	26	17660	2b	650	d
13	22172	2b	766*	c					
14	22060	2b	860	c					

(i) Mean  $\Delta\nu$  for solvent CHCl<sub>3</sub> : 260, 365, 641, 682, 766, 121, 1471 cm.<sup>-1</sup>(ii) Mean  $\Delta\nu$  for solute camphor : 129, 482, 573, 682, 717, 860, 927, 961, 1034, 1110, 1757, 2778, 2940 cm.<sup>-1</sup>

TABLE I(d)

Camphor in  $\text{CH}_3\text{OH}$ 

No.	$\nu$	I	$\Delta\nu$	Exciting $\nu$	No.	I	T	$\Delta\nu$	Exciting $\nu$
1	24061	1s	641	a	7	21486	od	1452*	c
2	23556	od band	1146	a	8	21203	od	1735	c
3	22390	1s	548	c	9	20176	2s	2782	c
4	22290	3s	648	c	10	20014	3 band	2024	c
5	22069	odb	869	c	11	19840	1s	3098	c
6	21771	1d band	1167	c					

(i) Mean  $\Delta\nu$  for solvent  $\text{CH}_3\text{OH}$ : 1452 cm.<sup>-1</sup>(ii) Mean  $\Delta\nu$  for solute camphor: 518, 645, 860, 1147, 1737, 2782, 2024, 3098 cm.<sup>-1</sup>

TABLE I(e)

Camphor in  $\text{CH}_3\text{COOH}$ 

No.	$\nu$	I	$\Delta\nu$	Exciting $\nu$	No.	$\nu$	I	$\Delta\nu$	Exciting $\nu$
1	24049	2s	653	a	6	21499	o band	1439	c
2	22275	4s	663	c	7	21203	o band	1735	c
3	22064	od band	874*	c	8	20156	2s	2782	c
4	21901	od band	947	c	9	19990	3 band	2948	c
5	21752	1 band	1186	c					

(i) Mean  $\Delta\nu$  for solvent  $\text{CH}_3\text{COOH}$ : 874 cm.<sup>-1</sup>(ii) Mean  $\Delta\nu$  for solute camphor: 658, 947, 1186, 1439, 1735, 2782, 2948 cm.<sup>-1</sup>

TABLE I(f)

## Solid camphor

No.	$\nu$	I	$\Delta\nu$	Exciting $\nu$	No.	$\nu$	I	$\Delta\nu$	Exciting $\nu$
1	22426	2b	512	c	4	21470	1s	1459	c
2	22285	3s	653	c	5	21200	2s	1738	c
3	21756	3b	1182	c	6	20001	3b	2937	c

Mean  $\Delta\nu$  for camphor: 512, 653, 1182, 1459, 1738, 2937 cm.<sup>-1</sup>

TABLE II  
Raman spectrum of camphor  
 $\omega_r$  in  $\text{cm}^{-1}$  of camphor

No.	In saturated solutions of				Mean value of $\frac{\omega_r}{\omega_c}$	Result of Jatkar and Padmanabhan.	Result of Thosar and Singh
	Carbon tetrachloride	Carbon disulphide	Chloroform	Methyl alcohol			
1	114 (rs)	—	130 (ss)	—	1.22	—	—
2	263 (cd)	251 (rd)	260 (ss)	—	—	—	—
3	—	295 (rb)	—	—	—	—	—
4	—	366 (cd)	360 (ss)	—	—	—	—
5	456 (cd)	357 (rb)	—	—	—	—	—
6	457 (cs)	476 (rs)	452 (rs)	—	—	—	—
7	536 (cs)	555 (rs)	573 (cb)	528 (rs)	—	—	—
8	603 (rd)	605 (rb)	623 (cc)	—	—	—	—
9	653 (cs)	653 (ss)	682 (ss)	645 (ss)	—	—	—
10	704 (rs)	705 (ss)	717 (rd)	685 (ss)	—	—	—
11	854 (rb)	849 (rb)	869 (cb)	874 (cd)	—	—	—
12	912 (rb)	—	927 (cb)	—	—	—	—
13	946 (rb)	936 (x band)	961 (cb)	—	—	—	—
14	1000 (rd)	1015 (rd)	1034 (cd)	—	—	—	—
15	1091 (rb)	1100 (rb)	1110 (rb)	—	—	—	—
16	1153 (sb)	1163 (qd)	1157 (x db)	1186 (x band)	—	—	—
17	1191 (gb)	1180 (qb)	1214 (cb)	—	—	—	—
18	1280 (ss)	—	—	—	—	—	—
19	1439 (cs)	1162 (rb)	1471 (2 band)	1452 (cd)	—	—	—
20	1739 (2s)	1743 (2s)	1757 (2s)	1737 (cd)	1.755 (cb)	1.740	1445 (s)
21	2782 (rb)	—	2776 (2s)	2762 (2s)	2.782 (2s)	—	1738 (2s)
22	2966 (4b)	—	2949 (gb)	2924 (3 band)	2.949 (3b)	2.946	2925 (5)
23	—	3114 (1s)	—	3098 (rs)	—	—	2963 (6)
				3114 (1s)	—	—	—

Notation : s = sharp, b = broad, d = diffuse.

in all the solutions of camphor in various solvents. Its structure is supposed to

depend on the number of C—H or X— $\overset{\text{H}}{\underset{\text{H}}{\text{C}}}$ —X groupings and is generally ascribed to them.

$2776 \text{ cm.}^{-1}$  is also due to the stretching of C—H bond.

$1712 \text{ cm.}^{-1}$  is the characteristic frequency of the keto group ( $\text{C}=\text{O}$ ). It is quite sharp in  $\text{CCl}_4$ ,  $\text{CS}_2$  and  $\text{CHCl}_3$  solutions, but is diffuse in  $\text{CH}_3\text{OH}$  and  $\text{CH}_3\text{COOH}$  solutions.

$1453 \text{ cm.}^{-1}$  is due to the deformation vibrations of the  $\text{CH}_2$  groups.

$1294 \text{ cm.}^{-1}$  is the deformation frequency due to the presence in the molecule of a single hydrogen atom attached to a carbon atom.

The double frequency  $1158$ ,  $1195 \text{ cm.}^{-1}$  is quite prominent and is attributed to  $\overset{\text{H}}{\underset{\text{H}}{\text{C}}}\text{—C}$  group. The frequencies  $918$ ,  $1016$ ,  $1100 \text{ cm.}^{-1}$  may be due

to the oscillations of C—C atoms in the chain

$920 \text{ cm.}^{-1}$  may be due to the vibration of the end methyl group against the rest of the molecule.

$658 \text{ cm.}^{-1}$  may be considered to be the characteristic of the nucleus of the camphor molecule consisting of  $\overset{\text{C}}{\underset{\text{C}}{\text{C}}}\text{—C}$  group of carbon atoms.

$472 \text{ cm.}^{-1}$  is generally due to  $\text{C}=\text{C}=\text{O}$  group

In order to explain the origin of the smaller frequencies observed in the solutions of camphor in its various solvents, the study of the state of polarisation of the various Raman lines would be necessary. Such a study may also explain some notable differences observed in the Raman frequencies for camphor in different solvents and also may throw light on the nature of interactions between the solute and the solvent molecules.

Our grateful thanks are due to Prof. J. B. Seth and Dr. P. K. Kichlu for the helpful interest they took in our work.

PHYSICS DEPARTMENT,  
GOVERNMENT COLLEGE,  
LAHORE.

#### R E F E R E N C E S

- 1 Jatkar, S. K. K. and Padmanabhan, R., *Ind. J. Phys.*, **10**, 55 (1936).
- 2 Thosar, B. V. and Singh, B. K., *Ind. Acad. of Sci.*, **6**, 105 (1937).
- 3 Anand, B. M., *Ind. Acad. of Sci.*, **4**, No. 5 (1936).
- 4 Anand, B. M., *J. Sci. Instruments*, **8**, 258 (1931).



# AN EXPERIMENTAL STUDY OF PARABOLIC WIRE- REFLECTORS ON A WAVE-LENGTH OF ABOUT 3 METRES

BY A. K. DUTTA, M.Sc., M. K. CHAKRAVARTY, M.Sc.,

AND

S. R. KHASTGIR, D.Sc.

Dacca University

*(Received for publication, May 5, 1939)*

## Plate X

**ABSTRACT.** The paper presents the results of an experimental study of parasitic wire-reflectors arranged in a parabolic array on a wave-length of about 3 metres. The array had a focal length of  $\lambda/4$  and the length of the wire-reflectors was  $\lambda/2$ . The primary antenna which was a grounded vertical  $\lambda/4$ -aerial connected to an ultra-short transmitter was placed at the focus of the parabola and the waves were received by a heterodyne receiving set constructed for the purpose. The relative field-strengths at a definite distance from the primary antenna were then measured for different orientations of the parabolic reflector. The polar distribution of the field-strengths was in this way studied :

- (1) with *varying* numbers of the wire-reflectors in the array with a *fixed* spacing between the contiguous wires,
- (2) with a *fixed* number of wire-reflectors of *varying* spacing values, and
- (3) with a *constant* value of the aperture for the parabolic array of *varying* numbers of wire-reflectors.

The experimental study yielded information about the dependence of *forward radiation*, *total directivity*, *forward-sector directivity* and *back radiation* on the number, spacing and aperture of the parasitic reflectors in the parabolic array. A theoretical discussion of the experimental results has also been given in the paper.

## I. INTRODUCTION

There are generally two types of multiple antenna systems employed in directional wireless transmission : (1) the directly excited system, and (2) the parasitically excited system. In the first type all the wire-elements of the antenna-array are interconnected by transmission lines so that the phases and the magnitudes of the currents in the radiating elements are under control. In

the second type there is a reflecting array of wires or metallic sheets which derives its energy through induction and radiation from the main or primary antenna or antenna-system. The relative dispositions of the wires in the reflecting array determine in this case the phases and magnitudes of the currents induced in the reflecting wires.

Much work has been done on the directional characteristics of antenna-arrays of the directly excited type and the results of these investigations have been utilised with much success in the commercial application of these arrays. Similar success has not, however, attended the use of parasitic wire-reflectors on a commercial scale, although this type of reflectors was first employed by Hertz<sup>1</sup> (1885-89) and afterwards by Marconi.<sup>2</sup> There may be many kinds of parasitic wire-reflectors, *e.g.*, single, double, trigonal, trapezoidal, plane and parabolic arrays. Some amount of work on these wire-reflectors has already been reported. Mention may be made of Dunmore and Engels<sup>3</sup> experiments with parabolic grid reflectors on a wavelength of 10 metres followed by Jones<sup>4</sup> who worked with similar reflectors on 3 metres. Englund and Crawford<sup>5</sup> investigated the effect of idle antennas in the neighbourhood of an excited one. More recently the directional characteristics of solid metal- and wire-reflectors were studied by Gresky<sup>6</sup> (2.08 metres), Kohler<sup>7</sup> (10.8 cm.), Beauvais<sup>8</sup> (15 to 17 cm.) and others and very recently by Nagy<sup>9</sup> (2.5 metres). The commercial possibilities of the parasitic reflectors were indicated by the work of Vagi,<sup>10</sup> Uda,<sup>11</sup> Meissner and Rothe,<sup>12</sup> Merconi and Franklin,<sup>13</sup> Clavier,<sup>14</sup> Esau and Hahnemann,<sup>15</sup> Wolff, Linder, and Biaden,<sup>16</sup> Kolster<sup>17</sup> and others.

In the present investigation an experimental study has been made of the intensity distribution in a horizontal plane due to the juxtaposition of a vertical antenna and parallel parasitic wires arranged in a parabolic array. It was thought desirable to obtain reliable information about the effect of the number and the spacing of the reflector-elements and of the aperture of the parabolic array on the directional characteristics of such an array. Adequate precaution was necessarily taken in the experimental arrangements to minimise extraneous radiation by placing horizontally, as far as practicable, all idle and current-carrying elements which did not form an integral part of the radiating unit. This resulted in a fair degree of symmetry of the polar radiation patterns so that the conclusions and deductions from these polar patterns are to a great extent reliable. Placing the primary antenna of a small-power ultra-short-wave transmitting set at the focus of the parabolic array, the polar energy distribution at some distance from the reflector was investigated for different values of the number and spacing of the wires and for different apertures of the parabolic system.

The results of these investigations are embodied in this paper and finally some approximate theoretical formulae for parabolic array of the parasitically excited type are discussed in the light of the experimental results.

2. EQUIPMENT

*The Parabolic Reflector*

The reflector-elements of the parabolic array consisted of S.W.G. No. 12 copper wires of length 150 cm. (approximately half the wave-length employed in this investigation). Two similar parabolic wooden frames of about 4 metres aperture, one fixed at a height of 70 cm. above the other in a parallel position, were fitted up with small ebonite discs 10 cm. apart and copper rods were inserted vertically through the holes drilled through the two sets of ebonite discs one above the other in the two wooden frames. Each rod could be fixed in position by a short stout wire inserted transversely at one end of the rod. The double wooden structure was held up at a convenient height by wooden supports so that the distance of the middle of each reflector wire from the ground was about 115 cm. The entire structure was so designed as to permit 360° rotation about a vertical axis through the vertex of the parabola. The focal length of the parabola was 75 cm., i.e., approximately a quarter of the wave-length employed in this work.

*The Transmitter*

The circuit diagram of the transmitting set is given in figure 1. A Telefunken R. E. 134 valve was connected to a single tuned circuit with capacitive retro-action. A voltage of above 250 volts was employed for the direct current supply for the anode circuit. Suitable choke coils having self-resonance at approximately the working wave-length were placed with their axes horizontal in all the D. C. supply leads to the valve electrodes. The transmitting aerial was practically a  $\frac{\lambda}{4}$ -aerial and the wave-length of the radiation was 2'88 metres.

The lower end of a straight S.W.G. No. 12 wire fixed in a vertical position was connected to one end of a small loop of wire which was also placed in a horizontal

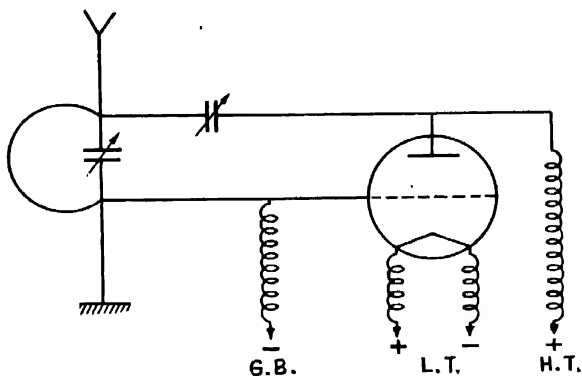


FIGURE 1

plane. This end was also connected to the retro-active condenser. The other end of the horizontal loop which was about 20 cm. above ground was connected to the earth by a straight vertical wire. Immediately above the loop was placed an ammeter to indicate the constancy of the aerial current. A sliding copper tube placed concentrically over the upper part of the vertical aerial was found convenient for the tuning purpose.

A light wooden frame with a horizontal wooden board on the top protected the components of the oscillator from wind and dust. The base board of the frame was fixed on four insulated supports. The aerial supported by a light wooden structure projected directly above the top board of the oscillator. Above this board the ammeter was fitted to the wooden structure supporting the aerial. The distance of the top end of the aerial from the ground was 77 cm. The photograph of the transmitter with the parabolic wire reflector is shown in figure 1(a), Plate X.

### *The Receiving Arrangement*

The receiver constructed for the measurements of relative field intensity comprised a detector-oscillator unit. This stage was used in an oscillating condition for the heterodyne reception of the waves from the transmitter. After rectification the beat-note of audible frequency was passed through an amplifying stage. A low frequency choke was inserted in the anode circuit of the amplifier and a pair of telephones was connected through a large condenser ( $1 \mu F$ ) to the anode end of the low frequency choke and the negative end of the low tension battery feeding the filament of the amplifier. The low frequency potential difference across the telephones was then measured in arbitrary units by means of a valve-voltmeter constructed for the purpose. The circuit diagram of the receiver is shown in figure 2(a). The detector-oscillator valve used was a Philip's T. C. 03/5 valve and the amplifying valve was a B 443 valve with a suitable bias voltage to the control grid. The receiving aerial was similar to the transmitting aerial. The distance of the top end of the aerial from the ground was 87 cm.

An A.C.S.G. valve fed by direct current was employed in the valve-voltmeter. After having applied suitable voltages to the anode and screen-grid the micro-ammeter which was in the plate circuit was balanced in the manner shown in figure 2(b). With the signal on, a change in the deflection of the micro-ammeter was observed. In all cases the readings of the micro-ammeter deflections were taken with a telescope placed at a distance of about 6 metres from the receiver. The complete receiving arrangement was fixed upon a wheeled carrier.

DUTTA, CHAKRAVARTY  
&  
KHASTGIR

PLATE X

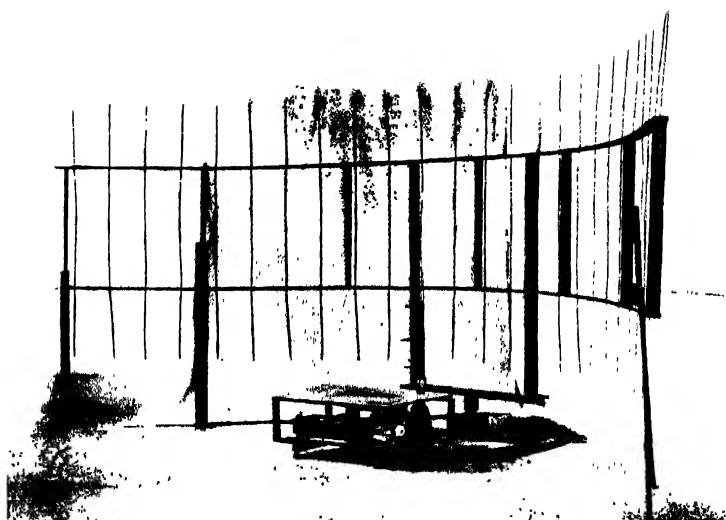


Figure 1 (a)



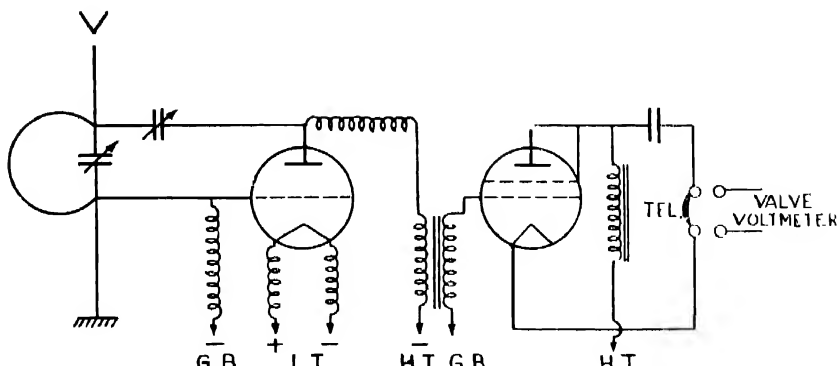


FIG. 2 (a).

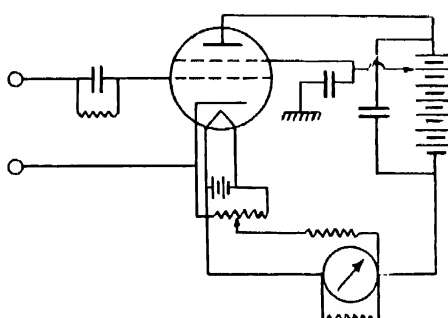


FIG. 2 (b).

To make the transmitting and receiving sets as light as possible, low tension batteries were used separately on insulated stands on the ground.

The tuning condenser in the detector-oscillator circuit was fitted with a long ebonite handle and once the adjustment of wave-length of the oscillation in the detector-oscillator circuit was made by turning this handle, the position of the tuning condenser was kept fixed throughout one set of observation of the micro-ammeter deflections.

The response curve of the receiver showing the change in the micro-ammeter deflection for different values of current in the transmitting aerial was found to be a straight line, except for extremely small aerial currents. The receiver current could, therefore, be taken as directly proportional to the field-strength due to the transmitter at a distance.

#### EXPERIMENTAL PROCEDURE

The experiments were carried out on level earth practically free from the disturbing effect of trees, underground circuits, etc. On the experimental site a circle of radius equal to 75 cm. was first marked out and the antenna of the transmitter was placed exactly at the centre. The receiver was placed at a distance of 10 metres from the transmitting antenna. The straight line joining the two antennas was taken as the zero degree line. Several diameters were

then marked on the circle, making different angles with the zero-line so that the parabolic reflector at its vertex could be placed tangentially along the circle with its axis oriented at different angles ( $0^\circ$  to  $360^\circ$ ) from the zero-line.

At first the measurement of the relative field-intensity was made without the parabolic reflector. After removing the reflector the aerial current of the transmitter was adjusted to some definite value. (The observation of the aerial current was made through a telescope situated at some distance from the transmitter.) The receiver was then adjusted and the change in the deflection of the micro-ammeter in the valve-voltmeter of the receiving set measured with the transmitter on and off. The parabolic reflector was then brought and placed tangentially at its vertex along the circle marked on the ground at the points corresponding to the ends of the diameters marked out previously. Thus for these different positions the axis of the parabola made different angles with the straight line joining the transmitting and the receiving antennas. Keeping the aerial current in the primary antenna the same as before, the changes of micro-ammeter deflections at the receiving end were then measured successively with the transmitter on and off for the different orientations of the parabolic reflector. The polar diagram of the distribution of the relative field-intensity in a horizontal plane was then constructed.

Three distinct cases were investigated :

- (1) Experiments with a *constant spacing* of the reflector-elements of *varying numbers* and consequently of varying apertures of the parabolic reflector.
- (2) Experiments with a *fixed number* of reflector-elements of *different spacing-values*.
- (3) Experiments with a *fixed aperture* of *varying numbers* of reflector-elements.

In all these cases the length of the wires was 150 cm.

#### EXPERIMENTAL RESULTS

The polar distribution of the radiation from the transmitting antenna without the reflector was first determined. The intensity distribution was found to be practically uniform in all directions. The experimental results with the parabolic reflector are given in three different sets.

##### Set I. Study of polar patterns of the parabolic reflector with a fixed spacing (20 cm.) of the reflector wires

The polar distribution of energy with 25, 19, 13, 7 and 3 wires of fixed spacing in the parabolic reflector was determined. A typical set of readings is shown in table I. The corresponding polar diagram is given in figure 3.

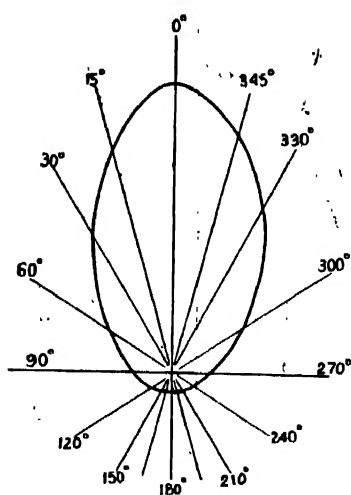


FIGURE 3

TABLE I

Spacing : 20 cm.

Number of wires : 13. Aperture : 224 cm. =  $78\lambda$

Primary aerial current: .21 amp.

Receiver current without reflector =  $8\mu\text{A}$

Orientation of the reflector.	Receiver current (micro-amps.).	Orientation of the reflector.	Receiver current (micro-amps.).
0°	18	90°	2
15°	14	270°	3
345°	16	120°	1
30°	10	240°	1
330°	12	150°	1
60°	4	210°	1
300°	6	180°	1

Figure 4 is constructed to represent graphically the change in the beam-shape with the change in the aperture of the reflector and consequently with the change in the number of wires when the spacing is kept constant. The receiver current  $I_\phi$  for any particular orientation  $\phi$  of the reflector is divided by the value of the

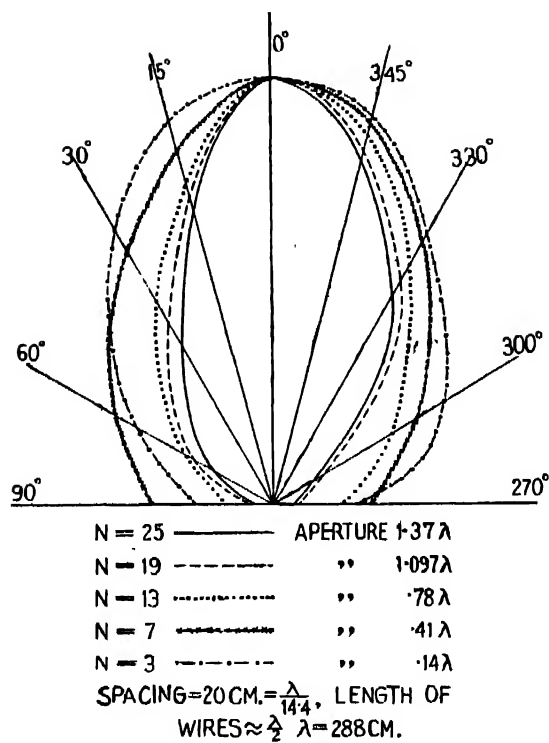


FIGURE 4

receiver current  $I$  without the reflector. This ratio is then expressed as a percentage of the maximum value  $I_0$  in the forward direction. These percentage values are then shown for different orientations of the reflector in the sector  $270^\circ$ ,  $0^\circ$  and  $90^\circ$ . The data for this comparison diagram prepared from the relevant readings of the different polar patterns are given in table II.

TABLE II

Orientation of the reflector.	Percentage values of : $\frac{I_\Phi}{I} / I_0$				
	N = 25	N = 19	N = 13	N = 7	N = 3
0°	100	100	100	100	100
15°	73.2	74.0	77.8	85.7	94.3
345°	86.7	85.1	88.9	92.8	94.3
30°	43.2	51.8	55.6	57.2	...
330°	60.6	66.7	66.6	71.4	60.3
60°	16.7	22.2	22.2	42.9	37.15
300°	13.2	14.7	33.3	...	37.15
90°	3.3	3.7	11.1	28.6	17.1
270°	3.3	7.3	16.7	21.4	22.9

The lateral and back radiation for the reflector within  $90^\circ$  and  $180^\circ$  are depicted in figure 5. The ordinates are the values of the receiver current in per cent. of the maximum forward radiation. In table III are given the data.

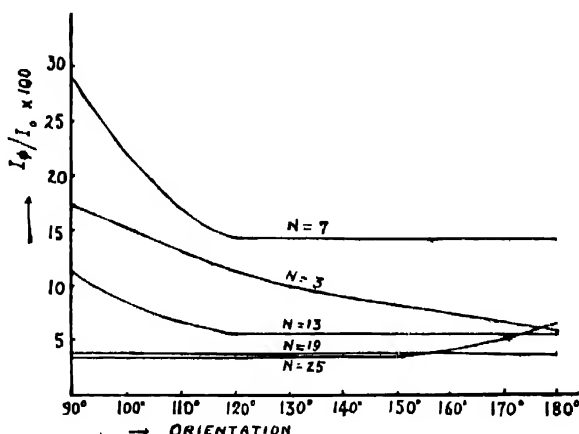


FIGURE 5

TABLE III

Orientation of the reflector.	Percentage values of $\frac{I_\phi}{I_0}$				
	N = 25	N = 19	N = 13	N = 7	N = 3
90°	3.3	3.7	11.1	28.6	17.2
120°	3.3	3.7	5.55	14.3	11.4
150°	3.3	3.7	5.55	14.3	8.6
180°	6.7	3.7	5.55	14.3	5.7

#### DEDUCTIONS FROM THE POLAR PATTERNS (Set I)

Before setting out the deductions from the above experimental study, the different symbols and terms used to characterise the directional properties of the parasitic reflector should be clearly defined :

$l$ =length of the reflector-element.

$S$ =separation of the reflector-elements.

$2a$ =aperture of the parabolic reflector, i.e., the straight-line distance between the two outermost elements in the array.

$N$  = number of reflector-elements in the array.

$\phi$  = orientation of the reflector from the  $0^\circ - 180^\circ$  axis.

$I$  = receiver current without reflector.

$I_\phi$  = receiver current with reflector for any value of  $\phi$ .

$I_0$  = forward radiation, i.e., receiver current when  $\phi=0$ .

$\mu$  = power amplification factor of reflector, i.e., the ratio of the receiver current with reflector for  $\phi=0$  to the receiver current without reflector,  $[\mu=I_0/I]$ .

$\delta$  = total directivity, i.e., the ratio of the area of a circle with radius  $I_0$  to the area of the entire polar pattern.

$\Delta$  = forward-sector directivity, i.e., the ratio of the area of a semi-circle with radius  $I_0$  to the area of the polar pattern contained within the sector  $270^\circ$ ,  $0^\circ$  and  $90^\circ$ .

$\beta$  = back radiation, i.e., the maximum value of the current in the sector  $90^\circ$ ,  $180^\circ$  and  $360^\circ$  expressed in per cent. of  $I_0$ .

$\beta_{180^\circ}$  = value of the receiver current for  $\phi=180^\circ$  in per cent. of  $I_0$ .

In table IV are given the values of  $\mu$ ,  $\delta$ ,  $\Delta$  and  $\beta$  for the polar patterns of Set I.

TABLE IV

$S = 20 \text{ cm.} = 0.069\lambda$ ;  $\lambda = 2.88 \text{ metres}$

No. of wires.	Aperture.	$\mu$	$\delta$	$\Delta$	$\beta_{180^\circ}$	$\beta$
25	$1.37\lambda$	3.3	7.9	3.9	6.7	6.7
19	$1.10\lambda$	3.0	7.1	3.6	3.7	7.4
13	$.78\lambda$	2.2	6.5	3.35	5.6	16.6
7	$.41\lambda$	1.8	4.4	2.5	14.3	28.5
3	$.14\lambda$	2.3	5.1	2.7	5.7	22.9

In figures 6(a) and 6(b) are illustrated the variation of  $\mu$ ,  $\delta$ ,  $\Delta$  and  $\beta$  with the change of aperture of the reflector.

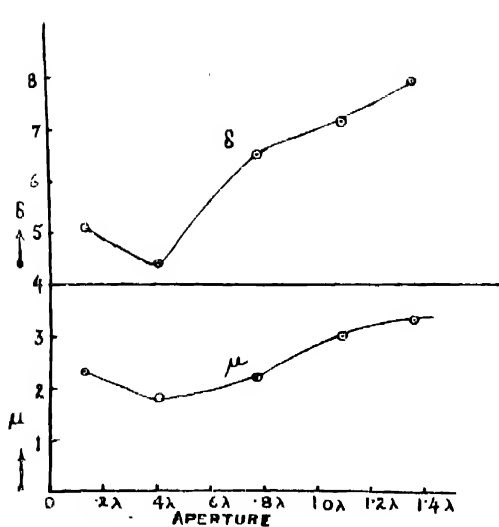


FIGURE 6(a)

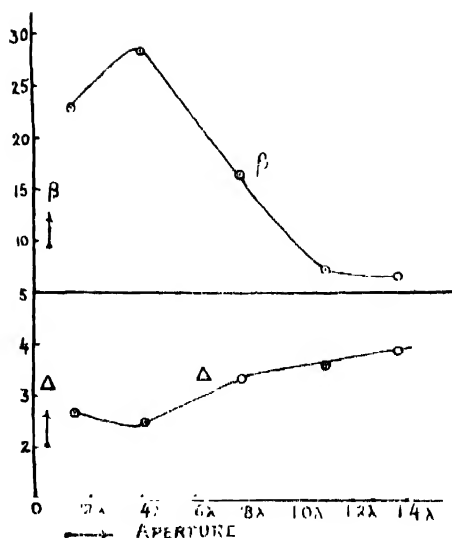


FIGURE 6(b)

The following is a summary of these results with conclusions and explanatory notes :

(1) With a constant spacing (20 cm.) and a constant length (150 cm.  $\approx \frac{\lambda}{2}$ ) of the wires, the forward radiation or the power-amplification factor of the reflector was found in general to increase with the increase of aperture. A diminution was, however, observed for  $0.41\lambda$  aperture. From considerations of phase relations it is evident that forward radiation may not continuously increase with the increase of aperture and may actually show a diminution for a certain increment of aperture. When the aperture is increased by the addition of an element to each side of the axis of the reflector, the phases of the field due to these added elements may be such as to cause 'destructive interference' so that the forward radiation may be 'nullified.' Additional elements will, however, compensate for this diminution and forward radiation will then increase with aperture till an unfavourable aperture-value is attained where the condition for destructive interference will prevail. The forward radiation is expected accordingly to reach a limiting value, when with further addition of wires the outermost reflector-elements will not materially contribute either additively or subtractively, since the induced currents in these outermost elements will necessarily be small. This limiting aperture according to Gresky, Kohler and Nagy is in the region of  $1.4\lambda - 1.5\lambda$ . It will be seen from figure 6(a) that the forward radiation tends to approach a constant value for the larger apertures.

(2) With the same spacing and the same wire-length, the forward-sector directivity increased in general with the increase of aperture and so also the total directivity. (See figure 6b.)

It is to be emphasised that the consideration of the phase-relationship is of prime importance. The aperture cannot, therefore, be always an index of amplification and directivity. It will be shown later that the amplification and the directivity of the reflector are altered by changing the number and the spacing of the elements even with the same aperture.

(3) Under similar reflector conditions the backward radiation seemed to be reciprocally related to the amplification and the directivity, i.e., a large amplification or directivity was found to be associated with a small back radiation. This is illustrated in figure 7 where the back radiation is plotted against amplification. It will, however, be shown later that this state is not generally true.

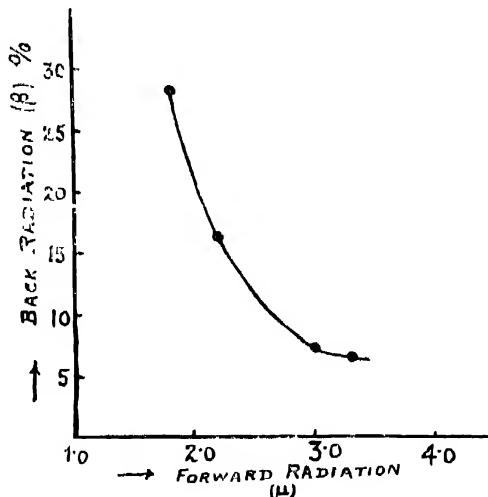


FIGURE 7

(4) Under similar conditions, the general nature of the variation of back radiation is a gradual diminution with the increase of aperture with a tendency to approach a steady value (figure 6a). This should be so, since back radiation is determined principally by the elements in the neighbourhood of the vertex of the parabolic array.

#### *Set II. Study of polar patterns of parabolic reflector having a constant number of reflecting wires with different spacings*

Polar patterns of a 7-wire parabolic array for six different spacings (10 cm., 20 cm., 30 cm., 40 cm., 50 cm. and 80 cm.) were constructed.

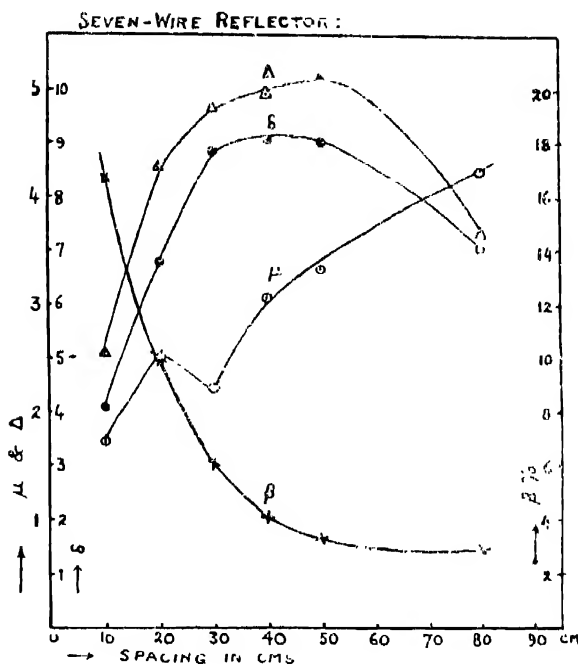


FIGURE 8

The power-amplification factor  $\mu$ , the total directivity  $\delta$ , the forward-sector directivity  $\Delta$  and the back radiation  $\beta$  are calculated from the experimental data. These are incorporated in table V. The results are illustrated in figure 8.

TABLE V

 7 wires  $\lambda = 2.88$  metres

Spacing.	Aperture.	$\mu$	$\delta$	$\Delta$	$\beta_{180^\circ}$	$\beta$
10 cm. = $0.35\lambda$	20.5 cm	1.71	4.09	2.54	16.7	25
20 cm. = $0.69\lambda$	40.4 "	2.50	6.79	4.26	10.0	20
30 cm. = $1.0\lambda$	50.3 "	2.23	8.87	4.84	6.1	10.20
40 cm. = $1.4\lambda$	80.1 "	3.06	9.09	4.96	4.0	12.24
50 cm. = $1.7\lambda$	100.0 "	3.33	9.05	5.1	3.3	10.0
80 cm. = $2.8\lambda$	395.5 "	4.25	7.08	3.65	2.94	5.88

## DEDUCTIONS FROM THE POLAR PATTERNS (SET III)

(1) Using a 7-wire reflector of constant wire-length, the power-amplification factor was found in general to increase with the increase of spacing. It is expected, however, from consideration of phases that the forward radiation may not always be an increasing function of spacing. In our experiment, the forward radiation for  $S=30$  cm. showed a diminution and increased again with the increase of spacing. (See figure 8.)

(2) With the same number of wires of constant length, the total directivity and the forward sector directivity were found to increase with the increase of spacing, each attaining a maximum in the region 50 cm. ( $17\lambda$ ) after which there was a diminution. (See figure 8).

(3) Under similar conditions, the back-radiation at  $180^\circ$  was found to diminish continuously with the spacing tending to approach a constant value. (See figure 8.)

*Set III. Study of polar patterns of the parabolic reflector of constant aperture with different numbers of wires*

Polar patterns of the parabolic array with  $1.37\lambda$  aperture (395.5 cm.) having 25 wires of spacing 20 cm., 13 wires of spacing 40 cm., 7 wires of spacing 80 cm. and 3 wires of spacing 240 cm. were constructed.

The values of power-amplification factor, total directivity, forward-sector directivity and back radiation calculated from the data are given in table VI.

TABLE VI

Aperture =  $1.37\lambda$  $\lambda = 2.88$  metres

No. of wires.	Spacing $S$	$\mu$	$\delta$	$\Delta$	$\beta_{180^\circ} \%$	$\beta \%$
25	20 cm.	3.33	7.7	3.02	6.06	6.06
13	40 cm.	3.5	6.93	3.56	3.6	7.1
7	80 cm.	4.25	7.08	3.65	2.94	5.88
3	240 cm.	3.125	12.08	9.1	16	16

These results are illustrative of the statement previously made, viz., the aperture is not always an index of amplification or directivity, for with the same aperture we see an increase or a decrease of forward radiation or directivity with different numbers of wires of varying separations. Again, it is not generally true that back radiation is small when the directivity is large or *vice-versa*. It is

clear from table VI that with 3 wires of 240 cm. spacing, the back radiation was considerable and the directivity was also large.

### S. THEORY OF PARABOLIC ARRAY OF PARASITIC WIRES

An approximate theory of the parabolic reflector has been worked out by A. Hund by the application of Huyghens' principle according to which the radiation can be imagined as being due to fictitious radiators which lie in the front face of the reflector. The directional characteristic (in a horizontal plane) of a vertical antenna with a parabolic reflector is accordingly given by

$$I_\phi = I_0 \cdot \frac{\sin \left[ \frac{2\pi}{\lambda} a \sin \phi \right]}{\sin \phi} \quad \dots \quad (1)$$

F. Ollendorff has also derived a similar formula for the field-strength in a horizontal plane of a parabolic array of vertical elements. Considering the effect of the reflector as equivalent to that of a metallic sheet carrying a current of constant amplitude, the expression for the field-strength is given by

$$I_\phi = K \left| \frac{\sin (2\pi/\lambda \cdot a \sin \phi)}{\sin \phi} \right| \quad (2)$$

where  $K = \frac{l_i}{\pi \epsilon_0 c r}$

$l$ =length of the reflector-element ;

$i$ =current density ;

$\epsilon_0$ =dielectric constant of vacuum ;

$r$ =distance from centre of aperture to receiver ;

$c$ =velocity of light ;

$a$ =half aperture of reflector ;

and  $\phi$ =orientation of reflector from the zero degree line.

We shall now examine Ollendorff's formula and see how far it agrees with our experimental results.

### I. Forward Radiation

By differentiating the numerator and the denominator of (2) separately, we can obtain the magnitude of the forward radiation from

$$I_\phi = K \frac{\cos\left(\frac{2\pi a}{\lambda} \sin \phi\right)}{\cos \phi} \cdot \frac{\frac{2\pi a}{\lambda} \cos \phi}{1 - \frac{2\pi a}{\lambda} \sin^2 \phi}$$

On putting  $\phi=0$ , we get  $I_0 = k.a$ , where  $k = \frac{2\pi K}{\lambda}$ . This relation is only approximately satisfied within a limited range of apertures as is evident from figure 9(b) where the results of our experiments (Set I) are compared with the results expected according to Ollendorff's formula.

### II. Forward-Sector Directivity

The values of forward-sector directivity  $\Delta$  are computed from the polar diagrams constructed according to Ollendorff. The theoretical and the experimental values in arbitrary units are shown for comparison in figure 9(a). The similarity only lies in the fact that both theoretically and experimentally there is an increase of  $\Delta$  with aperture.

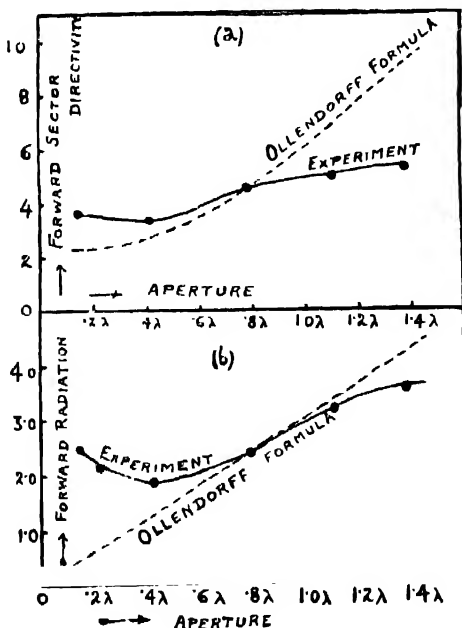


FIGURE 9

It should be remembered that, for Ollendorff's formula to hold, the arrays should produce effects similar to those of metallic sheets. According to Blake and Fountain<sup>20</sup> the spacing must then be  $\frac{\lambda}{30}$  or  $\frac{\lambda}{40}$ . Complete agreement with theory is not, therefore, expected since the spacing employed in the experiments, the results of which are considered here, is about  $\frac{\lambda}{4}$ .

#### 6. S U M M A R Y

The results of an experimental study of a parabolic wire-reflector on a wavelength of 2·88 metres are given in this paper. The parabolic array had a focal length of about  $\frac{\lambda}{4}$ . The main results of this study are enumerated below:—

(1) With a spacing of  $'069\lambda$  ( $= 20$  cm.) the a constant wire-length of  $\frac{\lambda}{2}$ , the forward radiation and the directivity were, in general, found to increase with the increase of aperture. A diminution was, however, noticed at a certain increment of aperture. The range of aperture was from  $'14\lambda$  to  $1'37\lambda$  and the number of wires was varied from 3 to 25. There was an indication of a limiting value of the forward radiation for the larger apertures.

(2) Under similar reflector conditions, a large amplification or a large directivity seemed to be associated with a small back-radiation and the latter was found in general to diminish with the increase of aperture.

(3) With a seven-wire parabolic reflector of the same wire-length as before, the forward radiation was found in general to increase with the increase of spacing. Under similar conditions the total directivity and the forward-sector directivity increased with the increase of spacing, each attaining a maximum in the region  $S = '17\lambda$  ( $= 50$  cm.). The back-radiation at  $180^\circ$  was found to diminish with the increase of spacing with a tendency to approach a constant value. The spacing ranged from  $'035\lambda$  to  $'28\lambda$ .

(4) The aperture was not always found to be an index of amplification and directivity; for, with the same aperture, an increase or a decrease of forward radiation and directivity was observed with different numbers of wires of varying spacing values.

(5) The statement in (2) is not also generally true, for working with a constant aperture, sometimes a large directivity with a relatively large amount of back-radiation was found, depending on the number and the spacing of the wires.

The experimental results have been used finally to discuss an approximate formula deduced by Ollendorff.

PHYSICS DEPARTMENT,  
DACCÀ UNIVERSITY.

#### R E F E R E N C E S

- 1 Hertz, *Electrical Waves*, Translated by Jones (1900).
- 2 Marconi, *Proc. I.R.E.*, **10**, 215 (1922).
- 3 Dunmore & Engels, *Bur. Stand. Sci. paper*, 469 (1923).
- 4 Zones, *QST*, May (1925).
- 5 Englund & Crawford, *Proc. I.R.E.*, **16**, 126, (1928).
- 6 Gresky, *Zeil für Hochfrequenz*, **32**, 144 (1938).
- 7 Kohler, *Hochfrequenz und Electroakustik*, **39**, 207 (1932).
- 8 Beauvais, *L'onde Electrique*, 184 (1930).
- 9 Nagy, *Proc. I.R.E.*, **24**, 233 (1936).
- 10 Yagi, *Proc. I.R.E.*, **16**, 715 (1928).
- 11 Uda, *Proc. I.R.E.*, **18**, 1047 (1930).
- 12 Meissner & Rothe, *Proc. I.R.E.*, **17**, 36 (1929).
- 13 Marconi, *Proc. I.R.E.*, **16**, 40 (1928); Franklin, *Electrician* (London), **6** (1933).
- 14 Clavier, *Electrical Communication*, 1931 (1933).
- 15 Eisen & Halmemann, *Proc. I.R.E.*, **18**, 471 (1930).
- 16 Wolff, Linder & Braden, *Proc. I.R.E.*, **23**, 11 (1935).
- 17 Kolster, *Proc. I.R.E.*, **22**, 1035 (1934).
- 18 Lund, A., *Phenomenon in High Frequency Systems*, 525 (1936).
- 19 Ollendorff, F., *Die Grundlagen der Hochfrequenz Technik*, 600, quoted in Nagy's paper, *Proc. I.R.E.*, **24**, 253 (1936).
- 20 Blake and Fountain, *Phys. Rev.*, **23** (1906).

# ON THE ABSORPTION AND EMISSION SPECTRA OF RARE EARTH CRYSTALS

By P. C. MUKHERJI,  
P. R. Student, Calcutta University

(Received for publication, May 26, 1939)

## Plate XI

**ABSTRACT.** In this paper the results of investigation of the emission and absorption spectra of the rare earth ions like  $\text{La}^{++}$ ,  $\text{Ce}^{+++}$ , etc., in crystals are given. An attempt has been made to correlate their absorption and emission spectra with special reference to  $\text{Ce}^{+++}$  ions.

It has been observed that the  $\text{La}^{++}$  ions in crystals do not fluoresce. The emission spectra due to  $\text{Ce}^{+++}$  ions in the chloride and the sulphate crystals consist of two discrete bands. The positions of the bands are slightly different in the two salts but they occupy almost the same positions whether the salts investigated are hydrated or dehydrated. The spectra due to  $\text{CeF}_3$  consist of three such emission bands; further on excitation with high frequency a weak luminescence appears on the long wave-side of the bands.

The strong and discrete emission bands have been supposed to be due to the true fluorescence of the  $\text{Ce}^{+++}$  ions. In conformity with the explanation of the absorption spectra due to  $\text{Ce}^{+++}$  ions by Bose and the writer, the origin of these emission bands has been ascribed to the transitions  $5D \rightarrow 4F$  in  $\text{Ce}^{+++}$  ions. The two bands in the chloride and the sulphate and the two lower frequency bands in the fluoride arise from the transitions  $5^2D_{5/2} \rightarrow 4^2F_{5/2, 7/2}$ , while the third band in  $\text{CeF}_3$  is due to  $5^2D_{3/2} \rightarrow 4^2F_{5/2}$ . It has been shown that there is a correlation between the frequency of the emission bands and the corresponding absorption frequencies. The absence of the third band in the other two crystals has been discussed.

The origin of the weak luminescence is not clearly understood. It has been suggested that it is due to an excitation of the  $\text{F}^-$  ion by a collision of the second kind, with the excited  $\text{Ce}^{++}$  ions, the process resembling somewhat a case of sensitized fluorescence.

## INTRODUCTION

In a previous paper \* the fluorescence spectra of a few rare earth ions, viz.,  $\text{La}^{+++}$ ,  $\text{Ce}^{+++}$ ,  $\text{Pr}^{+++}$  and  $\text{Nd}^{+++}$  in solution were investigated by the writer.

Zeit für Phys., 109, s 573 (1938).

It was observed that in solution all the ions give rise to a common diffuse band in emission, while in  $\text{Pr}^{+++}$  and  $\text{Nd}^{+++}$  ions there are respectively two and three additional diffuse bands. For the emission of the common fluorescence band by the four rare earth ions in solution, the following mechanism was proposed. The emission centres were assumed to be the metal complex ( $\text{Me}^{+++} \text{nH}_2\text{O}$ ), in which the  $\text{H}_2\text{O}$  groups are polarised in the field of the  $\text{Me}^{+++}$  ion. Even in the case of  $(\text{La}^{+++} \text{nH}_2\text{O})$ , which has no electron in the  $4f$  shell, the solution shows finite continuous absorption in the ultra-violet; the absorption of radiation is supposed to be by the complex as a whole leading to an excitation of the polarised  $\text{H}_2\text{O}$  group and re-emitted as fluorescence radiation. This fluorescence is similar in mechanism to that shown by uranyl groups  $[\text{UO}_2]^{++}$ . The fluorescence radiation emitted by the solutions containing  $\text{Ce}^{+++}$ ,  $\text{Pr}^{+++}$  and  $\text{Nd}^{+++}$  are much stronger than that by the La solution. This can be interpreted in the following way. In the case of  $(\text{Ce}^{+++} \text{nH}_2\text{O})$ , for example, besides the continuous absorption by the complex as a whole there are discontinuous absorption bands due to the absorption by the  $\text{Ce}^{+++}$  ions ( $4F \rightarrow 5D$ ). The corresponding ion is in a metastable excited state, and before it comes back to its ground state by the emission of radiation, it can transfer its energy by collision with other hydrated ions. These latter become excited and emit energy by  $\gamma$ -emission, with a frequency equal to that given by the lanthanum complex. If  $v_0$  represents the frequency associated with this transition, the presence of the additional bands was explained as having frequencies  $(v_0 \pm v_1)$  where  $v_1$  represents one or other of the characteristic frequencies of the  $\text{Me}^{+++}$  ion.

Later on, the fluorescence spectra of the same ions were investigated using crystals having different anions, both in the hydrated and in the anhydrous state. It was noticed that the width of the emission bands was much reduced; further the spectra of the different crystals having the same cations were found to be different. But no perceptible change could be found between the emission spectra of the same crystal when hydrated or in the dehydrated state. The purpose of the present paper is to study the correlations between the emission and absorption spectra of these ions in crystals and to attempt an explanation of the origin of the emission spectra in crystals with special reference to  $\text{Ce}^{+++}$  ion. But before we proceed to discuss the absorption and emission spectra of  $\text{Ce}^{+++}$  etc. ions, let us give a brief résumé of the previous knowledge of the fluorescence spectra of the rare earth crystals.

#### PREVIOUS KNOWLEDGE OF THE FLUORESCENCE SPECTRA OF THE RARE EARTHS

The true fluorescence of the rare earth ions was first observed by Tomaschek and Deutschbein<sup>1</sup> in pure hydrated crystals of Sm, Eu, Tb and Dy. The spectra

consist of groups of more or less sharp and diffuse lines in the visible region, which increased in sharpness on lowering the temperature of the crystals. Later on, Gobrecht<sup>2</sup> extended the investigations to the infra-red side and by considering the complete set of emission data was able to obtain some correlation between the emission and the absorption spectra of the respective ions.

In the rare earth ions the different combinations of the  $l$ - and  $s$ -vectors of the  $4f$  electrons according to the Russell-Saunders coupling give rise to a number of  $J$ -levels. Of these the term having the smallest inner quantum number consistent with the highest multiplicity and  $l$ -moment represents the ground state for the members in the first half of the series; for the latter half which have inverted terms the ground term will have the corresponding highest  $J$ -value. In the process of absorption the  $4f$ -electrons are excited from the ground state to the upper states allowed by the selection principle. In the crystals on account of the strong crystalline electric field the quadrupole radiation is also possible so that the selection rules will be due to both the dipole and the quadrupole radiation. Further in the strong inhomogeneous electric field each of the said  $4f$ -levels is perturbed and their degeneracy is partly removed ; so instead of a single line a group of lines arises out of each of those transitions.

In emission,\* on the other hand, the final state will be generally the ground state or some other state in its neighbourhood while the initial state may be the upper ones allowed by the selection rules. It is generally found that the transitions ending in the ground state give rise to the strong components in the emission spectra. Gobrecht has shown that for the four ions investigated there is an agreement between the number of strong emission groups and the multiplicity of the ground term. This is shown in table I. He also showed that the over-all splitting of the ground term obtained from the emission spectra leads to a correct value of the screening constant for the four ions investigated. Tomaschek and Melnert<sup>3</sup> recently observed the sharp fluorescence spectra in  $Gd^{+++}$  ions using hydrated sulphate crystals. It consists of one group of principal emission lines in the ultra-violet, which coincides in position with the group of absorption lines of lowest frequency due to the same ion. In  $Gd^{+++}$  ion having an  $^8S$ -term for its ground state only one group of emission lines is to be anticipated. It is thus clear that the fluorescence spectra observed in these five ions are explicable on the usual theory of emission spectra of such ions. But it is not understood, so far, why the sharp emission spectra are observed only in these five rare earth ions, while the absorption spectra of a similar nature are known to be present in all the members of the series excepting only  $Ce^{+++}$  and  $Yb^{+++}$ .

\* The mechanism of emission will be discussed more fully later on in the paper.

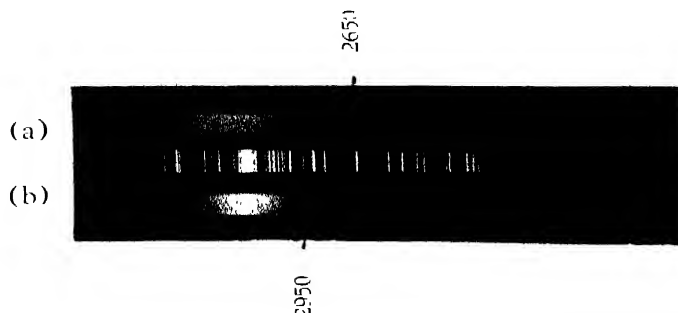
TABLE I

(Fluorescence spectra due to different rare earth ions in hydrated crystals)

Ion.	Ground State	Emission group.	Average intensity	Average position.	Final level.
$\text{Sm}^{++}$	$6H$	1	5	9,755 cm. <sup>-1</sup>	$6F_{7/2}$
		2	5	10,773 "	$6F_{5/2}$
		3	7	11,295 "	$6H_{11/2}$
		4	7	12,844 "	$6H_{13/2}$
		5	7	14,189 "	$6H_{11/2}$
		6	6	15,574 "	$6H_{9/2}$
		7	6	16,710 "	$6H_{7/2}$
		8	4	17,800 "	$6J_{5/2}$
$\text{Eu}^{+++}$	$7F$	1	9	12,215 cm. <sup>-1</sup>	$7F_6$
		2	4	13,330 "	$7F_5$
		3	5	14,340 "	$7F_4$
		4	5	15,325 "	$7F_3$
		5	9	16,240 "	$7F_2$
		6	8	16,877 "	$7F_1$
		7	3	17,108 "	$7F_0$
		*8	3	17,968 "	
		*9	3	18,711 "	
		*10	3	19,049 "	
$\text{Tb}^{+++}$	$7F$	1	8	14,734 cm. <sup>-1</sup>	$7F_0$
		2	7	14,938 "	$7F_1$
		3	5	15,399 "	$7F_2$
		4	6	16,145 "	$7F_3$
		5	6	17,076 "	$7F_4$
		6	9	18,334 "	$7F_5$
		7	5	20,483 "	$7F_6$
$\text{Dy}^{+++}$	$6H$	1	5	10,269 cm. <sup>-1</sup>	$6H_{5/2}$
		2	6	11,732 "	$6H_{7/2}$
		3	5	13,129 "	$6H_{9/2}$
		4	4	15,113 "	$6H_{11/2}$
		5	4	17,395 "	$6H_{13/2}$
		6	5	20,699 "	$6H_{15/2}$

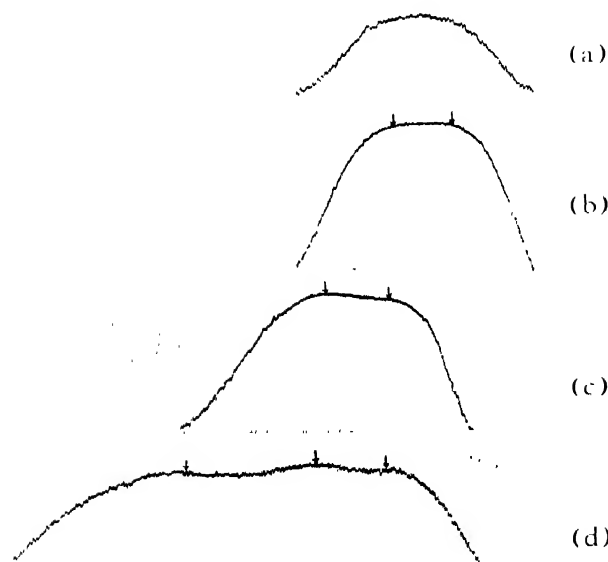
\* These groups are due to transitions from a level above the first excited state.

Figure 1.

Absorption spectra of  $\text{CeF}_3$ 

- (a) Using a very thin layer.
- (b) Using a thicker layer.

Figure 2.



## Microphtotometric records of fluorescence spectra.

- (a)  $\text{CeCl}_3$  soln.—one band with its centre at  $28,220\text{cm}^{-1}$
- (b)  $\text{CeCl}_3$  crystals—two bands at  $26,838$ ;  $29,631\text{ cm}^{-1}$
- (c)  $\text{Ce}_2(\text{SO}_4)_3$  crystals—two bands at  $29,655$ ;  $32,400\text{cm}^{-1}$
- (d)  $\text{CeF}_3$  crystals—three bands at  $29,655$ ;  $32,450$ ;  $36,095\text{cm}^{-1}$



FLUORESCENCE SPECTRA OF THE RARE EARTH IONS  
 INVESTIGATED

The fluorescence spectra of the first four ions of the rare earth series, *viz.*, La<sup>+++</sup>, Ce<sup>+++</sup>, Pr<sup>+++</sup> and Nd<sup>+++</sup> were investigated using hydrated and dehydrated crystals. The fluorescence was observed using monochromatic exciting radiations. A detailed account of the method of experimental investigation is given in a previous paper by the writer.<sup>4</sup> It was found that La<sup>+++</sup> ions in crystals do not fluoresce. In Ce<sup>+++</sup> ions, on the other hand, interesting results were obtained; both the position and the number of the bands were found to vary with the different anions used. The results are given in table II. The investigations with Pr<sup>+++</sup> and Nd<sup>+++</sup> ion are now being repeated with extra pure samples but no evidence of any fluorescence has been obtained in the near ultra-violet.\*

TABLE II

 Fluorescence bands of Ce<sup>+++</sup> ions in different hydrated and anhydrous crystals

Exciting radiation A.U.	Fluorescence radiation A.U.		
	Chloride (anhydrous).	Sulphate (hydrated and anhydrous).	Fluoride.
(a) 2750	3900-3200	1.3440-3305	1.3440-3305
		2.3205-2990	2.3206-2970
(b) 2550	"	1.3440-3305	1.3440-3305
		2.3205-2990	2.3205-2970
(c) 2300	"	1.3440-3305	1.3440-3305
		2.3205-2990	2.3200-2970
(d) 2100	"	1.3440-3305	1.3440-3305
		2.3205-2990	2.3200-2970
			3.2800-2740
			4085-3440

\* The investigation is now being carried on with Fluorite Spectrograph and Ilford's Q-plates.

$\text{La}^{+++}$  ions in solution fluoresce but not when they form part of a crystal. The continuous absorption and the fluorescence emission in the solution is by the metallic complex  $\text{La}^{+++} \cdot n\text{H}_2\text{O}$ . In the crystal, on the other hand, the absorption of radiation is by the lattice as a whole, and this is dissipated in the form of lattice oscillation. In order to understand the origin of the emission spectra due to  $\text{Ce}^{+++}$  ions in the different crystals it seemed necessary to investigate the absorption spectra of the respective crystals.

#### ON THE ABSORPTION SPECTRA DUE TO $\text{Ce}^{+++}$ IONS

The absorption spectra due to  $\text{Ce}^{+++}$  ions were observed by Bose and Datta<sup>5</sup> in solution and by Freed<sup>7</sup> using hydrated mixed crystals of Ce and La. It was found that the spectra consist of broad bands, which do not undergo any change with the lowering of temperature of the crystals. But the positions of the bands are altered slightly by changing the anions. These are shown in table III.

TABLE III

(Absorption spectra of  $\text{Ce}^{+++}$  ions in solution and in crystals)

Bands.	Position of the bands in A.U.		
	$\text{CeCl}_3$ soln. (1)	$\text{Ce}_2(\text{SO}_4)_3$ soln. (2)	$\text{La}(\text{Ce})\text{Cl}_6 \cdot 6\text{H}_2\text{O}$ (3)
I	2970	2960	3020
II	2525	2540	2775
III	2380	2400	2455
IV	2225	2230	2300

(1) By Bose and Datta.<sup>5</sup>

(2) By Roberts and Wallace.<sup>6</sup>

(3) By Freed.<sup>7</sup>

In course of the present work, the absorption spectra of  $\text{CeF}_3$  crystals were investigated. As single crystals of  $\text{CeF}_3$  could not be obtained, the investigation was carried on by the reflection method using extremely thin layer of the salt. In order to obtain a uniformly thin deposit, a small quantity of the salt was finely powdered and then shaken with distilled water in a beaker. After allowing some time for the heavier particles to settle down, a clean quartz plate was carefully introduced and kept suspended horizontally inside the water. After a

long time when the fine particles settled down, the clear water was siphoned out and the quartz disc was dried up. In this way uniform deposits of varying thickness were prepared. The absorption spectra, obtained by using a hydrogen discharge tube, is shown in plate XI. It was found that using even the thinnest deposit the absorption was of a continuous nature and so no definite conclusion could be reached. But it was noticed that on diminishing the thickness of the deposit the long wavelength limit of the continuous absorption shifts from about  $3100\text{A}^\circ$  to  $2600\text{A}^\circ$ . It indicates the existence of a very weak band in the neighbourhood of  $3000\text{A}^\circ$ .

In a recent paper by Bose and the writer<sup>8</sup> on the origin colour of paramagnetic ions in solution, the absorption spectra of  $\text{Ce}^{+++}$  ions in solution were explained to be due to the transition  $4^2F_{5/2} \rightarrow 5^2D_{5/2, 3/2}$ . In  $\text{Ce}^{+++}$  ions  $4F$  is the ground state and  $5D$  is the first virtual state whose average position in the case of vapour was taken to be at  $50,982 \text{ cm}^{-1}$  as given by Lang.<sup>9</sup> In solution the ground term  $4F$  being screened by the  $(5s, 1)$  octet shell remains unaffected, but the virtual ( $5d$ ) states are strongly perturbed by the influence of the neighbouring molecules.

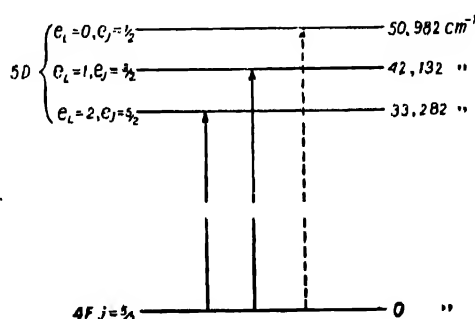


FIGURE 1

The scheme of energy levels proposed to explain the absorption spectra is shown in figure 1. The  $5D$  level is pictured as split up into three sub-levels. The relative positions of the sub-levels were calculated from the formula given below,

$$\Delta\nu = Ne \cdot \Delta e_L \cdot K'$$

where  $Ne$  = ionic charge,

$\Delta e_L$  = change in the electric quantum number,

$K'$  = a constant for all ions having a particular state.

putting  $Ne = 3$ ,  $e_L = 0, 1$  and  $2$  and  $K' = 2950 \text{ cm}^{-1}$

the average value of the constant for all ions having a  $D$ -state. In the process of absorption the  $4F$  electron may occupy one or other of the three  $5D$  levels and so three diffuse bands are expected as shown by the arrows. The agreement between the observed and the calculated positions is shown in table IV.

TABLE IV

Bands.	$\lambda(\text{A}.\text{\AA}.)$	$\nu(\text{Cm.}^{-1})$	C. G. ( $\text{Cm.}^{-1}$ )	$\nu(\text{Calcd.})$	Transitions.
I	2970	33,660	33,660	33,282 $\text{cm.}^{-1}$	$4F_{5/2} \rightarrow 5D_{5/2} (e_L = 2)$
II	2525	39,592			
III	2380	42,004	42,175	42,132 "	$4F_{5/2} \rightarrow 5D_{3/2} (e_L = 1)$
IV	2225	44,930		50,982 "	$4F_{5/2} \rightarrow 5D_{1/2} (e_L = 0)$

In table III it is found that the absorption spectra due to  $\text{Ce}^{+++}$  ions in hydrated crystals are, more or less, similar to that found in solution. It may be supposed, therefore, that the splitting up of the  $5D$  state in these hydrated crystals will be somewhat similar to that taking place in solution. So that a similar energy level diagram as shown in figure 1 will account for the absorption spectra of such crystals, only the value of the constant  $K'$  will be slightly modified by the different ions present.

#### ON THE EMISSION SPECTRA DUE TO $\text{Ce}^{+++}$ IONS IN CRYSTALS

The results of investigation on the fluorescence spectra of  $\text{Ce}^{+++}$  ions in crystal are given in table III. It was found that in  $\text{CeCl}_3$  crystals the emission band occupies the same position as in the corresponding aqueous solution. But from an examination of the microphotometric record of the spectrum it appeared to consist of two diffuse bands overlapping each other. In the sulphate crystals the two bands are more distinct and they occupy the same position whether obtained from the hydrated or the dehydrated crystals; but the position of the bands in either case is displaced slightly to the high frequency side as compared with that of  $\text{Ce}_2(\text{SO}_4)_3$  solution. The total width of the two bands is same in either of the above cases and is nearly equal to that of the common fluorescence band observed in solution. In  $\text{CeF}_3$  crystals three emission bands were noticed, of which the first two coincide in position with those due to the sulphate crystals. The third band on the higher frequency side appeared when the exciting frequency was high and along with this band a weak and diffuse luminescence appeared on

the longer wavelength side of the principal emission bands. The microphotometric records of the emission spectra are shown in plate XI. The centres of gravity of the bands obtained in the different crystals using the highest frequency used, viz.,  $48 \times 10^3$  cm.<sup>-1</sup> nearly are given in table V.

TABLE V

Centres of gravity of the Fluorescence bands due to Ce<sup>+++</sup> ions in crystals

Exciting Frequency.	Fluorescence bands emitted		
	Chloride.	Sulphate	Fluoride.
$48 \times 10^3$ cm. <sup>-1</sup>	(1) 26,838 cm. <sup>-1</sup> (2) 29,621 "	(1) 29,655 cm. <sup>-1</sup> (2) 32,400 "	(1) 29,655 cm. <sup>-1</sup> (2) 32,150 " (3) 36,095 "

The origin of these emission spectra will now be discussed in the light of the present theories of luminescence of solids. In the case of crystals like those investigated here, there are the following alternative possibilities, when light of suitable frequency is incident on them, viz.,

(1) The ultra-violet light may be absorbed by the Ce<sup>+++</sup> ions; (a) this may result in emission by the excited Ce<sup>+1+</sup> ions of the crystals. This gives rise to the true fluorescence; (b) there may be emission by transference of energy to the anion or a molecule attached to the Ce<sup>+1+</sup> ion by a collision of the second kind. This will be somewhat analogous to 'sensitized fluorescence.'

(2) Above a certain frequency the anion may begin to compete with the cation in absorption of radiation. At this stage no further emission levels of the cation may be excited by increasing the frequency of the exciting radiation.

#### ORIGIN OF THE FLUORESCENCE BANDS

In the different crystals containing Ce<sup>+++</sup> ion the stronger emission bands observed are evidently due to the true fluorescence of the cation. Their origin is, therefore, due to the possibility 1 (a), where Ce<sup>+++</sup> ions act as the absorbing and the emitting centres. In order to specify the different transitions in Ce<sup>+++</sup> ions, which may give rise to the respective emission bands, we shall discuss in brief the mechanism of fluorescence of solids as it is pictured now-a-days.

In the interior of a solid, an electron shares the vibration energy of the lattice and so the energy levels instead of being very sharp and discrete are spread over a band of energy. The spreading up of the energy states is also brought about by the resonance effect between the neighbouring cations, as they are much more closer to each other inside a solid than when in the vapour state. At the ordinary temperature the broadening in some cases increases to such an extent that there is overlapping of the two successive energy states. In such a case the Condon curves for the successive states will either touch or intersect each other. It was pointed out by Mott and Gurney<sup>10</sup> that this is an essential condition for the origin of phosphorescence or fluorescence in solids. In figure 2, let 'a' represent the Pot. E-curve for the ground state, while 'b' and 'b'' represent the

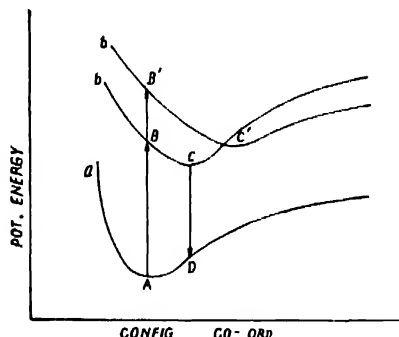


FIGURE 2

a—Ground states

b, b'—Successive excited states.

same for the two successive excited states. If A be the position of the absorbing centre when it absorbs, then, according to the Franck-Condon's principle, it can go to either B or B' by absorbing quanta Ab or Ab' respectively ; for there cannot be any change in the relative positions of the atomic nuclei during the absorption of a quantum of radiation. If it goes to B, then, by process of thermal collisions it will part with vibrational energy and come down to the configuration of lowest Pot. E as at C. From C an electronic transition to the ground state is possible by emitting the quantum of radiation represented by CD. This is the simplest case of fluorescence. When it is raised to B' it will come down in an exactly similar manner and reach the point P, where the two successive excited states are supposed to intersect. Thereafter it will either continue its motion along b' and reach C', the point of minimum Pot. E in b' or it may slip down into b through the point of intersection and reach the point C. In the latter case, there will be fluorescence emitting CD as before. In the former, there will be flores-

cence if  $C'$  is not beyond the curve 'a'; but, if the point  $C'$  lies outside the lower curve, no immediate transition is possible and so it will give rise to phosphorescence.

In order to understand the emission spectra due to the  $\text{Ce}^{+++}$  ions in crystals, we shall suppose that the energy bands due to the three sub-levels of  $5D_{3/2}$ , which give rise to the three strong absorption bands, overlap each other mutually as shown in figure 3. Now there is the possibility (a) that the energy band due to the lowest of these sub-levels may overlap that due to the state  $5D_{5/2}$  or (b) there may be a zone of separation between them.

The overlapping between the energy bands due to the successive excited states is, however, virtual, *i.e.*, it is not to be postulated until the  $4f$ -electron is excited to one of these states. So the frequencies of the selective absorption bands due to  $\text{Ce}^{+++}$  remain unaffected. If the incident radiation corresponds to any one of the absorption bands due to  $\text{Ce}^{+++}$  ion, the  $4f$ -electron will be excited to one or other of the upper states. But the excited electron will part with its energy in thermal collisions and gradually come down as has been pictured above. In case (a) the final level reached by the excited electron in this way will be the  $5D_{5/2}$ , and then there will be the transition of the electron to the ground term. In  $\text{Ce}^{+++}$  ion, the ground term is a doublet given by  $4^2F_{5/2, 7/2}$ . As transitions to either of them is possible from  $5D_{5/2}$ , two emission bands are to be expected in this case.

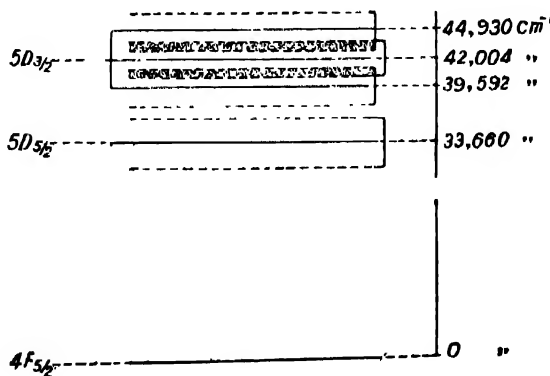


FIGURE 3

In case (b), on the other hand, transition is possible from either of the two states  $5D_{3/2}$  and  $5D_{5/2}$  to the ground term. This suggests that altogether there will be four emission bands here. But as the transition  $5D_{3/2} \rightarrow 4F_{7/2}$  involves a change of two units in ' $j$ ', this is much less probable. So that only three strong emission bands are to be anticipated.

The emission spectra observed in the different crystals will be qualitatively explained if it is supposed that in the chloride and sulphate crystals the energy-pattern is as in (a) while in  $\text{CeF}_3$  it is as in (b). It has to be shown now if there is any quantitative agreement between the positions of the emission bands observed and those expected from their absorption spectra. For this purpose the energy level diagrams for  $\text{Ce}^{+++}$  ions as revealed by a study of the emission spectra of the different salts are given in figures 4, 5 and 6.

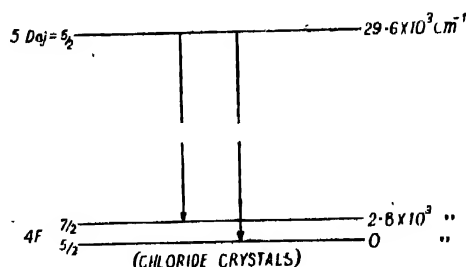


FIGURE 4

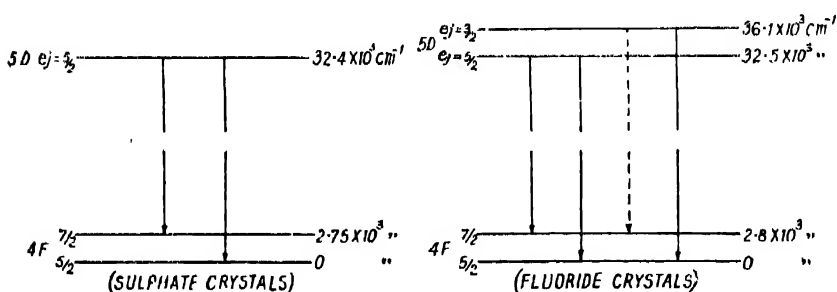


FIGURE 5

FIGURE 6

It is to be noted that in all the three figures the interval between the components of the ground term  $4^2F$  of  $\text{Ce}^{+++}$  is nearly the same, viz.,  $2,800 \text{ cm.}^{-1}$ . Also it is in fair agreement with the calculated value  $\Delta\nu = 2,500 \text{ cm.}^{-1}$  taking the usual value of the screening constant, viz.,  $\sigma = 34$ . As regards the position of the virtual states, it is found from figures 5 and 6 that in the sulphate and fluoride the state  $5D_{5/2}$  occupies almost the same position as is found in the case of absorption shown in figure 1. In chloride, the above energy level is slightly depressed. The position of the state  $5D_{3/2}$ , which is effective only in fluoride, could not be so correlated as the corresponding absorption spectra did not reveal any structure.

#### ORIGIN OF THE WEAK LUMINESCENCE

The origin of the weak luminescence (observed in  $\text{CeF}_3$ ) on the lower frequency side of the principal bands is not clearly understood. It appeared

when the exciting frequency was above  $40 \times 10^3$  cm. $^{-1}$  and gradually gained in intensity with the increase of the frequency of excitation. As in the sulphate and chloride crystals no such emission was observed even when excited with the high frequencies, it seems that Ce $^{++}$  ions alone are not responsible for its production. That is, the origin of this luminescence is not due to the process 1(a). Let us see if it may be due to the process 1(b) mentioned above. In that case one has to postulate that the ultra-violet radiation is first absorbed by Ce $^{++}$  ions and, when in the metastable state, they transfer their energy to the anions by collisions of the second kind, and the latter give rise to the luminescence. The process is then somewhat analogous to 'sensitized fluorescence' and it requires that the anion must possess excited states below the metastable state in question of the cation. But it is known that in LiF or in CaF<sub>2</sub>, the ultra-violet radiation up to a much higher frequency is transmitted undiminished. Since, however, the limit of absorption in CaF<sub>2</sub> (1400A°), is to the longer wave-length side of (1050A°) than in LiF, it may be (still more shifted to the longer wave-length side) in CeF<sub>3</sub>, where the polarisation of F $^-$  will be still greater on account of the triply charged cations; further, on account of the presence of defect places in the lattice, absorption may ensue at a still lower frequency.

On this hypothesis, however, one has to explain why such luminescence is absent in the chloride or the sulphate. It is well known that for either of the anions Cl $^-$  and SO<sub>4</sub> $^{--}$ , the continuous absorption begins at a lower wave-length than in F $^-$ . And, on account of the continuous absorption by the anions ensuing at much lower frequency, the requisite energy for sensitized fluorescence is not available to the cation. Further, the frequency of the transitions possible in these anions, in case of excitation, may not be within the spectral region investigated and thus may have escaped observation.

In conclusion the writer desires to express his grateful thanks to Prof. D. M. Bose, Ph.D., for his kind interest and helpful suggestions, and to Prof. M. N. Saha, D.Sc., F.R.S., for his kind encouragement during the progress of the work.

PALIT PHYSICAL LABORATORY,  
UNIVERSITY COLLEGE OF SCIENCE,  
CALCUTTA.

#### R. F. R. E. N. C. H. S

- <sup>1</sup> R. Tomascheck and O. Deutschbein, *Nature*, **131**, 473 (1933); *Zeit. für Phys.*, **34**, 374 (1933).
- <sup>2</sup> H. Gobrecht, *Ann. der Phys.*, **28**, s 673 (1937).
- <sup>3</sup> R. Tomascheck and Mehnert, *Ann. der Phys.*, **29**, s 306, (1937).
- <sup>4</sup> P. C. Mukherji, *Zeit. für Phys.*, **109**, s 573 (1938).
- <sup>5</sup> D. M. Bose and S. Datta, *Nature*, **128**, 270 (1931); *Phys.*, **80**, s 376 (1933).
- <sup>6</sup> R. W. Roberts and L. A. Wallace, *Nature*, **130**, 800 (1931).
- <sup>7</sup> S. Freed, *Phys. Rev.*, **38**, 2123 (1931).
- <sup>8</sup> D. M. Bose and P. C. Mukherji, *Phil. Mag.*, **26**, 757 (1937).
- <sup>9</sup> R. J. Lang, *Canadian J. Res.*, **14**, 127 (1936).
- <sup>10</sup> N. F. Mott and R. W. Gurney, *Proc. Phys. Soc.*, **49** (1936), Discussion on 'Conduction of Electricity in Solids.'
- <sup>11</sup> Schneider and O'Bryan, *Phys. Rev.*, **51**, 293 (1937).



# MEASUREMENTS BY MEANS OF THE ELECTRO-METER TRIODE

By J. A. N. THAES

(Received for publication, May 30, 1930)

**ABSTRACT.** Different purposes, for which Philips Electrometer Triode, type 4060, can be used, have been described with special references to the measurement of voltage. It is pointed out that when the voltage source has a high resistance, this particular tube can be used, in a circuit identical in principle with an ordinary valve voltmeter, in order to measure the voltage.

In engineering and in scientific research work where during the measurement it is often necessary to measure voltages, no current—or only a negligible amount of current—is drawn from the source. This necessity arises, for instance, in cases where the voltage source has a very high internal resistance or where any current taken by the measuring instrument would cause the voltage source to vary. For such measurements it is possible to use electrostatic voltmeters or electrometers (the electroscope, the quadrant electrometer, the string electrometer, etc.). These instruments, however, are very expensive and call for the most elaborate precautions if they are to give reliable results. Furthermore, they do not lend themselves to embodiment in a compact, transportable measuring device.

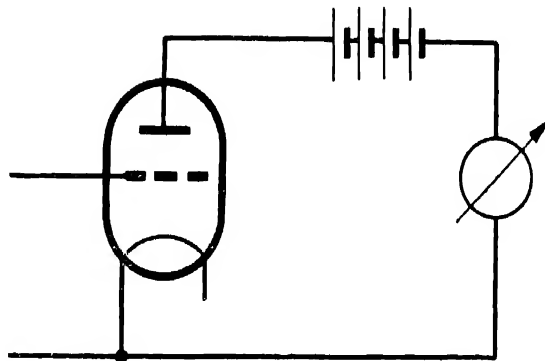


FIGURE I  
Theoretical circuit diagram

These disadvantages can be avoided by making use of an electronic valve. The electrometer triode is particularly suitable as a valve for the electrometer. A device incorporating a valve of this type is in the first place a more simple, robust and convenient arrangement. In addition it has a much smaller inertia and enables the voltage in question to be amplified to a practically unlimited

extent. A circuit embodying an electrometer valve (figure 1) is, in principle, identical with a "valve voltmeter" as used for the measurement of alternating voltages at radio frequencies. The voltage to be measured is applied to the grid of an electrometer valve. At the same time, a measuring instrument responding to current variations is connected in the anode circuit. Whilst an ordinary "valve voltmeter" is not usually subject to any special requirements in regard to its input resistance, a measuring device for the purpose mentioned above does have to fulfil certain conditions in this respect. In the case of a standard type electrometer, the input resistance—or the current taken by the instrument—is purely a question of the insulation of the various parts. In a measuring device embodying an electrometer valve, the amount of current taken is determined by the grid current of this valve, which consists of a very small ionic current and a leakage current across the insulation of the grid. The grid current in an ordinary radio valve is of the order of  $2 \times 10^{-7}$  amp., which is usually much too high for the present purpose. It is, therefore, necessary to use a special type of valve which is so constructed that the grid current is reduced to a minimum.

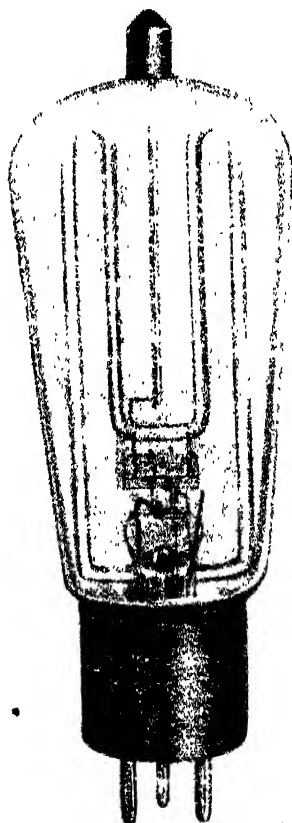


FIGURE 2  
Philips Electrometer triode, type 4060

Figure 2 shows the Philips Electrometer Triode, type 4060. The control electrode (the grid of an ordinary triode) is in this case constructed as a plate, like the anode. The filament is positioned between this control electrode and the anode. The control electrode is insulated by two glass "rods," each about 4 inches in length. With this construction the leakage path is very long. The ionic current is kept very small by taking steps to ensure a good vacuum and by using a very low anode voltage, *viz.*, about 4 volts. As a result of these precautions, the total grid current corresponding to point A in the characteristic of this valve (figure 3) is only about  $2 \times 10^{-15}$  amp. (mean value).

As already mentioned, electrometers are used chiefly in the following special cases: (1) if the use of an ordinary measuring instrument (*e.g.*, a galvanometer) would cause the voltage source to vary on account of the load; (2) if the voltage source has a very high internal resistance, and (3) if very small quantities of electricity have to be measured.

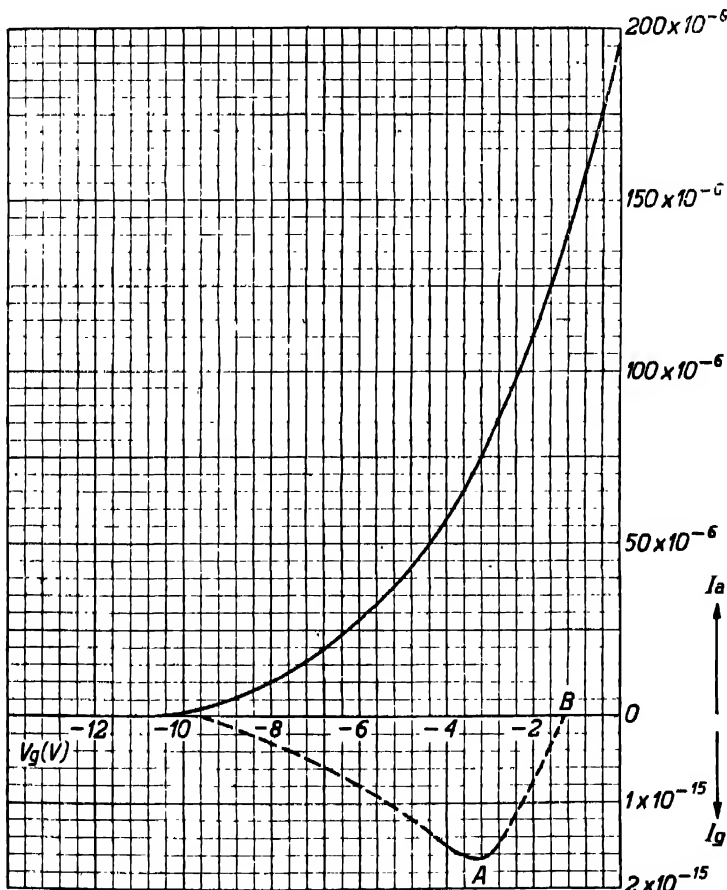


FIGURE 3  
Anode current and grid current as a function of the grid voltage of the  
electrometer triode, type 4060, at an anode voltage of 4 volts

Examples of case (1) are afforded by certain electrochemical measurements, for instance, pH measurements. The pH value of a solution is a measure of the concentration of hydrogen ions and hence an indication of the acidic or basic activity of the solution. This measurement is frequently carried out in chemical laboratories and works, in the laboratories of institutions for testing foodstuffs and agricultural products, in medical research work and in dairies. The pH value is found by measuring the rise of voltage which takes place between a "hydrogen electrode" immersed in the solution and another electrode. The hydrogen electrode is now frequently replaced by a glass electrode which offers many practical advantages but has a very high resistance. No current may be drawn from the electrode during the voltage rise, as this would cause polarisation of the solution and give an incorrect voltage reading. To make the measurement possible, a controllable voltage is connected in opposition and adjusted to such a value that a galvanometer in the circuit gives a zero indication. This counter-voltage is then measured with a voltmeter or by comparison with a standard cell. If there is a slight error in the adjustment of the counter-voltage, the current which flows will be determined by the difference between the voltage to be measured and the reference voltage and also by the resistance of the circuit. This current will cause a deflection of the galvanometer and polarisation will occur. In order to show the voltage difference while drawing practically no current from the source, an electrometer should be used. In the case of a glass electrode the resistance of the circuit is very high (several megohms), which alone justifies the use of an electrometer.

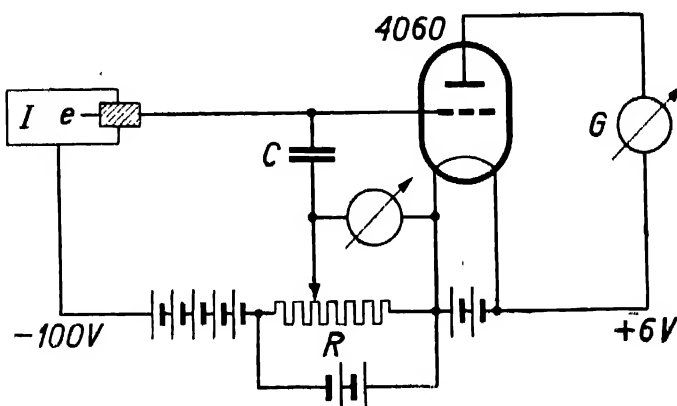


FIGURE 4

Circuit for measurement of minute quantity of electricity

An example of voltage measurement of a source having a very high internal resistance, is the measurement of very faint light intensities, for instance, when

taking photometric records of stars or of spectral lines. For this purpose a photo-electric cell is usually employed. The current delivered by this cell is proportional to the light intensity and in this case it is extremely small. In order to measure these very minute currents, a very high coupling resistance must be used. In such cases it is usual to work with liquid resistances of the order of  $10^9$  to  $10^{10}$  ohms. Currents of, say  $10^{-10}$  to  $10^{-11}$  amp., which are too small for measurement with a galvanometer, yield a voltage of about 0.1 volt on resistances of these magnitudes. The problem is how to measure this voltage without a shunt being formed by the measuring instrument across the coupling resistance. The electrometer answers this purpose ideally. A measuring device embodying the above-mentioned Electrometer Triode, type 1060, passes a current of less than  $10^{-14}$  amp., so that currents down to  $10^{-13}$  amp. can be measured with relatively high accuracy.

The third example : Measurement of very small quantities of electricity is met with in researches on radio-activity, providing in this case a means of counting the  $\alpha$ ,  $\beta$  and  $\gamma$  radiations. The charge measured indicates the intensity of the radiation. For these measurements the rays are trapped in an ionisation chamber, where they liberate gas ions. These gas ions are collected on an electrode in the ionisation chamber, and the increase of the electric charge of this electrode per unit of time is a measure of the radiation. The mean current produced by the ion-borne charge is extremely small, being of the order of  $10^{-12}$  amp. and again it is necessary to measure the voltage, without drawing current from the pick-up electrode. The usual procedure is to combine the electrode with a calibrated condenser which is very well insulated and to measure the voltage across the condenser after a certain time. From this voltage the value of the charge can be directly deduced. At the normal point of operation the grid current of the Electrometer Triode, type 1060, is a few times  $10^{-15}$  amp., which is very small compared with the electric charge of the condenser per unit of time. With most measurements the increase of voltage across the condenser is very slow, so that it is possible, by controlling an auxiliary voltage applied to the grid, to maintain the total grid voltage at such a value that the grid current is always nil (point B in figure 3). This method is described by Clay in *Physica* 4-1937, page 124 and page 654. The principle is indicated in figure 4. First the grid voltage is set at such a value that the grid current is nil. Under the action of the radiation to be measured, the chamber I becomes ionised and the liberated negative charges are attracted by the electrode. Condenser C is charged and the grid of the electrometer triode gradually becomes more negative. At the same time, however, the potentiometer R is controlled in such a manner that the galvanometer G in the anode circuit is maintained as nearly as possible at its initial deflection. At a moment when the anode current is absolutely identical with its initial value, the time

lapse is accurately measured and also the voltage on the potentiometer. It is then known that in this period of time the voltage on the condenser C has increased by exactly the same amount by which the voltage on the potentiometer was adjusted in order to keep the anode current constant. The amount of this adjustment can be read directly on a voltmeter connected across R.

By the application of this principle it is also possible to measure very small photo-electric currents.

PHILIPS LAMP WORKS,  
EINDHOVEN, HOLLAND.

# AN IMPROVED FORM OF VACUUM ARC MERCURY STILL FOR LABORATORIES

By M. V. SIVARAMAKRISHNAN

(Received for publication, August 15, 1938)

**ABSTRACT.** An apparatus for distilling mercury is described. Current flows through a short mercury arc and by the heat thus generated the mercury is heated and vaporised and is finally condensed in a water-cooled condenser connected to the middle of the arc.

Mercury, so largely used in laboratories gets contaminated easily by contact with foreign material and its cleaning is done in many ways but none so satisfactory as by distilling it in *vacuo*. To distil the mercury in *vacuo*, there are many forms of apparatus on the market but a convenient and simple form of it is the one constructed by Waran<sup>1</sup> in 1926. This has been found to have an

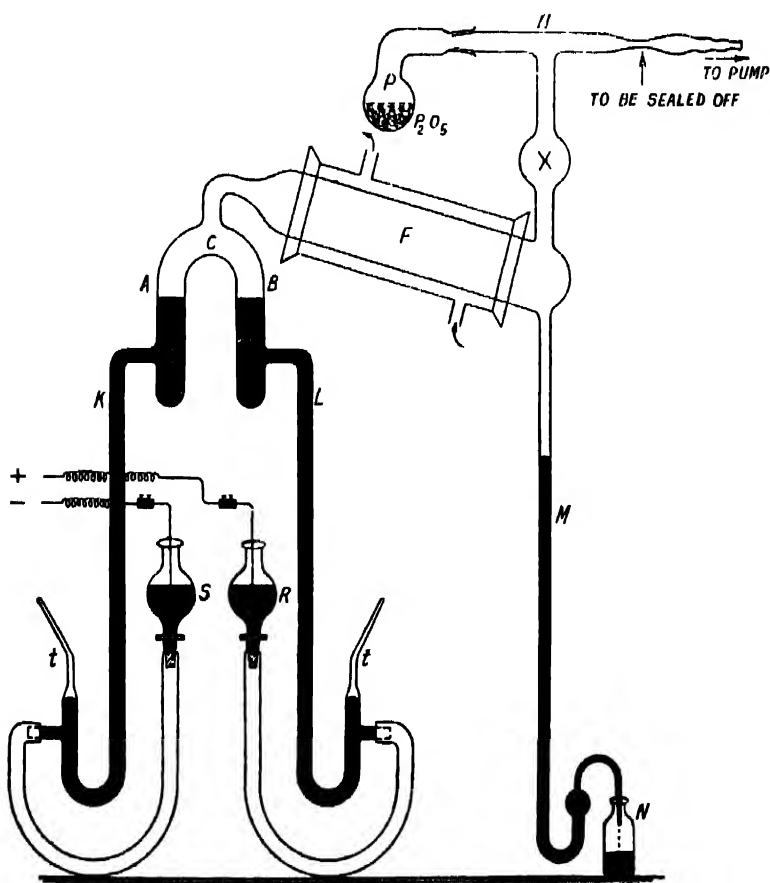


FIGURE 1

average yield of  $\frac{3}{4}$  lb. of distilled mercury per hour taking 5 amperes at 60 volts. The apparatus herein described is an improved form of the same. Any person with some skill in glass-blowing can easily make one and it is worth while making it in view of its prohibitive cost if we were to get it from outside and the risk involved in its transport from one place to another.

A C B is an inverted U-tube with a T-piece in the middle. The limbs A, B have vertically downward tubes K, L, about 72 cms. in length, and their lower ends are connected to mercury reservoirs by good pressure tubings. They are provided with air-traps  $t$ ,  $t$ . The T-piece at C is connected to the water-cooled condenser F, formed out of a thin-walled tube about 1" in bore and about 8" in length. From the other end of F, two tubes branch off. The vertically downward branch M is a small tube of not more than 2 mm. bore and over 100 cms. in length, bent round at the lower end as shown in figure 1. The upward branch has a bulb and is attached to the horizontal tube H, having a  $P_2O_5$  bulb at one end, the other end being connected to the pump. The whole of the apparatus is mounted on a backboard of wood. This mercury arc still operates as follows:—

The system is rapidly exhausted by a Cenco-Hyvac rotary oil pump instead of the Sprengal pump action used in the old form of apparatus. Mercury rises up in the two vertical tubes K, L to the barometric height and the height of the reservoirs is adjusted so that mercury occupies a few cms. above the side T joints of the U-piece. To start with, nozzle N of the small tube is closed and in a few minutes a vacuum of the order of '01 mm. of mercury is reached inside the apparatus. The  $P_2O_5$  in P is essential to remove the water vapour liberated as the mercury and the glass walls get heated up under the arc. Two stout copper rods with wire connectors at one end dip in the mercury of the reservoirs and form the leads for the current supplied by a 60-volts mains, with suitable rheostat in the circuit.

The switch being on, the reservoir, say S, is raised until the mercury rising in A flows in B. The mercury reservoir is now restored back to its shelf and as the contact with the mercury in B is broken at C, an arc plays between the two pools of mercury in A and B and the mercury is rapidly vaporized. The vapour evaporating from both the limbs goes down into F, where by air-cooling and water-cooling it condenses and trickles down into M. When the mercury from the condenser reaches the barometric height in M the end is broken and mercury is allowed to distil over smoothly.

The last stage in the process is sealing the arc distiller in the running condition. When the pressure inside the system is about '001 mm. or above, a condition necessary for the long life of the arc, the distiller may be sealed off at the thick narrow constriction of the horizontal tube with the help of a hand blow-pipe. When once the arc distiller has been set up in this way, all that one has to do is to pour in dirty mercury at one of the reservoirs, start the arc, and get it distilled as outlined above.

The present form is superior to the old form in several respects. The yield is practically doubled since the vapour from both the limbs is condensed in this form of the apparatus. We have dispensed with all electrode sealing which is frequently a source of damage to the apparatus when it cracks. Water-cooling adopted here is more efficient than the air-cooling adopted in the previous form, and thus enables a much higher arc current being employed without damaging the still. Thus the output from the still can be considerably increased with perfect safety. The following table gives the yield of mercury in pounds per hour approximately :—

Trial.	Time.	Current. (amps.)	Volts	Wt. of Hg distd. per hr. in gms	Wt. of Hg distd per hr. in lbs. (approx.)	Amount of Hg. per watt- hr (approx.)
1	1 hr.	2.6	60	2.17	1/2	1.6 gm.
2	"	3	"	3.24	2/3	1.8
3	"	3.5	"	3.80	5/6	1.8
4	"	4	"	4.12	1	1.8
5	"	4.5	"	5.20	1 <sup>1</sup> / <sub>6</sub>	1.9
6	"	5	"	5.75	1 <sup>1</sup> / <sub>3</sub>	1.9

Thus the average yield comes out to be  $1\frac{1}{2}$  lbs. per hour, taking 5 amperes at 60 volts or approximately 2 gms. of mercury per watt-hour, an output practically double that in the old form.

Incidentally, it may be mentioned that in a Physics Laboratory, such arc-distillers, when set up suitably, serve as bright sources of illumination for routine optical experiments in addition to serving the main purpose for which they are intended.

PHYSICS DEPARTMENT,  
PRESIDENCY COLLEGE.

R H F E R I N C E



# ON THE RAMAN SPECTRUM OF O-DIPHENYL-BENZENE

By S. K. MUKERJI, M.Sc., Ph.D. (LOND.),  
 Professor of Physics, Agra College, Agra

AND

S. ABDUL AZIZ, M.Sc.,  
 Agra University Research Scholar in Physics

(Received for publication, May 30, 1939)

## Plate XII

**ABSTRACT.** Results of the study of the Raman spectrum of *o*-diphenyl-benzene have been recorded for the first time in this paper. By employing suitable filters with the purest substance in the molten state and taking other precautions very clean spectra were obtained though the continuous background due to fluorescence still persisted. The substance has yielded thirty-three new lines, not recorded before, at frequencies 3196(0), 3059(6), 1608(8), 1595(10), 1577(1), 1503(5), 1471(1), 1430(1), 1288(10), 1247(4), 1180(2), 1158(6), 1059(2), 1032(7), 1005(8), 993(8), 874(1), 839(1), 774(5), 744(2), 708(5), 615(5 broad), 658(3), 521(2), 501 ?(1), 406(6), 359(5), 319(3), 253(1), 238(6 broad), 144(6 broad), 112(5 broad), and 73(5 broad) cm.<sup>-1</sup>

Seven anti-Stokes lines corresponding to frequencies 993, 708, 615, 406, 359, 238 and 144 cm.<sup>-1</sup> have been observed. The results have been discussed with reference to the Raman spectra of benzene and diphenyl.

## INTRODUCTION

Little or no work so far appears to have been done on the Raman effect of compounds with three benzene rings. In this investigation the Raman effect of *o*-diphenyl-benzene has been studied by us for the first time, and in a preliminary report<sup>1</sup> to 'Nature' the Raman lines yielded by this substance have been submitted. We have also reported in a previous communication<sup>2</sup> a large number of Raman lines due to diphenyl. Diphenyl is solid at the ordinary temperature and it consists of two benzene nuclei joined end on by C-C bond in the para direction. *o*-Diphenyl-benzene is also solid at the ordinary temperature but it consists of three benzene nuclei instead of two; two of these being joined to the third in the ortho direction. It is, therefore, interesting to obtain and compare the Raman spectra of this compound with those of diphenyl. With mercury arc

radiation this substance is found to be even more powerfully fluorescent than diphenyl and the continuous fluorescent background thus formed almost completely masked all traces of Raman lines on the plate. But using the substance in the molten state purified previously by repeated crystallisation from pure benzene and by employing  $\lambda 4358$  as the exciting line filtered through a concentrated solution of sodium nitrite, the continuous background has been considerably cut down and a large number of Raman lines have been obtained including seven anti-Stokes lines not recorded before. The results are given and discussed in the present paper. The Raman lines excited by  $\lambda 4358$  and also by  $\lambda 4347$  and  $\lambda 4339$  of mercury are given in the tables in this paper and the complete spectrum has been measured for the correct assignment of the lines recorded here.

#### E X P E R I M E N T A L

*o*-Diphenyl-benzene obtained from the research laboratory of Eastman Kodak Company after being purified by repeated crystallisation from pure benzene was distilled and the middle portion of the distillate was received directly into the Wood's tube. The tube containing the substance was then kept in an electrically heated oven and the temperature was kept slightly above its fusion point by adjusting the current flowing in the heating coil of the oven.

The other details of the experimental arrangement are practically the same as given in a previous communication by the authors. As mentioned before, the Raman spectrum of this substance gets completely masked by very powerful fluorescence but by employing  $\lambda 4358$  as the exciting line filtered through a concentrated solution of sodium nitrite the continuous background has been very considerably suppressed and a large number of Raman lines not recorded before have been obtained. The spectrograms were taken on Agfa Isochromic backed plates, speed H and D-4400, with a new Fuess glass spectrograph having a dispersion of about 21 Å.U. at  $\lambda 4358$ . The time of exposure was varied from 20 to 40 hours. Measurements were made, as usual, on a fairly accurate photomeasuring micrometer and the wave-lengths were calculated using Hartmann's dispersion formula.

In this investigation, the  $\lambda 4046$  excitation did not give a good photograph and showed very powerful fluorescence, the Raman lines being almost completely masked, giving only a few strong lines. But by employing  $\lambda 4358$  as the exciting line filtered through a concentrated solution of sodium nitrite, the continuous background was very much cut down and a fairly good photograph was obtained, bringing out a large number of weak lines in addition to the strong ones mentioned above. In table I are given the results obtained by the authors using only the mercury  $\lambda 4358$  radiation.

TABLE I

*o*-Diphenyl-benzene Frequencies

(With a filter of concentrated solution of sodium nitrite)

Number.	$\Delta\nu$ in cm. <sup>-1</sup>	Intensity. I	Number.	$\Delta\nu$ in cm. <sup>-1</sup>	Intensity.
1	3196	0	18	839	3
2	3059	6	19	774	6
3	1608	5	20	744	5
4	1595	10	21	708	3
5	1577	1	22	615	1
6	1503	5	23	558	6 (broad)
7	1471	1	24	521	6 "
8	1430	1	25	501 ?	5 "
9	1288	10	26	406	5 "
10	1247	4	27	359	4
11	1180	2	28	310	5
12	1180	6	29	253	2
13	1059	2	30	238	6
14	1032	7	31	144	5 (broad)
15	1005	8	32	112	3
16	993	8	33	73	2
17	874	1			

Anti-Stokes lines of the Raman frequencies, 993, 708, 615, 406, 350, 238 and 144 cm.<sup>-1</sup> recorded in table I, have also been observed.

The Raman frequencies due to benzene, diphenyl and *o*-diphenyl-benzene have also been included in table II, for a comparative study, as these three substances contain one, two and three benzene rings respectively in their compounds and have fairly strong common frequencies.

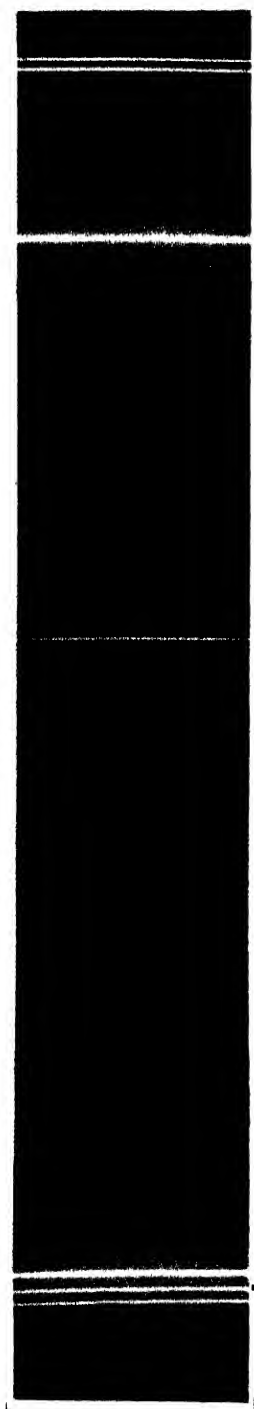
Complete tables showing assignments are given at the end of the paper in table V, and the exciting frequencies given in table IV.

The shifts for benzene are taken from the paper of Ananthakrishnan and the values for diphenyl are taken from the paper of the present authors.

The spectrogram is reproduced in Plate XII.

TABLE II

No.	Benzene.	Diphenyl.	<i>o</i> -Diphenyl-benzene.
1	3910 (o)	...	...
2	3187 (o)	3192 (o)	3196 (o)
3	3164 ( $\frac{1}{2}$ )	...	...
4	3064 (8)	3062 (5)	3059 (6)
5	3048 (4)	3047 (1)	...
6	2949 (5)	2961 (o)	...
7	2928 (od)	...	...
8	2617 ( $\frac{1}{2}$ )	...	..
9	2547 ( $\frac{1}{2}$ )	...	...
10	2457 ( $\frac{1}{2}$ )	..	...
11	2272 (o)	...	...
12	1605 (2)	1610 (10)	1608 (5)
13	1584 (3)	1590 (8)	1595 (10)
14	...	...	1577 (1) *
15	...	1506 (4)	1503 (5)
16	1480 (o)	...	1471 ( $\frac{1}{2}$ )
17	1445 (o)	1452 (1)	1430 ( $\frac{1}{2}$ )
18	1400 ( $\frac{1}{2}$ )	...	...
19	...	1376 (o)	...
20	...	1318 ( $\frac{1}{2}$ )	...
21	...	1283 (10)	1288 (10)
22	...	1241 (1)	1247 (4)
23	1175 (2)	1189 (3)	1180 (2)
24	...	1157 (4)	1158 (6)
25	...	1090 ( $\frac{1}{2}$ )	...
26	...	...	1059 (2)
27	1035 (o)	1032 (5)	1032 (7)
28	1006 ( $\frac{1}{2}$ )		
29	998 (1)	1003 (10)	1005 (8)
30	992.5 (10)	?	993 (8)
31	984 (1)	980 (1)	...



Raman spectrum of *o*-diphenyl benzene,  
 $\lambda$  4358 excitation with a filter of concentrated  
solution of  $\text{NaNO}_2$



TABLE II (*contd.*)

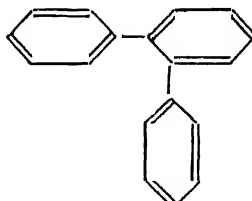
No.	Benzene	Diphenyl	<i>o</i> -Diphenyl-benzene
32	979 (1)	964 (1)	...
33	...	898 (1)	...
34	...	...	874 (1)
35	850 (2)	838 (4 br.)	839 (4)
36	801 (0)	...	...
37	778 (0)	779 (4)	774 (5)
38	...	740 (5)	744 (4)
39	...	...	708 (6)
40	688 (1)	...	...
41	606 (5)	614 (4)	615 (5 br.)
42	...	548 (1)	558 (3)
43	...	...	521 (2)
44	...	...	501 ? (1)
45	...	449 (0)	...
46	400 (rd)	408 (5 br.)	406 (6)
47	...	368 (0)	359 (5)
48	...	313 (4 br.)	319 (3)
49	...	267 (4 br.)	253 (1)
50	...	...	238 (6 br.)
51	...	193 (0,	...
52	...	140 (4 br.)	144 (6 br.)
53	...	...	112 (5 br.)
54	...	...	73 (5 br.)

br. indicates a broad line

## DISCUSSION OF RESULTS

Raman spectrum of diphenyl which consists of two benzene rings joined end on by C—C bond in the para-direction has been reported by us previously.<sup>3</sup> In this investigation we have studied *o*-diphenyl-benzene. This substance consists of three benzene nuclei, two of these being substituted in the third in the ortho position. The two benzene rings constituting the diphenyl molecule are preserved in *o*-diphenyl-benzene and we should expect the lines characteristic

of both diphenyl and benzene to be present in this compound. The three most prominent frequencies observed in *o*-diphenyl-benzene are at 1595, 1288 and 1005 cm.<sup>-1</sup> respectively. As the table II will show the frequency at 1595 cm.<sup>-1</sup> is



*o*-Diphenyl-benzene ( $C_{18}H_{14}$ )

present also both in benzene and diphenyl. But it may be noted that this frequency is comparatively weaker and is displaced towards the longer wave-length side in the case of benzene. The most prominent frequency observed in *o*-diphenyl-benzene is at 1288 cm.<sup>-1</sup> It is equally strong in diphenyl. This is evidently the characteristic frequency due to the C—C bond present in both these compounds. It will be seen in table II that diphenyl has given a very strong line at 1003 cm.<sup>-1</sup> Corresponding to this, *o*-diphenyl-benzene has given two equally strong lines at 1005 and 993 cm.<sup>-1</sup> respectively. The latter frequency is observed to be equally strong in benzene. The occurrence of this doublet only in *o*-diphenyl-benzene is, therefore, characteristic of this substance having three benzene nuclei, two of which being substituted in the third in the ortho position. The line at 1035 cm.<sup>-1</sup> is observed in all the three compounds but with marked changes in intensity. In benzene it is very weak, in diphenyl it is fairly strong and it is stronger still in *o*-diphenyl-benzene. As table II will show, there are also some fairly strong lines which are entirely due to *o*-diphenyl-benzene and are absent in benzene and also in diphenyl. These lines are at 1577, 1059, 708, 521, 501, 238, 112 and 73 cm.<sup>-1</sup> respectively. In addition to these, some very weak lines have been observed only in *o*-diphenyl-benzene. Since they are faint it cannot be said definitely that they are absent in one or the other of the compounds studied here. Evidently some of these differences may be due to the particular molecular configurations of these compounds. In benzene all the six carbon atoms are, so to say, free, in diphenyl one of the carbon atoms is loaded with a phenyl group and in *o*-diphenyl-benzene two consecutive carbon atoms are loaded with phenyl groups. The frequencies at 238, 112 and 73 cm.<sup>-1</sup> due to *o*-diphenyl-benzene which are absent in benzene and diphenyl may be due to the vibrations of the three benzene rings against one another.

Recently Birkett Clews<sup>4</sup> and Kathleen Lonsdale have studied the structure of this compound. From X-ray measurements together with an estimate of molecular susceptibility based on the magnetic anisotropy of benzene and the dimensions of the unit cell, they came to the conclusion that neither of the substituted phenyl

groups of this compound can be orthogonal to the parent nucleus, and that the most likely structure is one in which the two phenyl groups have their planes turned in the same direction out of the plane of the parent nucleus by about  $50^\circ$  or less. X-ray analysis<sup>5</sup> (Dhar, 1932) and also our investigation<sup>6</sup> (1938) tend to show that the molecule of diphenyl is planar in structure. An X-ray study of *p*-diphenyl-benzene, which consists of three benzene rings joined in the para-position, by L. W. Pickett<sup>7</sup> (1933), by the method of trial and error and Fourier analysis, tends also to show that the molecule of this compound is planar in form. It is only in the case of *o*-diphenyl-benzene amongst these three aromatic compounds which contain more than one benzene nucleus that the authors (Clews and Lonsdale) conclude that probably the two phenyl groups have their planes turned out of the plane of the parent nucleus. Looking at table II we find that practically all the strong Raman frequencies present in diphenyl are also present in *o*-diphenyl-benzene which has been investigated for the first time by us has not shown on any of our plates any strong line which is not also present in diphenyl, excepting the one at  $708 \text{ cm.}^{-1}$  and a few broad ones at very low frequencies. It seems, further comparison and study is required of other allied compounds before any further light can be thrown on the structure of this compound.

One of us (Mukerji) and Laksman Singh have just succeeded for the first time in obtaining a large number of Raman lines due to *p*-diphenyl-benzene which has been shown by L. W. Pickett,<sup>8</sup> referred to above, to be coplanar in form. This compound has also shown practically all the strong lines present in diphenyl and *o*-diphenyl-benzene in addition to a fair number of weaker lines not present in *o*-diphenyl-benzene or *m*-diphenyl-benzene which has also been investigated by us<sup>9</sup> for the first time. Details of the investigation on *p*-diphenyl-benzene will be published in a subsequent paper and it is possible that some further light may be thrown on the structure of compounds with three benzene rings, as a result of investigations on the Raman spectra of these compounds.

This investigation was carried on in the Physics laboratory, Agra College, with a new Fuess glass spectrograph kindly supplied by the authorities. One of the authors (S. Abdul Aziz) is also greatly indebted to the authorities of the Agra University for the award of a Research Scholarship.

TABLE IV

Exciting Line Å°.	Wave number $\text{cm.}^{-1}$	Notation.
4358·3	22938	Δ
4347·5	22995	Δ <sub>1</sub>
4339·2	23039	Δ <sub>2</sub>

TABLE V

## o-Diphenyl-benzene Frequencies

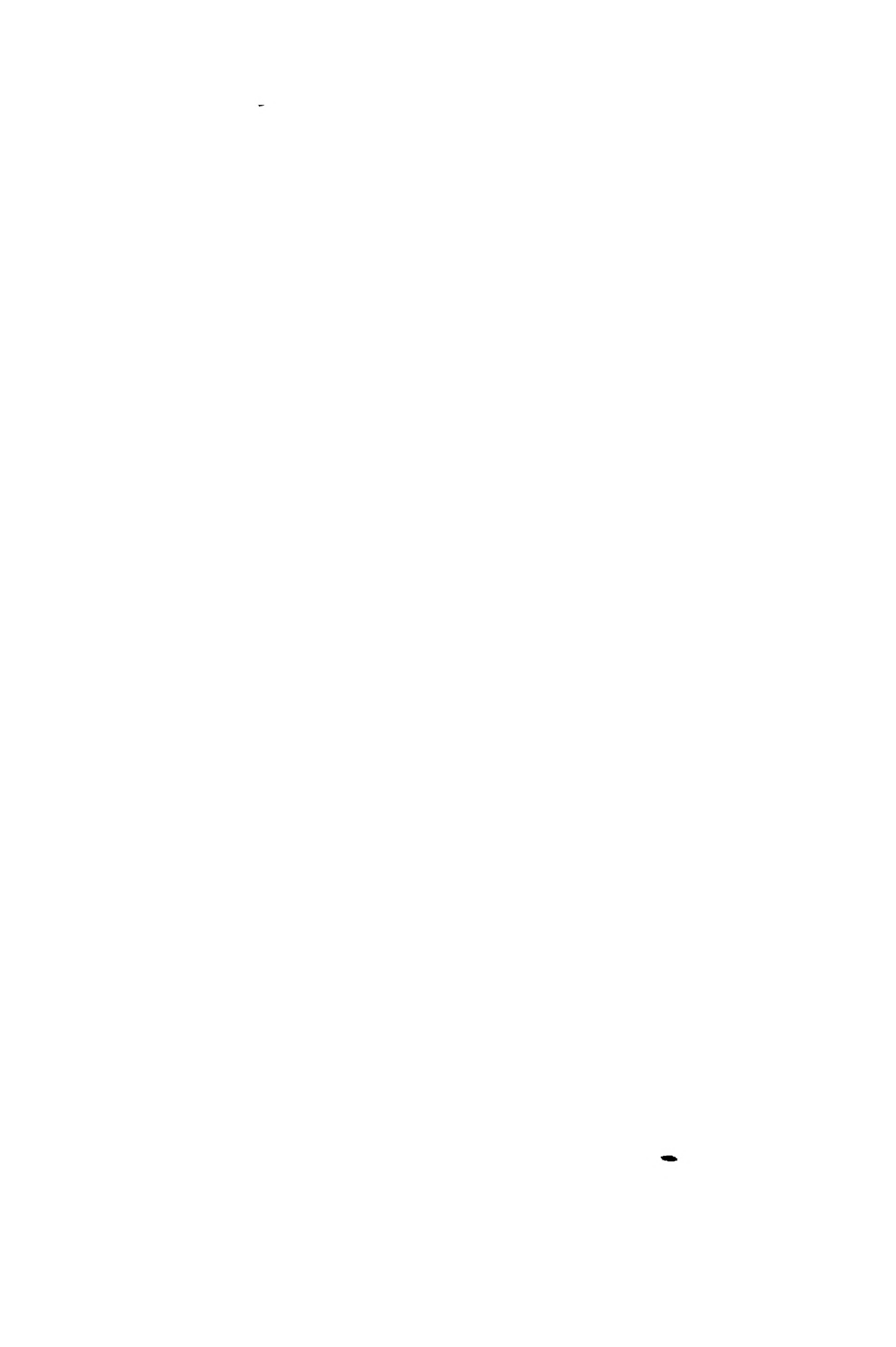
No.	Wave number cm. <sup>-1</sup>	Assignment.	Shift.	Intensity.
1	19742	A	3196	0
2	19879	A	3059	6
3	21330	A	1608	5
4	21343	A	1595	10
5	21361	A	1577	1
6	21400	A	1595	1
7	21435	A	1503	5
8	21467	A	1471	1½
9	21491	A	1504	1½
10	21508	A	1430	1½
11	21650	A	1288	10
12	21691	A	1247	4
13	21705	A	1290	1
14	21758	A	1180	2
15	21780	A	1158	6
16	21834	A	1161	1½
17	21879	A	1059	2
18	21906	A	1032	7
19	21933	A	1005	8
20	21945	A	993	8
21	21965	A	1030	1½
22	21992	A	1003	1½
23	22004	A	991	1½
24	22064	A	874	1½
25	22090	A	839	4
26	22164	A	774	5
27	22194	A	744	2
28	22230	A	708	6

TABLE V (contd.)

No.	Wave number cm. <sup>-1</sup>	Assignment.	Shift.	Intensity.
29	22323	A	615	5 br.
30	22380	A	558	3
31	22417	A	521	2
32	22437	A	501?	1
33	22532	A	406	6
34	22579	A	359	5
35	22619	A	319	3
36	22685	A	253	1
37	22700	A	238	6 br.
38	22794	A	144	6 br.
39	22826	A	112	5 br.
40	22865	A	73	5 br.
41	23082	A	144	2
42	23174	A	236	?
43	23298	A	360	2
44	23344	A	406	2
45	23555	A	617	1
46	23645	A	707	1
47	23932	A	994	½

br. indicates a broad line

R I<sub>1</sub> F I<sub>1</sub> R E N C R S<sup>1</sup> Mukerji and Aziz, *Nature*, **142**, 477 (1938).<sup>2</sup> Mukerji and Aziz, *Ind. J. Phys.*, **12**, 271 (1938).<sup>3</sup> Loc. cit<sup>4</sup> Birkett Clews and Kathleen Lonsdale, *Proc. Roy. Soc. A.*, **187**, 493 (1937).<sup>5</sup> Dhar, *Ind. J. Phys.*, **7**, 43 (1932).<sup>6</sup> Loc. cit.<sup>7</sup> Pickett, *Proc. Roy. Soc. A.*, **189**, 149 (1933).<sup>8</sup> Loc. cit.<sup>9</sup> Loc. cit.



# ON THE ORIGIN OF COLOUR OF PARAMAGNETIC IONS IN SOLUTION, II

## *Fine Structure of the Absorption Bands*

By D. M. BOSE

AND

P. C. MUKHERJI

*(Received for publication, June 2, 1939)*

In a previous paper<sup>1</sup> a theory was developed of the origin of the absorption bands in paramagnetic solutions giving rise to the colours shown by them. The paramagnetic ions belonging to the iron group of elements are in the S-, D- and F-states. It is supposed that the charge carried by these ions produce polarisation of the associated dipole water molecules, in whose field the ground term of the ion is split up into  $(L+1)$  equidistant levels, with each of which is associated an electric orbital number  $e_L = 0, 1, \dots, L$ . Due to transition between the ground level and the upper excited levels,  $L$  absorption bands will arise whose frequency  $\Delta\nu$  can be represented by the formula

$$\Delta\nu = \frac{Ne |\Delta e_L| K_o}{E} \quad (1)$$

where

$Ne$ —the ionic charge,

$E$ —the dipole moment of the molecules associated with the central ion,

$\Delta e_L$ —the change in the electric quantum number,

$K_o$ —a constant.

It was shown that the number and frequency of the absorption bands was better represented by the relation (1) than what was to be expected from the theory of splitting of ionic terms in a field of cubic symmetry as developed by Van Vleck,<sup>2</sup> Penney and Schlapp.<sup>3</sup> Further, it was found that most of the absorption bands showed a doublet structure whose frequency differences for the D- and F-terms are given below:—

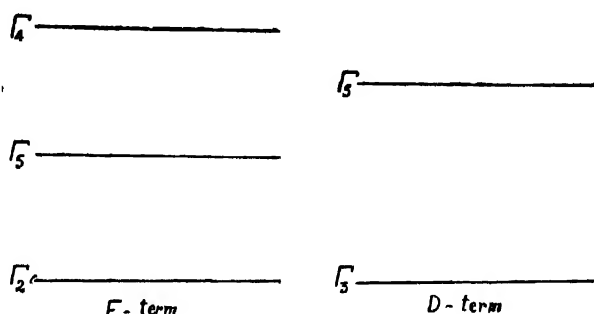
TABLE I

D-term Ions.		F-term Ions.	
Ti <sup>+++</sup>	-2836 cm. <sup>-1</sup>	V <sup>++</sup>	-859 cm. <sup>-1</sup>
Cr <sup>++</sup>	-2430 "		659 "
Fe <sup>++</sup>	-1180 "		
(MoO) <sup>+++</sup>	-1277 "	Cr <sup>+++</sup>	- 608 "
(WO) <sup>+++</sup>	-2380 "		874 "
Ce <sup>+++</sup>	-2408 "		
	2926 "		.

It is seen that the mean frequency difference is independent of the electric charge on the ion, but dependent on the  $L$ -quantum number of the latter, being of the order of  $2000 \text{ cm.}^{-1}$  for the D-term ions and  $750 \text{ cm.}^{-1}$  for the F-ions. It was apparent to us that such regularity in the doublet frequency difference and their dependence on the  $L$ -values must be due to the further splitting up of the ground terms of ions in the induced electric field due to the surrounding molecules. At the time of the writing of the paper it was not clear to us how the existence of an electric field of a lower order of symmetry could be accounted for in an electrolytic solution. We had only taken into account the immediate action of the field due to the polarisation of the six water molecules co-ordinated with the paramagnetic ion. According to Van Vleck, a field of cubic symmetry is to be expected under such conditions, but for our purpose we had assumed that a field of a different order of symmetry was produced. We had tacitly ignored the effect of the polarisation of the distant water molecules and also the influence on them of the charges on the anions. In a recent paper 'On the magnetic behaviour of Vanadium, Titanium and Chrome alums' Van Vleck<sup>4</sup> has shown that the observed spin-only values of susceptibility of all these alums, which belong to the cubic system, postulate the existence in addition to an electric field of cubic symmetry an additional crystalline field of a lower order of symmetry. Van Vleck discusses the various factors which contribute to the existence of such a field of a lower order of symmetry, and of the splitting produced by them on degenerate ground levels of  $\text{Ti}^{+++}$  and  $\text{V}^{+++}$  ions. He calculates the total splitting of the degenerate  $D\Gamma_5$  and  $F\Gamma_4$  levels due to the distribution of the various atoms surrounding the paramagnetic ions in the alums. According to the different assumptions made, the value of  $\Delta\nu$  for the  $D\Gamma_5$  term varies between 1450 to 2220  $\text{cm.}^{-1}$  and for  $F\Gamma_4$  it varies between 860 to 460  $\text{cm.}^{-1}$ . The values are strikingly of the same order of magnitude as the doublet separation observed in the D and F absorption bands mentioned above. It

seems, therefore, worthwhile to discuss in detail the contents of the Van Vleck's paper and to see how far the factors found to account for the low order field can be assumed to be possible in solutions of the paramagnetic ions.

We shall first give an account of Van Vleck's paper and then proceed to apply the results obtained to the case of solutions containing paramagnetic ions. If the crystalline field surrounding paramagnetic ions in a crystal is of cubic symmetry (the highest symmetry as yet considered) and represented by an equation of the form  $V = \Sigma f(r_i) + D(x^2 + y^2 + z^2)$ , the ground terms denoted by  $D$  and  $F$  are split up in such a field into Stark components according to the following pattern,



FIGURE

i.e., the number of levels is equal to the orbital moment number of the ground term and the separation between them is large as compared to  $kT$ . According to Bethe's<sup>5</sup> calculations, both the ground terms are non-magnetic; further,  $\Gamma_2$  is non-degenerate while  $\Gamma_3$  is doubly degenerate which is removed in a field of rhombic symmetry. Moreover, the coupling between the spin and the orbital moments of the paramagnetic ion breaks down, and the expression for the potential energy of the ion in a magnetic field is of the form:

$$V = f(r) + D(x^2 + y^2 + z^2) + \lambda(L.S) + \mu H(L + 2S) \quad (2)$$

The total paramagnetic susceptibility of such a crystal with a non-degenerate ground term will consist of the following components :

$$(i) \text{ a spin only value } \chi = \frac{4NS(S+1)\beta^2}{3kT} \quad (3)$$

where

$$\beta = \frac{e\hbar}{4\pi mc} = \text{the Bohr magneton}$$

(ii) a contribution due to the spin-orbit interaction between the lowest and the upper components of the ground term. This will produce a contribution to

$$\chi \sim \frac{N\beta^2}{kT} \left( \frac{\lambda}{D} \right)^2$$

(iii) a contribution to the magnetic moment, induced in the ground state 'a' by the high frequency terms 'k' of the form

$$2H \sum_k \frac{|\mu(ak)|^2}{hv(ka)}$$

This term contributes a magnetic moment which is independent of temperature.

A typical example of such a compound is chrome alum, whose susceptibility down to liquid air temperature has been measured by de Haas and Gorter<sup>6</sup>. This alum forms cubic crystals, in which each Cr<sup>+++</sup> ion has co-ordinated with it 6H<sub>2</sub>O molecules which are arranged in the shape of an octahedron. The electric field acting on Cr<sup>+++</sup> ion due to the induced polarisation of the water dipole molecules has cubic symmetry. The ground term of Cr<sup>+++</sup> is d<sup>3</sup> 4F Γ<sub>2</sub>. Ignoring for the present the influence of the high-frequency terms, Penney and Schlapp<sup>7</sup> find that the susceptibility can be very well represented by the formula

$$\chi = \frac{15N\beta^2}{3kT} \left( 1 - \frac{2\lambda}{5Dq} \right)^2$$

There are other paramagnetic alums, viz., vanadium and titanium alums whose susceptibility measurements have been made. The ground term of V<sup>++</sup> is d<sup>2</sup> 3F and Van Vleck has shown that the Stark levels in it is inverse to that for Cr<sup>+++</sup> and so the ground term is d<sup>2</sup> 3F Γ<sub>4</sub>. Ignoring for the present the effect of spin-orbital coupling, the susceptibility will, due to the independent orientations of the spin and the orbital vectors in the magnetic field, be of the form

$$\chi = \frac{4N\beta^2}{kT} \left\{ S(S+1) + L(L+1) \right\} \quad \dots \quad (4)$$

i.e., the susceptibility will depend not only on the spin value of the ground term but also on the orbital moment. The presence of spin-orbital coupling removes partially the degeneracy of the ground term, so that different orientations of the spin have different energies; but it is not possible to associate a definite axial quantisation of spin with each of the levels. Thus the spin is partially free and the orbital contribution will also be modified.

Similarly with the case of the titanium alum, Van Vleck considers the ground term of the Ti<sup>+++</sup> ion to be d<sup>1</sup> 2D Γ<sub>5</sub>. Here the term l<sub>5</sub> is also triply degenerate with non-vanishing magnetic moment. For both these alums belonging to the cubic system assuming the existence of a purely cubic field, we should expect a temperature dependence of susceptibility which cannot be

represented by a simple Bose-Stoner formula, but must contain in some complicated way the contribution of the orbital moment of the triply degenerate ground term. Experimentally determined values of the susceptibility of vanadium alum at room temperature shows the validity of the spin-only formula

$$\chi = \frac{4NS(S+1)\beta^2}{3kT}.$$

Since the cubic field is not sufficient to remove the degeneracy of the ground level, it is necessary to postulate the existence of an additional field of a lower order of symmetry. X-ray analysis shows that the field surrounding the paramagnetic ions in the alums has only trigonal symmetry. This is not incompatible with the cubic classification, as the microscopic symmetry of the local field need not be so great as the macroscopic symmetry.

Assuming the existence of such a trigonal field, the amount of whose splitting will be discussed later, we shall consider the splitting pattern produced on the triply degenerate  $\Gamma_4$  or  $\Gamma_5$  level by such a field. Van Vleck has given the following diagram.

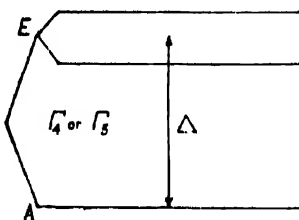


FIGURE 2

[The splitting of a triply degenerate cubic state in a trigonal field. The two components of  $\Gamma_5$  coincide unless magnetic forces are applied.]

This trigonal field arises as given by the results of X-ray analysis from the fact that the principal axes of the unit cell round each paramagnetic ion do not coincide with the principal axes of the octahedral arrangement of the six associated water molecules.

The effect of this additional trigonal field is to split up the triply degenerate  $\Gamma_4$  and  $\Gamma_5$  levels respectively with a single and a double degenerate levels, the latter being split up in the presence of an additional magnetic field. Thus according as the level A or E respectively is the lowest term in the case of  $Ti^{+++}$  and  $V^{+++}$  ions in the alums, will the susceptibility obey the spin only value (3) or show a deviation from it. Siegert<sup>8</sup> has discussed the conditions under which in both the ions a non-degenerate orbital state will be the lowest. The trigonal field consists of two parts, one a second order term and the other a fourth order one. He has shown that for a special range of values for the ratio of the second

order to the fourth order terms will the non-degenerate orbital state lie deepest both in  $Ti^{+++}$  and  $V^{+++}$ . Given the actual distribution of atoms in the unit cube of the alums round each paramagnetic ion, Van Vleck considers the factors which are responsible for the deviation of the crystalline field round the central ion from that of cubic symmetry. They are :

I. The direct action of the field from distant atom (*i.e.*, those outside the six water molecules)—The non cubic part of the field comes mainly from distant atoms, and they are known to be distributed with only trigonal symmetry.

II. The indirect action of the field from distant atoms—under their influence the associated water molecules may be somewhat disturbed from its normal octahedral arrangement, and so may exert a non-cubic field on the central paramagnetic ion.

III. The Jahn-Teller effect—which states that the most stable arrangement of a polyatomic molecule is always sufficiently unsymmetrical to lift any orbital degeneracy which may be present in the central atom. For qualitative purpose it will suffice to regard the cluster  $X^+ \cdot 6H_2O$  ( $X = Ti, V, Cr$ ) as a molecule embedded in a trigonal field of force.

The essence of the Jahn-Teller mechanism is that the potential or incipient degeneracy of the central paramagnetic ion has repercussions on the arrangement of the surrounding molecules.

Evaluation of the different contributing factors has been made as follows :—

I. The most important forces acting on the paramagnetic, ions apart from those due to the six associated water molecules, comes from the 32 oxygen and 8 sulphur atoms in the nearest eight ( $SO_4$ ) groups. Van Vleck has carried out his calculation of the forces on the following two assumptions :—

(a) in each ( $SO_4$ ), 'S' is uncharged and each 'O' carried  $-\frac{1}{2}e$  charge, *i.e.*, the action of each group is due to a charge distribution,

(b) each 'S' has  $ze$  and each 'O' has  $-e$ , *i.e.*, the action is due to dipoles having their seats in the ( $SO_4$ ) groups.

The truth lies between (a) and (b) and is probably closer to (a) than to (b). The second order effect is about the same for both (a) and (b). It gives a splitting of only  $40 \text{ cm.}^{-1}$  and of wrong sign for  $V^{+++}$ , *i.e.*, the degenerate state is the deepest. The fourth order effect with (a) is not large enough to overshadow the second order contributions and gives a substantial splitting of the proper sign in  $V^{+++}$ . The combined effect of these two is zero. With (b) the combined effect produces splitting of  $110 \text{ cm.}^{-1}$ , and is of such sign that the non-degenerate state is the lowest. With either (a) and (b) the non-degenerate state is the lowest in  $Ti^{+++}$ , and the splitting  $\Delta$  in figure 1 is  $400 \text{ cm.}^{-1}$  with (a) and  $330 \text{ cm.}^{-1}$  with (b).

II. Any small distortion of the water cluster comparable with the crystallographic trigonal symmetry, gives a sufficiently large ratio of the fourth order to

the second order term to make a non-degenerate ground state for both titanium and vanadium. The approximate validity of the spin-only value is due to the large contribution due to II over I.

For  $V^+$

(a) gives  $215 \text{ cm}^{-1}$

(b) gives  $425 \text{ } \text{,}$

III. In a separate paper<sup>9</sup> Van Vleck calculates the crystalline Stark splitting for clusters of the form  $\text{XY}_6$  due to Jahn-Teller effect. The final splitting produced by the three factors in the case of  $\text{V}^{+++}$  and  $\text{Ti}^{+++}$  is tabulated as follows:—

TABLE II

I	II	III	Total
$\text{V}^{+++}$ (a) 0	215	245	$460 \text{ cm}^{-1}$
(b) 0, (110)	425	435	$860 \text{ } \text{,}$
$\text{Ti}^{+++}$ (a) 400	500	1320	$2220 \text{ } \text{,}$
(b) 400	500	550	$1450 \text{ } \text{,}$

Having considered the splitting of the degenerate terms, we give below the Stark-levels in those paramagnetic alums in which the ground state of the ion is non-degenerate  $\Gamma_2$  and  $\Gamma_3$  respectively.

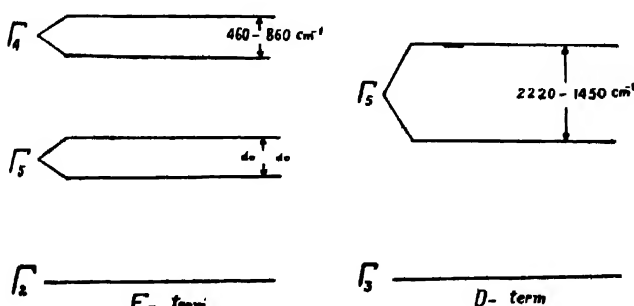


FIGURE 3

[In this case two absorption bands will be observed, each band a doublet with a mean frequency difference  $\Delta\nu$ ,  $460$  to  $860 \text{ cm}^{-1}$ ]

[One absorption band with a doublet with mean frequency difference  $\Delta\nu$ ,  $2220$  to  $1450 \text{ cm}^{-1}$ ]

From the above diagrams we draw the conclusion that if in crystals containing hydrated paramagnetic ions of the type ( $\text{X}^{+++}, 6\text{H}_2\text{O}$ ) we observe doublet struc-

ture in the absorption bands, whose frequency for the crystals containing ions with *F*-term  $\sim 460$  to  $860 \text{ cm.}^{-1}$  and for *D*-term  $\sim 2220$  to  $1450 \text{ cm.}^{-1}$  then we may conclude that the upper excited term of such ions are in the triply degenerate  $\Gamma_4, \Gamma_5$  states respectively, which are subject to a perturbation field of trigonal symmetry.

As mentioned in the introduction (Table I), aqueous solutions of paramagnetic salts do actually show structure which in the majority of cases is of a doublet nature, and the mean frequency difference for them agrees in the order of magnitude with those predicted by Van Vleck for the alums. The existence of doublet structure in the absorption band in such solutions forces us by analogy to postulate the existence of a perturbation field of trigonal symmetry in these solutions. It is known, from the similarity in the absorption spectra shown by paramagnetic ions in hydrated crystals and in aqueous solutions, that even in solution each ion carries a cluster of six coordinated water molecules. Similarly we may expect each of the anions to be associated with a cluster of water molecules. In between these cationic and anionic clusters are situated unattached water molecules which are subject to the polarising action of both these groups. In reference to the paramagnetic clusters, these intermediate water molecules play the part of distant molecules, corresponding to the part played by the  $8(SO_4)$  groups in the alums.

According to the Debye-Hückel theory of complete ionic dissociation, each ion of a given sign is surrounded by a spherical distribution of ions of the opposite sign. But recent absorption spectra evidence on rare earth solutions collected by Freed<sup>10</sup> goes to show that in them the anions occupy definite valence positions with respect to the cations and which are independent over a large range of the degree of dilution.\*

If this holds good in case of the electrolytes containing the elements of the other transition groups the directed positions of the anions with respect to the

\* The evidence is obtained as follows :—A particular group in the absorption spectra of  $\text{EuCl}_3$  in solution consists of four extremely sharp lines, which remain identical for all concentrations from  $1.5 \text{ M}$  to  $0.007 \text{ M}$ . But in  $\text{Eu}(\text{NO}_3)_3$  solutions it is found that the corresponding group consists of three lines which remain constant for all concentrations from  $1 \text{ M}$  to  $101 \text{ M}$ , while at greater dilution the chloride structure begins to appear. Although the total intensity changes, the relative intensity within the structure, their sharpness and their interval do not change during dilution. Further it was found that in the hydrated crystals of  $\text{Eu}$ -nitrate, the triplet appears and in the same position as in solutions. When the nitrate is dehydrated and then dissolved in anhydrous ether, the group appears as two strong lines.

The presence of these absorption lines due to  $\text{Eu}^{+++}$  in solutions seems to indicate that in solution the field round each  $\text{Eu}^{+++}$  ion is sharply defined in its intensity and orientation and depends partly on the nature of the solvent and partly on the nature of the anion. These results cannot be interpreted in terms of Debye-Hückel's theory of interionic action due to each ion of one sign being surrounded by diffuse atmosphere of ions of opposite sign, which change continually in extent and intensity with dilution.

cations may be the origin of the non-cubic perturbation field in aqueous solutions, and thus account for the type I and II of the perturbing forces. Further, the perturbing action of III, the Jahn-Teller forces, will be valid even in the case of hydrated paramagnetic ions in aqueous solution.

We shall now discuss what evidence the fine structure of the bands gives as to whether the Stark splitting of the *D*- and *F*-terms of the different ions in solution are upright or inverted.

TABLE III

	Upright level.	Inverted level.
For the <i>D</i> -term	One absorption band with doublet structure.	One absorption band, as according to the calculation of Van Vleck the $\Gamma_3$ term is not split up in a trigonal field.
For the <i>F</i> -term	More than one absorption band with a doublet structure.	The highest absorption band without structure the lower ones with doublet structure.

In the diagrams we have not taken into consideration the further splitting of the Stark levels due to spin-orbital coupling. If the energy of the spin-orbital coupling is of the same order of magnitude as that due to the effect of the trigonal field, then the structure of the absorption band may alter. An example of this is the occurrence of a triplet structure in the  $\text{Ce}^{+++}$  absorption band at 42,000 cm.<sup>-1</sup> nearly. Similarly, the absence of pronounced doublet structure in the absorption band due to  $\text{Ni}^{++}$  may be attributed to this cause.

Evidence from the absorption bands of the Stark level sequence in the different paramagnetic ions is given in table IV.

TABLE IV

*Ions with D-term :*

Ion.	Theoretical.*	Observed	Remarks.
$\text{Ti}^{+++}$	Inverted	Upright	Observed in $\text{HCl}$ solution of $\text{TiCl}_3$ , which may lead to an inversion of levels.
$\text{Cr}^{++}$	Upright	Upright	
$\text{Fe}^{++}$	Inverted	Upright	
$\text{Cu}^{++}$	Upright	Inverted	
$(\text{MoO})^{+++}$	Inverted	Upright	
$(\text{WO})^{+++}$	do	do	
$\text{Ce}^{+++}$	do	Inverted	Triplet observed due to the effect of large spin-orbital coupling.

As given by Van Vleck.

TABLE IV (*contd.*)*Ions with F-term :*

V <sup>++</sup>	Inverted	Upright
Cr <sup>++</sup>	Upright	do
Ni <sup>++</sup>	do	No decisive evidence
Co <sup>++</sup>	Inverted	do

## DISCUSSION

In the previous paper<sup>1</sup> we have shown that the number and frequency of absorption bands in the paramagnetic solutions (excluding those belonging to the rare earth group) can be more satisfactorily represented by the theory of Stark splitting of ionic levels given there than what could be deduced from the theory of Bethe and Van Vleck, in which it is assumed that in a hydrated metallic complex the field acting on the central ion has a predominantly cubic symmetry. On the other hand, the fine structure of these absorption bands both as regards their number of components and the amount of splitting is of the same order of magnitude, as calculated by Van Vleck for the degenerate orbital terms  $\Gamma_4$  and  $\Gamma_5$  of the paramagnetic ions in alums containing Ti, V and Cr. This splitting is assumed to be due to a trigonal field superposed on the original cubic field. The separation between the principal absorption bands was shown to be proportional to the charge on the paramagnetic ion. On the other hand, the doublet width of these bands is found to be independent of the ionic charge. This is due to the different origins of the primary and the trigonal fields.

Further, from the structure of the absorption bands of these ions in solution, the conclusion is drawn that in most of them the upper levels show degeneracy when placed in a cubic field (*i.e.*, the Stark levels are upright), contrary to the predictions of Van Vleck for these ions. Ce<sup>+++</sup> ions in solution show a triplet structure for the band at  $42 \times 10^3$  cm.<sup>-1</sup>, while according to the theory a doublet structure is expected. This may be due to the large spin-orbital coupling, whose energy is of the same order of magnitude as that due to the trigonal field superposed on it. The absorption bands both due to Ni<sup>++</sup> and Co<sup>++</sup> do not show a doublet structure (as expected for Ni<sup>++</sup>). This may also be due to the large values of spin-orbital coupling for these ions.

It would be of interest to determine the analytic expression for the field which produces the  $(L+1)$  equidistant levels by a splitting up of the ground term as required by our empirical formula. It is of the same nature as the

splitting produced by a uniform magnetic field on ions with the same orbital number, only the negative values of  $L$  are excluded. It follows that a conformal representation is possible by means of which both the electric moment of the ion and the induced field acting on it are transformed into a steady moment and a uniform field.

#### S U M M A R Y

In a previous paper the number and positions of the principal absorption bands of paramagnetic ions in solution were found to be capable of being accounted for by means of an empirical formula proposed by the authors.

Most of the bands were found to consist of doublets, whose frequency difference was of the order of  $2000\text{ cm.}^{-1}$  for the  $D$ -ions and of the order of  $750\text{ cm.}^{-1}$  for the  $F$ -ions.

In the present paper the doublet structure is accounted for as due to the presence of a superposed field of trigonal symmetry round the paramagnetic ions which is supposed to be due to the directed positions of the anions with respect to the cations in solution.

The splitting is found to be of the same order of magnitude as that calculated by Van Vleck for the  $D$ - and  $F$ -ions due to a trigonal field present in the alums containing these ions.

#### A D D E N D A

Since the completion of writing the above, we have been looking through the paper of Messrs S. Datta and M. Deb entitled "Light Absorption in Paramagnetic Crystals and Solutions" (*Phil. Mag.* XX, 1121, 1935), and it appears to us that there is definite optical evidence to settle the question whether the Stark splitting of the  $F$ -terms in  $\text{Co}^{++}$  and  $\text{Ni}^{++}$  are upright or inverted (see table IV). The authors have measured the absorption spectra of the crystals  $\text{CoCl}_2 \cdot 6\text{H}_2\text{O}$  and  $\text{NiCl}_2 \cdot 6\text{H}_2\text{O}$  by reflection from crystalline powders.

For the highest absorption band, the following results have been obtained.

	Position of absorption maxima.	$\Delta\nu$ .
$\text{Co}^{++}$	$505\text{ m}\mu$ 525 , , }	$750\text{ cm.}^{-1}$
$\text{Ni}^{++}$	410 , ,	

Thus the upper  $F$ -level of  $\text{Co}^{++}$  is split up into a doublet, the separation is of the order of magnitude to be expected for a  $F$ -level in a trigonal field, while that

in  $\text{Ni}^{++}$  is a singlet. This observation on hydrated crystals is supported by observations of the absorption spectra of aqueous solution of these compounds, which were made with the help of a Hilsch-Pohl double monochromator used in conjunction with a photo-electric cell.

In the  $\text{CoCl}_2$  solution, the  $515m\mu$  band is found to consist of at least two, if not three, sub-bands; while, in the  $\text{NiCl}_2$  solution, the band at  $407m\mu$  is very sharp with no trace of any structure, on the other hand the next band at  $650m\mu$  is broad with about three sub-bands. According to Van Vleck's calculations, the upper level of  $\text{Ni}^{++}$  is triply degenerate and of  $\text{Co}^{++}$  is non-degenerate in a cubic field. If it is accepted that the structure of the absorption bands in the hydrated paramagnetic crystals gives information about the sequence and splitting of the Stark levels of the paramagnetic ions containing them, on which their magnetic properties like susceptibility and anisotropy depend, then Van Vleck's interpretation of the origin of the large difference in anisotropy of similar crystals containing  $\text{Co}^{++}$  and  $\text{Ni}^{++}$  ions is no longer valid, and we have to seek other explanations to account for these properties. It is very desirable that a series of investigations on the absorption spectra of paramagnetic crystals specially of the alums and of other hydrated crystals should be undertaken.

#### R E F E R E N C E S

- 1 D. M. Bose and P. C. Mukherji—*Phi. Mag.*, **26**, 757 (1938).
- 2 J. H. Van Vleck—*Theory of Electric and Magnetic susceptibilities*; *Phys. Rev.*, **41**, 208 (1932).
- 3 W. G. Penney and R. Schlapp—*Phys. Rev.*, **42**, 666 (1932).
- 4 J. H. Van Vleck—*Jour. Chem. Phys.*, **7**, 61 (1939).
- 5 H. Bethe—*Ann. der. Phys.*, **3**, 133 (1929).
- 6 W. J. de Haas and C. J. Gorter—*Proc. Akad. Sci. (Amsterdam)*, **33**, 676 (1930), **36**, 158 (1933).
- 7 W. G. Penney and R. Schlapp—*loc. cit.*
- 8 Siegart—*Physica*, **3**, 85 (1936).
- 9 J. H. Van Vleck—*Jour. Chem. Phys.*, **7**, 72 (1939).
- 10 S. Freed—*Jour. Chem. Phys.*, **6**, 655 (1938); S. Freed and Weissman, *Jour. Chem. Phys.*, **8**, 297 (1938).

# NEW MEASUREMENTS OF ALUMINIUM MONOXIDE BANDS

By DEBESCHANDRA ROY, M.Sc.

(Received for publication, June 23, 1950)

## Plate XIII

**ABSTRACT.** The paper deals with new measurements of band-heads in the spectrum of aluminium monoxide, and reports the existence of several bands not yet recorded in literature. A new band head equation has also been derived.

## INTRODUCTION

It is well known that aluminium arc in air emits a bright band spectrum in the blue-green region between  $\lambda 4100$ - $\lambda 5700$ . The spectrum consists of a large number of bands with sharply defined heads degraded to the red and belongs to a single system due to a  $^2\Sigma \rightarrow ^2\Sigma$  transition.

These bands were first observed by Thalen in 1866. Since then they have been subjected to a number of investigations. A brief but complete review of these investigations till 1924 has been given by Mörikofer.<sup>1</sup> Most of them were concerned with the empirical representation of the band-edges or of the structure lines of bands or with the question of their emitter. Much doubt was expressed as to whether it is the metal or the oxide which is responsible for the emission of these bands. In 1925 Mulliken<sup>2</sup> proved definitely that their emitter is the diatomic oxide molecule, AlO. In the same year the quantum analysis of their vibrational structure was given independently by Birge<sup>3</sup> and by Mecke<sup>4</sup> from the band-head data of Mörikofer while that of their rotational structure was carried out by Eriksson and Hulthen.<sup>5</sup>

In the meantime many investigations have been made, notably by Pomeroy<sup>6</sup> and by Sen<sup>7</sup> to interpret correctly the band structure in the light of recent developments in the theory of band spectra of diatomic molecules. As a result of his new measurements of the structure lines of three of the most intense bands, viz., (1, 0), (0, 0) and (0, 1), from high-dispersion spectrograms, Pomeroy found the analysis previously given by Eriksson and Hulthen to be incorrect. Using a new method of locating uniquely the band-origins, he gave a correct quantum interpretation of the band structure and evaluated the important constants of the molecule. Very recently Sen has made further investigations on the rotational

structure of these bands. Employing a dispersion higher than that used by Pomeroy, he has studied the nature of spin-doubling in both the lower and the upper states of the band system.

It appears, however, from literature that since 1925 no further attempt has been made either to verify the correctness of the vibrational analysis of the bands and of the band-head equation given by Mecke or to extend the band system under improved conditions of excitation. In fact the differences between wave-numbers of band-heads as recorded by Mecke from the old data and those calculated from his band-head equation are in many cases appreciably large. This may be due to the fact that the wave-length data of band-heads are only approximate as they are given up to four figures. Hence fresh measurements of the band-heads are desirable to test the limit of accuracy of Mecke's equation.

In point of fact the present investigation was started with a view to search for new band systems in the spectrum of AlO, using different modes of excitation. For this purpose the first source employed was an aluminium arc in air operating from 220 volt D. C. mains but taking a current as high as eight amperes. For a preliminary survey of the spectrum in the region  $\lambda$  2200- $\lambda$  7000, photographs were taken with suitable quartz- and glass-prism spectrographs of large light-gathering power. Although no new band system was discovered in this region under the present mode of excitation, a number of yet unrecorded bands were observed in several sequences of the existing band system. The object of the present paper is to report the results of measurements of these new bands together with those of the existing ones and to derive a band-head equation which will represent the wave-numbers of band-heads within the limits of experimental error.

#### M E A S U R E M E N T S

Measurements of band-heads from high dispersion-spectrograms do not necessarily give always greater accuracy than when spectrograms of moderate dispersion are employed especially in the case of the weaker heads because of the difficulty of their exact location under the magnification of a comparator. Hence the bands were photographed in the first order of a 6 ft. concave grating set up on a Paschen mounting and having a dispersion of about 6 A. U. per mm. Suitable iron arc lines were taken as reference standards. The measurement was conducted in the usual way on a Gaertner precision-comparator from several plates photographed with different periods of exposure varying from a few seconds to about an hour. Individual measurements of band-head wave-lengths differed from one another by not more than  $\pm 0.02$  A.U. in any case. Their weighted mean is given in table II.

O-C VALUES OF BAND-HEAD WAVE-NUMBERS, USING  
 OLD DATA AND MECKER'S EQUATION

Table I includes the old data of band-heads with their  $v'$ ,  $v''$  assignments as given by Mecke, who derived the following band-head equation:—

$$\nu = 206.6 \cdot 0 + 866.1 \nu' - 4.0 \nu'^2 - 971.0 \nu'' + 7.2 \nu'^2.$$

TABLE I

$v', v''$	$\lambda$ (obsd.)	$\nu$ (obsd.)	$\nu$ (calcd.)	O-C (cm. <sup>-1</sup> )
4, 0	4158	24043.3	24046.4	-3.1
5, 1	4181	23011.0	23912.7	-1.7
6, 2	4202	791.5	785.4	6.1
7, 3	4223	673.2	664.5	8.7
8, 4	4243	561.6	550.0	11.6
9, 5	4261	462.1	441.9	20.2
10, 6	4279	363.4	340.2	13.2
3, 0	4308	200.1	208.3	-2.2
4, 1	4330	688.2	682.6	5.6
5, 2	4352	22071.8	21963.3	8.4
6, 3	4373	861.2	850.4	10.8
7, 4	4394	751.9	743.0	8.0
8, 5	4412	659.1	643.8	15.3
9, 6	4430	567.0	550.1	16.9
10, 7	4463	400.2	402.8	-6.6
2, 0	4470	365.1	362.2	2.9
3, 1	4494	245.7	244.5	1.2
4, 2	4516	137.3	133.2	4.1
5, 3	4537	034.8	028.3	6.5
6, 4	4557	21938.1	21929.8	8.3
7, 5	4576	847.0	837.7	9.3
8, 6	4594	761.4	752.0	9.4
9, 7	4610	685.9	672.7	13.2
10, 8	4625	615.6	599.8	15.8

TABLE I (*contd.*)

	$\lambda$ (obsd.)	$\nu$ (obsd.)	$\nu$ (calcd.)	$\Delta - C$ (cm $^{-1}$ )
1, 0	4648	21508.6	21508.1	0.5
2, 1	4672	308.1	308.4	-0.3
3, 2	4694	207.8	205.1	2.7
4, 3	4715	203.0	198.2	4.8
5, 4	4736	109.0	107.7	1.3
6, 5	4754	820.0	823.6	5.4
7, 6	4771	20954.1	945.9	8.2
8, 7	4788	879.7	874.6	5.1
9, 8	4801	823.2	809.7	13.5
0, 0	484	646.0	20616.0	0.9
1, 1	4866	545.0	544.3	0.7
2, 2	4888	412.6	449.0	-3.6
3, 3	4900	368.1	360.1	5.0
0, 1	5079	10683.4	10682.2	1.2
1, 2	5102	594.7	591.9	-0.2
2, 3	5123	514.1	514.0	0.4
3, 4	5143	438.5	439.5	-1.0
4, 5	5161	370.7	371.4	-0.7
5, 6	5177	310.8	309.7	1.1
6, 7	5192	255.0	254.4	0.6
7, 8	5205	207.0	205.5	1.5
0, 2	5337	18731.9	18732.8	-0.9
1, 3	5358	658.5	659.9	-1.4
2, 4	5376	596.0	593.4	2.6
3, 5	5394	534.0	5333.3	0.7
4, 6	5409	482.6	479.6	3.0
5, 7	5422	438.3	432.3	6.0
6, 8	5434	397.5	391.4	6.1
0, 3	5615	17804.5	17797.8	6.7



Figure 1.

AlO bands

Photographed with prism spectrograph.



TABLE I (*contd.*)

$v', v''$	$\lambda$ (obsd.)	$\nu$ (obsd.)	$\nu$ (calcd.)	O—C (cm. $^{-1}$ )
1, 4	5635	17741.3	17739.3	2.0
2, 5	5651	691.1	687.2	3.9
3, 6	5666	644.2	641.5	2.7
4, 7	5677	610.1	602.2	7.9
5, 8	5687	579.1	569.3	9.8

From the last column of table I, it is evident that the differences between the observed and the calculated values of band-head wave-numbers from Mecke's equation are in many cases well beyond the limits of experimental error, especially for bands of high  $v'$  and  $v''$  values. Hence it is necessary not only to secure new measurements of band-heads but also to derive a more approximate band-head equation than that given by Mecke. Incidentally, it may be noted that the assignment of  $v', v''$  value to the band-head at  $\lambda$  446.3 is incorrect. It should be assigned the value (11, 8) instead of (10, 7). With this new assignment, the O—C value is 19.3 cm. $^{-1}$  and is of the right order of magnitude.

#### O—C VALUES OF BAND-HEAD WAVE-NUMBERS, USING NEW DATA AND MECKE'S EQUATION

In table II are given the new data of band-heads. Column IV contains the O—C values using Mecke's band-head equation while the O—C values in column V are calculated using the new equation, *viz.*,

$$\nu_e = 20699.25 + 870.0(v' + \frac{1}{2}) - 3.80(v' + \frac{1}{2})^2 - 978.2(v'' + \frac{1}{2}) + 7.12(v'' + \frac{1}{2})^2$$

TABLE II

$v', v''$	$\lambda$ (air)	$\nu$ (vac.)	O—C (cm. $^{-1}$ ), using	
			Mecke's eqn.	present eqn.
4, 0	4156.80	24050.2	3.8	0.2
5, 1	4179.78	23918.0	5.3	0.0
6, 2	* 4201.81	23792.6	7.2	-0.1

TABLE II (*contd.*)

$v', v''$	$\lambda$ (air)	$\nu$ (vac.)	O-C (cm. <sup>-1</sup> , using Mecke's eqn)	O-C (cm. <sup>-1</sup> , using present eqn.)
7, 3	4222.85	23674.0	9.5	0.0
8, 4	4242.94	23561.9	11.9	-0.1
9, 5	4262.03	23456.4	14.5	-0.2
10, 6	4280.05	23357.7	17.5	-0.1
11, 7	4296.44*	23268.6	23.7	2.9
3, 0	4307.21	23210.4	2.1	0.0
12, 8	4312.79	23180.3	24.3	0.1
4, 1	4330.39	23086.1	3.5	0.1
5, 2	4352.64	22968.1	4.8	-0.2
6, 3	4373.78	22857.1	6.7	-0.1
7, 4	4393.84	22752.8	8.9	0.0
8, 5	4412.58	22650.1	12.3	1.1
9, 6	4430.31	22565.5	15.4	1.7
10, 7	4447.05*	22460.4	17.0	1.1
11, 8	4462.33	22403.5	21.6	2.1
2, 0	4470.38	22363.2	1.0	0.0
12, 9	4476.02*	22335.0	27.2	4.8
13, 10	4490.38*	22263.6	24.3	-2.0
3, 1	4493.82	22246.6	2.1	0.2
14, 11	4502.34	22204.5	26.9	-3.1
4, 2	4516.24	22136.1	2.9	-0.2
5, 3	4537.57	22032.1	3.8	-0.7
6, 4	4557.44	21936.0	6.2	0.0
7, 5	4576.26	21845.8	8.1	0.0
8, 6	4593.85	21762.2	10.2	0.0
9, 7	4610.07	21685.6	12.9	0.3
10, 8	4625.20	21614.6	14.8	0.4
11, 9	4638.77*	21551.4	17.7	0.0
1, 0	4648.08	21508.3	0.2	-0.1

TABLE II (*contd.*)

$v'$ , $v''$	$\lambda$ (air)	$\nu$ (vac.)	O-C (cm $^{-1}$ ), using	
			Mecke's eqn.	present eqn.
12, 10	4650.30*	21498.0	24.8	3.6
2, 1	4671.94	21398.4	0.0	-0.8
3, 2	4694.40	21296.0	0.9	-0.7
4, 3	4715.50	21200.7	2.5	-0.1
5, 4	4735.92	21109.3	1.6	-2.3
6, 5	4754.01	21028.9	5.3	-0.1
7, 6	4771.26	20953.0	7.1	0.0
8, 7	4787.10	20883.6	9.0	-0.1
9, 8	4800.92	20823.5	13.8	2.5
10, 9	4814.26*	20765.8	14.6	0.8
0, 0	4842.18	20646.1	0.1	0.1
1, 1	4866.23	20544.0	-0.3	-0.4
2, 2	4888.83	20449.1	0.1	-0.4
3, 3	4910.02	20360.8	0.7	-0.4
0, 1	5079.37	19682.0	-0.2	0.0
1, 2	5102.01	19594.7	-0.2	0.0
2, 3	5123.08	19514.0	0.0	0.0
3, 4	5142.60	19440.0	0.5	0.0
4, 5	5160.62	19372.1	0.7	-0.5
5, 6	5176.75	19311.8	2.1	0.0
6, 7	5191.44	19257.1	2.7	-0.6
7, 8	5204.25	19209.7	4.2	-0.5
8, 9	5216.20*	19165.7	2.3	-2.9
0, 2	5337.03	18731.8	-1.0	-0.5
1, 3	5357.75	18659.4	-0.5	0.2
2, 4	5376.93	18592.8	-0.6	0.0
3, 5	5394.27	18533.0	0.3	0.0
4, 6	5409.73	18480.1	0.5	0.3
5, 7	5422.70	18435.9	3.6	2.6

TABLE II (*contd.*)

$v, v'$	$\lambda$ (air)	$\nu$ (vac.)	O—C (cm. <sup>-1</sup> ), using	
			Mecke s eqn.	present eqn.
6, 8	5431.64	18395.4	4.3	2.0
7, 9	5445.05*	18360.2	3.3	0.0
8, 10	5453.52*	18331.7	2.9	-1.9
9, 11	5458.91	18313.5	6.4	-0.1
0, 3	5615.88	17801.7	3.9	4.9
1, 1	5635.60	17739.4	0.1	1.4
2, 5	5652.21	17687.3	0.1	1.5
3, 6	5666.62	17642.3	0.8	2.1
1, 7	5679.45	17602.5	0.3	1.2
5, 8	5690.20	17569.2	-0.1	0.2
6, 9	5698.47*	17543.7	0.4	0.4
7, 10	5701.41*	17525.4	2.7	1.0
8, 11	5708.80*	17512.0	3.0	0.0

The bands marked with asterisks in the preceding table are the new bands observed in the present investigation. Several of them are of very feeble intensity but they are undoubtedly present on all the plates taken with prism spectrographs of large light-gathering power which are especially meant for photographic Raman spectra.

#### DISCUSSIONS

From an inspection of the O—C values given in the last two columns of table II, it is evident that although the new equation does not materially differ from that of Mecke, it represents more approximately the new measurements of band-heads even for high values of  $v'$  and  $v''$ .

Using the new data, the energy of dissociation, D, of AlO in the lower and upper electronic states of the band system are found to be 4.03 and 6.04 volts respectively, while, from the old data, Lessheim and Samuel<sup>8</sup> had evaluated  $D''=4.15$  and  $D'=6.15$  volts. In either case, one finds that the dissociation-energy of the molecule increases on excitation. According to the view of the above authors, this is due to an increase in the number of electron pairs which in turn gives rise to an additional  $p-p$  bond in the upper electronic state of AlO.

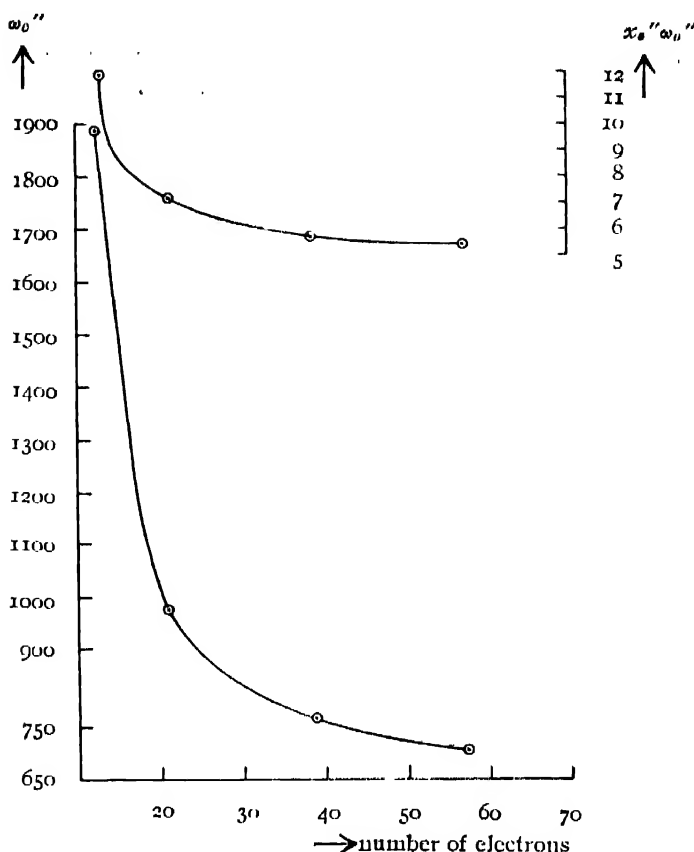


FIGURE 2

Excepting BO, the oxides of group IIIb elements are so far known to possess only one band system. Of course no band spectrum is yet recorded for thalium monoxide. No rotational analysis has been done of the bands of GaO<sup>0</sup> and InO<sup>1/2</sup>. Consequently there is much uncertainty about the nature of transition responsible for the emission of the band system in each case. It is, however, known that the ground states of BO is a  $^2\Sigma$  state which is the lower state of the  $\beta$ -bands. With a view to ascertain that the lower state of the band system for each of the oxides, *viz.*, AlO, GaO and InO is analogous to that of the  $\beta$ -bands of BO, variations of vibrational coefficients in the lower states of the band systems of BO, AlO, GaO and InO with increase of atomic number have been plotted in figure 2. The nature of each curve is what one should expect when all the states under question are analogous.

The author acknowledges with pleasure his best thanks to Mr. M. K. Sen, M.Sc., who had begun the work and taken several of the photographs used in the

present investigation and to Dr. P. C. Mahanti, for many helpful discussion and guidance. The author is finally indebted to Prof. P. N. Ghosh, for providing with every facility for the completion of the work.

SPECTROSCOPIC RESEARCH LABORATORY,  
DEPARTMENT OF APPLIED PHYSICS,  
UNIVERSITY COLLEGE OF SCIENCE & TECHNOLOGY,  
CALCUTTA.

#### R E F E R E N C E S

- <sup>1</sup> *Dissertation*, Basel (1925).
- <sup>2</sup> *Phys. Rev.*, **28**, 561 (1925).
- <sup>3</sup> *Phys. Rev.*, **28**, 240 (1925).
- <sup>4</sup> *Phys. Zeits.*, **26**, 217 (1925).
- <sup>5</sup> *Zeits. f. Phys.*, **34**, 775 (1925).
- <sup>6</sup> *Phys. Rev.* **29**, 59 (1927).
- <sup>7</sup> *Ind. J. Phys.*, **11**, 251 (1937).
- <sup>8</sup> *Zeits. f. Phys.*, **84**, 637 (1933).
- <sup>9</sup> *Helv. Phys. Acta*, **7**, 357 (1934); *Phys. Rev.*, **46**, 114 (1934); *Ind. J. Phys.*, **10**, 429 (1936).
- <sup>10</sup> *Phys. Rev.*, **80**, 607 (1936); Unpublished work of the present author.

# A SIMPLE METHOD OF COATING OPTICAL SURFACES WITH ALUMINIUM

By M. V. SIVARAMAKRISHNAN

*(Received for publication, June 12, 1939)*

**ABSTRACT.** A short history of the evaporation process for depositing metallic films on to mirrors is given. The apparatus herein described is found to be convenient for the deposition in high vacuum of most metals on various surfaces up to 6" in diameter. The metal to be deposited is evaporated from two straight parallel pieces of  $\frac{1}{2}$  mm. tungsten wire. At a pressure of  $10^{-4}$  mm of Hg the optical surface to be coated receives a good deposit when placed at a distance of about 10 cms. from the filament. The advantages of this process over chemical silvering, sputtering are discussed with special reference to the coating of optical surfaces with aluminium. The apparatus described is quite simple to be recommended for laboratory use. The author has introduced some important changes in the technique to facilitate easy repetitions of the process.

## INTRODUCTION

Optical surfaces, large and small, used in optical instruments such as reflectors in telescopes and interferometers are now being increasingly treated with chromium and aluminium instead of with silver for increasing their reflectivity. Chemical silvering done even with the best of care has been found to tarnish after some time. Surfaces coated with aluminium not only do not tarnish even after long intervals of time but possess the added advantage of increased reflectivity in the ultra-violet region,<sup>1, 2</sup> which property becomes so valuable in photographic work. So the problem of aluminising optical surfaces has been engaging the attention of many physicists in recent years and a good deal of data are now available for the successful coating of surfaces with aluminium. The present paper deals with a simple method developed in this laboratory for this process.

The method consists in enclosing the optical surface to be coated along with aluminium in high vacuum and vaporising the aluminium by passing a current through it. If the optical surface is suitably placed, the aluminium condenses on it and gives the surface the desired reflectivity. For supporting the aluminium wire in position and passing a current through it, tungsten wires of suitable thickness are used and the aluminium wire is supported on it as shown below.

## HISTORY OF THE EVAPORATION PROCESS

The evaporation process dates back to the time of Edison who in 1890 obtained patents in connection with it. The process was perfected by R. Ritschl at the Reichsanstalt particularly with a view to coating two interferometer mirrors simultaneously and equally to give the same reflecting power.

Cartwright and Strong<sup>4</sup> applied this process in 1931 for the deposition of many metals and non-metals including Al, Sb, Be, Ca, Cr, Co, Cu, Au, Fe, Pb, Mg, Mn, Ni, Se, Ag, Te, Sn, Zn, quartz, fluorite, the alkali halides and silver chloride on optical and other surfaces. They found this process much easier and it required less time than sputtering. Moreover, the thickness of the deposited film could be brought under more delicate control by weighing the amount of the material to be evaporated. This, therefore, permitted of an accurate reproduction of partially reflecting mirrors for the interferometers.

The coating of astronomical mirrors with aluminium was undertaken independently by Strong<sup>5</sup> and by Williams<sup>6</sup> in 1932. Since then, several other physicists, *viz.*, Sabine,<sup>1</sup> Cartwright,<sup>7</sup> Edwards,<sup>8</sup> and Yeagley<sup>9</sup> have used this technique for making mirrors for general experimental purposes.

## EVAPORATION TECHNIQUE FOR ALUMINIUM

An apparatus for evaporating the materials consists of some device for holding and heating the material to be evaporated, a vacuum-tight container, and an evacuating system to maintain the necessary high vacuum. Several arrangements were used in which these essential features were varied.

One of the problems encountered when evaporating metals in a vacuum is the choice of a proper heating element that will produce enough heat to vaporise the metal, without itself melting and snapping. Strong has described an evaporation process<sup>5</sup> where the heating element is a spiral of tungsten wire over which the aluminium wire is supported in the form of U-riders at a number of places. In this method, the disadvantages are that the aluminium derives its heat only by metallic contact and that the molten aluminium globules fall down in lumps from the support. A modification of this method by Edwards<sup>10</sup> involves the use of two parallel wires placed about one millimeter apart and in a horizontal position. The metal is simply laid upon the two wires and when it melts, it wets the tungsten and spreads out linearly between the two wires. Yeagley<sup>9</sup> has adopted a different method of heating where the filament is of adjustable overlapping type. The author has found this method more efficient.

## EXPERIMENTAL ARRANGEMENT

Figure 1 explains the parts and assembly of the evaporation chamber for aluminizing purposes. 'J' is a bell-jar 12" in height and 8" clear inside dia-

diameter, good enough for aluminising mirrors up to 6" in diameter. The base-plate 'P' is an ordinary 15" x 12" x  $\frac{1}{2}$ " glass plate. Two  $\frac{1}{4}$ " holes about 2" apart are drilled in the glass plate with carborundum and rotating pipe. The electrodes A, B, C entering the holes are made from  $\frac{1}{2}$ " brass rods. " 'A' is turned at one end and threaded to fit into the lower drilled and tapped portion 'B.' The 'L' shaped members C, C are bent from  $\frac{1}{4}$ " brass rods and held in place in the drilled holes in the upper part of 'B' by set screws. The horizontal portions in 'C' have  $\frac{1}{16}$ " holes and are split lengthwise by a hack-saw. Set screws at the sides serve to clamp the tungsten wires in these jaws."

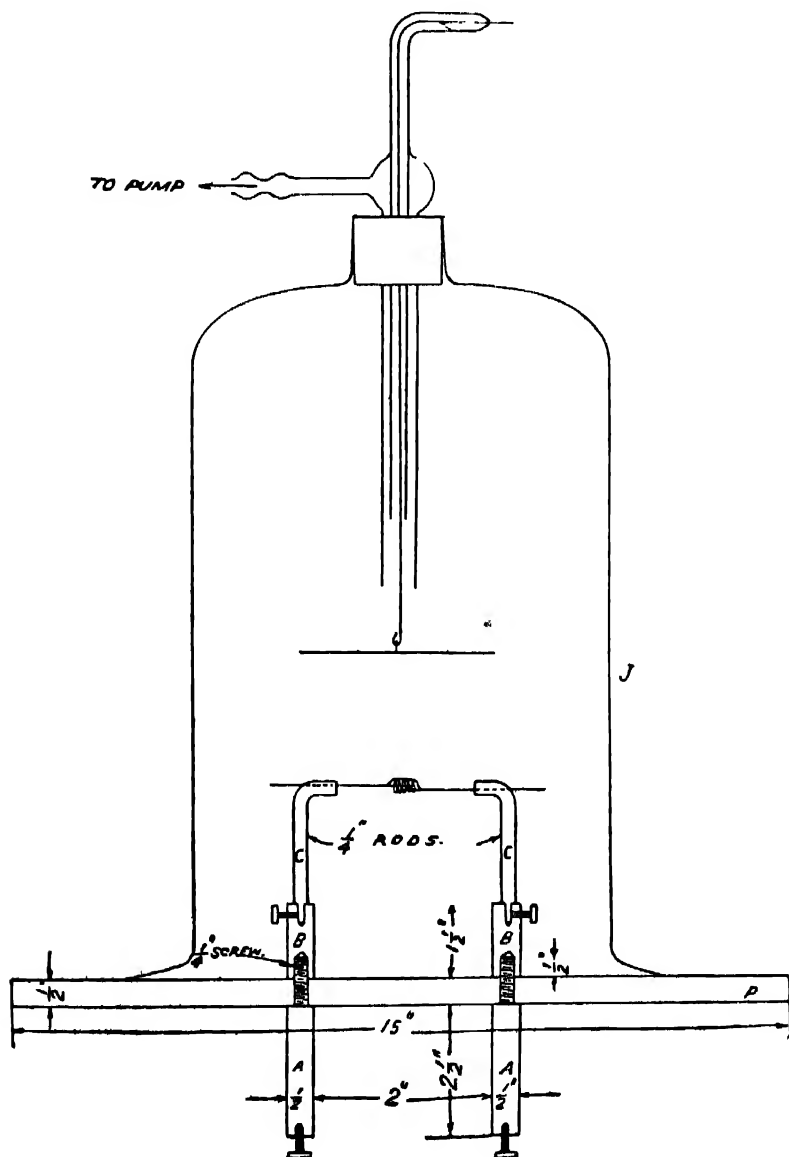


FIGURE I

It is found to be more convenient to evacuate from the top of the bell-jar. For this an internal joint is made from glass and fitted into the one-hole rubber cork of the bell-jar. An aluminium rod  $1/8''$  in diameter and about  $12''$  in length passes through the glass tube of the internal joint. It is sealed at one end with good sealing-wax and is provided with a hook at the other end. The aluminium rod serves two purposes, *viz.*, it forms one terminal for connecting the secondary of the induction coil. The other terminal of the secondary is connected to one of the electrodes. This procedure is useful in that we need not remove now and then the stray aluminium that may be deposited on the base plate, which, of course, becomes a necessity if the terminals for the electric discharge are provided at the base plate. The electric discharge is necessary to know the quality of the vacuum and for cleaning the optical surface to be aluminized. Secondly, the aluminium rod helps to hold small optical surfaces.

All joints, metal to glass, glass to rubber, are joined with good sealing-wax. The use of sealing-wax for fixing the bell-jar with the glass plate has been avoided. It is very often found difficult to seal vacuum tight with sealing-wax. Instead, the bell-jar is ground (lapped) with the glass plate with very fine carborundum and good vacuum grease is applied to the rim of the bell-jar and the space to be covered by the base of the bell-jar in the glass plate. After slightly warming the two, the bell-jar is pressed gently on the glass plate with slight rotation so that when the pump begins to work, there is no leakage there whatsoever. This procedure also helps considerably to remove the bell-jar from the base-plate very easily and thereby facilitates easy repetition of the process.

The filament is of overlapping, adjustable type. Two straight pieces of tungsten wire each about  $2''$  in length and  $'02''$  ( $\frac{1}{2}$  mm.) in diameter are clamped in the brass holders so that their near ends overlap about 4 mm. without touching each other. Four inches of thin aluminium wire (less than  $\frac{1}{2}$  mm.) are carefully wound tight on this overlapping portion

The surfaces to be coated are cleaned well first with alkali, then with concentrated  $HNO_3$ , and finally with distilled water. This order of cleaning<sup>11</sup> is essential to get rid of all traces of alkali for successful coating of aluminium.

#### V A C U U M T R C H N I Q U E

A Cenco-Hyvac rotary oil-pump in series with two apeizen oil-pumps of the Waren type<sup>12</sup> produces the necessary high vacuum. The vacuum in the system is measured by a McLeod gauge. "After pumping for about ten minutes, and after a possible leak has been healed, the discharge from the induction coil is found to soften into a patternless-grey-blue-glow." When the pressure as indicated by the McLeod gauge is about '001 mm. or above, the vacuum is found to be good enough for the successful evaporation of aluminium. It has been

found, however, that bright films cannot be obtained at pressures higher than  $10^{-4}$  mm. of Hg.

The heating is done by drawing current from a 60-volt D. C. supply with suitable carbon rheostat and ammeter in the circuit. The tungsten wire is found to glow when the current is about 10 amperes, and when it is adjusted to 15 amperes, the aluminium is found to melt and stick to the wire. On further increase of current, it is found to boil and condense on the surface to be coated. It is found that the optical surfaces receive a good deposit when placed at a distance of about 7 cms. from the heating filament, for a pressure of '001 mm. of mercury. The depth of the coat is easily and accurately controlled by observing through the top surface of the disc. About 5 to 10 minutes are required for complete aluminization.

Several plates have been aluminized including a 6" mirror. Attempts are now being made to make the apparatus simpler and suitable for aluminizing a 24" reflector, which has just been completed in the College, correctly figured, polished and parabolized.

I wish to express my thanks to Dr. H. Parameswaran, for suggesting the problem and to Professor P. S. Subramania Ayyar for allowing me facilities in carrying out this work.

PHYSICS DEPARTMENT,  
PRESIDENCY COLLEGE,  
MADRAS.

R E F R E N C E S

- <sup>1</sup> Williams and Sabine, *Astrophys. J.*, **77**, 316 (1933).
- <sup>2</sup> B. K. Johnson, *Nature*, 216 (1934).
- <sup>4</sup> Cartwright and Strong, *Rev. Sci. Inst.*, **2**, 189 (1931).
- <sup>5</sup> Strong, *Phys. Rev.*, **39**, 1012 (1932); **43**, 493 (1933).
- <sup>6</sup> Williams, *Phys. Rev.*, **41**, 255 (1932).
- <sup>7</sup> Cartwright, *Rev. Sci. Inst.*, **3**, 298 (1932).
- <sup>8</sup> Edwards, *Phys. Rev.*, **34**, 205 (1933).
- <sup>9</sup> Yeagley, *Scientific American* (1937), (July, August).
- <sup>10</sup> Edwards, *Rev. Sci. Inst.*, **4**, 449 (1933).
- <sup>11</sup> Strong, *Astrophys.* (1936).
- <sup>12</sup> Waren, *Jour. Sci. Inst.* (1923).



# RAMAN SPECTRUM OF DIPHENYL IN THE SOLID STATE

BY S. A. AZIZ, M.Sc.

(Received for publication, June 3, 1939)

## Plate XIV

**ABSTRACT** Raman spectrum of diphenyl in the solid state has been studied for the first time. In all 26 lines have been recorded. Many of the lines of molten diphenyl have appeared in the solid state of the substance. Most of the lines are observed to be shifted in frequency in passing from liquid to solid state, the shift, however, is not in the same direction for all the lines. In the region of small frequencies, four new lines have been recorded at 160, 93, 54, and 39  $\text{cm}^{-1}$ . The probable origin of these lines is pointed out.

## INTRODUCTION

Raman spectrum of diphenyl in the liquid state has been investigated in detail recently by Mukherji and Aziz.<sup>1</sup> The influence of change of state from liquid to solid on the Raman lines has been studied by Epstein and Steiner,<sup>2</sup> by Gross and Vink,<sup>3</sup> and by Sirkar<sup>4,5</sup> in the case of benzene and its other compounds with interesting results. Besides the appearance of some new lines characteristic of the solid state, the Raman lines show some changes in frequency and intensity in passing from liquid to solid state. It was thought worth while to study the Raman spectrum of diphenyl in the solid state and to compare it with that of diphenyl in the liquid state. The results obtained have also been compared with those of benzene.

## EXPERIMENTAL

Diphenyl obtained from the research laboratory of Eastman Kodak Company was purified by repeated distillation and the middle portion of the distillate was received directly into a clean Wood's tube which had been washed by the distillate. Particular care was taken to make the distillate dust-free. The distillate condensed into a semi-transparent crystalline mass and the Raman spectrum of this was photographed. The temperature was kept near about 25°C by circulating water in the jacket surrounding the Wood's tube. The drawn-out end was painted black from outside and stray light was cut down as much as possible.  $\lambda 4358\text{\AA}$  was used as the exciting line. The light of the quartz mercury lamp was filtered through a concentrated solution of sodium nitrite to suppress  $\lambda 4047\text{\AA}$ .

and the shorter wave-lengths, followed by another filter of a very dilute solution of iodine in carbon tetrachloride to suppress the continuous background between  $\lambda 4358\text{\AA}$  and  $\lambda 4916\text{\AA}$ . The time of exposure was about 80 hours on Agfa Isochroine backed plates H & D. 4400, with a Fuess glass spectrograph having a dispersion of about  $21\text{\AA}$  at  $\lambda 4358$ . The continuous spectrum was found to be more prominent as compared with the intensity of Raman lines in the case of the solid state of the substance. This continuous background is due to the reflection inside the spectrograph of the very strong Rayleigh line  $\lambda 4358$ . A complementary filter of a very dilute solution of potassium chromate suggested by Ananthakrishnan<sup>6</sup> was also used just before the slit of the spectrograph to weaken  $\lambda 4358$  before it entered the spectrograph.

Measurements were made with a Gaertner photo measuring comparator, fairly strong lines being correct within half an Angstrom and very weak ones within one Angstrom.

#### R E S U L T S A N D D I S C U S S I O N

The results are given in table I. For comparison, lines of diphenyl in the liquid<sup>1</sup> state are also added in the same table. Figures within brackets indicate visual estimates of intensity. Table III gives all the lines obtained along with their assignments.

TABLE I  
Diphenyl Frequencies

No.	Solid state (at $25^\circ\text{C}$ ).	Liquid state (slightly above fusion point).
1	...	3102 (o)
2	3063 (s)	3062 (s)
3	3043 (r)	3047 (r)
4	...	2961 (o)
5	1604 (ro)	1610 (ro)
6	1589 (ro)	1590 (s)
7	1506 (s)	1506 (s)
8	1459 (s)	1452 (s)
9	...	1376 (o)

TABLE I (*contd.*)

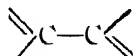
No.	Solid state (at 25°C).	Liquid state <sup>1</sup> (slightly above fusion point).
10	1326 (o)	1318 (4)
11	1273 (10)	1283 (10)
12	1201 (1)	1241 (1)
13	1164 (3)	1189 (3)
14	1146 (1)	1157 (1)
15	1097 (2)	1090 (4)
16	1033 (5)	1032 (5)
17	999 (8)	1003 (10)
18	...	980 (1)
19	...	964 (1)
20	...	898 (4)
21	846 (4)	838 (4 br.)
22	784 (2)	779 (4)
23	739 (3)	740 (5)
24	666 (2)	614 (4)
25	541 (o)	548 (1)
26	...	449 (o)
27	...	408 (5 br.)
28	...	368 (o)
29	320 (3)	313 (4 br.)
30	243 (2 diff.)	267 (4 br.)
31	...	193 (o)
32	169 (2 br.)	...
33	146 (4)	140 (4 br.)
34	93 (4 br.)	...
35	54 (3)	...
36	39 (1)	...

The lines of solid diphenyl are much sharper than the lines of liquid diphenyl, because of the absence of rotation of molecules in the solid

## S. A. Aziz

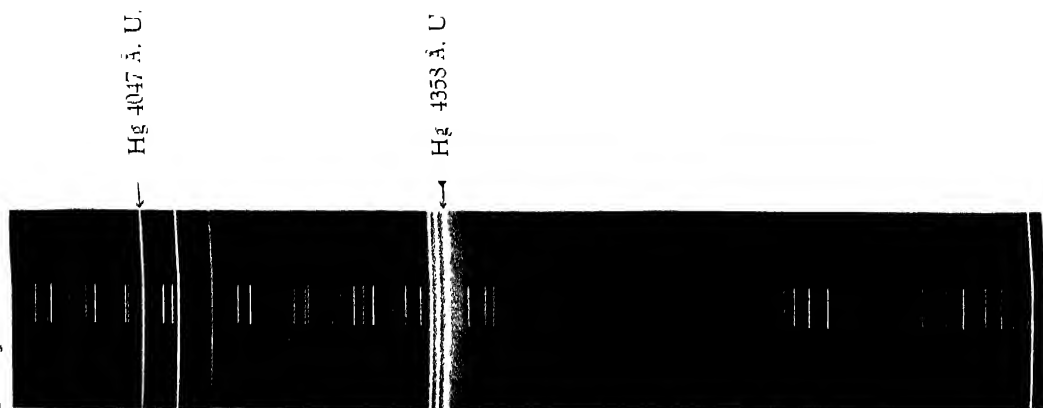
state, but the lines with  $\Delta\nu$ ,  $243 \text{ cm.}^{-1}$  and  $\Delta\nu$ ,  $169 \text{ cm.}^{-1}$  are somewhat diffuse. The line  $93 \text{ cm.}^{-1}$  is quite broad. From a study of table I, it will be noticed that a change from liquid to solid brings out some displacement in the position of the lines. A few lines however, at  $3063$ ,  $1589$ ,  $1506$ ,  $1033$  and  $739 \text{ cm.}^{-1}$ , do not show any appreciable change. The symmetrical hydrogen frequency at  $\Delta\nu$ ,  $3063 \text{ cm.}^{-1}$  suffers no change either in intensity or in frequency. This result is in accord with that of Sirkar<sup>5</sup> who observed that in benzene also this line shows no change. S. Bhagavantam and A. V. Rao,<sup>7</sup> however, have noticed it to change from  $3061$  in the liquid benzene to  $3069$  in the vapour state. The other hydrogen frequency  $3047$  of liquid diphenyl is shifted to  $3043 \text{ cm.}^{-1}$  in the solid state.

Out of the doublet  $1610$  and  $1500 \text{ cm.}^{-1}$  the former shows a definite decrease in frequency in the solid state and is shifted to  $1604$ . The latter shift suffers no change in frequency but gains in intensity in the case of the solid state. This line is somewhat diffuse in the liquid state but in the solid state it becomes quite sharp and the increase in intensity is partly due to the fact that in the solid state the whole intensity is distributed over a small width.

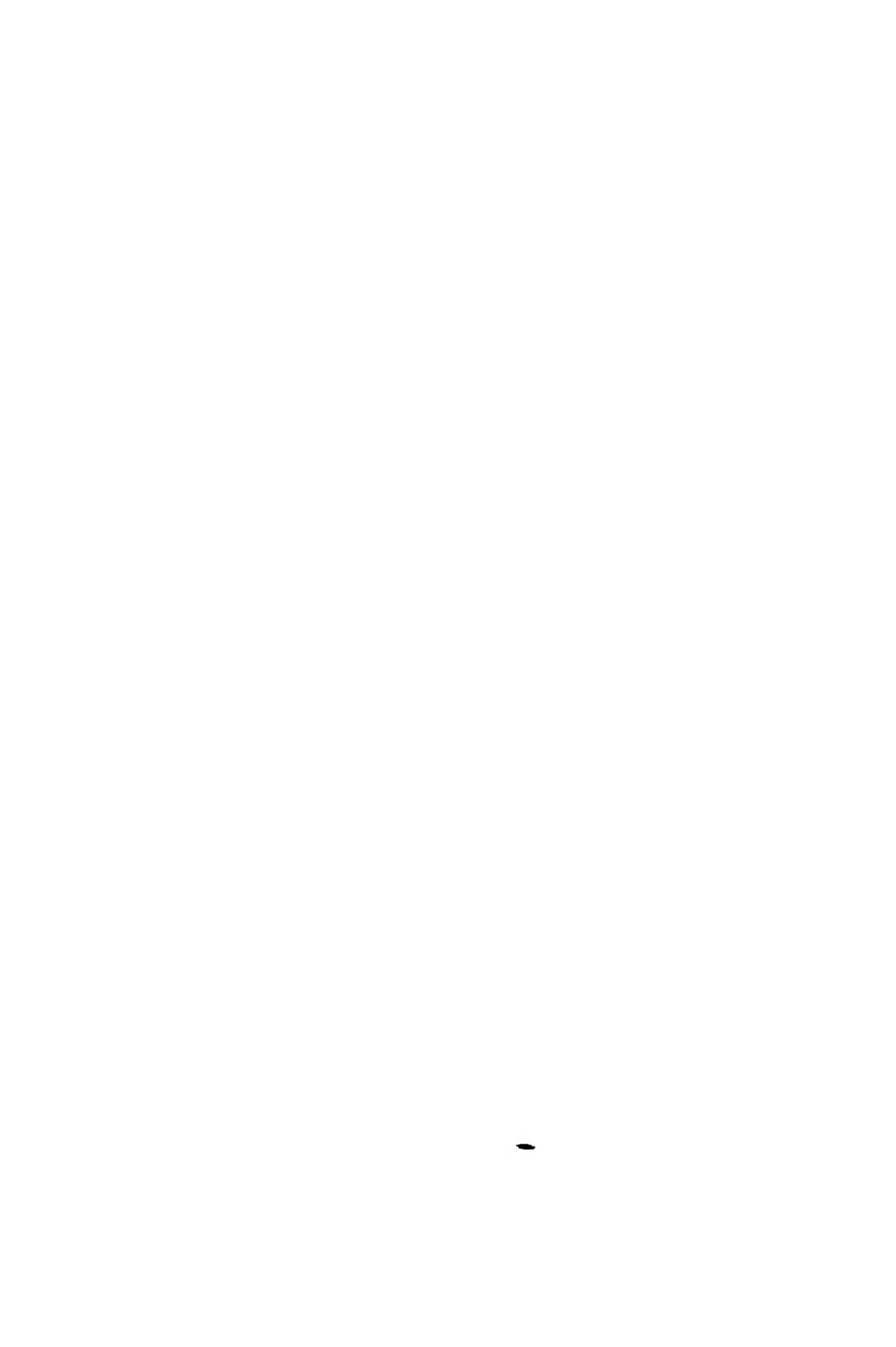
The other important frequency at  $1283 \text{ cm.}^{-1}$ , of liquid diphenyl is shifted to  $1273$  when it is in the solid state. Its intensity in the solid state is greater than that of  $999 \text{ cm.}^{-1}$ . Epstein and Steiner observed that the lines at  $983$ ,  $992$ ,  $1176$ , and  $1605 \text{ cm.}^{-1}$  of benzene were lowered by one to three wave-numbers in the solid state at low temperature. In the case of diphenyl also, the line  $1003$  due to C—C vibration of the benzene ring is lowered by four wave-numbers in the solid state. The other two lines  $1189$  and  $1157$  of liquid diphenyl are shifted to  $1164$  and  $1146$  respectively, the shifts however are much greater than those observed by Epstein and Steiner in the case of benzene. It will be noticed that the two symmetrical vibrations  $1003$  and  $1283$  of liquid diphenyl, both having their origin in the C—C vibration, the former characteristic of the benzene ring and the latter characteristic of  of diphenyl molecule behave similarly in passing from the liquid to the solid state so far as the displacement in frequency is concerned.

The displacement in frequency in passing from the liquid to the solid state is not in the same direction for all the lines. Whereas  $3062$ ,  $1590$ ,  $1506$ ,  $1032$ , and  $740 \text{ cm.}^{-1}$  do not show any appreciable shift in passing from the liquid state of the substance to the solid state, the lines  $3047$ ,  $1610$ ,  $1283$ ,  $1241$ ,  $1189$ ,  $1157$ ,  $1003$ ,  $614$ ,  $548$ , and  $267 \text{ cm.}^{-1}$  decrease in frequency in the solid state, but the lines  $1452$ ,  $1318$ ,  $1090$ ,  $838$ ,  $779$ ,  $313$ , and  $140 \text{ cm.}^{-1}$  increase.

The line  $408 \text{ cm.}^{-1}$  which is fairly strong and somewhat broad in the liquid state of the substance either grows extremely weak in the solid state or disappears



Raman spectrum of diphenyl in the solid state.



entirely. Also the lines 3192, 2961, 1376, 980, 964, 898, 449, 368, and 193  $\text{cm}^{-1}$  which are fairly weak in liquid diphenyl have not been recorded in the solid state.

In the region of small frequency shifts four new lines at 169, 93, 51, and 39  $\text{cm}^{-1}$  have been recorded in the solid state. Evidently they are characteristic of the solid state of diphenyl and compare fairly well with the lines found in other compounds of benzene in the solid state by Gross and Vuks,<sup>3</sup> and by Sirkar.<sup>5</sup> All of these contain the benzene nuclei and this may explain the common frequencies observed. The lines observed in diphenyl are due probably to the intermolecular oscillations in polymerised groups<sup>4</sup> of molecules of diphenyl in the solid state. Gross and Vuks,<sup>3</sup> however, ascribed the lines observed by them in benzene and other compounds in the solid state to vibrations characteristic of the crystal lattices of the respective molecules. Further evidence regarding the origin of the lines in the present case can be obtained if the substance be examined in solution for its Raman effect and the influence of temperature on these lines be studied.

The work was carried on in the Physics Laboratory, Agra College, Agra, and I wish to express my grateful thanks to Dr. S. K. Mukerji for suggesting the problem and for his continued guidance during the course of research, to Dr. N. K. Sethi for providing me with the facilities for the work and to the authorities of the Agra University for the award of a Research Scholarship.

TABLE II

## Exciting Lines

Exciting lines Å.	Notation.	Wave-number $\text{cm}^{-1}$
4358·3	A	22938
4347·5	A <sub>1</sub>	22905
4339·2	A <sub>2</sub>	23039

TABLE III

## Diphenyl Frequencies

No.	Wave-number $\nu$ .	Intensity.	Assignment.	$\Delta\nu$ in cm. $^{-1}$
1	19875	5	A	3063
2	19895	1	A	3043
3	21334	10	A	1604
4	21349	10	A	1589
5	21390	1	A <sub>1</sub>	1605
6	21407	1	A <sub>1</sub>	1588
7	21432	2	A <sub>2</sub>	1506
8	21451	0	A <sub>2</sub>	1588
9	21470	1	A	1459
10	21612	0	A	1326
11	21615	10	A	1273
12	21743	1	A <sub>1</sub>	1272
13	21737	1	A	1201
14	21763	0	A <sub>2</sub>	1276
15	21774	3	A	1164
16	21791	1	A	1146
17	21841	2	A	1097
18	21905	5	A	1033
19	21939	8	A	999
20	21961	0	A <sub>1</sub>	1034
21	21968	2	A <sub>1</sub>	997
22	22039	0	A <sub>2</sub>	1000
23	22092	2	A	846
24	22154	2	A	784
25	22199	3	A	739
26	22332	2	A	606
27	22397	0	A	541
28	22609	3	A	329
29	22695	2 diff.	A	243
30	22709	2 br.	A	169
31	22792	4	A	146
32	22845	4 br.	A	93
33	22884	3	A	54
34	22899	1	A	39

In the tables br. indicates a broad line and diff. a diffuse line

AGRA COLLEGE,  
AGRA, INDIA.

## REFERENCES

- 1 S. K. Mukerji and S. A. Aziz, *Ind. J. Phys.*, **12**, 271 (1938).
- 2 Epstein and Steiner, *Nature*, **138**, 910 (1934).
- 3 E. Gross and M. Vnks, *Nature*, **135**, 100, 431, 998 (1935).
- 4 S. C. Sirkar, *Ind. J. Phys.*, **10**, 109 (1926).
- 5 S. C. Sirkar, *Ind. J. Phys.*, **10**, 189 (1936).
- 6 R. Ananthakrishnan, *Proc. Ind. Acad. Sc. A.*, **5**, 76 (1937).
- 7 S. Bhagavantam and A. V. Rao, *Proc. Ind. Acad. Sc. A.*, **5**, 18 (1937).

# STUDIES OF THE IONOSPHERE AT CALCUTTA \*

By J. N. BHAR

(Received for publication, June 30, 1939)

## Plate XV

**ABSTRACT.** In the present paper the results of systematic ionospheric observations carried out at Calcutta ( $22^{\circ}33' N$ ) during the period January 1936 to April 1937 are described. The diurnal and seasonal variations of critical frequency for the E and F regions of the ionosphere are presented graphically and are discussed with reference to variations expected from the ultra-violet light theory. It is found that the observed variations of Region E<sub>1</sub> ionization are in general agreement with the theory of Chapman particularly during winter months. During summer months, however, there are deviations due presumably to the frequent occurrence of abnormal ionization associated with thunderstorms. The observed results are utilised for estimating the coefficient of recombination in the E region which is found to be of the order of  $10^{-9} \text{ cm.}^3/\text{sec.}$ . The phenomenon of abnormal E region ionization is discussed in detail and its association with the incidence of thunderstorms investigated.

The observed variations of Region F<sub>2</sub> ionization shows that the time of diurnal maximum shifts towards the afternoon in summer. There are two distinct maxima in the seasonal variation curves for the midday and the 1600 hours ionization. These seem to coalesce in the case of the 1900 hours seasonal ionization curve. The extreme day-to-day variability of the midnight ionization makes it difficult to form any idea as to the nature of its seasonal variation.

## 1. INTRODUCTION

Ionospheric investigation in common with all other geophysical investigations requires for its furtherance observational data collected over long periods and from different parts of the world. Proper collation of the data is only possible if there is international co-operation as in the case of the study of problems connected with transient variations of terrestrial magnetic elements. The importance of world-wide survey of the latter was recognised long ago and international organisations are now into existence for promoting synoptic study of this branch of geophysics. Need of similar co-operation for ionospheric investigations is also now recognised and the first step towards making planned observations was taken at the instance of the Union Radio Scientifique International in 1931 when the Union organised a subcommission for conducting radio research during the second International Polar Year 1932-33. The International Union of Geodesy and Geophysics have also recognised the need of such co-ordinating work and appointed in 1936 a joint committee of the Association of Terrestrial Magne-

\* Communicated by the Indian Physical Society.

tism and Electricity and of the U. R. S. I. with Prof. E. V. Appleton as Chairman.

Unfortunately, unlike the extended network of magnetic observatories, the number of ionospheric laboratories is extremely few and even those which exist are apparently working independent of one another without any co-ordinating scheme. The paucity of ionospheric data for different latitudes is still a severe handicap for formulating a complete theory of the ionosphere. It is therefore extremely desirable that new stations should be opened in different countries of the world and that those which are already in existence should carry on systematic observations on the variations of ionospheric characteristics over long continued periods.

So far as is known to the author the only station engaged on carrying out regular and systematic ionospheric observations at low northern latitudes is the one at Calcutta which was opened as early as 1930.\* The first systematic measurements on the ionosphere were started here in 1932 when observations on the heights of the ionospheric layers on a fixed frequency (1 Mc./sec.) at different hours of the day were made throughout the polar year (1932-33), in accordance with the programme formulated by the Polar Year Subcommission of the U. R. S. I. After the completion of the Polar Year programme the experimental equipment was developed to enable observations to be made by the ( $P'$ ,  $f$ ) curve method over a frequency range of 0.7 to 15 Mc./sec. This equipment was utilised for the measurement of the ion density of the ionospheric layers at different hours of the day for a period of about 16 months and the results obtained are presented and discussed in the present paper.

## 2 EXPERIMENTAL EQUIPMENT AND ESTIMATION OF CRITICAL FREQUENCY

### (a) Transmitter

The oscillatory circuit of the transmitter was of the conventional Hartley type employing a 250 Watt Philips TB 2/250 valve. The pulse modulation was normally at 200 per sec. and was accomplished by the well-known method of inserting a condenser and a grid leak in the grid circuit of the oscillator valve. We preferred this type of modulation to the now more commonly employed method of modulation at the frequency of the A. C. supply mains which is more convenient for automatic recording. The former has the advantage that if necessary the pulse recurrence frequency can be increased at will. Such increase becomes necessary when it is desired to resolve echoes of short delay.

The transmitter covered a frequency range of 0.7 to 15 Mc./sec. By suitably changing the tuning coils and the condenser setting the frequency over

\* Later, in 1934, a station at Allahabad has also been opened.

the entire range could be changed in steps of 0.15 Mc./sec. in the range 0.7 to 1.5 Mc./sec., of 0.25 Mc./sec. in the range 1.5 to 5 Mc./sec. and of 0.5 Mc./sec. in the range 5 to 15 Mc./sec.

(b) *Estimation of the critical frequency*

In estimating the critical frequency it is necessary to know which of the two—the ordinary or the extra-ordinary magnetically split echo—is being observed. The splitting being usually of the type known as stratification splitting, the longer delayed one is ordinary and the one with shorter delay the extra-ordinary for frequencies greater than the gyromagnetic frequency, which in our case is 1.27 Mc./sec. Our measurements were always confined to the ordinary ray and the critical frequency for a particular region was estimated by noting the frequency at which reflexions from this region just disappeared. In cases where splitting was not observed, as happened usually in the day time, it was presumed that the observed echo was due to the ordinary ray, the extra-ordinary ray being lost by greater absorption.

3. THEORETICAL IONIZATION CURVE FOR CALCUTTA

In order to interpret the observed data regarding the diurnal and seasonal variation of ionization which is now proved to be due to the varying inclination of the solar rays it is necessary to compare them with a set of representative curves which may be regarded as standard variation curves. Such standard curves may be drawn from Chapman's theoretical analysis<sup>1</sup> on the ionizing effect of monochromatic radiation on a rotating atmosphere. The main results of Chapman's analysis and the variation curves appropriate for the latitude of Calcutta calculated therefrom are given below.

(a) *Chapman's Analysis*

According to Chapman, the variation of N with time for a particular height  $h$  is given by the differential equation

$$\sigma_0 \frac{dv}{d\phi} + v^2 = \exp. [1 - z - \exp. (-z) f(R + z, \chi)]$$

where

$$v = N/N_0,$$

N—number of ions of each kind present per c.c.,

$N_0$ —maximum value of N above the equator at noon at the equinoxes,

$$\sigma_0 = \frac{1}{1.37 \times 10^4 a N_0},$$

$\alpha$ —coefficient of recombination,

$\phi$ —time reckoned from noon in radians

$\chi$ —zenithal distance of the sun,

$$z = \frac{h - h_0}{H},$$

$h$ —height at which the ionization is considered,

$h_0$ —height of the level above the equator at noon at the equinoxes,  
i.e.,  $\chi=0$ , where the rate of ion production is a maximum,

$H$ —“Scale height”, i.e., height of the homogeneous atmosphere,

$$R = \frac{a + h_0}{H},$$

$a$ —radius of the earth,

and  $f(R + z, \chi)$ —is a complicated function which approximates  $\sec \chi$  for values of  $\chi < 85^\circ$ .

The numerical value of  $R$  appropriate for a region at the level of the  $E_1$  layer is 650, as assumed by Chapman. The parameter  $\sigma_0$  which depends on  $N_0$  and the coefficient of recombination  $\alpha$  is uncertain. For reasons discussed in section (4c) we have taken  $\sigma_0 = 0.25$  for our calculation.

### (b) Theoretical Ionization Curves for Calcutta

Since in all ionization measurements the maximum electron density of a particular region is measured, it is necessary to calculate the variation of  $v_{\max}$  with  $\phi$ ,  $v_{\max}$  being the maximum value of  $v$  at any instant irrespective of height. Millington<sup>2</sup> has worked out an approximate numerical method of calculating  $v_{\max} - \phi$  curves from the above equation and has drawn a set of such curves appropriate for region  $F_2$ . Following the same procedure curves have been drawn depicting the diurnal variation of ionization of Region  $E_1$  at Calcutta for five specially chosen days of the year. These are given in figure 1.

Since we are specially interested in curves depicting the day-to-day variation of ionization throughout the year at a particular hour of the day, we derived a number of such curves from the five diurnal curves of figure 1. Two of these representing the seasonal variation of ionization at midday and at midnight are shown in figure 2,

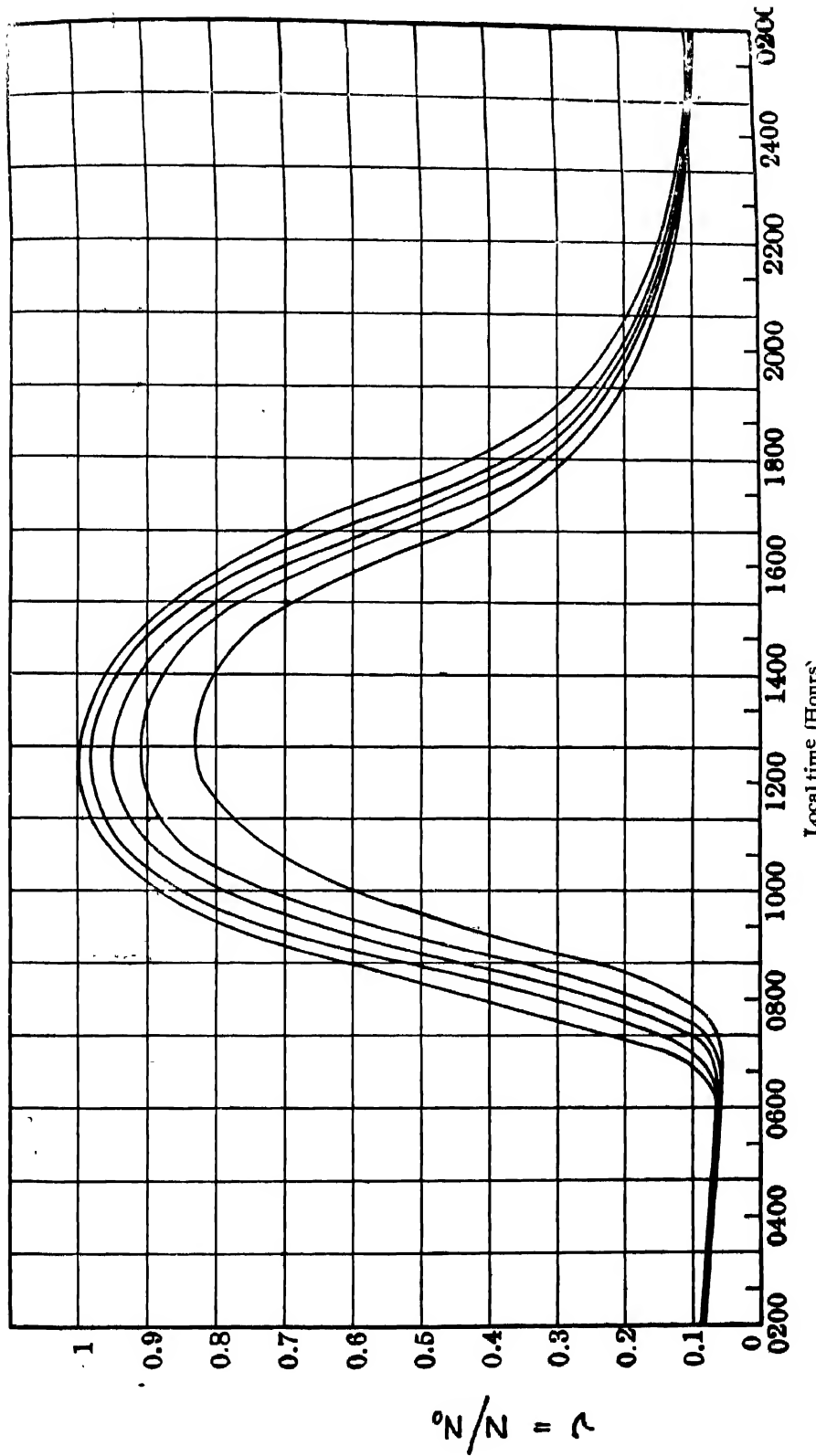


Fig. 1—Curves representing the diurnal variation of ionization at Calcutta for  $\sigma_0 = 0.25$ . Starting from above the curves successively correspond to  
 (i) Summer solstice, (ii)  $\delta = 10^\circ$ , (iii) Equinoxes, (iv)  $\delta = -10^\circ$  and (v) Winter solstice.

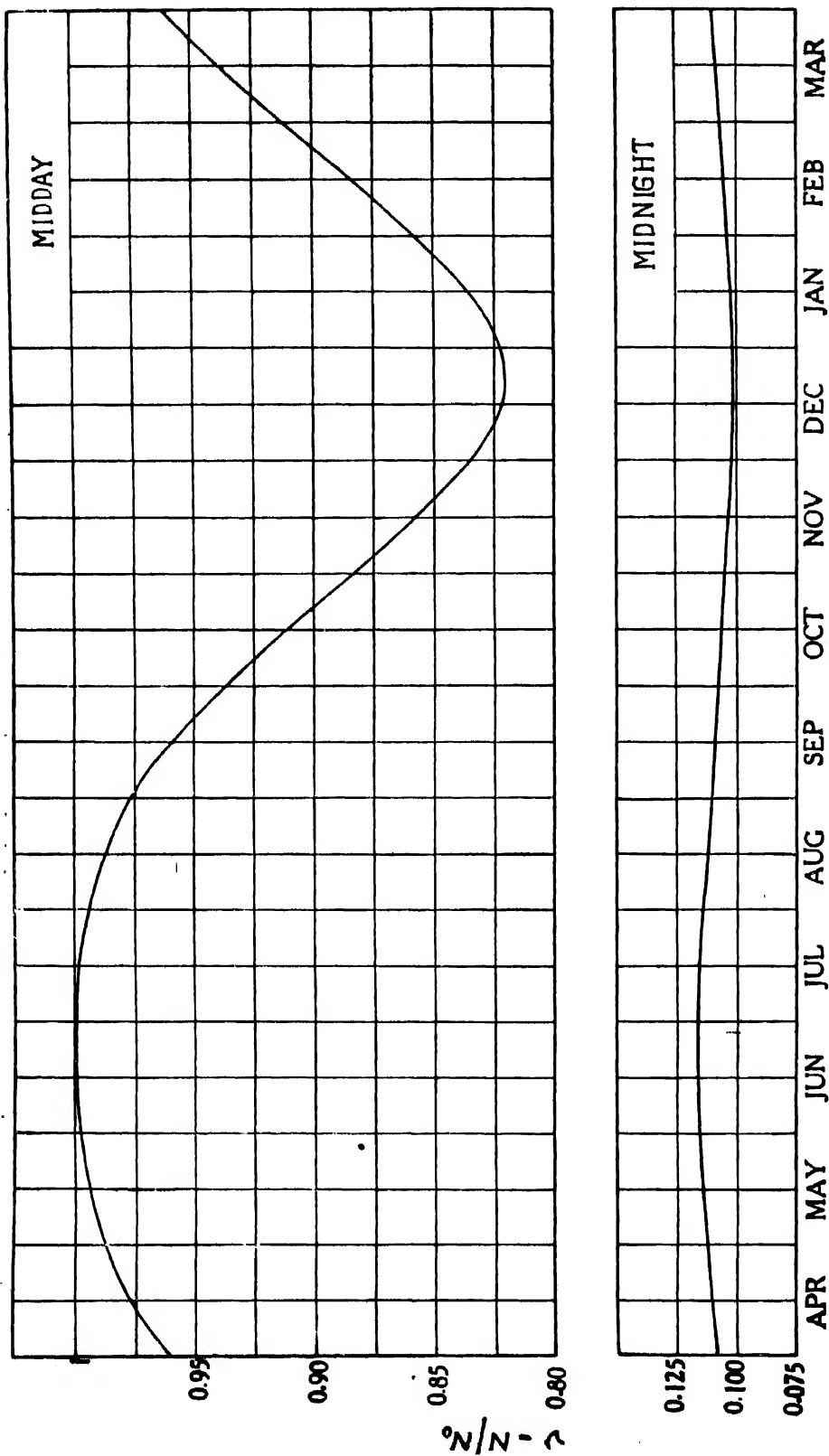


Fig. 2—Seasonal variation of midday and midnight ionization at Calcutta for  $\sigma_0 = 0.25$ .

An interesting point to be observed in connexion with the day-to-day variation of noon ionization (figure 2) is that the annual maximum is very flat compared to the relatively sharp minimum. It is also noteworthy that the amplitude of the seasonal variation is much greater for the noon ionization than for the midnight.

#### 4. STUDIES OF REGION E IONIZATION

It has been already mentioned that the critical penetration frequency for the region studied was always measured with reference to the ordinary wave component. It is known that the maximum electron density,  $N$ , of a particular region is related to the ordinary ray critical frequency,  $f$ , by the equation

$$N = 1.24 \times 10^{-8} f^2 \quad (1)$$

It has also been seen in sec. 3 that

$$\nu = \frac{N}{N_0} = \text{const.} \times N = \text{const.} \times f^2$$

Thus

$$f = \text{const.} \times \sqrt{\nu}$$

Measurements of this critical frequency for Region E<sub>1</sub> were made three days each week at noon, 1600 hours, 1900 hours and at midnight everyday. For reasons stated elsewhere additional observations were made at 1730 hours and at 2030 hours during the months of April to July. From the data obtained the following types of variation of ionization could be studied :

(i) Midday to midnight variation. For simplicity we will call this the diurnal variation.

(ii) Day-to-day variation of the ionization at certain fixed hours of the day, viz., noon, 1600 hours, 1900 hours and midnight throughout the year. We will call this the seasonal variation of ionization.

In what follows we shall discuss both these types of variation and compare them with theoretical deductions from Chapman's theory.

##### (a) Diurnal Variation

Plots of the four (sometimes six) daily observations made between midday and midnight (thrice every week) may be taken as a rough representation of the diurnal variations of ionization. In figs. 3 and 4 a number of such mean diurnal variation curves for the different months of the year ending April, 1937, are given. Each curve is drawn by taking the monthly mean of  $f_{E_1}^2$  for each hour of observation. Such mean values have the advantage that they tend to cancel out

occasional irregularities of ionization. The full line curve given in each case depicts the hourly variation of ionization as expected from the ultra-violet

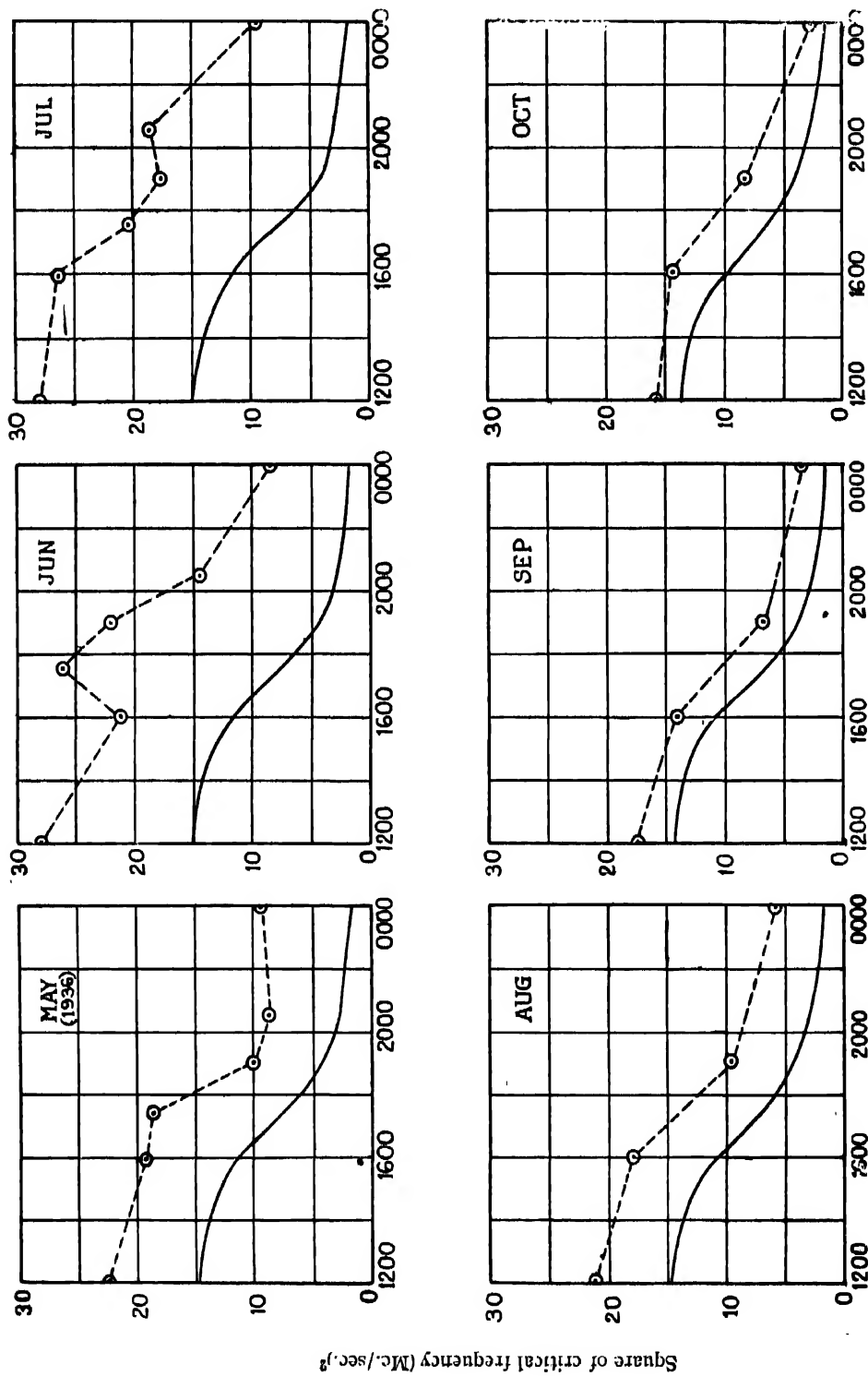


Fig. 3—Depicting the average variation of ionization of Region E<sub>1</sub> from midnight to midday to midnight in different months.—Theoretical variation of ionization.

theory. These are all drawn with reference to the theoretical value of  $v_{\text{noon}}$  at winter solstice as standard, the ordinate for the latter being adjusted to coincide

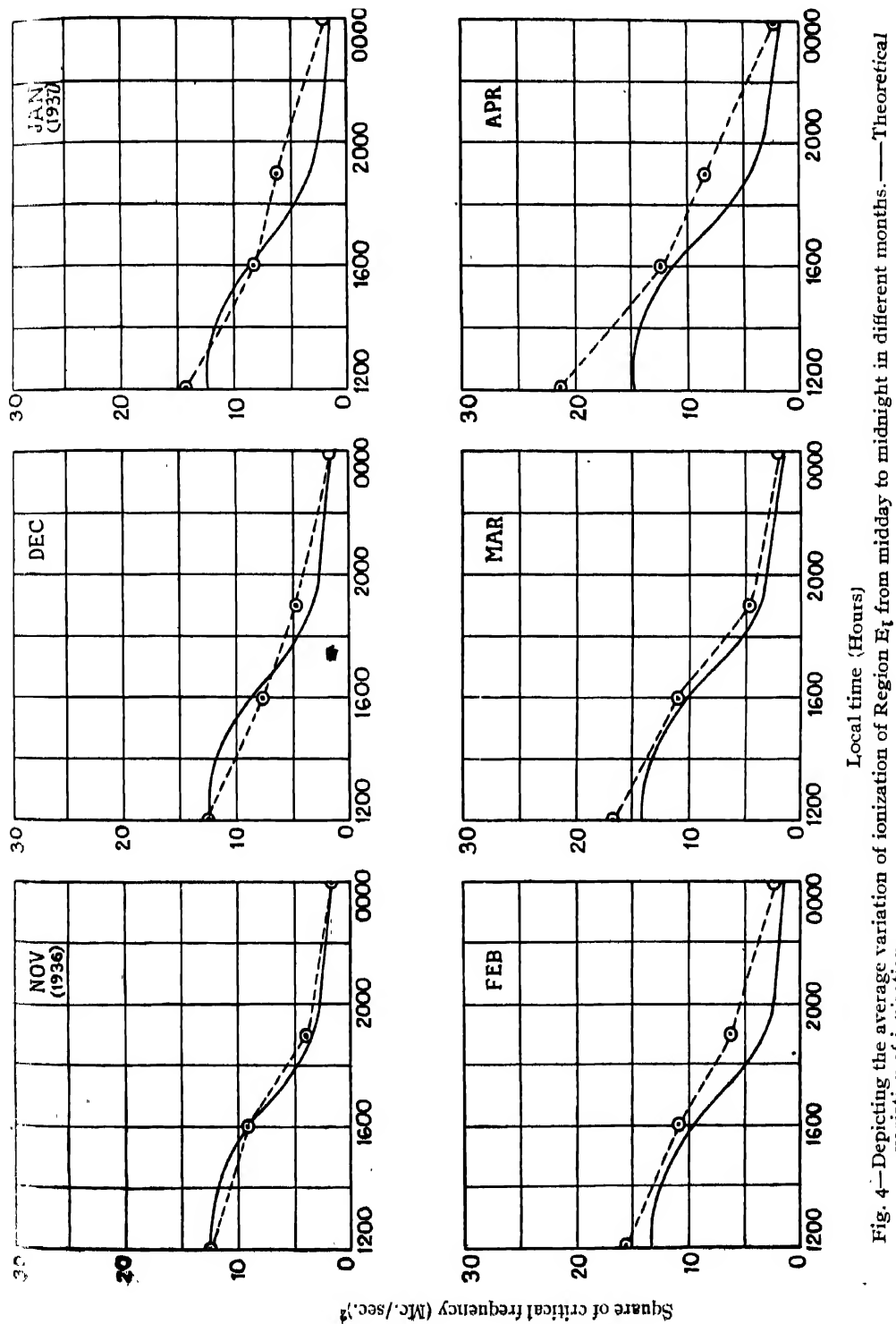


Fig. 4.—Depicting the average variation of ionization of Region  $E_t$  from midnight to midday in different months.—Theoretical variation of ionization.

## J. N. Bhar

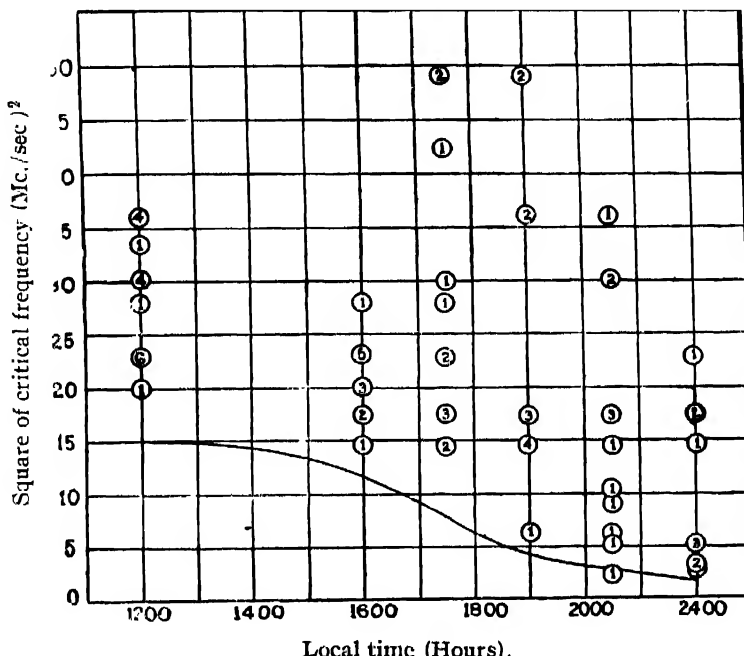
with that of the observed average value of  $f_{E_1}^2$  at midday in December. It will be seen that the general trend of variation in each month approximates more or less to the corresponding theoretical curve. The agreement between the theoretical and observed curves is very marked in the winter months. In summer, however, the curves diverge considerably. A quantitative estimate of the agreement or divergence between these curves in the different months of the year may be obtained from Table I in which the ratio of midnight to midday values of average  $f_{E_1}^2$  are tabulated.

TABLE

Months.	Observed.	Monthly mean of	$\frac{f_{E_1}^2}{f_{E_1}^2}$ (midnight)
		$f_{E_1}^2$ (midday)	
January (1937)	0.14		0.12
February	0.15		0.12
March	0.12		0.11
April	0.10		0.11
May (1936)	0.37		0.11
June	0.30		0.11
July	0.33		0.11
August	0.27		0.11
September	0.20		0.11
October	0.17		0.12
November	0.12		0.12
December	0.13		0.12

The very marked departures of the observed variations from the theoretically calculated values during the months May-September deserve special mention. It was observed that during these summer months the ionization of Region E<sub>1</sub> suffered frequent abnormal increases both by the day and also by the night. What was still more remarkable, the abnormal increases which occurred during the night were, in general, proportionately greater than those occurring in day-time. This point is illustrated in figure 5 in which the square of the observed critical frequency at each hour of observation is individually plotted for the

month of June (1936). It may be seen in the figure that at midnight the ratio of the observed maximum value of  $f_{E_1}^2$  to the corresponding normal value is about 1.2; but for midday this ratio is only about 2.4. The data for the other summer months show the same characteristics. Evidently this fact explains the large discrepancies encountered in these months as shown in Table 1.



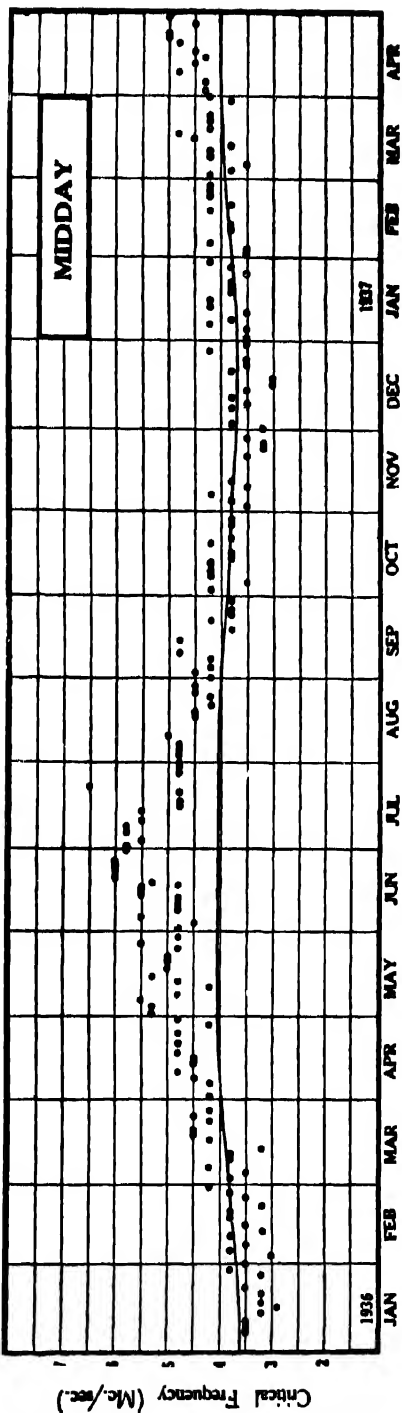


Fig. 6.—Seasonal variation of Region E<sub>1</sub> critical frequency. —Theoretical curve.

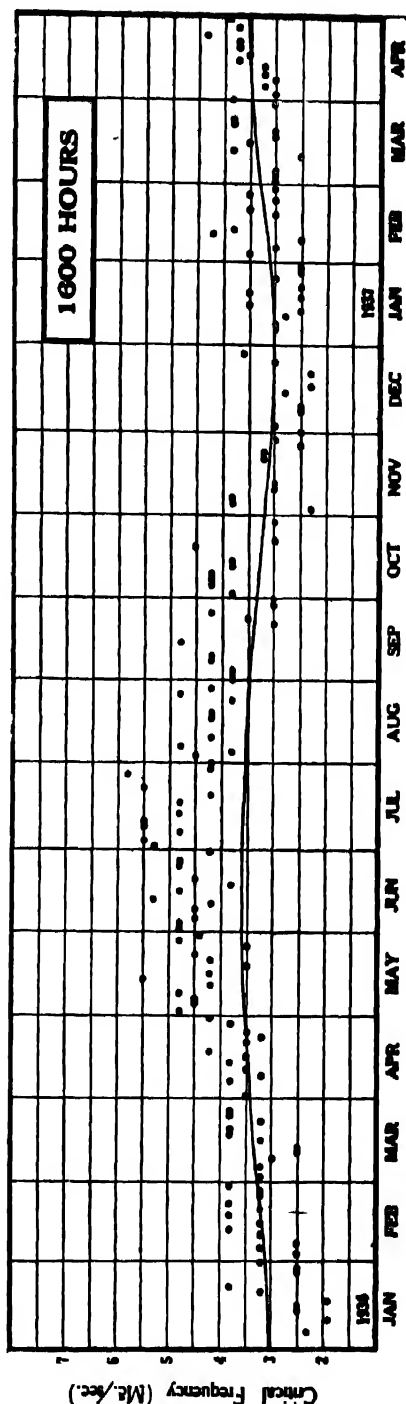


Fig. 7.—Seasonal variation of Region E<sub>1</sub> critical frequency. —Theoretical curve

for the winter months, there is considerable divergence between the two in summer. This divergence is least for the midday values and gradually increases as one proceeds from day to night. One interesting feature in the figure for midnight may be pointed out. The theoretical curve hardly shows any variation from

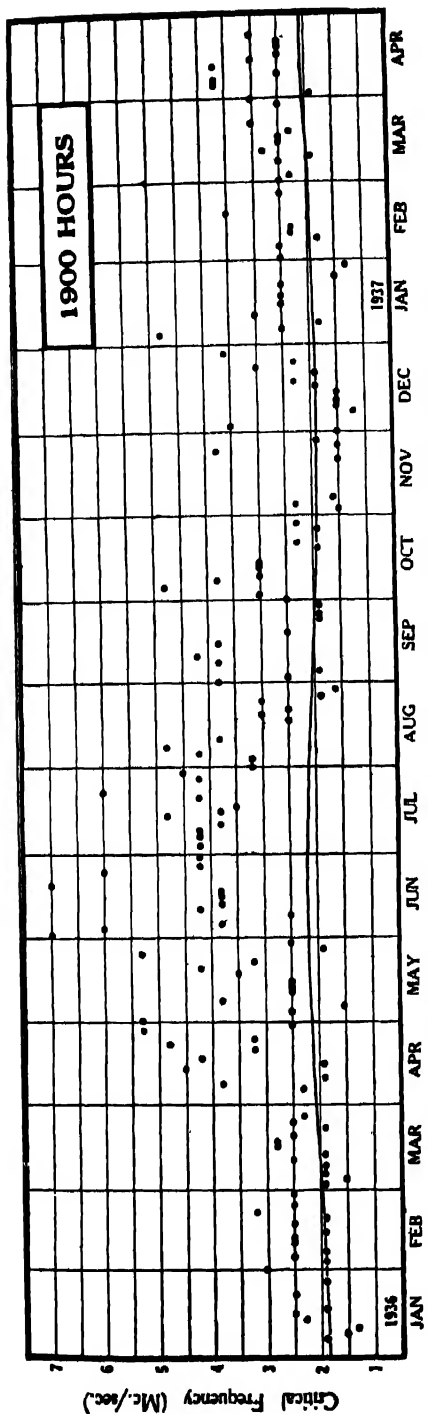


Fig. 8.—Seasonal variation of Region E<sub>1</sub> critical frequency — Theoretical curve.

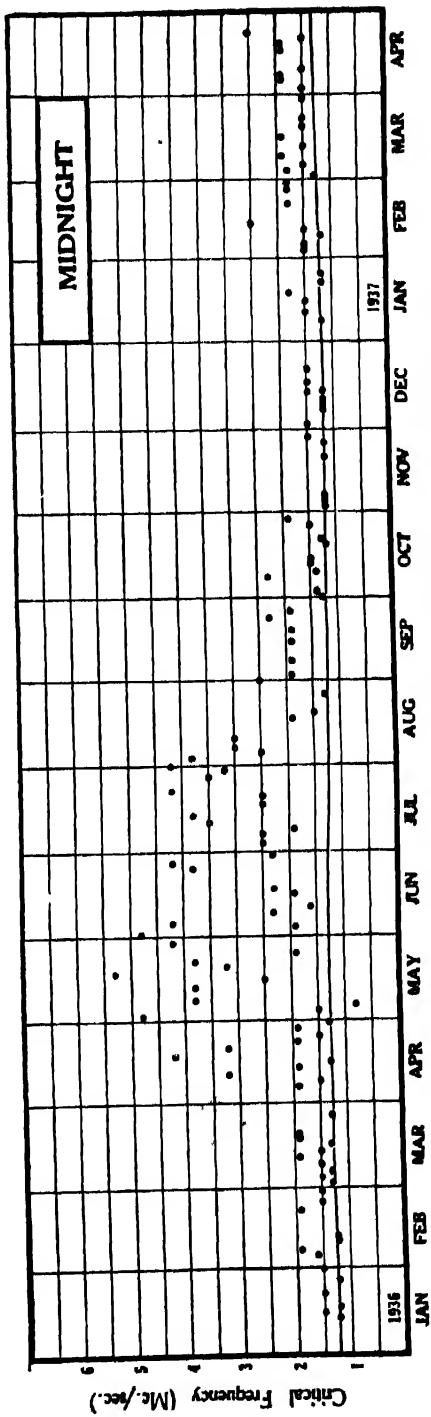


Fig. 9.—Seasonal variation of Region E<sub>1</sub> critical frequency—Theoretical curve.

month to month. The observed critical frequencies also show the same feature excepting, of course, that in the summer months they very often attain abnormally high values.

## (c) Coefficient of Recombination

We have seen in section (3a), that the parameter  $\sigma_0$  depends directly on the coefficient of recombination  $a$ . In order to find out the value of  $\sigma_0$  which would give the best fit of the calculated  $v-\phi$  curves with the observed ones, a number of such curves were drawn for the equinox with values of  $\sigma_0$  equal to  $0.05$ ,  $0.1$ ,  $0.25$ ,  $0.5$  and  $1$ . It was found that the curves with  $\sigma_0$  equal to  $0.25$  gave on the whole the best agreement. This particular value was therefore adopted in drawing all the curves reproduced in section 3. It is interesting to evaluate  $a$  from this value of  $\sigma_0$ . We know that

$$\sigma_0 = 1.37 \times 10^4 a N_0$$

Taking  $N_0 = 10^6$ , the maximum value of  $N$  above the equator at noon at the equinoxes, we obtain

$$a = 2.92 \times 10^{-10} \text{ cm.}^3 \text{ per sec.}$$

If  $N_0$  is taken to be equal to  $10^5$ , we get  $a$  equal to  $2.92 \times 10^{-9}$  cm. per sec. We may note that although this latter value is smaller than that obtained by others<sup>3,4</sup> during the day time, it is in good agreement with the value of  $a$  found under night-time conditions.

We will in passing make a rough estimate of the value of  $a$  from an entirely different set of observations. We had made<sup>5</sup> hourly measurements of Region E<sub>1</sub> critical frequency throughout several nights in connexion with our observations on the effect of meteoric showers on the ionosphere. An examination of these records showed that on the night of November 16–17, 1936 the rate of decay of ionization was particularly steady indicating that, in all probability, there had been no disturbing agency on this night affecting the ionization in an abnormal manner. We, therefore, utilised the records of observations of this particular night just by way of making a rough estimate of the value of the recombination coefficient. At night, when the sun's rays are withdrawn, we have

$$\frac{dN}{dt} = -aN^2$$

assuming that recombination is the only process of electron dissipation.

Hence  $\frac{d}{dt} (1/N) = -a$

If, therefore, we plot  $1/N$  against time, the slope of the curve will give  $a$ . Calculations made in this way showed that on the night in question  $a$  was equal to  $1.1 \times 10^{-9}$  cm.<sup>3</sup> per sec. It should be stressed, however, that it is not reasonable to attach any great importance to this value, for in order to claim accuracy in the measurement of  $a$  in this way the critical frequencies

should be determined more precisely than was possible with our method and also at more frequent intervals.

(d) *Abnormal Region E<sub>1</sub> Ionization*

As seen above, the ionization of Region E<sub>1</sub> attained abnormally high values, specially in the summer months both during the daytime as well as at night. Such abnormal conditions were first reported by Appleton<sup>6</sup> in 1930 and later on by many other workers<sup>7, 8, 9, 10</sup> who designated them in various ways, for example, "abnormal E," "sporadic E," "intense E" and so on. It is worth while to enquire, in view of the frequent occurrence of these phenomena, how far our observations in this connexion are related to similar phenomena observed by others. This is somewhat difficult because of the great variety of behaviour of these abnormal conditions observed by the different workers. The observational records in this connexion of Appleton and his co-workers<sup>11, 12</sup> are, however, best suited as a standard for comparison partly because their method of observation involved continuous variation of frequency and partly because they have given the most complete account of the behaviour of this phenomenon. We shall, therefore, compare our observations with the observations of these workers only.

A simplified reproduction of the type of ( $P'$ ,  $f$ ) records obtained by them at Slough is represented in figure 10. It may be seen that there is a sharp discontinuity at  $c$  in the lower part of the ( $P'$ ,  $f$ ) curve long before reflexions from the same equivalent height ceased altogether. The portion  $abc$  on the lower frequency side is believed by the above-mentioned workers to depict the normal trend of the equivalent height-frequency curve corresponding to the normal Region E<sub>1</sub>, so that the true critical frequency of this region is represented by  $c$ . The portion to the right of  $c$ , in which partial reflexion is evident,

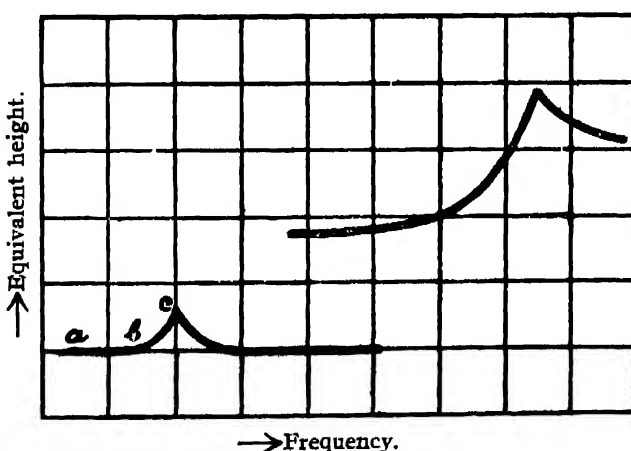


Fig. 10—Simplified equivalent height-frequency curve obtained at Slough at 07'30 G. M. T. on June 24, 1934.

represents "abnormal Region E<sub>1</sub> reflexion." Appleton and his co-workers believe that this portion has no connexion with the true critical frequency of the normal Region E<sub>1</sub> and hence cannot be taken as indicating the presence of abnormally high ionization.

We have not encountered the phenomena represented in the region *ab* of the ( $P'$ ,  $f$ ) curve of figure 10. The type of equivalent height-frequency curve as obtained under abnormal Region E<sub>1</sub> conditions is depicted in figure 11. It will be seen in the figure that reflexion from the level of Region E<sub>1</sub> occurred up to a frequency as high as 6.9 Mc./sec. and that the corresponding ( $P'$ ,  $f$ ) curve was apparently continuous up to this frequency after which complete penetration took place. This may possibly be due to the fact that the ( $P'$ ,  $f$ ) curves, in our case, were obtained, as mentioned before, by observing the equivalent paths on a number of fixed frequencies spaced at definite intervals so that any sharp discontinuity like that at *c* in figure 10 might have been missed in one of the frequency steps in which the whole range was covered. Whether the absence of the discontinuity is real or is due to the incompleteness of our observations

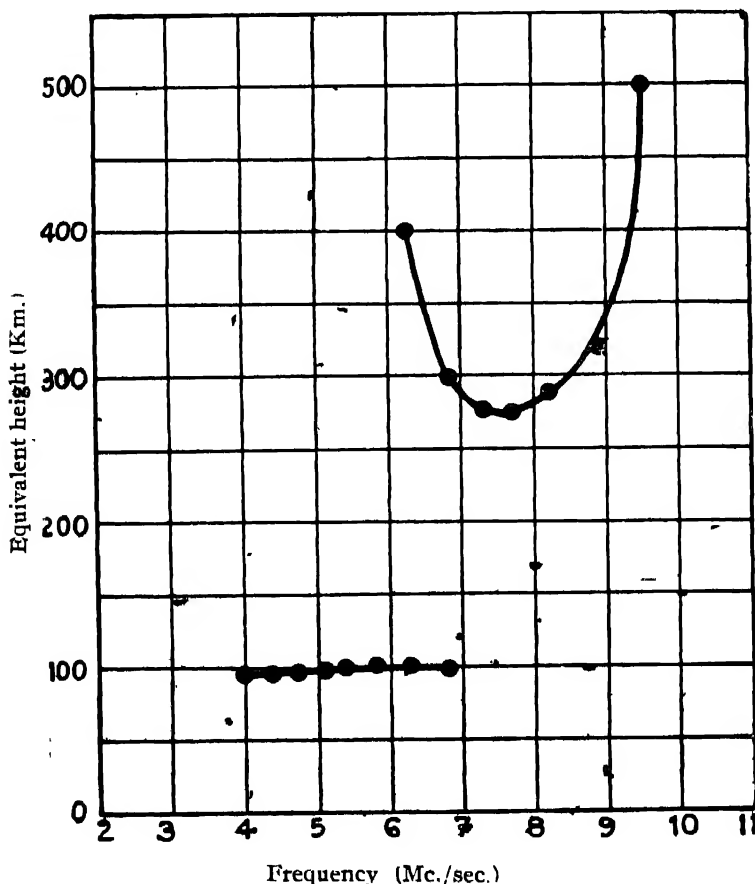


Fig. 11—Equivalent height-frequency curve obtained at Calcutta at 1600 hours local time on July 15, 1936.

is a question which can be decided only if measurements at our place are also made by continuous frequency variation method. Until this is done, there is no other alternative for us than to believe that all such records indicate abnormally high ionization of the normal Region E<sub>1</sub>.

(e) *Correlation between Abnormal Region E<sub>1</sub> Ionization and Thunderstorms*

Attempts have been made from time to time to correlate the occurrence of such abnormal increases of Region E<sub>1</sub> ionization with the incidence of thunderstorms. The results of the attempts made by different workers <sup>3, 8, 13, 14</sup> do not seem, however, to agree with one another. The present author in collaboration with Syam<sup>15</sup> carried out a series of observations in 1935 and found that the occurrence of thunderstorms and abnormal increases in Region E<sub>1</sub> ionization are markedly associated with each other. The actual value of the correlation coefficient between these two phenomena found by them was C<sub>1</sub>=0.5. The regular observations made during 1936-37 offered us an opportunity of examining anew this problem. It is for this reason that additional observations at 1730 hours and 2030 hours were made in the months of April-July. The results of these observations were studied statistically in the same manner as described in the paper <sup>15</sup> above referred to. For convenience of comparison, the results of the two sets of association tests between thunderstorms and abnormal increases in Region E<sub>1</sub> ionization carried out in 1935 and in 1936 are given below in tabular form (Table 2).

TABLE 2

Test of Association between Thunderstorm and Abnormal Ionization.	Magnetically Quiet Days.			Magnetically Disturbed Days.	
	Year	$\chi^2$	C <sub>1</sub>	$\chi^2$	C <sub>1</sub>
1935	41.55	0.504	19.75	0.474	
1936	17.78	0.31	4	0.19	

The table shows at once that while in 1935 the observed association between thunderstorms and abnormal ionization was marked on both magnetically quiet and disturbed days, that in 1936 was appreciable only on magnetically quiet days.

(f) *Ionization of Region E<sub>2</sub>*

In course of the investigation, echoes from a virtual height of about 150 kms. were occasionally observed. The region from which these echoes are

which is termed Region  $E_2$ . Since our observations were particularly directed towards the study of the main Regions  $E_1$  and  $F_2$ , only few measurements on

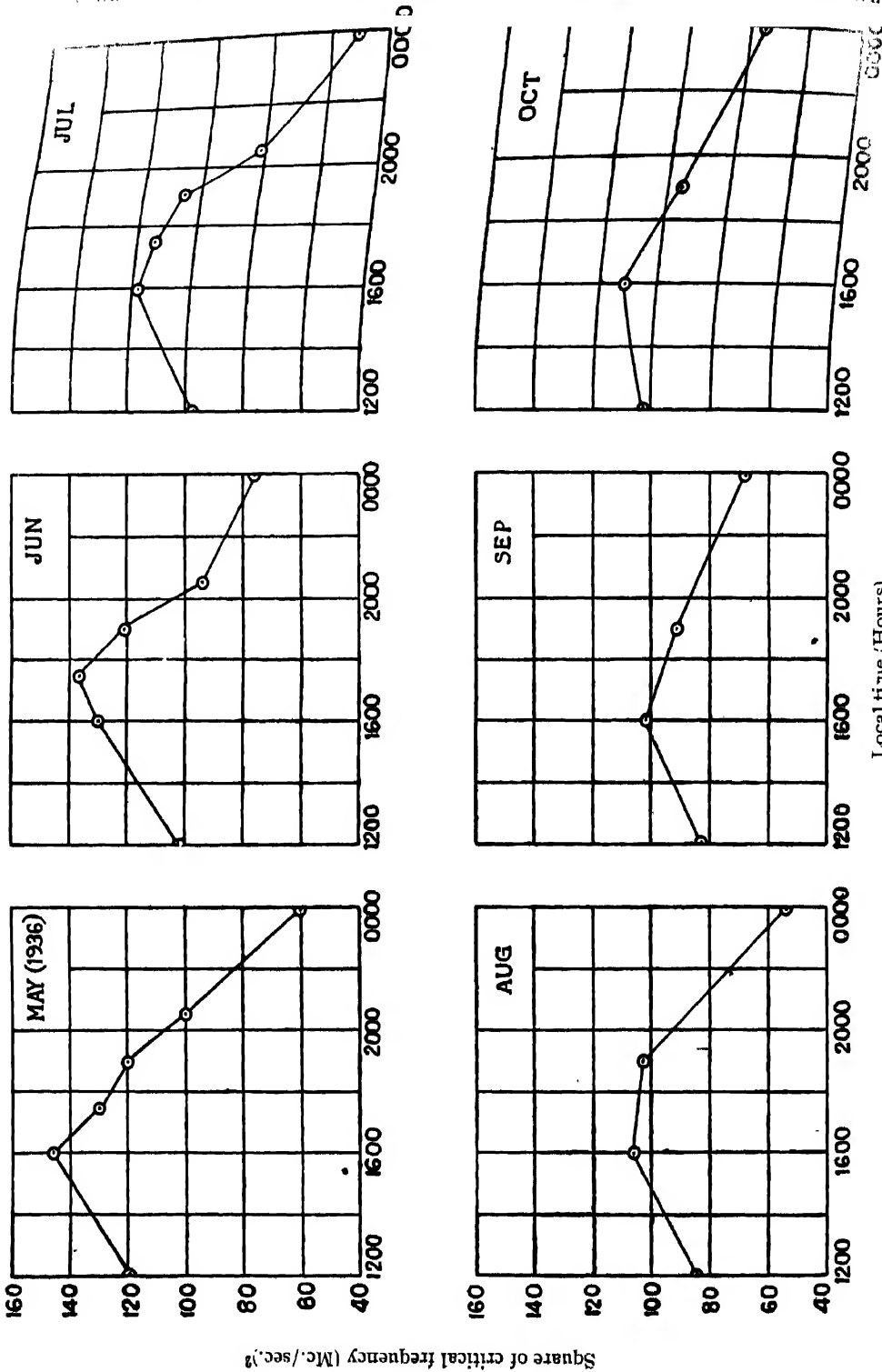


FIG. 12.—Depicting the average variation of ionization of Region  $F_2$  from midday to midnight in different months.  
Local time (Hours).

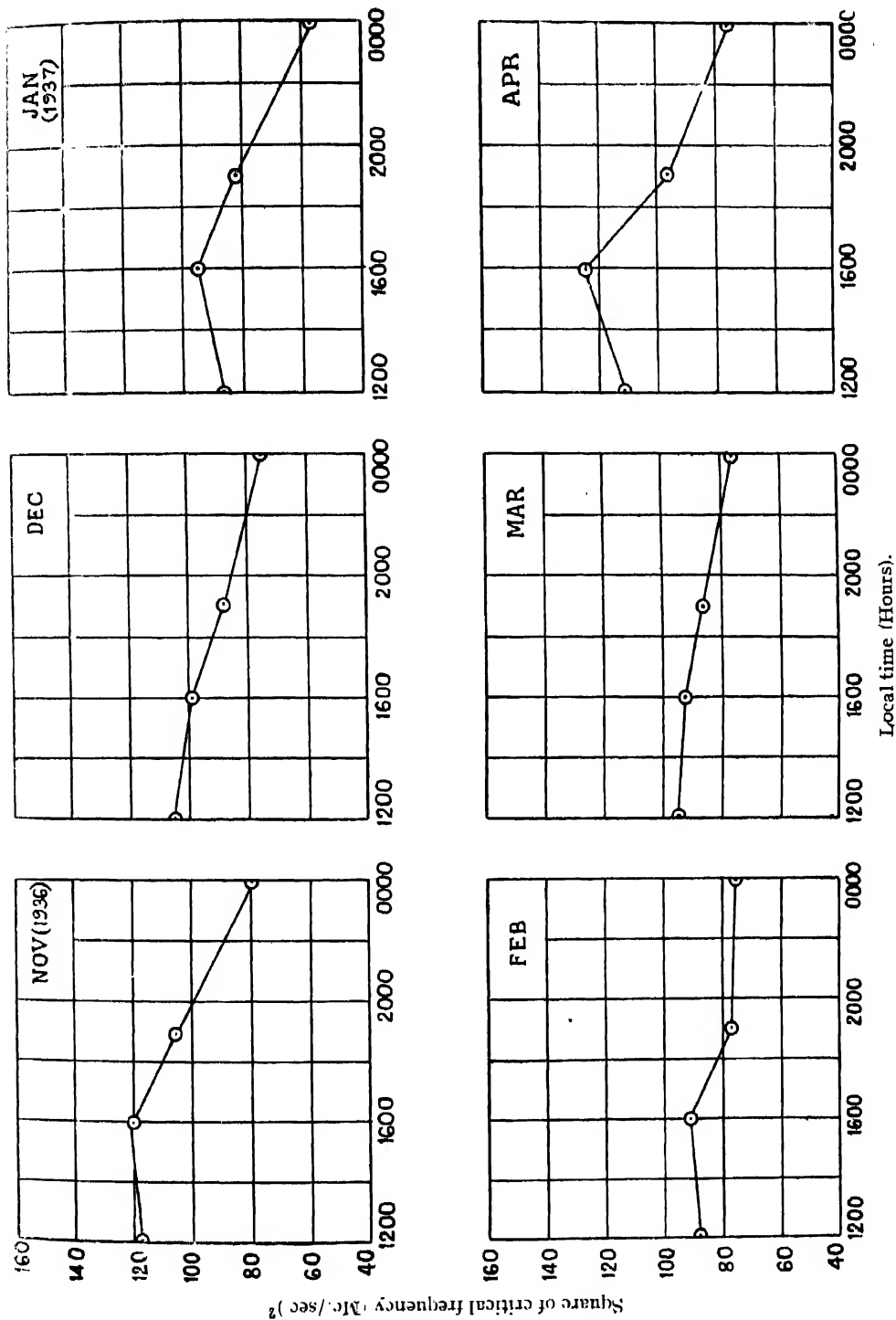


Fig. 13—Depicting the variation of ionization of Region F<sub>2</sub> from midday to midnight in different months.

this subsidiary region were made in course of our regular observations. So far as can be gathered from these measurements, we may summarise briefly the following results :

(i) The electron density of Region  $E_2$  was usually about 20-40 per cent. higher than that of Region  $E_1$ . The percentage difference was relatively greater when the ionization of Region  $E_1$  was greater than when it was less.

(ii) The variation of the equivalent height with frequency could not be ascertained with accuracy since the frequency band on which the echoes could be obtained was always very narrow. The virtual heights usually observed ranged between 150-170 kms. approximately.

(iii) Reflexion from the level corresponding to this region were detected usually during the daytime. Occasionally, however, echoes could be obtained also in the night though these latter were somewhat irregular in occurrence.

### 5 STUDIES OF REGION F IONIZATION

Measurements of the ordinary ray critical frequency for Region  $F_2$  were made simultaneously with Region  $E_1$ . The results obtained are presented in this section.

#### (a) Diurnal Variation

The average variation of the critical frequency from midday to midnight is plotted for each month from May, 1936 to April, 1937, in figs. 12 and 13. It will be evident from these figures that the maximum ionization was observed distinctly after noon in most of the months. In fact, in the summer months, the records show that the maximum was deferred till a little before sunset. As winter approached this afternoon maximum became less and less pronounced until in mid-winter (December) the maximum appeared to occur near noon. It seems as if the time of diurnal\* maximum tends to shift towards noon as the sun recedes away from the zenith in its annual course.

These results are evidently not in accord with the observed as well as the theoretical variation of ionization for Region  $E_1$ . It should be remembered, however, that Region  $E_1$  and  $F_2$  differ from one another both in location as well as in physical conditions. It is, therefore, interesting to see if these differences modify the theoretical  $v - \phi$  curves in such a way as to correspond to the observed variation of Region  $F_2$  ionization. We have already mentioned that a number of such curves appropriate for Region  $F_2$  at a height of about 300 kms. are available in Millington's paper.<sup>2</sup> An examination of figs. 4 to 6 of this paper will show that for the latitude of  $20^\circ$ ,  $v$  attains its maximum value more than two hours after noon both in summer as well as at the equinoxes while in winter the maximum shifts appreciably towards noon. These curves are for  $\sigma_0$  equal to 1. It may be seen by actual calculations that as  $\sigma_0$  is increased beyond unity, the time

\* Strictly speaking, the maximum of the period between midday and midnight.

of maximum is more and more deferred towards sunset. For  $\sigma_0$  equal to 2 and for latitude  $20^\circ$  the maximum value of  $v$  actually occurs near about sunset at the equinoxes. It ought to be noted in this connexion that taking  $N_0$  equal to  $10^6$  electrons per c.c., the value of  $\sigma_0 = 2$  requires that  $a$  should be equal to  $3.6 \times 10^{-11}$  cm.<sup>3</sup> per electron per sec. This value of  $a$  is not at all unreasonable as may be judged from other considerations which we need not discuss here.

We thus see that the occurrence of the diurnal maximum in late afternoon can be explained on the basis of Chapman's theory. But there are certain features of the variation of Region F<sub>2</sub> ionization which this simple theory is inadequate to

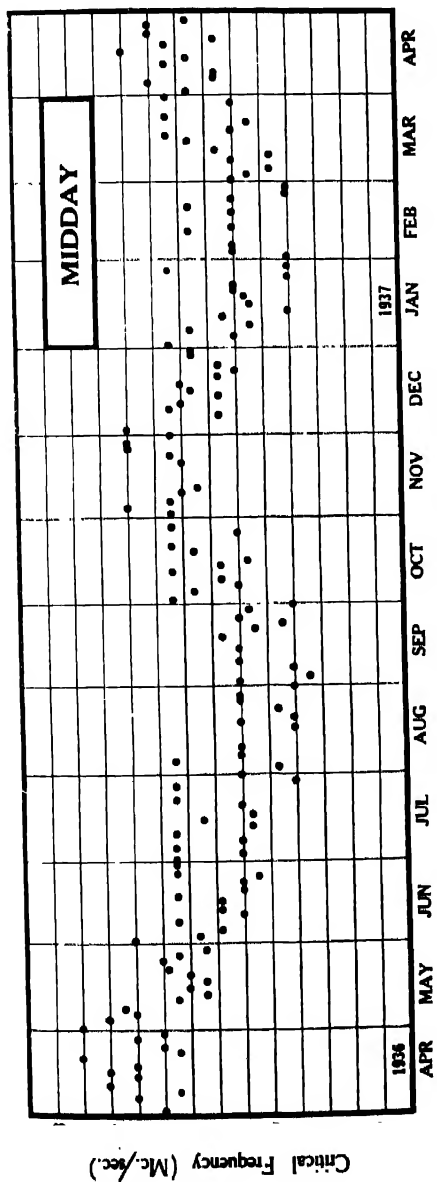


Fig. 14—Seasonal variation of Region F<sub>2</sub> critical frequency.

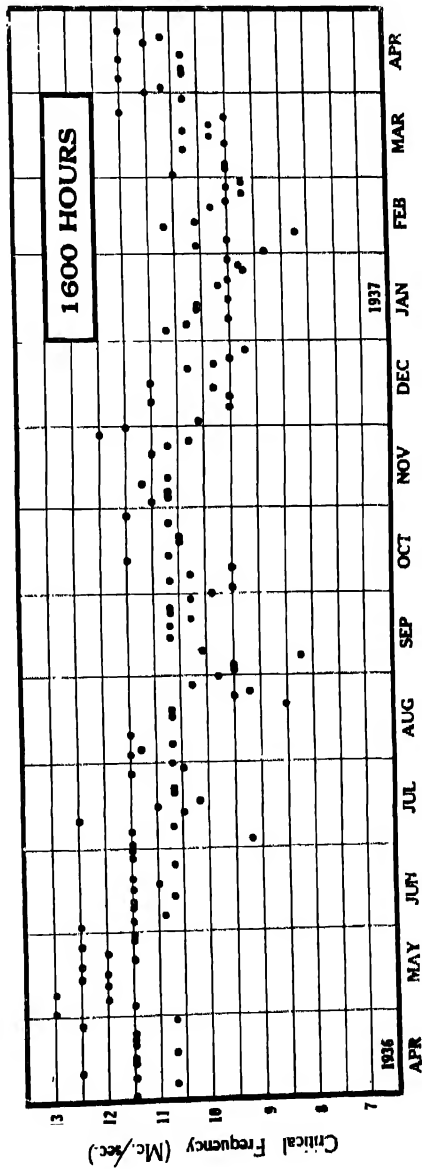
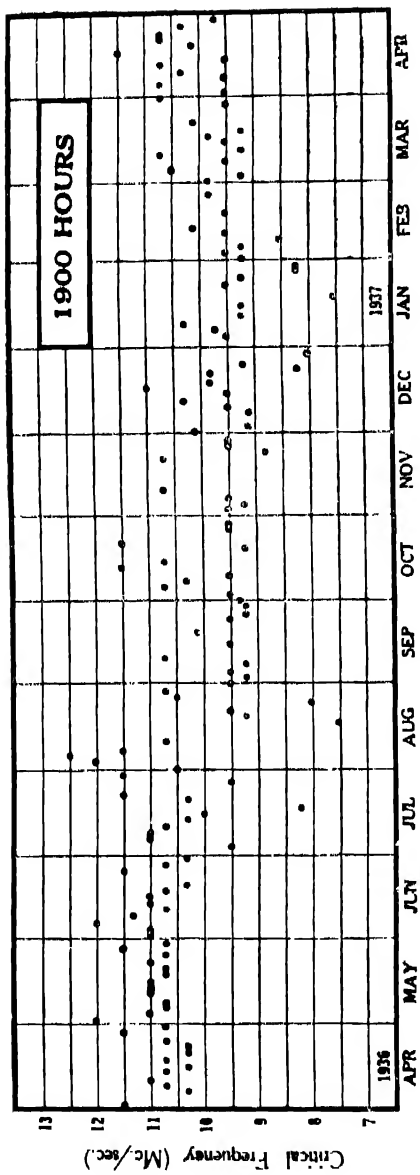
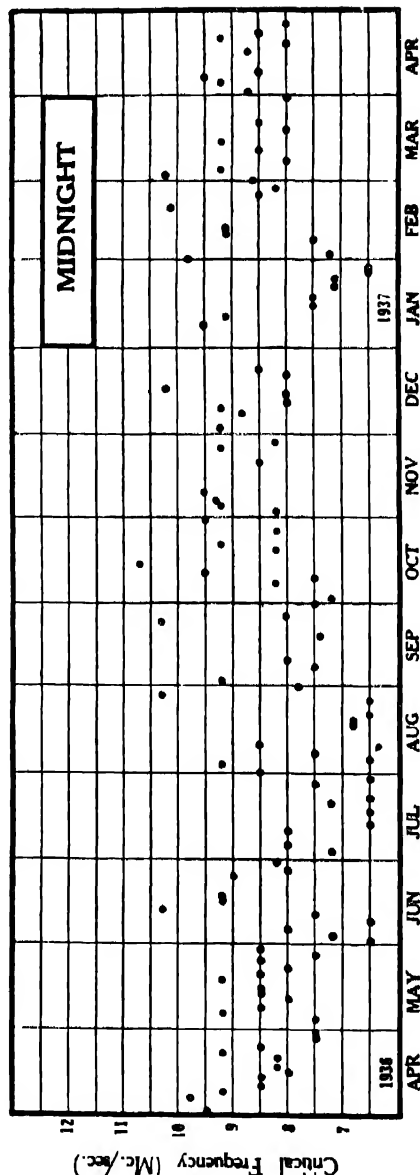


Fig. 15—Seasonal variation of Region F<sub>2</sub> critical frequency.

Fig. 16—Seasonal variation of Region  $F_2$  critical frequency.Fig. 17—Seasonal variation of Region  $F_2$  critical frequency.

account for. We may, for example, cite the two maxima observed by various investigators in the diurnal and seasonal variation curves.

#### (b) Seasonal Variation

Figs. 14—17 represent the seasonal variation of Region  $F_2$  critical frequency for the ordinary ray for four different hours of the day and night. It will be seen that the plots are altogether different from those for Region  $E_1$  depicted in figs 6—9. The critical frequency values show much greater day-to-day variation. Further, the general nature of the seasonal variation is quite different from what

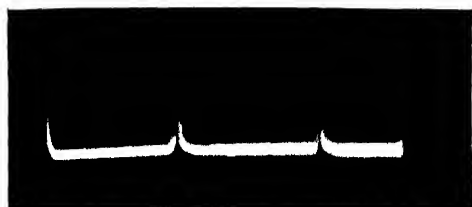


Fig. 18 -Anomalous reflexion coefficient of region  $F_2$



Fig. 19—Magneto-ionic double-splitting.

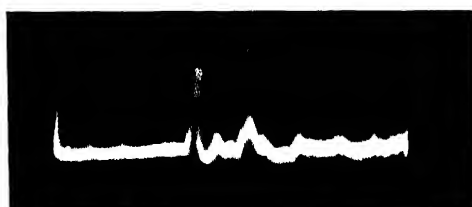


Fig. 20 -Complex echoes.

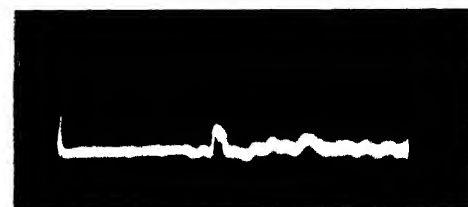


Fig. 21--Complex echo appearing as evidence of triple-splitting.



we would expect from Chapman's simple theory. Instead of the expected maximum in summer, there are two distinct maxima in the whole year, one in April and the other in November for the midday (Fig. 14) and the 1600 hours (Fig. 15) critical frequencies. But for 1900 (Fig. 16) hours the two maxima are apparently replaced by a single maximum in early summer. As regards the midnight values (Fig. 17) the day-to-day variation is seen to be most marked making it very difficult to form any idea as to the nature of any seasonal variation.

### (c) *Reflexion Coefficient, Magnetic Splitting and Complex Echoes*

The intensity of the echoes reflected from Region  $F_2$  increased enormously from day to night. The abundance of multiple reflexions from this region during and after sunset, the occurrence of anomalous values of the reflexion coefficient (values greater than 1) at the approach of darkness are all features in common with Region  $E_1$ . In figure 18 (Plate XV) are reproduced photographs of echo patterns depicting this phenomenon.

Magneto-ionic splitting of the F-echoes was very frequently observed specially during the night time. The amplitudes of these components were comparable to one another, except when one of them was about to disappear. Figure 19 represents photographs depicting this phenomenon.

Some times complex echoes of the type discussed by Appleton and Builder<sup>16</sup> and others were observed at night. It was very difficult to ascertain the respective heights of reflexion of the several components constituting the complex group on account of the fact that their intensity fluctuated very rapidly. Second order reflexions of such complex groups were also frequently obtained. These complex reflexions sometimes persisted over considerable frequency ranges. For example, on February 12, 1937, at midnight, a complex group associated with its second order reflexion was observed over a frequency band extending from 2.68 to 9.0 Mc./sec. although the amplitudes of the reflexions gradually decreased and some of the components actually disappeared as the frequency was gradually increased. In figure 20, photographs of such complex echoes are reproduced.

Occasionally, complex echoes having a structure comparatively simpler than those discussed above were also noticed. One such record, for instance, obtained on October 14, 1936, at 1900 hours on a frequency of 6.3 Mc./sec. showed that the group consisted of four components, all of which were relatively steady in intensity. Measurement of the equivalent heights corresponding to these four components revealed that these were 335, 360, 398 and 450 kms. respectively. Sometimes three distinct components were visible on the screen which may be easily taken as evidence of triple splitting claimed to have been first observed by Toshniwal.<sup>17</sup> Figure 21 represents a record of this type obtained on April 9, 1937, at 1900 hours on a frequency of 3.75 Mc./sec. We cannot, however, say definitely whether this was due to magneto-ionic triple splitting or due to partial reflexions from three distinct ionized strata as we had no means for testing the polarization of the individual components.

(d) *Ionization of Region F<sub>1</sub>*

Reflexions from equivalent heights ranging from 190-220 kms. were frequently observed in course of our investigations. These echoes are believed to have been returned from Region F<sub>1</sub>, which is sometimes called the "lower shelf of Region F." Although observations on this region were not included in our regular programme, we made occasional measurements of the critical frequency of this region. These records show that the ionization of this region was considerably greater than those of Regions E<sub>1</sub> and E<sub>2</sub>. In contrast with the pronounced seasonal variation of ionization of the main Regions E<sub>1</sub> and F<sub>2</sub>, the average midday ionization of Region F<sub>1</sub> did not show, on the whole, any marked variation throughout the year. We, however, make this inference with some hesitation bearing in mind the insufficiency of data in our hand. The critical frequencies at midday varied from 6 to 8 Mc./sec. approximately throughout the year. Reflexions from this region were observed both during the daytime as well as at night.

## ACKNOWLEDGEMENTS

The investigations described in this communication were undertaken at the suggestion of Prof. S. K. Mitra and formed part of the thesis submitted by the author for the degree of Doctor of Science of the University of Calcutta. I take this opportunity of recording my sincere thanks to Prof. Mitra for his advice and guidance in conducting the investigations.

I also wish to acknowledge my indebtedness to Dr. H. Rakshit for his valuable assistance and for many helpful discussions.

WIRELESS LABORATORY,  
UNIVERSITY COLLEGE OF SCIENCE,  
92, UPPER CIRCULAR ROAD,  
CALCUTTA

## REFERENCES

- 1 Chapman, *Proc. Phys. Soc.*, **43**, 26 and 483 (1931).
- 2 Millington, *Proc. Phys. Soc.*, **44**, 580 (1932).
- 3 Best, Farmer and Ratcliffe, *Proc. Roy. Soc. A.*, **164**, 96 (1938).
- 4 Appleton, *Proc. Roy. Soc. A.*, **162**, 451 (1937).
- 5 Bhar, *Ind. Jour. Phys.*, **11**, 109 (1937).
- 6 Appleton, *Proc. Roy. Soc. A.*, **126**, 567 (1930).
- 7 Schaefer and Goodall, *Proc. I. R. E.*, **20**, 1131 (1932).
- 8 Ratcliffe and White, *Proc. Phys. Soc.*, **48**, 399 (1933) and **48**, 107 (1934).
- 9 Kirby and Judson, *Proc. I. R. E.*, **23**, 733 (1935).
- 10 Kirby, Berkner and Stuast, *Proc. I. R. E.*, **22**, 481 (1934).
- 11 Appleton and Naismith, *Proc. Roy. Soc. A.*, **118**, 685 (1935).
- 12 Appleton, Naismith and Ingram, *Phil. Trans.*, **236**, 119 (1937).
- 13 Appleton and Naismith, *Proc. Phys. Soc.*, **48**, 389 (1933).
- 14 Berkner and Wells, *Terr. Mag.*, **42**, 73 (1937).
- 15 Bhar and Syam, *Phil. Mag.*, **28**, 513 (1937).
- 16 Appleton and Builder, *Proc. Phys. Soc.*, **46**, 208 (1933).
- 17 Toshniwal, *Nature*, **138**, 471 (1935).

# DYNAMICS OF THE PIANOFORTE STRING AND THE HAMMER, PART III. (GENERAL THEORY)

BY MOHINIMOHAN GHOSH

Burdwan Raj College (Bengal)

(Received for publication, July 3, 1939)

**ABSTRACT.** The dynamics of the pianoforte string and the elastic hammer has been worked out, following the operational method, that was developed in parts I and II. Here the method has been extended, to cover the most general case, when the elastic hammer strikes at any point of a string of finite length. This is the exact problem relating to the acoustics of the pianoforte string, and no fruitful attempt was made previously, to solve it. The general expressions for the displacement of any point on the string, and the pressure exerted by the hammer during impact, are given. The time-displacement shadow-graph of a point, on the shorter segment of the string was taken by some of the previous workers. It is found that there are smaller kinks, superposed on the hump produced by the impact of the hammer on the string. It is a clear evidence of the excitation of vibration in the shorter segment of the string during impact. But the theories given by the previous workers, fail to explain the same. Using the data supplied by Banerjee and Ganguli (*Phil. Mag.*, 7, 347, 1929), in the theoretical expression of the displacement obtained in this paper, time-displacement curves are drawn. These curves are found to be identical in form and in the number of kinks present with the shadow-graph obtained by the experiments cited above. This shows a remarkable quantitative agreement of the theory with the experiment. Further the values of the duration of contact worked out for some particular cases are found to be in very good agreement with those obtained experimentally.

## INTRODUCTION

In parts I and II, the dynamics of the pianoforte string struck by hard<sup>1</sup> or elastic<sup>2</sup> hammer was built up. However only the cases in which the hammer strikes near the end of a semi-infinite string, and the mid-point of a finite string, were considered. In the present paper, the dynamics will be extended to the most general case, when the hammer strikes at any point of a string of finite length. It should be of course noted, that, this is the actual case of the pianoforte. Previously P. Dass and R. N. Ghose studied the problem of the pianoforte string and the hammer theoretically, but none of them was able to solve the exact problem. Das<sup>3</sup> considered, that, the effect produced by the hammer when it struck a finite string, at a point, dividing it into two unequal segments, was equal to the sum of two partial effects, produced by the hammer on two semi-infinite strings by striking at finite distances, which were equal to the two segments

respectively. But this idea of Das as was shown by the author<sup>4</sup> previously, leads to results, different from that of Kaufmann, in the case when the struck point divides the string into two equal segments. The difference appears after the time, equal to the period of free vibration of the string, measured from the beginning of the impact. The difference evidently, arises, because, the above idea of Das does not incorporate the effect, *equivalent* to the coupling of the two segments. In other words he has completely ignored the effect of successive reflections of the waves from one end, which had already suffered reflection from the opposite end. R. N. Ghosh has recently made an attempt to study the vibration of the loaded string excited by impulse, where he also ignores the coupling effect of the two segments.

The powerful and elegant operational method adopted here gives the complete solution of the exact problem.

#### EXPLANATION OF THE SYMBOLS USED

$l$ =Length of the string= $a+b$ .

$a$ =Shorter segment of the string.

$b$ =Longer segment of the string.

$t$ =Variable time.

$x$ =Variable, measured along the length of the string, the string is fixed at  $x=0$  and  $x=l$ .

$x_1=x-a$ .

$y$ =Displacement at any point at the string at a given time  $t$ .

$y_a$ =Displacement of the struck point,  $x=a$ .

$y_1$ =Displacement at any point  $x < a$ .

$y_2$ =Displacement at any point  $x > a$ .

$\rho$ =Linear density of the string.

$M_1$ =Mass of the shorter segment of the string= $\rho a$ .

$M_2$ =Mass of the longer segment of the string= $\rho b$ .

$M$ =Mass of the string= $\rho l=M_1+M_2$ .

$m$ =Mass of the hammer.

$c$ =Velocity of the transverse wave motion along the string.

$T$ =Tension along the string= $c^2 \rho$ .

$\Theta$ =Period of the free vibration of the string= $2l/c$ .

$$\theta_1 = \frac{2a}{c} = \Theta \frac{a}{l}$$

$$\theta_2 = \frac{2b}{c} = \Theta \frac{b}{l}$$

$$t_n = t - n\Theta_1$$

$$v_o = \text{Velocity of impact.}$$

$$J = mv_0.$$

$u$  = The compression of the hammer.

$z = y_a + u$  = Displacement of the hammer.

$E$  = Elastic constant for the material of the hammer.

$P$  = Pressure exerted by the hammer.

$$D = \text{Operator } \frac{d}{dt}.$$

The equation of motion of the string is,

$$\frac{d^2y}{dt^2} = c^2 \frac{d^2y}{dx^2}, \quad \dots \quad (1)$$

which is equivalent to,

$$\frac{d^2y}{dx^2} = \frac{D^2}{c^2} y, \quad \dots \quad (1.1)$$

The elastic hammer strikes at  $x=a$ , and if  $y_a$  is the displacement of the struck point, we get,

$$y_1 = y_a \cdot \frac{\sinh \frac{Dx}{c}}{\sinh \frac{Da}{c}}, \quad \dots \quad (1.2)$$

$$y_2 = y_a \cdot \frac{\sinh \frac{D(l-x)}{c}}{\sinh \frac{Db}{c}}, \quad \dots \quad (1.3)$$

The effect of the elastic hammer on the string during impact is same as that of a hard load backed by a weightless spring, the pressure  $P$  exerted by the load is given by,

$$P = m \cdot \frac{d^2z}{dt^2} = - E u \quad (\text{By Hooke's law}) \quad \dots \quad (19)$$

and subsequent motion of the load is given by the equation. (cf. eq. 2)

$$m \cdot \frac{d^2z}{dt^2} = T \cdot \Delta \left( \frac{dy}{dx} \right)_{x=a}, \quad \dots \quad (19.1)$$

$$\text{where, } z = y_a + u \quad \dots \quad (19.2)$$

Now with the help of eqs. (19.2), (1.2) and (1.3), eqs. (19) and (19.1) can be written in the form,

$$\left[ mD^2 + D \frac{T}{C} \left( \coth \frac{Da}{c} + \coth \frac{Db}{c} \right) \right] y_a + mD^2 u = JD, \quad \dots \quad (20)$$

$$mD^2 y_a + (mD^2 + E) u = JD. \quad \dots \quad (20.1)$$

On solving the simultaneous eqs. (20) and (20·1) for  $y_a$ . and  $u$  we get,

$$y_a = -\frac{1}{F(D)} \cdot v_o, \quad \dots \quad (21)$$

$$\begin{aligned} u &= \left( \coth \frac{Da}{c} + \coth \frac{Db}{c} \right) \cdot \frac{D}{F(D)} \cdot \frac{v_o T}{Ec}, \\ &= \frac{T}{Ec} \left( \coth \frac{Da}{c} + \coth \frac{Db}{c} \right) D y_a. \text{ From eq. (21)} \quad \dots \quad (21\cdot1) \\ &= \frac{T}{Ec} \left( \coth \frac{Da}{c} + \coth \frac{Db}{c} \right) y'_a, \quad \dots \quad (21\cdot2) \end{aligned}$$

$$\begin{aligned} \text{where } F(D) &= D + \left( \frac{T}{Ec} \cdot D^2 + \frac{T}{mc} \right) \left( \coth \frac{Da}{c} + \coth \frac{Db}{c} \right), \\ &= D + \left( \frac{T}{Ec} \cdot D^2 + \frac{T}{mc} \right) \left[ \frac{1 + e^{-D\theta_1}}{1 - e^{-D\theta_1}} + \frac{1 + e^{-D\theta_2}}{1 - e^{-D\theta_2}} \right]. \quad \dots \quad (21\cdot3) \end{aligned}$$

So

$$\begin{aligned} y_a &= \frac{(q+p)}{D_1 D_2} (1 - e^{-D\theta_1} - e^{-D\theta_2} + e^{-D\Theta}) \left[ 1 - \frac{(q+p)D}{D_1 D_2} e^{-D\theta_1} \right. \\ &\quad \left. - \frac{(q+p)D}{D_1 D_2} e^{-D\theta_2} - \left\{ 1 - 2 \frac{(q+p)D}{D_1 D_2} \right\} e^{-D\Theta} \right]^{-1} v_o. \quad \dots \quad (48) \end{aligned}$$

The general term (*i.e.*, the  $r^{th}$  term) of the multinomial expansion of

$$\left[ 1 - \frac{(q+p)D}{D_1 D_2} e^{-D\theta_1} - \frac{(q+p)D}{D_1 D_2} e^{-D\theta_2} - \left\{ 1 - \frac{2(q+p)D}{D_1 D_2} \right\} e^{-D\Theta} \right]^{-1},$$

is

$$\frac{\Gamma(\alpha+\beta+\gamma+1)}{\Gamma(\alpha+1)\Gamma(\beta+1)\Gamma(\gamma+1)} \cdot \left\{ \frac{(q+p)D}{D_1 D_2} \right\}^{\alpha+1} \left\{ \frac{(q+p)D}{D_1 D_2} \right\}^{\beta} \left\{ 1 - \frac{2(q+p)D}{D_1 D_2} \right\}^{\gamma} e^{-D(\alpha\theta_1 + \beta\theta_2 + \gamma\Theta)} \quad \dots \quad (49)$$

where  $r = \alpha + \beta + \gamma$ , and  $D_1 = D + q$ ,  $D_2 = D + p - q$  and  $-p$

being the roots of the eq.  $D^2 + \frac{Ec}{2T} D + \frac{E}{m} = 0$

On multiplying the above by

$$\frac{(q+p)v_o}{D_1 D_2} \left( 1 - e^{-D\theta_1} - e^{-D\theta_2} + e^{-D\Theta} \right)$$

and putting different values for  $\alpha$ ,  $\beta$ ,  $\gamma$  from zero to any positive integer and collecting the useful terms which will occur within the time  $t=0$  and  $t=2\Theta$ , as hammer always leaves the string, long before  $t=2\Theta$ , we get from (48) [*vide* appendix (2), Part II],

$$\begin{aligned}
 y_a = & f_1 + (f_2 - f_1)e^{-D\theta_1} + (f_3 - f_2)e^{-D^2\theta_1} + \dots + (f_{n+1} - f_n)e^{-D.n\theta_1} \\
 & + (f_2 - f_1)e^{-D\theta_2} + (f_3 - f_2)e^{-D^2\theta_2} + \dots + (f_{n+1} - f_n)e^{-D.n\theta_2} \\
 & + (2f_3 + 4f_2 + 2f_1)e^{-D\Theta} \\
 & + (3f_4 - 7f_3 + 5f_2 - f_1)e^{-D(\Theta + \theta_1)} + (4f_5 - 10f_4 + 8f_3 - 2f_2)e^{-D(\Theta + 2\theta_1)} \\
 & + \dots + \{(n+2)f_{n+3} - (3n+4)f_{n+2} + (3n+2)f_{n+1} - nf_n\}e^{-D(\Theta + n\theta_1)} \\
 & + (3f_4 - 7f_3 + 5f_2 - f_1)e^{-D(\Theta + \theta_2)} + (4f_5 - 10f_4 + 8f_3 - 2f_2)e^{-D(\Theta + 2\theta_2)} \\
 & + \dots + \{(n+2)f_{n+3} - (3n+4)f_{n+2} + (3n+2)f_{n+1} - nf_n\}e^{-D(\Theta + n\theta_2)} \\
 & + (6f_5 - 18f_4 + 20f_3 - 10f_2 + 2f_1)e^{-D^2\Theta} \quad \dots \quad (50)
 \end{aligned}$$

where [vide appendix (2) Part II]

$f_n$  stands for  $f_n(t)$

$$= \frac{(q+p)^n}{D_1^n D_2^n} \cdot v_o. \quad \dots \quad (51)$$

With the help of appendix (2) Part II, eq. (50) becomes,

$$\begin{aligned}
 y_a = & f_1(t) + \sum_1^n [f_{n+1}(t - n\theta_1) - f_n(t - n\theta_1)] + \sum_1^n [f_{n+1}(t - n\theta_2) - f_n(t - n\theta_2)] \\
 & + 2f_3(t - \Theta) - 4f_2(t - \Theta) + 2f_1(t - \Theta) \\
 & + \sum_1^n [(n+2).f_{n+3}(t - \Theta - n\theta_1) - (3n+4).f_{n+2}(t - \Theta - n\theta_1) \\
 & \quad + (3n+2).f_{n+1}(t - \Theta - n\theta_1) - nf_n(t - \Theta - n\theta_1)] \\
 & + \sum_1^n [(n+2).f_{n+3}(t - \Theta - n\theta_2) - (3n+4).f_{n+2}(t - \Theta - n\theta_2) \\
 & \quad + (3n+2).f_{n+1}(t - \Theta - n\theta_2) - nf_n(t - \Theta - n\theta_2)] \\
 & + 6f_5(t - 2\Theta) - 18f_4(t - 2\Theta) + 20f_3(t - 2\Theta) \\
 & \quad - 10f_2(t - 2\Theta) + 2f_1(t - 2\Theta). \quad \dots \quad (52)
 \end{aligned}$$

Eq. (52) is the general expression for the displacement of the struck point during impact.

#### General expression for the pressure

From eqs. (21-2) and (19) we have,

$$-P = Eu = \frac{T}{C} \left( \coth \frac{Da}{c} + \coth \frac{Db}{c} \right) y'_a, \quad (53)$$

where  $Dy_a = y'_a$ , and from eq. (50),

$$\begin{aligned}
 y'_a &= f'_1 + \Sigma(f'_{n+1} - f'_n)e^{-Dn\theta_1} + \Sigma(f'_{n+1} - f'_n)e^{-Dn\theta_2} \\
 &\quad + (2f'_3 - 4f'_2 + 2f'_1)e^{-D\Theta} \\
 &\quad + \Sigma[(n+2)f'_{n+3} - (3n+4)f'_{n+2} + (3n+2)f'_{n+1} - nf'_n]e^{-D(\Theta+n\theta_1)} \\
 &\quad + \Sigma[(n+2)f'_{n+3} - (3n+4)f'_{n+2} + (3n+2)f'_{n+1} - nf'_n]e^{-D(\Theta+n\theta_2)} \\
 &\quad + [6f'_5 - 18f'_4 + 20f'_3 - 10f'_2 + 2f'_1]e^{-D2\Theta} \quad \dots \quad (54)
 \end{aligned}$$

$$\text{and } \frac{T}{C} \left( \coth \frac{Da}{c} + \coth \frac{Db}{c} \right) = \frac{2T}{c} \left[ 1 + \sum_1^{\infty} e^{-rD\theta_1} + \sum_1^{\infty} e^{-rD\theta_2} \right] \quad \dots \quad (55)$$

Now with the help of eqs. (54) and (55), and after collecting useful terms that will occur during the interval  $t=0$  and  $t=2\Theta$  eq. (53) becomes,

$$\begin{aligned}
 P &= -\frac{2T}{c} [f'_1 + \sum_1^n f'_{n+1}e^{-D\theta_1} + \sum f'_{n+1}e^{-D\theta_2} + 2(f'_3 - f'_2)e^{-D\Theta} \\
 &\quad + \sum_1^n \{(n+2)f'_{n+3} - 2(n+1)f'_{n+2} + nf'_{n+1}\}e^{-D(\Theta+n\theta_1)} \\
 &\quad + \sum_1^n \{(n+2)f'_{n+3} - 2(n+1)f'_{n+2} + nf'_{n+1}\}e^{-D(\Theta+n\theta_2)} \\
 &\quad + (6f'_5 - 12f'_4 + 8f'_3 - 2f'_2)e^{-D2\Theta}].
 \end{aligned}$$

Or with the help of appendix 1-2 Part II,

$$\begin{aligned}
 P &= -\frac{2T}{c} [f'_1(t) + \Sigma f'_{n+1}(t - n\theta_1) + \Sigma f'_{n+1}(t - n\theta_2) + 2f'_3(t - \Theta) - 2f'_2(t - \Theta) \\
 &\quad + \Sigma \{(n+2)f'_{n+3}(t - \Theta - n\theta_1) - 2(n+1)f'_{n+2}(t - \Theta - n\theta_1) \\
 &\quad \quad + nf'_{n+1}(t - \Theta - n\theta_1)\} \\
 &\quad + \Sigma \{(n+2)f'_{n+3}(t - \Theta - n\theta_2) - 2(n+1)f'_{n+2}(t - \Theta - n\theta_2) \\
 &\quad \quad + nf'_{n+1}(t - \Theta - n\theta_2)\} \\
 &\quad + 6f'_5(t - 2\Theta) - 12f'_4(t - 2\Theta) + 8f'_3(t - 2\Theta) - 2f'_2(t - 2\Theta)]. \quad \dots \quad (56)
 \end{aligned}$$

The eq. (56) gives the general expression for the pressure exerted by the hammer. It is evident that any function in the above general expressions will appear only from the time obtained, by equating the corresponding argument to zero. This will be easily understood by considering some special cases.

## (i) The hammer strikes at the mid-point

Here  $a = b$  and  $b = 2a$  which gives  $\theta_1 = \theta_2 = \frac{\Theta}{2}$  and we have from eq. (52),

$$\begin{aligned}
 y_a &= f_1(t) + 2 \sum_1^4 [f_{n+1}(t - n\theta_1) - f_n(t - n\theta_1)] \\
 &\quad + 2f_3(t - \Theta) - 4f_2(t - \Theta) + 2f_1(t - \Theta) \\
 &\quad + 2 \sum_1^2 \{(n+1)f_{n+3}(t - \Theta - n\theta_1) - (3n+4)f_{n+2}(t - \Theta - n\theta_1) \\
 &\quad \quad + (3n+2)f_{n+1}(t - \Theta - n\theta_1) - nf_n(t - \Theta - n\theta_1)\} \\
 &\quad + 6f_5(t - 2\Theta) - 18f_4(t - 2\Theta) + 20f_3(t - 2\Theta) - 10f_2(t - 2\Theta) \\
 &\quad \quad + 2f_1(t - 2\Theta), \quad \dots \quad (57)
 \end{aligned}$$

as the impact terminates during  $2\Theta < t < \frac{5\Theta}{2}$ ; whence we get,

$$0 < t < \theta_1, \quad \dots \quad (57.1)$$

$$y_a = f_1(t) \quad \dots \quad (57.1)$$

$$\theta_1 < t < 2\theta_1, \quad \dots \quad (57.2)$$

$$y_a = y_a, (0 < t < \theta_1) + 2f_2(t_1) - 2f_1(t_1) \quad \dots \quad (57.2)$$

where

$$t_1 = t - \theta_1$$

$$2\theta_1 < t < 3\theta_1,$$

$$y_a = y_a, (\theta_1 < t < 2\theta_1) + 4f_3(t_2) - 6f_2(t_2) + 2f_2(t_2),$$

where

$$t_2 = t - 2\theta_1.$$

$$3\theta_1 < t < 4\theta_1,$$

$$y_a = y_a, (2\theta_1 < t < 3\theta_1) + 8f_4(t_3) - 16f_3(t_3) + 10f_2(t_3) - 2f_1(t_3),$$

where  $t_3 = t - 3\theta_1$ , and so on.

The expression for the pressure exerted by the hammer is obtained from the eq. (56),

$$\begin{aligned}
 -P &= \frac{2T}{c} [f'_1(t) + 2 \sum f'_{n+1}(t - n\theta_1) + 2f'_3(t - \Theta) - 2f'_2(t - \Theta) \\
 &\quad + 2 \sum \{(n+2)f'_{n+3}(t - n\Theta_1 - n\theta_1) - 2(n+1)f'_{n+2}(t - \Theta - n\theta_1) \\
 &\quad \quad + nf'_{n+1}(t - \Theta - n\theta_1)\}] \\
 &\quad + 6f'_5(t - 2\Theta) - 12f'_4(t - 2\Theta) + 8f'_2(t - 2\Theta) - 2f'_1(t - 2\Theta), \quad \dots \quad (58)
 \end{aligned}$$

whence the expression for the pressure at different intervals are easily obtained;

$$P_1 = \frac{2T}{c} f'_1(t) \quad \dots \quad (58 \cdot 1)$$

$$P_2 = P_1 + \frac{4T}{c} f'_2(t_2) \quad \dots \quad (58 \cdot 2)$$

$$P_3 = P_2 + \frac{4T}{c} [2f'_3(t_2) - f'_2(t_2)] \quad \dots \quad (58 \cdot 3)$$

$$P_4 = P_3 + \frac{4T}{c} [4f'_4(t_3) - 4f'_3(t_3) + 2f'_2(t_3)] \quad \dots \quad (58 \cdot 4)$$

and so on.

(ii) The hammer strikes at a distance  $a$  from one end of the string, other segment  $b$  is taken to be very large; so when  $b$  is taken to be infinite compared to  $a$ , eqs. (52) and (56) become identical with the eqs. (29·4) and (32) (*vide Part II*).

(iii) The hammer strikes at a point away from the centre, i.e., when  $a < b < 2a$  we have,

$$y_a = f_1(t), \quad 0 < t < \theta_1;$$

$$y_a = f_1(t), + f_2(t_1) - f_1(t_1), \dots \theta_1 < t < \theta_2;$$

$$y_a = f_1(t), + f_2(t_1) - f_1(t_1), + f_2(t - \theta_2) - f_1(t - \theta_2).$$

$$+ f_3(t_2) - f_2(t_2), \dots 2\theta_1 < t < \Theta;$$

as  $2l < 4b < 6a$

$$y_a = f_1(t), + f_2(t_1) - f_1(t_1), + f_2(t - \theta_2) - f_1(t - \theta_2),$$

$$+ f_3(t_2) - f_2(t_2), + 2f_3(t - \Theta) - 4f_2(t - \Theta)$$

$$+ 2f_1(t - \Theta), \dots \Theta < t < 2\theta_2;$$

$$y_a = y_a (\Theta < t < 2\theta_2) + f_3(t - 2\theta_2) - f_2(t - 2\theta_2), \dots 2\theta_2 < t < 3\theta_1 \quad \dots \quad (59)$$

and so on.

From eq. (56), the corresponding expression for the pressure exerted by the hammer are obtained as follows:

$$P_1 = \frac{2T}{c} f'_1(t), \quad \text{during} \quad 0 < t < \theta_1;$$

$$P_2 = P_1 + \frac{2T}{c} f'_2(t_1) \quad \dots \quad \theta_1 < t < \theta_2;$$

$$\begin{aligned}
 P_3 &= P_2 + \frac{2T}{c} f'_2(t - \theta_2) & \theta_2 < t < 2\theta_1; \\
 P_4 &= P_3 + \frac{2T}{c} f'_3(t_2) & 2\theta_1 < t < \Theta; \\
 P_5 &= P_4 + \frac{4T}{c} [f'_3(t - \Theta) - f'_2(t - \Theta)], & \Theta < t < 2\theta_2; \\
 P_6 &= P_5 + \frac{2T}{c} f'_3(t - 2\theta_2), & 2\theta_2 < t < 3\theta_1; 
 \end{aligned} \tag{60}$$

and so on.

(iv) The hammer strikes at  $\frac{a}{l} = \frac{1}{3}$  which gives  $l = 3a$  and  $b = 2a$ . Substituting these values of  $l$  and  $b$  in eq. (52) and (56)

$$\begin{aligned}
 y_a &= f_1(t), & \text{during } 0 < t < \theta_1; \\
 y_a &= y_a(0 < t < \theta_1) + f_2(t_1) - f_1(t_1), & \dots \quad \theta_1 < t < 2\theta_1; \\
 y_a &= y_a(\theta_1 < t < 2a) + f_3(t_2) - f_2(t_2), & \dots \quad 2\theta_1 < t < 3\theta_1; \\
 y_a &= y_a(2\theta_1 < t < 3\theta_1) + f_4(t_3) + f_3(t_3) - 4f_2(t_3), \\
 &\quad + 2f_1(t_3), \dots \quad 3\theta_1 < t < 4\theta_1
 \end{aligned} \tag{61}$$

and so on.

And the corresponding expressions for the pressures are

$$\begin{aligned}
 P_1 &= \frac{2T}{c} f'_1(t), \\
 P_2 &= P_1 + \frac{2T}{c} f'_2(t_1), \\
 P_3 &= P_2 + \frac{2T}{c} [f'_3(t_2) + f'_2(t_2)] \\
 P_4 &= P_3 + \frac{2T}{c} f'_4(t_3) + \frac{4T}{c} [f'_3(t_3) - f'_2(t_3)] \quad \dots \tag{62}
 \end{aligned}$$

and so on.

In this way, we can find out the expressions giving the exact value of  $y_a$  and  $P$  when the hammer strikes at any point of a finite string. Thus the problem is completely solved. It may be noted here that none of the previous theories known, could solve this problem completely except some special cases.

DISPLACEMENT AT ANY POINT DURING IMPACT  
ON THE FINITE STRING

Now expressing the right hand side of the eq. (1.2) and (1.3) in terms of equivalent exponential, and expanding we have,

$$\begin{aligned} y_1 &= y_a + \sum_{r=1}^n \left[ e^{\frac{D}{c}(x_1 - r - 1 + 2a)} - e^{-\frac{D}{c}(x_1 + r + 2a)} \right], \\ y_2 &= y_a + \sum_{r=1}^n \left[ e^{-\frac{D}{c}(x_1 + r - 1 + 2b)} - e^{\frac{D}{c}(x_1 + r + 2b)} \right]. \end{aligned} \quad \dots \quad (63)$$

Substituting the value of  $y_a$ , the displacement for the struck point, from eqs. (52) in eqs. (63) and collecting the useful terms which will occur during the interval  $t=0$  to  $t=2\Theta$ , we have

$$\begin{aligned} y_1 &= f_1 \left( t + \frac{x_1}{c} \right) + \Sigma f_{n+1} \left( t + \frac{x_1}{c} - n\theta_1 \right) - \Sigma f_n \left( t - \frac{x_1}{c} - n\theta_1 \right) \\ &\quad + \Sigma [f_{n+1} - f_n] \left( t + \frac{x_1}{c} - n\theta_2 \right) \\ &\quad + |f_2 - f_1| \left\{ \left( t + \frac{x_1}{c} - \Theta \right) - \left( t + \frac{x_1}{c} - \Theta \right) \right\} \\ &\quad + |2f_3 - 4f_2 + 2f_1| \left( t + \frac{x_1}{c} - \Theta \right) \\ &\quad + |2f_3 - 3f_2 + f_1| \left\{ \left( t + \frac{x_1}{c} - \Theta - \theta_1 \right) - \left( t - \frac{x_1}{c} - \Theta - \theta_2 \right) \right\} \\ &\quad + \Sigma [(n+2)f_{n+3} - (3n+4)f_{n+2} + (3n+2)f_{n+1} - nf_n] \left\{ \left( t + \frac{x_1}{c} + \Theta - n\theta_1 \right) \right. \\ &\quad \left. + \left( t + \frac{x_1}{c} - \Theta - n\theta_2 \right) \right\} \\ &\quad + \Sigma [(n+2)f_{n+3} - (2n+3)f_{n+2} + (n+1)f_{n+1}] \left\{ \left( t + \frac{x_1}{c} - \Theta - n\overline{+1} \cdot \theta_1 \right) \right. \\ &\quad \left. - \left( t - \frac{x_1}{c} - \Theta - n\overline{+1} \cdot \theta_1 \right) \right\} \\ &\quad + \Sigma [f_{n+2} - f_{n+1}] \left\{ \left( t + \frac{x_1}{c} - \Theta - n\theta_2 \right) - \left( t - \frac{x_1}{c} - \Theta - n\theta_2 \right) \right\} \end{aligned}$$

$$+ [3f_4 - 6f_3 + 4f_2 - f_1] \left\{ \left( t + \frac{x_1}{c} - \theta_2 \right) - \left( t - \frac{x_1}{c} - \theta_2 \right) \right\} \\ + [6f_5 - 18f_4 + 20f_3 - 10f_2 + 2f_1] \left( t + \frac{x_1}{c} - \theta_2 \right), \quad \dots \quad (64)$$

and the value for  $y_2$  is same as that for  $y_1$  but we are to read  $-x_1$  for  $x_1$ ,  $\theta_1$  for  $\theta_2$  and  $\theta_2$  for  $\theta_1$ .

The expressions within the first bracket represents the arguments of the functions within third brackets, as,

$$[f_{n+1} - f_n] \left\{ \left( t - \frac{x_1}{c} - n\theta_2 \right) + \left( t + \frac{x_1}{c} - n\theta_2 \right) \right\} \\ = f_{n+1} \left( t - \frac{x_1}{c} - n\theta_1 \right) - f_n \left( t - \frac{x_1}{c} - n\theta_1 \right) + f_{n+1} \left( t + \frac{x_1}{c} - n\theta_2 \right) \\ - f_n \left( t + \frac{x_1}{c} - n\theta_2 \right). \quad \dots \quad (65)$$

If we put  $x=a$ , i.e.,  $x_1=0$  in the expressions for  $y_1$  and  $y_2$  as in eqs. (64), each of them is reduced to the expressions for  $y_n$  as is given by the eq. (52).

In the above expressions (*vide* eqs. 52, 56 and 64),  $\sum_n$  does not represent an infinite series but is used as an abbreviation in working out a finite number of terms, that will occur during different intervals, so long as the hammer is in contact with the string.

#### SPECIAL CASES

When the hammer strikes at a finite distance  $a$  of the string from one end,  $b$  being the other segment of the string of length  $l$  which is taken to be very large, we put  $b \rightarrow \infty$ ,  $l \rightarrow \infty$  in eq. (64), and in the corresponding eqs. for  $y_1$  and  $y_2$ . We get during the first interval,

$$y_1 = f_1 \left( t + \frac{x_1}{c} \right), \quad \text{and} \quad y_2 = f_1 \left( t - \frac{x_1}{c} \right);$$

during second interval,

$$y_1 = f_1 \left( t + \frac{x_1}{c} \right) + f_2 \left( t + \frac{x_1}{c} - \theta_1 \right) - f_1 \left( t - \frac{x_1}{c} - \theta_1 \right), \\ y_2 = f_1 \left( t - \frac{x_1}{c} \right) + f_2 \left( t - \frac{x_1}{c} - \theta_1 \right) - f_1 \left( t - \frac{x_1}{c} - \theta_1 \right);$$

during third interval,

$$\begin{aligned}
 y_1 = & f_1\left(t + \frac{x_1}{c}\right) + f_2\left(t + \frac{x_1}{c} - \theta_1\right) + f_3\left(t + \frac{x_1}{c} - 2\theta_1\right), \\
 & -f_1\left(t - \frac{x_1}{c} - \theta_1\right) - f_2\left(t - \frac{x_1}{c} - 2\theta_1\right); \\
 y_2 = & f_1\left(t - \frac{x_1}{c}\right) + f_2\left(t - \frac{x_1}{c} - \theta_1\right) + f_3\left(t - \frac{x_1}{c} - 2\theta_1\right) \\
 & -f_1\left(t - \frac{x_1}{c} - \theta_1\right) - f_2\left(t - \frac{x_1}{c} - 2\theta_1\right) \quad \dots \quad (66)
 \end{aligned}$$

and so on.

When the hammer strikes at the mid-point we must put  $a=b$  and  $l=2a$  in the general expression for  $y_1$  and  $y_2$  given by eq. (64).

From the above values of  $y_1$  and  $y_2$  we find that the string sets in vibration as soon as the hammer comes in contact with the string. The fact that the shorter segment of the string vibrates during impact was observed by Kaufmann, Banerjee and Ganguli<sup>6</sup> and afterwards by R. N. Ghosh. In addition to the hump due to impact of the hammer, it is found that, there are smaller kinks superposed on it. This fact proves, that, the vibration is started in the string as soon as impact begins. R. N. Ghosh<sup>5</sup> in order to explain the existence of the kinks added an arbitrary series  $\sum_r P_r \sin \frac{r\pi x}{a} \cdot \sin \frac{r\pi ct}{a}$  to the expression duly obtained for  $y_1$  with the assumption of Kaufmann, that the shorter segment behaves like a rigid rod during impact. His explanation is, however, not complete.

The present theory explains the kinks quantitatively, the displacement of any point  $x$  for different values of  $t$ , within duration of impact, is calculated from eq. (64). Here we calculate for some particular cases, for the string struck by a hard hammer only where  $E$  is taken to be equal to infinity, as sufficient data for the elastic hammer are not available. The different values of  $y_1$  in arbitrary units, are plotted against the corresponding values of  $ct$  as the magnification of the time displacement curve obtained by different experimenters are never given in their papers. From the graphical representation of the same, we shall at present be able to study, the exact form and the number of kinks developed therein, in addition to the hump due to the impact of the hammer. The study of the harmonics present in the vibration set up during impact will be reported in a different paper.

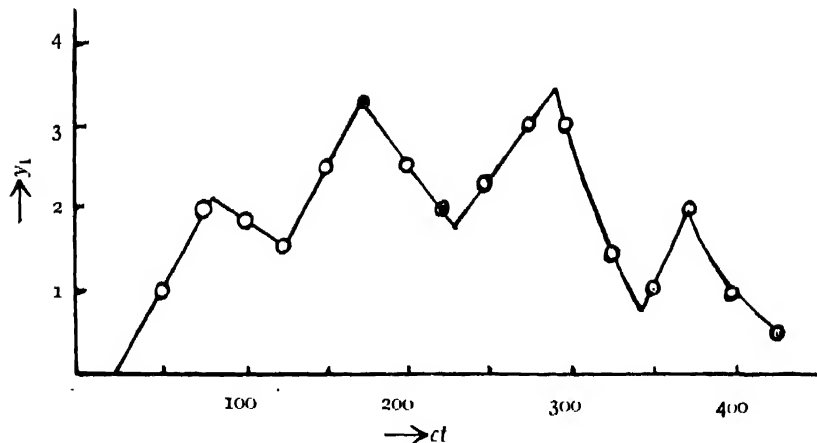


FIGURE 1

Figure 1 represents the time displacement curve for  $m = 21.2$  gms.,  $\rho = 0.5$  gm./cm.,  $v_0 = 45.5$  cm./sec.,  $c = 2.75 \times 10^4$  cm./sec.,  $a = 50$  cms.,  $l = 600$  cms.,  $v = 25$  cms. Here it is found that the impact terminates before any disturbance from the remote end overtakes the hammer.

FIGURE 2(a)

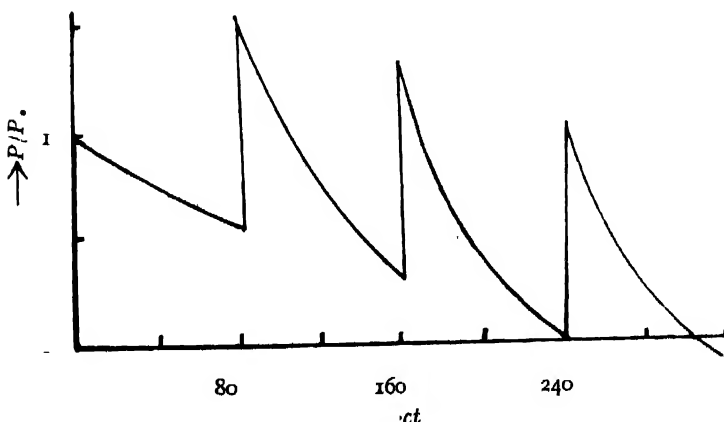
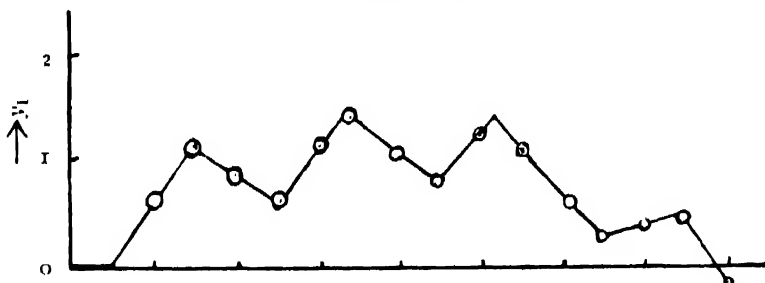


FIGURE 2(b)

Banerjee and Ganguli<sup>6</sup> have supplied experimental data and photographs (Figures 7, 4 and 5 of their paper) which are used in testing the theory. They have used a string 240 cms. long and of mass 16.4 gms. stretched under tension 10.903 kilogrammes. The figure (7) in the paper cited, is the displacement-time shadow-graph for  $m=13.4$  gm.,  $x=20$  cm.,  $a=40$  cm. The value of  $a$  is not given in the paper but is obtained from the latter author in a private consultation. Figure (2a) of this paper represents the same in arbitrary unit. Here we find with the help of eq. (64), that there exist four regularly arranged prominent kinks similar to those given in the photograph. Figure (2b) is the pressure time curve of the hammer whence the value of the duration of impact is found to be equal to '021 sec. and the value obtained experimentally is '0205 sec. This shows a very striking agreement. It is found that no disturbance from the remote end overtakes the hammer before the impact terminates.

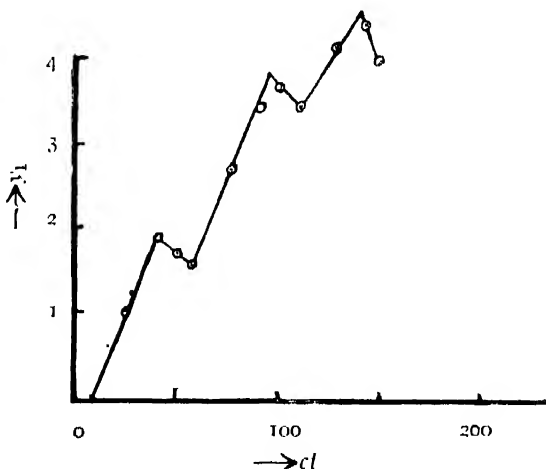


FIGURE 3

Figures (3) and (4a) of this paper correspond to shadow-graph (4) and (5) in the paper cited above for  $m=46$  gms. and for  $a=25$  cms.,  $x=17$  cms. and  $a=32$  cms.,  $x=25$  cms. respectively. Figure (3) is drawn only up to  $ct=150$  cms. Here also the hammer leaves the string just before the disturbance from the remote end overtakes it. But in the case represented by figure (4) the hammer leaves the string long after it is overtaken by a succession of disturbances from the remote end. The figure (4b) represents the pressure time curve of the hammer, as given by the general expression (56). The duration of contact of the hammer as calculated graphically is '0364 secs. and the corresponding observed value is '0369 secs. But if we on the other hand ignore like Das, the effect of the disturbances that overtake the hammer from the remote end, the pressure would have terminated to zero at the point A instead of at the point B. The corresponding duration of impact would have been '9314 secs. This is too low a value.

Further, the number and arrangement of kinks represented in figure (4a) are same as those given in the photograph (5) of the paper cited.

FIGURE 4(a)

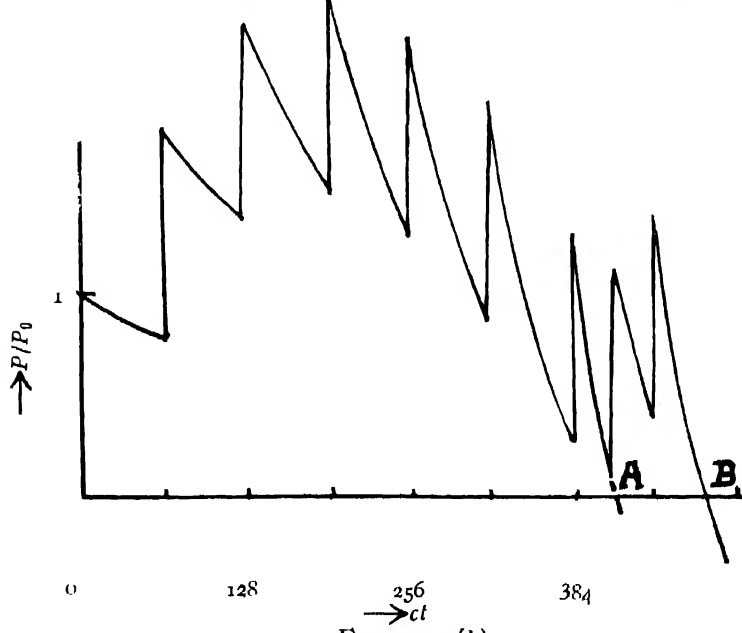
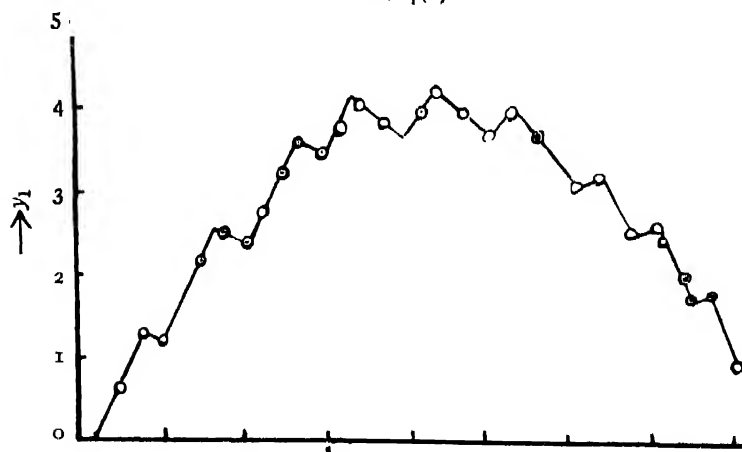


FIGURE 4(b)

My best thanks are due to Prof. K. C. Kar, D.Sc., of Presidency College, Calcutta, who has taken lively interest in this work.

PHYSICAL LABORATORY,  
BURDWAN RAJ COLLEGE,  
BURDWAN.

#### R E F E R E N C E S

- <sup>1</sup> Ghosh, M., *Ind. Jour. Phys.*, **12**, 317 (1938), (Part I).
- <sup>2</sup> Ghosh, M., *Ind. Jour. Phys.*, **12**, 437 (1938), (Part II).
- <sup>3</sup> Das, P., *Proc. Ind. Asso. Cal.*, **9**, 913 (1926).
- <sup>4</sup> Kar, K. C. and Ghosh, M., *Phil. Mag.*, **9**, 306 (1930).
- <sup>5</sup> Ghosh, R. N., *Phil. Mag.*, **9**, 1174 (1930).
- <sup>6</sup> Banerjee, D. and Ganguli, R., *Phil. Mag.*, **7**, 347 (1929).
- <sup>7</sup> Ghosh, M., *Ind. Jour. Phys.*, **7**, 365 (1932).



# SURFACE TENSION AND LINDEMANN FREQUENCY

By L. SIBAIYA, M.Sc., F.A.Sc.

AND

M. RAMA RAO, M.Sc.

Department of Physics, University of Mysore, Central College, Bangalore

(Received for publication, July 12, 1939)

**ABSTRACT.** Assuming as in the theory of liquid viscosity by Andrade that the molecules of a liquid at its melting-point continue to oscillate with Lindemann frequency  $\nu$ , the surface tension  $\gamma$  of a liquid is here considered to be given by the energy of the oscillating molecules in unit area of its surface of unimolecular thickness. The relation to which this assumption leads, viz.,  $\gamma = k^2 m \nu^2$ , where  $m$  is the mass of the atom or molecule, has been examined in the light of available data for fortyfive substances including elements and compounds; and it is found that the constant  $k$  has a mean value 2'34. Experimental results, which show that viscosity influences the rotational "wings" in light-scattering, necessitate a view-point of viscosity independent of relative motion; assuming tentatively that the total momentum transferred per oscillation by the molecules across unit area gives the value of viscosity, and inserting the value of  $k$  obtained from surface tension data therein, Andrade's expression for viscosity is shown to follow quantitatively. The variation of surface tension with temperature is explained on the basis of Macleod's relations; several empirical relations requiring verification have been obtained.

Attempts at explaining the phenomena of surface tension in liquids from the molecular standpoint have been made by a number of investigators.<sup>1</sup> Any satisfactory theory of capillarity should ultimately be capable of explaining many of the well established empirical relations. Andrade<sup>2</sup> has put forward an elegant theory of viscosity based on the fact that substances at their melting-points possess certain properties characteristic of the solid state; the molecules for instance are considered to retain at their melting-point their oscillations with the Lindemann frequency. An approach to the study of the liquid state from the solid state is essentially correct; for the viscosity of liquids like the rigidity of solids decreases with rise of temperature; on the other hand the viscosity of gases increases with rise of temperature. Again in the study of capillarity the solid and the liquid alike have free surfaces of their own. Thus in developing a theory of surface tension in liquids we assume—an assumption that has been amply justified in the viscosity of liquids—that at the melting-point the molecule continues to oscillate with the Lindemann frequency about a slowly displaced equilibrium position. The energy of the oscillating molecule is on the average

equally distributed between the kinetic and the potential energies. Now let us assume that the surface tension of a liquid can be defined as being equal to the total energy of the molecules in a surface layer of unit area of unimolecular thickness. The correctness of the assumption can only be established by the results deduced therefrom which are capable of experimental verification. A preliminary note in support of our assumptions has already appeared in Nature.<sup>3</sup>

On the basis of the assumptions made above, the surface tension at the melting-point,

$$\gamma = \frac{\sum m (2\pi\sigma v)^2}{1 \text{ sq. cm.}}$$

$$= \frac{2\pi^2 a^2}{\sigma^2} m v^2,$$

where

$\sigma$  = mean distance between two molecular centres,

$a$  = amplitude of vibration,

$v$  = Lindemann frequency,

$m$  = mass of the atom or the molecule.

Assuming that  $\frac{a}{\sigma}$  is constant we get

$$v = k \sqrt{\gamma/m}$$

Calculating the Lindemann frequency<sup>4</sup> both for elements and compounds from the relation  $v = 2.8 \times 10^{12} \sqrt{\frac{T_s}{MV^{\frac{5}{3}}}}$ , where  $T_s$  is the melting-point,  $V$  the atomic or the molecular volume,  $M$  the atomic or molecular weight and dividing the frequency so obtained by  $\sqrt{\frac{\gamma}{m}}$  we get the value of  $k$ :

$$k = 2.8 \times 10^{12} \sqrt{\frac{T_s}{MV^{\frac{5}{3}}}} / \sqrt{\frac{\gamma}{m}} \quad \dots \quad (1)$$

Table (1) gives the value of  $k$  calculated from (1) and shows that it is fairly constant with a mean value of 2.34.

Since  $\frac{M}{m} = N$  (Avagadro number) and is constant, it follows that

$$\frac{T_s}{\gamma V^{\frac{5}{3}}} = \text{constant} = \frac{\rho^{\frac{5}{3}} T_s}{\gamma M^{\frac{5}{3}}}.$$

Similar results have been obtained from entirely different considerations by Weng Wen-Po.<sup>5</sup>

TABLE I

Sl. No.	Substance.	Lindemann frequency $\nu \times 10^3$	$\sqrt{\frac{\gamma}{m}} \times 10^2$	$k$ .
1	Antimony	3.00	1.32	2.27
2	Oxygen	1.7	0.71	2.40
3	Lead	1.84	1.14	1.61
4	Tin	2.24	1.59	1.40
5	Mercury	1.25	1.29	0.97
6	Cadmium	3.00	1.84	1.63
7	Bismuth	1.50	1.05	1.53
8	Gallium	2.50	1.76	1.42
9	Zinc	4.36	2.64	1.65
10	Silver	4.36	2.12	2.06
11	Gold	3.40	1.75	1.94
12	Copper	6.70	3.24	2.07
13	Potassium	2.30	2.52	0.91
14	Sodium	3.96	2.78	1.42
15	Platinum	4.36	2.38	1.83
16	Argon	1.32	0.45	2.95
17	Bromine	1.70	0.54	3.25
18	Chlorine	2.24	0.75	2.98
19	Hydrogen	4.36	1.32	3.31
20	Nitrogen	2.50	1.94	1.29
21	Sulphur	3.96	1.06	3.74
22	Selenium	2.70	0.71	3.64
23	Helium	0.66	0.23	2.87
24	Silver Bromide	1.76	0.63	2.81
25	Calcium Chloride	2.37	0.91	2.60
26	Barium Chloride	1.47	0.71	2.13
27	Silver Chloride	2.74	0.73	2.93
28	Lithium Chloride	4.29	1.40	3.06
29	Sodium Chloride	4.00	1.09	3.68
30	Sodium Bromide	2.72	0.78	3.44
31	Potassium Chloride	3.13	0.88	3.54
32	Potassium Bromide	2.34	0.66	3.54
33	Propyl Acetate	0.77	0.40	1.93
34	Methyl Formate	1.20	0.34	3.57
35	Propyl Iodide	0.61	0.27	2.29
36	Propyl Chloride	0.88	0.48	2.31
37	Propyl Bromide	0.72	0.31	2.30
38	Pentane	0.81	0.31	2.37
39	Octane	0.71	0.35	2.03
40	Ethyl Benzene	0.74	0.42	1.74
41	Ethyl Sulphide	0.81	0.42	1.92
42	Benzene	1.19	0.48	2.47
43	Carbon Tetrachloride	0.78	0.33	2.34
44	Carbondisulphide	1.03	0.53	1.95
45	Chloroform	0.86	0.38	2.25

*Effect of Temperature on Surface Tension:*—While the Lindemann frequency is of the order  $10^{12}$ , the collision frequency in gases is of the order  $10^8$ . Assuming, that in the liquid state the molecular frequency suffers a gradual decrease with rise of temperature from its value (Lindemann frequency) at the melting-point, Macleod<sup>6</sup> has shown that the frequency at temperature T,

$$\nu_T = \nu \frac{v_s - v_o}{v_T - v_o} \sqrt{\frac{T}{T_s}},$$

where  $v_s$  is the specific volume of the liquid at the melting-point,  $v_T$  the specific volume of the liquid at temperature  $T$ ,  $v_0$  a constant. Since  $v_T - v_0$  increases more rapidly than  $\sqrt{T}$ ,  $v_T$  decreases with rise of temperature. Thus the surface tension at any temperature,  $T$ ,

$$\gamma \propto m v^2 \left( \frac{v_s - v_0}{v_T - v_0} \right)^2 \frac{T}{T_s} \propto \frac{T}{(v_T - v_0)^2} \quad \dots \quad (2)$$

The value of  $v_0$  calculated from (2) is of the same order of magnitude as  $v_0$  calculated from viscosity data by Macleod.

Assuming after Eödser<sup>7</sup> that the energy of a molecule is inversely proportional to the  $m$ th power of the mutual distance between two molecular centres, it follows that—

$$\gamma \propto \frac{1}{r^{m+2}}$$

The distance between two molecular centres is proportional to  $V^{1/3}$  where  $V$  is the molecular volume of the liquid ; and hence

$$\gamma V^{\frac{m+2}{3}} = \text{constant.} \quad \dots \quad (3)$$

This equation reduces to Sugden's parachor when  $m=10$ , evidence for which value will be given in what follows. Again combining (3) with Eötvös rule we get

$$V^{\frac{m}{3}} (T_c - T) = \text{constant,} \quad \dots \quad (4)$$

which gives the relation between the volume and temperature of a liquid below the critical temperature. Equation (4) readily yields for the value of the co-efficient of volume expansion at temperature  $T$ ,

$$\alpha_T = \frac{3}{m(T_c - T)} \quad ,$$

wherein it has been shown previously by one of us<sup>8</sup> that agreement with experimental results is obtained when  $m=10$ . It has also been shown that if  $\alpha_0$  is the co-efficient of expansion at  $0^\circ\text{C}$ , the critical temperature on the centigrade scale is given by

$$T_c = \frac{3}{10\alpha_0} \quad .$$

From Eötvös rule and (3) it follows that  $\gamma \propto (T_c - T)^{\frac{m+2}{m}}$  and according to Ferguson<sup>9</sup> the index is nearly 1.2, whence also it is seen that  $m$  should be equal to 10. A further instance is given later on,

A P P L I C A T I O N O F S U R F A C E T E N S I O N D A T A T O  
V I S C O S I T Y

Recent work on light scattering by Ramam and Venkateswaran<sup>10</sup> in four different liquids of varying viscosity has shown that increase of viscosity plays an important rôle in suppressing rotational "wings" accompanying Rayleigh lines. Enhanced viscosity arising from increased concentration in solutions has also led to the same results (L. Sibaiya & H. S. Venkataramiah : in publication). Viscosity, which is therefore an inherent property of a liquid even when at rest, should admit of an alternative description apart from the one usually given on the basis of relative motion in layers. We shall assume that viscosity or the internal friction of a liquid is given by the momentum transferred by oscillating molecules across a layer of unit area of the liquid to other molecules. The suppression of the "wings" should then be traced to cases where the molecular rotation frequency is less than the frequency of the momentum-transfer type collision ( $2\nu$ ). On the bases of the assumptions made in the case of surface tension, the total energy of the vibrating molecule,

$$E = 2\pi^2 m a^2 \nu^2 ;$$

the momentum in the equilibrium position =  $\sqrt{2mE} = 2\pi m a \nu$ . Assuming that the vibrating molecule transfers momentum twice per oscillation, the total momentum transferred per oscillation is  $4\pi m a \nu$ . By the assumption made above

$$\eta = \frac{4\pi m a \nu}{\sigma^2} = 4\pi \left( \frac{a}{\sigma} \right) \frac{m \nu}{\sigma} ,$$

where  $\eta$  is the viscosity of liquid at the melting-point. From surface tension

$$\frac{\sqrt{2\pi a}}{\sigma} = \frac{1}{2 \cdot 34} ,$$

whence

$$\eta = \frac{4}{3 \cdot 3} \frac{m \nu}{\sigma} .$$

A comparison with Andrade's expression  $\eta = \frac{4}{3} \frac{m \nu}{\sigma}$  shows that the value of

$\frac{\sqrt{2\pi a}}{\sigma}$  deduced from surface tension data is essentially correct.

If as before we assume that the energy of the oscillating molecule is proportional to  $\frac{1}{\sigma^{m_i}}$ , it readily follows from the above consideration that

$$\eta \propto \frac{1}{\sigma^{\frac{m+4}{2}}} ,$$

or  $\eta V^{\frac{m+4}{6}} = \text{constant}$  for a given liquid.

Combining our expression for surface tension with Andrade's expression for viscosity and with Sugden's parachor it is easily shown that

$$\eta V^{\frac{7}{3}} = \text{constant},$$

whence also it follows that  $m=10$ . It can be shown that for any liquid, its surface tension at any given temperature is directly proportional to  $\frac{12}{7}$ th power of its viscosity at the same temperature. These relations require verification.

Our thanks are due to Professor A. Venkat Rao Telang for his kind encouragement.

#### R E F E R E N C E S

- <sup>1</sup> Laplace, "Mecanique Celeste," suppl. to Book 10 (1806); Young, "Cohesion of Fluids," *Phil. Trans. A.*, **96**, 65 (1805); Sutherland, *Phil. Mag.*, **24**, 113 (1887); Kleeman, *Phil. Mag.*, **19**, 783 (1910), Bakker, *Zeits f. Phys. Chem.*, **68**, 684 (1910); Edser, *Fourth Report on the Progress of Colloid Chemistry* (1922).
- <sup>2</sup> Andrade, *Phil. Mag.*, **17**, 497 (1934).
- <sup>3</sup> L. Sibaiya and M. Rama Rao, *Nature*, **143**, 723 (1939).
- <sup>4</sup> L. Sibaiya and M. Rama Rao, *Cur. Sc.*, **8**, 12 (1939).
- <sup>5</sup> Weng Wen-po, *Phil. Mag.*, **23**, 33 (1937); also **25**, 111 (1938).
- <sup>6</sup> Macleod, *Proc. Phys. Soc.*, **53**, 88 (1938).
- <sup>7</sup> Edser, *Fourth Report on the Progress of Colloid Chemistry* (1922).
- <sup>8</sup> L. Sibaiya, *Current Science.*, **6**, 329 (1938).
- <sup>9</sup> Ferguson, *Trans. Far. Soc.*, **19**, 408 (1923).
- <sup>10</sup> Raman and Venkateswaran, *Nature*, **143**, 798 (1939).

## LIQUID DROPS

By L. D MAHAJAN, M.Sc., Ph.D., F.Inst.P (LONDON)

(Received for publication, July 13, 1939)

**ABSTRACT.** A general mathematical relation between the life of the drops floating on the surface of the same liquid and the viscosities of the mother liquid and of the surrounding medium is deduced, which is applicable for all viscosities and under all conditions.

Many papers<sup>1</sup> have already been published by the author on the various aspects of the phenomenon of the liquid drops floating on the surface of the same liquid, but so far no plausible mathematical relation has been given between the life of the drops and the viscosities of the liquids and of the surrounding medium. In his previous paper on the theory<sup>2</sup> of the drops, three relations were deduced which are to be used for three different stages of viscosities. No single relation could satisfy the results in all the three stages. But in this paper, the author has deduced a general mathematical relation between them which is applicable in all conditions.

## DISCUSSIONS

The following observations are recorded from the Table I of the paper "Eine Theorie der Erscheinung Von flüssigen Tropfen auf der Oberfläche derselben Flüssigkeit," Von L. D. Mahajan, Kolloid Zeitschrift, Band 65, Heft 1 (1933), pp. 20-23.

TABLE I

No. of observation.	Life of the primary drops in seconds.	Life of the secondary drops in seconds.	Viscosity of the mother liquid (in C.G.S. Units).
1	1.2	3.4	0.013
2	2.3	5.8	0.018
3	2.4	4.6	0.019
4	3.4	3.5	0.023
5	4.5	3.5	0.029
6	about 2	2.3	0.045
7	1.2	1.2	0.066
8	about 1	almost no life	0.104
9	about 1	no splashing	0.223
10	nil.	no splashing	0.768

These observations show that the life of a drop depends upon the viscosity of the mother liquid and is independent of its density or surface tension. The life of the drop increases with the increase of viscosity up to a certain limit and at this viscosity the life is maximum. If the viscosity is still further increased, the life decreases with the increase of viscosity, till it becomes almost zero, and formation of the drop becomes impossible.

A graph, if plotted to show the relation between the viscosity of the mother liquid and the life of the floating drop, takes the shape of a parabola with its latus rectum equal to ' $a$ ', and can be represented by the following equation :—

$$(X - m)^2 = -a(Y - n) \quad \dots \quad (1)$$

which can be shown by the curve given in figure 1.

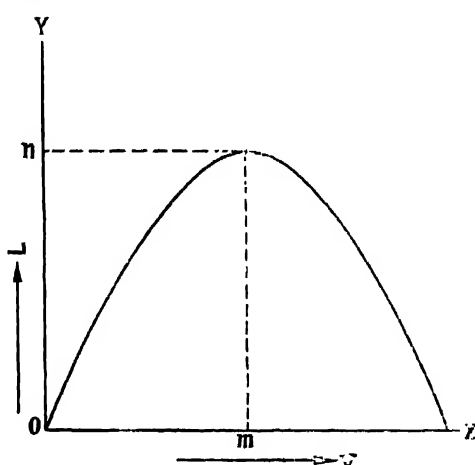


FIGURE 1

Now in the equation (1), 'X' can be represented by 'v' the viscosity of the mother liquid, and 'Y' by L, the life of the drop in seconds, hence we get :—

$$(v - m)^2 = -a(L - n) \quad \dots \quad (2)$$

where 'm' is the viscosity of the mother liquid which when used for the formation of the drops gives the drops of maximum life whatever method for its formation is applied. Now if the viscosity of the mother liquid is varied (increased or decreased) the life of the drop decreases in a certain order. Thus there are two viscosities at which the drops may have the same life.

In equation (2), 'n' stands for the maximum life of the drop for the corresponding liquid, ' $a$ ' is a constant depending upon the nature of the method applied for the formation of the drops, the condition of the weather when the experiment is performed and the nature of the surrounding medium. From equation (2), we get :—

$$L = n - \frac{1}{a} (v - m)^2 \quad \dots \quad (3)$$

Whereas the following observations are taken from Table II, of the same paper as mentioned above.

TABLE II

No. of observa- tion.	Mother liquid.	Viscosity of the mother liquid in C.G.S. Units.	Surrounding medium.	Viscosity of the surrounding medium in C.G.S. Units.	Life of the primary drops in sec.
1	Water	0.01	Air	$1.84 \times 10^{-3}$	about 0.04
2	"	"	Petroleum	0.020	" 4
3	"	"	Aniline at 50°C	0.0185	" 4
4	"	"	" at 23°C	0.0396	" 8
5	"	"	Olive oil at 98°C	0.0167	" 10
6	"	"	Olive oil at 80°C	0.0604	" 12
7	"	"	Olive oil at 78°C	0.0851	" 18
8	"	"	Olive oil at 66°C	0.1461	" 30
9	"	"	Olive oil at 54°C	0.2532	" 50

These observations clearly indicate that the life of the drop depends upon the viscosity of the surrounding medium, and is directly proportional to it. Hence

$$L \propto V \quad \dots \quad (4)$$

where 'V' is the viscosity of the surrounding medium. By combining (3) and (4) we get the general equation

$$L = \frac{V}{V_{air}} \left\{ n - \frac{I}{a} (v - m)^2 \right\} \quad \dots \quad (5)$$

where  $V_{air}$  is the viscosity of the air. When there are two different surrounding media, we get :—

$$\frac{L_1}{L_2} = \frac{V_1 \left\{ n - \frac{I}{a} (v_1 - m)^2 \right\}}{V_2 \left\{ n - \frac{I}{a} (v_2 - m)^2 \right\}} \quad \dots \quad (5a)$$

where  $V_1, v_1$  and  $V_2, v_2$  are corresponding viscosities for  $L_1$  and  $L_2$  respectively, and  $V_{air}$  is eliminated.

(i) When  $v = m$ ,

$$L = \frac{V}{V_{\text{air}}} n \quad \text{and} \quad \frac{L_1}{L_2} = \frac{V_1}{V_2} \quad \dots \quad (6)$$

(ii) When  $V = V_{\text{air}}$

$$L = \left\{ n - \frac{1}{a} (v - m)^2 \right\} \quad \dots \quad (7)$$

(iii) When  $V = V_{\text{air}}$  and  $v = m$ , we get :—

$$L = n \quad \dots \quad (8)$$

In the above formula (5) the value of 'a' is to be found out either by taking known values of 'n,' 'v,' 'm' and then calculating 'a,' or from the curve by drawing it for a number of observations, between 'v' and 'L.'

The absolute values of the constants 'a,' 'n' and 'm' can be deduced from three observations taken with a certain liquid or solution, by varying its viscosity as follows :

#### *The value of 'm'*

Let  $L$ ,  $L'$ , and  $L''$  be the lives of the drops for the corresponding viscosities  $v$ ,  $v'$ , and  $v''$ , and let the surrounding medium be air. Then we get from the general equation (5),

$$L = \frac{V}{V_{\text{air}}} \left\{ n - \frac{1}{a} (v - m)^2 \right\} \quad \dots \quad (5)$$

when medium is air,  $\therefore L = n - \frac{1}{a} (v - m)^2$

and  $L' = n - \frac{1}{a} (v' - m)^2$

$$\text{Therefore, } L - L' = \frac{1}{a} (v'^2 - 2v'm + v^2 + 2vm) \quad \dots \quad (9a)$$

Similarly, for  $L$  and  $L''$ , we get

$$L - L'' = \frac{1}{a} (v''^2 - 2v''m + v^2 + 2vm) \quad \dots \quad (9b)$$

$$\text{Therefore, } \frac{L - L'}{L - L''} = \frac{v'^2 - 2v'm + v^2 + 2vm}{v''^2 - 2v''m + v^2 + 2vm} \quad \dots \quad (9c)$$

Therefore, from (9c), by cross-multiplication and simplification, we get the value of  $m$  as follows:—

$$m = \frac{1}{2} \frac{(L - L')(v^2 - v'^2) + (L - L'')(v''^2 - v^2)}{(L - L')(v - v') + (L - L'')(v' - v)} \quad \dots \quad (9)$$

The equation (9) gives the value of the constant 'm,' i.e., the viscosity of the liquid, at which the liquid gives the drops of maximum life, in terms of the known factors  $L$ ,  $L'$ ,  $L''$  and  $v$ ,  $v'$  and  $v''$ .

### *The value of 'n'*

Now, in order to find out the value of 'n,' the maximum life of the drop of the liquid at its viscosity 'm,' consider the first two observations. Let  $L$  and  $L'$  be the lives of the drops at the corresponding viscosities  $v$  and  $v'$ , the surrounding medium being again air. From the general equation (5), we get :—

$$\begin{aligned} L &= \frac{V}{V_{\text{air}}} \left\{ n - \frac{I}{a} (v - m)^2 \right\} \\ &= n - \frac{I}{a} (v - m)^2 \quad \dots \quad (10a) \end{aligned}$$

$$\text{Similarly } L' = n - \frac{I}{a} (v' - m)^2 \quad \dots \quad (10b)$$

From (10a) and (10b) we get

$$L - n = - \frac{I}{a} (v - m)^2$$

and

$$L' - n = - \frac{I}{a} (v' - m)^2$$

or

$$\frac{L - n}{L' - n} = \frac{(v - m)^2}{(v' - m)^2} \quad \dots \quad (10c)$$

From equation (10c) by cross-multiplication and simplification, we get the value of  $n$  as follows :

$$n = \frac{L'(v - m)^2 - L(v' - m)^2}{v^2 - v'^2 - 2vm + 2v'm} \quad \dots \quad (10)$$

By substituting the value of 'm' found by the equation (9), and the known values of  $L$ ,  $L'$ ,  $v$  and  $v'$  in this equation, find the absolute value of 'n,' the maximum life of the drop of the solution or liquid under consideration corresponding to its viscosity 'm.'

### *The value of 'a'*

Having known the values of 'm,' and 'n,' we substitute them in equation (10a), and get

$$L = n - \frac{I}{a} (v - m)^2$$

$$n - L = \frac{1}{a} (v - m)^2$$

$$\therefore a = \frac{(v - m)^2}{n - L} \quad \dots \quad (11)$$

wherein, the values of 'm' and 'n' have been found in the equations (9) and (10), and the values of 'v' and L are taken as known for a certain observation.

Thus we get the absolute values of 'a,' 'm' and 'n.' By substituting their values in the general equation (5), we can find out the life of the drop of any liquid or solution, having viscosity 'v' in the C.G.S. Units, and the viscosity of the surrounding medium 'V.' These equations satisfy all the results obtained by any method.

In the equations (9) and (10) there should be sufficiently large difference between the two values L and L', in order that the results may be accurate. The values found with the help of these equations are almost the same as those found experimentally.

PHYSICS LABORATORY,  
MOHINDRA COLLEGE, PATIALA, INDIA.

<sup>1</sup> L. D. Mahajan, *Phil. Mag.*, **7**, 247 (1928); *Nature*, **126**, 761 (1930); *Phil. Mag.*, **10**, 383 (1930); *Nature*, **127**, 70 (1931); *Current Science*, **1**, 100 (1932); **1**, 128 (1932); *Zeits. f. Phys.*, **79**, 380 (1932); *Current Science*, **1**, 162-163 (1932); *Zeits. f. Phys.*, **81**, 605 (1933); **84**, 676 (1933); *Kolloid-Zeit. Leipzig*, **68**, 20 (1933); **69**, 16, (1934); **68**, 22 (1934); *Zeit. f. Phys.*, **91**, 633 (1934).

<sup>2</sup> L. D. Mahajan, *Kolloid-Zeit.*, **68**, 20 (1933).

# EVAPORATION FROM EARTHEN JUGS

BY HAZARILAL GUPTA

AND

ABINASH CHANDRA

(University of Delhi)

*(Received for publication, July 20, 1939)*

**ABSTRACT.** A theory of the evaporation of water from earthen jugs has been given and the results expected according to the theory have been found to agree fairly with those observed experimentally by the authors.

The present paper is concerned with the study of the evaporation of water from earthen jugs.<sup>4</sup> In section 1, the theory of the process is discussed. This is based on the theory of wet- and dry-bulb hygrometer.<sup>1</sup> In section 2, the experimental results and their comparison with the theory is given.

§1. When water is kept in an earthen jug the cooling produced by evaporation keeps it cooler than its surroundings. The poor thermal conductivity of the clay plays an important part in preventing the flow of heat from the surroundings to the cooler jug, and in fact because of this thermal insulation the temperature of the water in the jug approaches to within half a degree the temperature of the wet-bulb thermometer, and the wet-bulb temperature represents the lowest attainable by cooling due to free evaporation in the atmosphere.

As in the case of the wet-bulb thermometer we shall here assume that the air in contact with the jug becomes saturated at the temperature of the jug. Let  $m$  denote the mass of the jug,  $S$  the specific heat† of the clay composing it,  $M$  the mass of the water contained in the jug, and  $T$  the absolute temperature of the jug (and the water in it). Let  $T'$  and  $T''$  denote the absolute temperatures of the dry- and wet-bulb thermometers respectively, and  $x'$ ,  $x''$  and  $x$  the humidity mixing ratios for the normal air, the air saturated at the

During summer months in India drinking water is invariably kept in earthen jugs.

† The specific heat was determined by the usual method and was found to be 0.22.

wet-bulb temperature  $T'$  and the air saturated at the temperature  $T$  of the jug respectively. The normal air contains  $x'$  grams of water vapour per gram of dry air, and, therefore, when  $(1+x')$  grains of normal air come in contact with the jug, its temperature changes from  $T'$  to  $T$  and it becomes (as we have assumed) saturated at the temperature of the jug, i.e., the amount of water vapour associated per gram of dry air increases from  $x'$  to  $x$ . The amount of heat given out in the process by  $(1+x')$  grams of air is  $(C_p + x' C_{p'}) \times (T' - T)$ , and the amount of heat required to saturate it will be  $(x - x') L$ , where  $C_p$  is the constant-pressure specific heat of dry air,  $C_{p'}$  that for water vapour and  $L$ , the latent heat for evaporation corresponding to temperature  $T$ . For every  $(1+x')$  grams of the normal air the amount of water evaporating from the jug is  $(x - x')$ , and hence if  $\frac{dM}{dt}$  represents the rate of evaporation of water from the jug, the amount of normal air coming in contact with the jug per second will be

$$\frac{x}{(x - x')} = \frac{dM}{dt} (1 + x'),$$

and the equation expressing energy conservation will become

$$-(M + Sm) \frac{dT}{dt} = \frac{dM}{dt} \left\{ L_e - \frac{(T' - T)}{x - x'} (C_p + C_{p'} x') \right\} \quad \dots \quad (1)$$

As  $C_{p'}/C_p$  is about 2 and  $x'$  rarely exceeds 0.025,  $C_{p'} x'$  may be neglected compared to  $C_p$  in the last term on the right-hand side of the above expression. Again as a first approximation we may substitute

$$v = e \frac{e'}{p - e}; \quad x' = e \frac{e'}{p - e'} \quad \dots \quad (2)$$

where  $e'$  is the vapour pressure of normal air,  $e$  the saturated vapour pressure for temperature  $T$ ,  $p$  the total pressure and  $\epsilon$  the ratio of the densities of water vapour and dry air at the same temperature and pressure. We thus obtain

$$-(M + Sm) \frac{dT}{dt} = \frac{dM}{dt} \left\{ L_e - \frac{C_p p}{\epsilon} \cdot \frac{T' - T}{e - e'} \right\}, \quad \dots \quad (3)$$

or 
$$-(M + Sm) \frac{dT}{dM} = L_e - \frac{C_p p}{\epsilon} \cdot \frac{T' - T}{e - e'} \quad \dots \quad (4)$$

It may be noted that  $\frac{C_p p}{e} = 300$ , where  $p$  (and also  $e$ ,  $e'$ ) is in mm. of mercury. Equation (4) is fundamental to our study.\* When the steady state is reached  $\frac{dT}{dM} = 0$ , and if  $T''$  denotes the temperature of the jug in the steady state then

$$e'' - e' = \frac{C_p p}{e} (T' - T'') \quad \dots \quad (5)$$

This is the usual expression for the wet- and dry-bulb hygrometer and thus, as is also otherwise obvious, the temperature of water in an earthen jug approaches the wet-bulb temperature and as the wet-bulb temperature remains the same for the "same air mass" (c.g., outside and inside of a room provided with *khas-taties*), the same result holds for the temperature of water in an earthen jug. The next section deals with the experimental results.

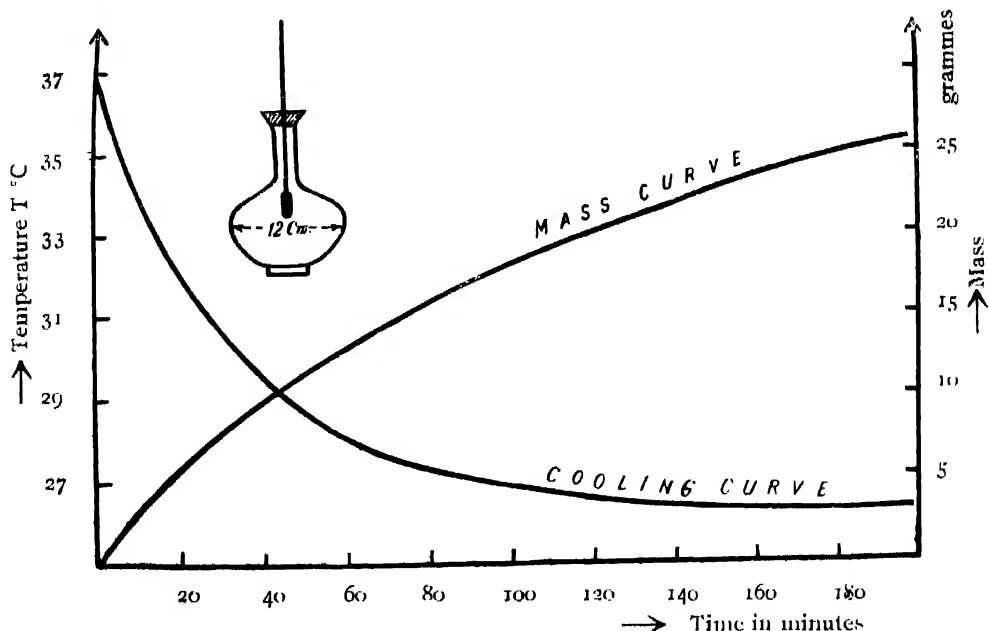


FIGURE 1

§2. In the experiment we used ordinary earthen jugs, but of rather small size (diameter about 5"). They were filled with water a few degrees above the room temperature and cooling curves were plotted, the water being continuously stirred. The weight was also determined every five minutes. Figure 1 shows a

\*  $\frac{dM}{dt}$  will depend upon a number of factors, i.e., the porosity of the clay, the movement of the surrounding air, etc.

typical cooling curve and also the corresponding mass-curve showing the amount of water evaporating in a given time. (The dimensions of the jug are given in the inset). The dry-bulb temperature was  $32^{\circ}\text{C}$ , the wet-bulb temperature  $26^{\circ}\text{C}$ , and the humidity corresponding to these readings 65%.

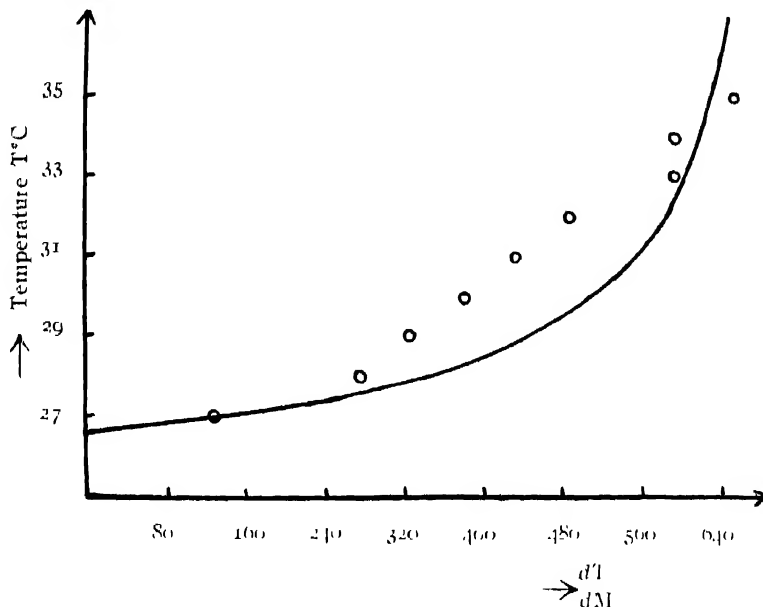


FIGURE 2

In figure 2, the curve is theoretical and represents the relation between  $\frac{dT}{dM}$  and  $T$  as given by the expression (4) for  $T^v = 32 + 273^{\circ}\text{K}$  and  $c' = 23 \text{ mm.}$  corresponding to a humidity of 65%. The observed points as computed from figure 1 are indicated by circles. Considering the nature of the experiment and the assumptions and approximations involved in the theory the agreement is not altogether bad.\*

We hope to undertake later a detailed study of the problem discussed here.

Our thanks are due to Dr. D. S. Kothari for suggesting the problem and for his guidance.

DELHI UNIVERSITY,  
DELHI, INDIA.

\* As a means for keeping water cool, the earthen jug is really efficient,—its temperature almost approaches the wet-bulb temperature.

#### R E F E R E N C E S

<sup>1</sup> Normand, *Mem. Indian Met. Dept.*, 28, 1 (1921). A good account is given in Brunt, *Physical and Dynamical Meteorology* (1934), Art. 47 and 48, and this is followed here.

<sup>2</sup> Brunt, *loc. cit.*

# ABSORPTION SPECTRA OF COMPOUNDS OF PHOSPHORUS

BY SH. NAWAZISH ALI

*(Received for publication, July 12, 1939)*

## Plate XVI

**ABSTRACT.** The absorption spectra of solutions of  $\text{HPO}_3$ ,  $\text{H}_3\text{PO}_4$ ,  $\text{K}_3\text{PO}_4$ ,  $\text{K}_2\text{HPO}_4$ ,  $\text{KH}_2\text{PO}_4$ ,  $\text{H}_4\text{P}_2\text{O}_7$  and  $\text{K}_2\text{HPO}_3$  and of vapours of  $\text{HPO}_3$ ,  $\text{H}_3\text{PO}_4$  and  $\text{KPO}_3$  have been studied experimentally. Absorption maxima have been observed in the case of the solutions in the region from 2600 Å U. to 3000 Å U. and in the case of the vapours diffuse maxima of absorption have been observed in the region 2100–2550 Å U. From the observed behaviour of the bands with the change of concentration of the solutions it is concluded that there is no essential difference in behaviour or structure between the acids, salts and esters formed by phosphorus and those formed by nitrogen. The significance of these results is discussed in the light of the theories of chemical combination.

## INTRODUCTION

In order to extend the work done by Franek<sup>1</sup> and his collaborators, some recent investigations in this laboratory have been directed towards the study of the transition from covalent to electrovalent linkage in the case of more complex chemical structures. The absorption spectra of nitrates and sulphates in the vapour state<sup>2</sup> indicate clearly that these salts exhibit a covalent bond between metal and oxygen as isolated individual molecules, *i.e.*, in the absence of outside forces such as those of hydrolysis or the crystal lattice, which may turn the ionic potential curve into a repulsive one and at the same time into that of the lowest electronic term of the system. At the same time it is shown,<sup>3</sup> that nitrogen is also penta-covalent in solutions of high concentrations of tetra-alkyl ammonium salts. We have, therefore, tried to extend such experiments to phosphates and the following is a report on the results obtained in this connection.

It was obvious from the very beginning that the study of phosphates and the derivatives of other acids of phosphorus will be more difficult than that of nitrates. Nitrogen, for instance, forms only one kind of acid in its penta-covalent state and one kind of salt, *i.e.*, nitric acid and nitrates, with the structural formula  $\text{O} \begin{matrix} \nearrow \\ \searrow \end{matrix} \text{N} = \text{O} - \text{M}$ . A similar structure prevails in meta-phosphoric acid  $\text{HPO}_3$ , but

in ortho-phosphoric acid  $H_3PO_4$  one of the double bonds is replaced by two OI groups. This results in the presence of altogether three hydrogen atoms or, in the salts, up to three metal atoms, which may become electrovalent one after the other. Naturally the dissociation constants for the second and third of these bonds must be lower than those for the first, but inspite of that there should be equilibrium between the ions such as  $PO_4'''$ ,  $HPO_4''$ ,  $H_2PO_4'$ , in any solution. It follows, therefore, that only those solutions for which the equilibrium has been shifted very much to one of such ions can be taken into account, and all others have to be disregarded. A typical instance is that of a solution of  $P_2O_5$  in water, which contains not only the ions due to  $H_3PO_4$  but also those produced by  $H_4P_2O_7$  and  $HPO_3$ . The absorption spectrum, therefore, varies with concentration and age of the solution. Another consequence of the existence of three electrovalent bonds is that the ionic forces between the lattice points of the crystal are multiplied resulting in a very high melting-point, and it is, therefore, possible to obtain a vapour pressure high enough to study the absorption spectrum of the vapour only in some cases such as  $KPO_3$  or  $HPO_3$  itself, whereas for compounds with two or three electrovalent bonds such as  $K_3PO_4$  sufficient vapour pressure cannot be produced at a temperature which excludes the possibility of thermal decomposition of the molecule. A further difficulty is that the indicator of beginning of decomposition, *i.e.*, bands comparable with those of  $NO_2$  and  $NO$  in the case of nitrates and  $SO_2$  in the case of sulphates is missing for the compounds of phosphorus. Furthermore, no quantitative measurements of solutions of acids of phosphorus can be found in literature which could be used as a guide as in the case of nitric acid and nitrates.

We present, therefore, in the following only those results for which we can be reasonably sure that the spectra really refer to a particular molecule or ion alone, disregarding all doubtful cases. It can be seen that they permit certain conclusion with respect to the structure and the character of the bonds.

#### EXPERIMENTAL PROCEDURE

For the absorption spectra of solutions various experimental procedures have been worked out which are all similar in this respect that a spectrum of the solution of defined concentration and thickness of absorbing layer is compared with a spectrum through the solvent only. The spectrum through the solvent is weakened by various mechanical devices by a defined percentage and if a wavelength is found for which both spectra have equal intensities on the same plate the extinction coefficient can be calculated easily for such a frequency. When only such sources were available for the ultra-violet region which gave either a continuous spectrum or one with many lines, but were unstable or had a variable intensity, both the spectra (twin spectra), *i.e.*, one through the solution and the other through the solvent had to be taken simultaneously by means of the various

optical and mechanical arrangements. Nowadays, however, the continuous spectrum of hydrogen provides a source of light not only entirely continuous but also quite stable provided such a construction of the discharge tube is employed which works with stagnant gas. For these investigations the hydrogen tube devised by Lau<sup>1</sup> was employed as a source of light. The intensity of light given by this tube remains constant for long periods even if the transformer is run on the mains and the exposure time is not too short so that the ordinary small changes of voltage have time to counterbalance themselves. Hilger's E<sub>2</sub>-spectrograph was employed as the resolving instrument. Values of extinction coefficients for the various compounds were calculated by the formula of Bunsen and Roscoe based on the assumption of Lambert's Law and Beer's Law :

If  $I_0$  = the intensity of the incident light,

$I$  = the intensity after transmission through the solution,

$c$  = the concentration per mol per litre, taken as 'one,'

$d$  = the thickness of the solution layer in cms.,

$k$  = the extinction coefficient, i.e., the reciprocal of the thickness of the solution the passage of light through which reduces the intensity of the incident light to  $1/10$  th.

Then

$$I/I_0 = 10^{-kcd}$$

$$\log I/I_0 = -kcd$$

$$k = -(\log I/I_0)/cd.$$

The time of exposure for transmission of light through the solvent was taken as  $1/10$ th of the time through the solution so that the intensity of light was reduced ten times giving the value of  $\log 1/I_0 = -\log 10 = -1$  in the above formula; and  $k = 1/cd$ .

Several twin spectra corresponding to different values of  $d$ , the thickness of the solution with a known concentration  $c$  were taken on the same plate by means of a Hartmann's diaphragm, the time of exposure for the solvent being  $1/10$ th of that for the solution. On each of the twin spectra wave-lengths corresponding to equal intensity points were determined and the values of

$\log k = \log (I/cd)$  were plotted on a graph paper with wave-lengths as abscissæ. This procedure was adopted for strong solutions of concentration  $c=1$ .

For weaker solutions of concentrations  $c=1/10$  the maxima were at very low  $\log k$  values and absorption cells of lengths 10 cms. to 100 cms. were required. Working with such long tubes was not considered quite satisfactory because it introduced an error of optical adjustment and it was extremely difficult to maintain the intensity of light during an exchange of the tubes. We have therefore measured these solutions by taking a spectrum through the solutions together on the same plate with spectra of the solvent of various exposure times. All the spectra thus obtained were then measured by the recording photometer. The spectra through the solvent only were utilised as intensity marks. Combining the above equation  $I = I_0 e^{-kd}$  with Schwarzschild equation  $I_1 t_1^p = I_2 t_2^p$ , we obtain  $kcd = p(\log t_1 - \log t_2)$ . The intersections of the photometer curves due to the solvent on the photometer records with the curves due to the solution then defined  $k$  for that wave length if  $c$  and  $d$  are known. Figure 1 (Plate XVI) is an example of the spectrum for M/10 solution of  $H_3PO_4$ . The three more or less parallel curves are due to three exposures through the solvent with exposure times 360, 180, and 30 secs. respectively and the fourth curve is due to the solution with an exposure time of 360 secs. It can be seen that the solvent curve with 30 secs. intersects the solution curve just on the maximum and the  $\log k$  value is therefore  $-6$  for the maximum. Taking into account the known positions of the maxima with  $c=1$  and the density or blackness of the plates judged visually about three or four intensity marks are generally enough to obtain a fairly accurate value of  $\log k$ .

To obtain the absorption spectra of vapours the following method was employed :—

On account of the high melting-point of most of the compounds a rather long absorption-tube of dimensions  $80 \times .4$  cms. was employed. A small quantity of the substance taken in a china boat was introduced into the absorption-tube and the usual manometer arrangement for creating a vacuum was fitted up. The absorption-tube after being placed in an electric furnace was first evacuated and the comparison spectrum taken. Then the temperature was raised to about  $100^\circ C$  and kept constant for about an hour with the pump running in order to expel all water vapour from the salt. Then the temperature was raised steadily up to about  $1000^\circ C$  and the spectra taken at different temperatures. The hydrogen discharge tube mentioned above was used as a source of continuous spectrum and Hilger's quartz-spectrograph, E<sub>3</sub> was used as the resolving instrument. The positions of the maxima of absorption were determined from the micro photometer records in comparison with copper lines taken directly on the original plates.

The results of the experiments are listed in table 1.

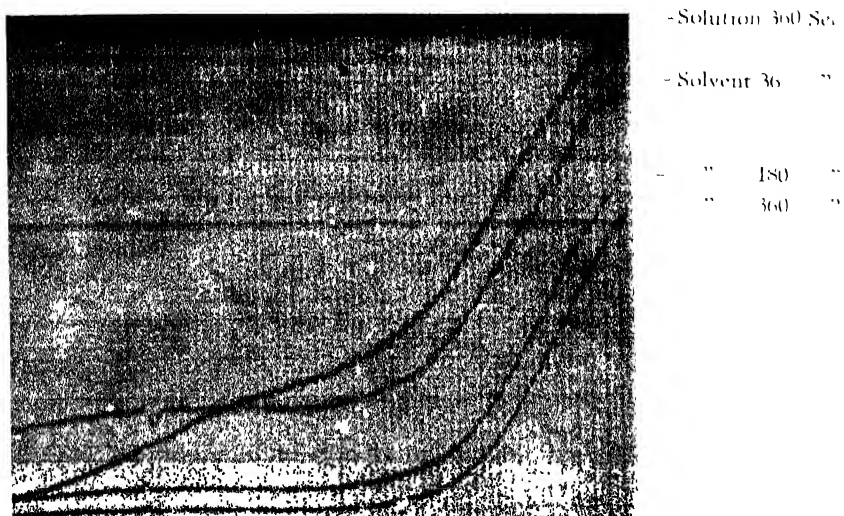


Figure 1.  $H_3PO_4$ ,  $M'_{10}$  Solution.

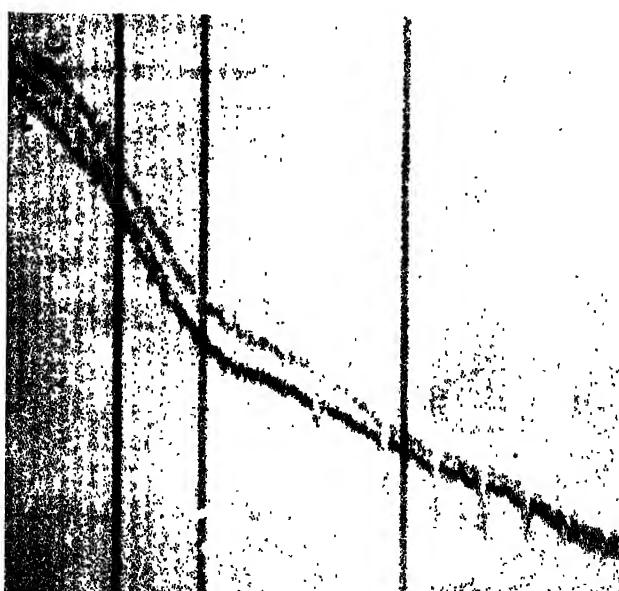


Figure 2.  $KPO_4$  Vapour.  
a - Room temperature, 30°C  
b—Vapour at 508°C  
c— " " 900°C



TABLE I

## A. Solutions

(Maxima of absorption)

	Wave-lengths in A.U.	$\log k, c = 1\text{ mol}$	$\log k, c = 0\cdot 1$
$\text{HPO}_3$	2630	-0.3	-0.2
$\text{H}_3\text{PO}_4$	2630	-0.2	-0.1
$\text{K}_3\text{PO}_4$	2720	-0.1	...
$\text{K}_2\text{HPO}_4$	2860	-0.2	0.0
$\text{KH}_2\text{PO}_4$	2700	-0.7	...
$\text{H}_4\text{P}_2\text{O}_7$	2550	...	...
$\text{K}_2\text{HPO}_3$	2970	...	...

## B. Vapours

(Diffuse maxima of absorption)

	Wave lengths in A.U.	$\log k, c = 1\text{ mol}$	$\log k, c = 0\cdot 1$
$\text{HPO}_3$	4440	...	...
$\text{H}_3\text{PO}_4$	2440	...	...
$\text{KPO}_3$	2500	...	...

## DISCUSSION

Metaphosphoric acid,  $\text{HPO}_3$ , whose structure is similar to that of nitric acid was studied first. In solution it passes slowly into the ortho-acid. At room temperature, however, this change takes place in several days. In solutions of  $c = 1\text{ mol}$ ,  $\text{HPO}_3$  shows a maximum of absorption at  $\lambda 2630$ , in the same position as  $\text{H}_3\text{PO}_4$ , but the region of selective absorption is much broader than that of  $\text{H}_3\text{PO}_4$  and the minimum lies at  $\lambda 2400$ , while that of  $\text{H}_3\text{PO}_4$  is at  $\lambda 2540$ . Furthermore, weak solutions of  $\text{H}_3\text{PO}_4$  do not show this maximum and in 1 mol  $\text{HPO}_3$  only a small percentage of  $\text{H}_3\text{PO}_4$  can be present in the beginning. This maximum, therefore, if it does not belong to  $\text{HPO}_3$  entirely, at least will be composed of that of  $\text{H}_3\text{PO}_4$  along with a maximum of selective absorption at slightly longer waves than  $\lambda 2630$ . In a solution of concentration  $c = 0\cdot 1$ , this

maximum has been considerably weakened, and at the same time in the vapour state the selective absorption is shifted to shorter waves with a point of inflection at  $\lambda 2440$ . This curve can be due to the covalent  $\text{HPO}_3$  molecule and resembles that of  $\text{HNO}_3$  very much, only shifted slightly to higher frequencies.

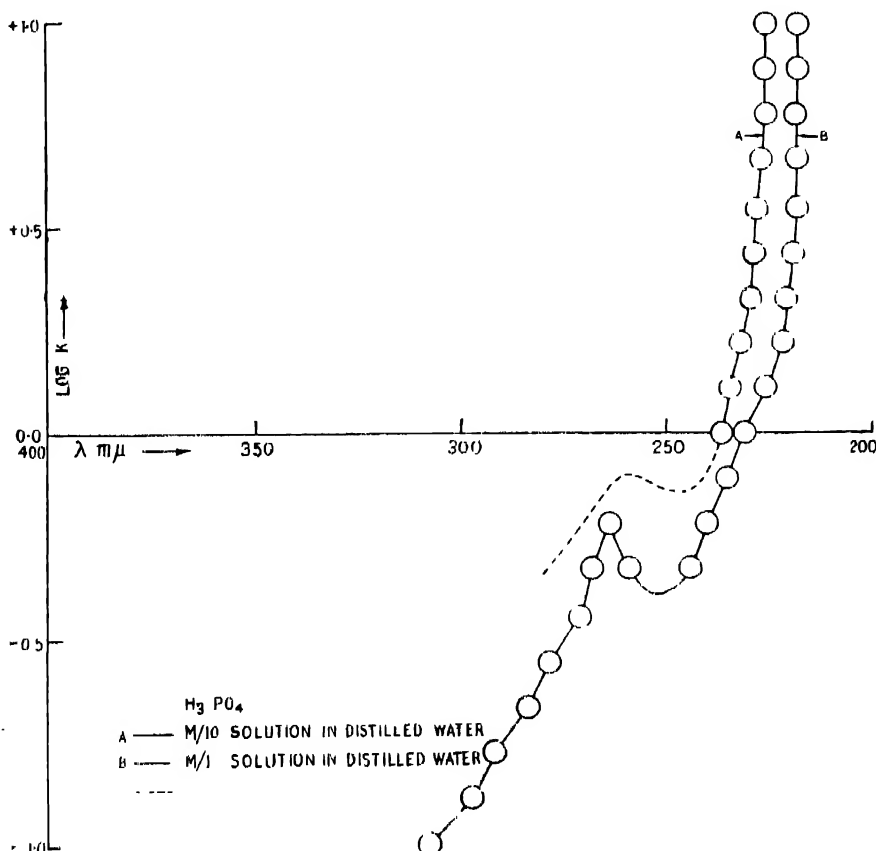


FIGURE 3

Again  $\text{KPO}_3$ , obtained by calcinating  $\text{KH}_2\text{PO}_4$ , shows an exactly similar absorption curve in the vapour state and we conclude that the isolated molecules  $\text{HPO}_3$  and  $\text{KPO}_3$  are both covalent and resemble strongly the corresponding nitrogen compounds, whereas the results obtained in solution are not quite conclusive on account of the transformation to orthophosphoric acid and the existence of a polymeric form.

Attention may now be drawn to the ortho-acid. It possesses a steep and small maximum at  $\lambda 2630$  for  $c=1^{\circ}$  which slowly disappears on dilution. From the constants of electrolytic dissociation,  $k_1=1.1 \times 10^{-2}$ ;  $k_2=5.6 \times 10^{-8}$ ; and  $k_3=1.2 \times 10^{-12}$ , it is obvious that with dilution the equilibrium of the solution is shifted in the order  $\text{H} + \text{H}_2\text{PO}_4^- \rightarrow 2\text{H} + \text{HPO}_4^{2-} \rightleftharpoons 3\text{H} + \text{PO}_4^{3-}$ . This maximum, therefore, belongs to the  $\text{H}_2\text{PO}_4^-$  ion.

In solutions of  $\text{KH}_2\text{PO}_4$  the same maximum lies at  $\lambda 2700$  and in  $\text{K}_2\text{HPO}_4$  at  $\lambda 2860$ . In those of  $\text{K}_3\text{PO}_4$  it lies at  $\lambda 2720$ , but is much broadened and it is known that solutions of  $\text{K}_3\text{PO}_4$  contain various ions, particularly  $\text{H}_2\text{PO}_4^-$  ions, on account of hydrolysis. Provisionally we correlate this maximum to the  $\text{P}-\text{O}$  bond, which we take as the chromophoric group producing selective absorption at about  $\lambda 2700$ .

The covalent molecules on the other hand, i.e.,  $(\text{C}_2\text{H}_5)_3\text{PO}_4$ ,  $(\text{C}_2\text{H}_5)_2\text{HPO}_4$  and  $\text{H}_3\text{PO}_4$  possess a diffuse absorption region only in the vapour state with a point of inflection at about  $\lambda 2500$ .

A first survey, therefore, leads to the conclusion that conditions are very much the same as in the nitrates. These show selective absorption with a maximum at  $\lambda 3000$  as long as the O—M bond is electrovalent, but a continuous end-absorption with a point of inflection at about  $\lambda 2650$  only, as soon as this bond is of covalent nature. In the same manner we obtain a maximum at  $\lambda 2630$  in solutions of  $\text{HPO}_4^2-$  and similar maxima due to the various ions formed by  $\text{H}_3\text{PO}_4$  dissolved in water, but continuous end-absorption only in the vapours of  $\text{KPO}_4$ , the two acids and their organic esters. The main difference which still has to be

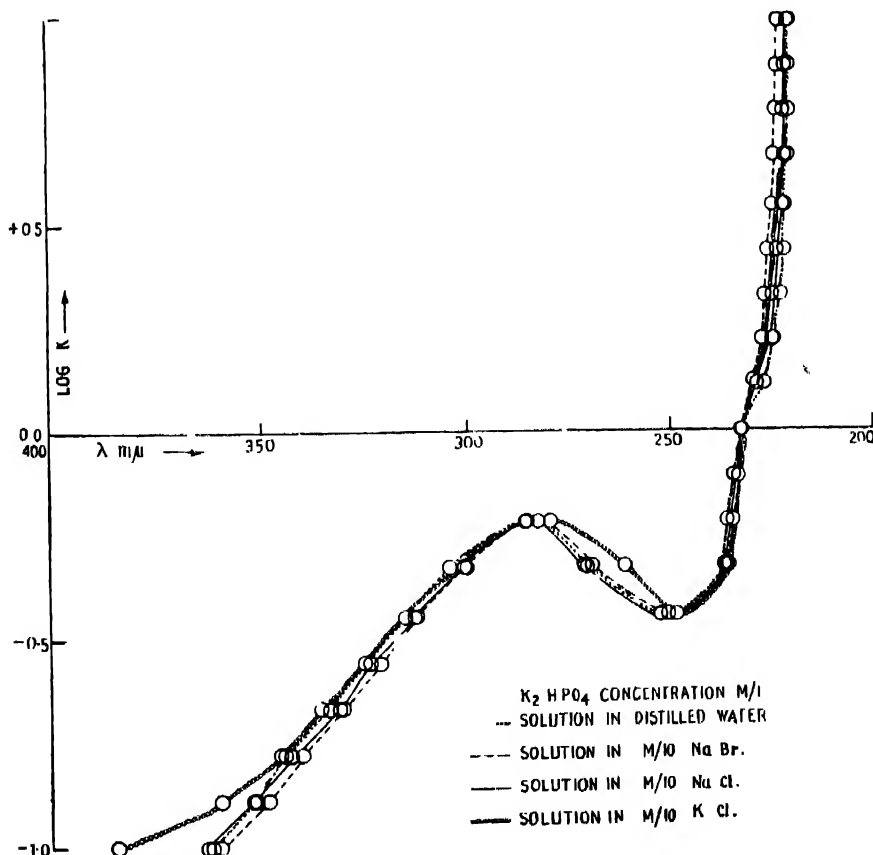


FIGURE 4

accounted for, is that the maximum of the nitrate ion always shows the same wavelength in the same solvent whereas here the wave-length varies. This fact appears to be connected with the varying number of P—O—M bonds in the same molecule.

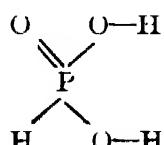
In order to establish that indeed an anion acts as chromophoric group for the maximum at about  $\lambda_{2700}$ , we have measured the absorption of  $K_2HPO_4$  in aqueous solutions in the presence of various foreign ions. In water alone the maximum lies at  $\lambda_{2870}$  (fig. 4); in a solution of NaBr (the concentration of NaBr being 0·1) at  $\lambda_{2840}$ ; in NaCl solution of concentration 0·1 at  $\lambda_{2850}$ , these two curves being close together. In a solution of KCl of concentration 0·1 the maximum is at  $\lambda_{2800}$  and this curve is quite clearly shifted towards the shorter wave-lengths. This shows that the change of the positive ion produces a change in the absorption curve whereas a change in the negative ion Cl or Br has little or no influence. The chromophoric group, therefore, will be a negative ion, since particularly at such low concentrations, only a negative ion can be surrounded by a cloud of positive ions like those of  $Na^+$  or  $K^+$ .

Finally the results in solutions of  $c=0\cdot1$ , compared with those of  $c=1\cdot0$  which have been listed above, show that the selective maximum increases in intensity (log  $k$  values) with dilution in all compounds, none of them obeying Beer's law. This certainly indicates that the maximum belongs to an electrovalent form, the percentage of which is increased with dilution.

Hence it is assumed that also  $H_2PO_4^-$  and its salts behave exactly like  $HNO_3$  and  $HPO_4^{2-}$  and their salts respectively. The electrovalent form possesses a sharp selective maximum in the quartz ultra-violet, the covalent a diffuse one only at shorter wave-lengths. With increasing concentration the number of molecules of the covalent form increases. In the vapour state the ortho-acid is entirely covalent and so are its organic esters. The fact that each molecule can possess more than one electrovalent bond does not essentially change the behaviour of the molecule.

This conclusion is supported by the fact that also pyro-phosphoric acid  $H_4P_2O_7 = HO_2=P=\overset{\parallel}{O}=\overset{\parallel}{O}—P(OH)_2$  shows a similar maximum at  $\lambda_{2550}$

although here one of the OH bonds is replaced by an O—P bond. Moreover also  $K_2HPO_4$ , i.e., the ion  $HPO_4^{2-}$  must have essentially the same structure since it shows a similar maximum at  $\lambda_{2970}$ . This agrees very well with the dibasicity of the acid known from chemical reactions and thermochemical experiments and is a further indication that phosphorous acid is a derivative not of trivalent but of pentavalent phosphorus with the formula



About the difference in the actual position of the maxima not much can be said. It is obvious that again the various effects, described in a previous paper,<sup>5</sup> will play a rôle and will counter-act each other. We may assume that both the solutions of  $\text{KH}_2\text{PO}_4$  and  $\text{H}_3\text{PO}_4$  will be made up in the main by  $\text{H}_2\text{PO}_4^-$  ions, the maxima, however, are not at the same position but at  $\lambda\lambda$  2760 and 2630 respectively. This will be due to the fact, that the one solution contains  $\text{K}^+$ , the other  $\text{H}^+$  ions. The hydrogen ion will collect a greater number of water molecules and, therefore, have the bigger dehydrating effect, which, as has been seen, is bound to shift the maximum towards shorter wave-lengths. On the other hand the maximum of  $\text{K}_2\text{HPO}_4$ , i.e., of the  $\text{HPO}_4^{2-}$  ion lies at still longer waves, viz.  $\lambda$  2860. This must be due to the deforming influence by which the two ionic bonds act on each other. It has been seen in part I that according to the rule of Fajans and Joos a negative ion in the field of a positive one consolidates its electronic structure and all energies of excitation getting increased, the maxima are shifted towards shorter waves. This is the normal behaviour of ions of unlike charges forming pairs in strong solutions. Here now it happens that two negative ions of like charge are kept together and cannot increase the distance between them because both belong to the same complex molecule. The opposite condition, therefore, becomes true; the electronic configuration gets loosened and the maximum for that molecule which possesses two electrovalent bonds is shifted towards red if compared with that which exhibits only one of them. These few remarks, however, do not aim at an explanation; the amount of available data is still much too small and theoretical interpretation of this more complicated phenomenon cannot be given. It just shows in which direction an explanation should be looked for at a later date.

One fact, however, appears to be worthy of note. Generally it is found that the spectra of homologous molecules, as a whole, shift towards longer waves with increasing mass and decreasing excitation or bond energies. Numerous examples, from the halogen molecules to the complicated organic molecules, can be quoted as instances. Here, however, we see that the selective absorption of the electrovalent form as well as the continuous end-absorption of the covalent form are at shorter waves than those of the nitrates. For these it has been assumed provisionally that the spectra correspond to a splitting-off of an oxygen atom which occurs for the covalent form, e.g.,  $\text{N}_2\text{O}_5$  or nitro-compounds with an energy of 69 K cal/mol. Reliable thermochemical data for a comparison with the corresponding compounds of phosphorus are not available. The heat of formation of  $1/2 \text{P}_2\text{O}_5$  is measured to 185 K cal/mol but for  $1/2 \text{Q}(\text{P}_2\text{O}_3)$  Mellor mentions two values of Berthelot and Ogier respectively, i.e., 37 and 122 K cal/mol, and both are given as unreliable. It can be seen, however, that the energy difference  $1/2 \text{D}(\text{P}_2\text{O}_5) - 1/2 \text{D}(\text{P}_2\text{O}_3)$  with both figures yields a value higher than the corresponding value of 69 K cal/mol for nitrates.

Setting up Born's cycle to obtain the atomic energies of formation for both

the molecules, all figures will cancel with the exception of  $1/2 D(O_2)$  and the energies of sublimation of the two molecules. Assuming the latter ones to be of the same order, we form the differences of the Q values, i.e.,  $185 - 37 = 148$  and  $185 - 122 = 63$  and add  $1/2 D(O_2) = 58$ . The energy for the splitting-off of an oxygen atom will, therefore, be on the basis of these figures; either 206 or 121 K cal/mol, i.e., higher than for the nitrates. This may explain the shift of the spectrum towards shorter waves, but, of course, it does not explain why the P=O bond shall be stronger than the N=O bond. Other thermochemical data are, however, not available for compounds formed by trivalent phosphorus. In view of the fact, however, that the absorption is connected essentially with the bond between oxygen and metal (or hydrogen) and that the structure of the molecule plays a small rôle only, to our mind it is by no means clear yet whether the dissociation process really concerns a P=O bond.

The main result of the present piece of work, therefore, is that between the acids, salts and esters formed by phosphorus and those formed by nitrogen there is no essential difference in behaviour or structure. This is quite interesting in itself. As has been mentioned in part I, there exists in chemistry a school of thought that claims an exception for the atoms of the period Li to F which shall exhibit fewer covalencies than those of the higher periods, e.g., Na to Cl. This exception originally derived from the octet rule appeared to be supported by certain wavemechanical considerations of London. According to the theory of Heitler<sup>3</sup> and London<sup>4</sup>, chemical combination is brought about by the coupling of spin vectors of the constituent atoms. Since the maximal population of a p shell is six, only three electrons with unpaired spins are possible in it and any numerical valency higher than three has to make use of the next d shell, e.g., sulphur in its ground level  $3s^2 3p^4$  possesses only two electrons with unpaired spin, the other two p electrons forming a closed orbital and London assumed that tetra valency of S involves the configuration  $3s^2 3p^3 3d$ . Phosphorus with  $3s^2 3p^3 4s$  is accordingly trivalent and becomes pentavalent only by fissuring the  $s^2$  group. The excitation of an s electron, however, does not bring it to  $3p$  where it would counterbalance the spin of one of the other ones but yields according to this conception the configuration  $3s 3p^3 3d$ . Since a 2d shell does not exist, a similar procedure is not possible for nitrogen and it was thought that this supports a theory in which N is not able to exhibit five covalent bonds while this is possible for P. The whole conception is, however, not quite correct. It is valid for diatomic molecules only and indeed the higher number of p-p bonds ever observed in diatomic molecules is three. In polyatomic molecules, however, where the field possesses more than one favoured direction, other rules for the unpairing of spins are brought about by Pauli's principle. This can be seen, e.g., from the ground level of  $S_2$ , which possesses two unpaired electrons inspite of the fact that it involves two S atoms in their ground level in which no d electron is present. Indeed such a modification of London's conception for poly-atomic

molecules has already been made use of and will be discussed in detail in a forthcoming paper from this laboratory. In poly-atomic molecules the  $p$  shell can exhibit up to five  $p-p$  bonds according to the number of  $p$  electrons present and pentavalency obtains for P from the configuration  $3s\ 3p^4$  and for N from  $2s\ 2p^4$ . There is no difference any longer between these atoms and no difference in behaviour can be expected. It is gratifying to note that such a difference at least is not supported by the absorption spectra of various acids of pentavalent phosphorus and its salts.

PHYSICS DEPARTMENT,  
MUSLIM UNIVERSITY,  
ALIGARH.

#### R E F E R E N C E S

- <sup>1</sup> J. Franck, *Trans. Farad. Soc.*, **21**, 526 (1925) and literature mentioned there.
- <sup>2</sup> M. I. Haq and R. Samuel, *Proc. Ind. Acad. Sc.*, **3**, 487 (1936).
- <sup>3</sup> *Proc. Ind. Acad. Sc.*, **3**, 390 (1936).
- <sup>4</sup> R. Lau, *Zs. f. Inst. Kunde*, **48**, 284 (1928) und **60**, 581 (1930).
- <sup>5</sup> See ref. 2.
- <sup>6</sup> W. Heitler and F. London, *Z. f. Phys.*, **44**, 155 (1927); F. London, *Z. f. Phys.*, **46**, 455 (1928).



# LINEAR EXTENSION OF REFLECTED IMAGE PRODUCED BY A SURFACE TRAVERSED BY WAVES

By F. C. AULUCK

Lecturer in Mathematics, Dyal Singh College, Lahore

*(Received for publication, August 22, 1930)*

**ABSTRACT.** The formation of the image of a light source by reflection at a sheet of disturbed water has been investigated theoretically. The image is extended and the extension has been expressed in terms of the angle subtended by the image at the eye. Expressions have been derived for this extension for two different conditions, *viz.*, (a) when the observer is facing the source, and, (b) when his back is towards the source.

1. It is a matter of common experience that the image of a light source in a sheet of disturbed water appears to be extended. This extension depends upon the nature of the waves produced by the disturbance and the positions of the observer and the source. We shall consider the extension as measured by the angle subtended by the image at the eye. It is the object of this paper to study this angle of extension. The intensity and the state of polarisation of the reflected light will be studied in the papers to follow. For the sake of simplicity we shall take simple harmonic waves and the observer in the plane containing the source and the direction of propagation of waves.

2. In what follows  $h_1$  and  $h_2$  denote the heights of the observer O and the source of light S respectively above the undisturbed surface. Let  $d$  denote the horizontal distance between S and O. The axis of  $x$  is taken in the undisturbed surface in the direction of propagation of the waves and the axis of  $y$  vertically upwards through O.  $y=f(x)$  is the equation of the section of the disturbed surface by the plane (xy).

There are two methods of dealing with the problem :—

(i) Find the caustic for the given curve  $y=f(x)$  and the given position of the source. Then find the angle between the tangents drawn to the caustic from the point of observation.

(ii) Find the family of aplanatic\* curves for the points S and O, and then the points where the given curve  $y=f(x)$  touches any aplanatic curve. Light striking at such points will, after reflection, pass through O. We, then, find the maximum angle subtended at O.

\* An aplanatic curve for S and O is such that any ray from S after reflection at the curve must pass through O. Any ellipse with S and O for its foci is an aplanatic curve.

We shall use the second method in this paper.

3.  $P(x, y)$  is a point on the given curve  $y=f(x)$ . Let the tangent at  $P$ ,  $PO$  and  $SP$  make angles  $\psi$ ,  $\alpha$  and  $\beta$  with the positive direction of the axis of  $x$ .

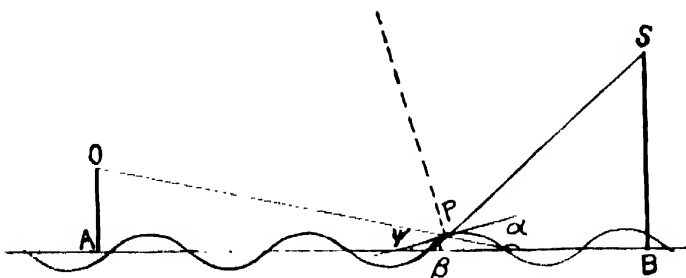


FIGURE 1

Then assuming the laws of reflection we obtain

$$2\psi = \alpha + \beta + \pi, \quad \alpha + \beta, \quad \text{or} \quad \alpha + \beta - \pi.$$

In all these three cases

$$\tan 2\psi = \tan (\alpha + \beta) \quad \dots \quad (1)$$

It may be remarked here that by taking tangents of both sides of the above equation, we have introduced an ambiguity. If of a value of  $\psi$ , say  $\psi_0$ , satisfies the equation (1),  $\psi_0 + \frac{\pi}{2}$  will also satisfy it.

Now

$$\left. \begin{aligned} \tan \alpha &= \frac{h_1 - y}{x} \\ \tan \beta &= \frac{h_2 - y}{d - x} \end{aligned} \right\} \quad \dots \quad (2)$$

and since  $p \equiv \frac{dy}{dx} = \tan \psi$ , equation (1) reduces to

$$\frac{2p}{1 - p^2} = \frac{x(h_1 + h_2 - 2y) - (h_1 - y)d}{(h_1 - y)(h_2 - y) + xd - x^2} \quad \dots \quad (3)$$

This is the differential equation for the family of aplanatic curves for the points  $S$  and  $O$ .

A simple harmonic progressive wave is represented by

$$y = a \sin \theta$$

where  $\theta = \frac{2\pi}{\lambda}(x - vt)$ ,  $a$  the amplitude,  $\lambda$  the wave-length,  $v$  the velocity of wave propagation and  $t$  the time. We have now to find out the points where any aplanatic curve touches the given curve. In equation (3), therefore, we substitute

$y = a \sin \frac{2\pi}{\lambda} (x - vt) = a \sin \theta$  and  $p = \frac{dy}{dx} = \frac{2\pi a}{\lambda} \cos \theta$  and thus obtain

$$\frac{\frac{4\pi a}{\lambda} \cos \theta}{1 - \frac{4\pi^2 a^2}{\lambda^2} \cos^2 \theta} = \frac{x(h_1 + h_2 - 2a \sin \theta) - (h_1 - a \sin \theta)d}{(h_1 - a \sin \theta)(h_2 - a \sin \theta) + xd - x^2} \quad (4)$$

For a given value of  $t$ , say  $t_0$ , the solution of (4) will give us those values of  $x$  where an aplanatic curve touches the displacement curve  $y = a \sin \frac{2\pi}{\lambda} (x - vt_0)$  at time  $t_0$ . Alternatively, if (4) is solved for any given value of  $\theta$ , say  $\theta^*$ , then the solution will represent those values of  $x$  where an aplanatic curve touches the displacement curve at time  $t^*$  such that

$$\frac{2\pi}{\lambda} (x^* - vt^*) - \theta^* \quad (5)$$

and at time  $t^*$ , therefore, a ray reflected at  $x^*$  will be received at O making with the horizontal an angle  $a$ , where

$$\tan a = - \frac{h_1 - a \sin \theta^*}{x^*} \quad (6)$$

For every value of  $\theta$  we can, therefore, evaluate the points of contact between the displacement curve  $y = f(x)$  and an aplanatic curve and calculate the angles  $a$  that the rays reflected at these points and passing through O will make with the horizontal. But as we are interested in finding the maximum and minimum values of  $a$ , the angular extension of image being  $a_{\max} - a_{\min}$ , we can do this straightforwardly by substituting for  $x$  in (4) from (6), and then determine the maxima and minima of  $\tan a$ , treating  $\theta$  as an independent variable.

We shall assume that the amplitude of the waves is very small compared to the distance between the source and the observer. Then putting

$$\delta = \pi - a$$

and

$$\tan \delta = Z,$$

we have on substituting for  $x$  in equation (4) from equation (6)

$$q = \frac{(h_1 + h_2 - 2a \sin \theta)Z - Z^2 d}{(h_2 - a \sin \theta)Z^2 + Zd - (h_1 - a \sin \theta)} \\ = \frac{(h_1 + h_2)Z - Z^2 d}{h_2 Z^2 + Zd - h_1} + O\left(\frac{a}{d}\right) \quad (7)$$

where

$$q = - \frac{\frac{4\pi a}{\lambda} \cos \theta}{1 - \frac{4\pi^2 a^2}{\lambda^2} \cos^2 \theta} \quad (8)$$

Solving (7) for  $Z$  we have

$$Z = \tan \delta = \frac{h_1 + h_2 + qd \pm \sqrt{(h_1 + h_2 - qd)^2 + 4h_1 q(h_2 q + d)}}{2(h_2 q + d)} + O\left(\frac{a}{d}\right) \dots \quad (9)$$

Since  $\frac{a}{d} \ll 1$ , the maximum and minimum values of  $Z$  and hence  $\delta$  are not appreciably affected by omitting the second term  $O\left(\frac{a}{d}\right)$ , provided  $h_1$  and  $h_2$  are not both zero.

The equation

$$q = \frac{(h_1 + h_2)Z - Z^2 d}{h_2 Z^2 + Z d - h_1} \dots \quad (10)$$

represents a cubic curve in the plane  $(q, Z)$ . The cubic has the following three asymptotes

$$\left. \begin{aligned} q &= -\frac{d}{h_2} \\ Z &= \frac{\sqrt{d^2 + 4h_1 h_2} - d}{2h_2} \\ Z &= -\frac{\sqrt{d^2 + 4h_1 h_2} + d}{2h_2} \end{aligned} \right\} \dots \quad (11)$$

Every line parallel to  $q$ -axis cuts the cubic in one and only one point and every line parallel to  $Z$ -axis meets it in two points.

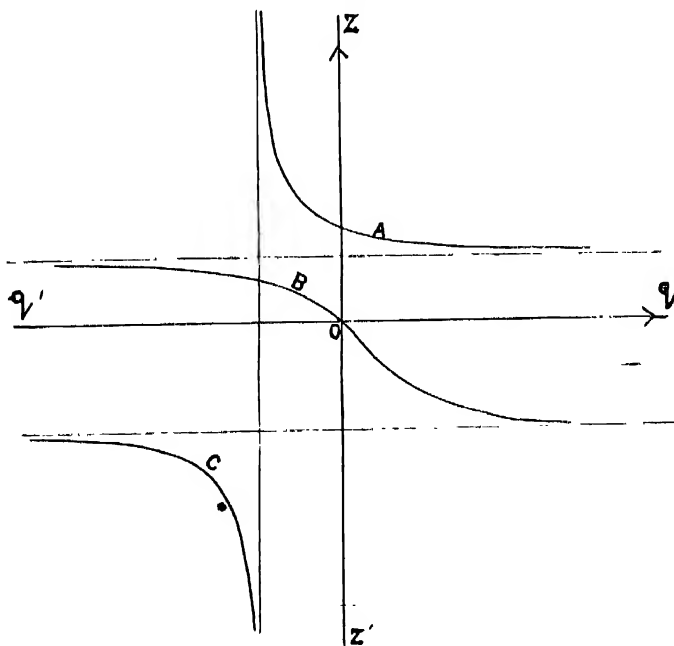


FIGURE 2

Consider the part of the cubic represented by

$$Z = \frac{h_1 + h_2 - qd + \sqrt{(h_1 + h_2 - qd)^2 + 4h_1 q(h_2 q + d)}}{2(h_2 q + d)} \quad (12)$$

It passes through the point  $(q=0, Z = \frac{h_1 + h_2}{d})$  and  $\frac{dq}{dz}$  at this point

$$= -\frac{(h_1 + h_2)d^2}{h_2\{(h_1 + h_2)^2 + d^2\}}. \text{ Hence } Z \text{ is a decreasing function of } q \text{ at this point.}$$

Moreover as  $q$  increases,  $Z$  increases and tends to the value  $\frac{\sqrt{d^2 + 4h_1 h_2} - d}{2h_2}$

as  $q \rightarrow \infty$ . It cannot increase at any point, for, then, we can find a value of  $Z$ , which will correspond to two values of  $q$ , which is impossible. When  $q$  decreases

from 0 to  $-\frac{h_2}{d}$  along this branch,  $Z$  increases and tends to  $\infty$  as  $q \rightarrow -\frac{h_2}{d}$ .

When  $q$  is less than  $-\frac{h_2}{d}$ ,  $Z$  is negative and increases from  $-\infty$  to

$$-\frac{d + \sqrt{d^2 + 4h_1 h_2}}{2h_2} \text{ as } q \rightarrow -\infty.$$

Now consider the curve

$$Z = \frac{h_1 + h_2 - qd - \sqrt{(h_1 + h_2 - qd)^2 + 4h_1 q(h_2 q + d)}}{2(h_2 q + d)} \quad (13)$$

It passes through the point  $(q=0, Z=0)$  and at this point  $\frac{dq}{dz} = -\frac{h_1 + h_2}{h_1}$ . It can

be shown that  $Z$  decreases from  $\frac{\sqrt{d^2 + 4h_1 h_2} - d}{2h_2}$  to  $-\frac{\sqrt{d^2 + 4h_1 h_2} + d}{2h_2}$

continuously as  $q$  varies from  $-\infty$  to  $\infty$ . In figure 2 A and C represent the equation (12) and B represents (13).

Now if the reflecting surface were a plane (i.e.,  $a=0$ ), there would have been only one point-image corresponding to  $q=0$ ;  $\tan \delta = \frac{h_1 + h_2}{d}$ . We shall take this as a boundary condition. Let  $\delta_{\max}$  and  $\delta_{\min}$  denote the maximum and minimum values of  $\delta$ .

#### Determination of $\delta_{\min}$

When  $\frac{a}{\lambda} < \frac{1}{2\pi}$ ,  $p$  can have all values between  $-\frac{2\pi a}{\lambda}$  and  $\frac{2\pi a}{\lambda}$  and  $q$

varies from  $-q_0$  to  $q_0$ ,

where

$$q_0 = \frac{\frac{4\pi a}{\lambda}}{1 - \frac{4\pi^2 a^2}{\lambda^2}}$$

To every value of  $q$ , there correspond two values of  $Z$ , one corresponding to  $p = \frac{2\pi a}{\lambda} \cos \theta$  and the other corresponding to  $p = -\frac{\lambda}{2\pi a \cos \theta}$ . The second must be rejected, for this gives  $|p| > 1$  which is a contradiction because  $|p| \leq \frac{2\pi a}{\lambda} < 1$ . Since when  $a=0$ ,  $q=0$  and  $\tan \delta = \frac{h_1 + h_2}{d}$ , the point  $(q, Z)$  moves on the branch A and therefore  $\delta_{\min}$  can be calculated by putting  $q=q_0$  in (12).

But when  $\frac{a}{\lambda} > \frac{1}{2\pi}$ ,  $q_0$  becomes negative. Putting  $q = \frac{1}{r}$ , the L. H. S. of (12) becomes

$$\frac{(h_1 + h_2)r - d + \sqrt{[(h_1 + h_2)r - d]^2 + 4h_1(h_2 + rd)}}{2(h_2 + rd)}.$$

Denoting this expression by  $f(r)$ , we notice that  $f(0) = -d + \frac{\sqrt{d^2 + 4h_1h_2}}{2h_2}$  which is not zero in general. Hence the radical does not change its sign as  $r$  passes through the value  $r=0$ . When  $r$  becomes negative and equal to  $-R$ ,

$$f(r) = \frac{(h_1 + h_2)R + d - \sqrt{[(h_1 + h_2)R + d]^2 + 4h_1(h_2 - Rd)}}{2(Rd - h_2)}$$

$$\begin{aligned} &= \frac{h_1 + h_2 + \frac{d}{R} - \sqrt{\left(h_1 + h_2 + \frac{d}{R}\right)^2 + 4\frac{h_1}{R}\left(-d + \frac{h_2}{R}\right)}}{2\left(d - \frac{h_2}{R}\right)} \\ &= \frac{h_1 + h_2 - qd - \sqrt{(h_1 + h_2 - qd)^2 + 4h_1q(h_2q + d)}}{2(h_2q + d)} \end{aligned}$$

where  $q$  is negative.

Hence if  $\frac{a}{\lambda} > \frac{1}{2\pi}$ ,  $\delta_{\min}$  is given by putting  $q=q_0$  in (13).

#### Determination of $\delta_{\max}$

An argument similar to that used above shows that when  $\frac{a}{\lambda} < \frac{1}{2\pi}$ ,  $\delta_{\max}$  is

calculated by putting  $q = -q_0$  in (12) and when  $\frac{a}{\lambda} > \frac{1}{2\pi}$ ,  $\delta_{\max}$  is given by putting  $q = -q_0$  in (13). Hence

$$\delta_{\max} = \tan^{-1} \left\{ \frac{h_1 + h_2 + q_0 d + e \sqrt{(h_1 + h_2)^2 + q_0^2 d^2 + 4h_1 h_2 q_0^2 + 2(h_2 - h_1) q_0 d}}{2(d - h_2 q_0)} \right\} \quad (14)$$

and

$$\delta_{\min} = \tan^{-1} \left\{ \frac{h_1 + h_2 - q_0 d + e \sqrt{(h_1 + h_2)^2 + q_0^2 d^2 + 4h_1 h_2 q_0^2 - 2(h_2 - h_1) q_0 d}}{2(d + h_2 q_0)} \right\} \quad (15)$$

where

$$e = +1 \quad \text{if } \frac{a}{\lambda} < \frac{1}{2\pi}$$

and

$$e = -1 \quad \text{if } \frac{a}{\lambda} > \frac{1}{2\pi}.$$

If

$$\frac{a}{\lambda} = \frac{1}{2\pi},$$

$$\delta_{\max} = \pi - \tan^{-1} \frac{\sqrt{d^2 + 4h_1 h_2 + d}}{2h_2}$$

and

$$\delta_{\min} = \tan^{-1} \frac{\sqrt{d^2 + 4h_1 h_2 - d}}{2h_2}$$

$\gamma = \delta_{\max} - \delta_{\min}$  is the angle of extension.

From (14) and (15) we deduce the following results :—

$$(i) \text{ If } h_1 = h_2, \quad \gamma = \tan^{-1} q_0.$$

In this case, the apparent extension is independent of the height of the observer and the distance between the source and the observer.

(ii) If  $h_2 = nh_1$  and  $n \neq 1$ ,  $\gamma$  depends upon  $n$ ,  $h_1$ , and  $d$ . Figures 3 and 4 show the relation between  $\gamma$  and  $\frac{h_1}{d}$  for  $n = \frac{1}{10}$  and 10. The curves become parallel for sufficiently large values of  $\frac{h_1}{d}$ .

(iii) Let  $n \rightarrow \infty$

$$\text{then} \quad \gamma \rightarrow 2 \tan^{-1} q_0 \quad \text{if } \frac{a}{\lambda} \geq \frac{1}{2\pi}$$

$$\text{and} \quad \gamma = \pi \quad \text{if } \frac{a}{\lambda} \geq \frac{1}{2\pi}$$

provided  $h_1 \neq 0$

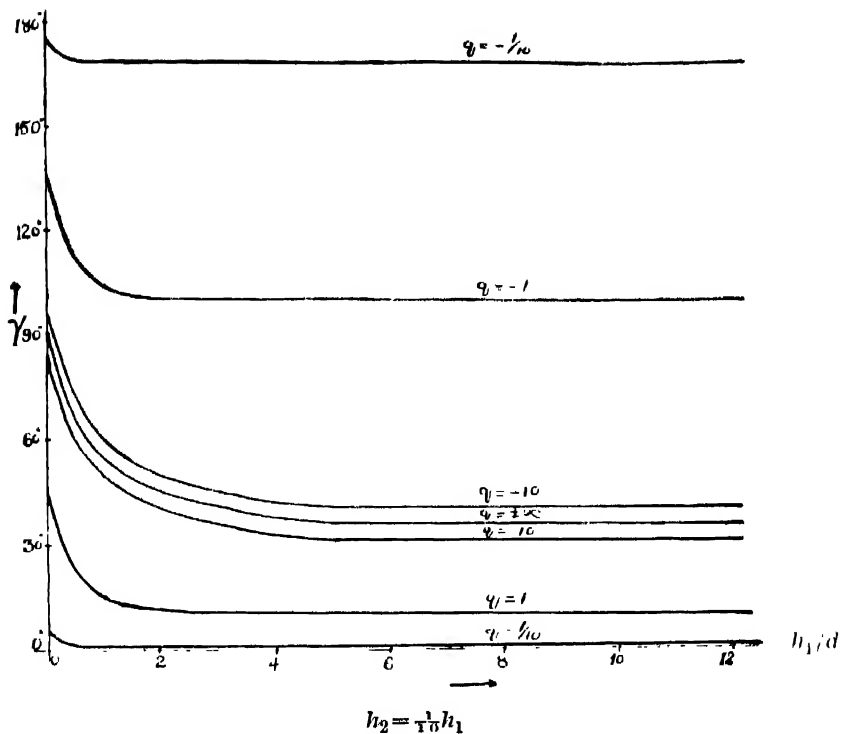


FIGURE 3

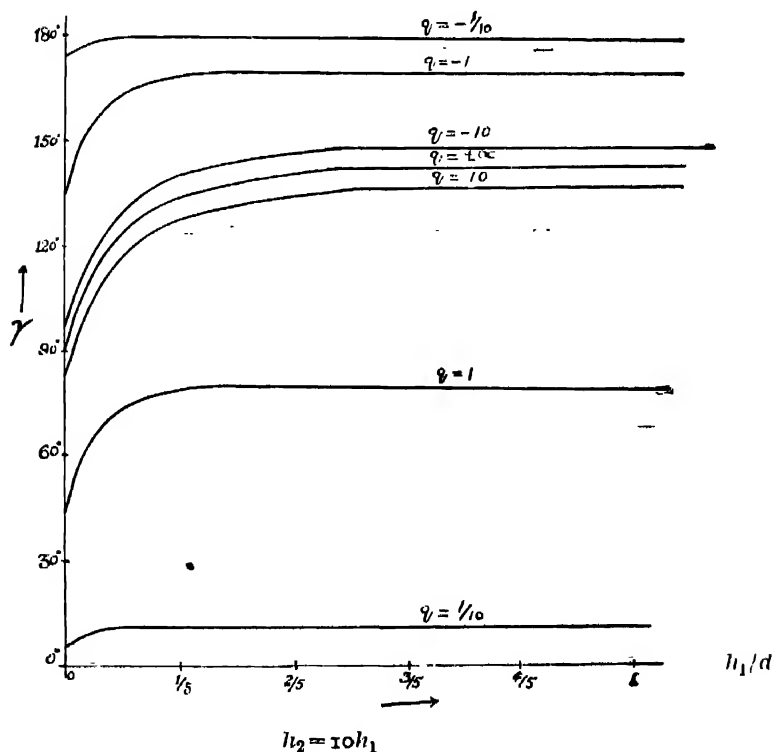


FIGURE 4

(iv) Let  $n \rightarrow 0$

$$(a) \text{ If } \frac{a}{\lambda} < \frac{1}{2\pi}$$

$$\gamma = 0 \quad \text{if } q_0 \leq \frac{h_1}{d}$$

and

$$\gamma = \tan^{-1} q_0 - \tan^{-1} \frac{h_1}{d} \quad \text{if } q_0 \geq \frac{h_1}{d}$$

$$(b) \text{ If } \frac{a}{\lambda} > \frac{1}{2\pi}$$

$$\gamma = \tan^{-1} q_0 - \tan^{-1} \frac{h_1}{d} \quad \text{if } q_0 \leq -\frac{h_1}{d}$$

and

$$\gamma = 2 \tan^{-1} q_0 - \pi \quad \text{if } q_0 \geq -\frac{h_1}{d}$$

$$(c) \text{ If } \frac{a}{\lambda} = \frac{1}{2\pi}$$

$$\gamma = \tan^{-1} \frac{d}{h_1}$$

(v) Now we shall consider the two cases .

(a) Observer facing the source.

(b) Observer with his back to the source.

(a) When the observer is facing the source, the maximum angle which the reflected ray through the eye of the observer can make with the horizontal is  $\frac{\pi}{2}$ .

The angle of extension is  $\delta_{\max} - \delta_{\min}$  if  $q_0 < \frac{d}{h_2}$  and is  $\frac{\pi}{2} - \delta_{\min}$  if  $q_0 > \frac{d}{h_2}$  or if  $q_0$  is negative.

(b) In this case the minimum value of  $\delta$  can be  $-\frac{\pi}{2}$ . The image cannot be

observed if  $q_0$  is less than  $\frac{d}{h_2}$  and positive. If  $q_0$  is greater than  $\frac{d}{h_2}$ , or is nega-

tive, the extension  $= \delta_{\max} - \frac{\pi}{2}$ .

It is a pleasure to record my thanks to Dr. D. S. Kothari (University of Delhi) for suggesting the problem and helpful discussions.



# ISOTOPE EFFECT IN THE BAND SPECTRUM OF TIN MONOXIDE

By P. C. MAHANTI

AND

A. K. SENGUPTA

(Received for publication, September 20, 1939)

## Plate XVII

**ABSTRACT.** From high-dispersion spectrograms of the (0,1) band of the A system of tin monoxide, quantitative evidence of the existence of less abundant tin isotopes of masses 116, 118, 122 and 124 has been secured. The observed intensities of the different isotopic lines are in most cases in conformity with their relative abundances. But no trace of lines due to isotopes of masses 117 and 119, which according to the mass spectrograph data of Aston, are more abundant than the isotopes of masses 122 and 124, could be found even in regions in which they are expected to be resolved from the neighbouring isotopic lines.

## INTRODUCTION

Tin, according to the recently corrected mass-spectrograph results of Aston,<sup>1</sup> consists of ten isotopes, whose atomic weights and relative abundances (given in parentheses in percents) are as follows :—112(1.1), 114(0.8), 116(15.5), 117(9.1), 118(22.5), 119(9.8), 120(28.5), 122(5.5) and 124(6.8).

It is, therefore, to be expected that in the spectra of the diatomic molecules of different tin compounds, the branch lines situated favourably in a band with respect to its origin as well as to the system-origin, should be split up, under suitable dispersion, into ten components due to tin isotopes alone. Each band head should also be resolved into a similar number of isotopic heads. Of these isotopic components of branch lines or of heads, at least five should be more prominent than the others. But, if the dispersion employed is relatively low, one is not likely to observe more than a broadening or diffuseness of the branch lines or of heads owing generally to the small magnitude of the separation between the different isotopic components.

Using a dispersion of about 7.4 A.U. per mm. in the first order of a 2'4 m. concave grating, such a broadening or diffuseness due to unresolved tin-isotope effect was first noticed by Jevons<sup>2</sup> in 1926 in several band heads associated with SnCl<sup>35</sup> and SnCl<sup>37</sup> in the more refrangible band system of tin monochloride

(SnCl). In the meantime, band spectra due to SnO, SnS, SnSe, SnF and SnBr have been identified. Although the values of  $\nu$  for the various tin isotopes are larger for SnSe and SnBr than for the others, there is in literature no mention of tin-isotope effect on either the band heads or the structure lines in the spectra of these two molecules. But in cases of SnO, SnS and SnF, evidence for the existence of tin-isotope effect has been secured. Loomis and Watson<sup>3</sup> observed the heads of bands, particularly those remote from the system-origin, very diffuse in character, so much so, that it was difficult for them to obtain accurate measurements in such cases. In the spectrum of SnS, Rochester<sup>4</sup> also noticed several diffuse band heads and found the observed width of their diffuseness approximately equal to the calculated total spread of the isotope pattern due to the more abundant isotopes. He thus obtained a little more than qualitative evidence for the existence of tin-isotope effect. Very recently in the spectrum of SnF Jenkins and Rochester<sup>5</sup> have observed for the first time the resolution of the tin-isotope effect in band heads which are, in favourable cases, split up into five nearly, equally-spaced components. These components have been identified as due to tin isotopes of atomic weights, 116, 118, 120, 122 and 124 and their observed intensities are also in conformity with the relative abundances of these isotopes. Isotopic heads due to the two isotopes of atomic weights 117 and 119, which are, according to the mass-spectrograph data of Aston, more abundant than the isotopes of masses 122, and 124 have not, however, been observed by Jenkins and Rochester. They are very likely unresolved from the neighbouring isotopic heads. But it is of interest to ascertain whether they are actually unresolved or entirely absent. Hence it is desirable to search for their existence under conditions more favourable than what has hitherto been secured. Undoubtedly the study of isotope effect on the rotational structure of a band favourably situated with respect to the system-origin is very suitable for the purpose.

It may here be mentioned that Loomis and Watson, who photographed the far ultra-violet bands of SnO under high dispersions obtainable in the first and second orders of a 21-ft. concave grating, observed the isotope effect of tin on the structure lines. They found that, as one should expect theoretically, the branch lines of a band favourably situated with respect to the system-origin are fairly sharp and single in the region in which the vibrational and the rotational isotopic displacements exactly or approximately cancel each other. On the other hand, for a band for which these displacements are additive, the branch lines are generally diffuse in the neighbourhood of the origin, but a little away from it they are split up into about five components. Finally the isotope splitting becomes so large that the isotopic components of the successive lines greatly overlap each other, thereby rendering the structure analysis practically impossible. In the absence of such an analysis, it was not therefore possible for Watson and Loomis to identify the different isotopic components of the branch lines. Practically similar features have also been recently observed in the band structure of

the visible system of SnS by Shawhan,<sup>6</sup> who has evaluated the rotational constants of the molecule from the partially resolved structure of the (0,0) and (1,0) bands. It was, therefore, thought worthwhile to investigate the tin-isotope effect on the branch lines of the A system of tin monoxide in view of the simple structure of the bands which are of the two branch types involving a  $^1\Sigma \rightarrow ^1\Sigma$  transition, as has been reported recently by the authors.<sup>7</sup> From high-dispersion spectrograms it has been found that, as in the case of the visible SnS system, the branch lines of the (1,0) band are diffuse near the head, the width of their diffuseness gradually decreasing as one proceeds towards the tail because of the cancellation of the constant vibrational displacement by the gradually increasing rotational displacement due to the different tin isotopes. In the (0,0) band, the lines appear fairly sharp near the head but become increasingly diffuse towards the tail of the band. On the other hand, a little further from the head, the lines of the two branches of the (0,1) band are split up into a number of components, three of which are clearly discernible in most cases while two others can be definitely located in regions free from any overlapping of successive lines. The object of the present paper is to report, as far as possible, detailed results of measurements of the isotopic components in the two branches of this band, thus recording for the first time the resolution of Sn-isotope effect in band structure.

#### EXPERIMENTAL

The band under investigation was photographed in the first and second orders of a 21-ft. concave grating in a Paschen mounting. This grating is ruled with 30,000 lines per inch on a 6-inch ruled surface. The dispersion in the region  $\lambda 3480-\lambda 3520$  is about  $1.285 \text{ \AA/mm.}$  in the first order.

The light source employed was a carbon arc in air, the lower positive electrode containing chemically pure metallic tin. The arc was operated from a d.c. 220V circuit and a current of about 4 amps. developed the band with optimum intensity. With an effective exposure of about four hours, good first-order plates were obtained, while, in the second order, more than double this time was necessary. Fine-grained plates were used for securing the best definitions of the structure lines.

Using iron-arc lines as standards of comparison, measurements were made on a Gaertner comparator (M1201A) readable directly to 0'001 mm. and estimable to 0'0001 mm. Several sets of measurements on independent plates were carried out and reduced to wave-lengths in the usual manner. In most cases the individual wave-length data do not differ from their mean value by more than 0'005  $\text{\AA}$  for any particular line. Reductions to vacuum wave-numbers were made with the aid of Kayser's "Schwingung Zahlen."

*The Theory of Isotopic Separations*

From the theory of isotope effect in electronic band spectra of diatomic molecules, it is now well known that in a  $v'$ ,  $v''$ -band due to a mixture of two isotopic molecules, the lines in a given branch of the less abundant one, although similar to those of the more abundant molecule, are weaker in intensity and displaced from them in position. The lines due to the more abundant molecule are easily measurable because of their intensity. They are, therefore, used as points of reference for the measurement of the isotopic displacement which is the wave-number interval between lines with the same J- or K-numbering for a particular branch in the band.

According to the theory, the difference in the total energy of two isotopic molecules in a given electronic state is given by

$$\begin{aligned} E^i - E \\ = (E_e^i - E_e) + (E_v^i - E_v) + (E_r^i - E_r), \end{aligned} \quad \dots \quad (1)$$

and the corresponding difference in energy terms is

$$\begin{aligned} T^i - T \\ = (T_e^i - T_e) + (G^i - G) + (F^i - F). \end{aligned} \quad \dots \quad (2)$$

Hence the isotopic displacement,  $v^i - v$ , of a line in a given  $v'$ ,  $v''$ -band is

$$\begin{aligned} v^i - v \\ = (T_e^i - T_e) - (T' - T'') \\ = (v_e^i + v_v^i + v_r^i) - (v_e + v_v + v_r) \\ = (v_e^i - v_e) + (v_v^i - v_v) + (v_r^i - v_r). \end{aligned} \quad \dots \quad (3)$$

In general, the electronic isotope displacement,  $v_e^i - v_e$ , is negligibly small in magnitude. Hence, for all practical purposes, the observed isotopic displacement of a line may be assumed to be the algebraic sum of only the vibrational and rotational displacements.

The vibrational isotopic displacement,  $v_v^i - v_v$ , of a given  $v'$ ,  $v''$ -band is expressed in several ways, the exact expression being

$$\begin{aligned} v_v^i - v_v \\ = (\rho - 1) [\omega_e'(v' + \frac{1}{2}) - \omega_e''(v'' + \frac{1}{2})] \\ - (\rho^2 - 1) [\omega_e' \omega_e'(v' + \frac{1}{2})^2 - \omega_e'' \omega_e''(v'' + \frac{1}{2})^2] + \dots \end{aligned} \quad \dots \quad (4)$$

But for a band with low values of both  $v'$  and  $v''$ , the displacement can be calculated with sufficient accuracy by the help of the following approximate equation :

$$\begin{aligned} v_v^i - v_v \\ \therefore (\rho - 1) \times \Delta v_v, \end{aligned} \quad \dots \quad (5)$$

where  $\Delta v_v$  is the wave-number interval between the band-origin,  $v_v$ , and the system-origin,  $v_e$ . It is thus evident that the vibrational isotopic displacement is the

same for the head as for the origin of a band and is therefore constant for a given band. But it changes in sign and magnitude according to the position of the band with respect to the system-origin.

The rotational isotopic displacement,  $\nu_r^i - \nu_r$ , of a line in a given branch of a band is expressed by

$$\begin{aligned} & \nu_r^i - \nu_r \\ & = (\rho^2 - 1) [B_r' N'(N' + 1) - B_r'' N''(N'' + 1)], \end{aligned}$$

neglecting the terms involving  $a$ ,  $D$  and higher powers of  $\rho$ . So that in a band due to  ${}^1\Sigma \rightarrow {}^1\Sigma$  transition,

$$\begin{aligned} & \nu_r^i - \nu_r \\ & = (\rho^2 - 1) [B_r' K'(K' + 1) - B_r'' K''(K'' + 1)]. \quad \dots \quad (6) \end{aligned}$$

But for a line of a  $K$ -value not very high, the rotational displacement can be calculated by the following approximate equation:

$$\begin{aligned} & \nu_r^i - \nu_r \\ & \doteq (\rho^2 - 1) \times \Delta\nu_r, \quad \dots \quad (7) \end{aligned}$$

where  $\Delta\nu_r$  is the wave-number interval between that line and the band-origin,  $\nu_0$ . Hence the rotational isotopic displacement vanishes at the band-origin and changes in sign and magnitude according to the position of a line of the main or more abundant molecule with respect to the band-origin.

The observed isotopic displacement of a line in a given branch of a  $v', v''$ -band is therefore the algebraic sum of the constant vibrational displacement and the varying rotational displacement, assuming the electronic effect to be negligible.

Equation (3) can now be expressed in terms of equations (5) and (7), so that we have

$$\begin{aligned} & \nu^i - \nu \\ & = [(\rho - 1)\Delta\nu_v + (\rho^2 - 1)\Delta\nu_r]. \quad (8) \end{aligned}$$

In equations (1) to (8), the different symbols have their usual significance<sup>8</sup> unless otherwise stated. The superscript  $i$  distinguishes the symbols associated with the less abundant molecule from those of the more abundant one. The value of  $\rho$  is given by

$$\begin{aligned} \rho & = \sqrt{\mu/\mu'} \\ & = \sqrt{\frac{MM'}{M + M'}} \sqrt{\frac{M'M'}{M' + M'}} \\ & = \sqrt{\frac{M(M' + M')}{M'(M + M')}}, \quad \dots \quad (9) \end{aligned}$$

where  $M$  and  $M'$  are respectively the masses of the more and less abundant isotopes of an atom.  $M'$  is the mass of other component atom of the diatomic molecule.  $M$ ,  $M'$  and  $M'$  may be replaced by the atomic weights  $A$ ,  $A'$  and  $A''$  respectively when calculating the actual masses.

It is now easily seen that if a band is due to a mixture of a number of isotopic molecules, then its head or its branch lines should be resolved under favourable conditions into the same number of components due to isotopes alone because of as many different values of  $\rho$ .

#### IDENTIFICATION OF TIN ISOTOPES

It has been noted in a previous section that in the high-dispersion spectrograms of  $(1,0)$ ,  $(0,0)$  and  $(0,1)$  bands of the  $\Lambda$ -system of tin monoxide, there exists definite indication of tin-isotope effect on their structure lines. In the  $(1,0)$  band which lies on the shorter wave-length side of the system-origin, the lines appear most diffuse near the head but as one proceeds towards the tail, the diffuseness decreases to a minimum and then tends to increase. On the other hand, the lines of the  $(0,0)$  band are comparatively sharper near the head than those away from it. These features are qualitatively in accord with the theoretical expectations when the dispersion employed is not large enough to resolve the isotopic components of the structure lines because of very low values of separations between the different components. In the  $(0,1)$  band (Fig. 1), however, the branch lines are resolved into a number of finer components. But there is so much overlapping and superposition between the components of the neighbouring P- and R-branch lines that it is very difficult to identify them merely from a visual inspection. In the region beyond  $\lambda 3500$ , where only the P-branch lines are prominent, the isotopic components are, however, easily discernible. They are found to occur in groups of four and further on towards the tail of five nearly-equally-spaced lines, the two high-frequency ones being much weaker than the other three which are almost of the same intensity. Hence this band offers the best opportunity for the identification of tin isotopes from a measurement of its structure lines.

Although considerable difficulty was experienced in sorting out the lines of the P- and R- branches associated with the main molecule,  $^{120}\text{SnO}$ , once this was achieved, it was then only a matter of calculation of the values of isotopic displacements,  $v^i - v$ , with respect to these lines for identifying those due to the less abundant molecules. On the low-frequency side of the band-origin, the displacement is positive for molecules heavier than  $^{120}\text{SnO}$  while it is negative for the lighter ones. In calculating the displacements, the values of  $v_e = 29630 \text{ cm.}^{-1}$  and  $v_o = 28687 \text{ cm.}^{-1}$ , obtained respectively from the vibrational analysis of the band system and from the structure analysis of the  $(0,1)$  band, have been



Figure 1.

A portion of the (0, 1) band of  $\text{SnO}$ , A-system.



used. The observed displacements together with their O-C values for the lines of the several less abundant isotopic molecules identified in the present investigation are given in Tables II and III. The values of  $\rho$  and  $\rho^2$  for these molecules are included in Table I. No consideration has, however, been made regarding the isotopic nature of oxygen atom, whose atomic weight is taken as 16.

TABLE I

Molecule	$\rho$	$\rho^2$
$^{184}\text{SnO}$	0.996101	0.996205
$^{187}\text{SnO}$	0.999000	0.998071
$^{118}\text{SnO}$	1.000996	1.001994
$^{116}\text{SnO}$	1.002027	1.004057

Finally the complete data of the structure lines of the band in question are included in Table IV.

TABLE II

Isotopic Displacements (in  $\text{cm}^{-1}$ ) in the R-branch

K	$^{184}\text{SnO}$		$^{123}\text{SnO}$		$^{118}\text{SnO}$		$^{116}\text{SnO}$	
	Obs.	O-C	Obs.	O-C	Obs.	O-C	Obs.	O-C
24	-	-	-	-	0.90	0.05	1.93	0.04
28	-	-	-	-	0.94	0.02	1.94	0.00
36	-	-	-	-	0.96	0.00	1.96	-0.01
27	-	-	-	-	0.98	-0.02	1.89	0.07
28	-	-	-	-	0.97	0.00	1.91	0.05
29	-	-	-	-	0.96	0.01	2.01	-0.07
30	-	-	-	-	0.98	-0.01	2.00	-0.04
31	-	-	-	-	0.98	0.00	(1.90)	(0.08)
32	-	-	-	-	1.00	-0.02	(1.96)	(0.03)
33	-	-	-	-	0.96	0.02	(2.08)	(0.08)
34	-	-	-	-	0.98	0.01	1.94	0.07
35	-	-	-	-	0.98	0.01	2.00	0.02
36	-	-	-	-	0.96	0.04	1.98	0.05

TABLE II (*contd.*)

K	$^{124}\text{SnO}$		$^{122}\text{SnO}$		$^{118}\text{SnO}$		$^{116}\text{SnO}$	
	Obs.	O-C	Obs.	O-C	Obs.	O-C	Obs.	O-C
		—		—		—		—
37	—	—	—	—	0.98	0.02	1.98	0.06
38	—	—	—	—	1.04	-0.03	2.05	0.00
39	—	—	—	—	0.98	0.03	2.04	0.01
40	—	—	—	—	1.00	0.02	2.06	0.01
41	—	—	—	—	1.02	0.00	2.07	0.01
42	—	—	—	—	1.03	0.00	2.08	0.01
43	—	—	—	—	1.05	-0.02	2.10	0.00
44	—	—	—	—	1.03	0.01	2.11	0.00
45	—	—	—	—	1.04	0.00	2.15	-0.03
46	—	—	—	—	1.02	0.03	2.18	-0.05
47	—	—	—	—	1.09	0.06	2.18	-0.03
48	—	—	—	—	1.01	0.05	2.14	0.02
49	—	—	—	—	1.05	0.02	2.13	0.04
50	—	—	—	—	1.08	-0.01	2.20	-0.01
51	—	—	—	—	1.08	0.00	2.20	0.00
52	—	—	—	—	1.11	-0.02	2.24	-0.03
53	—	—	—	—	1.12	-0.02	2.22	0.01
54	—	—	—	—	1.12	-0.02	2.23	0.01
55	—	—	—	—	1.12	-0.01	2.24	0.02
56	—	—	—	—	1.10	0.02	2.27	0.01
57	—	—	—	—	1.12	0.01	2.30	-0.01
58	—	—	—	—	1.08	0.06	2.32	-0.01
59	—	—	—	—	1.14	0.00	2.33	-0.01
60	—	—	—	—	1.14	0.01	2.31	0.03
61	—	—	1.22	-0.07	1.11	0.05	2.29	0.07
62	—	—	1.07	0.09	1.15	0.02	2.33	0.05
63	—	—	1.15	0.02	(1.21)	(-0.03)	2.40	0.00
64	—	—	1.23	-0.05	(1.11)	(-0.08)	2.33	0.08

TABLE III  
Isotopic Displacements (*in cm.<sup>-1</sup>*)  
in the P-branch

K	<sup>114</sup> SnO		<sup>112</sup> SnO		<sup>118</sup> SnO		<sup>116</sup> SnO	
	Obs.	O-C	Obs.	O-C	Obs.	O-C	Obs.	O-C
20	—	—	—	—	1'10	+0'10	—	—
21	—	—	—	—	1'08	+0'08	—	—
22	—	—	—	—	1'02	+0'01	—	—
23	—	—	—	—	1'06	+0'05	—	—
24	—	—	—	—	1'04	+0'03	—	—
25	—	—	—	—	0'90	-0'12	1'92	0'15
26	—	—	—	—	0'96	-0'07	1'99	0'09
27	—	—	—	—	1'05	-0'02	2'10	-0'01
28	—	—	—	—	1'05	-0'01	2'08	0'03
29	—	—	—	—	1'11	-0'07	2'15	-0'03
30	—	—	—	—	1'10	-0'05	2'12	0'01
31	—	—	—	—	1'06	-0'01	2'22	-0'08
32	—	—	—	—	1'08	-0'20	2'27	-0'12
33	—	—	—	—	1'08	-0'01	2'16	0'01
34	—	—	—	—	1'08	-0'01	2'18	0'00
35	—	—	—	—	1'11	-0'03	2'16	0'03
36	—	—	—	—	1'12	-0'03	2'22	-0'01
37	—	—	—	—	1'10	-0'01	2'21	0'01
38	—	—	—	—	1'10	0'00	2'22	0'02
39	—	—	—	—	1'11	0'00	2'25	0'00
40	—	—	—	—	1'11	0'01	2'28	-0'01
41	—	—	—	—	1'18	-0'06	2'27	0'01
42	—	—	—	—	1'13	0'00	2'29	0'01
43	—	—	—	—	1'14	0'00	2'42	-0'11
44	—	—	—	—	1'15	0'00	2'33	0'00
45	—	—	—	—	1'16	0'00	2'24	0'11

TABLE III (*contd.*)

K	<sup>114</sup> SnO		<sup>112</sup> SnO		<sup>116</sup> SnO		<sup>118</sup> SnO	
	Obs.	O-C	Obs.	O-C	Obs.	O-C	Obs.	O-C
46	-	-	-	-	1.16	0.00	2.40	-0.03
47	-	-	-	-	1.18	-0.01	2.36	0.02
48	--	--	1.21	-0.04	1.19	-0.01	2.37	0.03
49	--	-	1.11	0.07	1.22	-0.03	2.37	0.05
50	-	-	1.14	0.05	1.19	0.01	2.31	0.13
51	-	-	1.08	0.10	1.22	-0.01	2.52	-0.06
52	--	-	1.07	0.14	1.28	-0.06	2.51	-0.06
53	--	-	1.10	0.06	1.26	-0.03	2.55	-0.05
54	-	-	1.00	0.14	1.20	-0.04	2.57	-0.06
55	-	-	1.10	0.14	1.22	0.03	2.48	0.06
56	--	--	1.30	-0.05	1.32	-0.06	2.60	-0.04
57	--	-	1.19	0.07	1.29	-0.02	2.55	0.03
58	--	-	1.16	0.11	1.29	-0.01	2.61	-0.01
59	--	-	1.28	0.00	1.28	0.01	2.64	-0.02
60	-	-	1.41	-0.11	1.37	-0.07	2.64	0.00
61	-	-	1.33	-0.03	1.31	0.00	2.66	0.00
62	--	--	1.26	0.05	1.32	0.00	2.67	0.02
63	-	-	1.43	-0.11	1.35	-0.02	2.71	0.00
64	--	--	1.38	-0.05	1.35	-0.01	2.72	0.01
65	--	-	1.36	-0.02	1.41	-0.05	2.78	-0.02
66	--	--	1.48	-0.13	1.43	-0.06	2.69	0.09
67	-	-	1.29	0.08	1.32	0.06	2.83	-0.02
68	2.35	0.09	1.52	-0.14	1.47	-0.07	2.76	0.08
69	2.38	0.08	1.45	-0.06	1.39	0.02	2.81	0.05
70	2.34	0.14	1.28	0.12	1.41	0.01	2.86	0.03
71	2.32	0.18	1.24	0.18	1.42	0.01	2.81	0.10
72	2.43	0.09	1.34	0.09	1.45	0.00	2.91	0.03

TABLE III (contd.)

K	$^{124}\text{SnO}$		$^{122}\text{SnO}$		$^{118}\text{SnO}$		$^{116}\text{SnO}$	
	Obs.	O-C	Obs.	O-C	Obs.	O-C	Obs.	O-C
73	2.50	0.03	1.28	0.16	1.30	0.10	2.85	0.12
74	2.61	0.06	1.33	0.13	1.30	0.11	2.84	0.15
75	2.62	-0.05	1.27	0.20	1.41	0.08	2.88	0.14
76	2.72	-0.13	1.45	0.03	1.50	-0.08	2.07	0.08
77	2.74	-0.13	1.40	0.01	1.50	0.02	2.00	0.18
78	2.78	-0.15	1.46	0.05	1.50	0.03	2.00	0.11

TABLE IV

## Structure of (o,1) Band

Wave-numbers ( $\nu$ in cm. $^{-1}$ )	Identification	Wave-numbers ( $\nu$ in cm. $^{-1}$ )	Identification
28687.56	$^{120}\text{R}(16)$	28676.00	$^{118}\text{R}(26)$
86.84	$^{120}\text{R}(17)$	75.46	$^{120}\text{R}(27)$
86.06	$^{120}\text{R}(18)$	75.00	$^{116}\text{R}(26)$
85.20	$^{120}\text{R}(19)$	74.48	$^{118}\text{R}(27)$
84.26	$^{120}\text{R}(20)$	73.87	$^{110}\text{R}(28)$
83.24	$^{120}\text{R}(21)$	73.57	$^{116}\text{R}(27)$
82.14	$^{120}\text{R}(22)$	72.90	$^{116}\text{R}(28)$
80.97	$^{120}\text{R}(23)$	72.22	$^{120}\text{R}(29)$
79.72	$^{120}\text{R}(24)$	71.96	$^{116}\text{R}(28)$
78.82	$^{118}\text{R}(24)$	71.26	$^{118}\text{R}(29)$
78.38	$^{120}\text{R}(25)$	70.48	$^{120}\text{R}(30)$
77.80	$^{118}\text{R}(24)$	70.18	$^{116}\text{R}(29)$
77.44	$^{118}\text{R}(25)$	69.50	$^{118}\text{R}(30)$
76.96	$^{120}\text{R}(26)$	68.68	$^{120}\text{R}(31)$
76.44	$^{116}\text{R}(25)$	68.48	$^{116}\text{R}(30)$

TABLE IV (*contd.*)  
Structure of (0,1) Band

Wave-numbers ( $\nu$ in cm. <sup>-1</sup> )	Identification	Wave-numbers ( $\nu$ in cm. <sup>-1</sup> )	Identification
28667.70	$^{118}\text{R}(31)$	28550.28	$^{118}\text{R}(39)$
66.78	$^{120}\text{R}(32)$ ; $^{116}\text{R}(31)$	49.50	$^{120}\text{P}(24)$
65.78	$^{118}\text{R}(32)$	49.22	$^{116}\text{R}(39)$
64.82	$^{120}\text{R}(33)$ ; $^{116}\text{R}(32)$	48.72	$^{120}\text{R}(40)$
63.86	$^{118}\text{R}(33)$	48.52	$^{118}\text{P}(24)$
62.74	$^{120}\text{R}(34)$ ; $^{116}\text{R}(33)$	47.72	$^{118}\text{R}(40)$
61.70	$^{118}\text{R}(34)$	46.97	$^{120}\text{P}(25)$
60.80	$^{116}\text{R}(34)$	46.66	$^{116}\text{R}(40)$
60.60	$^{120}\text{R}(35)$	46.07	$^{120}\text{R}(41)$ ; $^{118}\text{P}(25)$
59.62	$^{118}\text{R}(35)$	45.95	$^{118}\text{R}(41)$ ; $^{116}\text{P}(25)$
58.96	$^{120}\text{P}(20)$	44.34	$^{120}\text{P}(20)$
58.60	$^{116}\text{R}(35)$	44.00	$^{116}\text{R}(41)$
58.36	$^{120}\text{R}(36)$	43.35	$^{120}\text{R}(42)$ ; $^{118}\text{P}(26)$
57.86	$^{118}\text{P}(20)$	42.35	$^{118}\text{R}(42)$ ; $^{116}\text{P}(26)$
57.40	$^{118}\text{R}(36)$	41.63	$^{120}\text{P}(27)$
56.72	$^{120}\text{P}(21)$	41.30	$^{116}\text{R}(42)$
56.38	$^{116}\text{R}(36)$	40.58	$^{120}\text{R}(43)$ ; $^{118}\text{P}(27)$
56.08	$^{120}\text{R}(37)$	39.53	$^{118}\text{R}(43)$ ; $^{116}\text{P}(27)$
55.64	$^{118}\text{P}(21)$	38.81	$^{120}\text{P}(28)$
55.10	$^{118}\text{R}(37)$	38.48	$^{116}\text{R}(43)$
54.44	$^{120}\text{P}(22)$	37.76	$^{120}\text{R}(44)$ ; $^{118}\text{P}(28)$
54.10	$^{116}\text{R}(37)$	36.73	$^{118}\text{R}(44)$ ; $^{116}\text{P}(28)$
53.72	$^{120}\text{R}(38)$	35.92	$^{120}\text{P}(29)$
53.42	$^{118}\text{P}(22)$	35.65	$^{116}\text{R}(44)$
52.68	$^{118}\text{R}(38)$	34.81	$^{120}\text{R}(45)$ ; $^{118}\text{P}(29)$
52.02	$^{120}\text{P}(23)$	33.77	$^{118}\text{R}(45)$ ; $^{116}\text{P}(29)$
51.67	$^{116}\text{R}(38)$	32.92	$^{120}\text{P}(30)$
51.26	$^{120}\text{R}(39)$	32.66	$^{116}\text{R}(45)$
50.96	$^{118}\text{P}(23)$	31.82	$^{120}\text{R}(46)$ ; $^{118}\text{P}(30)$

TABLE IV (contd.)

Wave-numbers ( $\nu$ in cm <sup>-1</sup> )	Identification	Wave-numbers ( $\nu$ in cm <sup>-1</sup> )	Identification
8630·80	$^{118}\text{R}(46)$ ; $^{116}\text{P}(30)$	28613·48	$^{120}\text{P}(36)$
29·92	$^{120}\text{P}(31)$	13·28	$^{118}\text{R}(51)$
29·64	$^{116}\text{R}(46)$	12·36	$^{118}\text{P}(36)$
28·86	$^{118}\text{P}(31)$	11·95	$^{120}\text{R}(52)$
28·70	$^{120}\text{R}(47)$	11·26	$^{118}\text{P}(36)$
27·70	$^{118}\text{R}(17)$ ; $^{116}\text{P}(31)$	10·81	$^{118}\text{R}(52)$
26·78	$^{120}\text{P}(32)$	10·00	$^{120}\text{P}(37)$
26·52	$^{116}\text{R}(47)$	09·71	$^{116}\text{R}(52)$
25·70	$^{118}\text{P}(32)$	08·90	$^{118}\text{P}(37)$
25·52	$^{120}\text{R}(48)$	08·32	$^{120}\text{R}(53)$
24·51	$^{118}\text{R}(48)$ ; $^{116}\text{P}(32)$	07·70	$^{116}\text{P}(37)$
23·50	$^{120}\text{P}(33)$	07·20	$^{118}\text{R}(53)$
23·38	$^{116}\text{R}(48)$	06·40	$^{120}\text{P}(38)$
22·51	$^{118}\text{P}(33)$	06·10	$^{116}\text{R}(53)$
22·23	$^{120}\text{R}(49)$	05·30	$^{118}\text{P}(38)$
21·43	$^{116}\text{P}(33)$	04·66	$^{120}\text{R}(54)$
21·18	$^{116}\text{R}(49)$	04·18	$^{116}\text{P}(38)$
20·28	$^{120}\text{P}(34)$	03·54	$^{118}\text{R}(54)$
20·10	$^{116}\text{R}(49)$	02·72	$^{120}\text{P}(39)$
19·20	$^{118}\text{P}(34)$	02·43	$^{116}\text{R}(54)$
18·00	$^{120}\text{R}(50)$	01·61	$^{118}\text{P}(36)$
18·10	$^{116}\text{P}(34)$	00·84	$^{120}\text{R}(55)$
17·82	$^{118}\text{R}(50)$	00·47	$^{116}\text{P}(30)$
16·96	$^{120}\text{P}(35)$	509·72	$^{118}\text{R}(55)$
16·70	$^{116}\text{R}(50)$	08·06	$^{120}\text{P}(40)$
15·85	$^{118}\text{P}(35)$	08·60	$^{116}\text{R}(55)$
15·48	$^{120}\text{R}(51)$	07·85	$^{118}\text{P}(40)$
14·80	$^{116}\text{P}(35)$	06·97	$^{120}\text{R}(56)$
14·40	$^{118}\text{R}(51)$	06·68	$^{116}\text{P}(40)$

TABLE IV (contd.)

Wave-numbers ( $\nu$ in cm. <sup>-1</sup> )	Identification	Wave numbers ( $\nu$ in cm. <sup>-1</sup> )	Identification
28595 S <sub>7</sub>	118R(56)	28574'80	120P(46)
95'12	120P(41)	73'90	116R(61)
94'70	118R(56)	73'64	118P(46)
93'94	118P(41)	72'83	122R(62)
93'00	120R(57)	72'40	116P(46)
94'85	118P(41)	71'76	120R(62)
91'88	118R(57)	70'61	118R(62)
91'23	120P(42)	70'42	120P(47)
90'70	118R(57)	69'43	118R(62)
90'10	118P(42)	69'24	118P(47)
88'94	120R(58); 116P(42)	68'43	122R(63)
87'86	118R(58)	68'06	116P(47)
87'22	120P(43)	67'48	120R(63)
86'62	118R(58)	66'07	120P(48); 118R(63)
86'08	118P(43)	64'88	118P(48); 116R(63)
84'80	120R(59); 116P(43)	63'91	122R(64)
83'66	118R(59)	63'70	116P(48)
83'15	120P(44)	62'68	120R(64); 122P(49)
82'47	116R(50)	61'57	120P(49); 118R(64)
82'00	118P(44)	60'35	118P(49); 116R(64)
80'82	116P(44)	59'20	116P(49)
80'54	120R(60)	58'15	122P(50)
79'40	118R(60)	57'01	120P(50)
79'00	120P(45)	55'82	118P(50)
78'23	116R(60)	54'70	116P(50)
77'84	118P(45)	53'16	122P(51)
77'41	122R(61)	52'38	120P(51)
76'76	116P(45)	51'16	118P(51)
76'19	120R(61)	49'86	116P(51)
75'08	118R(61)	48'71	122P(52)

TABLE IV (contd.)

Wave-numbers ( $\nu$ in cm. <sup>-1</sup> )	Identification	Wave-numbers ( $\nu$ in cm. <sup>-1</sup> )	Identification
28547.64	120P(52)	28509.38	116P(59)
46.36	118P(52)	08.00	122P(60)
45.10	116P(52)	06.59	120P(60)
43.97	122P(53)	05.22	118P(60)
42.81	120P(53)	03.95	116P(60)
41.55	118P(53)	02.39	122P(61)
40.26	116P(53)	01.06	120P(61)
39.00	122P(54)	499.75	118P(61)
37.91	120P(54)	98.40	116P(61)
36.63	118P(54)	96.69	122P(62)
35.34	116P(54)	95.43	120P(62)
34.04	122P(55)	94.11	118P(62)
32.92	120P(55)	92.76	116P(62)
31.70	118P(55)	91.13	122P(63)
30.44	116P(55)	89.70	120P(63)
29.14	122P(56)	88.35	118P(63)
27.84	120P(56)	86.99	116P(63)
26.52	118P(56)	85.26	122P(64)
25.24	116P(56)	83.88	120P(64)
23.84	122P(57)	82.53	118P(64)
22.65	120P(57)	81.16	116P(64)
21.36	118P(57)	79.30	122P(65)
20.10	116P(57)	77.94	120P(65)
18.67	122P(58)	76.53	118P(65)
17.41	120P(58)	75.16	116P(65)
16.12	118P(58)	73.39	122P(66)
14.80	116P(58)	71.91	120P(66)
13.30	122P(59)	70.48	118P(66)
12.02	120P(59)	69.22	116P(66)
10.74	118P(59)	67.07	122P(67)

TABLE IV (*contd.*)

Wave-numbers ( $\nu$ in cm. $^{-1}$ )	Identification	Wave-numbers ( $\nu$ in cm. $^{-1}$ )	Identification
28465.78	$^{120}\text{P}(67)$	28428.92	$^{124}\text{P}(73)$
64.46	$^{118}\text{P}(67)$	27.70	$^{122}\text{P}(73)$
62.95	$^{114}\text{P}(67)$	26.42	$^{120}\text{P}(73)$
61.17	$^{124}\text{P}(68)$	25.06	$^{118}\text{P}(73)$
60.34	$^{122}\text{P}(68)$	23.57	$^{116}\text{P}(73)$
58.82	$^{120}\text{P}(68)$	22.25	$^{124}\text{P}(74)$
57.35	$^{118}\text{P}(68)$	20.97	$^{122}\text{P}(74)$
56.06	$^{116}\text{P}(68)$	19.64	$^{120}\text{P}(74)$
54.92	$^{124}\text{P}(69)$	18.28	$^{118}\text{P}(74)$
53.99	$^{122}\text{P}(69)$	16.80	$^{116}\text{P}(74)$
52.54	$^{120}\text{P}(69)$	15.38	$^{124}\text{P}(75)$
51.15	$^{118}\text{P}(69)$	14.03	$^{122}\text{P}(75)$
49.73	$^{116}\text{P}(69)$	12.76	$^{120}\text{P}(75)$
48.60	$^{124}\text{P}(70)$	11.35	$^{118}\text{P}(75)$
47.54	$^{122}\text{P}(70)$	09.88	$^{116}\text{P}(75)$
46.26	$^{120}\text{P}(70)$	08.50	$^{124}\text{P}(76)$
44.85	$^{118}\text{P}(70)$	07.23	$^{122}\text{P}(76)$
43.40	$^{116}\text{P}(70)$	05.78	$^{120}\text{P}(76)$
42.00	$^{124}\text{P}(71)$	04.19	$^{118}\text{P}(76)$
40.92	$^{122}\text{P}(71)$	02.81	$^{116}\text{P}(76)$
39.68	$^{120}\text{P}(71)$	01.44	$^{124}\text{P}(77)$
38.26	$^{118}\text{P}(71)$	00.19	$^{122}\text{P}(77)$
36.87	$^{116}\text{P}(71)$	398.70	$^{120}\text{P}(77)$
35.43	* $^{124}\text{P}(72)$	97.21	$^{118}\text{P}(77)$
34.34	$^{122}\text{P}(72)$	95.80	$^{116}\text{P}(77)$
33.00	$^{120}\text{P}(72)$	94.30	$^{124}\text{P}(78)$
31.55	$^{118}\text{P}(72)$	92.98	$^{122}\text{P}(78)$
30.09	$^{116}\text{P}(72)$	91.52	$^{120}\text{P}(78)$

The structure analysis of the D bands observed for the first time by Loomis and Watson is nearly complete and will be reported in a subsequent communication.

The authors acknowledge their best thanks to Prof. Dr. P. N. Ghosh, the Head of the Department, for allowing all facilities to complete the investigation and for his interest and useful criticism during the progress of the work.

SPECTROSCOPIC RESEARCH LABORATORY,  
DEPARTMENT OF APPLIED PHYSICS,  
CALCUTTA UNIVERSITY.

R E F E R E N C E S

- <sup>1</sup> F. W. Aston, *Nature*, **137**, 613 (1936).
- <sup>2</sup> W. Jevons, *Roy. Soc. Proc. (A)*, **110**, 365 (1926).
- <sup>3</sup> F. W. Loomis and T. F. Watson, *Phys. Rev.*, **45**, 805 (1934).
- <sup>4</sup> G. D. Rochester, *Roy. Soc. Proc. (A)*, **150**, 668 (1935).
- <sup>5</sup> F. A. Jenkins and G. D. Rochester, *Phys. Rev.*, **52**, 1134 (1937).
- <sup>6</sup> E. N. Shawhan, *Phys. Rev.*, **48**, 521, (1935); **49**, 810 (1936).
- <sup>7</sup> P. C. Mahanti and A. K. Sen Gupta, *Zeits. f. Phys.*, **109**, 39 (1938).
- <sup>8</sup> W. Jevons, *Report on Band-Spectra of Diatomic Molecules* (1932).



# "ON THE POLARISED FLUORESCENCE OF ORGANIC COMPOUNDS"

By SACHINDRAMOHAN MITRA

(Received for publication, October 6, 1939)

**ABSTRACT.** The variation of the polarisation of fluorescence of the dyestuffs with the change of (a) the viscosity of the solution, (b) the temperature of the solution, and (c) the concentration of the dyestuffs has been investigated experimentally. In all the cases it has been observed that the degree of polarisation tends to vanish at low viscosities or high temperatures or at high concentrations of the dyestuffs while at very high viscosities or low temperature or at very low concentrations of the dyestuffs, the polarisation tends to reach asymptotically a certain limiting value which is dependent on (a) the nature of the dyestuffs, (b) the wave-length of the exciting radiation, and (c) the nature of the solvent. These results have been discussed on the basis of Perrin's theory. The variation of the polarisation with the wave-lengths of the exciting radiations has also been investigated in detail. It was found that the polarisation first decreases with the increase of the wave-length of the exciting radiation and increases again after reaching a minimum value which is negative and occurs at the exciting wave-lengths which are characteristic for the molecules of the dyestuff.

Besides the investigations mentioned above, the average life of the dyestuff molecules in the excited states, the absorption spectra of a large number of dyestuffs in glycerine solution in the ultra-violet region, the influence of one dyestuff molecule on the polarisation of fluorescence of another dyestuff molecule and the quenching of the fluorescence of the dyestuffs in solution by the addition of foreign substance have been investigated.

## GENERAL INTRODUCTION

A large amount of experimental work has been done, especially during recent years, on the fluorescence of dyestuffs in solution.<sup>1</sup> Much of the work, however, has been more or less of a qualitative nature; even where quantitative measurements have been attempted, the results obtained by the various experimenters differ so widely from one another that they can be considered only as giving the order of magnitude of the quantities measured. This is especially so in the case of measurements on the polarisation of fluorescence. It is now definitely known from the work of Weigert,<sup>2</sup> Wawilow,<sup>3</sup> Schmidt,<sup>4</sup> Perrin,<sup>5</sup> Gaviola and Pringsheim<sup>6</sup> and others that the degree of polarisation of the fluorescent radiations emitted by solutions of dyestuffs depends among others on the following factors:—the temperature and the viscosity of the solution, the concentration of the dyestuff and the wave-length of the exciting radiations. For most of the measurements on polarisation, however, sufficient data regarding

these factors are not available to enable us to know the exact conditions to which the measurements refer.

At the same time it is generally recognised that accurate measurements on the polarisation are likely to throw considerable light on the nature of fluorescence, which would be highly welcome in view of the unsatisfactory nature of the various theories that have been proposed from time to time—not one of them being capable of explaining satisfactorily even the essential facts of the phenomenon.

A few years ago it was, therefore, felt desirable to make systematic measurements on the polarisation of the fluorescence of some typical organic compounds for different wave-lengths of monochromatic excitation, at various temperatures, for different concentrations of the compound and also the influence of foreign substances. The present report gives the results of our further measurements<sup>7-14</sup> with a critical discussion of the results obtained so far.

#### THE OPTICAL ARRANGEMENT

The light from a quartz mercury lamp, automatic copper, cadmium and zinc arcs, rendered monochromatic by passage through a Hilger constant deviation quartz monochromator, was used, in general, as the source of excitation. In order to eliminate the uncertain polarisation introduced by the crystal-quartz parts of the monochromator, the light issuing from the monochromator was allowed to pass through a polarising prism before incidence on the fluorescent solution. The polarising prism was of the Glan type, and was transparent to the ultra-violet. The fluorescent solution was contained in a rectangular cell with windows of fused silica. By keeping the exit slit of the monochromator very wide, and shifting the telescope lens of the instrument suitably towards the slit, it was possible to focus the radiations of any required wave-length at the centre of the cell containing the fluorescent solution. The light so focussed was naturally in the form of a vertical thin sheet, which, when viewed from above, looked, especially in the neighbourhood of the focus, like a thin parallel pencil of light. This direction of observation was, therefore, very convenient for measurements on "transverse" fluorescent radiations.

The partial polarisation of the fluorescent light was measured in the usual manner by the Cornu method. Since the fluorescence was in the visible region for the dyestuffs studied here, the measurements could be made visually: where the intensity was very feeble, and sometimes also in other cases for a corroboration of the visual measurements, the measurements were made by photographing the tracks by their fluorescent light. Since the technique of these measurements is well known, it is unnecessary to describe here the details. In some cases the measurements of the polarisation were made by a Savart plate in the usual way.

DEPENDENCE OF POLARISATION ON THE WAVE-LENGTH  
OF THE EXCITING RADIATIONS

Before proceeding to the results obtained, it is necessary to explain the notation adopted by us. The incident light is linearly polarised, and the measurements refer to the fluorescent radiations along a direction normal to the plane containing the direction of vibration and the direction of propagation of the incident light. The fluorescent light is in general partially polarised, its vibrations along the direction of propagation being usually less intense than the vibrations in the perpendicular direction. The polarisation is then taken as positive and is measured as usual by the ratio of the difference in the intensities of the two vibrations to the sum of the two intensities, the ratio being expressed as a percentage. When the vibrations along the direction of propagation are more intense than those along the perpendicular direction, as happens in some cases, the polarisation is taken, consistently with the above notation, as negative.

The results of our measurements of the polarisation of fluorescence excited by different wave-lengths after correcting for the polarised fluorescence of glycerine,<sup>9</sup> are given in the following tables and are graphically shown by the accompanying curves. The tables and the figures conclusively show that the polarisation generally decreases to a minimum value as the wave-lengths of the exciting radiations decrease and then increases on the further decrease of the wave-lengths. This minimum value is negative and is reached when the exciting light is near about  $\lambda 3131 \text{ A}$ .

It may be mentioned here in passing that Jablonski<sup>15</sup> reported recently that in the cases of various colouring matters in glycerine solutions, the polarisation of the fluorescence progressively decreases with the decrease of the wave-length of the exciting radiation and under the ultra-violet excitation the polarisation practically vanishes. Later on Grisebach<sup>16</sup> observed that the polarisation attains the maximum negative value at two wave-lengths\* of the exciting radiation in the case of eosin instead of at one which we observe at about  $\lambda 312 \text{ m}\mu$ . He also claims that the polarisation is zero when the exciting wave-length is at about  $\lambda 365 \text{ m}\mu$  and  $326 \text{ m}\mu$ . But our measurements of the polarisation for various exciting wave-lengths do not agree with those of the aforesaid workers.

\* We shall further return to this point at a later part of the paper.

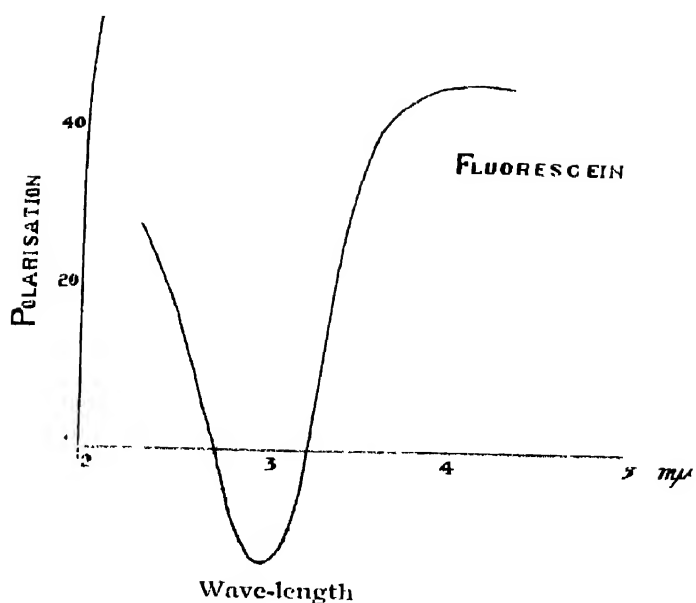


FIGURE 1

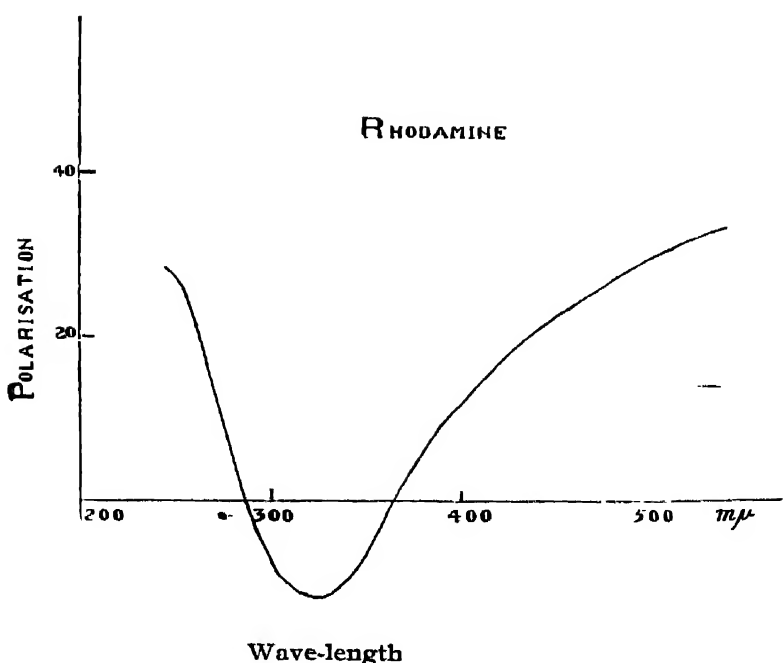


FIGURE 2

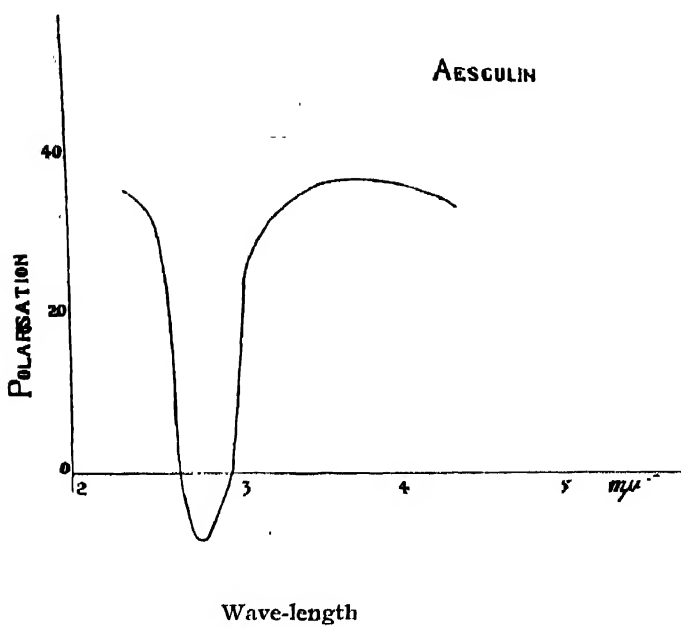


FIGURE 3

TABLE I

Percentage of Polarisation of Fluorescence in Glycerine.

Concentration of the compound =  $4 \times 10^{-5}$  gm./c.c.Temperature =  $28^{\circ}$ — $30^{\circ}$ C

Wave-length in $m\mu$	Fluorescein	Succinyl-fluorescein.	Rosin.	Succinyl eosin.	Magdalal red.	Rhodamine.	Erythrosin.
546	—	—	43	40	41	34	50
535	—	—	44	42	40	33	—
517	42	—	46	43	38	32	—
509	43	40	47	44	36	31	49
480	—	—	48	—	34	27	—
466	—	—	48	—	—	25	47
436	45	45	47	45	26	20	45
405	45	45	42	—	—	13	—
365	42	40	27	25	10	0	27
326	4	0	-7	-8	-6	-12	-8
313	-10	-8	-9	-9	-6	-10	-9
298	-14	-9	-7	-6	0	-6	-4
278	-5	6	0	7	11	8	14
265	6	20	9	—	—	20	25
254	17	29	16	34	25	27	38
233	28	—	35	38	31	29	45

TABLE I (*contd.*)

Percentage of Polarisation of Fluorescence in Glycerine.

Concentration of the compound =  $4 \times 10^{-5}$  gm./c.c.Temperature =  $28^{\circ} - 30^{\circ}\text{C}$ 

Wave-length in $m\mu$	Acro- flavine.	Aesculin.	Naphthyl- amine.	Sodium salicylate.	<i>o</i> -Amino benzoic acid.
436	38	34	22	42	14
405	35	—	—	—	—
365	23	37	18	37	16
326	0	33	16	35	14
313	-10	29	15	30	10
298	-12	0	0	0?	0
278	0?	-9	-8	-7	-5
265	8	0	0	5	-3
254	15	31	10	19	7
233	28	36	20	23	12

## POLARISED FLUORESCENCE IN OTHER SOLVENTS

In order to find out whether this change of the percentage of polarisation, especially of the negative value, is due to the influence of the nature of the solvent, we undertook a detailed investigation on the effect of the exciting wave-lengths on the polarisation of the fluorescence of the compounds in various solvents. The solvents used were sugar solution, castor oil, glycerine-water mixture, collodion-ether mixture. The results of our measurements are given below.

TABLE II

Percentage of Polarisation of Fluorescence in Castor oil.

Concentration of the compound =  $4 \times 10^{-5}$  gm./c.c.Temperature =  $28^{\circ} - 30^{\circ}\text{C}$ 

Wave-lengths in $m\mu$ .	Fluorescein.	Eosin.	Aesculin.	Rhodamine.	Magdala red.
546	—	45	—	—	42
535	—	45	—	—	41
517	—	—	—	—	32
509	—	—	—	31	31
480	—	—	—	28	29
466	—	46	—	—	—
436	45	47	30	26	27
405	44	40	—	12	—
365	40	28	37	0	15
326	-10	-6	35	-12	-8
313	-15	-10	33	-12	-8
298	-13	-7	0	-6	-6
278	0	2?	-6	7	0
265	9	10	0	25	6
254	17	31	20	33	12
233	26	—	24	35	20

TABLE III

Percentage of Polarisation of Fluorescence in Collodion-ether mixture.  
Concentration of the compound =  $4 \times 10^{-5}$  gm./c.c.

Temperature =  $28^{\circ} - 30^{\circ}\text{C}$ 

Wave-lengths in $\text{m}\mu$ .	Fluorescein.	Nosin	Asculin.	Rhodamine.	Magdala red.
546	—	45	—	42	40
535	—	44	—	41	—
517	—	44	—	39	39
509	—	43	—	38	38
480	—	—	—	—	36
436	46	42	35	28	31
405	44	40	—	—	26
365	36	26	32	9	18
326	0	-7	30	-10	-7
313	-10	-8	28	-12	-8
298	-12	-6	11	-6	-4
278	—	—	-5	—	—
265	9	11	5	18	5
254	15	20	20	27	10
233	22	23	29	34	19

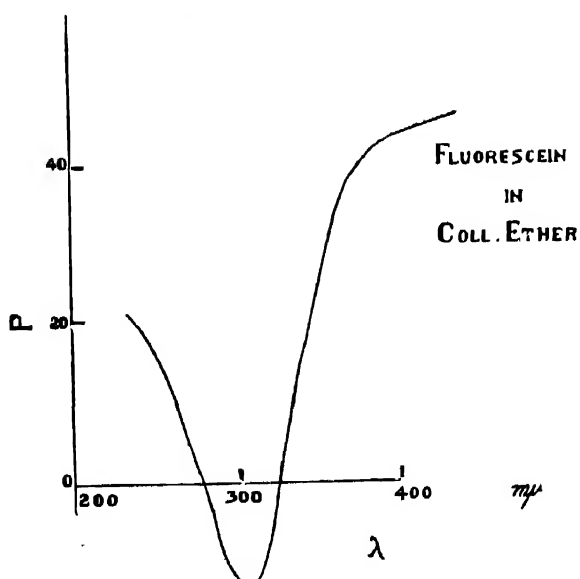


FIGURE 4

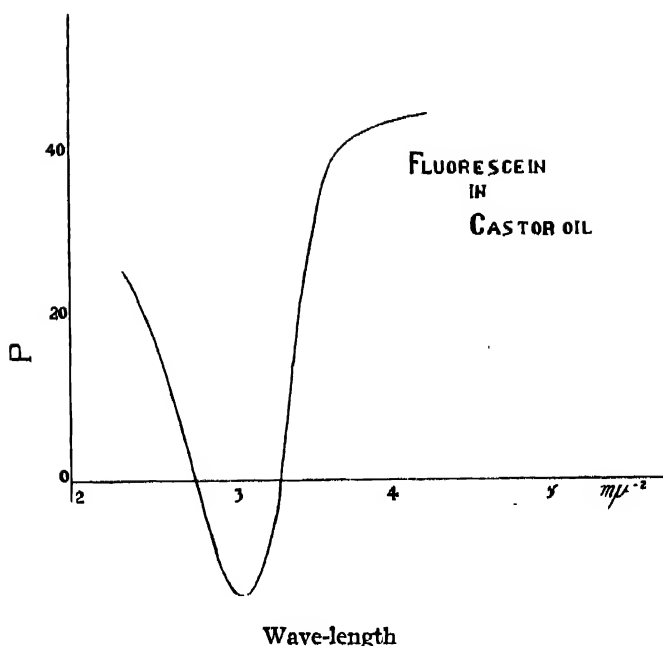


FIGURE 5

The tables and the curves conclusively exhibit that though the value of  $P$  is different for different solvents, the general nature of the graphs practically remains the same and the negative values persist in all the cases.

#### POLARISED FLUORESCENCE IN THE SOLID STATE

We have also measured the polarisation of fluorescence in the solid solution. A measured quantity of gelatine was added with a small quantity of water in a test-tube. They are then gently warmed till there was a very thick emulsion. To this was added a measured amount of stock solution of the fluorescent organic compound. The whole was stirred vigorously so as to make a uniform solution of the organic compound. This emulsion of gelatine was poured on a flat glass plate. On being dried the film exhibited an intense fluorescence.

Measurements of the "polarisation were made in the forward direction with the plane of the film perpendicular to the path of the exciting light, in order to avoid the influence of the polarisation due to the reflection at the surfaces, which would affect the measurements along other directions; complementary colour filters were used to cut off the incident exciting light. The results are given in the Table IV.

TABLE IV

Percentage of Polarisation of the Dyestuffs in solid solution.

Concentration =  $4 \times 10^{-5}$  gm./c.c.

Temperature = 28°C

Wave-length in <i>mμ.</i>	Fluorescein.	Eosin.	Rhodamine R.	Magdala Red.
546	—	22	12	21
436	24	10	10	12
405	20	8	8	18
365	12	5	0	7
326	-4	-2 ?	-5	-3
313	-8	-3	-5	-3
298	-6	-2 ?	0	0
278	5	0	4	3
265	13	—	7	5
254	19	15	10	8

INFLUENCE OF THE VISCOSITY OF THE SOLUTION  
ON THE POLARISATION

In a well-known paper Perrin has investigated the dependence of polarisation on the viscosity of the fluorescing solution, and has deduced on the basis of the theory of the Brownian rotation of molecules an expression for the above dependence. The essential principle of the calculation is as follows:—

Assuming that the molecules are rigidly fixed in space, if an incident polarised light excites fluorescence in the medium, the polarisation of fluorescence will have a certain value  $\rho_0$  which is characteristic of the substance. If on the other hand, as in the actual experiments, the molecules are rotating, the mean square of the angle of rotation per second can be calculated in terms of the viscosity of the solution and its temperature from Einstein's theory of the Brownian motion; hence the "expectation" of rotation for a time  $\tau$  can be calculated, where  $\tau$  is the mean duration of the molecules in the excited states. The smaller this angle of rotation, the more closely would the actually observed value of the polarisation approximate to the ideal value, *viz.*,  $\rho_0$ . Thus for very large viscosity or very low temperatures  $\rho$  should reach asymptotically the limiting value  $\rho_0$ , while at high temperatures or low viscosities the polarisation ought to reach again asymptotically zero value.

We will quote here only the final expression obtained by Perrin,<sup>17</sup> *viz.*

$$p = p_0 \cdot \frac{1}{1 + (1 - \frac{1}{2}p_0) \frac{RT}{\eta V} \cdot \tau}$$

where  $p$  is the degree of polarisation observed under the actual condition of the experiment and  $p_0$  the value for the same molecules *when they are not allowed to rotate* from their initial orientations;  $p_0$  would evidently be limiting value of  $p$  when either the viscosity is very large or the temperature very low.  $R$  is the gas constant for gram molecule and  $V$  the gram-molecular volume of the dyestuff,  $\tau$  is the absolute temperature and  $\eta$  is the coefficient of viscosity.  $\tau$  gives the mean duration of the fluorescing molecules in the excited state (defined as usual by the relation  $I = I_0 e^{-t/\tau}$ ) under the actual conditions of the experiment; if the excited molecules are in an isolated state, i.e., free from collisional and other influences of the neighbouring molecules, the duration will be that due to the radiational resistance alone, and can be readily calculated. For example, when the fluorescent band is in the green at about  $5000\text{\AA}^\circ$ , calculation gives for  $\tau$  the value  $11.1 \times 10^{-9}$  secs. in vacuum, or in glycerine solution for which the refractive index is about 1.47 the value of  $\tau$  would be equal to  $7.5 \times 10^{-9}$  sec.

TABLE V

Polarisation of Fluorescence in Succinyl Fluorescence excited by  $\lambda 4358\text{\AA}$ 

Percentage by wt. of glycerine.	Viscosity in Poises.	Percentage of polarisation [ $P = p \times 100$ ]		
		Concentration $c = 0.8 \cdot 10^{-5}$ gm/c.c.	Concentration $c = 8 \cdot 10^{-6}$ gm/c.c.	Concentration $c = 1 \cdot 10^{-5}$ gm/c.c.
99	5.7	50	47	45
92.7	1.8	46	42	37
86.3	.74	40	35	29
80.8	.39	34	27	21
75.9	.21	28	21	12
71.6	.17	23	16	—
67.8	.13	18	12	5
64.9	.10	15	9	...
61.2	.086	12	5	...
58.3	.071	10	...	...
55.8	.052	7	...	...
53.4	.052	3	...	...
51.2	.047	0	...	...

But actually there may be other channels through which the energy of the fluorescent molecule can be dissipated—other than radiation—as for example collisions of the second kind, etc., all of which will effectively tend to diminish the mean duration in the excited state.

In order to be able to get some information regarding the duration of the excited state measurements were made on the polarisation of fluorescence of fluorescein solutions in glycerine-water mixtures whose relative proportions and hence the viscosity could be varied over a wide range. The concentration of the dyestuff per c.c. of the solution was kept the same in all cases. The results of the measurements are tabulated in the following tables.

The values for the viscosity given in column two of the table are calculated from the recent extensive measurements by Muller (International Critical tables) on viscosity at different temperatures and various concentrations, by graphical interpolation.

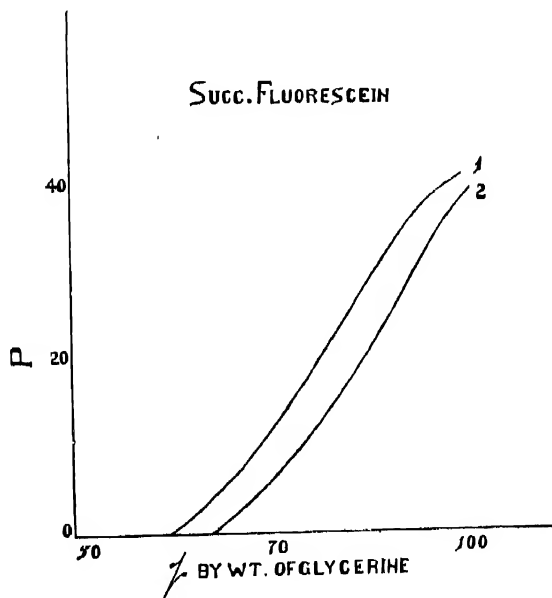


FIGURE 6

$$1 - c = 8 \times 10^{-5} \text{ gm./c.c.}$$

$$2 - c = 4 \times 10^{-5} \text{ " " }$$

TABLE VI

Polarisation of Fluorescence in Succinyl Fluorescein excited by  $\lambda$  3650 A

Percentage by wt. of glycerine.	Viscosity in Poises.	Percentage of Polarisation "P"	
		Concentration $4 \cdot 10^{-6}$ gm./c.c.	Concentration $8 \cdot 10^{-6}$ gm./c.c.
99	5.7	40	42
92.7	1.8	32	38
86.3	.74	20	30
80.8	.39	14	22
75.9	.21	10	13
71.6	.17	3	8
67.8	.13	0	5
64.9	.10	—	0

The values of P for the two concentrations are plotted in the accompanying figures. It will be seen from the curves that at high dilutions, *i.e.*, at low viscosities the values of P tend to zero and at high viscosities to the limiting value  $P_0$ , as we should expect from Perrin's expression.

In order to have some idea about the mean life of the fluorescent molecules in the excited state,  $\tau$  was calculated from the relation —

$$\tau = \frac{p_0 - p}{(1 - \frac{1}{2}p_0) \cdot \frac{RT}{V\eta} \cdot p},$$

the following gives the results of our calculation.

TABLE VII

$\tau \cdot 10^9$  sec. for Succ. Fluorescein in Glycerine water.  
Exciting wave length  $\lambda$  4358 A

Viscosity in Poises.	$\tau \cdot 10^9$ in sec.		
	Concentration $0.8 \times 10^{-6}$ gm./c.c.	Concentration $8 \times 10^{-6}$ gm./c.c.	Concentration $1 \cdot 10^{-5}$ gm./c.c.
.74	3	5	9
.39	• 3	5	9
.21	3	5	8
.17	3	5	9
.13	3	5	—
.10	4	—	—

TABLE VIII  
 $\tau \cdot 10^9$  sec. for Suc. Fluorescein in Glycerine water. Exciting- $\lambda$  3650 A

Viscosity in Poises.	$\tau \cdot 10^9$ in sec.	
	Concentration $4 \cdot 10^{-5}$ gm./c.c.	Concentration $8 \times 10^{-5}$ gm./c.c.
1.8	15	...
.78	15	5
.39	15	6
.21	...	5

TABLE IX  
Values of  $\tau \cdot 10^9$  in seconds for Fluorescein in Glycerine water. Exciting- $\lambda$  4358 A

Viscosity in Poises.	$\tau \cdot 10^9$ in sec.	
	Concentration $1 \cdot 10^{-5}$ gm./c.c.	Concentration $0.8 \cdot 10^{-5}$ gm./c.c.
5.7	9	3
1.8	9	4
.78	8	3
.21	8	3
.17	9	3
.13	...	3
.10	...	3
.086	...	4

TABLE X  
Values of  $\tau \cdot 10^9$  in seconds for Fluorescein in Glycerine water mixture.  
Exciting wave-length  $\lambda$  3650 A

Viscosity in Poises.	$\tau \cdot 10^9$ in sec.	
	Concentration $1 \cdot 10^{-5}$ gm./c.c.	Concentration $0.8 \cdot 10^{-5}$ gm./c.c.
1.8	9	3
.78	9	3
.39	8	3
.21	...	3
.17	...	3

Thus we find that within the limit of the experimental errors the values of  $\tau$  is practically the same for all the viscosities, though the values are widely different for the different concentrations of the fluorescent compounds. Moreover, the values of  $\tau$  as calculated from the Perrin's equation are independent of the exciting wave-length.

DEPENDENCE OF THE POLARISATION ON THE  
TEMPERATURE

The influence of temperature on  $p$  will be two-fold ; directly owing to the greater thermal agitation at higher temperatures the 'expectation' of rotation of the molecules after excitation, from their initial positions, will be the greater and hence the value of  $p$  correspondingly smaller. It also affects indirectly by changing the viscosity of the solution, the effect of which is also in the same direction as the previous effect, viz., to diminish as higher temperatures. Both of these influences are taken into consideration in Perrin's theory. If these are the effects of temperature,  $p$  calculated from Perrin's expression ought to be independent of temperature. Conversely this independence, if established experimentally, may be taken as an indirect proof that there are no other effects of temperature, e.g., through increased collisions between molecules, etc.

Experimentally the value of  $p$  was measured for temperatures from  $0^{\circ}\text{C}$  to about  $100^{\circ}\text{C}$ . The technique of the measurements is very simple and need not be described here. The solution was kept in a glass bulb inside a water tank whose temperature could be regulated as desired. The entrance as well as the observation sides were double walled and the space between the two walls was maintained dry by pieces of calcium chloride kept inside. This prevented the condensation at low temperatures of moisture on the walls of the vessel, which otherwise would diffuse the light and render accurate measurements impossible. A small heating coil in these two chambers served to maintain the outer wall at the room temperature.

The results of the measurements are tabulated below, and the values of  $p$  are plotted in the accompanying curves (Fig. 7).

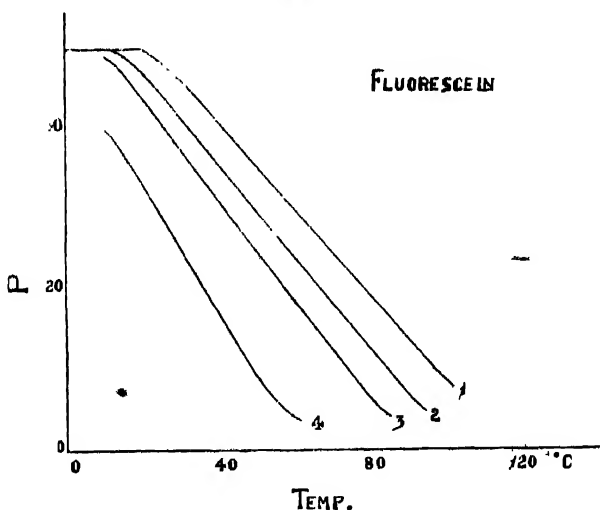


FIGURE 7

1— $c=1 \times 10^{-5} \text{ gm./c.c.}$  2— $c=4 \times 10^{-6} \text{ gm./c.c.}$  3— $c=8 \times 10^{-6} \text{ gm./c.c.}$  4— $c=12 \times 10^{-6} \text{ gm./c.c.}$

TABLE XI

Values of  $p_{100}$  for Fluorescein in Glycerine. Excitation by  $\lambda 4358 \text{ A}$ 

Temperature °C.	$c = 12 \cdot 10^{-6} \text{ gm./c.c.}$	Percentage of Polarisation.			
		$8 \cdot 10^{-5}$ .	$4 \cdot 10^{-5}$ .	$1 \cdot 10^{-5}$ .	$0.8 \cdot 10^{-5}$ .
0	—	50	50	50	...
10	41	50	50	50	...
20	34	...	48	50	50
30	26	37	48	45	50
40	17	32	36	42	49
50	8	25	29	39	45
60	5	20	26	32	39
70	3	12	20	26	34
80	Almost zero	5	13	20	26
90	"	Almost zero	5	9	17
98	"	"	...	7	13

TABLE XII

Values of  $p_{100}$  for Fluorescein in Glycerine. Excitation by  $\lambda 3650 \text{ A}$ 

Temperature °C.		Concentration of dyestuff in $10^{-5} \text{ gm. per c.c.}$	
		8	4
10		45	45
20		45	45
30		37	41
40		34	32
50		27	26
60		20	18
70		12	...
80		5	...
90		4	..
98	Almost zero		...

TABLE XIII

Values of  $p_{100}$  for Succinyl Fluorescein in Glycerine Excitation by  $\lambda 4358 \text{ A}$ 

Temperature in °C.	Concentration of dyestuff in $10^{-5} \text{ gm./c.c.}$			
	II	8	4	I
0	50	50	50	50
10	48	50	50	50
20	42	45	50	50
30	28	37	45	48
40	19	32	36	40
50	8	25	30	37
60	5	20	28	32
70	3	12	22	24
80	Almost zero	5	15	18
90	"	Almost zero	5	15
98	...	...	...	10

TABLE XIV

Values of  $p_{100}$  for Succinyl Fluorescein in Glycerine. Excitation by  $\lambda 3650 \text{ A}$ 

Temperature in °C.	Concentration of dyestuff in $10^{-5} \text{ gm./c.c.}$			
	II	8	4	I
0	42	42	42	42
10	42	42	42	42
20	40	42	42	42
30	28	32	37	40
40	17	23	28	33
50	10	17	21	26
60	4	12	15	20
70	Almost zero	7	11	14
80	0	...	6	10
90	...	...	0	10

TABLE XV

Values of  $p \times 100$  for Rhodamine B in Glycerine. Excitation by  $\lambda 5461$  A

Temperature in °C.	Concentration of dyestuff in $10^{-5}$ gm./c.c.			
	8	4	2	.5
0	...	41	41	41
10	39	41	41	41
20	37	41	41	41
30	32	34	39	41
40	27	29	36	37
50	21	26	31	34
60	14	21	27	29
70	9	17	23	...
80	7	15	19	24
90	5	12	14	17
97	0	5	7	14

TABLE XVI

Value of  $p \times 100$  for Rhodamine B in Glycerine. Excitation by  $\lambda 4358$  A

Temperature in °C.	Concentration of dyestuff in $10^{-5}$ gm./c.c.			
	8	4	2	.5
0	22	22	22	22
10	22	22	22	22
20	22	22	22	22
30	19	20	22	22
40	15	17	19	20
50	10	13	15	17
60	7	11	13	15
70	4	8	10	13
80	0	5	7	11
90	...	...	...	8

The general form of the curves is the same as for the curves representing the variation  $\rho$  with viscosity. At low temperatures  $\rho$  tends to reach asymptotically limiting value  $\rho_0$  as for very high viscosities, while at high temperatures  $\rho$  tends to vanish. On calculating the values of  $\tau$  on the basis of Perrin's expression we get the following results.

It is obvious from the nature of the expression that for values of  $\rho$  very near  $\rho_0$  as also very near zero, the calculated value of  $\tau$  cannot be reliable. Hence  $\rho$  has been calculated only for values other than these.

TABLE XVII  
Values of  $\tau \times 10^9$  for Fluorescein in Glycerine in secs.  
Excitation by  $\lambda 4358 \text{ \AA}$

Temperature in °C.	Concentration of dyestuff in $10^{-5} \text{ gm/c.c.}$			
	12	8	1	0.8
30	83	18	9	
40	75	19	8	
50	72	18	8	4
60		17	8	3
70			6	3
80			6	4

TABLE XVIII  
Values of  $\tau \times 10^9$  sec. for Fluorescein in Glycerine.  
Excitation by  $\lambda 3650 \text{ \AA}$

Temperature in °C.	Concentration of dyestuff in $10^{-5} \text{ gm/c.c.}$	
	8	4
30	17	—
40	18	15
50	17	16
60	19	16
70	18	12

TABLE XIX

Values of  $\tau \times 10^9$  sec. for Succinyl Fluorescein in Glycerine.Excitation by  $\lambda$  4358 Å

Temperature in °C.	Concentration of dyestuff in $10^{-5}$ gm/c.c.			
	10	8	4	1
30	81	18	—	—
40	75	19	15	9
50	70	18	16	9
60	—	19	16	8
70	—	18	16	9

TABLE XX

Values of  $\tau \times 10^9$  in sec. for Succinyl Fluorescein in Glycerine.Excitation by  $\lambda$  3650 Å

Temperature in °C.	Concentration of dyestuff in $10^{-5}$ gm/c.c.	
	8	4
30	18	—
40	17	15
50	18	16
60	18	15

It is interesting to note that though the value of  $\tau$  shows a very striking dependence on the concentration of the dyestuff, it is practically independent of temperature except in the case of the strongest solution, viz., of concentration  $12 \times 10^{-5}$  gm. per c.c. This shows definitely that only effects of raising the temperature are through increased thermal agitation and the consequent larger value of expectation of Brownian rotation of the dye-molecule per second and through diminished viscosity.

In the case of the very strong solutions, however, the value of  $\tau$  tends to diminish with rise of temperature (see Table XVII, Col. 2).

Measurements have also been made with other solvents excited by different wave-lengths. The results are included in the following tables and the changes with temperatures are graphically shown in the accompanying curves (Figs. 8, 9).

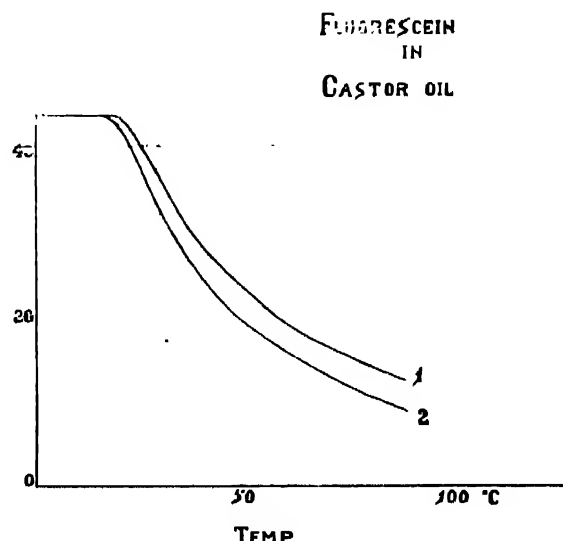


FIGURE 8

1— $c = 4 \times 10^{-5}$  gm/c.c.  
2— $c = 8 \times 10^{-5}$  , ,

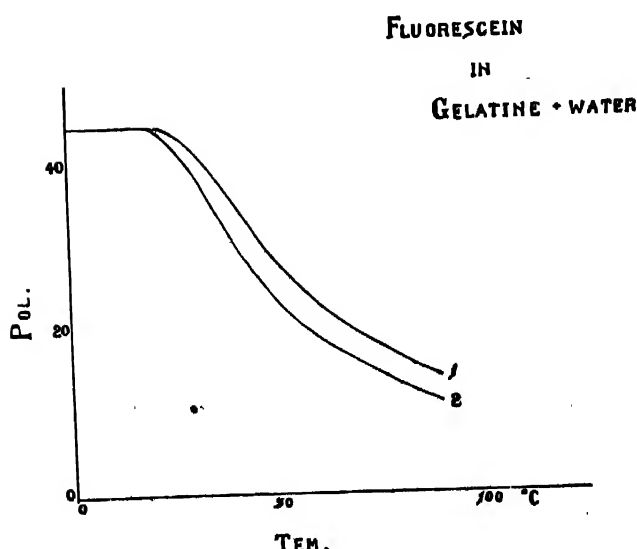


FIGURE 9

TABLE XXI  
Values of P for Fluorescein in Castor oil.  
Excitation by  $\lambda$  4358 Å

Temperature in °C.	Concentration of dyestuff in $10^{-6}$ gm/c.c.		
	8	4	2
0	45	45	45
10	45	45	45
20	44	45	45
30	36	42	43
40	27	32	38
50	20	26	34
60	15	22	30
70	11	19	27
80	8	16	25
90	5	14	23

TABLE XXII  
Values of P for Fluorescein in Sugar mixture.  
Excitation by  $\lambda$  4358 Å

Temperature in °C.	Concentration of dyestuff in $10^{-6}$ gm/c.c.		
	8	4	2
0	45	45	45
10	45	45	45
20	42	45	45
30	34	38	41
40	25	29	31
50	20	24	27
60	17	20	23
70	14	17	20
80	11	15	18
90	9	12	14

TABLE XXIII

Values of  $\tau \cdot 10^9$  for Fluorescein in Castor oil.  
Excitation by  $\lambda 4358 \text{ A}$

Temperature in $^{\circ}\text{C}$	Concentration of dyestuff in $10^{-5} \text{ gm./c.c.}$	
	8	4
30	14	9
40	15	11
60	14	10

We have also calculated the value of  $\tau$  in the case of fluorescein in castor oil, collodion ether and gelatine water mixtures. The following table gives the values of  $\tau$  for fluorescein in different solvents when excited by  $\lambda 4358$ , the concentration of the dye and the temperature being same in all the cases ( $c=8 \times 10^{-5} \text{ gm./c.c.}$ ).

TABLE XXIV

Values of  $\tau \cdot 10^9 \text{ Sec.}$  for Fluorescein in various solvents.  
Excitation by  $\lambda 4358 \text{ A}$

Solvent.	$\tau \cdot 10^9 \text{ Sec.}$
1. Glycerine	18
2. Castor oil	14
3. Ether collodion	16
4. Gelatine water	20

This shows that the average life depends on the solvents.

#### INFLUENCE OF CONCENTRATION OF THE FLUORESCING COMPOUND ON THE POLARISATION.

We have already seen that the polarisation of fluorescence shows a conspicuous change with the change of the concentration of the fluorescing compound. The results of our measurement are given in the following tables and are graphically shown by the accompanying curves (Figs. 10, 11),

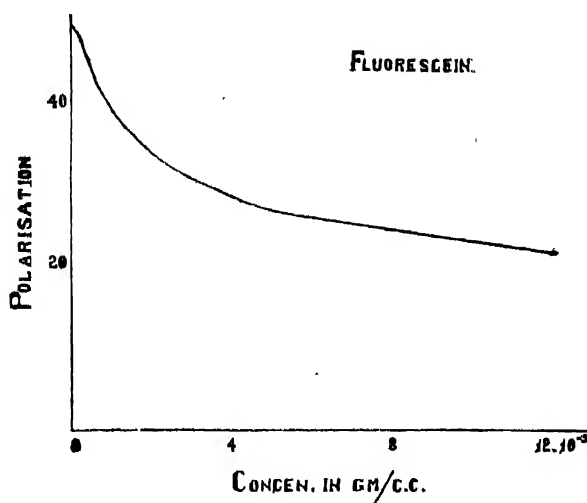


FIGURE 10

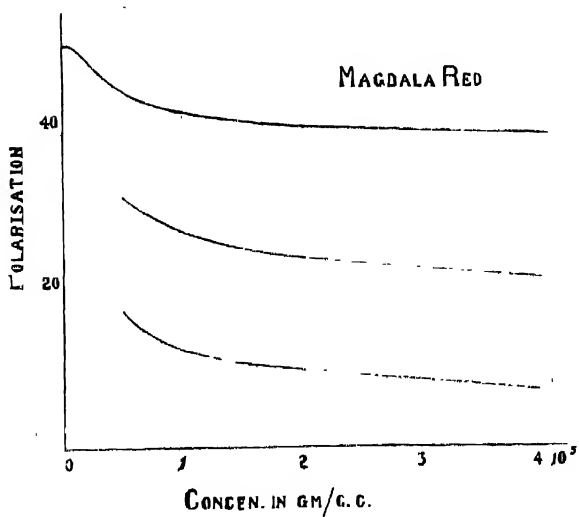


FIGURE 11

TABLE XXV

Fluorescein at  $30^\circ \text{ C}$ 

$c \times 10^5 \text{ gm./c.c.}$		8	4	2	1	.5	.25	.14	.07
Percentage of polarisation for	4358	37	42	44	45	46	50	50	50
3650		36	41	42	43	45	45	45	45

TABLE XXVI  
Fluorescein at 50° C

$c \times 10^5$ gm/c.c.		8	4	2	.08
Percentage of polarisation for	4358	25	29	39	45

TABLE XXVII  
Rhodamine B at 30° C

$c \times 10^5$ gm/c.c.		8	4	2	.5
Percentage of polarisation for	5461	32	34	39	41

TABLE XXVIII  
Eosin at 30° C

$c \times 10^5$ gm/c.c.		4	2	1	.5	.25	.16	.08
Percentage of polarisation for	5461	37	41	44	44.5	45	46	47
	4358	41	44	45	46	47	50	50
	3650	22	22	24	25	27	29	—

TABLE XXIX  
Magdala red at 30°C

$c \times 10^5$ gm/c.c.		4	2	1	.5	.25	.16	.08
Percentage of polarisation for	5461	39	41	42	44	47	50	—
	4358	21	24	27	31	—	—	—
	3650	7	10	12	17	—	—	—

TABLE XXX  
Succinyl Fluorescein at 30° C

$c \times 10^5$ gm/c.c.	11	8	4	1	8	'08
Percentage of polarisation for	4358	28	37	45	47	50

TABLE XXXI  
Succinyl Fluorescein at 70° C

$c \times 10^5$ gm/c.c.	11	8	4	1
Percentage of polarisation for	4358	3	12	22

It will be seen from the graphs and the tables that with increase of concentration the value  $\rho$  tends to vanish, while at very small concentrations it tends to reach asymptotically the same limiting value  $\rho_0$  as is reached by  $\rho$  at large viscosities or low temperatures.

This result is very surprising. We would naturally expect that when we increase the concentration of the fluorescent dyestuff, either the effective value of  $\tau$  remains unaltered or probably due to increase in the number of collisions between excited molecules there will be a small tendency for the excited molecules to dissipate their energy in the form of kinetic energy of translation of the molecules. This would be equivalent to diminishing the mean period of duration of the molecules in the excited state. This is indeed the case as is shown by the direct measurements on the duration of the excited state.

This diminution in the mean life of the molecules in the excited state at high concentration of dyestuff would conduce on the basis of Perrin's theory to an increase in the value of the polarisation, since the molecule would not have sufficient time to rotate far from its original orientation where it was excited; and thus the polarisation will approximate closer to its upper limiting value. But our experimental results show quite the opposite effect.

TABLE XXXII  
Variation of  $\tau$  with the concentration of fluorescein in glycerine at 40° C

Concentration $\times 10^{-5}$ gm/c.c.	$\tau \cdot 10^9$ sec $\lambda 4358 \text{ A}$
--	--

12	72
8	18
4	17
1	7
'08	3

TABLE XXXIII

Variation of  $\tau$  with concentration of Succinyl  
Fluorescein in Glycerine water at 30°C.

Concentration $\times 10^{-4}$ gm/c.c.	$\tau \times 10^8$ sec.	
	$\lambda 4358\text{A}$	$\lambda 3658\text{A}$
.08	3	
.8	5	6
1	9	15

TABLE XXXIV

Variation of  $\tau$  with the concentration of Succinyl  
Fluorescein in Glycerine at 40°C.

Concentration $\times 10^{-6}$ gm/c.c.	$\tau \times 10^8$ sec. $\lambda 4358\text{A}$
11	75
8	19
4	15
1	9

ON THE MAXIMUM VALUE OF THE POLARISATION " $p_0$ "

We have already mentioned that the value of  $p_0$  is the value of the polarisation when the molecule is not allowed to rotate from its initial orientation, which is also evidently the limiting value of  $p$  when the viscosity is very large or the temperature very low. The following table shows the values of  $p_0$  for the various dyestuffs in various solvents when excited by radiations of various wavelengths as obtained experimentally:—

TABLE XXXV

'The values of "P<sub>0</sub>" ( $P_0 \times 100$ )

Dyestuffs	Solvents	Exciting	Wave-length	
		5461	4358	3650A.
Fluorescein	Glycerine	—	50	45
	Castor oil	—	45	41
	Sugar & water	—	45	40
	Gelatine & water	—	45	38
	Collodion & ether	—	40	35
Succinyl fluorescein	Glycerine	—	50	42
	Collodion & ether	—	35	30
Rhodamine B	Glycerine	41	25	15
	Collodion & ether	44	30	10
Aesculin	Glycerine	—	40	45
	Collodion & ether	—	35	41
Eosin	Glycerine	47	50	42
	Castor oil	45	48	30
	Sugar & water	45	48	30
	Collodion & ether	40	45	31

The foregoing table conclusively shows that this limiting value of the polarisation "P<sub>0</sub>" depends on the following factors, viz.:—

- (a) On the wave-length of the exciting radiations ;
- (b) On the nature of the fluorescent molecules ;
- (c) On the nature of the solvents.

#### ULTRA-VIOLET ABSORPTION OF THE DYESTUFFS IN SOLUTION AND THE NEGATIVE POLARISATION

The literature on the absorption spectra of the dyestuffs in solution reveals that the great majority of the investigators in that particular dominion confined their investigation within the visible region of the spectrum in order to establish correlation between the absorption, colour and the structure of the molecules,

Very few systematic quantitative measurements have been made in the ultra-violet region. It might not be out of place to mention here in passing that Grisebach<sup>18</sup> measured the absorption coefficients in the ultra-violet region of a few dyestuffs in solution and tried to establish a relation between the absorption curves and the polarisation curves of the fluorescence emitted by them in solution. In view of the scanty data as well as to find out whether there is actually any relation between the absorption and the polarisation curves as reported by Grisebach, we carried out detailed quantitative measurements on the absorption of the dyestuffs in glycerine solution, the following gives graphically the results of our measurements.

The absorption coefficients were determined by a calibrated rotating sector photometer used in conjunction with an Adam Hilger quartz spectrograph. The results were, however, further verified by the measurements of absorption with a sensitive Moll thermopile and a galvanometer system. A parallel beam of light from a point source of mercury-quartz lamp was allowed to fall on a cell containing dye-solution through a combination of filters, which allowed a monochromatic radiation to pass. The incident and transmitted radiations were measured with the help of a Moll thermopile and galvanometer. The absorption coefficients,  $\alpha$ , were calculated from the relation.

$$I_{\text{transmitted}} = I_{\text{incident}} e^{-\alpha d}$$

where  $d$  is the thickness of the cell.

The results from thermoelectric measurements and photographic method are given below for comparison. The agreement, as will be evident from the following tables, is within the experimental errors:—

TABLE XXXVI

Dyestuffs.	Absorption coefficient for $\lambda 313 \text{ m}\mu$	
	Thermoelectric method.	Photographic method
1. Fluorescein	.50	.498
2. Eosin	.657	.656
3. Aesculin	.568	.56
4. Rhodulin orange	.41	.415
5. Acriflavin	.138	.13
6. Magdal red	.576	.58

In the accompanying graphs are drawn the absorption coefficient curves as well as the polarisation curves. (Figs. 12-18.) In the case of fluorescein, we find that the position of the maximum negative polarisation corresponds to the junction of the two adsorption bands in the ultra-violet, as was observed by Grisebach. (See Fig. 14.) But in the case of eosin and magdala red it corresponds to the first adsorption maximum in the near ultra-violet. (See Figs. 12, 13.)

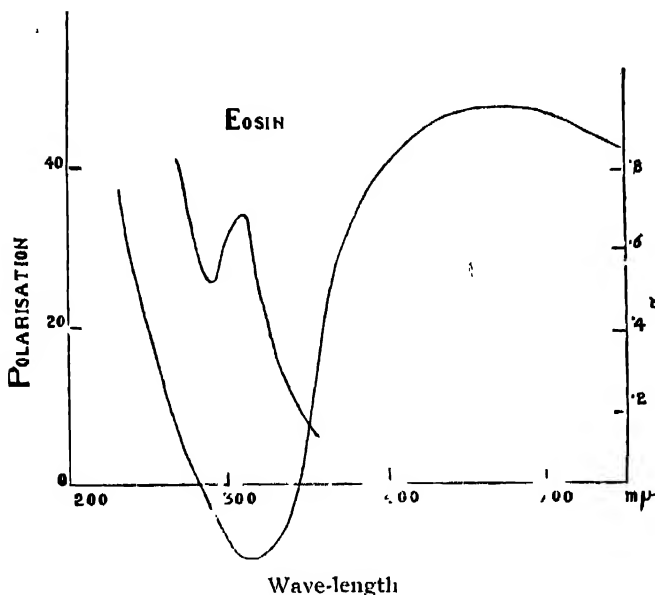


FIGURE 12

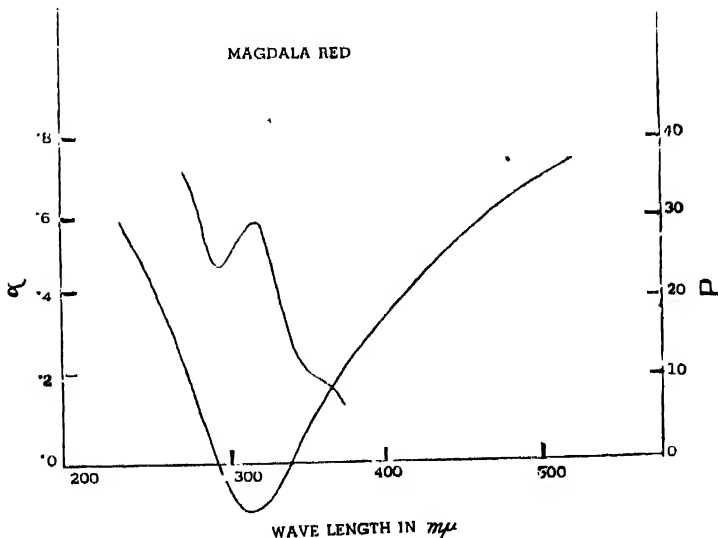


FIGURE 13

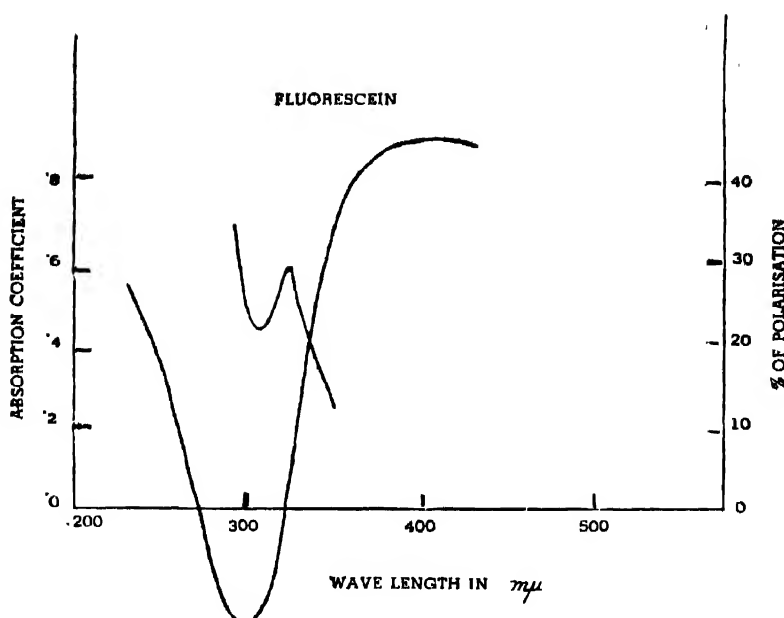


FIGURE 14

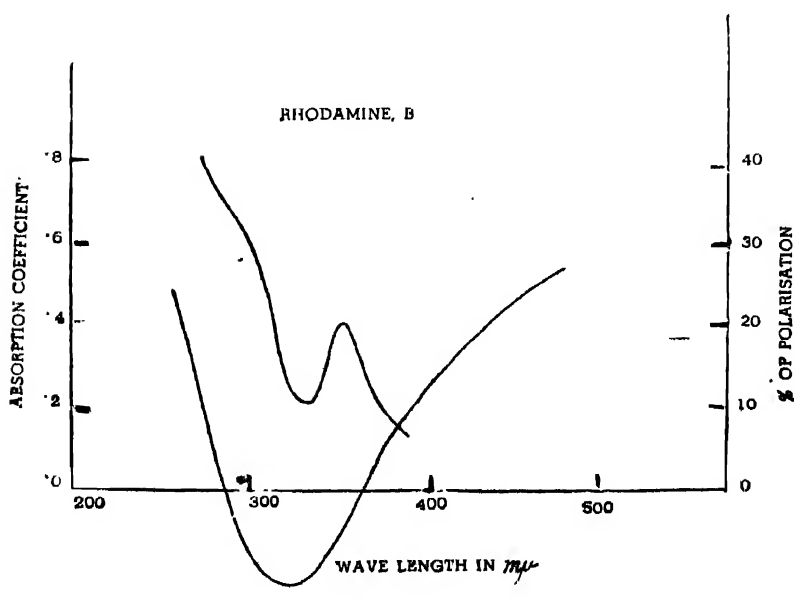


FIGURE 15

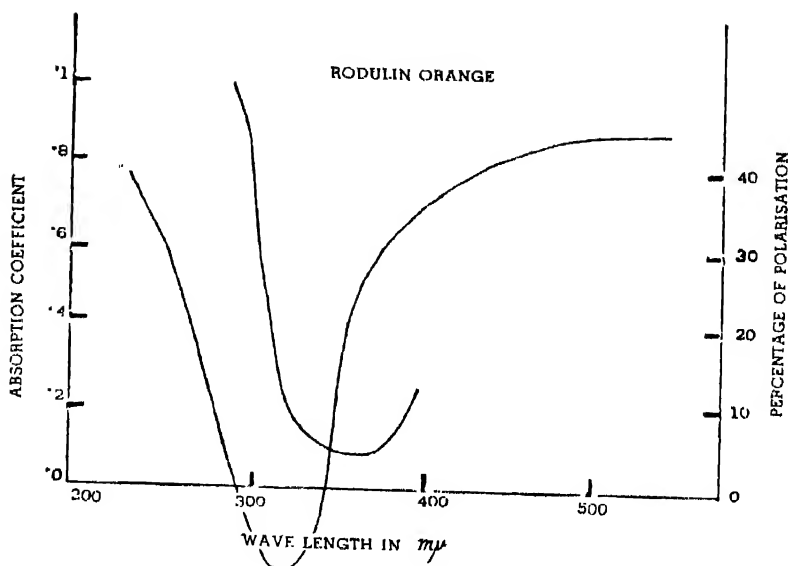


FIGURE 16

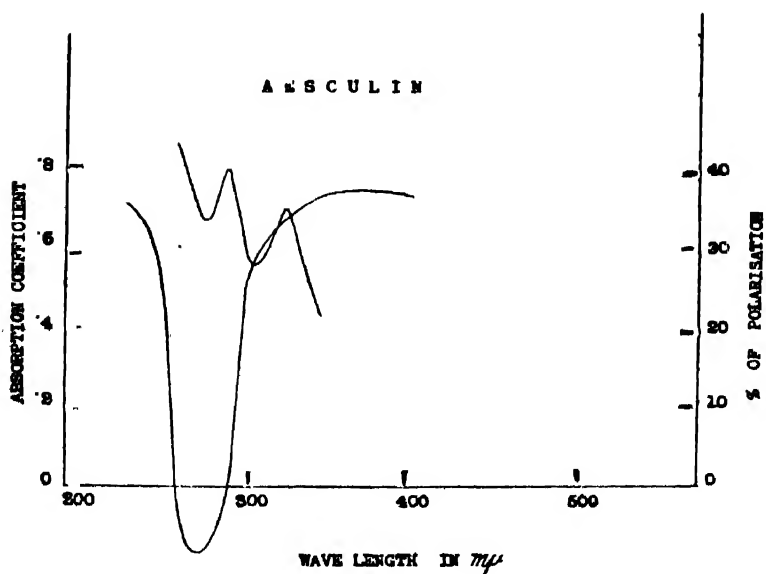


FIGURE 17

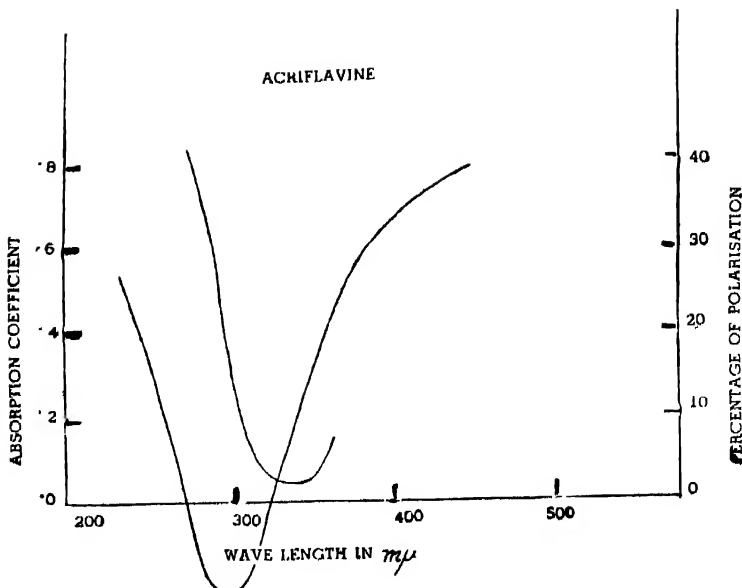


FIGURE 18

RELATION BETWEEN FLUORESCENT BAND, ABSORPTION BAND AND MAXIMUM NEGATIVE POLARISATION

We have seen that the value of the polarisation decreases as the wave-length of the incident exciting radiation is decreased and then increases with the further decrease of the wave-length of the exciting light. This minimum value is negative and the maximum negative value is reached for wave-lengths which are different for different dyestuffs as will be evident from the following table : —

TABLE XXXVII

Dyestuff in Glycerine solution $c = 4 \times 10^{-5}$ gm/c.c.	Wave-length for the excitation of the fluorescence of the max. negative polarisation in $m\mu$	Band maxima in $m\mu$	
		Fluorescent.	Absorption.
Aesculin	275	459	
Fluorescein	300	512	500
Eosin	312	535	525
Rhodamine B	325	560	535

The table reveals certain interesting points, namely, as the fluorescent, consequently the absorption band maxima shift towards the greater wave-length side, the wave-length for the excitation of fluorescence of the maximum negative polarisation also shifts towards the greater wave-length side.

**INFLUENCE OF A FLUORESCENT DYESTUFF MOLECULE  
ON THE POLARISATION OF FLUORESCENCE OF  
ANOTHER DYESTUFF IN SOLUTION**

It is now a well-known phenomenon that the fluorescence of organic compounds in solution is quenched by the addition of foreign substances with a simultaneous increase in the polarisation. This quenching is generally explained as due to the collision of the second kind between the molecules of the excited dyestuff and those of the foreign substance as a result of which the excited molecules come down to the unexcited state without emitting any fluorescent radiation.

We have already investigated the effect of the addition of potassium iodide to the fluorescence of fluorescein, eosin and others, and have observed that this fluorescent intensity decreases with the addition of the iodide together with the simultaneous increase of the value of the polarisation. We have also observed that this polarisation never exceeds the maximum value  $p_0$ .

Now it might be of interest to investigate the influence of a dyestuff on the polarisation of the fluorescence of another dyestuff molecule in solution. For this investigation we have taken the following :

1. Aesculin, and rhodamine B.
2. Fluorescein and rhodamine B.

These were taken in order to study the influence of aesculin and fluorescein on the polarisation of the fluorescence of rhodamine excited by  $\lambda 5461$  Å.

3. Aesculin and eosin.
4. Fluorescein and eosin.

These were taken in order to investigate the influence of aesculin and fluorescein on the polarisation of fluorescence of eosin in solution excited by  $\lambda 5461$  Å.

Lastly the influence of fluorescein on the polarisation of magdala red excited by  $\lambda 5461$  was also investigated by adding different quantities of fluorescein to the magdala red solution. The solvent used was, in all the cases glycerine.

The results of our measurements are given in the accompanying tables and graphs (Figs. 19, 20, 21, 22).

TABLE XXXVIII

Influence of Fluorescein on the polarisation of Eosin.  $c = 1 \times 10^{-5}$  gm/c.c.

Exciting.	Concentration of fluorescein $\times 10^5$ gm/c.c.								
	0	.25	.5	1	2	4	8	12	
5461 A	44	42	40	38	35	31	26	22	

TABLE XXXIX

Influence of Aesculin on the polarisation of Eosin  $c = .08 \times 10^{-5}$  gm/c.c.

Exciting.	Concentration of aesculin $\times 10^5$ gm/c.c.								
	0	.12	.25	.5	1	2	4	8	12
5461 A	47	46	44	40	36	32	26	16	14

TABLE XL

Influence of Aesculin on the polarisation of Rhodamine B

Concentration  $= 2 \times 10^{-5}$  gm/c.c.

Exciting in A. U.	Concentration of Aesculin $\times 10^5$ gm/c.c.					
	0	.5	1	2	4	8
5461	39	35	33	31	30	28

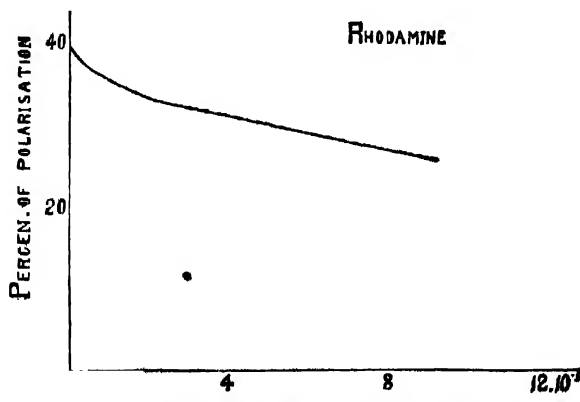


FIGURE 19

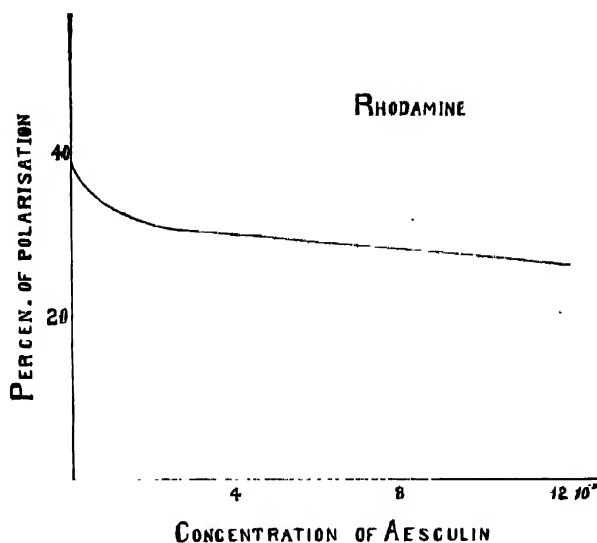


FIGURE 20

TABLE XLI

Influence of Fluorescein on the polarisation of Rhodamine B  
Concentration =  $2 \times 10^{-5}$  gm/c.c.

Exciting in A. U.	Concentration of fluorescein $\times 10^5$ gm/c.c.						
	0	.25	.5	1	2	4	8
5461	39	38	37	36	33	31	27

TABLE XLII

Influence of Fluorescein on the polarisation of Magdala red  
Concentration =  $2 \times 10^{-5}$  gm/c.c.

Exciting in A. U.	Concentration of fluorescein $\times 10^5$ gm/c.c.						
	0	.5	1	2	4	8	12
5461	47	43	41	39	38	36	35

Here we also find that in all the cases the value of the P tends to decrease with the increase of the concentration of the foreign dyestuff.

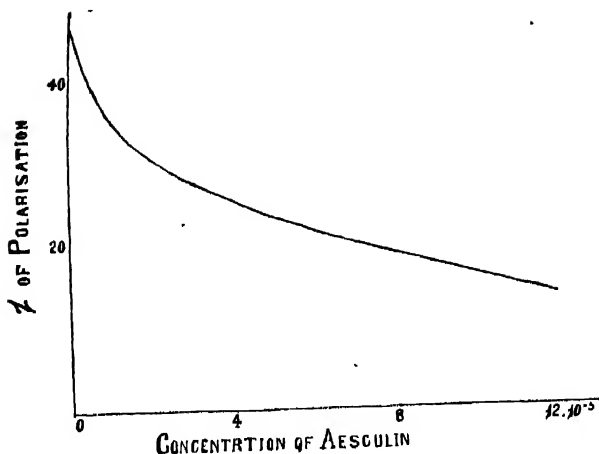


FIGURE 21

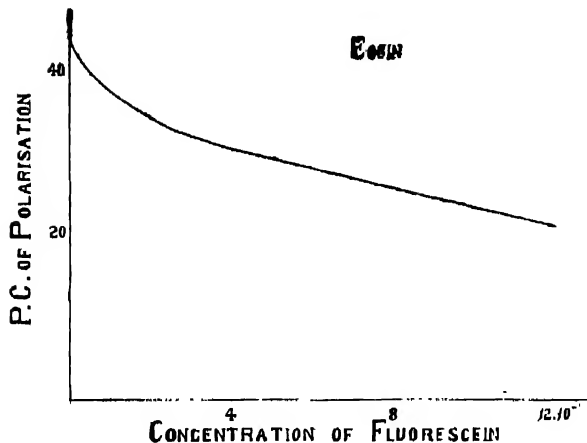


FIGURE 22

#### ON THE QUENCHING OF FLUORESCENCE OF ORGANIC COMPOUNDS IN SOLUTION BY FOREIGN SUBSTANCE

It is well known that the addition of small quantities of a foreign substance to a fluorescent solution causes a quenching of its fluorescent radiation with a simultaneous diminution of its efficiency. This phenomenon of the quenching of the fluorescence of the dye solution has been investigated by a number of workers and some of them are at present inclined to the view that the quenching effects is due to the deactivation of the excited molecule with a molecule of the foreign substance through the collision of the second kind. The principal argument in favour of this physical interpretation of the quenching effect is the increase of polarisation by quenching, which was first observed by Perrin<sup>19</sup> and afterwards by the present author<sup>20</sup> and others.

The theory of collisions of the first kind was first postulated by Wawilow<sup>21</sup> on the basis of the theory of the Brownian motion, and later on in order to explain the non-linear dependence of the quenching action on the concentration of the quencher and on the viscosity of the solvent Wawilow and Frank<sup>22</sup> modified the same and recently the theory was further modified by Wawilow and Sveshnikoff.<sup>23</sup>

In our present investigation, undertaken with a view to throw more light on the subject, which includes the following two points,—(a) dependence of the quenching on the concentration of the quencher, and (b) dependence of the quenching on the wave-length of the exciting light, all the measurements of the efficiency were done with the help of a spectrophotometer in the usual way. The sources of the exciting light was a quartz mercury arc for the radiations  $\lambda$  2537, 3131, 3650, 4047, 4358 and 5461 Å. The excitation of fluorescence was produced by polarised monochromatic radiation, which was separated by means of suitable filters and observations were made at right angles to the direction of the incident light.

As we have seen that when the concentration of the dyestuffs is large, the addition of a foreign substance causes a considerable deformation of the absorption band, due to formation of perhaps "complex molecules," so we have used in our present investigation a very dilute aqueous solution (concentration of the order of  $10^{-6}$  gm/c.c.).

(a) *Dependence of the quenching on the concentration of the quencher*—The quenching of fluorescence with potassium iodide had been investigated by many workers. But their results show such great differences that a repetition of those experiments was felt desirable and hence the present measurements were undertaken. Our values of  $I_0/I$  (where  $I_0$  and  $I$  are respectively the efficiencies of fluorescence, i.e., ratios of emitted to absorbed energy, in the absence and the presence of the quencher) for the various concentrations of the quencher are given in the tables.

(b) *Dependence of quenching on the wave-length of the exciting radiation*—It was Wawilow who first investigated the influence of the exciting wave-length on the quenching action and found the same independent of the exciting-light. This was confirmed by Sveshnikow.<sup>24</sup> Wawilow carried out his investigation in viscous medium, whereas the later worker Sveshnikow used a less viscous medium. The aforesaid worker used only two wave-lengths for the exciting radiation. But in the region of the higher concentrations of the quencher, West and Jetty<sup>25</sup> found a great dependence on the wave-lengths of the exciting radiations. In view of the great importance of the problem on the whole mechanism of fluorescence, we considered it prudent to investigate the point using a number of monochromatic radiations for the excitations of the fluorescence.

TABLE XLIII

Variation of  $I_0/I$  for Fluorescein in water due to the addition of KI. Concentration of the dyestuff =  $4 \times 10^{-4}$  gm./c.c.

Exciting	Concentration of the quencher in $10^{-3}$ gm/c.c.													
	0	1	2.5	5	10	20	50	100	200	300	350	500	600	650
436	1	1.03	1.18	1.40	1.75	2.72	5.56	12.02	26.51	50.1	70.5	110.2	122.8	132.6
405	1	1.08	1.21	1.38	1.76	2.75	5.50	12.03	26.53	50.1	70.6	110.8	123.1	132.5
365	1	1.05	1.22	1.39	1.78	2.73	5.61	12.01	26.52	50.2	70.3	110.8	122.6	132.7
313	1	1.07	1.18	1.43	1.77	2.75	5.63	12.02	26.51	50.7	70.8	110.8	122.7	133.1
254	1	1.05	1.19	1.41	1.76	2.73	5.58	12.05	26.51	50.2	70.6	110.6	122.8	132.8

TABLE XLIV  
Variation of  $I_0/I$  for Eosin in water by the addition of KI. Concentration of the dyestuff =  $4 \times 10^{-5}$  gm./c.c.

Exciting	Concentration of the quencher in $10^{-3}$ gm./c.c.										
	0	1	2	3	5	10	15	20	25	30	35
546	1	1'25	1'50	1'75	2'30	4'20	6'70	10'25	15'72	22'81	32'61
436	1	1'20	1'45	1'74	2'32	4'15	6'68	10'31	15'68	22'75	32'50
405	1	1'21	1'48	1'72	2'31	4'18	6'69	10'30	15'70	22'78	32'58
365	1	1'25	1'49	1'73	2'32	4'22	6'70	10'28	15'75	22'79	32'60
313	1	1'23	1'47	1'74	2'30	4'21	6'71	10'26	15'72	22'80	32'59

The result of our measurements of  $I_0/I$  are given in the aforesaid Tables XLIII, XLIV. The quencher employed was potassium iodide.

It might be mentioned here in passing that we can consider, in fact many investigators have considered, the act of quenching as something like a quantum mechanical resonance if we look at it in the light of collision process of the second kind. If now on undergoing different excitations with different wave-lengths, the excited molecules had different excited states and hence a different mean life and different probabilities of quenching some dependence of the quenching on the excitation wave-lengths should be observed.

But experimentally we find, as revealed from the aforesaid tables, that there is no dependence of the quenching action on the exciting wave-lengths. This conclusively shows that the excited molecules have all the same energy level during the excited state. This conclusion is also in agreement with our former conclusion, namely the independence of the average life  $\tau$  on the exciting wave-lengths, which we have arrived at from our polarisation measurements.

#### S U M M A R Y

It is now definitely known from the investigations of Wawilow, Perrin, Pringsheim, Gaviola and others that the fluorescent radiations emitted by the dyestuffs in solution are polarised and this polarisation depends among others on the following facts—the viscosity and the temperature of the solution, the concentration of the dyestuff and the wave-length of the exciting radiations. For most of the measurements on the polarisation, however, sufficient data regarding these factors are not available to enable us to know the exact conditions to which the measurements refer. Moreover the conclusions arrived at by the various workers from time to time, are sometimes highly contradictory.

At the same time, it is generally recognised that accurate measurements on the polarisation are likely to throw considerable light on the nature of fluorescence, which would be highly welcomed in view of the unsatisfactory nature of the various theories that have been proposed from time to time—not one of them being capable of explaining even the essential facts of the phenomenon. It was therefore felt desirable to make a systematic measurements on the polarisation of some typical dyestuffs in solution.

The present paper describes the measurements on the variation of the polarisation of the fluorescence of the dyestuffs with the change of the following factors among others :—

- (a) the viscosity of the solution,
- (b) the temperature of the solution,
- (c) the concentration of the dyestuffs.

In all cases the variation is of the same type; the degree of the polarisation tends to vanish at low viscosities, or high temperatures or high concentrations of the dyestuffs, while at very high viscosities or low temperature or at very low concentrations of the dyestuffs the polarisation tends to reach asymptotically a certain limiting value which is dependent on the following factors:—

- (a) the nature of the dyestuffs,
- (b) the wave length of the exciting radiation,
- (c) the nature of the solvent.

These results are discussed on the basis of the Perrin's theory and it is shown that while the variation of the polarisation with viscosity and the temperature are satisfactorily explained by this theory, the theory definitely breaks down when applied to the variation of the degree of polarisation with the concentration of the dyestuff. Indeed the predictions are just the reverse of what is obtained experimentally.

The variation of the polarisation with the wave-lengths of the exciting radiations has also been investigated in details. It was found that the polarisation decreases with the increase of the wave-lengths of the exciting radiation and then increases with further decrease of the exciting wave-length. This minimum value is negative and is reached at the exciting wave-lengths which are characteristic of the dyestuff molecules. It was also observed that as the band maxima of the fluorescent bands of the dyestuffs shift towards the longer wave-lengths, the position of the maximum negative value of the polarisation also shifts towards the same direction. This contradicts the observations of Wawilow, who found that the negative value (maximum value) is reached when the exciting wave-length is near about  $3131\text{ \AA}$  in all the cases of the dyestuffs (fluorescein, eosin rhodamine B, magdala red). Further in the case of the aesculin he did not observe the negative polarisation at all. Whereas we found that the maximum negative polarisation occurs when the exciting wave-length is  $278\text{ m}\mu$ .

The average life of the dyestuff molecules in the excited states has also been calculated with the help of the Perrin's expression and it has been found to be independent not only of the viscosity and the temperature but also of the wave-lengths of the exciting light. This same conclusion has also been arrived at from our measurements of the quenching of the fluorescent radiation by foreign substances of varying concentrations, which has been observed to be independent of the exciting wave-length. These conclusions show conclusively that all the molecules have the same energy level in the excited state.

The absorption spectra of a large number of dyestuffs in glycerine solution in the ultra-violet region were also investigated in details with a view to find out whether there is any relation between the absorption and the negative polarisa-

tion. No general relationship was observed but in the cases of the fluorescein, eosin, magdala red and rhodamine B it was observed that in the region of the wave-lengths which produce the negative polarisation when excited by them (*i.e.*, in the region  $326 \text{ m}\mu$  to  $298 \text{ m}\mu$ ) the absorption coefficient increases, then decreases and again increases as the wave-length decreases.

The influence of one dyestuff molecule on the polarisation of the fluorescence of another dyestuff molecule has also been investigated in details. The polarisation instead of increasing with the amount of the foreign dyestuff molecules, was found to decrease. The influence of the foreign dyestuff seems to be the same as that observed by increasing the concentration of the fluorescing dyestuff molecule itself.

The quenching of the fluorescence of the dyestuffs in solution by the addition of the foreign substances has also been investigated. The quenching, though depending on the concentration of the foreign substance, was found to be independent of the exciting wave-length.

Finally the author thanks Prof. S. N. Bose and Dr. K. S. Krishnann for their great interest in the work and in helping him in various ways during the course of the work.

PHYSICS LABORATORY,  
DACCÀ UNIVERSITY.

#### R E F E R E N C E S

- <sup>1</sup> For a good account of the earlier works on the subject see Pringsheim, "Fluorescence and Phosphorescence."
- <sup>2</sup> Weigert, *Verh. Phys. Gesell.*, **1**, 100 (1921); **2**, 531 (1922); *Phys. Zett.* **23**, 232 (1922).
- <sup>3</sup> Wawilow and Lewschin, *Phys. Zett.*, **23**, 173 (1922); Wawilow, *Zell. für Phys.*, **68**, 690 (1929).
- <sup>4</sup> Schmidt, *Phys. Zett.*, **23**, 233 (1922).
- <sup>5</sup> Perrin, *Ann. der Phys.*, **12**, 169 (1929).
- <sup>6</sup> Pringsheim and Gaviola, *Phys. Zett.* **24**, 24 (1924).
- <sup>7</sup> Mitra, *Current Science*, **2**, 126 (1933).
- <sup>8</sup> Mitra, *Current Science*, **2**, 176 (1933).
- <sup>9</sup> Mitra, *Ind. J. Phys.*, **8**, 171 (1933).
- <sup>10</sup> Mitra, *Ind. J. Phys.*, **8**, 445 (1934).

- 11 Mitra, *Current Science*, **2**, 347 (1934).
- 12 Mitra, *Zell. fur Phys.*, **92**, 61 (1934).
- 13 Mitra, *Zell. fur Phys.*, **97**, 137 (1935).
- 14 Mitra, and Krishnam, *Nature*, **181**, 204 (1933).
- 15 Jablonski, *Acad. Pol. Sci. et letters.—Bull.*, **1-2A**, 14 (1934)
- 16 Grisebach, *Zell. fur Phys.*, **101**, 13 (1936)
- 17 Perrin, *Fluorescence duree elementaire d' emission lum.* Hermann, Paris (1931)
- 18 Grisebach, *l.c.*
- 19 Perrin, *Thesis* (1929), Paris.
- 20 Mitra, *Zell. fur Phys.*, **92**, 61 (1934).
- 21 Wawilow, *Zell. fur Phys.*, **80**, 52 (1928); **53**, 665 (1929).
- 22 Wawilow and Frank, *Zell. fur Phys.*, **89**, 100 (1931).
- 23 Wawilow and Seveshnikoff, *Acta. Phys. Chim., U.R.S.S.*, **3**, 257 (1935).
- 24 Seveshnikoff, *Acta. Phys. Chim., U.R.S.S.*, **3**, 453 (1936).
- 25 West and Jetty, *Proc. Roy. Soc.*, **121A**, 199, 313 (1928).

# RAMAN EFFECT IN ARSENATES AND HEAT OF DISSOCIATION OF AS-O

By S. M. MITRA

(Received for publication, October 6, 1939)

**ABSTRACT.** The Raman spectra of arsenates in solution have been investigated and the four lines with  $\Delta\nu$  equal to 349, 827, 878 and 463  $\text{cm}^{-1}$  have been assigned to the  $\text{AsO}_4$  ion. The binding force between As and O has been calculated and then the heat of dissociation has been determined.

## INTRODUCTION

After the discovery of the Raman effect, several organic and inorganic substances have been studied with the object of interpreting the frequency shifts in the Raman spectra in terms of their grouping of atoms.

The correlation of the frequency shifts in the inorganic compounds with the groupings of atoms and their characteristic oscillation frequencies was first brought about by the works of Pringsheim, Rosen and Carelli<sup>1</sup> on several inorganic nitrates in solution and the same results were virtually obtained by other investigators. As regards the investigation of salts containing ion of the type  $\text{XO}_4$ , it was carried out successfully by Krishnamurti,<sup>2</sup> Nishi<sup>3</sup> and others. But a few gaps, however, remain to be filled up, i.e.,  $\text{AsO}_4^{4-}$  ions do not appear to have been investigated in a rigid way. Ghose and Kar<sup>4</sup> attempted to study a few arsenates in solution without much success.

In the present investigation the author attempts to study the Raman effect of a few arsenates in solution and from the Raman shifts the heat of dissociation of the bond As-O is calculated.

## EXPERIMENTAL ARRANGEMENTS

The substances were studied in aqueous solution and they were all of Merck's preparation further purified by recrystallisation. Solution was made with redistilled water and was rendered free from the suspended matter by repeated filtration. The method of illumination was virtually the same as that of Wood. The solution was put in an inner tube placed inside a vertical outer jacket. The whole arrangement was clamped upright and a vertical quartz-mercury lamp was placed alongside, so that the light scattered at right angles, emerged along the axis of the vertical inner tube. The scattered beam was totally reflected by a rectangular

## Fluorescein

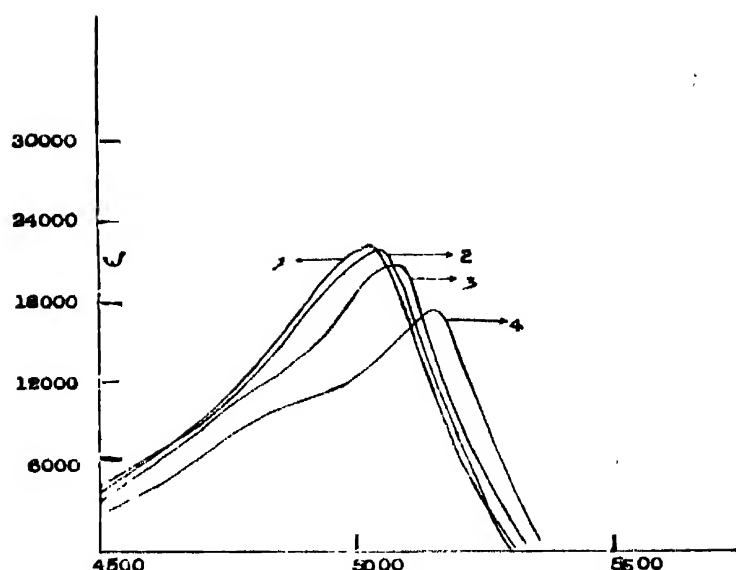


**FIGURE 3**  
Fluorescein

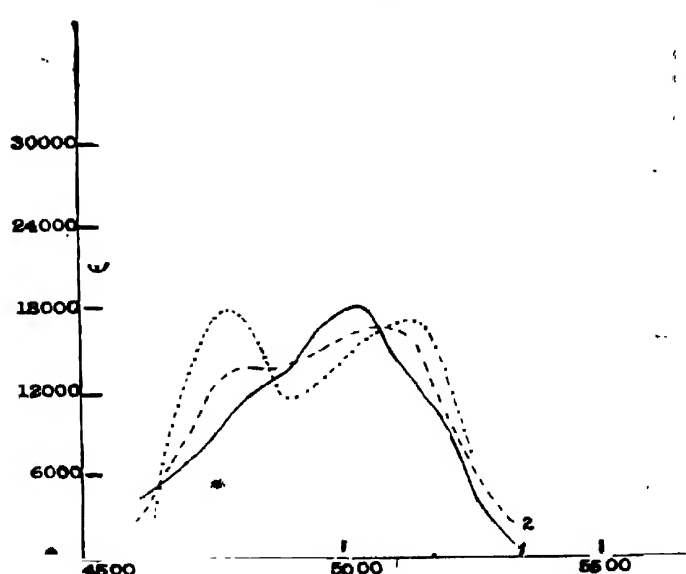


**FIGURE 4**

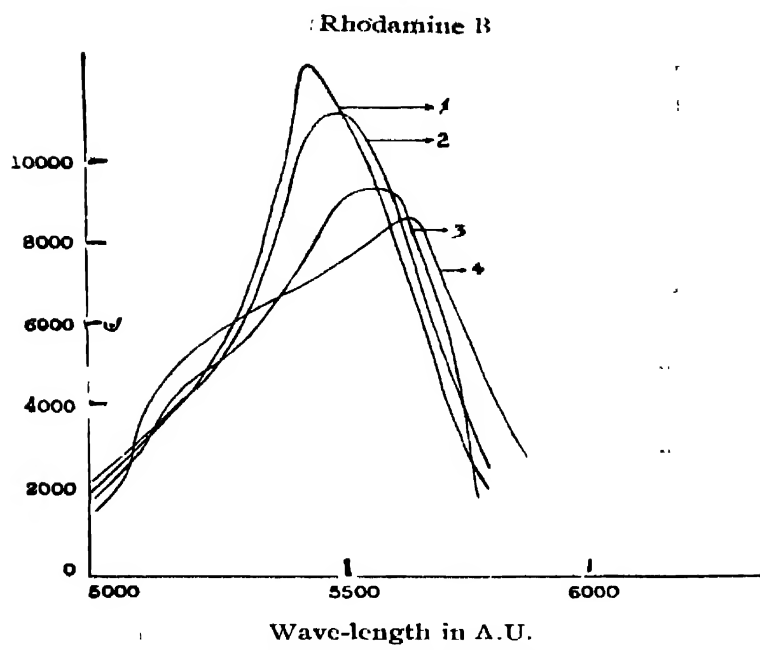


FIGURE 5  
Rhodamine B

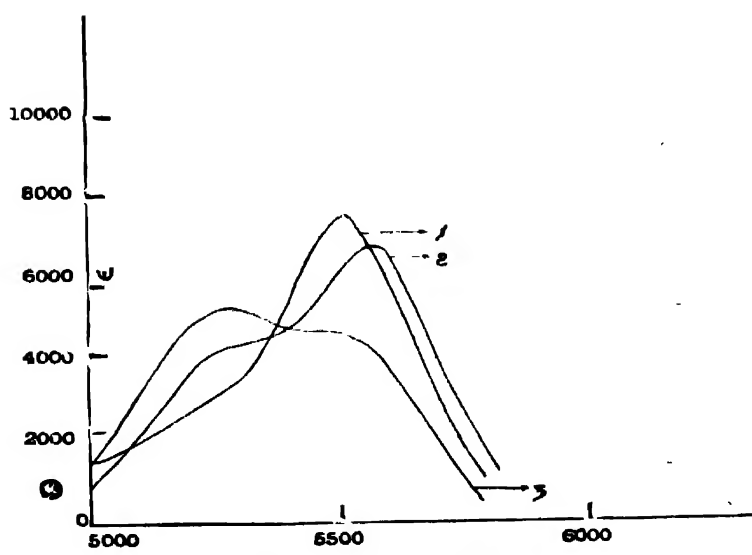
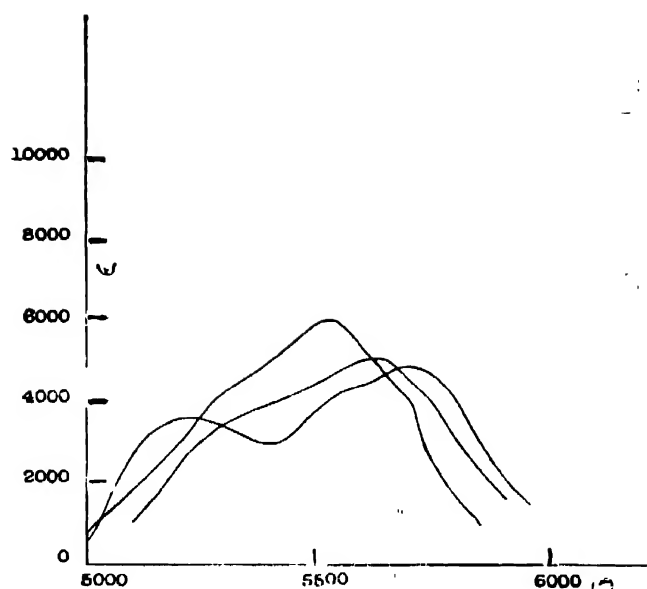
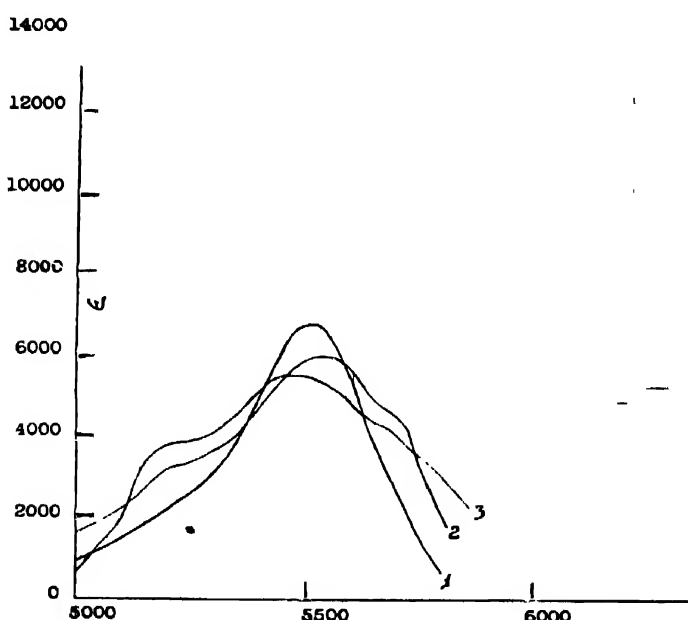


FIGURE 6

## Rhodamine B



Wave-length in A.U.

Concentration of rhodamine B =  $1 \times 10^{-4}$  gm./c.c.Concentration of KI = 0      2.      Concentration of KI =  $0.02$  gm./c.c.3.      Concentration of KI =  $0.10$  gm./c.c.FIGURE 7  
Rhodamine B

Wave-length in A.U.

Concentration of rhodamine B =  $1 \times 10^{-5}$  gm./c.c.

1.      Measurement made just after the addition

2.      "      "      "      "      1 hour

3.      "      "      "      "      3 hours

FIGURE 8

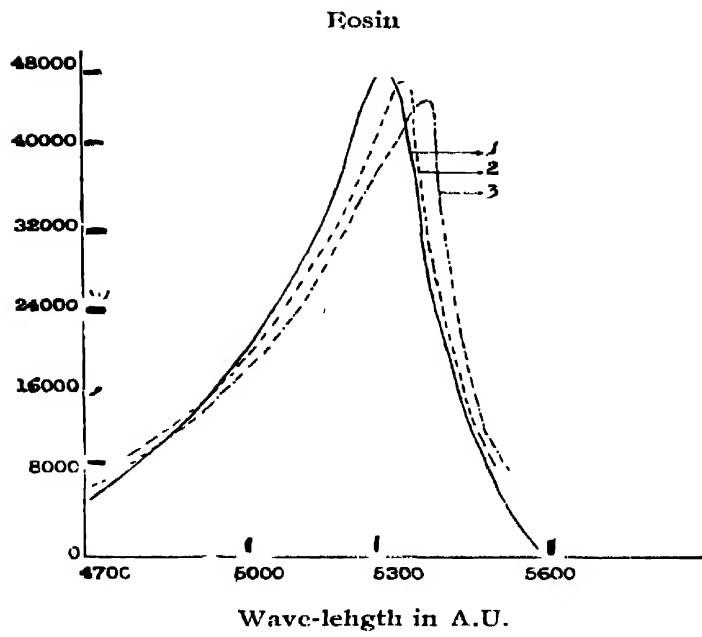


FIGURE 9  
Eosin

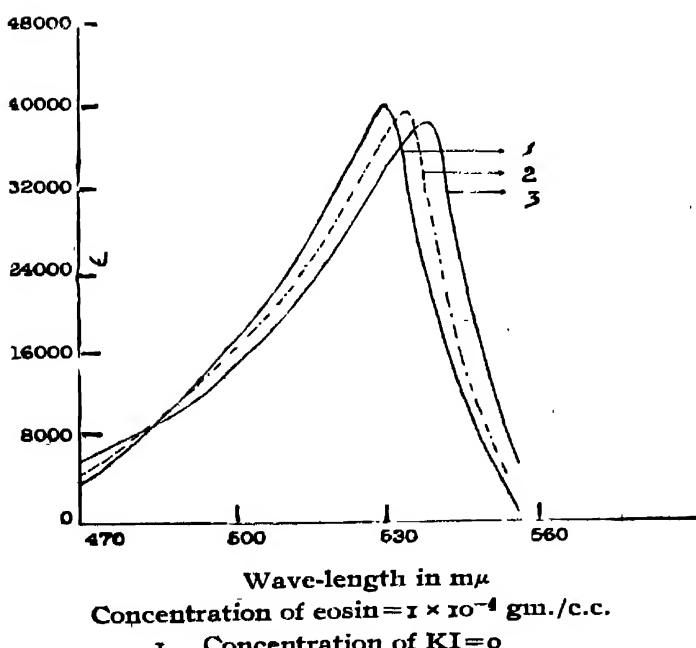


FIGURE 10

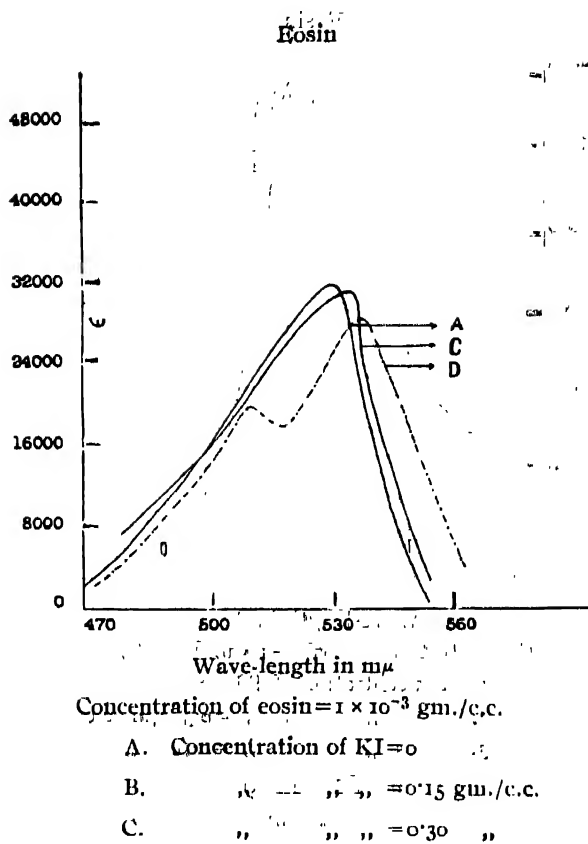


FIGURE 11

(b) The maximum value of the extinction coefficient decreases.

(c) Nature of the curve changes; with the increase in the concentration of potassium iodide the fundamental maximum of the absorption band becomes flat concurrently with the growth of another maximum on the short wave-length side.

In the case of rhodamine B, the nature of the absorption band changes a little on the addition of even traces of potassium iodide even when the concentration of the dyestuff is very small (of the order of  $10^{-6}$  gm./c.c.) (see fig. 5). This change consists in the displacement of the whole spectrum towards the longer wave-length side and in an appreciable change in the value of the maximum extinction co-efficient. But when the concentration of the dyestuff is higher than this (*i.e.*, of the order of  $10^{-5}$  gm./c.c.) addition of potassium iodide brings about a profound change in the absorption spectrum (see figs. 6, 7) similar to that observed in case of fluorescein. Moreover the extinction coefficients in this case were found to vary with time, when the concentration of the dyestuff is of the order of  $10^{-5}$  gm./c.c. or more. (See fig. 8.)

In the case of eosin at concentration  $10^{-5}$  gm./c.c. and  $10^{-4}$  gm./c.c. (see figs. 9, 10) the absorption curve was observed to shift a little towards the red on adding potassium iodide, the nature of the curve remaining the same. This shift was greater in the case of eosin than in that of fluorescein. But when the concentration of the dyestuff was of the order of  $10^{-3}$  gm./c.c., there was also a profound change in the nature of the absorption curve on the addition of potassium iodide (see fig. 11) showing the formation of "complex molecules."

In conclusion the author thanks Prof. S. N. Bose for his kind interest in the work.

PHYSICS LABORATORY,  
DACCA UNIVERSITY.

#### R E F E R E N C E

*Thesis*, Berlin.



# A WEAK RADIO-ACTIVE SUBSTANCE

(*A preliminary note*)

BY RAJENDRALAL DE

(Received for publication, October 9, 1939)

## Plate XVIII

**ABSTRACT.** The radio-active property of one of the constituents described in the author's pamphlet, "Twin Elements in Travancore Monazite," has been detected. The constituent appears to emit  $\alpha$ -rays. A rough estimate of its average life has been given.

The mineral monazite contains two interesting constituents possessing similar chemical properties. Their similarity, being also manifested in the formation of gaseous and volatile derivatives, facilitates their separation from the remaining constituents of the mineral. One of the two constituents is weakly radio active, but its radio-activity is masked when it remains mixed with the other constituent. Its radio-activity has been detected with the  $\alpha$ -electroscope and with the help of the photographic plates as well.

An electro-chemical deposit of the substance on aluminium was employed for detecting its radio-activity. In connection with the electroscope employed for the purpose of detection the stage in the ionization chamber, used for placing a radio-active source had to be fixed within a few millimetres from the upper disc carrying the leaf of the electroscope. The radio-activity found with such an arrangement and using a source, 8 cms. in diameter, was about 2 units (arbitrary scale) while the natural leak of the instrument was about 5 units (of the same scale). For the purpose of photographic detection a source of the above kind and also a solution of a gaseous electrolytic product obtained from the same radio-active substance, put directly in contact with a photographic plate and thus infected, were employed. In the former case the photographic plate was placed at about 3 mm. above the source, and was exposed to its radiation with or without an intervening screen for a period (in most cases) of 60 days. Figure 1, plate XVIII refers to a case of an intervening screen, made with two strips of aluminium foil of  $10\mu$  in thickness and placed in the form of a cross, almost touching the photographic plate. The shadow cast by the strips appears in the plate. Figure 2 refers to a case without any intervening screen. The plate appears apparently blank, but under a microscope it shows a number of dots as shown by figure 3, a micro-photograph of these dots. The micro-photograph shows however two kinds of dots, large and small. The large dots can be conveniently seen even with a magnification of 50 times. A count of these large dots has been made.

In a particular plate the dots were distributed in the following manner, count being made at different distances from a point corresponding to the centre A of the source :

at 2 cms. an average of 0.81 per sq. mm.

at 4 " " 0.71 " "

at 6 " " 0.71 " "

Similar count in two different plates, exposed to the same source for the same period of 60 days but one period following the other, has given the following values.

One exposed from the 1st April to 3rd June gave an average of 1.62 dots per sq. mm. while the other exposed from the 13th August to the 12th October gave an average of 0.81 dots per sq. mm. The mean interval of time between the two exposures is 123 days, i.e., 13 days less than the half-value period of polonium *viz.*, 136 days. Presuming each dot to represent an impact with one  $\alpha$ -particle, the large dots may reasonably be ascribed to polonium, since they seem to diminish by one-half during about the interval of the half-value period of polonium.

The small dots have been ascribed to a different variety of the  $\alpha$ -rays. By infecting a photographic plate with a solution of the same radio-active material after it was allowed to stand for a few months before it was so used, two kinds of  $\alpha$ -ray tracks, long and short, have been found. Figure 1 refers to a plate infected with a gaseous product of electrolysis, obtained from the said radio active material, and kept (after being infected) in the dark for a period of three months. For the observation of the tracks a magnification of seven to eighteen hundred times has been employed. It appears that the length of the short track is almost half the length of the long one. Ascribing the long tracks to polonium, the average life of its associate giving short tracks comes out to be very much longer than  $10^{20}$  years.

It may be remarked that the photographic plate relating to figure 2, exposed without an intervening screen, is clear and practically free from fog. The absence of fog indicates the absence of the  $\beta$ -radiation. There exists, however, a dark background in the photograph relating to figure 1, exposed with an intervening screen. The darkening effect is evidently due to the  $\delta$  rays emerging from the aluminium foil and arising from its impact with the  $\alpha$ -rays from the source.

We may mention that the radio-active material is responsive to some of the chemical tests of polonium, visible to the naked eye, and has a reference to the substance described in author's pamphlet, "Twin elements in Travancore Monazite" where its radio-activity has been anticipated.

In conclusion I beg to thank Mr. C. R. Bose for helping me by counting the dots relating to figure 2 and also Mr. B. C. Shome and Dr. S. Hedayetullah of the Manipur Agricultural Farm, Dacca, for the micro-photographs.

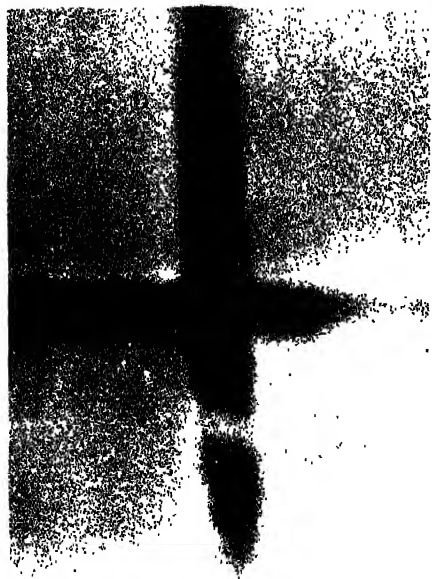


Figure 1.

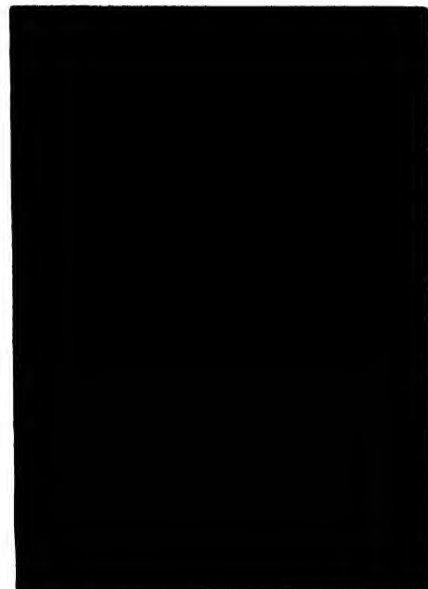


Figure 2.

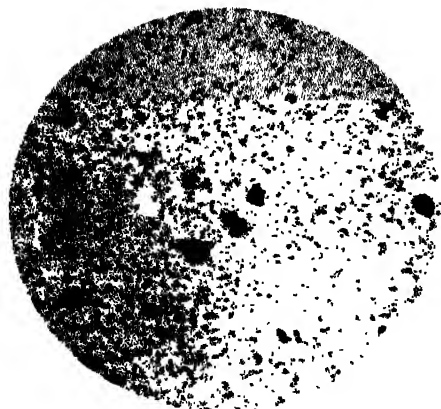


Figure 3.

S represents small dots  
L „ large „

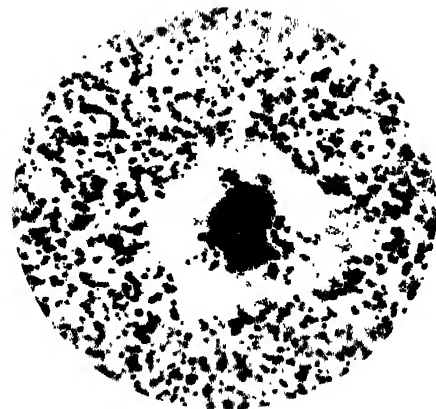


Figure 4.

LL represents long track  
S „ short „



# NOTE ON MAINTENANCE OF ELECTRON EMISSION IN COSSOR VALVES AFTER THE LOW-TENSION SUPPLY IS DISCONNECTED

By N. S. PANDYA

AND

P. D. PATHAK

*(Received for publication, September 22, 1930)*

**ABSTRACT.** The persistence of the anode current, even after the low-tension supply is disconnected as observed previously by Narsimhaiya with some Cossor valves, has been studied in detail with a few Cossor 2-volt battery valves.

In a paper by Narsimhaiya<sup>1</sup> it is stated that in some Cossor valves anode current persisted even after disconnecting the low-tension supply when it reached a certain minimum value, viz., 15% of the normal filament-current.

We studied this phenomenon with several Cossor 2-volt battery valves under static conditions. The grid was given a potential of 2 volts and the anode potential was gradually increased up to 300 volts but no persistence of anode current was observed when the filament current was switched off. The maximum anode current was 80 milliamperes. Later the grid was given an increasing positive voltage from 0 to 50 volts and the anode voltage was kept at 20, 40, 60, and 80 volts respectively. Even here no persistence was observed except in the case of 210 H. F. (when the grid was at +50 volts) probably due to the breaking of the inductive circuit. The anode current in this case was 88 m.A. and persisted at 63 m.A. for about a minute under one set of conditions. The highest anode current in the other valves was 109 m.A. and the grid current 83 m.A.

Three different potentials, viz., 20, 30 and 40 volts were also applied to the grid and plate shorted. Out of the two sources of potential used, viz., D. C. mains and a high-vacuum rectifier giving smoothed 400 D. C. voltage with a potentiometer arrangement, the former failed to exhibit the phenomenon while the latter curiously did in the case of almost all the Cossor valves, viz., 220P., 25 H.F., 210 H.L., 210 R.C., 215 S.G., 215 P. and 220 S.V.G. When the filament current is switched off the anode current tries to fall, thus immediately increasing the potential difference between the plate and the filament. Probably this rising voltage checks the falling current and a balance between

the two is obtained. The persistence was noted for over 15 minutes in all the cases (after 15 minutes the H.T. supply was removed fearing the valves might get damaged). The anode current varied between 74 to 100 m.A. for different valves and the value of the persistence current was about 70 to 80% of these values.

The above-named valves include even those that were discarded by Narsinhaiya. Narsinhaiya explained this persistence by assuming that the filament remained hot by the passage of the anode current through it. The filament coating is the same in all the Cossor valves tried, as reported to us by the manufacturers, and hence there is no reason why some of them should behave differently.

Further work is being carried on to investigate this in detail and also to study the same under dynamic conditions. An attempt is also being made to correlate this behaviour with circuit arrangement and the temperature of the filament.

We thank Dr. C. C. Shahi for sympathetic guidance and Prof. N. K. Aptc for suggestions and facilities in this work.

PHYSICS LABORATORY,  
BARODA COLLEGE,  
BARODA.

R B F R R E N C B

<sup>1</sup> *Proc. Inst. Radio Engineers.* **23**, 252 (1935)

# ON THE LONDON-VAN DER WAALS FORCES BETWEEN TWO DISC-LIKE PARTICLES\*

By G. P. DUBE  
(Balwant Rajput College, Agra)

AND  
H. K. DASGUPTA  
(Institut des Mécaniques, Paris)

*(Received for publication, November 2, 1939)*

**ABSTRACT.** The London-van der Waals interaction energy has been calculated between two disc-like particles. Only two cases are dealt with : i) when the two discs are in the same plane, (ii) when their planes are parallel to each other but perpendicular to the line of centres. In the first case the interaction energy for small interparticle distances varies inversely as  $5^{1/2}$  power of the shortest distance between the edges of the discs and in the second case it varies inversely as the quadratic power of the distance between their centres. These results may be used in explaining the arrangement of particles in thixotropic pastes.

Many of the characteristic physical properties of the colloidal solutions are undoubtedly explained by the nature of the interaction forces acting between the particles of the sol. or gel. In general there will be contributions to the interaction energy from forces of three types (i) from the electrical forces arising due to the electrical double layer of the particles, (ii) from attractive forces acting between two molecules, (iii) due to hydration and electrostrictive effects. Nothing practically is known about the hydration effects and moreover it will only be important at high concentrations. We, therefore, entirely neglect it. The contribution due to the electrical double layer has already been investigated in detail by one<sup>1</sup> of us (G. P. Dube) by using the approximate Debye-Hückel equation in the theory of strong electrolytes and the readers are requested to refer to the original papers. Besides these we should also consider the attracting forces which play an important rôle in establishing the properties of a colloidal system. Kallmann and Miss Willstatter<sup>2</sup> have definitely shown that the attraction cannot be caused by van der Waals' forces (e.g., Keesom orientation effects ; Debye induction effects) which decrease so strongly with increasing distance that they practically vanish for interparticle distances of the order of molecular dimensions. How-

\* Communicated by the Indian Physical Society.

ever, London,<sup>3</sup> using wavemechanical concepts, has conclusively shown that the short-lived electronic displacements caused when two molecules approach each other lead to the development of attractive forces which have an additive character, act over much more than molecular dimensions, are independent of the position of the molecules and the temperature. Their additive character makes them valuable in the discussion of the colloidal phenomena. The interaction between two particles is, therefore, the sum of the interactions of all the molecules or ions involved. For small interparticle distances it will depend on the actual shape and surface structure of the particles.

The interaction energy between two particles containing  $q$  atoms per c.c. is given by,

$$U = - \int \int_{v_1 v_2} dv_1 dv_2 q^2 \lambda \quad (1)$$

where  $r$  is the distance between the volume elements  $dv_1$ ,  $dv_2$  of the two particles and  $\lambda$  is the van der Waals constant. For the case of spherical particles this integral has been calculated approximately by Bradley<sup>4</sup> and accurately by Hamaker.<sup>5</sup>

It is well known that colloidal systems, exhibiting thixotropic phenomena, generally consist of non-spherical<sup>6</sup> particles. They are rod-shaped in the thixotropic sols. of vanadium pentoxide ( $V_2O_5$ ), disc-like in the sols. of iron-oxide and paste of clay. It may be of interest, therefore, to derive the expression for the van der Waals interaction energy between two non-spherical particles. There are many difficulties of mathematical nature involved in the evaluation of the integral.<sup>1</sup> However, we have been able to find a convenient expression for the case of two disc-like particles.

Let us consider the case of two circular discs of radii  $a$  and  $b$ , with their centres at a distance  $c$  apart. There are two interesting cases : (a) the discs are in the same plane, (b) the planes of the discs are parallel to each other, but perpendicular to the line of centres. If  $\delta l_1$ ,  $\delta l_2$  be the thicknesses of the two discs ;  $dS_1$ ,  $dS_2$  be the surface elements, the van der Waals interaction energy becomes

$$U = - q^2 \lambda \delta l_1 \delta l_2 \int \int_{S_1 S_2} dS_1 dS_2 \quad (2)$$

To evaluate the integral, we proceed by an indirect method. We first determine the potential energy due to the first disc of radius  $a$ , at a point P whose co-ordinates are  $(x, 0, z)$  referred to the centre of the disc as origin. (See fig. 1).

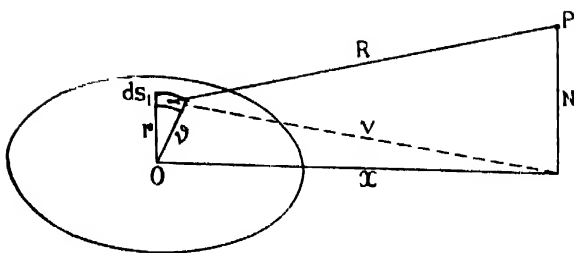


FIGURE 1

This potential energy is given by

$$u = -2q\lambda\delta l_1 \int_{-\pi}^{\pi} \int_{-\infty}^{\infty} \frac{dr d\theta}{R^6} \quad (3)$$

where

$$\begin{aligned} R^2 &= r^2 + x^2 + z^2 = r^2 + x^2 - 2xr \cos \theta + z^2 \\ &= (r - x)^2 + z^2 + 2xr(1 - \cos \theta) \\ &= (r - x)^2 + z^2 - 2xr(1 + \cos \theta). \end{aligned}$$

To evaluate the integral, transform the variable such that

$$p\xi = \cot \frac{\theta}{2},$$

where

$$p^2 = \frac{(x - r)^2 + z^2}{(r - x)^2 + z^2} = \frac{[*]}{(*)}.$$

It is easy to verify that

$$R^2 = [*] \cdot \frac{1 + \xi^2}{1 + p^2 \xi^2}$$

$$d\theta = -\frac{2pd\xi}{1 + p^2 \xi^2}$$

where the limits of  $\xi$  are from infinity to zero. Hence the integral (3) becomes

$$u = -4q\lambda\delta l_1 \int_0^\pi \int_0^\infty \frac{r dr p d\xi (1 + p^2 \xi^2)^2}{[*]^3 (1 + \xi^2)^3}.$$

The integration with respect to  $\xi$  can be carried out by the method of residues and then we get

$$u = -\frac{\pi}{4} q\lambda\delta l_1 \int_0^\pi \frac{r dr p (3p^4 + 2p^2 + 3)}{[*]^3}.$$

The integration over  $r$  is elementary but rather tedious. We shall not go into details here. It is easy to verify that the integrand can be written in the form

$$-\frac{d}{dr} \left\{ \frac{1}{[*]^{\frac{3}{2}} - (*)^{\frac{1}{2}}} + \frac{1}{[*]^{\frac{1}{2}} - (*)^{\frac{3}{2}}} \right\} - \frac{x}{z^2} \frac{d}{dr} \left\{ \frac{x-r}{[*]^{\frac{1}{2}} - (*)^{\frac{3}{2}}} + \frac{x+r}{[*]^{\frac{3}{2}} - (*)^{\frac{1}{2}}} \right\} \\ - \frac{1}{z^4} \frac{d}{dr} \cdot \frac{x^2 - r^2 - z^2}{[*]^{\frac{1}{2}} - (*)^{\frac{1}{2}}}.$$

Hence,

$$u = \frac{\pi}{4} q \lambda \delta l_1 \left\{ \frac{1}{[*]^{\frac{3}{2}} - (*)^{\frac{1}{2}}} + \frac{1}{[*]^{\frac{1}{2}} - (*)^{\frac{3}{2}}} + \frac{x}{z^2} \left( \frac{x-r}{[*]^{\frac{1}{2}} - (*)^{\frac{3}{2}}} + \frac{x+r}{[*]^{\frac{3}{2}} - (*)^{\frac{1}{2}}} \right) \right. \\ \left. + \frac{x^2 - r^2 - z^2}{z^4 [*]^{\frac{1}{2}} - (*)^{\frac{1}{2}}} \right\}_o \\ = - \frac{\pi}{4} q \lambda \delta l_1 \left\{ \frac{1}{z^4} - \frac{1}{(*)\sqrt{-}} - \frac{1}{[+] \sqrt{-}} - \frac{x}{z^2} \left( \frac{x-a}{(*)\sqrt{-}} + \frac{x+a}{[+] \sqrt{-}} \right) - \frac{x^2 - a^2 - z^2}{z^4 \sqrt{-}} \right\} \quad (4)$$

where  $(-) = (x-a)^2 + z^2$ ;  $[+] = (x+a)^2 + z^2$ ;  $\sqrt{-} = [+]^{\frac{1}{2}} (-)^{\frac{1}{2}}$ .

#### Case (a) Two discs in the same plane

If we put  $z=0$  in the above expression, we can find out the potential energy at any point lying in the plane of the disc and at a distance  $a$  from the centre and it is given by

$$u_a = -\frac{\pi}{2} q \lambda \delta l_1 a^2 \cdot \frac{a^2 + 2x^2}{(x^2 - a^2)^4} \quad \dots \quad (5)$$

To obtain the interaction energy between the two discs, we multiply the above expression by  $q \delta l_2 dS_2$  and integrate over the surface of the second disc of radius  $b$ .

$$I_a = -q^2 \lambda \delta l_1 \delta l_2 \frac{\pi a^2}{2} \int_{S_2} \frac{a^2 + 2x^2}{(x^2 - a^2)^4} dS_2.$$

Introducing polar co-ordinates  $(r, \theta)$  with respect to the centre of the second disc, we have,  $x^2 = c^2 + r^2 - 2cr \cos \theta$  and so,

$$I_a = -q^2 \lambda \delta l_1 \delta l_2 I_a = -q^2 \lambda \delta l_1 \delta l_2 \pi a^2 \int_0^b \int_0^\pi \frac{r dr d\theta (a^2 + 2x^2)}{(x^2 - a^2)^4}.$$

Integration over  $\theta$  can be carried out by using the same trick as before. Putting

$$p_1 \xi = \cot \frac{\theta}{2}$$

where

$$p_1^2 = \frac{(c+r)^2 - a^2}{(c-r)^2 - a^2},$$

the integral can be written as

$$I_a = 2\pi a^2 \int_0^b \frac{p_1 r dr}{\{(c+r)^2 - a^2\}^3} \int_0^\infty \left\{ \frac{3a^2(1+p_1^2\xi^2)^3}{\{(c+r)^2 - a^2\}(1+\xi^2)^4} + \frac{2(1+p_1^2\xi^2)^3}{(1+\xi^2)^3} \right\} d\xi.$$

We can now proceed by the method of residues and thus obtain

$$\begin{aligned} I_a &= \frac{3\pi^2 a^4}{16} \int_0^b p_1 \frac{(5+3p_1^2+3p_1^4+5p_1^6)}{\{(c+r)^2 - a^2\}^4} r dr + \frac{\pi^2 a^2}{4} \int_0^b \frac{p_1 (3+2p_1^2+3p_1^4)}{\{(c+r)^2 - a^2\}^3} r dr, \\ &= I_2 + I_1. \end{aligned}$$

The integral  $I_1$  has already been evaluated, the only difference being in the definition of the brackets [ ] and ( ), which now become  $(c+b)^2 - a^2$ ,  $(c-b)^2 - a^2$  respectively and are denoted by [ ]<sub>1</sub>, ( )<sub>1</sub>. Similarly we can evaluate  $I_2$ . The results obtained are :—

$$\begin{aligned} I_1 &= \frac{\pi^2 a^2}{4} \left[ \frac{1}{a^4} - \frac{1}{(\ )_1 \sqrt{1}} - \frac{1}{[ ]_1 \sqrt{1}} + \frac{c}{a^2} \left\{ \frac{c-b}{(\ )_1 \sqrt{1}} + \frac{c+b}{[ ]_1 \sqrt{1}} \right\} + \frac{b^2 - a^2 - c^2}{a^4 \sqrt{1}} \right] \\ I_2 &= \frac{\pi^2 a^2}{4} \left[ -\frac{1}{a^4} - \frac{3a^2}{4} \left( \frac{1}{[ ]_1^2 \sqrt{1}} + \frac{1}{(\ )_1^2 \sqrt{1}} \right) + \frac{3c}{4} \left( \frac{c-b}{(\ )_1^2 \sqrt{1}} + \frac{c+b}{[ ]_1^2 \sqrt{1}} \right) \right. \\ &\quad \left. + \frac{c^2 - a^2}{[ ]_1 (\ )_1 \sqrt{1}} - \frac{c}{a^2} \left\{ \frac{c-b}{(\ )_1 \sqrt{1}} + \frac{c+b}{[ ]_1 \sqrt{1}} \right\} - \frac{b^2 - a^2 - c^2}{a^4 \sqrt{1}} \right]. \end{aligned}$$

Adding the two and making necessary simplifications this gives

$$\begin{aligned} I_a &= \frac{\pi^2 a^2 b^2}{16 \sqrt{1}} \left\{ 3 \left( \frac{c-b}{(\ )_1^2} - \frac{c+b}{[ ]_1^2} \right) - \frac{2b}{[ ]_1 (\ )_1} \right\} \\ &= \frac{\pi^2 a^2 b^2}{2} \cdot \frac{\{c^2(2c^2 - a^2 - b^2) - (b^2 - a^2)^3\}}{\{(c+b)^2 - a^2\}^{\frac{5}{2}} \{(c-b)^2 - a^2\}^{\frac{5}{2}}}. \quad \dots (6) \end{aligned}$$

The expression is symmetrical between  $a$  and  $b$ , as it ought to be. In the particular case of equal radii,  $a=b$ , the interaction energy becomes

$$E_a = -q^2 \lambda \delta l_1 \cdot \delta l_2 \cdot \frac{c^2 - a^2}{c^3(c^2 - 4a^2)^{\frac{5}{2}}}.$$

Putting  $c/a=s$ , where  $s=2$  denotes contact, the above expression becomes

$$E_a = -q^2 \lambda \delta l_1 \cdot \delta l_2 \cdot \frac{\pi^2}{a^2} \cdot \frac{s^2 - 1}{s^3(s^2 - 4)^{\frac{5}{2}}}. \quad \dots (7)$$

$$= -B \cdot \frac{s^2 - 1}{s^3(s^2 - 4)^{\frac{5}{2}}}. \quad \dots (8)$$

Hence  $E_a$  varies as  $1/\delta^2$  for small  $\delta$ , where  $\delta$  is the shortest distance between the edges of the two particles, i.e.,  $s=2+\delta$ .

## Case (β)

The discs have their planes parallel and these are also perpendicular to the line of centres. The potential energy at any point  $(r, \theta)$  of the second disc due to the first is obtained by putting  $z=c$  and  $x=r$  in (4). Integration over the angle  $\theta$  then simply gives a factor  $2\pi$  and the interaction energy is given by

$$E_\beta = -q^2 \lambda \delta l_1 \delta l_2 \frac{\pi^2}{2} \int_0^b \left[ \frac{1}{c^4} - \frac{1}{(r-a)^2 \sqrt{(r-a)^2 + c^2}} - \frac{1}{(r+a)^2 \sqrt{(r+a)^2 + c^2}} - \frac{r^2 - c^2 + a^2}{c^4 \sqrt{(r^2 - c^2 + a^2)}} \right] r dr$$

The brackets  $[ ]$ ,  $( )$  now denote  $(r-a)^2 + c^2$ ,  $(r+a)^2 + c^2$

On integrating, we obtain,

$$\begin{aligned} E_\beta &= -q^2 \lambda \delta l_1 \delta l_2 \frac{\pi^2}{2} \left[ \frac{r^2}{2c^4} + \frac{r^2 + c^2 + a^2}{2c^2 \sqrt{(r^2 + c^2 + a^2)}} - \frac{1}{2c^4 \sqrt{(r^2 + c^2 + a^2)}} \right]_0^b \\ &= -q^2 \lambda \delta l_1 \delta l_2 \frac{\pi^2}{4c^4} \left[ (b^2 + a^2) - \frac{(b^2 - a^2)^2 + c^2(a^2 + b^2)}{\{(b+a)^2 + c^2\}^{\frac{3}{2}} \{(b-a)^2 + c^2\}^{\frac{3}{2}}} \right]. \quad \dots \quad (9) \end{aligned}$$

In the particular case of equal radii  $a=b$ , using  $c/a=s$  this becomes

$$\begin{aligned} E_\beta &= -q^2 \lambda \delta l_1 \delta l_2 \frac{\pi^2}{2a^2} \left\{ \frac{1}{s^4} - \frac{1}{s^3(s^2+4)^{\frac{3}{2}}} \right\} \\ &= -\frac{B}{2} \left\{ \frac{1}{s^4} - \frac{1}{s^3(s^2+4)^{\frac{3}{2}}} \right\}. \quad \dots \quad (10) \end{aligned}$$

For very small distances between the two discs,

$$E_\beta \text{ varies as } \frac{1}{s^4}.$$

The results obtained in these cases differ from that obtained in the case of two spheres, where  $E$  varies inversely as the first power of the distance. It is to be observed that the range of the London-van der Waals forces in case (a) is greater than that in the case (β). It may therefore be probable that the particles in a thixotropic paste arrange themselves according to the case (a), i.e., in the form of chains or some honey-comb structures. Such structures have been observed in some cases. For details on the experimental data the readers are requested to refer to Buzagh's Colloid Systems Sec. 25 (b) p. 150, (1937), the Technical Press Ltd., London.

This work was completed during my (G. P. Dube) stay at the Institut Henri Poincaré, Paris and a note to this effect has already been published in Comptes Rendus de l'Académie des Sciences, Paris, p. 340, tome 209 (1939).

My thanks are due to Prof. Louis de Broglie and Prof. Francis Perrin for the hospitality enjoyed by me during my stay there.

N.B.--For the definition of the range of van der Waals forces in colloidal systems consult Hamaker, Recueil des Travaux Chimiques des Pays-Bas t. 57, p. 70 (1938.) According to the first definition range is the distance at which energy equals  $kT$  and according to the second, range is the distance at which the force equals the weight of the particles or to a certain multiple of the weight.

#### R E F E R E N C E S

- <sup>1</sup> G. P. Dubé and S. Levine, *Comptes Rendus*, **208**, 1812 (1939). Two papers in *Trans. Faraday Soc.*, **34**, 1125, 1141 (1939). General Math Theory. *Phil. mag.* . . . in press.
- <sup>2</sup> Kallmann and Miss Willstätter. *Naturwiss.* **20**, 952 (1932)
- <sup>3</sup> London, *Zeit. Physik. Chem.*, B, **11**, 246 (1936). *Trans. Faraday Soc.*, **33**, 8 (1937).
- <sup>4</sup> Bradley, *Phil. Mag.*, **13**, 853 (1932)
- <sup>5</sup> Hamaker, *Physica*, **4**, 1058 (1937).
- <sup>6</sup> See Freundlich's *Thixotropy*. Actualités Scientifiques et Industrielles No 267, Hermann and Cie, Paris (1935) p. 10. This book contains a wealth of information on the thixotropic phenomena.



# PRESSURE WAVES AND BOUNDARY SURFACES IN THE FREE ATMOSPHERE \*

By D. S. SUBRAHMANYAM, M.A.,  
A. C. College, Guntur

(Received for publication, November 28, 1939)

**ABSTRACT.** Assuming that an element of air keeps its volume constant in small displacements and that the atmosphere is characterised by boundary surfaces each of which divides the atmosphere into two regions—the upper and the lower, between which there is no mixing of air, a simple theory of canal waves of air is developed on the basis that the wave form is similar to the equilibrium form. A result is obtained connecting the height of 'the ground layer' with the velocity of the wave, which is similar to that for a canal of water. Several interesting results follow :

- (1) The boundary surface corresponding to the semi-diurnal vibration resembles the Tropopause of the atmosphere.
- (2) There is possibility for mixing of air between the ground and this boundary surface so that convection can take place up to it and not beyond. Convective equilibrium can therefore prevail in the ground layer which therefore resembles the Troposphere.
- (3) The possibility for a number of boundary surfaces between that corresponding to  $n$  equal to 2 and  $n$  equal to infinity of the polar component explains the possibility of this region of the atmosphere to be divided into strata between which there can be no motion of air, i.e., the possibility of a 'Stratosphere.'
- (4) The boundary surface corresponding to the travel of a wave along a great circle will be at a height of 21.85 km. at all points on the globe and should be an isobaric surface. This compares well with the observed fact that at about 20 km. height the pressure at all points on the globe and at all times of the year is the same.
- (5) Possibility has also been shown for other higher boundary surfaces corresponding to higher possible modes of oscillation. The heights deduced for three of them (87.4 km., 196.7 km. and 49.2 km. respectively) are rather close to the heights of the E, F, and D ionised layers of the atmosphere.

## INTRODUCTION

Investigations of the upper atmosphere by means of sounding balloons and radio waves have revealed the fact that the free atmosphere is divided into a number of layers of a permanent nature, the boundary between two consecutive layers being in many cases sharp. There is first the meteorological boundary surface, the Tropopause, discovered by Tisserenc de Bort,<sup>1</sup> which divides the atmosphere into two thermally distinct regions—"the lower, known as the Troposphere, in which the temperature decreases steadily with height and an upper region, the Stratosphere, in which the temperature remains constant or increases slightly with height." The Tropopause "is at a height which varies

\* Communicated by the Indian Physical Society.

from about 18 km. at the equator to about 11 km. over Southern Europe and to 6 km. at the poles. The height at the poles cannot be specified with accuracy, mainly on account of paucity of observations, in the polar regions. The rate of diminution of temperature with height known as the lapse rate does not diminish steadily to zero at the Tropopause but retains approximately its normal value right up to the limit of the Tropopause and then suddenly changes to zero or even changes sign.<sup>22</sup> Further, Shaw "has shown that at 9 km. above the surface, the wind blows horizontally, that no mass of air passes from the Troposphere to the Stratosphere and consequently no mixing of air in the two regions takes place."<sup>23</sup> Another meteorological boundary may also be said to exist at a height of about 20 km. where it is found that the pressure is the same at all points on the globe and at all times of the year. Besides these meteorological divisions there are the ionised layers of the atmosphere : the E layer at a height of about 90 km., the F layer at a height of about 200 km., and the D layer at a height of about 55 km. The lower boundaries of these layers are also considered to be sharp.<sup>1</sup> Thus division into layers marked by sharp boundaries seems to be a very important characteristic of the atmosphere.

There is so far no theory which explains any of these sharp divisions in the atmosphere in a satisfactory manner, not to speak of a comprehensive theory which takes into account all or many of them. Theories of the ionised layers explain the ionisation from the conditions of air obtaining there, but not their sharp lower boundaries. Even though attempts have been made to explain the transition at the Tropopause, the theories offered do not account for the suddenness of the change. The theories put forward by Humphreys<sup>2</sup> and Gold<sup>3</sup> that the Stratosphere is in radiative equilibrium are not entirely satisfactory even in regard to the explanation that they give for the isothermal condition of the Stratosphere.<sup>7</sup>

The present paper attempts to connect these discontinuities in the atmosphere with the pressure oscillations that are taking place in it. Analysis of pressure observations made at different places on the globe has shown that there are several of these pressure oscillations and that the semi-diurnal oscillation is the most predominant of them. This oscillation, according to Schmidt<sup>8</sup>, takes place in two ways :

"(a) Firstly a vibration parallel to the circle of latitude which resolves itself into two complete waves travelling east to west. The amplitude of this vibration is greatest over the equator and decreases towards each pole where it becomes zero."<sup>9</sup> This vibration is called by Simpson "*the equatorial vibration.*"

"(b) And secondly a vibration between the equator and the poles along the circles of longitude. This vibration is caused by a stationary wave so that the pressure increases and decreases at the same absolute time at all places on the polar sides of latitude 35° 16' N. and S., and changes at the same time but in opposite direction between these latitudes and the equator. The amplitude of the pressure changes is greatest at the neighbourhood of the poles where it is

much larger than the amplitude produced there by the equatorial vibration, so that it becomes there the predominant cause of pressure changes." This is called "the polar vibration" by Simpson.<sup>9</sup> Combining the two modes of oscillation, Simpson finds that the semi-diurnal pressure oscillation can be represented by

$$p_2 = 0.937 \sin^3 \theta (\sin 2t + 154^\circ) + 0.137 (\cos^2 \theta - \frac{1}{3}) (\sin 2t - 2\phi + 105^\circ)$$

where  $\theta$  denotes the co-latitude,  $t$  the local time in degrees,  $\phi$  the longitude and the unit is 1 mm. of mercury.

Besides this 12-hourly oscillation, there is also an important 8-hourly oscillation as pointed out by Whipple<sup>10</sup> and Chapman,<sup>11</sup> and a 6-hour component as mentioned by the latter. While the pressure oscillations, the periods of which are related to the solar day of 24 hours, are so prominent, the lunar tides are found to be irregular and practically insensible.

The theoretical study of the oscillations of the atmosphere has been made by Laplace,<sup>12</sup> Kelvin,<sup>13</sup> Margules,<sup>14</sup> Lamb,<sup>15</sup> Chapman,<sup>16</sup> Taylor,<sup>17</sup> Pekeris<sup>18</sup> and others. These investigators considered the oscillations of the atmosphere as a whole, treating the air as a compressible medium. The chief subject for examination by the later workers has been whether the atmosphere possesses a free period of 12 hours so that the 12-hour solar component could be magnified by resonance; but it cannot be said that this has been established yet. Pekeris in his paper tries to resolve the difficulties met with earlier,<sup>19</sup> by showing that it is possible for the atmosphere to have two modes of oscillation, one of period 10½ hours and the other of period 12 hours. However he finds it necessary to adjust 'the top' of the atmosphere by giving it a fall of temperature above the 60 km. level, which does not seem to be supported by observation. On the other hand, Appleton<sup>20</sup> finds from the study of the diurnal and seasonal changes in the maximum ionisation density in the upper atmosphere, that the temperature at great heights (200 km. to 400 km.) should be surprisingly high "that the absolute temperature at a level of 300 km. must be at least 1200°A on a summer day." The subject of atmospheric oscillations may therefore be considered to be still open for study. Recent investigations of ionospheric phenomena by Ranzi,<sup>21</sup> Colwell<sup>22</sup> and Bajpai and Pant<sup>23</sup> show that there are correlations between those phenomena and the atmospheric pressure at the ground. The influences which make the solar component predominant must therefore be considered to have been not yet understood. However, taking the principal features of the oscillations as they are, it would be interesting to examine whether the subject can be treated in a different way and whether such a treatment would yield any interesting results. The present paper is an attempt made in this direction. The principal assumptions made in the development of the theory are as follows :

(a) An element of air tends to keep its volume constant in the movements of the atmosphere when the displacements of the element are not great. Such an assumption made in a recent paper by the author<sup>24</sup> has led to a satisfactory explanation of the constant lapse rate in the free atmosphere and it is but logical

that the hypothesis should be tested by applying it to other movements in the free atmosphere also.

(b) Another departure from the other theories of atmospheric oscillations is the hypothesis that the atmosphere is characterised by layers between which there is no mixing of air. Mention has already been made of the Troposphere and the Stratosphere which are separated by the Tropopause and the ionised layers with their sharp lower boundaries. This hypothesis would therefore take into account, and bring into the compass of theory, these several boundary surfaces in the atmosphere which are apparently disconnected.

#### 'CANAL WAVES OF AIR'

A simple type of oscillations which lend themselves to easy analysis is considered. If we imagine, say, a vertical section of the fluid surrounding the earth along the equator and a tide-generating body to lie in that plane, the horizontal tidal force (per unit mass) on particles of the fluid in the same vertical line may be considered to be independent of the height of the fluid when it is not great. In the equilibrium theory it is assumed that this tide-generating force is balanced by the horizontal gradient of pressure so that this gradient which is

equal to  $\frac{1}{\rho} \cdot \frac{\partial p}{\partial x}$  ( $x$  denoting the horizontal direction in this section,  $\rho$  the density and  $p$  the pressure at a point) should also be independent of height whatever be the nature of the fluid, whether it be compressible or incompressible, uniform or varying in density. Suppose now that the tide-generating force ceases to act. The fluid would start to move due to the gradient of pressure which is independent of height. The horizontal acceleration of all the particles in the same vertical would therefore be of the same value. If we want the wave generated by the dynamical motion now to be similar to the equilibrium form in its subsequent motion also, the same condition should be satisfied throughout the motion; for if the tidal force be re-introduced at any future instant, the same condition of equality should obtain between the tidal force and the horizontal gradient of pressure for equilibrium to prevail. In the theory developed here, the simple case of a wave that is similar to the equilibrium tide in form is considered so that the assumption is made throughout that

$\frac{1}{\rho} \cdot \frac{\partial p}{\partial x}$  is the same for all particles that lie on a vertical line.

To begin with, the propagation of a disturbance in one direction along the horizontal is considered there being no motion in a perpendicular direction. This is in a line with Schmidt's analysis of the equatorial vibration along the parallels of latitude and the polar vibration along the meridians, when each is taken to be independent of the other. The theory so developed may be said to be that of 'canal waves of air.'

Imagine the atmosphere between two close parallel vertical walls of infinite height, separated by a distance  $b$ . This shall be hereafter called a canal of air. Let the axis of  $x$  be horizontal and parallel to the length of the canal, that of  $y$  vertical and upwards, and let the motion take place in these two directions  $x$ ,  $y$ . Let  $P$  be a point in the canal (figure 1) and  $APB$  a vertical section passing through  $P$  at right angles to the length of the canal. Now, in accordance with what has been stated above, it shall be assumed that for all points in this section

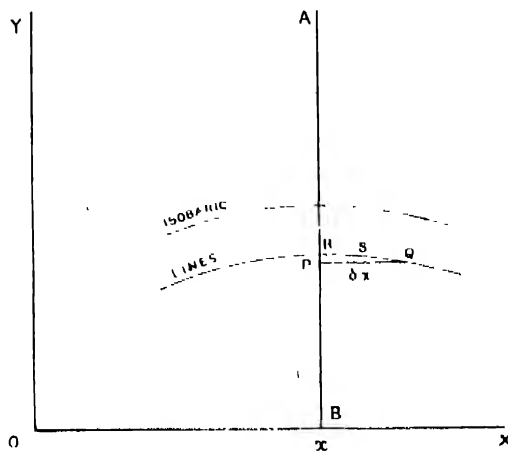


FIGURE 1

$\frac{I}{\rho} \cdot \frac{\partial p}{\partial x}$  has the same value, provided the height of  $P$  above the ground  $OBX$  is not great. Applying the equation of horizontal motion at  $P$ , we have for  $u$ , the velocity of air particles along the  $x$ -axis,

$$\frac{\partial u}{\partial t} + u \frac{\partial u}{\partial x} = - \frac{I}{\rho} \cdot \frac{\partial p}{\partial x}. \quad \dots \quad (1)$$

In the case of small motions the above equation may be written as

$$\frac{\partial u}{\partial t} = - \frac{I}{\rho} \cdot \frac{\partial p}{\partial x} \quad \dots \quad (2)$$

(since  $u \frac{\partial u}{\partial x}$  is a quantity of the second order). If  $g$ , the acceleration due to gravity, be assumed to be a constant independent of height (which will be true when the height of  $P$  is not great as compared to the radius of the earth), we may put

$$\frac{I}{\rho} \cdot \frac{\partial p}{\partial x} = g \cdot \frac{\partial \eta}{\partial x} \quad \dots \quad (3)$$

where  $\frac{\partial \eta}{\partial x}$  is again a quantity which is independent of height and the significance of which shall be seen presently. Then equation (2) may be written as

$$\frac{\partial u}{\partial t} = -g \cdot \frac{\partial \eta}{\partial x}. \quad \dots \quad (4)$$

The meaning that we may attach to  $\frac{\partial \eta}{\partial x}$  is obtained as follows : Let P and

Q (figure 1) be points in the same horizontal line separated by a small distance  $\delta x$ . Let RSQ be an isobaric line passing through Q which meets the vertical APB at the point R. Then the difference of pressure between P and Q is equal to the difference between P and R, i.e., to the weight of a column PR on unit cross-section. The density of the fluid is not a constant but varies with height. However, if  $\rho_a$  be the average density of air in the element PR,

$$\delta p = \rho_a \cdot g \cdot PR.$$

Now, when Q is taken very close to P, the point R approaches the point P and the average density  $\rho_a$  approaches  $\rho$ , the density at P, so that in the limit

$$\frac{\delta p}{\delta x} = \rho \cdot g \cdot \frac{PR}{\delta x}$$

or  $\frac{\partial p}{\partial x} = \rho \cdot g \cdot \frac{\partial Y}{\partial x} \quad \dots \quad (5)$

where Y is the equation of the isoergic line passing near the point P. Hence from (3) and (5), we have

$$\frac{\partial Y}{\partial x} = \frac{\partial \eta}{\partial x} \quad \dots \quad (6)$$

so that  $\frac{\partial u}{\partial t} = -g \cdot \frac{\partial \eta}{\partial x} = -g \cdot \frac{\partial Y}{\partial x}. \quad \dots \quad (7)$

Now, if  $\xi$  is the time integral of the displacement past the section  $x$ , up to the time  $t$ ,

$$\xi = \int u \cdot dt$$

In the case of small motions, this will, to the first order of small quantities, be equal to the displacement of particles which occupy it at time  $t$ . Equation (7) may therefore be written as

$$\frac{\partial u}{\partial t} = \frac{\partial^2 \xi}{\partial t^2} = -g \cdot \frac{\partial \eta}{\partial x} = -g \cdot \frac{\partial Y}{\partial x}. \quad \dots \quad (8)$$

Let us now make the hypothesis that, of all the isobaric lines that may be drawn, there is one across which there is no transference of air. As the disturbance takes place, this line would divide the atmosphere into two separate parts and would therefore have the properties of a boundary. If  $Y_1$  is the y co-ordinate of a point on this isobaric boundary line in the section at  $x$ , the above relation holds good for this line also and therefore

$$\frac{\partial Y_t}{\partial x} = \frac{\partial \eta}{\partial x} \quad (9)$$

Integrating, we get  $Y_t = h + \eta$ , where  $h$  is a constant.  $\eta$  is the variable part of  $Y_t$ , and we may therefore readily identify  $h$  to be the height of this boundary at  $x$ , in its equilibrium position and  $\eta$  its displacement from this position at the instant  $t$ .

The equation of continuity may now be applied by considering the fluid that has entered the space below this boundary, lying between the sections at  $x$  and  $x + \delta x$  up to the time  $t$ , time being reckoned from the instant when  $\eta$  is zero at  $x$ . If we make the hypothesis that elements of air retain their volume unchanged in the movements of the free atmosphere, the equation of continuity becomes analogous to that of water and if  $\eta$  be not great, we get

$$-\frac{\partial}{\partial x} (\xi, h, b.) \delta x = \eta, b. \delta x$$

$$\text{or } \eta = -h \cdot \frac{\partial \xi}{\partial x} \quad \dots \quad (10)$$

$$\therefore \frac{\partial \eta}{\partial x} = -h \cdot \frac{\partial^2 \xi}{\partial x^2}. \quad \dots \quad (11)$$

Eliminating  $\eta$  between (8) and (11), we have

$$\frac{\partial^2 \xi}{\partial t^2} = g \cdot h \cdot \frac{\partial^2 \xi}{\partial x^2} \quad \dots \quad (12)$$

$$= c^2 \cdot \frac{\partial^2 \xi}{\partial x^2} \quad \dots \quad (13)$$

$$\text{where } c = \sqrt{g \cdot h}. \quad \dots \quad (14)$$

This is the well-known equation for wave propagation, the velocity of propagation in the  $x$  direction being equal to  $c$ . Hence if the wave travel with a velocity  $c$ , in the  $x$ -direction, the height of the isobaric boundary surface (which divides the atmosphere into two parts and between which there is no mixing of air) above the ground is  $h$ , where

$$h = \frac{c^2}{g} \quad \dots \quad (15)$$

$$= \frac{\lambda^2}{T^2 \cdot g} \quad \dots \quad (16)$$

and where  $\lambda$  is the wave-length and  $T$  the period of oscillation,  $h$  may be called the height of the 'ground layer.'

A relation is thus obtained connecting the height of the layer with the mode of oscillation that is propagated in it. It should be noted that in developing

in the theory, it is assumed that  $\frac{1}{\rho} \cdot \frac{\partial p}{\partial x}$  is the same at all points in a vertical line.

From this, it follows that  $\frac{\partial \eta}{\partial x}$  or  $\frac{\partial Y}{\partial x}$  is the same for all isobaric lines along a vertical. This means that the isobaric lines are parallel. The same result, as is obtained above, will also follow, if we start with this alternative assumption that as the disturbance is propagated the isobaric lines remain parallel.

#### EQUivalence BETWEEN A GROUND LAYER AND AN OCEAN OF WATER OF THE SAME DEPTH

The result deduced above can be seen to be a particular case of the correspondence between the oscillations that can take place in a ground layer and those that can take place in an ocean of incompressible fluid like water. Provided the assumptions made above hold good, i.e.,

- (1) the surface of the ground layer is an isobaric surface,
- (2) all isobaric surfaces are parallel, and
- (3) an element of air retains its volume constant in its movements in the free atmosphere,

the oscillation in a layer of height  $h$  of the atmosphere are equivalent to those in an ocean of water of the same depth. This may be taken as a principle which can be applied for studying readily the different modes of oscillation in the atmosphere, for the tidal oscillations of an ocean of water have already been studied in great detail.

#### LAYER CORRESPONDING TO THE SEMI-DIURNAL EQUATORIAL VIBRATION

The theory developed above not only shows the possibility of layers in the atmosphere but also enables us to calculate the height from the mode of oscillation. The semi-diurnal equatorial vibration is the most dominant oscillation in the atmosphere and the height of the layer corresponding to it may be now calculated. This vibration travels along the parallels of latitude making one complete circuit in a day and therefore the canal theory developed above may be applied to the vibration along a parallel.

Assuming the earth to be a sphere of radius  $a$ , the length of a parallel of latitude  $\lambda$  is  $2\pi a \cos \lambda$  and the velocity  $C_\lambda$  at this latitude becomes

$$C_\lambda = \frac{2\pi a \cos \lambda}{24 \times 60 \times 60} \quad (17)$$

Hence from (15) it follows that the height of the ground layer at this latitude is

$$h_\lambda = \frac{C_\lambda^2}{g} = \frac{4\pi^2 a^2 \cos^2 \lambda}{g \cdot (24 \times 60 \times 60)^2} \quad (18)$$

or

$$h_\lambda = h_0 \cdot \cos^2 \lambda \quad \dots \quad (19)$$

(assuming that  $g$  is constant over the whole globe) where  $h_0$  is the height of the layer where  $\lambda=0$ .

i.e.,

$$h_0 = \frac{4 \cdot \pi^2 \cdot a^2}{g(24 \times 60 \times 60)^2} .$$

$h_0$  thus becomes the height of the ground layer at the equator.

Assuming  $a$  to be 6368 km., and  $g$  to be 981 cm/sec.<sup>2</sup>,  $h_0$  may be calculated.

$$h_0 = \frac{4\pi^2 \cdot 6368^2}{(24 \times 60 \times 60)^2 \times 981 \times 10^{-5}} = 21.85 \text{ km.} \quad \dots \quad (20)$$

At the equator therefore the height of the ground layer is 21.85 km. From equation (19) the height at any other latitude can be calculated. It is seen that the height gradually decreases as we go away from the equator to the poles and at the poles it is zero. At  $\lambda = 45^\circ$ , the height is 10.93 km. At Greenwich ( $\lambda = 51^\circ$ ),  $h = 8.7$  km. The way in which the height of the layer varies with latitude is shown by curve 1 in figure 2.

Corresponding to the equatorial oscillation it is thus seen that there is a ground layer of the atmosphere which is separated from the region above it by a boundary surface, the height of which above the ground decreases from the equator to the pole. The equatorial vibration is very prominent and therefore it is to be expected that the boundary surface of the ground layer will be very marked and produce perceptible effects. The effects it will produce may be easily deduced to be as follows:

(1) There is no mixing of air below with that above. Consequently the upper region of the atmosphere cannot receive heat by convection from below.

(2) The boundary surface of a fluid has the property that at the boundary the velocity of the fluid perpendicular to the boundary is zero. Hence motion of air near the boundary will be parallel to it. The boundary surface of the ground layer slopes down from a height of about 22 km. at the equator to zero at the poles in a distance of 10,000 km., so that in a limited region it may be considered to be sensibly horizontal. Consequently air masses above and below this boundary surface will, to this extent, move in a horizontal direction, vertical motion being absent.

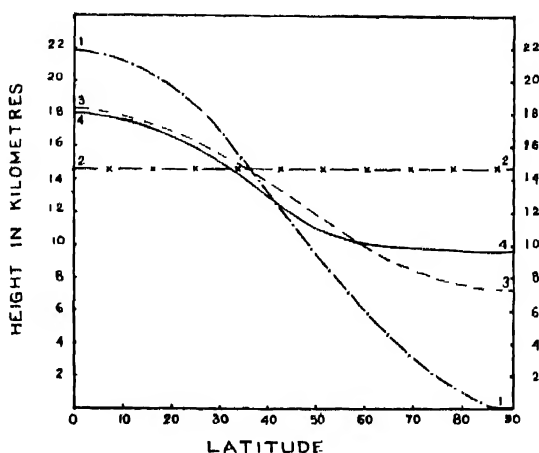
(3) As a consequence of (1) and (2) above, heat can be transferred from below to the region above only by conduction and radiation, convection from the ground taking place only up to the boundary surface. Since convection is a more effective method of transfer of heat than conduction or radiation, heat transfer in the ground layer may be considered to be mainly governed by convection so that the equilibrium that prevails there would be convective equilibrium for which there is a uniform lapse-rate of 6.84°C. per km., as discussed by the author in a previous paper.<sup>24</sup> This lapse-rate which is a consequence of convection

should prevail up to the boundary surface. The temperature distribution above this surface, being governed by conduction and radiation, will be different from that below.

(4) The transition from the lower region to the upper region at this boundary surface will not be gradual but sudden.

(5) The height of such a boundary surface above the ground will vary from the equator to the pole, being about 22 km. at the equator and zero at the poles.

FIGURE 2.



- 1. - - - - - Curve showing height corresponding to equatorial vibration
- 2. - x - x - x - " " " polar "
- 3. - - - - - Auxiliary curve showing mean of the above two heights
- 4. - - - - - Curve showing height of Tropopause  
(mean value from Ramanathan's diagram 2a)

#### IS THE BOUNDARY SURFACE OF THE EQUATORIAL OSCILLATION THE TROPOAUSE OF OUR ATMOSPHERE?

It has been stated in the introduction that the atmosphere is divided thermally into two regions, the Troposphere and the Stratosphere, at the Tropopause, and that so far there has been no satisfactory explanation for it. The chief features that are seen at the Tropopause have also been described. When these features are compared with the effects mentioned above, a very close similarity between the two is found. Effects (1) and (2) agree with Shaw's observations that there is no mixing of air between the lower and upper regions and that air movements are horizontal at the Tropopause. Effect (3)—a constant lapse rate due to convective equilibrium—is what is found as the chief feature of the Troposphere. An explanation may also be obtained for the isothermal condition of the lower Stratosphere from what has been stated above. Since convection from below is not possible into the upper region across the boundary, heat can

be transferred from below only by conduction and radiation. Transfer of heat by conduction, however, is very slow and consequently cannot influence the temperature above. Further, since according to this theory, it is not radiation that balances the effects of convection and stops it at the boundary surface, it is even possible to assume that the optical density<sup>25</sup> of the upper region is equal to zero, which means that radiation has no effect upon the temperature there. Consequently when once isothermal conditions are established, radiative processes cannot destroy it. An adequate explanation may thus be obtained for the isothermal condition of the lower Stratosphere even when the transfer of heat from below only is considered, as is usually done in discussions on this subject. Effect (4)—the suddenness of transition—is what is characteristic of the change at the Tropopause, a feature which has not been explained until now. Effect (5) again is in good qualitative agreement with the way in which the Tropopause varies in height with latitude. The theoretical boundary surface varies from about 22 km. at the equator to 0 at the poles, while the Tropopause varies from about 18 km. at the equator to about 6 km. at the poles. If it is remembered that there has so far been no theory which explains in a comprehensive manner all the features that are observed at the Tropopause, the explanation that this simple theory offers cannot but be considered to be remarkable.

It may also be seen why there is want of quantitative agreement between the height of the boundary surface of the theory and the height of the Tropopause. In the theory developed above, the vibration is considered to take place along the parallels of latitude. When the polar vibration is also taken into account, the resultant vibration is modified and it will no longer be along the parallels except where the amplitude of the polar vibration is zero. It will be of interest therefore to examine how the polar vibration would itself divide the atmosphere.

#### THE POLAR VIBRATION

Considering motion along meridians only and following the close analogy with tidal oscillations in water, the polar vibration may be studied as follows: Let  $u$  be the velocity of particles along the meridians, the velocity at right angles being considered to be zero. Consider an element between closed meridians at a point the co-latitude of which is  $\theta$ . If  $\eta$  is the displacement of the isobaric boundary surface in the direction of the vertical and  $h$  the height of this surface above the ground at this point, the equation of motion and the equation of continuity can be written down to be<sup>26</sup>

$$\frac{\partial u}{\partial t} = -g \cdot \frac{\partial \eta}{a \cdot \partial \theta}$$

$$\frac{\partial \eta}{\partial t} = -\frac{1}{a \sin \theta} \left\{ \frac{\partial (h \cdot u \cdot \sin \theta)}{\partial \theta} \right\}.$$

In the case of simple harmonic motion, the time factor being  $e^{i(\sigma t + \epsilon)}$ , the equations take the form :

$$\eta = \frac{i}{\sigma \cdot a \cdot \sin \theta} \left\{ \frac{\partial (h \cdot u \cdot \sin \theta)}{\partial \theta} \right\}$$

$$u = \frac{i \cdot g}{\sigma \cdot a} \cdot \frac{\partial \eta}{\partial \theta}.$$

If we assume that  $h$  is uniform

$$\eta = - \frac{h \cdot g}{\sigma^2 \cdot a^2 \cdot \sin \theta} \cdot \frac{\partial}{\partial \theta} \left( \sin \theta \cdot \frac{\partial \eta}{\partial \theta} \right)$$

or  $\frac{1}{\sin \theta} \cdot \frac{\partial}{\partial \theta} \left( \sin \theta \cdot \frac{\partial \eta}{\partial \theta} \right) + \frac{\sigma^2 \cdot a^2}{h \cdot g} \cdot \eta = 0.$

This is identical with the equation for zonal harmonics if we put<sup>27</sup>

$$\frac{\sigma^2 \cdot a^2}{h \cdot g} = n \cdot (n+1). \quad \dots \quad (21)$$

The solution of the above equation will be  $\eta = Z_n$ , where  $Z_n$  is the zonal harmonic of order  $n$ .

From (21) the height of the isobaric surface from the ground may be deduced for the semi-diurnal oscillation for which  $n=2$  and

$$\sigma = \frac{2\pi}{12 \times 60 \times 60}; \quad \frac{\sigma^2 \cdot a^2}{h \cdot g} = 2 \cdot (2+1)$$

or  $h = \frac{\sigma^2 \cdot a^2}{6g} = \frac{4\pi^2 \cdot a^2}{6(12 \times 60 \times 60)^2 \times g} = \frac{4}{3} h_o = 14.57 \text{ km.} \quad \dots \quad (22)$

where  $h_o$  is given by equation (20). Since the oscillation is the same along each meridian, the height of the corresponding boundary surface will be the same at all points on the globe and it will be equal to 14.57 km. The theory presented above is in conformity with Schmidt's hypothesis, for there is a nodal circle at latitude given by  $\cos^2 \theta = \frac{1}{3}$  for the zonal harmonic of the second order, or since  $\theta$  and  $\lambda$  are complementary angles,

$$\sin^2 \lambda = \frac{1}{3}$$

or  $\lambda = 35^\circ 16'.$

At this latitude, the polar vibration is zero and the equatorial vibration alone is present. Consequently the height of the ground layer will not be affected by the former. It is equal to

$$\begin{aligned} h &= h_o \cdot \cos^2 \lambda = h_o (1 - \sin^2 \lambda) \\ &= h_o (1 - \frac{1}{3}) = \frac{2}{3} h_o \\ &= 14.57 \text{ km.} \end{aligned}$$

Along this latitude therefore the height of the ground layer will be 14.57 km., the same as for the polar vibration. Since the polar vibration is absent at this latitude and the equatorial vibration alone is present, the motion of particles is along the parallel and the canal theory developed above should be strictly applicable. The height of the boundary surface above the ground should therefore be 14.57 km. at this latitude. Observations show that the height of the Tropopause at this latitude does not differ appreciably from this value. According to Ramanathan's diagram <sup>28</sup> it is about 14.8 km. in summer and 12.8 km. in winter so that the mean value comes to about 13.8 km. which differs from the above theoretical value by about 6%. The agreement between the two may be taken to be fair.

At other latitudes the canal theory cannot strictly be applied, since the resultant of the two vibrations one along the parallels and the other along the meridians will not be linear in general. The theory of these oscillations presents some difficulties which will have to be further studied and it is therefore left for the present. However, it is seen that the height of the layer due to the equatorial vibration is greater in latitudes lower than 35° 16', and less in latitudes higher than 35° 16' than that due to the polar vibration. Consequently, in the lower latitudes, the boundary surface due to the resultant vibration may have to be higher than 14.57 km. but it may not reach the value corresponding to the equatorial vibration. At the equator, therefore, the boundary surface may have to be intermediate between 14.57 km. and 21.85 km. Actually the Tropopause is at a height of about 18 km. at the equator. Similarly, in the higher latitudes the height due to the resultant vibration may have to be greater than that due to the equatorial vibration but less than 14.57 km. This may be the reason for the height of the Tropopause not being zero at the poles. The auxiliary curve 3 in figure 2 shows fair agreement with the Tropopause except in the polar regions.

From the very close similarity between the effects deduced for the boundary surface of the theory and the features observed at the Tropopause, the fair agreement that is found between the height of the Tropopause and the calculated height of the boundary surface at the nodal circle of 35° 16', and the qualitative agreement between them at other latitudes, it may be concluded that the Tropopause is no other than the boundary surface of the theory, being a consequence of the very prominent semi-diurnal oscillation of the atmosphere.

Several other questions arise when such a hypothesis is made. The boundary surface of the theory is an isobaric surface, so that the question comes up whether the Tropopause is such a surface. Confining our attention to the equatorial vibration, it is seen that it is only necessary for the pressure to be the same along parallels of latitude on the Tropopause, for the waves travel along parallels. The Tropopause as a whole need not be an isobaric surface. This seems to have a bearing on the height of the Tropopause and the pressure at the ground. If the Tropopause is low at a place, the height of the ground layer becomes less at the place than at other places lying on the same isobaric line of the Tropopause. The pressure at the ground at that place will therefore be less than the pressures at these other places at the ground. A low Tropopause consequently means a comparatively lower pressure at the ground. This agrees with the well-observed fact that when the pressure is low at the ground the Tropopause is low and when the pressure is high the Tropopause is high. A more detailed examination of the question will have to be undertaken later.

Another question is whether other large-scale disturbances in the atmosphere will not go to obliterate the effects of the disturbance due to the semi-diurnal oscillation. In answer to this it may be said that :

Firstly, the semi-diurnal oscillation is not weak. It is very prominent and is observed at all stations over the globe.

Secondly, whether the large-scale disturbance upsets the normal conditions and obliterates the Tropopause or not depends on the nature of the disturbance. If the disturbance is one of penetrative convection, the Tropopause will be broken through and the effects of the discontinuity would disappear. If, however, the disturbance is one of cumulative type in which air masses are pushed up due to accumulation below and air motion is similar to that in long waves of water, the discontinuity will persist but the position where it occurs would be different from the normal. It is shown in a previous paper <sup>24</sup> by the author that it is this type of convection that prevails in the free atmosphere. Consequently, there is possibility for the discontinuity to remain intact even when there are disturbances (of this type) in the free atmosphere.

There are also several other questions connected with the Tropopause like the variation of its height with seasons and with the presence of cyclones and anti-cyclones in the atmosphere, which demand an explanation from the theory. These questions are left for the present for future discussion.

#### THE 'STRATOSPHERE'

The effect of the semi-diurnal oscillation has so far been discussed. But it is known that there are other modes of oscillation also which have been referred to in the introduction. The other possibilities corresponding to these modes may now be discussed. If we take the 8-hour oscillation to travel along the parallels of latitude, the height of the corresponding layer will not be different

from what it is for the 12-hour oscillation as  $\frac{\lambda}{T}$  will have the same value. But in the case of the polar vibration it is not so; for if we put  $n$  equal to 3 in equation (21)

$$h = \frac{\sigma^2 \cdot a^2}{g(n+1)n} = \frac{\sigma^2 \cdot a^2}{g \cdot 3 \cdot 4}$$

$$= \frac{4\pi^2 \cdot a^2}{g \times 3 \times 4 \times (8 \times 60 \times 60)^2} = \frac{3}{4} h_o.$$

Similarly for the 6-hour oscillation : while the height corresponding to the equatorial vibration is not altered, that corresponding to the polar vibration will be

$$h = \frac{4}{5} h_o.$$

For the 4-hour oscillation this will be

$$h = \frac{6}{7} h_o.$$

Thus the height corresponding to the polar vibration increases as the mode of oscillation becomes higher. Consequently the heights of the boundary surfaces, corresponding to the resultants of these higher modes will also gradually increase. However, there is one limiting value for this height. It is seen from equation (21) that when  $n$  is equal to infinity the value of  $h$  is equal to  $h_o$  (i.e., 21.85 km.). From the minimum height corresponding to  $n$  equal to 2 to the maximum height corresponding to  $n$  equal to infinity, there is a possibility for a number of intermediate boundary surfaces to exist. But as there can be no motion at right angles to a boundary surface the air in this region will possibly have to move horizontally, being confined to strata between consecutive boundary surfaces. The name 'Stratosphere' then becomes specially appropriate.

#### B O U N D A R Y S U R F A C E A T 21.85 K.M.

The height corresponding to the travel of a vibration along a great circle is the maximum possible height of the boundary surface at any point on the globe and this height is the same for all points on it. The isobaric boundary surface corresponding to this extreme mode would, therefore, present a discontinuity at a height of 21.85 km. above the ground at all places on the earth which may become marked by presenting some interesting features. An important observation that has attracted the attention of meteorologists and that has led to the explanation of several interesting facts is that "the pressure at 20 km. above the surface is practically constant (the value being about 55 mb.) all over the globe and at all seasons."<sup>20</sup> Discussing the law of temperature difference that

where the upper strata are warm the lower strata are cold and *vice versa*, Geddes states that "this is bound to follow from the uniformity of pressure at 20 km. For this uniformity of pressure depends almost entirely on the mean temperature of the air from the surface to 20 km. The mean temperature must, therefore, be the same not only for cyclones and anti-cyclones of mean latitudes but also for all parts of the globe so that the temperature in the Stratosphere over the equator must be very much lower than in the high latitudes which is in agreement with observation." <sup>30</sup>

#### OTHER POSSIBLE HIGHER LAYERS

Another interesting possibility may also be discussed, *viz.*, the waves propagated being along great circles of the earth. For a vibration that travels round the earth periodically and continuously it is easily seen that a great circle should comprise either 1 wave or 2 waves or 3 waves or 4 waves, etc. Thus if  $\lambda$  be the wavelength of a wave, we may write

$$\lambda_1 = 2\pi a$$

$$\lambda_2 = \frac{2\pi a}{2}$$

$$\lambda_3 = \frac{2\pi a}{3}$$

$$\lambda_4 = \frac{2\pi a}{4}$$

... (22)

Again the period of oscillation is in terms of the solar day of 24 hours so that taking that as the period of the fundamental, the periods of the harmonics will be 12 hours, 8 hours, 6 hours, etc. Thus the possible periods are

$$T_1 = 24 \text{ hours}$$

$$T_2 = 12 \text{ } ",$$

$$T_3 = 8 \text{ } ",$$

$$T_4 = 6 \text{ } ",$$

... (23)

Now the velocity of propagation  $C$  is equal to  $\frac{\lambda}{T}$ , so that combining the possible values of  $\lambda$  with the possible values of  $T$  we get a number of possible values of  $C$ . Corresponding to each value of  $C$  again we have a possible height of the boundary surface  $h$ .

$$h = \frac{C^2}{g} = \frac{\lambda^2}{T^2 \cdot g} \quad \dots \quad (24)$$

The height  $h_0$  that has been calculated to be 21.85 km. above corresponds to  $C_0$ , where

$$C_0 = \frac{\lambda_2}{T_2} = \frac{\lambda_1}{T_1} = \frac{\lambda_3}{T_3} = \dots$$

and  $h_0 = \frac{\lambda_2^2}{T_2^2 \cdot g} = \dots \dots = \frac{C_0^2}{g} = 21.85 \text{ km.}$  ... (25)

Some other possible velocities and heights of boundary surfaces may therefore be easily found out.

$$(1) \quad C_1 \text{ (say)} = \frac{\lambda_1}{T_2} \left( = \frac{\lambda_2}{T_4} \right) = 2C_0.$$

The corresponding height of the boundary surface is

$$h_1 = \frac{C_1^2}{g} = \frac{4C_0^2}{g} = 4h_0 \quad \dots \quad (26)$$

$$= 87.4 \text{ km.} \quad \dots \quad (27)$$

$$(2) \quad \text{Again, } C_2 \text{ (say)} = \frac{\lambda_1}{T_3} = 3C_0.$$

The corresponding height of the boundary surface is

$$h_2 = \frac{C_2^2}{g} = \frac{9C_0^2}{g} = 9h_0 \quad \dots \quad (28)$$

$$= 196.7 \text{ km.} \quad \dots \quad (29)$$

$$(3) \quad \text{Further, } C_3 \text{ (say)} = \frac{\lambda_2}{T_3} = \frac{3}{2} \cdot C_0.$$

The corresponding height of the boundary surface is

$$h_3 = \frac{C_3^2}{g} = \frac{9C_0^2}{4g} = \frac{9}{4} \cdot h_0 \quad \dots \quad (30)$$

$$= 49.2 \text{ km.} \quad \dots \quad (31)$$

In a similar way the heights of other possible higher layers may also be calculated but those calculated above are the most important as they involve the first few higher orders up to 3. It should be noted in this connection that these values require some correction as some of the assumptions made, like the constancy in the value of  $g$ , will not hold good strictly at these heights. It is, however, remarkable that the heights  $h_1$ ,  $h_2$ ,  $h_3$ , deduced above are very close to the values of the heights observed for the E, F, and D ionised layers of the atmosphere which are about 90 km., 200 km. and 55 km. respectively from the ground. It is not known whether the corresponding oscillations, for which a possibility has been seen, do actually exist in the atmosphere. It would greatly strengthen the hypothesis of this paper if they are discovered.

## CONCLUSION

The theory presented above cannot be said to be complete. Only the case of canal waves of air has been satisfactorily dealt with and the horizontal pressure gradient  $\rho \cdot \frac{\partial p}{\partial x}$  is assumed to be independent of height. Even with these limitations, several important and interesting results have been deduced, the most important one being the possibility for the atmosphere to be divided into layers, the transition from the lower to the upper one being very sharp. There is no mixing of air between the two layers and the height of the ground layer depends upon the mode of oscillation to which it corresponds. Several other results followed which are :

- (1) The boundary surface corresponding to the semi-diurnal vibration has a resemblance to the Tropopause in the atmosphere.
- (2) There is possibility for mixing of air between the ground and this boundary surface so that convection can take place up to it and not beyond. Convective equilibrium can therefore prevail in the ground layer up to the boundary surface. In this respect the ground layer resembles the Troposphere of our atmosphere.
- (3) The possibility for a number of boundary surfaces between that corresponding to  $n$  equal to 2 and that corresponding to  $n$  equal to infinity of the polar component explains the possibility of this region of the atmosphere to be divided into strata between which there can be no vertical motion of air i.e., the possibility of a 'Stratosphere.'
- (4) The boundary surface corresponding to the travel of a wave along a great circle will be at a height of 21.85 km. at all points on the globe and should be an isobaric surface. This compares well with the observed fact that at 20 km. height the pressure at all points of the globe and at all times of the year is the same.
- (5) Possibility has also been shown for other higher boundary surfaces corresponding to the principal possible modes of oscillation. The heights deduced for three of these are found to be very close to the heights of the E, F and D layers of the atmosphere.

Thus the results deduced from the theory find corresponding facts of observation and it is a question whether these coincidences are fortuitous. It may, however, be seen that the coincidences are rather close and that they are also not one or two. Further, it may be noted that the theory is based on the assumption that in the movements of the free atmosphere an element of air tends to keep its volume constant (provided the displacements are not great) and this assumption has also led to a satisfactory explanation of the uniform lapse-rate in the free Troposphere and to the vertical motion in cyclonic and anti-cyclonic systems. Taking all these things together, the theory presented here may be taken to be

a new approach to the understanding of some very important phenomena in the free atmosphere which have not yet been completely understood.

In conclusion, the author takes great pleasure in expressing his grateful thanks to Mr. V. Ch. John, the Principal, and Rev. Dr. H. H. Sipes, the Bursar, of his college for their kind encouragement and to Dr. I. Ramakrishna Rao of the University College, Waltair, for the great interest he has been taking in the author's work.

#### R E F E R E N C E S

- 1 Teisserenc de Bort : Communication to *Socie \* te \* de Physique*, 1899.
- 2 Brunt, *Physical and Dynamical Meteorology*, p. 17.
- 3 Geddes, *Meteorology*, p. 276.
- 4 Syam, *Ind. J. Phys.*, **10**, 13 (1936).
- 5 Humphreys, *Astrophys. Journal*, **29**, 14 (1909).
- 6 Gold, *Proc. Roy. Soc. A.*, **82**, 43 (1909).
- 7 Brunt, *Ibid*, p. 142.
- 8 Schmidt, *Met. Zs. Braunschweig.*, **7**, 182 (1890).
- 9 Simpson, *Quart. Journal Roy. Met. Soc.*, **44**, 1 (1918).
- 10 Whipple, *Quart. Journal Roy. Met. Soc.*, **44**, 20 (1918).
- 11 Chapman Pramanik and Topping, *Beitrage Zur. Geophysik*, **33**, 246 (1931).
- 12 Laplace, *Mechanique Celeste*.
- 13 Kelvin, *Proc. Roy. Soc. Edinburgh*, **11** (1882).
- 14 Margules, *Wien. Sitz. Ber. Ak. Wiss.*, **99**, 204 (1890); **101**, 1369 (1892); **102**, 11 (1893).
- 15 Lamb, *Hydrodynamics*.
- 16 Chapman, *Quart. Journal Roy. Met. Soc.*, **50**, 165 (1924).
- 17 Taylor, G. I., *Proc. Roy. Soc. A.*, **186**, 318 (1936).
- 18 Pekeris, *Proc. Roy. Soc. A.*, **188**, 650 (1937).
- 19 Taylor, *Proc. Roy. Soc. A.*, **126**, 169, 728 (1929).
- 20 Appleton and Naismith, *Proc. Roy. Soc. A.*, **160**, p. 685.
- 21 Ranzi, *Nature*, **180**, 545 (1932).
- 22 Colwell, *Proc. Inst. Rad. Eng.*, **21**, 721 (1933).
- 23 Bajpai and Pant, *Ind. J. Phys.*, **13**, 57 (1939).
- 24 Subrahmanyam, *Ind. J. Phys.*, **13**, 43 (1939).
- 25 Brunt, *Ibid*, p. 138; p. 140.
- 26 Lamb, *Ibid*, 4th Edn. p. 295.
- 27 Lamb, *Ibid*, p. 106.
- 28 Brunt, *Ibid*, p. 18.
- 29 Geddes, *Ibid*, p. 232.
- 30 Geddes, *Ibid*, p. 276.



# RAMAN SPECTRA OF COUMARINS AND CHROMONES

By (Miss) ASIMA MOOKERJEE

AND

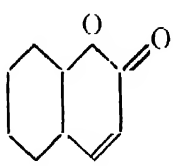
JAGANNATH GUPTA

(Received for publication, November 30, 1939)

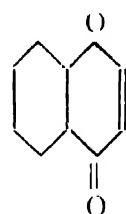
## Plate XIX

**ABSTRACT.** The Raman spectra of three coumarins and two chromones, including the parent bodies, have been recorded. A significant difference of more than fifty wavenumbers has been observed in the maximum non-hydrogen frequencies ( $1600\text{-}1700\text{ cm}^{-1}$ ) of the two series of compounds. It has been suggested that the examination of Raman spectra can be undertaken to easily differentiate a chromone body from a coumarin, even if they are strictly isomeric, either of which may be formed in some well-known synthetic reactions of organic chemistry.

The Pechmann method<sup>1</sup> of condensing phenols with  $\beta$ -ketonic esters in presence of sulphuric acid, and the allied method of Simonis<sup>2</sup> using phosphorus pentoxide as the condensing agent, give rise occasionally to benzo  $\alpha$ -pyrones or coumarins and benzo  $\gamma$ -pyrones or chromones.



Coumarin skeleton



Chromone skeleton

A considerable volume of work has accumulated studying the influence of different substituents in the benzene nucleus on the formation of these pyrone bodies, and empirical rules have been formulated whereby to anticipate the formation of one or other of these in a condensation process.<sup>3</sup> The purely chemical method of testing a chromone or a coumarin is based upon alkaline hydrolysis of the compound and examination of the hydrolysed products obtained. The distinction is made by degradation to an  $\alpha$ -hydroxy ketone or -acid or an  $\alpha$ -methoxy cinnamic acid, or for 2-methyl chromones by the formation of styrene derivatives. Further, the coumarins, being of simple lactonic nature, do not give rise to semicarbazones, oximes or phenylhydrazones, indicating absence of any ketonic character of the C=O group present in it; while

the chromones are known to give rise to oximes and oxonium salts. These chemical methods are not always simple, and negative evidences are often of little value.<sup>4</sup>

Simple physical methods for differentiating the two closely related series of compounds have not yet been developed. A study of Baker and Eastwood<sup>5</sup> on the constitution and power to form gels in dilute alkali with different  $\gamma$ -pyrone derivatives did not yield any fruitful results. Tasaki and Rakower's studies<sup>6</sup> on the absorption spectra are restricted to coumarin and its derivatives, and have not been pursued further. Measurements of electric moment by Rau<sup>7</sup> indicate the existence of mesomerism in the pyrone derivatives, and do not appear to be useful for purposes of differentiation.

It may be noted that the physical methods summed up here do not, in general, reveal any characteristics of the carbonyl group present in all pyrone compounds. Chemical evidences indicate difference in nature and activity of the carbonyl group present in the  $\alpha$  and  $\gamma$  series. It was argued that coumarins and chromones should be characterizable by studying the physical properties of this carbonyl group, even when they were strictly isomeric. The carbonyl linkage, it may be mentioned, is found in acids, acyl halides, esters, anhydrides, aldehydes and ketones, and the corresponding Raman inner frequencies occur in the region of  $1645\text{-}1800\text{ cm}^{-1}$ , not very crowded with other frequencies even in poly-atomic molecules. Existing data also indicate variations in the value of the  $\text{C=O}$  frequencies depending on the location of the group in differently constituted compounds, corresponding to known differences in chemical behaviour. Consequently, with a view to detecting the difference, if any, that might exist in the magnitude of the carbonyl frequencies of the two series of compounds a number of similar coumarins and chromones have been prepared and their Raman spectra examined, the results of which are being communicated in the present paper.

The attribution of the many frequencies recorded of these highly complex heterocyclic compounds to individual modes of vibration, although very interesting, was not the object of the present work, and has not been attempted here.

#### E X P E R I M E N T A L

*Chromone*—It has been obtained from *o*-hydroxy acetophenone and oxalic ester by modifying the method of Kostanecki and his co-workers.<sup>8</sup>

*o*-Hydroxy acetophenone was prepared from phenyl acetate by Frie's rearrangement. Anhydrous  $\text{AlCl}_3$  (200 g.) was taken, cooled in ice, and phenyl acetate (106 g.) slowly added. The reaction started at once with a strong evolution of  $\text{HCl}$ . When the reaction subsided, the mass was heated for half an hour in an oil-bath at  $110\text{-}112^\circ\text{C}$ . The red mass was cooled, decomposed with ice-water, and distilled in steam for 56 hours. The turbid distillate was taken up

with ether, which was then removed. The liquid residue, *o*-hydroxy acetophenone, was purified by vacuum distillation (distils at 107-110°C/1 mm).

Molecular sodium (6 g.) was kept under ether (30 c.c.) cooled in freezing mixture, and oxalic ester (20 g.) was added, followed by a cooled mixture of *o*-hydroxy acetophenone (16 g.) and oxalic ester (20 g.). The flask was kept all the time under a reflux condenser, through which ice-cold water circulated. A vigorous reaction took place, after which the flask was kept undisturbed for 2½ hours. The orange pasty mass was then treated with alcohol, acidified with dilute acetic acid and shaken up with ether. The liquid residue obtained from the ether extract, 2-oxy benzoyl pyruvic ester, was dissolved in 100 c.c. alcohol and hydrolysed to chromone carboxylic acid by refluxing with conc. HCl (20 c.c.) for four hours. The alcohol was removed and the carboxylic acid after washing and crystallizing from dilute alcohol, was decarboxylated by heating at 255-260°C for two hours. The tarry liquid obtained was distilled in vacuum when chromone distilled over (110-112°C/1 mm). It was recrystallized from dilute methyl alcohol. (M.P. 58°C).

*2:3-dimethyl 7-hydroxy chromone*—This was obtained by the method of Pechmann and Duishberg,<sup>9</sup> and was purified by crystallization from alcohol. (M.P. 262°C).

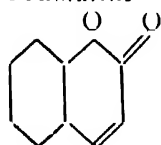
*Coumarin*—Schering's purest sample was recrystallized from alcohol. (M.P. 67°C).

*3:4-dimethyl 7-hydroxy coumarin*—This was obtained by the method of Kostanecki and Lloyd,<sup>10</sup> and was further purified by recrystallization from alcohol. (M.P. 255-257°C).

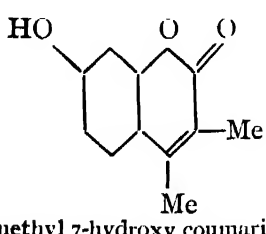
*β-Methyl umbelliferone methyl ether*—This compound, obtained by methylation of *β*-methyl umbelliferone synthesized by the method of Chakravarti,<sup>11</sup> was kindly lent by him to the present authors, and was subsequently purified by crystallization from alcohol. (M.P. 159°C).

The chemical structures of the compounds examined in the present work are as follows :—

*Coumarins*

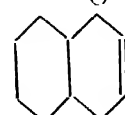


I. Coumarin

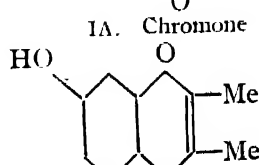


II. 3:4-dimethyl 7-hydroxy coumarin

*Chromones*



III. Chromone



III. 2:3-dimethyl 7-hydroxy chromone

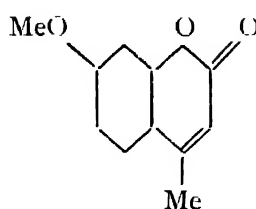
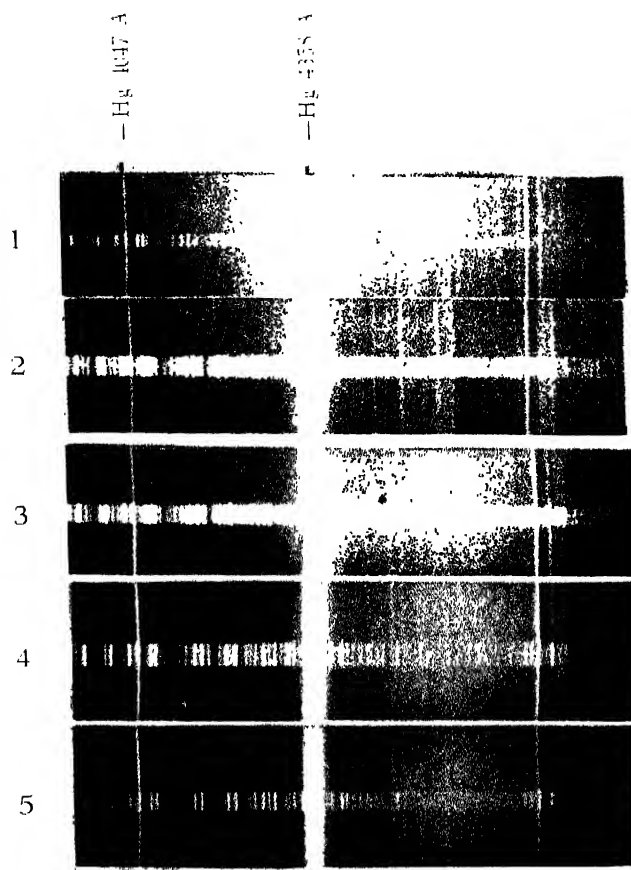
III.  $\beta$ -methyl umbelliferone methyl ether

TABLE I  
*Coumarin and Chromone*

Raman frequencies in  $\text{cm}^{-1}$  (200-2000). Figures in parenthesis indicate relative intensities

Coumarin.		Chromone.			Molten.
Solid <sup>12</sup> (1000-2000).	in $\text{CHCl}_3$ <sup>12</sup> (1000-2000).	in $\text{CH}_3\text{OH}$ .	in $\text{CH}_3\text{OH}$ .	in $\text{CHCl}_3$	
1030	1030	1034	234 (1)	361 (1)	
1100	1096	1112	283 (1)	432 (1)	
1128	1123	1179	496 (1)	498 (1)	
1156	1156		716 (4)	710 (2)	708 (1)
1181	1181		761	812 (6)	
1228	1229	1225	868 (1)	944 (4)	
1260	1262	1263	1037 (10)	1039 (1)	1121 (1)
1328	1332	1324	1129 (2)	1121 (4)	1179 (1)
1457	1460	1446	1193 (2)		
1486	1493	1484	1249 (2)		
1567	1569	1558	1300 (1b)		
1604	1609	1609	1324 (8)		1335 (1)
1620	1631	1717	1354 (8)		
1708	1720		1560 (2)		
1731			1646 (6)	1450 (4)	
			1657 (3)		1647 (2)



Raman spectra of Coumarins and Chromones.

1. Coumarin in methyl alcohol.
2. Chromone " " "
3. 2 : 3 dimethyl 7-hydroxy chromone in  $\text{CHCl}_3$ .
4. 3 : 4 dimethyl 7-hydroxy coumarin " " "
5.  $\beta$ -methyl umbelliferone methyl ether " " "



The parent bodies, *viz.*, simple coumarin and chromone, were examined by dissolving them in different solvents. Usually the best solvent was chloroform, and the solution during exposure was kept electrically heated to keep larger quantities of the substances in solution. *m*-Dinitrobenzene filter was used to cut off the 4046 Å group of lines and lines of shorter wave-length from the incident radiation, to avoid any undesirable fluorescence. Chromone was melted in vacuum in a thick-walled pyrex test tube, and kept molten during the exposure by heating electrically. Ilford Special Rapid plates were preferred for the good contrast in the recorded spectrum. The usual exposure varied from 20 to 40 hours. The results are tabulated below.

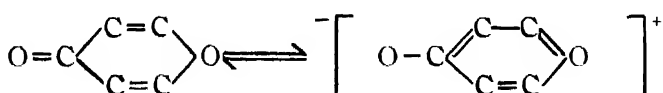
TABLE II  
Coumarin and Chromone Derivatives in Chloroform

II A	II	III
365	360	365
422	424	438
	470	487
812	808	811
948	942	939
1122	1140	1149
	1211	1210
1339	1338	1330
1448	1449	1451
1596	1548	1549
	1603	1603
	1702	1700

#### DISCUSSION

The photographs of some of the spectra recorded are reproduced in the plate. It may be easily seen from the results obtained, that the carbonyl frequency in the coumarins has a normal value, nearabout 1700, although it changes slightly in different solvents, quite possibly owing to hydrogen bond formation.<sup>13</sup> The maximum frequency however, leaving the hydrogen oscillations, has a considerably lower value in the chromones, being of the order of 1600-1650. That this lower value is not due to damping of the inner frequency of the carbonyl group bonded to a hydrogen atom of the solvent molecule is certain, because the value

does not change greatly in molten chromone and in the solutions of the same in different solvents. Some of the higher frequencies (1500-1650) in the coumarins and chromones are doubtless due to inner vibrations of the benzene ring ( $\nu_0$  and  $\nu'_0$ )<sup>14</sup> attached to the heterocyclic, and the question whether the frequencies nearabout 1600 are due to such vibrations of the benzene ring or that of a carbonyl group has to be settled. The possibility of the latter case arises from a ketone-betaine mesomerism in chromones of the type



as postulated by Le Fevre and Le Fevre on the strength of electric moment data.<sup>15</sup>

The systematic difference, however, of more than fifty wavenumbers between the maximum non-hydrogen frequencies in the two series of compounds—a difference which persists even when two pairs of isomeric compounds are chosen from the two series—is very interesting, and indicates the possibility of utilizing the Raman spectra of these compounds for the purpose of differentiating a chromone from a coumarin. Further verification with a larger number of known isomeric coumarins and chromones is desirable.

The authors are indebted to Prof. M. N. Saha, Palit Professor of Physics, for kindly providing all facilities of his laboratory, and to Dr. S. C. Sirkar and Dr. P. K. Bose for their constant interest in the work. Their grateful thanks are due also to Dr. D. Chakravarti, for lending some of his compounds.

CHEMICAL LABORATORIES,  
UNIVERSITY COLLEGE OF SCIENCE, CALCUTTA.

#### R E F E R E N C E S

- <sup>1</sup> Pechmann *et al.*, *Ber.*, **16**, 2119 (1883), *et seq.*
- <sup>2</sup> Simonis *et al.*, *Ber.*, **46**, 2015 (1913); **47**, 697 (1914).
- <sup>3</sup> Chakravarti, *Proc. Nat. Inst. Sci. Ind.*, **5**, 235 (1939); Heilbron, Hey and Lythgoe, *J. Chem. Soc.*, 1936, 295.
- <sup>4</sup> Kelkar, *Rasayanam*, **1**, 68 (1936); Chakravarti, *loc. cit.*
- <sup>5</sup> Baker and Eastwood, *J. Chem. Soc.*, 1929, 2897.
- <sup>6</sup> Tasaki, *Acta Phytochim.*, **3**, 21 (1927); Rakower, *Acta Phys. Polon.*, **3**, 415 (1934).
- <sup>7</sup> Rau, *Proc. Ind. Acad. Sci.*, **4A**, 687 (1936).
- <sup>8</sup> Kostanecki *et al.*, *Ber.*, **33**, 471 (1900); **38**, 859, 861, 2547, 2887 (1901).
- <sup>9</sup> Pechmann and Duishberg, *Ber.*, **16**, 2119 (1883).
- <sup>10</sup> Kostanecki and Lloyd, *Ber.*, **34**, 2948 (1902).
- <sup>11</sup> Chakravarti, *J. Ind. Chem. Soc.*, **12**, 536 (1935).
- <sup>12</sup> Murti and Seshadri, *Proc. Ind. Acad. Sci.*, **8A**, 519 (1938).
- <sup>13</sup> Farad. Soc. Discussions, (1937) 200.
- <sup>14</sup> Magat, A.T.C. Tables, 1936, 70.
- <sup>15</sup> Le Fevre and Le Fevre, *J. Chem. Soc.*, 1937, 196.

# SUPERSONIC VELOCITY IN GASES AND VAPOURS.

## PART IX. SPECIFIC HEATS AND DISPERSION OF SUPERSONIC VELOCITY IN ORGANIC VAPOURS

BY S. K. KULKARNI JATKAR

(Received for Publication, Nov 18, 1939)

**ABSTRACT.** It has been shown that the recent results obtained by Railston for the supersonic velocity at lower temperatures are in agreement with the author's results at higher temperatures in the case of benzene, ethyl alcohol and ethyl ether. The methyl alcohol and carbon tetrachloride vapours appear to have lost the vibrational specific heats below 100 Kc./sec. In the case of benzene and carbon disulphide vapours the value of  $V_0$  and  $V_1$  or  $V_2$  at  $90^\circ$  are 200 m./sec., 208 m./sec. and 203 m./sec. and 216 m./sec. respectively. The corresponding values of the specific heats are in agreement with the theoretical values calculated on the basis of the assumption that in the case of benzene, the deformational vibrational terms and in the case of carbon disulphide, both the deformational and longitudinal vibrational terms disappear from the acoustic cycle.

The supersonic velocities in vapours of acetone, chloroform, methylene chloride and ethyl alcohol yield specific heat values, which are higher than those calculated from spectroscopic data on account of uncertain corrections due to saturation.

### INTRODUCTION

It was shown in previous parts of this series<sup>1</sup> that the molecular heats of vapours of several organic compounds calculated from the velocities at supersonic frequencies between 50-127 Kc./sec. were in most cases in fair agreement with those found by thermal methods and with those calculated from spectroscopic data. Since all polyatomic molecules have vibrational energy they should show supersonic dispersion if there is a time lag between the rotational and vibrational specific heats. In line with this idea the author found that in the case of molecules which are increasingly anisotropic, there is a dropping out of deformational and vibrational degrees of freedom in the acoustic cycle in the frequency range below 50 Kc./sec. The results of the author also indicated that the molecules of the AXB<sub>3</sub> type appeared to have suffered transition in the velocity of sound below 50 Kc./sec. As polyatomic molecules have large vibrational specific heats, other vapours might show dispersion at frequencies higher than the range studied till now.

The possibility of multiple transitions in supersonic velocity which was originally put forth by Bourgin and Richards was thus partially substantiated by the results of the author. According to this idea the velocity of sound at low

frequency may remain at a value  $V_1$ , in which the translational, rotational and vibrational frequencies of the molecules take their full share in the adiabatic cycle. At higher frequencies the velocity passes through the first dispersive region and remains at a constant value  $V_1$  owing to the time lag between the rotational and transverse vibrational specific heats. When the frequency is further increased the time period may be too short to permit the transformation of translational and rotational energy into the energy of vibrations, both transverse and longitudinal, when the velocity will reach a terminal value  $V_\infty$ . The specific heat of even the most complex molecules will then consist of only translational and rotational terms. The possibility of a partial degradation of rotational specific heat terms in supersonic waves has also been shown to be possible by the present author.

Further support to the existence of transitions in supersonic velocity in comparatively low frequency range was found by the author in the calculations of specific heats based upon the recent supersonic velocity measurements in vapours by Railston<sup>2</sup> at lower temperature. Railston found that it was more difficult to work with vapours than with gases, especially with vapours of benzene, acetone and ether, which stopped the oscillations of the crystals within 20 to 30 minutes after admission into the apparatus. Two of the vapours, benzene and carbon disulphide, showed change of velocity with frequency, which was more than his experimental error (0.5% at 97.8 Kc., 1% at 465 Kc., 1.3% at 695 Kc., and 2.5% at 1000 Kc.). The measurements were carried out at comparatively lower temperatures, where the compressibility corrections were large and uncertain. The reason for the increased error at higher frequency is not mentioned and is obviously due to complexity of the wave form, and no attempt has been made by Railston to calculate the specific heats for several of the vapours.

The object of the present paper is to calculate the specific heats of the various vapours using the velocity data obtained by Railston and compare the results with those calculated by the spectroscopic method used by the author, in order to find out whether the velocities at supersonic frequencies were normal ( $V_0$ ), or showed any transition ( $V_1$  and  $V_\infty$ ).

A comparison of the velocity measurements obtained by Railston (*loc. cit.*) with those already measured by the author at higher temperatures by calculating the temperature coefficients using the linear law of the type  $V_t = V_0(1 + \alpha_t)^{\frac{1}{2}}$ , connecting the values of the velocity at different temperatures, is given in table 1.

The values of the temperature coefficient obtained from the results of the author are given in column 1. In the case of carbon disulphide the temperature coefficient has been calculated from the result of Railston at 45° and the author's result at 92°. The values of  $\alpha$  are in most cases near theoretical value for gases, *viz.*, 0.0037. A comparison of the velocity calculated from the temperature coefficient, with the values observed by Railston shows that linear law

TABLE I

	$\alpha$	V	Temp. °C.	V, meters/sec.		
				Author.	metres/sec.	Calculated.
Carbon disulphide	.0034	190.9	45		203.0	203
Benzene	.0041	170.9	90		200.0	198
Chloroform	.0036	147.7	70		169.9	154
Methylene chloride	.0031	179.0	43		190.5	177
Ethyl alcohol	.0046	223.9	80		261.5	262
Acetone	.0041	201.9	58		224.7	210
Carbon tetrachloride	.0047	120.3	77		140.4	151
Ethyl ether	.0041	174.7	35		186.8	188
Methyl alcohol	.0030	285.7	67		320.8	338

holds good in the case of the vapours of benzene, ethyl alcohol and ethyl ether. In the case of carbon tetrachloride and methyl alcohol the results of Railston are too high, probably due to the fact that at lower temperatures these vapours have already undergone a transition. In the case of methylene chloride, chloroform and acetone, Railston's results are too low, which seem to indicate that the compressibilities in these vapours are very much higher than those given by the equation of state.

The specific heats were calculated from the velocity of sound by the ratio  $C_p/C_v = \gamma$ , which is given by the expression  $\frac{V^2 M}{R T} \phi$ , where  $\phi$  is given by

$$\phi = 1 - \frac{9}{64} \pi \tau (1 - 6\tau^2)$$

in which  $\pi = P/P_c = \text{actual pressure/critical pressure}$ ,

$\tau = T_c/T = \text{critical temperature/actual temperature}$ ,

$M = \text{molecular weight}$ ,

$R = \text{the gas constant } (8.3156 \times 10^7)$

and  $V = \text{velocity of sound in cms./sec.}$

The corresponding value of  $(C_p - C_v)$  is

$$(C_p - C_v) = R(1 + 27/16 \pi \tau^3).$$

The derivation of the above factors is given by the Berthelot's equation of state. The details of the calculations of specific heats from the various factors is

given in table 2. The specific heats observed from the velocity of sound are compared with those calculated by the method of Bennewitz and Rossner<sup>3</sup> from the spectroscopic data. These authors found that the experimental results for specific heats of organic vapours of non-linear molecules, containing carbon, hydrogen and oxygen, could be expressed by the equation

$$(C_v)_{p=0} = 3R + \sum q_i E_{v_i} + \frac{(3n - 6 - \sum q_i)}{\sum q_i} \sum q_i E_{\delta_i},$$

where  $\sum q_i$  = number of valence bonds in the molecule,  $n$  = total number of atoms in molecule,  $E_{v_i}$  and  $E_{\delta_i}$  = Einstein's functions for a given bond with characteristic vibration frequencies  $v_i$  and  $\delta_i$ . The numerical value of  $v$  for each bond was determined from infra-red or light-scattering data. The values for  $\delta_i$  were

TABLE II  
Specific Heats of Organic Vapours

	°C	M	P <sub>h</sub>	t <sub>h</sub>	V	$\frac{V^2 M}{RT} -$	φ	γ	C <sub>p</sub> - C <sub>v</sub>	C <sub>p</sub>
									obs.	cal
Benzene	90	78.08	47.89	288.5	200	1.014	1.061	1.076	2.248	25.7
	"	"	"	"	208	1.120	"	1.188	"	14.6
Carbon disulphide	45	76.12	72.90	273.0	203	1.186	1.055	1.252	2.330	11.9
	"	"	"	"	216	1.341	"	1.419	"	8.2
Ethyl ether	35	74.10	35.61	193.8	186	1.001	1.077	1.079	2.317	32.6
Methyl alcohol	67	32.04	78.50	240.0	338	1.292	1.034	1.336	2.136	8.7
Carbon tetrachloride	77	153.84	45.00	283.2	152	1.216	1.070	1.301	2.287	10.3
Chloroform	70	119.39	53.80	262.9	154	0.992	1.060	1.048	2.227	49.5 (?)
Acetone	58	58.06	60.00	237.0	211	0.938	1.048	0.984?	—	19.6
Ethyl alcohol	80	46.06	62.96	243.1	266	0.966	1.039	1.004	2.156	30.2
Methylene chloride	43	84.94	60.90	245.1	178	1.025	1.057	1.083	2.230	29.4 (?)

determined empirically from the experimental values of molecular heats for some known substances by a step-by-step calculation. This equation yielded results in excellent agreement with their own experimental data obtained by the method of continuous-flow calorimeter, and with that of other investigators. In order to reduce the values to atmospheric pressure the following equation was used :

$$(C_p)_{p \approx p} = (C_v)_{p \approx v} + R \left[ 1 + \frac{81}{32} \pi \tau^3 \right].$$

When allowance is made for the moderate accuracy in the velocity measurements claimed by Railston and for the lack of exact equation of state, the velocity 200 m./sec. in benzene at 90° and at 46.5 Kc., observed by Railston, gives a value of  $C_p$ , which is in fair agreement with that calculated, and therefore represents the  $V_\infty$  stage. This is also borne out by the velocity measurement at audible frequencies. The lower value 198 m./sec. observed by Railston at 97.8 Kc./sec. is difficult to explain. The value of 208 m./sec. at 1800 Kc./sec. gives 14.6 calories as the value of  $C_p$ , which is in agreement with the calculated value from the spectroscopic data by dropping out 7.2 calories, which is the share of the deformation oscillations.

The velocity 203 m./sec. in carbon disulphide vapour at 97.8 Kc./sec. obviously represents the  $V_\infty$  stage. The velocity observed at 1800 Kc./sec. 216 m./sec., gives 8.2 calories as the value of specific heat, which indicates the disappearance of all vibrational specific heats from the acoustic cycle.

The remarkably low values of  $C_p$  for methyl alcohol and carbon tetrachloride, as compared with those calculated from the spectroscopic data, would also seem to indicate a transition to  $V_\infty$  and  $V_1$  stage respectively in the lower supersonic range at lower temperatures. It is interesting to point out that both these molecules come under the same category as chloroform, *iso*-propyl alcohol and *tert*-butyl alcohol, which were found by the author to show partial disappearance of the share of rotational and deformational oscillations at higher temperatures.

Ethyl ether shows nearly the normal specific heat even at 1000 Kc./sec.

The calculated specific heats of the other vapours are too high. This is due to the fact that at lower temperatures molecules are associated and the Berthelot's equation of state no longer holds good. The increase in the specific heat with the association of molecules is to be expected.

The dispersion observed by Railston in the case of benzene is in harmony with the findings of Richardson<sup>4</sup> who pointed out the connection between the strong Raman spectra and Tyndall's scattering of carbon dioxide, nitrous oxide, sulphur dioxide and carbon disulphide vapours and their supersonic dispersion and absorption.

DEPARTMENT OF PURE AND APPLIED CHEMISTRY,  
INDIAN INSTITUTE OF SCIENCE,  
BANGALORE (INDIA).

#### R E F E R E N C E S

- <sup>1</sup> *J. Ind. Inst. Soc.*, **22 A**, 19-110 (1939).
- <sup>2</sup> *J. Acoust. Soc. Amer.*, **11**, 107 (1939).
- <sup>3</sup> *Zeit. f. Phys. Chem. B*, **39**, 126 (1938).
- <sup>4</sup> *Proc. Roy. Soc. A.*, p. 535 (1935).



## UNUSUAL SOLAR ACTIVITY

BY MD. SALARUDDIN, B.A., M.Sc.

AND

B. G. NARAYAN, B.Sc.

*(Received for publication, Nov. 29, 1939)*

### Plates XX & XXI

**ABSTRACT.** The paper describes briefly the outstanding features of a recent persistent solar activity observed in Kodaikanal.

Attempts have been made to correlate the bright chromospheric eruptions with the terrestrial effects. It is suggested that until many more data are obtained, judgment must be withheld regarding the nature of the relation between the eruptions and terrestrial magnetic disturbances.

Persistent solar activity was observed for about three weeks commencing from the 26th August, 1939, and one of its remarkable features was that it was practically confined to a zone in the neighbourhood of latitude  $15^{\circ}$  in the southern hemisphere. The first signs of this spell of activity were noticed simultaneously with the appearance of the spot group Kodaikanal No. 7152 at the east limb at latitude  $15^{\circ}$ S. This long-lived spot group had already gone round the sun twice before without showing much activity. On the 26th August, however, a flocculus in the neighbourhood of this spot brightened up and showed considerable Doppler displacements. The maximum Doppler shift observed in the flocculus was  $2\text{.}4\text{ \AA}$  to red at  $8^{\text{h}}45^{\text{m}}$  I.S.T., indicating a velocity of recession (with respect to the observer) of the order of 110 Km./sec. A prominence connected with the spot group was also active and showed a displacement of  $1\text{ \AA}$  to violet. On the same day, eruptions were observed in the neighbourhood of spot groups Nos. 7148 and 7150, the latter of which was near latitude  $15^{\circ}$  S, but the former was in the northern hemisphere.

The spot group No. 7152 continued to be very active throughout its passage across the solar disc and gave rise to eruptions almost every day. The most extensive of these occurred on August the 30th, its area being 500 millionths of the sun's visible hemisphere. The region of the spot group was showing signs of activity even from the morning. A dark marking to the north of the spot group showed displacements of  $2\text{ \AA}$  to violet and  $2\text{ \AA}$  to red at different points at  $8^{\text{h}}35^{\text{m}}$ . A point to the south of the group brightened up at  $9^{\text{h}}0^{\text{m}}$  but subsided to its normal brightness at  $9^{\text{h}}55^{\text{m}}$ . But the eruption proper began at  $11^{\text{h}}30^{\text{m}}$  and very soon

extended all round in long streaks. Its intensity as measured with a graduated step-wedge was 3 times that of the undisturbed disc. The eruptive area showed good Doppler displacements, the maximum displacement being  $2.4 \text{ \AA}$  to red at  $11^h 55^m$ . In the accompanying plate spectro-heliogram 1 (a) shows the region of the spot group at  $8^h 26^m$  before the eruption began and the spectro-heliograms 1 (b) to 1 (e) show the region at the time of the eruption between  $11^h 49^m$  and  $11^h 52^m$ .

Another eruption was observed on September 1. Though smaller in area, this was very much brighter than that of August 30. The H $\alpha$  and K spectro-heliograms taken before  $8^h 0^m$  showed no appreciable activity in the region of the spot group and nothing extraordinary was noted by the spectro-helioscope observer till  $8^h 25^m$  when suddenly the flocculus adjacent to the leading spot of the group brightened up and became eruptive. It soon extended in a narrow column towards the east and joined up with one of the following spots of the group. At the same time there was another bright column seen starting up from one of the following spots and extending in a southwestwardly direction. The eruption attained its maximum brightness at about  $8^h 45^m$  and then the intensity fell off gradually, the whole activity subsiding by  $9^h 30^m$ . No Doppler displacement was noticeable in the eruptive area but two small dark markings lying to the north and south of the spot group showed some displacements.

From observations with the spectro-helioscope it was found that this large spot group was very active on the morning of the 2nd September. No less than three eruptions were observed between  $8^h 10^m$  and  $11^h 20^m$  in the large flocculus surrounding the spot, the times of maximum intensity for these three outbursts being  $8^h 28^m$ ,  $10^h 12^m$  and  $10^h 50^m$ . In this case the eruption obviously took the form of a series of brightenings of different parts of the flocculus.

A very bright eruption occurred in the same region on September 6. The eruption began at  $8^h 17^m$ , reached its maximum intensity at  $8^h 27^m$  and faded away at about  $9^h 0^m$ . Doppler displacements of  $1.0 \text{ \AA}$  to violet at  $8^h 17^m$  and  $2.0 \text{ \AA}$  to red at  $8^h 30^m$  were noted in the region by the spectro-helioscope observer.

The spot group gave rise to active and metallic prominences at the west limb on the 7th and 8th September. The spectroscope showed most of the lines belonging to sodium, iron and magnesium usually observed in the prominences. Doppler displacements of about  $2 \text{ \AA}$  to both red and violet were observed. Photographs of these prominences in calcium light taken on the 7th and 8th September are reproduced here in figures 2 (a) and 2 (b) respectively (see plate XX).

Two other very active spot groups that crossed the sun's disc during the period are the Kodaikanal Nos. 7157 and 7159. These spots were also situated in the neighbourhood of latitude  $15^\circ$  in the southern hemisphere. The spot No. 7157 gave rise to an eruptive prominence on September 1. The prominence was not visible in the earlier photographs but suddenly appeared at about  $9^h 0^m$  and showed extraordinary activity, attaining a height of more than  $4'$  (perhaps  $5'$

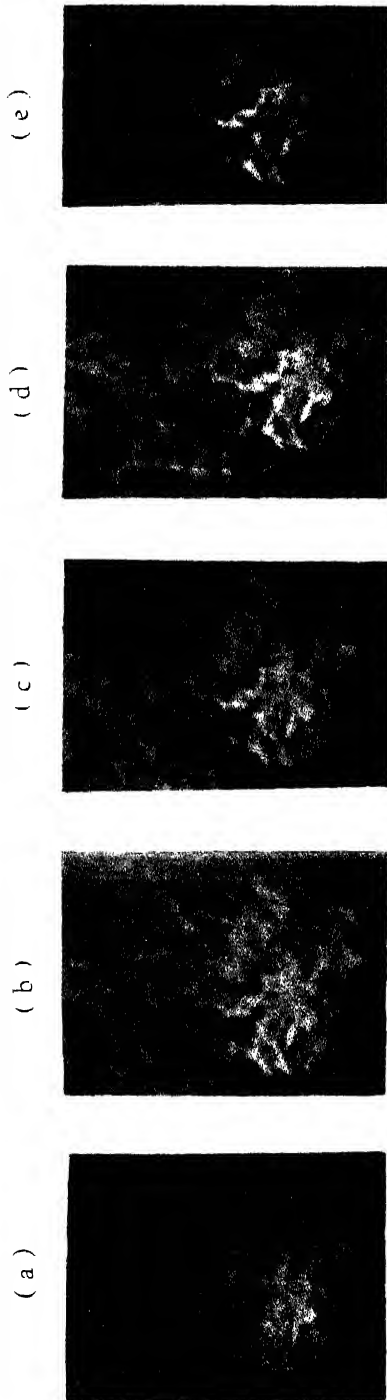
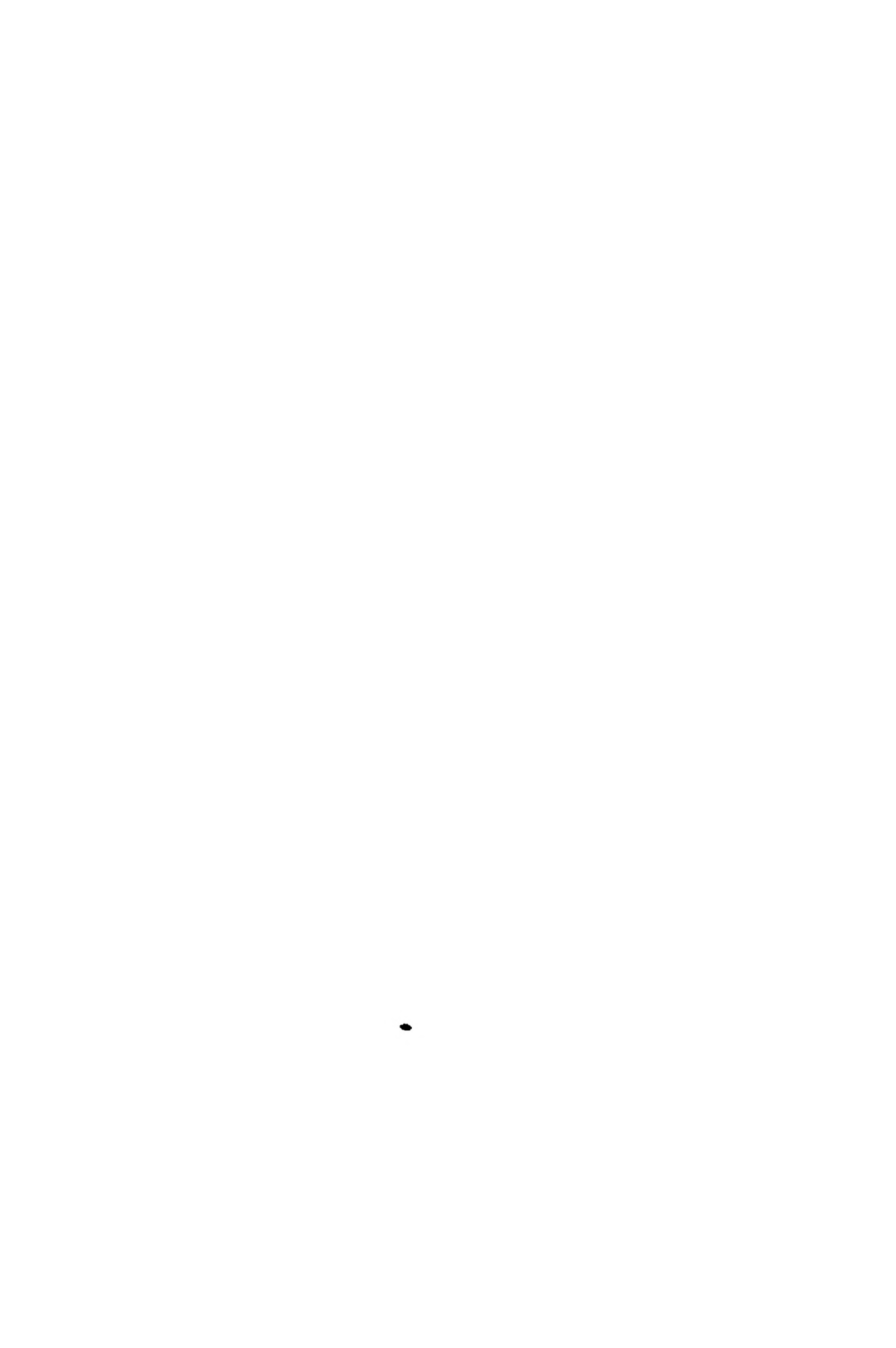


Fig. 1.



Fig. 2



which is equal to 217,500 Kms.) during a very short time. The prominence was metallic and all the lines usually observed were seen in the spectroscope. The maximum displacements observed in the prominence were  $6 \text{ \AA}$  to red (velocity of recession 275 Km./sec. and  $9 \text{ \AA}$  to violet (velocity of approach 410 Km./sec.) at  $9^h 25^m$ . The prominence completely disappeared at  $9^h 55^m$ .

A number of eruptions were also associated with the spot group No. 7159 and as many as three of these occurred on the morning of the 6th September alone. The first one began at  $8^h 32^m$ , attained its maximum brightness at  $8^h 35^m$  and subsided by  $9^h 0^m$ . Another eruption was observed to begin at  $9^h 28^m$  and it lasted till  $9^h 40^m$  reaching its maximum intensity at  $9^h 36^m$ . The third eruption in the same region, which was the brightest of all, began at  $9^h 45^m$  and though it attained its maximum intensity at  $9^h 50^m$  did not subside till two hours later. A series of 21 spectro-heliograms of this eruption was obtained in  $\text{H}\alpha$  light and the more important ones are reproduced in figures 3 (a) to 3 (c) (see plate XXI).

Apart from these eruptions, the other important phenomena noted during the period are the breaking up of  $\text{H}\alpha$  dark markings. Instances of breaking up of markings were observed on the 26th August and on the 2nd and 12th September. The last of these was remarkable in as much as a big marking, which was seen for a number of days, completely disappeared in a very short interval. This marking is shown by means of an arrow head in the spectro-heliogram figure 4 (a) taken at  $8^h 17^m$  on September 12. It is seen that the northern end of the marking is connected with the spot No. 7157, the other end of the marking establishing a contact with the spot group No. 7159. Nothing special was noted in the marking till about  $9^h 32^m$ , when suddenly the end of the marking close to the spot group No. 7159 began to show a displacement of about  $1.2 \text{ \AA}$  to violet indicating an outward rush of matter from one of the spots of the group. At the same time a displacement of  $1.0 \text{ \AA}$  to red in the portion of the marking about the middle, i.e., nearest the west limb was observed indicating that the matter coming out of the spot was moving towards the limb. The displacement towards red gradually increased and was about  $2.5 \text{ \AA}$  at  $9^h 45^m$ . A streak was clearly seen starting from this point of the marking and advancing towards the limb giving rise to a prominence which is reproduced here in figure 4 (b). The maximum height attained by the prominence was about 3'. Perhaps its height was actually much greater, but it could not be measured as the top was cut off in all the three photographs taken that morning. After a short time the prominence as well as the dark marking completely disappeared. As can be seen from the spectro-heliogram figure 4(c) taken at  $10^h 26^m$ , there is no trace of the dark marking, but on the other hand there is a bright marking exactly in the same place where the dark marking was before. The bright marking is clearly the base of the prominence that disappeared and is a good example in support of the conclusions arrived at in a previous bulletin<sup>1</sup> that the lowest parts of a prominence being much brighter than the surrounding disc show themselves by emission, and

that only the higher portions of a prominence show themselves by absorption on the disc.

It is a well-known fact that photographs of the sun's disc taken in monochromatic light show decided contrast between the intensity of a sunspot and that of the surrounding region on the disc. If it is assumed that these brilliant chromospheric outbursts are associated with exceptionally high temperature, they should show themselves conspicuously in the monochromatic images taken at the time of their occurrence. Photographs taken at this observatory on several occasions in regions free from absorption lines fail to show any images corresponding to the eruptions shown in the photographs taken in H $\alpha$  line or the line of calcium. It seems therefore reasonable to conclude that the active agent producing both the eruption and the observed terrestrial effects originates in layers lower than the chromosphere, below the eruptive patch.

Correlations between solar eruptions and disturbances in terrestrial magnetic elements have been cited by A. G. McNish<sup>2</sup> who found that the magnetic disturbances produced by the chromospheric eruptions are unique and that in almost every case they are augmentations of the normal diurnal variations in geomagnetism. Although the persistent activity with frequent appearance of unusually bright and extensive eruptions mentioned in the present study extended over several days, Alibag magnetic records did not reveal any magnetic disturbance of sufficient importance. It would appear that the connection between the eruptions and the magnetic effects is not a simple one and there is need for further careful studies of the diurnal variations accompanying solar outbursts.

It has not been possible to study the connection between these solar flares and the associated radio effects, as continuous series of daily records regarding the behaviour of the ionosphere are not available in India.

In conclusion the authors wish to express their thanks to the Director and Assistant Director for their helpful criticisms and suggestions.

THE SOLAR PHYSICS OBSERVATORY,  
KODAIKANAL.

#### R E F E R E N C E S

<sup>1</sup> T. Royds, *Kodaikanal Observatory Bulletin* No. 89.

<sup>2</sup> A. G. McNish *Phys. Rev.*, 52, 155-160 (1937). *Cinquième Rapport de la Commission Pour L'ictude*, pp. 105-110, 1938.

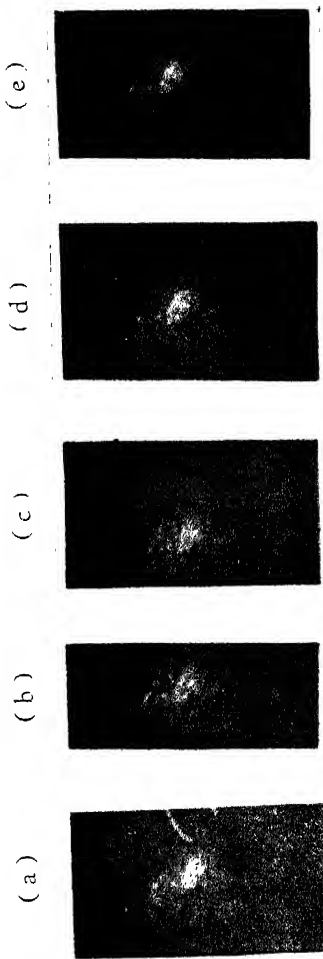


Fig. 3.

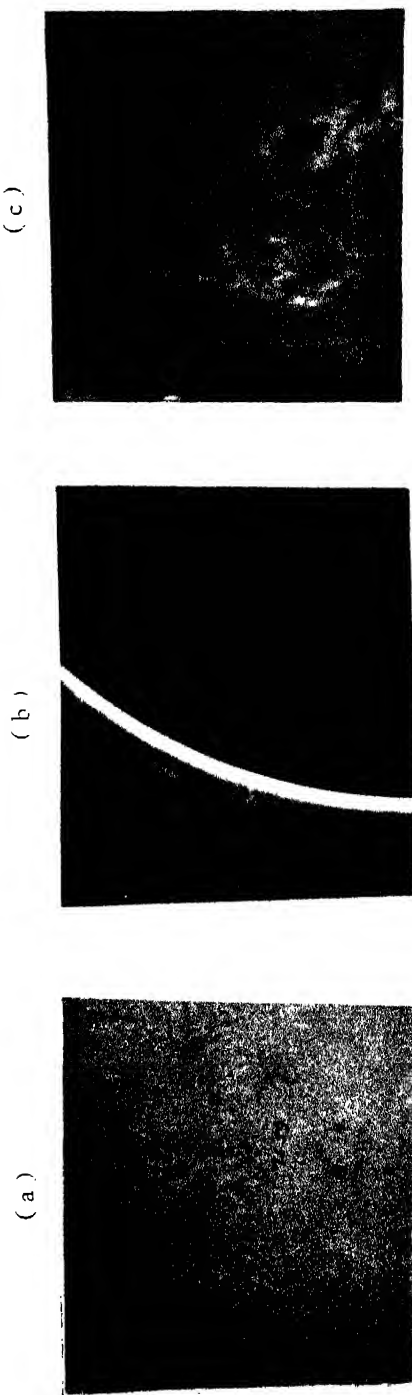


Fig. 4



# On the Origin of Colour in Paramagnetic Salts and Solutions

D. M. BOSE.

I have to thank the members of the Indian Physical Society for electing me your President. I have been officially connected with the Society since its foundation in 1935, and it is an honour which I greatly appreciate being asked to preside over the affairs of the Society. I regret very much that pressure of other work prevents me from coming down to Madras and attend this annual meeting of our Society.

You have before you the report presented by the Council on the work of the Society during the past year. We have reason to congratulate ourselves on the satisfactory progress we have achieved during the five years of our existence, but we are aware that there is room for further improvement, in increasing the membership of the Society and also in making the latter more adequately represent the interests and activities of the physicists in India. The Council invite your suggestions and co-operation in achieving this aim.

Mention has been made in the annual report of the very interesting lecture on Cosmic Ray which Prof. Millikan gave before a meeting of the Indian Physical Society. We cordially welcome the presence of the distinguished physicist and his co-workers to this country, and we look forward to a very successful outcome of the investigations undertaken by them here.

The visit of these scientists to India, has raised in our minds the question of the possibility of locally initiating Cosmic Ray investigation in this country. India is surrounded by high mountains, and it will not be difficult to install permanent observation stations at altitudes up to 14,000 ft., which are not very far from centres of electrical and mechanical power supply. Further the extended land area and the favourable meteorological conditions during certain parts of the year, make this country specially suitable for balloon flight investigation. The Indian Meteorological Department is giving valuable assistance to Prof. Millikan and his party in their investigations, and we hope later on the same help will be available to Indian physicists when they take up this line of work. Scientific

workers in India have made valuable contributions to the sciences of geodesy, meteorology and recently to our knowledge of the ionosphere. We look forward to a time when equally important contributions will be made from this country to our knowledge of the Cosmic Ray phenomena.

It is customary at such annual gathering for your president to deliver an address on some topic selected by him. A certain amount of latitude is given to him, and after some hesitation I have decided to place before you a connected account of a subject in which I have been interested for several years, it is on the origin of colour in paramagnetic crystals and solutions. The reason for my hesitation is that the President of the Physics section of the Indian Science Congress, who is an authority on the subject of crystal magnetism will probably deal with the subject of crystal magnetism in his presidential address, and there may be some overlapping between the subject matter of his discourse and mine. Still I hope I may be able to present you with a different way of approaching the investigation of the crystalline field present in paramagnetic crystals and solutions, whose influence is felt in diverse subjects like paramagnetic susceptibility, anisotropy, paramagnetic rotation and even colour.

In my address I shall first discuss how the concept of a molecular field, which is of electrostatic origin, arose gradually from a study of paramagnetic susceptibility, then how an elegant analytic method of investigating this crystalline field was developed by Bethe, Van Vleck and his fellow workers. Next it will be shown how a test of the optical consequence of Van Vleck's theory was undertaken by a study of the band absorption in paramagnetic crystals and solutions. Such a study led to the proposal of an empirical formula which appears better to account for the Stark splitting responsible for the absorption bands in these paramagnetic substances. A theoretical deduction of the empirical formula is given, which permits of a fairly approximate calculation of the number and frequencies of the absorption bands in terms of the known constants of the paramagnetic ion and of the associated dipole molecules.

The discovery of the law of temperature variation of paramagnetic susceptibility is due to Curie's investigation with oxygen, when it was found that

$$\chi = \frac{C}{T}; \text{ where } \chi \text{ is the molar susceptibility.}$$

The theoretical interpretation of this relation was given by Langevin, who assumed that each oxygen molecule was the seat of a permanent magnetic dipole of moment  $\mu$ . Langevin found that in a not too intense magnetic field  $\chi = \frac{N\mu^2}{3kT}$ ; if we further take into consideration the tempera-

ture independent susceptibility observed in many substances, which are partly of diamagnetic and partly of paramagnetic origin then

$$\chi = \frac{N\mu^2}{3kT} + N\alpha \quad \dots \quad \dots \quad \dots \quad (1)$$

Weiss investigated the temperature dependence of the paramagnetic susceptibility of crystals and solutions, and showed that over fairly large ranges of temperature the Curie law in the modified form  $\chi = \frac{C}{T - \Delta}$  holds. Weiss interpreted the correction factor  $\Delta$  as due to the presence of an inner magnetic field of molecular origin. It was Debye who first showed that this molecular field was most probably of electrostatic origin.

The next line of investigation which again pointed to the presence of this crystalline field began with the quantum theory interpretation of the origin of the magnetic moment  $\mu$  of the ions. According to the quantum theory the magnetic moment of a free ion with inner quantum number  $j$  is  $\mu = j\beta$  where  $\beta = \frac{e\hbar}{4\pi mc}$  is the Bohr's unit of magnetic moment. This value of  $\mu$  is not a constant, but depends upon the state of excitation of the ion. If the energy difference between the ground and the excited states of the ion is large compared to  $kT$  then the ions at the temperature  $T$  are all in the ground state, and in a field of strength  $H$  the  $2j+1$  fold state of degeneracy of the ion is removed, and the average moment of the ion is  $\mu = \sqrt{j(j+1)}\beta$ .

This relation first deduced by Hund was well verified in the case of the ions of the rare earth elements, *viz.* the experimentally determined values of  $\mu$  agreed well with those calculated from spectroscopic data. When the same formula was tried to account for the measured magnetic moments of the ions of the iron group of elements, there was a total lack of agreement. It was pointed out by me in 1927 that the magnetic moment of a large number of simple and complex compounds of the iron group of element could be explained on the assumption that the orbital moments of these ions were completely quenched by the interaction with its neighbouring atoms in solids and solutions, so that the spin moment of the ions were alone free to orient in a magnetic field.

This leads to the formula

$$\chi = \frac{4S(S+1)}{3kT} N\beta^2 \quad \dots \quad \dots \quad \dots \quad (2)$$

In deducing the formula the analogy of the quenching of the temperature variation of dielectric polarisation on solidification, observed in polar liquids, was used.

The investigation of the mechanism of the quenching of the orbital moment of ions in paramagnetic crystals or rendering them partially ineffective was the starting point of a series of important communications by Van Vleck and his fellow workers.

### **Van Vleck's Theory.**

We have seen that the  $2j+1$  fold degeneracy of an ion is totally removed by an axial magnetic field. If the ion forms part of a crystal, then due to the regular arrangement of other ions and atoms round it, an electric field of a given symmetry acts on the ion and thereby either partially or totally removes the degeneracy of the orbital moment of the ion, depending upon the symmetry properties of the crystalline field. Thus a Stark effect separation of the degenerate state of the ground term of the paramagnetic ion is produced. On the magnitude and degree of this separation will depend the future behaviour of the paramagnetic crystal in a superposed magnetic field. If the separation is small compared to the multiplet separation of the ground term of the ion, and also to the latter's spin orbital coupling, the inner quantum number of the ion retains its significance and Hund's formula will fairly represent the temperature variation of the susceptibility of such crystals. This is the case with the rare earth crystals, in which the incomplete  $4f$  shell responsible for the paramagnetism of the rare earth ion is inside the  $5s, p$  octet shell; the latter shields the former more or less effectively from the outer crystalline field.

In the case of the salts of the iron group of elements the  $3d$  shell is the carrier of the paramagnetic effect and is fully exposed to the crystalline field. If the potential energy of the latter is large compared to the energy of the spin orbital coupling  $\lambda(LS)$ , then the latter breaks down and a Stark effect splitting of the  $L$  moment of the ion takes place, since an electric field has no direct effect on the spin moment.

Bethe in 1929 published an important investigation on the Stark splitting of the ground term of ions with S, P, D, F orbital quantum numbers. For example in a field of cubic symmetry the D term is split up into two components  $\Gamma_3$  and  $\Gamma_5$ , the former is doubly degenerate and non magnetic, and the latter triply degenerate. The F term is split into three components  $\Gamma_2, \Gamma_5$  and  $\Gamma_4$  of which  $\Gamma_2$  is non degenerate and non magnetic, while the two others are both triply degenerate. In a rhombic field, all the degeneracies of the ground term are completely removed. In a magnetic field, the spin and orbital moment of the ion will, upto the factor of spin orbital coupling, be free to orient independently—the orbital moment so far as its degeneracy has not been removed by the crystalline

field. Many of the paramagnetic salts like chrome alum belong to the cubic system, while in the case of others belonging to the hydrated crystals of the rare earth group, it is found that it is sufficient to take a predominantly cubic field. Such a field is however not capable of accounting for the observed paramagnetic anisotropy of the hydrated crystals containing  $\text{Fe}^{++}$ ,  $\text{Co}^{++}$ ,  $\text{Ni}^{++}$  and  $\text{Cu}^{++}$  ions. Penney and Schläpp suppose that an additional field of rhombic symmetry of low intensity is superposed on the dominant cubic field in these hydrated crystals. While in the case of certain other paramagnetic Alums Van Vleck has assumed the existence of a small trigonal field. The most general expression for the energy of an ion in a superposed crystalline and magnetic field of strength  $H$  is :

$$V = \Sigma [D(x_i^4 + y_i^4 + z_i^4) + Ax_i^2 + By_i^2 - (A+B)z_i^2] + \lambda(L.S) + \beta H(L+2S) \dots \dots \quad (3)$$

where  $x_i$ ,  $y_i$  and  $z_i$  represent the coordinates of an electron in the d-shell of the ion, and the summation is over all the electrons present in the latter. The first term represents the dominant cubic field, the second represents the rhombic field,  $\lambda$  is the constant of the spin orbit interaction.

Fig 1. gives the term levels for the D and F ions.

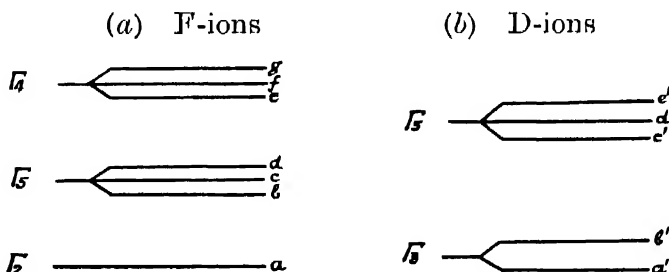


FIG. 1

(Upright in  $\text{Ni}^{++}$ , inverted in  $\text{Co}^{++}$ ) (Upright in  $\text{Cu}^{++}$ , inverted in  $\text{Fe}^{++}$ )

We shall first consider the conditions under which a paramagnetic crystal will have a spin only value for its susceptibility. They are :

- (i) the ground term is non degenerate and non magnetic like  $T_2$  of F
- (ii) the crystalline field is essentially cubic
- (iii) the distance between the ground and the upper terms is very large compared to  $kT$ .
- (iv) the spin orbital coupling is negligible and
- (v) the magnetic moment induced in the ground state  $a$  by the higher energy states like  $k$  which is of the form  $2H \sum_k |\mu(ak)|^2 / h \cdot v(ka)$  is negligible.

Chrome alum is found to be magnetically isotropic with a magnetic susceptibility almost perfectly represented by formula (2). Penney and Schlapp find that the susceptibility is better represented by the formula  $\chi = \frac{15N\beta^2}{3kT} \left(1 - \frac{2\lambda}{5Dq}\right)^2$ ; the correction term represents the effect of spin orbital interaction.

Next we consider the case of the Nickel salts. Their susceptibility e.g. of the hydrated sulphate is greater than the spin only value, and its magnetic anisotropy is about 30 per cent. Here it is assumed that the term sequence is the same as that in the chromic salts, only the separation is less, and there is a small rhombic field. In this case the induced magnetic moment due to the interaction with the triplet terms of  $I'_{3}$  and  $I'_{4}$  are comparatively large, and we have a temperature independent susceptibility which is dependent upon the direction of the magnetic axis. Therefore the value of the induced moment is different along the three magnetic axes of the crystal, and this is the origin of the anisotropy of Nickel salts.

Penney and Schlapp have calculated the splitting of the F term in the cubic field and obtained the following values of the 3 Stark terms 0,  $8Dq$  and  $18Dq$  where  $q$  is the multiplicative factor of D in equation (3) for a system of  $n$  electrons.

The value of  $\bar{\chi}$  the mean susceptibility of  $\text{Ni}^{++}$  is found to be

$$\chi = \frac{8N\beta^2}{3kT} \left[ 1 + \left( \frac{8\lambda}{3} - kT \right) (\alpha_1 + \alpha_2 + \alpha_3) \right]$$

where  $\alpha_1$ ,  $\alpha_2$ , and  $\alpha_3$  are certain constants, proportional to the intensities of the rhombic field along the three magnetic axes.

Comparison of this expression after certain simplifications, with the magnetic data enables the values of  $Dq$  to be calculated, which comes out to be  $1485 \text{ cm}^{-1}$  for  $\text{Ni}^{++}$  salts and  $3730 \text{ cm}^{-1}$  for  $\text{Cr}^{+++}$ . A knowledge of these constants enables us to calculate the Stark term separation for the F ion, they come out to be of the order of  $10^4 \text{ cm}^{-1}$ .

Now  $\text{Co}^{++}$  ( $d^7 4F$ ) has the same orbital term as  $\text{Ni}^{++}$  ( $d^8 3F$ ) and carry the same ionic charge, but they differ greatly in their magnetic properties, viz. the susceptibility of  $\text{Co}^{++}$  shows a very large deviation from the Bose Stoner value, and the anisotropy of hydrated cobalt sulphate crystal is about 70%. Van Vleck shows that from theoretical consideration the term level in  $\text{Co}^{++}$  is inverse to that in  $\text{Ni}^{++}$  so that the ground term in the former is the triply degenerate  $I'_{4}$  with a residual orbital moment. The contribution of the latter accounts for the larger deviation from the

spin only value of susceptibility in cobalt salts. Assuming the existence of rhombic field,  $I'_4$  is split up into three sub levels, and then the large anisotropy in Cobalt salts can at least be qualitatively interpreted.

So far nothing has been said of the way in which the triply degenerate  $I'_4$  and  $I'_5$  levels can be split up. We find that more detailed specification is necessary to account for the spin only values of the paramagnetic susceptibilities of the alums of Vanadium and Titanium. This is only possible if the ground terms of both these ions are non-degenerate and also non-magnetic.

In Table I are given the various D and F ions and how they split up into upright or inverted terms in a cubic field according to Van Vleck's classification. The general principle underlying this tabulation appears to be that pairs of ions with the same orbital quantum number, the sum total of whose d electrons are either 5, 10, or 15 have opposite sequences of term.

According to this Table the ground term of  $Ti^{++}$  is  $d^1 \text{ } ^2D \text{ } I'_5$  and of  $V^{+++}$  is  $d^2 \text{ } ^3F \text{ } I'_4$ , both of which are triply degenerate; and as such their magnetic susceptibilities ought to deviate largely from the spin only values.

TABLE I.

## Ions with D-term :

## Ions with F-term

Ion.	Theoretical.*	Ion.	Theoretical?
$Ti^{++}$	Inverted	$V^{+++}$	Inverted
$Cr^{++}$	Upright	$Cr^{+++}$	Upright
$Fe^{++}$	Inverted	$Ni^{++}$	do
$Cu^{++}$	Upright	$Co^{++}$	Inverted
$(MoO)^{++}$	Inverted		
$(WO)^{++}$	do		
$Ce^{+++}$	do		

To account for the spin only value of magnetic susceptibility of these alums the following assumptions are necessary.

(i) that in these alums a field of lower symmetry than cubic exists in which the triply degenerate ground term  $I'_5$  and  $I'_4$  are split up. This assumption was not necessary in the case of Chrome alum since the lowest level in  $Cr^{++}$  is the non-degenerate  $I'_2$ .

(ii) that in both cases the lowest of these terms is non-magnetic. If the lowest term is non-degenerate but has an orbital moment, then in the expression for magnetic susceptibility a term independent of temperature is added.

\* As given by Van Vleck.

1. Van Vleck shows that in the alums an additional field of trigonal symmetry exists, which arises as shown by X-ray analysis from the fact that the principal axes of the unit cell round each paramagnetic ion do not coincide with the principal axes of the octahedral arrangement of the six associated water molecules. The Stark splitting in a trigonal field of  $\Gamma_4$  and  $\Gamma_5$  term is shown in fig. 2.

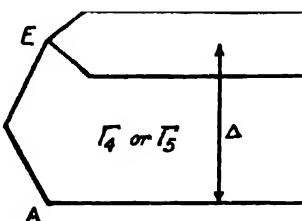


FIG. 2

(The splitting of a triply degenerate cubic state in a trigonal field. The two components of E coincide unless magnetic forces are applied).

2. Siegert has shown that in the most general type of trigonal field it cannot be expected that the non degenerate orbital level will be the deepest both for  $Ti^{+++}$  and  $V^{++}$ . Under some special type of potential function for a trigonal field will this arise.

The general formula of the alums is  $AMe(SO_4)_3 \cdot 12H_2O$  where A is an alkali atom, Me is a trivalent atom. In the paramagnetic alums each paramagnetic ion is embodied in an octahedral arrangement of six water molecules, round which the  $SO_4$  ions, the remaining  $H_2O$  molecules and the alkali atoms are grouped.

Van Vleck assumes that the cubic part of the field arises from the action of the six oriented dipole water molecules round each paramagnetic ion. Penney, Schlapp and others have calculated the value of  $Dq$  for the paramagnetic ions  $Cr^{+++}$ ,  $Ni^{++}$ ,  $Cu^{++}$ , the value is found to vary from  $1480$  to  $3730$   $cm^{-1}$ . Van Vleck assumes a reasonable value  $Dq = 1500$   $cm^{-1}$ , and from it he finds that the dipole moment of the oriented water molecules. In this theory the effect of the polarisation of these molecules due to the charge on the paramagnetic ions plays no part.

From calculations made by Penney and Schlapp, in a cubic field a F ion is split up into three Stark levels with separations  $8Dq$  and  $18Dq$  for the upright ions like  $Cr^{+++}$  and  $Ni^{++}$  and  $10 Dq$  and  $18Dq$  for inverted ions like  $Co^{++}$ , while for a D-ion like  $Cu^{++}$  the separation between  $\Gamma_3$  and  $\Gamma_5$  is  $10Dq$ .

Having obtained a clue of the origin of the cubic part of the crystalline field, Van Vleck proceeds to evaluate the splitting of the doubly

degenerate  $T_3$  and the triply degenerate terms  $T_4$  and  $T_5$  in the trigonal field. According to him the latter arises from

(i) the direct action of the distant atoms *i.e.*, those beyond the six associated water molecules

(ii) the indirect action of these distant atoms on the associated water molecules, the latter become somewhat disturbed from their normal octahedral arrangement

(iii) the Jahn-Teller effect—which states that the most stable arrangement of a polyatomic molecule is always sufficiently unsymmetrical to lift the orbital degeneracy which may be present in the central atom.

Calculations made by Van Vleck show that the total splitting produced by this trigonal field is for  $V^{++}$  ion ( $T_4$  term) from  $460-860\text{ cm}^{-1}$  and the  $Ti^{++}$  ion ( $T_5$  term) from  $1450-2200\text{ cm}^{-1}$ , according to the special assumptions made.

### Optical Test of Van Vleck's theory.

In fig. 3 is given the energy diagram of the Stark splitting of the D and F ions due to a combined cubic and trigonal fields as present in the paramagnetic alums. It will be seen that in all hydrated paramagnetic

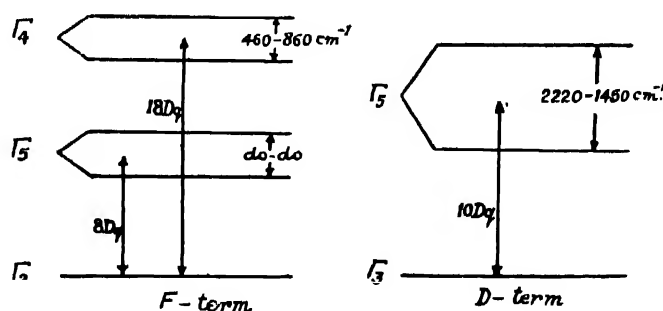


FIG. 3  
 $Dq \sim 1500\text{ cm}^{-1}$  according to Van Vleck

crystals the separation between the Stark levels is of the order of  $10^4\text{ cm}^{-1}$ ; transitions between them will produce absorption and emission spectra lying between the infra red and ultra violet regions and as such can be capable of optical verification. Another consequence of the theory is that according as the Stark levels of the ions are upright or inverted the highest absorption bands will show a doublet structure or a singlet structure. The latter will be a little complicated by the superposition of the spin orbital coupling. This will be specially noticeable in the absorption spectra due to  $Co^{++}$  and  $Ni^{++}$  ions. The investigation of the optical consequences of Van Vleck's theory has been undertaken by P. C.

Mukherji and myself<sup>1)</sup><sup>2)</sup>, the results of which are given in two papers recently published. The conclusions drawn by us are that (i) Van Vleck's theory is unable to represent the number and frequencies of the principal absorption bands ; (ii) on the other hand the doublet separation shown by some of these bands agree fairly well with predictions made by Van Vleck for the paramagnetic alums ; (iii) the structure of the absorption bands to a large extent do not conform to the classification by Van Vleck into upright and inverted Stark levels. In the first paper<sup>1)</sup> we have proposed an empirical formula which appears to us to give a better representation of the number and frequencies of these absorption bands, and we have discussed the assumptions on which such a formula could be based. In a subsequent paper<sup>3)</sup> I have attempted a theoretical deduction of this formula.

Before proceeding further it will be desirable at this stage to say a few words about the general nature of the absorption bands shown by hydrated paramagnetic crystals and solutions. Most of them are coloured, with one or two absorption bands in the visible part of the spectrum. In those crystals and solutions whose infra red absorption spectra have been investigated like those of Nickel and Cobalt, we find absorption bands in the neighbourhood of  $1.2\mu$ . Some of the absorption spectra like that due to  $\text{Cu}^{++}$  show a single broad absorption band, others like that due to  $\text{Ti}^{+++}$  show a doublet structure. Under large dispersion the absorption bands due to  $\text{Co}^{++}$  and  $\text{Ni}^{++}$  ions appear to consist of a number of fine absorption bands. We shall for the present confine our attention to the mean frequencies of the broad absorption bands and of their prominent doublet structures.

The position of the absorption bands are dependent upon the nature of the solvent in which the crystals are dissolved, e.g. water, ammonia, alcohol, etc. It is assumed that in such solvents they form hydrated, ammoniated, alcoholated complexes, and the change in the position of the absorption bands in these solvents is to be attributed to the different strength of the crystalline fields which the associated water, ammonia, alcohol dipole molecules exert on the central paramagnetic ion. From a study of these principal absorption bands we find that the following empirical formula fairly represent their number and frequencies.

$$\Delta \nu = ne. | \Delta e_L | . C.P. \dots \dots \quad (4)$$

The assumptions underlying the above formula are that

- (i) the ionic charge  $ne$  in a paramagnetic ion induces a polarisation proportional to  $P$  in the associated dipole molecules

- (ii) in the electric field due to the polarisation of the dipole molecules, the paramagnetic ion which has an electric moment proportional to its orbital quantum number  $L$ , can occupy  $L+1$  discrete energy levels each characterised by an electric quantum number  $e_L$  such that  $0 \leq e_L \leq L$
- (iii) transitions between the ground term and the  $L$  upper levels will give rise to  $L$  absorption bands, whose frequencies are given by formula (4)

where  $C$  is a numerical constant

$P$ , as we shall see later, is dependent both on the dipole moment  $\mu$  and the polarisability  $\gamma$  of the associated dipoles.

Some of the consequences of this formula which can be verified are :

- A. For the same kind of associated dipole molecules, e.g., water
- (i) For the same ion the ratio of the absorption frequencies will be as       $1 : 2$       for D-ions  
 $1 : 2 : 3$    for F-ions

According to the theory of cubic splitting the frequency ratio will be for F ions either 8 : 18 or 10 : 18 according as the term sequence in the ion is upright or inverted.

(ii) For the D resp. F-ions, the separation of the corresponding bands in different ions will be as  $nc$ ; for doubly and triply charged ions the ratio will be as 2 : 3.

(iii) For the different ions

$$K' = ecP = \frac{\Delta \nu}{n \cdot \Delta e_L} \quad \text{ought to come out as a constant.}$$

B. For the same ion associated with two different kinds of dipole molecules like water and ammonia, the ratio of their absorption frequencies will be proportional to their polarisability, i. e.,

$$\frac{\Delta \nu_{H_2O}}{\Delta \nu_{NH_3}} = \frac{P_{H_2O}}{P_{NH_3}}$$

In Tables II, III are collected the data for the known absorption bands due to paramagnetic ions with D and F orbital numbers. It will be seen that the conclusions (i) and (ii) are fairly verified, while the values of (e. C. P.) for D term varies between 2,580 to 3,380  $\text{cm}^{-1}$  with a mean value of 2,950  $\text{cm}^{-1}$  which is fairly good. For the F terms the agreement is not so good, the value of the constant varying from 2,640 to 4,130  $\text{cm}^{-1}$ .

TABLE II.

Ions.	Configura-tion.	Ground term.	$\lambda$ (A. U.)	Selective Absorption. $\nu$ (cm. <sup>-1</sup> )	Centre of gravity (cm. <sup>-1</sup> )	Transitions.	$K' = \frac{\Delta\nu}{N \cdot \Delta e_L}$ .	Observers.
Ti <sup>+++</sup> .....	$3d^1$	$^2D_{5/2}$	6100	16,369 19,225 17,336 18,513	17,807	0-2	2,968 cm. <sup>-1</sup>	{ Bose and Datta. <sup>†</sup>
(MoO) <sup>+++</sup> ...	$4d^1$	$^2D_{3/2}$	5200 5800 5400		17.875	0-2	2,979 "	Kato <sup>‡</sup> .
(W0) <sup>+++</sup> .....	$5d^1$ •	$^2D_{3/2}$	7000	14,282	15,472	0-2	2,579 "	"
(V, O) <sup>++</sup> .....	$3d^1$	$^2D_{3/2}$	6000	16,660	15,510	0-2	3,377 "	"
Cr <sup>++</sup> .....	$3d^4$	$^3D_0$	7400 7300—	18,695 16,125	14,910	0-2	3,423 "	"
			6200 4510 4100	22,216 24,368 16,385	*	—	—	Topp   .
			6120 4000	25,000	†	—	—	Dreisch <sup>¶</sup> .
Co <sup>++</sup> .....	$3d^6$	$^5D_4$				C-2	2,483 "	Dreisch and Trommer <sup>§</sup> .
Fe <sup>++</sup> .....	$3d^6$	$^5D_4$	10700	9,348 10,523	9,933	C-2	2,483 "	
Cu <sup>++</sup> .....	$3d^9$	$^2D_{5/2}$	9500 8200	12,192	12,192	2-0	3,064 "	
					Mean = 2,950 "			

\* The doublet band is perhaps due to Cr.<sup>++</sup><sup>†</sup> Loc. cit.<sup>‡</sup> Dissert. Münster (1928)<sup>||</sup> Zeits. f. Phys. Chem. xxxvii. p. 37 (1937).<sup>¶</sup> This is discussed in detail later (see Table III).<sup>§</sup> Loc. cit.<sup>¶</sup> Zeits. f. Phys. xl. p. 714 (1927).

## D. M. Bose

TABLE III

Ion.	Configura-tion.	Ground term.	Selective $\lambda$ (A. U.)	Absorption $\nu$ (cm. <sup>-1</sup> ).	Centre of gravity (cm. <sup>-1</sup> ).	Ratio.	Transi-tion.	$K' = \frac{\Delta\nu}{N_e \Delta \nu}$ .	Observers.	
V <sup>+</sup> +	.....	3d <sup>1</sup>	<sup>3</sup> F <sub>2</sub>	6100	16,359	16,389	2 : 3	0—2	2,731 cm. <sup>-1</sup>	Kato *.
				4200	23,803	23,803	..	0—3	2,645 ..	"
V <sup>++</sup>	.....	3d <sup>4</sup>	<sup>4</sup> F <sub>3/2</sub>	8200	12,192	12,620	..	0—2	3,155 ..	"
				7660	13,051	..	2 : 3	..	..	
				5600	17,852	18,180	..	0—3	3,055 ..	"
				5400	18,513	..	..	..	..	
Cr <sup>+++</sup>	.....	3d <sup>3</sup>	<sup>4</sup> F <sub>5/2</sub>	6380	15,670	15,976	..	0—2	2,668 ..	Datta and Deb †.
				6140	16,280	..	2 : 3	..	..	
				4470	22,365	22,807	..	0—3	2,667 ..	Datta and Deb †.
				4300	23,249	..	..	..	..	Dreisch ‡.
Co <sup>++</sup>	.....	3d <sup>7</sup>	<sup>4</sup> F <sub>7/2</sub>	12500	8,000	8,000	..	..	..	
				7700	12,982	12,982	..	3—1	3,245 ..	" †.
				5150	19,413	19,413	..	3—0	3,235 ..	" †.
Ni <sup>++</sup>	.....	3d <sup>8</sup>	<sup>5</sup> F <sub>4</sub>	12100	8,262	8,262	1 : 2	0—1	4,131 ..	Houston §.
				6870	14,552	14,552	..	0—2	3,638 ..	"
				4050	24,654	24,684	..	0—3	4,114 ..	"

\* Loc. cit.  
† Zeits. f. Phys. xl p. 714 (1927).

† Loc. cit.  
‡ Proc. Roy. Soc. Edin. xxxi. pp. 530, 538 (1910).

TABLE IV.

Ground state of the ion.	Substance.	Centres of selective absorption	Ratio $\frac{P_{NH_3}}{P_{H_2O}}$
D-state.....	$CuSO_4 \cdot 5H_2O$ $[Cu(NH_3)_6]Cl_2 \cdot H_2O$	12,297 cm. <sup>-1</sup> 14,160 „ Ratio..... '87	
F-state.....	$[Cr(II_2O)_6]Cl_3$ $[Cr(NH_3)_6]Cl_3$	18,200 cm. <sup>-1</sup> , 24,100 cm. <sup>-1</sup> 21,500 „, 23,500 „ Ratio..... '85 '85	
	$[Ni(II_2O)_6]Cl_2$ $[Ni(NH_3)_6]Cl_2$	8,497 cm. <sup>-1</sup> , 15,870 cm. <sup>-1</sup> , 25,510 cm. <sup>-1</sup> 10,804 „, 17,200 „, 27,900 „ Ratio..'79 '89 '91	
G. or H state.....	$[Co(II_2O)_6]Cl_3$ $[Co(NH_3)_6]Cl_3$	16,340 cm. <sup>-1</sup> , 25,000 cm. <sup>-1</sup> 10,460 „, 28,650 „ Ratio..... '84 '87	

In Table IV is given the ratio of the frequencies of absorption of the same ion when associated with water and ammonia dipoles. The value of this ratio varies between '79 to '91, while according to the theoretical formula to be deduced later this ratio is '78 for D terms and '74 for F terms (see p. 15, formula (6)). We may consider the agreement as fairly satisfactory.

We shall now briefly indicate the theoretical deduction of the empirical formula given above. It is assumed that round each paramagnetic ion six dipole molecules are completely oriented, occupying the six faces of a cube at distances  $R = 2\Lambda^\circ$ . The intensity of the field at the centres of these molecules is  $E = \frac{ne}{R^3}$ . Under the action of this field, the axis of each of the dipoles will point towards the ion, and also a polarisation  $\gamma E$  will be induced on each of them. The combined effect of these two for each dipole will be a field of intensity F at the centre of the ion where

$$F = \frac{2\mu}{R^3} + \frac{2\gamma ne}{R^5}$$

The resultant field due to the six oriented dipole molecules can be written as equal to  $CF$ . It is difficult to calculate the value of C; we shall determine its value from experimental data. *A priori* it can be seen that  $C < 1$ , due to the fact that the fields of the six dipoles acting on the central ion, will to a large measure neutralise each other. We assume that the ion has an electric moment  $M_L^E$  proportional to the orbital number L, and the

energy of orientation of the ion in the field of a single dipole molecule is taken to be

$$dW = M_L^E \cdot \frac{e_L}{I_L} \cdot C \cdot F.$$

If the frequency of absorption due to a transition from the ground term is

$$\Delta v, \text{ then } \Delta v = \frac{\Delta W}{h} = -\frac{M_L^E}{I_L} \cdot |\Delta e_L| \cdot C \cdot n e P \quad \dots \quad (5)$$

$$\text{where } P = \frac{2}{R^5 h} (\gamma + \frac{R^2}{ne} \cdot \mu)$$

From experimental data we find that  $\frac{M_L^E}{I_L}$  is independent of  $I_L$  and we shall

put  $M_L^E = \bar{r} \cdot e \cdot L$ , where  $r$  is the mean radius of the three quantum Hydrogen like ion with charge  $ne$ .

We shall determine the value of  $C$  from the absorption data for  $Ti^{++}$  ion.

We take  $n=3$ ;  $\bar{r}=1.08 \times 10^{-8}$  cm. approximately and it is found  $F=19.9 \times 10^5$

The calculated value of  $\Delta v = C \cdot 94.6 \times 10^3 \text{ cm}^{-1}$

While the observed value =  $17.8 \times 10^3 \text{ cm}^{-1}$ .

So that,  $C \sim \frac{1}{6}$  which appears to be quite plausible.

We shall next proceed to deduce a result of which we have previously made use, viz., we shall determine the ratio of the absorption frequencies, when the same paramagnetic ion has either water or ammonia molecules associated with it. The ratio comes,

$$\frac{\nu_{H_2O}}{\nu_{NH_3}} = \frac{2n_1\gamma_1 e + \frac{2\mu_1}{R^3}}{2n_2\gamma_2 e + \frac{2\mu_2}{R^3}} \quad \dots \quad (6); \quad \begin{array}{ll} \text{for water} & \mu_1 = 1.84 \times 10^{-18} \\ & \gamma_1 = 1.49 \times 10^{-24} \\ \text{for ammonia} & \mu_2 = 1.46 \times 10^{-18} \\ & \gamma_2 = 2.26 \times 10^{-24} \end{array}$$

Taking  $R=2 \times 10^{-8}$  cms. the value of this ratio comes to be 0.78 for D ions and 0.74 for F ions ( see p. 14 for verification ).

I hope the above discussion will convince you that we have a fairly satisfactory basis for a theory of the origin of colour shown by hydrated paramagnetic salts and solutions. I will not overtax your attention by discussing the rough model on which I have made it plausible why the quantum number  $L$  is restricted between 0 and  $L$  and not between  $\pm L$ .

It is useful at this stage to compare the two different methods of approach adopted by the school of Bethe and Van Vleck, and by the present writer. In the former from the consideration of symmetry an analytic expression for crystalline field which is suited to account for the paramagnetic phenomenon is deduced and by methods of group theory the number of Stark levels are calculated and their relative separation expressed in terms of an undetermined constant  $D$ . The latter is determined from the temperature variation of susceptibility or paramagnetic anisotropy of these crystals. Then by choosing a suitable mean value for this constant, it is found that the crystalline field is alone due to the dipole moment  $\mu$  of the associated molecule. The effect of the central charge  $ne$  of the paramagnetic ion and the polarisability of the associated molecule play no part in the theory. This theory cannot, therefore, explain the greater frequencies of absorption in ammoniated as compared to the hydrated ion, since  $\mu_{NH_3} < \mu_{H_2O}$ , nor the dependence on the ionic charge. While in our method of approach we have started with the scrutiny of experimental data and shown how they can be best fitted to an empirical formula, of which a theoretical deduction is next attempted.

I next propose to show how the splitting of triply degenerate terms  $T_4$  and  $T_5$  in paramagnetic alums as calculated by Van Vleck can be experimentally verified.

Doublet structure of the bands—In Table V have been collected the doublet separation for the principal absorption bands for D and F ions. It will be noticed that the doublet separation lies within the limits calculated by Van Vleck for the splitting of the D and F terms. As some of

TABLE V.

D-term Ions.		F-term Ions.
Ti <sup>+++</sup>	—2886 cm. <sup>-1</sup>	V <sup>+ +</sup> —859 cm. <sup>-1</sup>
Cr <sup>++</sup>	—2430 „	659 „
Fe <sup>+ +</sup>	—1180 „	Cr <sup>+ + +</sup> —608 „
(MoO) <sup>++ +</sup>	—1277 „	874 „
(WO) <sup>++ +</sup>	—2880 „	Co <sup>+ +</sup> —750 cm. <sup>-1</sup>
Ce <sup>++ +</sup>	—2408 „	Ni <sup>+ +</sup> no structure for the highest absorption band.

the data contained in the above tables are taken from absorption data for hydrated crystals and partly from paramagnetic solutions, we may conclude that some or all of the factors which according to Van Vleck produce the trigonal field in the alums are also effective in other hydrated crystals and solutions. Further discussion of these results are given in our second paper. Another interesting conclusion, which can be drawn from the fine structure of the absorption bands, is on the sequence of the Stark splitting in the ions responsible for them i.e. whether the splitting is upright or inverted.

In Table VI are collected the data of the Stark level sequences in different D and F ions as calculated by Van Vleck and as deduced from absorption data. It will be seen that in most of them Van Vleck's sequence

TABLE VI.

*Ions with D-term :*

<i>Ion.</i>	<i>Theoretical.<sup>a</sup></i>	<i>Observed</i>	<i>Remarks.</i>
$Ti^{++}$	Inverted	Upright	Observed in $HCl$ solution of $TiCl_3$ , which may lead to an inversion of levels.
$Cr^{++}$	Upright	Upright	
$Fe^{++}$	Inverted	Upright	
$Cu^{++}$	Upright	Inverted	
$(MoO)^{++}$	Inverted	Upright	
$(WO)^{++}$	do	do	
$Ce^{+++}$	do	Inverted	Triplet observed due to the effect of large spin-orbital coupling.

*Ions with F-term :*

$V^{+++}$	Inverted	Upright	
$Cr^{+++}$	Upright	do	
$Ni^{++}$	do	Inverted	
$Co^{++}$	Inverted	Upright	

is not followed. The crucial case is the reversal of the sequences in  $Co^{++}$  and  $Ni^{++}$ , on which the whole theory of the large anisotropy of  $Co^{++}$  salts compared to that of  $Ni^{++}$  salts was based.

\* As given by Van Vleck.

The point raised here is whether the interpretation of the origin of of the absorption bands, in hydrated paramagnetic crystals and solutions given above is valid ; also whether it is legitimate to apply the Stark level scheme deduced from it to the interpretation of paramagnetic anisotropy, and other magnetic properties.

I hope I may interest some of you to take up the study of light absorption in paramagnetic salts and solutions, specially with a view to the determination of the fine structure of the absorption bands. Many important problems as to the nature of the crystalline field in crystals and solutions await investigations, and can be attacked by the absorption spectra method.

### References

1. D. M. Bose & P. C. Mukherji—Origin of Colour of Paramagnetic Ions in Solution, Phil. Mag. XXVI, p. 757, 1938.
2. Ibid—On the Colour of Paramagnetic Ions in Solution II. Fine Structure of the Absorption Bands, Ind. Jour. Phys. XIII, p. 219, 1939.
3. D. M. Bose—On the origin of the crystalline field acting on Paramagnetic ions in hydrated crystals and aqueous solutions—Trans. Bose Res. Inst. Vol. XIII, 47.